GLOBAL MAPPING OF HUMAN SETTLEMENT

Experiences, Datasets, and Prospects

Taylor & Francis Series in Remote Sensing Applications

Series Editor

Qihao Weng

Indiana State University
Terre Haute, Indiana, U.S.A.

Global Mapping of Human Settlement: Experiences, Datasets, and Prospects, *edited by Paolo Gamba and Martin Herold*

Hyperspectral Remote Sensing: Principles and Applications, *Marcus Borengasser, William S. Hungate, and Russell Watkins*

Remote Sensing of Impervious Surfaces, *Qihao Weng*

Multispectral Image Analysis Using the Object-Oriented Paradigm, *Kumar Navulur*

GLOBAL MAPPING OF HUMAN SETTLEMENT

Experiences, Datasets, and Prospects

Edited by
Paolo Gamba *and* Martin Herold

CRC Press
Taylor & Francis Group
Boca Raton London New York

CRC Press is an imprint of the
Taylor & Francis Group, an **informa** business

CRC Press
Taylor & Francis Group
6000 Broken Sound Parkway NW, Suite 300
Boca Raton, FL 33487-2742

CRC Press is an imprint of Taylor & Francis Group, an Informa business

No claim to original U.S. Government works

Printed in the United States of America on acid-free paper
10 9 8 7 6 5 4 3 2 1

International Standard Book Number: 978-1-4200-8339-2 (Hardback)

Library of Congress Cataloging-in-Publication Data

Global mapping of human settlement: experiences, datasets and prospects / Paolo Gamba, Martin Herold, editors.
p. cm. -- (Taylor & Francis series in remote sensing applications ; v.4.)
Includes bibliographical references and index.
ISBN 978-1-4200-8339-2 (alk. paper)
1. Human settlements. 2. Human geography. 3. Human beings--Migrations. 4. Rural-urban migration. 5. Remote sensing. 6. Aerial photography. 7. World maps, Physical. 8. Maps, Comparative. I. Gamba, Paolo. II. Herold, Martin.

GF101.G57 2009
304.2022'3--dc22 2009019416

Visit the Taylor & Francis Web site at
http://www.taylorandfrancis.com

and the CRC Press Web site at
http://www.crcpress.com

Contents

PART III Mapping and Monitoring Projects and Research

PART IV Critical Issues and Avenues for Future Research

Series Foreword

Remote sensing refers to the technology of acquiring information about the Earth's surface (land and ocean) and atmosphere using sensors onboard airborne (aircraft, balloons) or spaceborne (satellites, space shuttles) platforms. Since the end of World War II, the technology of remote sensing has gradually evolved into a scientific subject. Its early development was driven mainly by military uses. Later, remotely sensed data became widely applied to civilian usages. Remote sensing applications cover a range of topics including archaeology, agriculture, cartography, civil engineering, meteorology, climatology, coastal studies, emergency response, forestry, geology, geographic information systems, natural and man-made hazards, land use, land cover, natural disasters, oceanography, and water resources. Recently, with the advent of high spatial-resolution imagery and more capable techniques, commercial applications of remote sensing are rapidly gaining interest in the remote sensing community and beyond.

The Taylor & Francis Series in Remote Sensing Applications is dedicated to recent developments in the theories, methods, and applications of remote sensing. Written by a team of leading authorities, each book is designed to provide up-to-date developments in a chosen sub-field of remote sensing applications. Each book may vary in format, but often contains similar components, such as a review of theories and methods, analysis of case studies, and examination of the methods for applying remote sensing techniques to a specific practical area. This book series may serve as guide or reference books for professionals, researchers, scientists, and alike in academics, governments, and industries. College instructors and students may also find them to be excellent sources for textbooks or a supplement to their chosen textbooks.

This book, *Global Mapping for Human Settlement: Experiences, Datasets, and Prospects,* focuses on urban remote sensing at the global scale, and intends to provide an overview of datasets, approaches, and important lessons in the use of remotely sensed data to map human settlements regarding land cover, land use, and human population. Mapping human settlements is a topic of worldwide interest due to its importance in various aspects of urban planning, environmental management, quality of life, and decision making. The focus on global cities reflects awareness of the increasing percentage of the world population that lives in urban areas, and growing concerns over the Earth's environment. The evolving sensor technology and digital image processing algorithms continue to drive users' interest in better quality and globally consistent land use and land cover data from remote sensing imagery. Because previous efforts in mapping human settlements were concerned largely with the regional and local scales, this book fills a unique niche in the field of urban remote sensing.

Professors Gamba and Herold have extensive experience in conducting research, and publishing results in top remote sensing journals. By coordinating the efforts of a group of leading figures in urban remote sensing, this edited volume is expected to have a great impact on global land mapping for many years to come.

I hope that the publication of this book will promote a better use of remote sensing data, science, and technology, and will facilitate the monitoring and assessing of the global environment and sustaining our common home — the Earth.

Qihao Weng, Ph.D.
NASA
Huntsville, Alabama

Preface

According to United Nations predictions, by the year 2030 60% of the world's population will live in cities. Although urban areas occupy only approximately 3% of the Earth's surface, their impact on surrounding rural areas is rapidly increasing, and they drive and change natural and human systems at all geographic scales. Any operational efforts tailored at sustainable and desirable future development have to consider urban dynamics as one of the key human-induced processes for understanding and managing our fast-changing world. Earth observation has been focused on mapping, monitoring, and understanding these urban phenomena for many years, but with more emphasis on local to regional scales. Global mapping of human settlements is particularly challenging because of the spatial and spectral heterogeneity of urban environments, as well as their small and fragmented spatial configuration.

The aim of this book is to provide a comprehensive overview of experiences, methodologies, datasets, and approaches related to the use of remotely sensed data to map human settlements. The focus is on global- and coarse-scale analyses, and as such on global and regional datasets, with applications to land cover/land use and population mapping. The unprecedented capability of remote sensing technologies to provide global coverage for observing human settlements with sufficient spectral, spatial, and temporal resolution has resulted in several attempts to extract global mapping products or refine existing ones. A complete and exhaustive list of such projects and their approaches does not exist yet. This book aims to fill this gap by further considering the improving global observing capacities, the growing demand for consistent and continuous global data advocated by political initiatives such as the Group on Earth Observation (GEO) and Global Monitoring for Environment and Security (GMES), and evolving operational land monitoring programs. This book will provide students, researchers, and practitioners a milestone reference point that summarizes the state of the art and discusses future needs that are still to be fulfilled.

The target audience for this book is diverse. The book should be useful in several different ways for graduate-level education and capacity building:

1. As part of curricula dealing with remote sensing, geographic information system (GIS) and spatial analysis, and global monitoring and assessments. Several chapters provide the technical basics and approaches to coarse-scale urban remote sensing and monitoring.
2. As a part of urban geography, ecology, and planning curricula, because it shows how remote sensing could be used to improve the knowledge for urban planning and management beyond the local scale, or to compare human settlements through consistent global observation perspective.
3. In the evolving fields of global environmental change and sustainability studies.
4. For international capacity building and to support related applications intending to make use of techniques and datasets described and applied.

The book includes perspectives from users and producers of global data. It offers a valuable source of information for global international organizations, researchers, and practitioners. Furthermore, it is very important for those who want to exploit existing datasets and use them as part of their research or work, because it explains the methodology behind the datasets, allowing the reader to understand the potentials and perhaps limitations of each dataset, to compare them, and to use one that best serves their purpose.

In addition to the text, a DVD with key global datasets described and referred to in several chapters of the book is provided. Although most of these data are freely available on the Web, they are presented here in a common format and are intended to help the interested readers take a closer look or use them for educational or capacity-building purposes.

Thus, potential readers will benefit from several factors: the written background documentation in this book, appropriate references to existing datasets summarized in one source, the available datasets provided in the accompanying DVD, the methodologies behind these datasets introduced and discussed in separate chapters, potential applications of these datasets analyzed by leading experts in the field, and the directions for research highlighted in the final section of the book.

The chapters are subdivided into four parts. Each one addresses some of the above-mentioned needs of the audience. Part I is devoted to analyzing the requirements for global and regional urban remote sensing, and thus maintains a general point of view on the topic. The two chapters by Karen Seto and Martin Herold provide a general background of global urban issues and outline some general observation and assessment requirements, and how they relate to current initiatives on the international policy and strategic levels.

Part II describes the characteristics of human settlements as seen and mapped from remote sensors, either at regional or global scale. The spectral variety, the spatial scales, and the nighttime appearance as key remote sensing indicators of these environments are discussed in the subsequent chapters by Martino Pesaresi, Daniele Ehrlich and Chris Small. The contribution by Annemarie Schneider and her colleagues describes a comprehensive approach using Moderate Resolution Imaging Spectroradiometer (MODIS) sensor remote sensing data to derive consistent global urban extent data.

Part III describes some of the most acclaimed and important projects and programs carried out in the past or present for urban mapping and monitoring. Examples are presented at global and regional scales and involve examples from the developing and developed world. The focus of the chapters in this part highlights the impressive amount of information available and the processing and analysis techniques used to extract such data from several data sources including satellite imagery. Experiences and approaches from the Global Rural Urban Mapping Project, ongoing for many years, are discussed in the chapter by Deborah Balk. The contribution by John Latham et al. highlights results and examples from regional urban monitoring examples for Africa as part of the efforts of the Global Land Cover Network (GLCN) and the Food and Agricultural Organization (FAO). The Urban Environmental Modeling project focuses on 100 cities worldwide, an effort that is further explained by Elizabeth Wentz and her colleagues. The MEGACITIES project, presented in the chapter by

Hannes Taubenböck et al., has a focus on risk management and how Earth observation data contribute to such efforts. Furthermore, there are a number of Earth observation initiatives on the European level with different projects of Monitoring Land Use/Cover Dynamics, and GMES Urban Services, and recent efforts in the context of GMES. The chapter by Frank Martin Seifert advocates their scope, achievements, and future plans.

Part IV presents some of the future challenges and lines of research that should be actively pursued in the near future. Issues relating to semantic characterization of human settlement areas are discussed in the chapter by Louisa Jansen. A closer look into a suite of existing global urban maps is taken by David Potere and Annemarie Schneider. They analyze and compare them to improve our current level of understanding on existing global map products. Two chapters deal with the potential arising from the evolving Earth observation technology. The chapter by Fabio Dell'Acqua discusses the role of synthetic aperture radar sensors in this context. From a broader perspective, the contribution by Manfred Ehlers advocates an integrated perspective for global urban monitoring. The issue of multidate urban observations and approaches to study and analyze this new level of high-temporal data is discussed in the chapter by Alexandre Boucher and Karen Seto.

Research on applications and use of remote sensors for human settlement mapping and monitoring is a rather recent effort compared to other global mapping efforts. Research aimed at achieving useful results at a regional or global level has only recently reached a suitable level of maturity. This book stems from the results of the work of those who started these efforts in the past decade. It is commonly understood that future efforts will be more driven by issues such as "interoperability," "operational and efficient global monitoring," and "international coordination and cooperation" for developing and exchanging datasets, improving models, and links to decision making and urban planning and management. Thus, we would like the reader to understand this book as community message advocating the comprehensive level of understanding on how to approach global urban monitoring, how different efforts have led to a number of suitable products, and the obvious path forward to make global urban monitoring an operational component of such efforts as GEO and GMES, and to stimulate further research.

Paolo Gamba and Martin Herold

Acknowledgments

The idea for this book materialized in Brazil, more specifically in the wonderful town of Florianopolis, where the editors were invited to provide a tutorial within the XIII Simposio Brasileiro de Sensoriamento Remoto (SBSR). The venue was spectacular, the location gorgeous, and the relaxing environment instrumental for discussing the idea and finding the right approach to this book. For this reason, we are greatly indebted to Instituto Nacional Pesquisas Espaciais (the Brazilian Institute for Space Research), organizer of the SBSR series, and especially to Claudia Almeida, our host. We would further like to thank Qihao Weng for helping and stimulating the efforts in preparing this book. The editors would also like to thank Susann Kuenzl for her administrative support.

Editors

Dr. Martin Herold received his B.S. degree in geography in 2000 from Friedrich Schiller University of Jena, Germany, and Bauhaus University of Weimar, Germany. In 2004, he completed his Ph.D. in geography at the University of California–Santa Barbara, with a dissertation entitled "Remote Sensing and Spatial Metrics for Mapping and Modeling of Urban Structures and Growth Dynamics." Since 2004, Dr. Herold has been coordinating the European Space Agency Global Observation for Forest and Land Cover Dynamics project office at Friedrich Schiller University, where his interests include harmonization and validation of global land cover datasets, and development and implementation support for large land cover monitoring systems within the context of the United Nations Framework Convention on Climate Change (UNFCCC) (Global Climate Observing System implementation plan and reducing emissions from deforestation), the GEO, GLOBCOVER, Integrated Global Observations for Land, and FAO's Forest Resources Assessment 2010 remote sensing survey. He has recently become a partner in the Vanuatu Carbon Credits Project and acts as technical advisor to the Vanuatu UNFCCC delegation and government.

Paolo Gamba is currently an associate professor of telecommunications at the University of Pavia, Italy. He received his B.S. degree in electronic engineering from the University of Pavia, Italy, in 1989. He also earned his Ph.D. in electronic engineering in 1993 from the same university. He is the organizer and technical chair of the biennial Geoscience and Remote Sensing Society/International Society for Photogrammetry and Remote Sensing (ISPRS) Joint Workshops on Remote Sensing and Data Fusion over Urban Areas from 2001 to 2007. He is a senior member of the Institute of Electrical and Electronics Engineers (IEEE), associate editor of *IEEE Geoscience and Remote Sensing Letters*, and is currently the chair of the Data Fusion Committee of the IEEE Geoscience and Remote Sensing Society. He has published more than 40 papers on urban remote sensing in peer-reviewed journals, and has presented more than 100 papers on the same subject at workshops and conferences. He was likewise invited to give tutorials about urban remote sensing at the International Geoscience and Remote Sensing Symposium (IGARSS) in 2004, and the Brazilian Symposium on Remote Sensing in 2007.

Contributors

Babikar Fadl El Seed El Siddig Adam is a Ph.D. candidate in remote sensing at the University of Khartoum and a consultant at the Remote Sensing Centre in Khartoum.

Deborah Balk is the associate director of the City University of New York (CUNY) Institute for Demographic Research, and associate professor at the Baruch School of Public Affairs and the CUNY Graduate Center (in the sociology and economics Programs). Her expertise lies in spatial demography and the integration of Earth and social science data and methods to address interdisciplinary policy questions. Her current research focus is on urbanization, population, poverty, and environmental interactions (such as climate change). Before coming to Baruch, she was a research scientist at the Center for International Earth Science Information of Network at Columbia University. There, she was also lead project scientist for the NASA-funded Socioeconomic Data and Applications Center, where she worked on large-scale data integration and analysis of geographic, survey, and administrative data. She received her Ph.D. in demography from the University of California at Berkeley, and her M.S. in public policy and B.A. in international relations from the University of Michigan, Ann Arbor. She is currently a member of the International Union for the Scientific Study of Population working group on urbanization and recently completed service to two National Research Council panels.

Kimberly E. Baugh is a staff scientist at NOAA's NGDC in Boulder, Colorado. She manages and develops strategies, algorithms, and protocols for the creation, storage, and dissemination of DMSP OLS-derived data products.

Alexandre Boucher received a B.Eng. in geological engineering from Ecole Polytechnique of Montreal, Canada, an M.Phil. in mining geostatistics from University of Queensland, Australia and a Ph.D. in geostatistics from Stanford University. His research interests include remote sensing and probabilistic modeling of spatio-temporal phenomena. He is currently an acting assistant professor in the Department of Environmental Earth System Science at Stanford University where he teaches geostatistics.

Anthony J. Brazel holds a Ph.D. in geography from the University of Michigan. He is co-principal investigator for the Central Arizona–Phoenix Long-Term Ecological Research site, for which he served as leader of the Climate Ecosystem Interactions Program Area, and a member of the Climate Science team of the Decision Center for Desert City, while working as a faculty member and associate director of the School of Geographical Sciences at Arizona State University. His research interests include the climatology of the Southwest United States and urban climatology with applications

to understanding urban heat islands, development of mitigation strategies, and global and regional climate change.

Renato Cumani is an environment officer with the Environment, Climate Change, and Bioenergy Division of FAO. His main research activities are related to the use of geospatial information for environmental assessments that contribute to the responsible management of natural resources as key to attaining sustainable agricultural and rural development. In addition, he contributes to GIS and remote sensing and mapping activities, GeoNetwork portal, GLCN program, GTOS, and various FAO technical cooperation projects in several developing countries.

Stefan Dech received his diploma in geography, sociology, and political science in 1987 and his Ph.D. in geography in 1990 from the University of Würzburg, Germany. From 1987 to 1998, he was a researcher at the DLR-DFD, of which he became director in 1998. In addition, he has been lecturing since 1991 at the Universities of Eichstätt, München and Würzburg. Since 2001, he has been serving as chair of Remote Sensing at the University of Würzburg. His scientific interests lie mainly in the fields of terrestrial remote sensing (biophysical parameters, land cover, urban areas, and development of early warning systems for natural hazards).

Fabio Dell'Acqua received his B.S. in electronics engineering (cum laude) from the University of Pavia in 1996. In 1999 he defended his Ph.D. thesis at the same university, after 3 years work on the processing of meteorological satellite images for disaster forecasting.

In the year 2000, he worked as an assistant researcher at the Division of Informatics, University of Edinburgh, Scotland, UK, on a training and mobility of researchers (TMR) project aimed at the reconstruction of 3-D environments from laser range data. In 2001, he was appointed as an assistant professor at the University of Pavia.

Since the academic year 2003–2004, he has been in charge of three remote sensing courses every year at the University of Pavia. He tutors on average 10–15 students a year, both graduate and undergraduate, and he has established strong links with companies in the remote sensing market.

Dr. Dell'Acqua has been actively involved in the organization of a successful series of biannual IEEE/ISPRS conferences named URBAN on remote sensing and data fusion over urban areas, since the first event was held in Rome in 2001. He is or has been on the technical committee of several conferences: Pattern Recognition in Remote Sensing, IGARSS, and European Association of Remote Sensing Laboratories (EARSeL) symposia, and is cochair of the EARSeL Special Interest Group on radar remote sensing. He has coauthored about 30 papers in peer-reviewed journals, contributions in several books, and more than 80 conference papers. His research interests include change analysis in satellite images of disaster events and extraction of features from high-resolution optical and SAR images.

Manfred Ehlers is a full professor of GIS and remote sensing at the University of Osnabrueck, Germany. He is the director of the University's Institute for Geoinformatics and Remote Sensing, and is the current president of the Society for Geoinformatics (a scientific society in Germany, Austria, and Switzerland). He is also the chairman of the GiN in North Germany, a public–private partnership association. He holds an M.S. in mathematics, and a Ph.D. and Habilitation degree (*venia legendi*) in surveying engineering with emphasis on remote sensing, digital image processing, and GIS.

Dr. Ehlers teaches courses in geoinformatics, GIS, remote sensing, digital image processing, environmental monitoring, and environmental information systems. He has held academic appointments at various universities and research institutions in Germany, the United States, and the Netherlands. His research interests focus on the concepts for integrated geographic analysis and modeling techniques, especially the integration of GIS and remote sensing. Other research areas include geoinformatics concepts, data fusion techniques, and advanced techniques for image analysis.

Over the past 10 years, Dr. Ehlers has been principal investigator or co-principal investigator on more than 50 funded research grants totaling more than €7.5 million. He was the chairman of several international working groups on GIS and remote sensing for the ISPRS, and has organized and chaired a number of national and international conferences and workshops. He has published about 300 papers on GIS, mapping, digital image processing, remote sensing, geoinformatics, digital photogrammetry, and environmental monitoring, and has given more than 300 presentations at scientific and professional meetings and conferences.

Daniele Ehrlich holds a B.S. degree in forestry from the University of Padua, Italy (1984), as well as an M.S. (1989) and Ph.D. (1992) in geography from the University of California–Santa Barbara, USA. He worked as a postdoctoral researcher at the United Nations Environment Programme (UNEP)/Global Resource Information Database (GRID) node hosted at the EROS/Data center in Sioux Falls, and later as a consultant in southern California. In 1994, he joined the JRC of the EC as a postdoctoral researcher and was subsequently awarded a position as a scientific officer with management tasks at the JRC Centre for Earth Observation. He is currently a senior staff of JRC, Support to External Security Unit, where from 2002 to 2007 he co-led the Information Support for Effective and Rapid External Action team. In his scientific and professional career he has used Earth observation and geographical information systems for regional crop area estimations, continental tropical deforestation and land cover change assessments, crisis management with focus on population enumeration, and vulnerability assessments. The focus of his current work is on the use of very high resolution satellite imagery for quantifying built-up stock and disaster risk to physical infrastructure and on postdisaster damage assessments.

Christopher D. Elvidge received his Ph.D. in applied Earth sciences from Stanford University in 1985. He was a National Research Council postdoctoral fellow at the National Space Aeronautics Administration's (NASA) Jet Propulsion Laboratory from 1985 to 1987 and was on the Biological Sciences faculty at the Desert Research

Institute in Reno starting in 1988. In 1994, he moved to the National Oceanic and Atmospheric Administration's (NOAA) National Geophysical Data Center (NGDC) in Boulder, Colorado, to lead an effort to construct global maps of fires and lights using the low-light imaging data from the U.S. Air Force Defense Meteorological Satellite Program (DMSP) Operational Linescan (OLS) system. He currently leads NGDC's Earth Observation Group.

Mark A. Friedl is a professor of geography and environment at Boston University, where he has taught for 15 years. He received his B.S. in physical geography from McGill University in 1986, and his Ph.D. in geography from the University of California at Santa Barbara in 1993. He is the principal investigator for the MODIS Global Land Cover Product and his research focuses on global land cover mapping, land surface climate processes, remote sensing of vegetation phenology, and land–atmosphere interactions.

Tilottama Ghosh is a third-year Ph.D. student in the Geography Department of the University of Denver. She finished her M.S. in geography from Presidency College, Calcutta, India, and an M.S. in population studies from the International Institute for Population Sciences, Mumbai, India. Her Ph.D. dissertation investigates the possibility of using nighttime imagery in concert with spatial models to provide an alternative estimate of the size of the informal economy in such nations as Mexico, India, and China. She also works as a professional research assistant at NGDC, NOAA.

Barbara Huddleston served as chief of FAO's Food Security Service for 18 years, before her retirement in 2002. Her educational background includes international affairs, economic history, and agricultural economics; before joining FAO, she was a research fellow with the International Food Policy Research Institute in Washington, D.C. Since 2002, she has undertaken various consultancy assignments in the fields of food security, sustainable agricultural and rural development, and climate change response, and has advised FAO on the use of geospatial information for decision support in these fields.

Louisa J.M. Jansen earned her bachelor's degree in agricultural and environmental sciences at Wageningen University, the Netherlands. She has gained considerable international experience in land change dynamics and semantics, natural resources management, land use planning and policy, and land tenure reform. In the course of her work, she combines knowledge management with information technology for informed decision making. She has worked for the EC and EU Phare program, FAO, the Dutch International Institute for Geo-Information Science and Earth Observation, the Italian Cooperation and the Agronomic Institute for Overseas Areas of the Italian Ministry of Foreign Affairs, the Nordic Council of Ministers, the Dutch Royal Tropical Institute, and the World Bank. She currently works in the Spatial Development and Consultancy Division of the Cadastre, Land Registry and Mapping Agency of the Netherlands.

John Latham is the program director of the Global Terrestrial Observing System (GTOS), which is hosted by FAO. In addition, he coordinates the GIS and poverty mapping activities of FAO and runs numerous projects and initiatives such as the FAO/UNEP GLCN, an initiative supported by the government of Italy.

Antonio Martucci finished his B.S. in agronomic sciences (majoring in rural planning) in 1996 from the University of Bari, Italy. After obtaining his M.S. in the use of remote sensing and GIS for environmental studies, he spent 6 years in the United States (Louisiana) refining his knowledge and experience on the development of information systems to support the decision-making process. In 2003, he joined FAO, where he has been working on global programs and field projects dealing with geospatial information, focusing on the implementation of innovative solutions for information dissemination and sharing.

Matthias S. Möller is a professor and head of the geoinformatics and remote sensing research group at the University of Bamberg, and research associate with the Austrian Academy of Sciences, GIScience, Salzburg, Austria. He received his Ph.D. in environmental sciences from the University of Vechta, Germany, in 2002. From 2002 until 2003, he established the Center of Excellence (GiN) for the Ministry of Science and Culture in the state of Lower Saxony. Starting in 2003, he worked for 2 years as a postdoctoral research assistant at ASU, Global Institute of Sustainability, in the National Science Foundation–founded project, Agricultural Landscapes in Transition. He was chair for cartography and geoinformatics at the University of Bonn for three terms from 2006 until 2007. His main research interests focus on processing and analysis of extremely high-resolution remote sensing images, development of new digital geodata visualization methods, and integration of geoinformation in teaching concepts.

Maik Netzband earned his degree in applied physical geography from the University of Trier, Germany, and his Ph.D. at the Technical University of Dresden, Germany. While undertaking research in urban ecology and urban planning at the Institute for Ecological and Regional Research in Dresden, and later on, at the University of Leipzig and at ASU, he also intensified his methodological knowledge on remote sensing techniques when approaching questions of urban ecology and urban planning. In particular, problems associated with urban land use, climate, soil imperviousness, land consumption, green areas, and open spaces caught his attention. His special research interest lies in monitoring and evaluating these complex issues with methods of remote sensing and geoinformation. He is currently working with the Helmholtz Centre for Environmental Research in Leipzig, Germany, on various urban-related and international geoinformation research projects.

Nihad El Nogoumy is a satellite photo interpreter employed by Environmental & Remote Sensing Services, an Egyptian firm based in Cairo. He is currently providing consultancy services to FAO for the systematic assessment of urban change in Africa.

Martino Pesaresi completed his course in town and regional planning at the Venice University Institute of Architecture in 1991–1992. He pursued research activities involving the use of remotely sensed data in urban analysis with the Centre d'Analyse et de Mathématique Sociales, the EHESS, Paris, in 1991–1992; with the Laboratoire d'Informatique Appliquée of ORSTOM (Paris) in 1992–1993; and for the University of Venice until 1995. In 1992–1997, he served as a consultant for public and private companies as well as professionals involved in town and regional planning activities. From 1997 to 2000, he was under a research contract with the former European Commission Joint Research Centre (EC JRC) Space Applications Institute. During 2001–2004, he worked in the map production industry, leading the digital mapping sector of the Environmental Technologies and Services Area, INFORM Srl, Padova, Italy. He has been working since 2004 at the EC JRC IPSC, Support to External Security Unit, and has been leading the Information Support for Effective and Rapid External Action team of the same institute since September 2007.

David Potere is completing his Ph.D. in demography at Princeton University's Office of Population Research with a dissertation entitled "Mapping the World's Cities: an Examination of Global Urban Maps and Their Implications for Conservation Planning." Before starting at Princeton, David completed his M.S. in remote sensing and GIS at Boston University's Department of Geography and Environment with a thesis entitled "Patterns in Forest Clearing Along the Appalachian Trail Corridor." David's interests center on the application of remote sensing and GIS to human and environment interactions.

Ilaria Rosati holds a Ph.D. in image processing and pattern recognition. She has been a consultant with FAO since 1996, working as a remote sensing and GIS expert, mainly for the GLCN and GTOS projects. Her field of expertise is cover analysis, and particularly in processing/interpretation of satellite images, mapping, and analysis of datasets.

Achim Roth received his B.S. in geodesy from the Technical University of Karlsruhe, Germany in 1987. He joined the DLR in 1988, in particular, the synthetic aperture radar (SAR) development group of the German Processing and Archiving Facilities for the European Remote Sensing and Shuttle Imaging Radar-C and X-Band SAR missions. He leads the "topography and urban analysis" team at the DFD, focusing on such research topics as SAR geocoding, generation of digital relief information (DEMs), SAR coherence analysis, analysis of urban characteristics based on high-resolution optical and SAR data, and vulnerability studies. In addition, he is currently the science coordinator of the TerraSAR-X mission.

Mirella Salvatore is an economist and a Ph.D. statistician who joined FAO in December 2002 as a consultant for the GIS unit in FAO. She has been responsible for the creation and maintenance of statistical and GIS databases for analyzing poverty and malnutrition in rural residents and evaluating their relationship with the physical environment, and has been an important contributor to the development of FAO's Urban and Rural Population Database. She is currently the bioenergy officer of the

Bioenergy and Food Security project at FAO, which integrates food security concerns into the assessment of bioenergy potentials in various developing countries.

Annemarie Schneider received her B.S. from the University of Wisconsin–Madison, and her M.A. and Ph.D. in geography from Boston University. After her first faculty appointment at the University of California–Santa Barbara's Geography Department, she joined the Center for Sustainability and the Global Environment at the University of Wisconsin–Madison in 2007, with a joint affiliation with the Department of Geography. Her current projects focus on transforming the study of urban areas from local investigation to one of comparative analysis in support of global change research. She leads the 40 Cities Project, an effort to compare/contrast the rates, patterns, and drivers of land use change in a global cross section of metropolitan areas. As part of this project, she focuses on characterizing urban expansion in cities in China and developing simulations of future changes under different policy scenarios. To help understand the impacts of urbanization on the regional and global environment, her work also includes mapping urban land surface properties globally using the fusion of remote sensing data types. Her overall research interests include the urban environment, land cover change, urban geography, and the human dimensions of global environmental change.

Frank M. Seifert is a Earth Observation Application Engineer at the Earth Observation Programme Directorate of the European Space Agency (ESRIN) in Rome, Italy.

Karen C. Seto is an associate professor in the School of Forestry and Environmental Studies at Yale University. Her research is on the dynamics of land use change and focuses on three broad themes: (1) monitoring, measuring, and forecasting urban form and growth patterns; (2) identifying and comparing the drivers of urban growth; and (3) analyzing the environmental and social consequences of land use change and urban expansion. A geographer by training, her research provides an interdisciplinary evaluation of 21st century urban growth dynamics by combining research approaches and conceptual frameworks from the fields of urban studies, geography, economics, and policy studies. Her geographic region of specialization is China, where she has worked on urban development issues for more than 10 years. She has also had research projects in India, Vietnam, Qatar, and the United States. Professor Seto is cochair of the Urbanization and Global Environmental Change Project of the International Human Dimensions Programme of Global Environmental Change, and Global Thematic Leader on Ecosystem Management Tools for the International Union for Conservation of Nature's (IUCN) Commission on Ecosystem Management. She is the executive producer of *10,000 Shovels: Rapid Urban Growth in China*, a short documentary film that highlights the unprecedented urban changes occurring in South China.

Christopher Small is a geophysicist at the Lamont–Doherty Earth Observatory of Columbia University. Before receiving his Ph.D. from the Scripps Institution of Oceanography in 1993, his formative experiences ranged from shipboard studies

of the circulation of the Chesapeake Bay with the University of Maryland to satellite mapping for frontier petroleum exploration with the Exxon Production Research Company. His current research interests focus on measuring changes of the Earth's surface and understanding the causes and consequences of these changes. Details are available online at http://www.LDEO.columbia.edu/~small.

William L. Stefanov holds a Ph.D. in geology from ASU. He was lead remote scientist for the Central Arizona–Phoenix Long-Term Ecological Research site and Urban Environmental Monitoring Project while a faculty research associate at ASU. In 2004, he became senior geoscientist for the International Space Station Crew Earth Observations payload at NASA's Johnson Space Center, Houston, Texas, USA. His research interests include the application of remotely sensed data to investigation of surface mineralogy, geomorphology, and geohazards in urban/periurban areas on Earth, with applications to future outposts on the Moon and Mars; biophysical aspects of urban heat islands and development of mitigation strategies; ecological disturbance mechanisms and patterns; and the role of humans as geological agents on the landscape.

Paul C. Sutton received his Ph.D. in geography from the University of California at Santa Barbara. He is an associate professor and director of graduate studies in the Department of Geography at the University of Denver. His research interests are primarily in the area of human–environment–sustainability problems with particular emphasis on ecological economics and developing innovative applications using nocturnal imagery of the Earth from space. These applications include developing urban sprawl and environmental sustainability metrics, mapping and modeling population density, and making disaggregate maps of economic activity.

Hannes Taubenböck earned his bachelor's degree in geography with minors in remote sensing, GIS, and environmental planning from the Ludwig Maximilians University München, Germany in 2004. He joined the German Remote Sensing Data Center (DFD) at the German Aerospace Center (DLR) in 2005, working on the topic "Mega Cities and Natural Disasters." He received his Ph.D. from the Julius Maximilians University of Würzburg, Germany in 2008. Since autumn 2007, he has been working at the University of Würzburg for the project "Last-Mile Evacuation — Numerical Tsunami Early Warning and Evacuation System."

Benjamin T. Tuttle is an associate scientist at the Cooperative Institute for Research in Environmental Sciences at the University of Colorado, Boulder, Colorado, and a Ph.D. student in the Department of Geography at the University of Denver, Colorado, USA. He holds a B.A. in geography and a B.A. in environmental studies from the University of Colorado, and an M.S. in geographic information science from the University of Denver. His primary research interests include remote sensing of human–environment interactions, nighttime lights, satellite wildfire monitoring, and the geospatial Web. He has coauthored articles in several journals, including

Remote Sensing of Environment, *Environmental Management*, and *ISPRS Journal of Photogrammetry and Remote Sensing*.

Elizabeth A. Wentz is an associate professor of geography at Arizona State University (ASU). She teaches introductory and advanced courses in geographic information science, spatial analysis, and physical geography. Her research publications are related to advancing the analytical capabilities of GIS, such as: "Development and Testing of a Trivariate Shape Measure for Geographic Analysis" in *Geographical Analysis*, and "Geographic Representation in Geographic Information Systems and Spatial Analysis" in the *Annals of the Association of American Geographers*. She also has research interests in the urban environment. She, along with colleagues, investigated elevated levels of carbon dioxide in the Phoenix metropolitan area. Professor Wentz earned a Ph.D. in geography from Pennsylvania State University (1997) and an M.A. in geography (1989) and a B.S. in mathematics (1987) from The Ohio State University.

Part I

Requirements for Urban Remote Sensing

Part I

Requirements for Urban Remote Sensing

1 Global Urban Issues
A Primer

Karen C. Seto

As we enter the 21st century, the world is becoming increasingly urban, both in terms of human population and the Earth's surface. Although cities have existed for centuries, the urbanization processes today are different from urban transitions of the past in three significant ways (Cohen, 2004). First, the magnitude of urbanization is extraordinary. The global proportion of urban population was a mere 13% in 1900 (UN, 2006). It rose gradually to 29% in 1950. By 2030, the world's urban population is expected to nearly double from 2.86 billion in 2000 to almost 5 billion (Figure 1.1). There are now 400 cities with populations of 1 million or greater, compared with only 16 cities with populations of 1 million or greater at the turn of the 20th century. The scale of urban land area is also extraordinary. Neoliberal reforms, demographic transitions, and economic development have created new cities and megapolitan regions of extraordinary size. The two biggest metropolitan regions, New York and Tokyo–Yokohama, together encompass an area of greater than 15,000 km^2, an area the size of one and one-half Jamaicas.

Second, the rapidity with which landscapes and populations are urbanizing is faster than during other periods in history. China and India, the two most populous countries in the world, regard urbanization as a critical component of their development process and have ambitious goals to build a vast network of new cities to fuel their industrialization goals (Song and Ding, 2007; Kennedy, 2007). In the next two decades, China will create nearly 30 new cities of 1 million inhabitants; India is expected to add 26 cities of this size during the same period. In contrast, the United States has only nine cities with populations of 1 million or greater. Together, China and India are projected to have almost one-third of the world's urban dwellers by 2030 (UN, 2006).

A third characteristic of the urban transition underway today is that it will take place primarily in Africa and Asia (UN, 2006). Whereas the urbanization levels in the Americas and Europe are already high, 80% in South America and 75–78% in Europe and North America, the urban populations in the continents of Africa and Asia are less than 40% of total population. Over the next two decades, the urban populations of both continents are expected to increase to more than 50%. A majority of these new urban residents will be poor, with estimates that between one-quarter and one-third of all urban households in the world live in absolute poverty (UNCHS, 2002).

Although there is uncertainty about urban population forecasts, especially for countries where data are not readily available or nonexistent, given the scale of the global urban transition of the 21st century, there is an urgent need for spatially

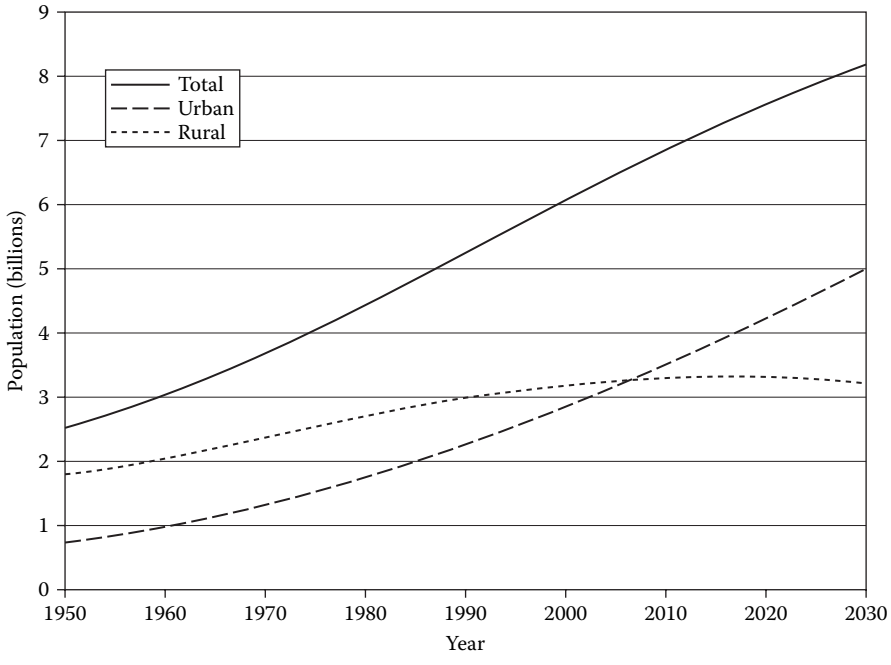

FIGURE 1.1 Global population and composition, 1950–2030 (Source: UN, 2006).

explicit information on urban areas (Cohen, 2004; Montgomery, 2007). With estimates that the global urban population will increase to 6 billion by 2030, the number and size of urban areas will need to grow significantly to house the world's growing urban population. The growth of these urban areas will likely come at the expense of agricultural land, pastures, forests, savannas, and countrysides. Thus, information about *where* urban areas will likely expand or be developed will be critical for forecasting impacts on natural resources (e.g., energy, water, building materials), food security, biodiversity, and conservation of flora and fauna. Satellite remote sensing can provide accurate and timely information on urban land use, its location and spatial configuration, as well as growth rates and patterns. The internally consistent measurements and long observational record of satellite sensor data make it an attractive source of reliable information on urban extent and form.

Human settlements are dominantly coastal. Globally, approximately 400 million people live within 20 m of sea level and within 20 km of a coast (Small and Nicholls, 2003). Many large cities occupy coastal locations that are often flood-prone and vulnerable to extreme events. There is a growing need to understand the distribution of vulnerability across landscapes, and to differentiate risk among different communities within cities (Parnell et al., 2007). Hurricane Katrina and the 2004 Asian tsunami showed that all cities — even those in wealthy countries — are vulnerable to global environmental change and disasters. However, the coping capacity and resilience differs significantly among communities. Hurricane Katrina revealed that the poorest communities within New Orleans suffered disproportionately, and

inadequate timely information about the spatial distribution of urban population and urban infrastructure impeded emergency relief efforts.

Urban areas and socioeconomic processes within them will be increasingly important in affecting and being affected by global environmental change. Locally, the conversion of vegetated surfaces to urban areas modifies the exchange of heat, water, trace gases, aerosols, and momentum between the land surface and overlying atmosphere (Crutzen, 2004), leading to the "urban heat island effect," often characterized by elevated daytime and nighttime temperatures in and near urban areas (Oke, 1974; Arnfield, 2003) and reduced rainfall in some regions (Kaufmann et al., 2007). These changes imply that urban land use and urban land-use change can affect local, regional, and global climate at diurnal, seasonal, and long-term scales. The term "metro-agro-plex" has emerged to describe regions where there is a tight coupling of the agricultural and urban-industrial activities within a geographic region (Chameides et al., 1994). Metro-agro-plexes are a major force in the world economy and also in global environmental change. Globally, they are also major sources of atmospheric pollutants such as carbon dioxide, nitrogen oxides, and sulfur oxides.

The urban heat island effect is well established, but the relationship between urban land-use change and its impact on local and regional precipitation and temperature is less understood. The Intergovernmental Panel on Climate Change (Trenberth et al. 2007) notes a growing interest in understanding the contribution of urban land cover/land use and pollution to climate change. Of particular importance, Chapter 3 (Section 3.3.2.4) reviews a growing body of research that links urban-related processes and regional precipitation. Although urban land use modifies surface roughness, energy flows, and water flow, global change studies have not considered fully the interactions between urban areas and biophysical processes at regional or global scales. It is assumed that the urban heat island effect is a local phenomenon with little effect on global climate. As such, general circulation models (GCMs) have not included urban processes, and most are so spatially coarse that they render geographic information within urban areas useless (McGuffie and Henderson-Sellers, 2005). The spatial resolution of most GCMs is between 250 and 600 km. For example, the HadCM3 developed at the Hadley Center in the United Kingdom has a horizontal resolution of 2.5° (latitude) by 3.75° (longitude), which is equivalent to 417 × 278 km at the equator and 295 × 278 km at 45° latitude (Gordon et al., 2000). This coarse spatial resolution means that the representation of land surfaces — such as urban extent and urban form — are greatly simplified. There are many spatial downscaling techniques to derive finer resolution climate information from these coarse GCMs (Hewitson and Crane, 1996; Wilby and Wigley, 1997). With finer downscaling of these models, it will soon be possible to incorporate detailed information on urban areas, including texture, form, building material, and vertical structure. Only then will we understand the extent to which aggregated expansive and rapid urban growth modifies regional and global climate.

The connections and interactions between these urbanization processes and global environmental change are increasingly intertwined and complex. Several new international initiatives and research networks have now been established to explore the relationship between urbanization and global change. For example, the Resilience Alliance's (2007) Urban Program focuses on the major challenges facing urban

systems and their landscapes. The Urban Climate Change Research Network (http://www.uccrn.org) is a consortium of institutions and individuals that pursue the analysis of climate change and energy issues from an urban perspective, with a primary objective of creating open discourse and information exchange among researchers and decision makers on cutting-edge scientific, economic, and planning-related research. Another such initiative is the International Human Dimensions Programme on Global Environmental Change Urbanization and Global Environmental Change Project (UGEC) seeks to develop a better understanding of the interactions and feedbacks between global environmental change and urbanization at local, regional, and global scales (Sanchez-Rodriguez, 2005).

One of the key research questions of the UGEC is, "How does urban land use and urban land-use change affect global environmental change?" Urban form is the physical manifestation of the interactions among global, regional, and local forces in a single geographic space. The size, scale, and form of cities and their likely future growth trajectories will be critical to global environmental change. The environmental challenges posed by the spatial configuration of urban land use have been and will continue to be enormous: infrastructure requirements of extensive versus compact cities, energy implications of commuting patterns, impact of urban expansion on global food security. The conversion of natural and agricultural ecosystems to urban uses has massive implications for Earth system functioning, and although there are numerous regional and local case studies, the global rate and extent of urbanization as a transformation of the landscape are poorly documented. There is tremendous opportunity for the remote sensing community to contribute information and insight into the urban land use, urban growth, and their interactions with ecosystem processes. For example, how does urban growth in coastal zones impact on aquatic food chains and water quality? How does the aggregate impact of conversion of land to urban uses affect regional and global hydrological cycles? Particularly in semiarid areas, to what extent does groundwater extraction cause salinization and consequent land-use/cover change that in turn contribute to global environmental alterations through changes in surface albedo, or rainfall?

Another process for which the urban remote sensing community can offer better understanding is peri-urbanization. Peri-urbanization is the process where rural areas both close to but also distant from city centers become enveloped by, or transformed into, extended metropolitan regions (Simon et al., 2004; Aguilar and Ward, 2003). These changes are generally stimulated by exogenous investments in industry, real estate speculation, or residential development. Almost always, they result in a tight mosaic of traditional and agricultural areas juxtaposed with modern and industrial land uses. As a physical phenomenon, peri-urbanization involves the conversion of agricultural land, pastures, and forests to urban uses. As a social phenomenon, peri-urbanization involves cultural and lifestyle adjustments of agrarian communities as they become absorbed into the sphere of the urban economy. In most developing countries, peri-urbanization is the most prominent form of urban growth and urbanization, with different characteristics across countries and regions. In some regions, peri-urbanization is driven by foreign investments and increased commerce and manufacturing, whereas in others, it is driven by interregional migration, infrastructure development, and domestic investments. Whatever the cause, different outcomes

result on the landscape: thriving and economically robust satellite towns distant from large cities or stagnant industrial outputs with the potential of deindustrialization. Remote sensing studies can shed light on the peri-urbanization process and provide critical information for policy-makers and planners.

The physical process of urban land-use change is most commonly described as either a change in the absolute area of urban space (a measure of extent) or the pace at which nonurban land is converted to urban uses (a measure of rate). The extent and rate of urban growth provide indications of the aggregate size of cities and the rate at which other land uses such as agriculture are converted to urban uses. However, aggregate growth rates give limited information regarding spatial patterns of urbanization or the underlying processes that shape human settlements. The spatial configuration of urban landscapes is as much a reflection of past as it is an indicator of current socioeconomic processes and interactions. For any period, the spatial arrangement of urban areas provides a snapshot of various economic, social, and political factors that influenced land use decisions. Our understanding of how cities grow or expand is poor (Batty, 2008). And although there are a number of remote sensing studies of urban morphology (Ridd, 1995; Herold et al., 2002, 2003; Benediktsson et al., 2003; Seto and Fragkias, 2005; Rashid et al., 2005), more research is needed to understand *how* and *why* cities grow, and the role of urban form on biophysical processes, infrastructure and transport needs, energy demands, and environmental impacts.

Throughout history, infectious diseases have had a significant impact on human populations. In the mid-1300s, the bubonic plague killed more than 100 million people, wiping out one-third of Europe's population and half of China's population. This was without air travel, modern-day dense settlements, and relatively smaller cities. More recently, outbreaks of severe acute respiratory syndrome (SARS) and avian influenza remind us of the speed and extent with which diseases and viruses can spread globally, especially in and across densely populated regions. Climate change is expected to expand the potential transmission zone of malaria (van Lieshout et al., 2004). Urbanization in the global south is expected to increase the risks of disease, including dengue fever, plague, and yellow fever (Gubler, 1998). Conditions within cities such as poor drainage, inadequate sanitation, overcrowding, and slum housing could further exacerbate disease risk and increase transmission rates. Additionally, urban land-use change will disturb ecosystems that in turn will lead to changes in disease vectors and parasite populations. The confluence of these factors — growth in urban populations, climate change, and urban land-use change — may foster conditions favorable for an increased prevalence of some infectious diseases and a global health epidemic.

At local scales, a growing body of research suggests a relationship between urban form and public health (Jackson, 2003; Frumkin, 2002; Frank, 2000). Low-density urban development has led to more automobile travel, less physical activity, and less use of public transportation (Frank and Pivo, 1995; Kenworthy and Laube, 1999). More sedentary lifestyles including less walking and bicycling, combined with poor diets, are contributing to higher obesity rates and higher risk for cardiovascular disease and stroke. Although low-density urban development does not directly lead to higher mortality rates, urban sprawl is associated with decreased physical activity. As obesity increasingly becomes a global public health issue, synoptic information

on urban form and urban morphology can help target public health interventions, be it planting trees, provision of sidewalks, or mixed-use zoning.

As cities continue to attract the bulk of the world's population, there is a growing need to understand urban land use processes. Cities are complex entities of interconnected economic, social, and political systems. Remote sensing information on human settlements can be the common linkage among research, policy, and practice that will be integral to successfully solving pressing urban and global change issues.

REFERENCES

Aguilar, A., and Ward, P., Globalization, regional development, and megacity expansion in Latin America: Analyzing Mexico City's peri-urban hinterland, *Cities*, 20, 3–21, 2003.

Arnfield, A.J., Two decades of urban climate research: A review of turbulence, exchanges of energy and water, and the urban heat island, *International Journal of Climatology*, 23, 1–26, 2003.

Batty, M., The size, scale, and shape of cities, *Science*, 319, 769–771, 2008.

Benediktsson, J.A., Pesaresi, M., and Arnason, K., Classification and feature extraction for remote sensing images from urban areas based on morphological transformations, *IEEE Transactions on Geoscience and Remote Sensing*, 41, 1940–1949, 2003.

Chameides, W.L., Kasibhatla, P.S., Yienger, J., and Levy, H., II, Growth of continental-scale metro-agro-plexes, regional ozone pollution and world food production, *Science*, 264, 74–77, 1994.

Cohen, B., Urban growth in developing countries: A review of current trends and a caution regarding existing forecasts. *World Development,* 32 (1): 23–51, 2004.

Crutzen, P.J., New directions: The growing urban heat and pollution "island" effect — impact on chemistry and climate, *Atmospheric Environment*, 38, 3539–3540, 2004.

Frank, L.D., and Pivo, G., Impacts of mixed use and density on utilization of three modes of travel: Single-occupant vehicle, transit, and walking, *Transportation Research Record*, 1466, 44–52, 1995.

Frank, L.D., Land use and transportation interaction: Implications on public health and quality of life, *Journal of Planning, Education and Research*, 20, 6–22, 2000.

Frumkin, H., Urban sprawl and public health, *Public Health Reports*, 117, 202–217, 2002.

Gordon, C., Cooper, C., Senior, C.A., Banks, H., Gregory, J.M., Johns, T.C., Mitchell, J.F.B., and Wood, R.A., The simulation of SST, sea ice extents and ocean heat transports in a version of the Hadley Centre coupled model without flux adjustments, *Climate Dynamics*, 16, 147–168, 2000.

Gubler, D.J., Resurgent vector-borne diseases as a global health problem, *Emerging Infectious Diseases*, 4, 442–450, 1998.

Herold, M., Scepan, J., and Clarke, K.C., The use of remote sensing and landscape metrics to describe structures and changes in urban land uses, *Environment and Planning A*, 34, 1443–1458, 2002.

Herold, M., Goldstein, N.C., and Clarke, K.C., The spatiotemporal form of urban growth: Measurement, analysis and modeling, *Remote Sensing of Environment*, 86, 286–302, 2003.

Hewitson, B.C., and Crane, R.G., Climate downscaling: Techniques and application. *Climate Research*, 7, 85–95, 1996.

Jackson, L.E., The relationship of urban design to human health and condition, *Landscape and Urban Planning*, 64, 191–200, 2003.

Kaufmann, R.K., Seto, K.C., Schneider, A., Zhou, L., and Liu, Z., Climate response to rapid urban growth: Evidence of a human-induced precipitation deficit, *Journal of Climate*, 20, 2299–2306, 2007.

Kennedy, L., Regional industrial policies driving peri-urban dynamics in Hyderabad, India, *Cities*, 24, pp. 95–109, 2007.

Kenworthy, J.R., and Laube, F.B., *An International Sourcebook of Automobile Dependence in Cities, 1960–1990*, University Press of Colorado, Boulder, 1999.

McGuffie, K., and Henderson-Sellers, A., *A Climate Modelling Primer*, John Wiley and Sons, New York, 2005.

Montgomery, M.R., The urban transformation of the developing world, *Science* 319: 761–764, 2007.

Oke, T.R., Review of urban climatology 1968–1973, WMO Tech. Note 143, WMO No. 383, Geneva, 1974.

Parnell, S., Simon, D., and Vogel, C., Global environmental change: Conceptualizing the growing challenge for cities in poor countries, *Area*, 39, 357–369, 2007.

Rashid, T., Weeks, J.R., Stowe, D., and Fugate, D., Measuring temporal compositions of urban morphology through spectral mixture analysis: Toward a soft approach to change analysis in crowded cities, *International Journal of Remote Sensing*, 26, 699–718, 2005.

Resilience Alliance, Urban Resilience: A Research Prospectus, 2007, http://www.resalliance.org/files/1172764197_urbanresilienceresearchprospectusv7feb07.pdf.

Ridd, M.K., Exploring a V-I-S (Vegetation-Impervious Surface-Soil) model for urban ecosystem analysis through remote sensing: Comparative anatomy for cities, *International Journal of Remote Sensing*, 16, 2165–2185, 1995.

Sanchez-Rodriguez, R., Seto, K.C., Simon, D., Solecki, W., Kraas, F., and Laumann, G., *Urbanization and Global Environmental Change Science Plan*, International Human Dimensions Programme on Global Environmental Change (IHDP) Report No. 15. Bonn, Germany, 2005.

Seto, K.C., and Fragkias, M., Quantifying spatiotemporal patterns of urban land-use change in four cities of China with time series landscape metrics, *Landscape Ecology*, 20, 871–888, 2005.

Simon, D., McGregor, D., and Nsiah-Gyabaah, K., The changing urban-rural interface of African cities: Definitional issues and an application to Kumasi, Ghana, *Environment and Urbanization*, 16, 235–247, 2004.

Small, C., and Nicholls, R.J., A global analysis of human settlement in coastal zones, *Journal of Coastal Research*, 19, 584–599, 2003.

Song, Y., and Ding, C., eds., *Urbanization in China: Critical Issues in an Era of Rapid Growth*, Lincoln Institute of Land Policy, 2007.

Trenberth, K.E., Jones, P.D., Ambenje, P., Bojariu, R., Easterling, D., Tank, A.K., Parker, D., Rahimzadeh, F., Renwick, J.A., Rusticucci, M., Soden, B., and Zhai, P., Observations: Surface and atmospheric climate change. In: Solomon, S., Qin, D., Manning, M., Chen, Z., Marquis, M., Averyt, K.B., Tignor, M., and Miller, H.L., eds., *Climate Change 2007: The Physical Science Basis*, Cambridge University Press, Cambridge, United Kingdom, 2007.

UNCHS, *The State of the World's Cities Report 2001*, United Nations Centre for Human Settlements Habitat, 2002.

United Nations, *World Urbanization Prospects: The 2005 Revision*, UN Press, New York, 2006.

van Lieshout, M., Kovats, R.S., Livermore, M.T.J., and Martens, P., Climate change and malaria: Analysis of the SRES climate and socio-economic scenarios, *Global Environmental Change*, 14, 87–99, 2004.

Wilby, R.L., and Wigley, T.M.L., Downscaling general circulation model output: A review of methods and limitations, *Progress in Physical Geography*, 21, 530–548, 1997.

2 Some Recommendations for Global Efforts in Urban Monitoring and Assessments from Remote Sensing

Martin Herold

CONTENTS

2.1 INTRODUCTION

The persisting dynamic urban change processes, especially the tremendous worldwide expansion of urban population and urbanized area, affect and drive natural and human systems at all geographic scales. Although urban areas occupy only about 3% of the Earth's surface, their impact on surrounding rural areas is also rapidly increasing. Urbanization not only concentrates people (and therefore the demand for all social and economic services they require); it also creates hot spots for energy consumption, natural resource consumption, and emissions of pollutants and greenhouse gases, and acts as nodes linking communications and transport infrastructure — themselves all too often a source of pressure on the surrounding environment.

Urbanization is the trigger for a variety of land change processes in natural and seminatural environments. Any operational efforts tailored at sustainable and desirable future development have to consider urban dynamics as one of the key human-induced processes for understanding and managing our fast-changing world.

Thus, there is no doubt that global urban monitoring is an essential requirement to derive suitable information for understanding and management of urban processes to address problems of worldwide urgency. In this chapter, I am going to review some of the issues relating to a "global urban monitoring and assessment." Such an effort not only includes continuous, consistent, and accurate observations and monitoring, but also a process that links with political and strategic initiatives to ensure its relevance and legitimacy, and, ultimately, societal benefits. For the Earth observation domain, several such initiatives are ongoing. I will discuss several lessons learned from previous global environmental assessments and urban remote sensing exercises, and introduce international Earth observation initiatives to suggest a number of recommendations to the global observation community.

2.2 GLOBAL ENVIRONMENTAL ASSESSMENTS

Global environmental assessments have become an important element in international, national, and local policy and decision making. They are a prominent means for scientists providing input to address environmental problems on the policy level, in addition to more traditional options such as peer-reviewed publications, popular media, or private advice to relevant actors (Clark et al., 2006). The global nature of such efforts emphasizes their role in addressing problems that require cooperation among different countries, between scientists and policy makers, and across different scales. There are numerous examples of such assessments (Mitchell et al., 2006) including the Millennium Ecosystem Assessment (MEA), the Intergovernmental Panel on Climate Change assessment reports, United Nations Environment Programme's (UNEP) Global Environmental Outlook, or the Forest Resources Assessments conducted by the Food and Agriculture Organization (FAO). There is no doubt that good scientific information is essential for environmental decision making (Sutherland et al., 2006). However, mechanisms to link scientific research to policy level discussions and decisions are not an easy matter. For example, there is temporal dependence, and an evolution cycle between scientific findings, establishment of an observation and monitoring program, and related policy and public awareness and actions, referred to as the "issue attention cycle" (Kingdon, 1995). Furthermore, global assessments involve a social communication process in which scientists, decision makers, advocates, and the media interact and interpret findings in particular ways. Thus, it is to be recognized that the impact of a global assessment not only depends on the science being robust and technically believable (credibility). Any users must view the assessment as "salient" and "legitimate" as well as "credible" (Clark et al., 2006). When potential users believe that the information generated by an assessment process is relevant to their decision making it can be considered salient (Cash et al., 2002; Clark et al., 2006). Legitimacy is provided if the process is perceived as fair and took account of the concerns and insights of relevant stakeholders (Cash and Clark, 2001). In this context, five general issues

have been advocated for practitioners to implement efficient global and regional assessments (Clark et al., 2006):

- Focus on the process, not the report.
- Focus on salience and legitimacy as well as credibility.
- Assess with multiple audiences in mind.
- Involve stakeholders and connect with existing networks.
- Develop influence over time.

The suggested rules are similarly relevant for a case of global urban monitoring and assessment efforts that, besides providing the data and observations, should engage in international processes to make any findings and results more relevant and accepted. This paper discusses some of these issues. The reader is also referred to contributions from Moreno et al. (this volume) and Seto et al. (this volume).

2.3 URBAN REMOTE SENSING

Remote sensing provides the most suitable systematic approach for collecting spatial information on human settlements. Earth observation has been focused on mapping, monitoring, and understanding urban phenomena for many years, but with more emphasis on local to regional scales. Global mapping of human settlements is particularly challenging because of the spatial and spectral heterogeneity of urban environments, as well as their small and fragmented spatial configuration. In fact, there is large disagreement between urban land represented in different global land cover products (Figure 2.1; see also Schneider et al., 2003; Potere and Schneider, this volume). Different reasons can be cited: challenges in mapping urban areas with coarse-scale Earth observation systems; different definitions of "urban" and varying mapping standards; issues with integrating different data sources; problems in precise geolocation of spatial datasets; and the importance of update information because urban areas are evolving quickly. Thus, global urban mapping can, in most cases, currently only marginally deliver what is needed to approach the multitude of challenges resulting from continuous urbanization and population growth.

The recent proliferation of new sources of data and tools for data processing, analysis, and modeling has provided and opened up avenues for significant progress toward global observations of urban patterns and dynamics. Because of the heterogeneity of global urban characteristics, the key issue is to combine Earth observation indicators for characteristics and change in human settlements. Sensors such as Moderate Resolution Imaging Spectroradiometer (MODIS) or LANDSAT give spectral evidence for built-up areas and the land cover configuration within urban environments; nighttime observations by Defense Meteorological Satellite Program (DMSP) are a strong indicator of populated areas and population distribution; synthetic aperture radar (SAR) measurements emphasize the three-dimensional characteristics of urban surfaces; thermal infrared data contain information about energy fluxes and local climatic conditions.

Previous global activities have applied a variety of data sources, mapping and monitoring strategies, and analysis methods to study urban phenomena on global scales.

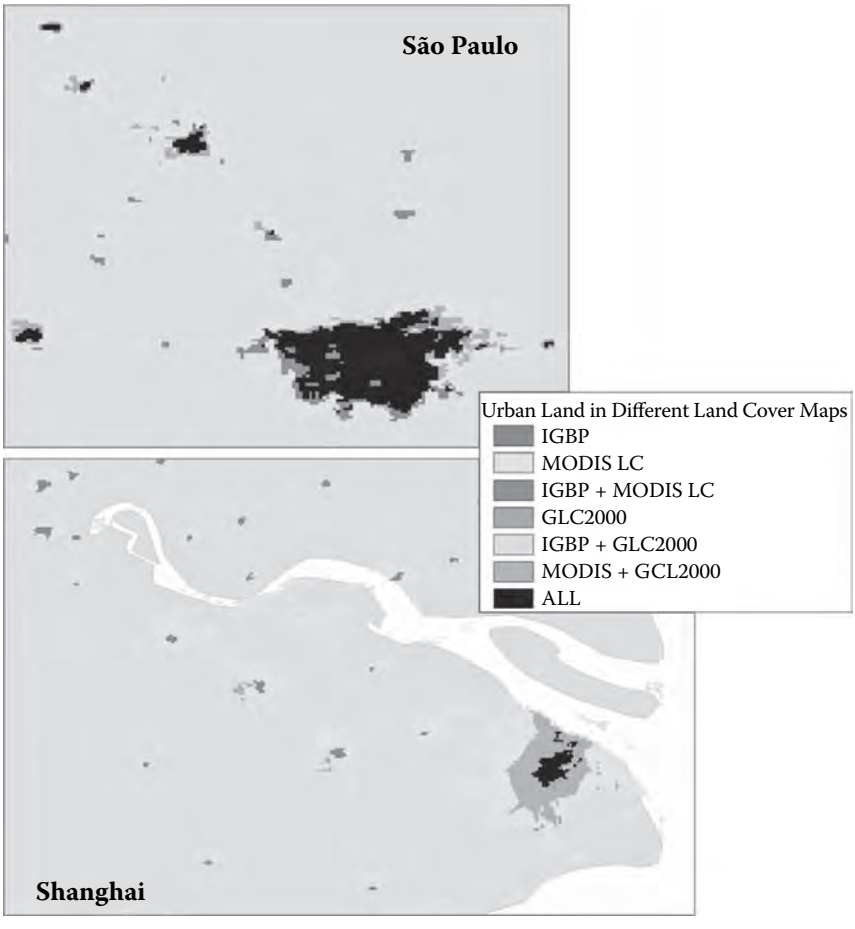

FIGURE 2.1 Comparison and agreement of urban land in three different global land cover products: International Geosphere-Biosphere Programme-Data Information System (urban areas from digital chart of the world), MODIS land cover [urban areas from MODIS (2000), DMSP (1994–1995), and ancillary data], and GLC2000 [urban areas from the Defense Meteorological Satellite Program (1994–1995)].

The most comprehensive information on global urban dynamics has been derived from statistical datasets describing demographic, socioeconomic, and economic indicators of urban characteristics and quality. On global scales, this information usually exists in rather coarse spatial precision, with large time steps for updating, and sometimes the data are not consistently available for specific regions (e.g., developing countries). More details can be provided by Earth observation. Remote sensing data sources for coarse scale urban mapping have been multifaceted: optical data (Schneider et al., 2003), thermal measurements (Hafner and Kidder, 1999), active radar data (Henderson and Xia, 1997; Grey et al., 2003; see also Dell'Acqua, this volume), and nighttime-lights DMSP data (Imhoff et al., 1997; Henderson et al., 2003). The data sources have been used to study a variety of urban phenomena such as urban ecosystems (Miller and

Small, 2003), urban climates (Voogt and Oke, 2003; Trana et al., 2006), urban population (Sutton et al., 1997; Small, 2003; Liu et al., 2006), health and disease (Tatem and Hay, 2004), urban growth and change processes (Phinn et al., 2002; Seto and Kaufmann, 2003; Herold et al., 2003), and others. Despite the availability of several global land cover datasets including urban areas (see Potere, this volume), comprehensive global urban monitoring programs have so far been studying selected representative cities in high spatial and temporal detail. The observations and analysis provide general assumptions about ongoing processes on coarser scale (Lavalle et al., 2001; Beckel et al., 2002). Often, Earth observation mapping and monitoring offers sufficient information for analysis of urban form and spatial processes toward support and improvement of urban modeling, management, and planning efforts, and advances in understanding urban phenomena in a theoretical context (Herold et al., 2007).

2.4 INTERNATIONAL LAND OBSERVATION INITIATIVES AND PROGRAMS

Several international Earth observation initiatives are currently active and connected for global and regional scale observations. Figure 2.2 outlines their relationships and roles; the initiatives will be discussed in more detail in this section. Their general goal is continuity and consistency for observations providing high-quality data and information in support of sustainable development and natural resource management. There are high level and political processes — that is, the Group on Earth Observations (GEO) and the United Framework Convention on Climate

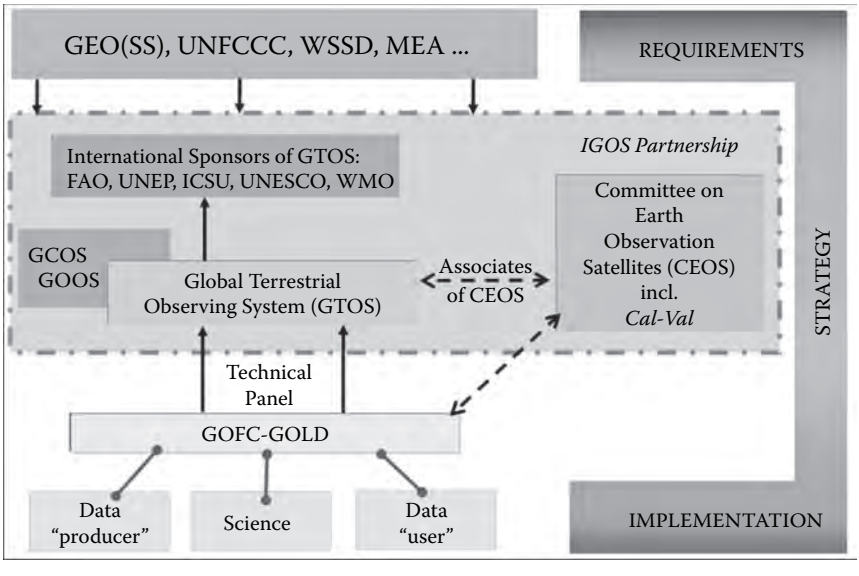

FIGURE 2.2 The big "picture" in global Earth observations: organizations and agencies involved in defining requirements, strategies, and implementation activities.

Change (UNFCCC) — that specify requirements as frame for efforts on the more strategic Earth observation level. The Integrated Global Observing System (IGOS) Partnership involves a number of partners that formulate observation strategies and technical implementation guidelines for implementation by national or international agencies and organizations. On the implementation level, there are organizations such as Global Observation of Forest Cover and of Land Dynamics (GOFC-GOLD; http://www.fao.org/gtos/gofc-gold). As the technical panel of Global Terrestrial Observing System (GTOS; http://www.fao.org/gtos), it provides the interface between the strategic and the implementation level. GOFC-GOLD provides a communication and cooperation platform for actors involved in global Earth observation including data producers (e.g., space agencies, land cover facilities), the scientific community, and data users (FAO, UNEP, global modeling community, etc.). GOFC-GOLD has proposed a program of annual coarse resolution (250–1000 m) Earth observations, fine-scale land cover mapping (~25 m) on a 5-year cycle, and integration with in situ observations on global scales (Townshend and Brady, 2006). Perhaps, the programs and processes on Earth observation are not solely targeted at urban monitoring. Their role and approaches in addressing urban issues will be discussed in the following sections.

2.4.1 Group on Earth Observations

The GEO (http://earthobservations.org/) followed a G8 initiative that called for strengthened cooperation and coordination among global observing systems and research programs for integrated global observations. GEO emerged in 2003 from a consensus among governments and international organizations that, while supporting and developing existing Earth observation systems, more can and must be done to strengthen global cooperation and Earth observations. The GEO vision was formulated in the Washington Declaration adopted at the Earth Observation Summit of 2003. Since this declaration in 2003, the GEO process has resulted in a variety of Earth Observation Summits, the latest a ministerial summit at Cape Town in November 2007. As its most comprehensive early achievement, GEO has defined nine areas of societal benefits where society can directly benefit from Earth observation.

The GEO process has outlined a framework document calling on Global Earth Observation System of Systems (GEOSS). Although not legally binding, this document marks a crucial step in developing the 10-Year Implementation Plan for the creation of a comprehensive, coordinated, and sustained Earth observation system or systems. For implementation, there is a GEO 2007–2009 work plan in place.

Given the current draft of the GEOSS implementation plan (GEOSS, 2005), global urban mapping is mentioned in several circumstances (Table 2.1). Several aspects of urban mapping are described as areas of societal benefit. It should be noted that some of these observation requirements are beneficial to several of these areas and are not mentioned twice. Urban extent and land use/land cover maps are considered to be not yet widely available or not yet adequately monitored globally but could be within 2–10 years. One parameter not mentioned in Table 2.1 is transportation infrastructure that also is called on in the GEOSS implementation plan.

TABLE 2.1
GEO-Defined Areas of Societal Benefits and Earth Observation Objectives for Urban Mapping on Global Scales

Societal benefit area	Global Earth observation requirements referring to urban areas
Disasters	Human infrastructure
Health	Urban heat island and air quality
	Population density
	Land cover
Energy	Land use and land cover
	Urban extent
Climate	Land cover
Water	Land use
	Industrial water demand
	Population density
Ecosystems	Population density
Agriculture	Land cover
	Population density

Most of the urban mapping features (e.g., urban extent, land use, land cover, etc.) are considered to be not yet widely available or not yet adequately monitored globally but could be within 2–10 years. The GEOSS plan also emphasizes the need for integrative analysis of the Earth observation mapping products, that is, gaps exist in the integration of relevant existing observation systems, for example, integrating the global urban land observations with data that characterizes the built environment, chemical emission, and with indicators of environmental quality, health, and disease. Despite the relevance emphasized in the GEOSS Implementation Plan (GEOSS, 2005), and a specific GEO task dealing with global land cover (Herold, 2007), current GEO implementation lacks activities relating to land use and urban issues.

2.4.2 Integrated Global Observations of Land

The Integrated Global Observing Strategy (IGOS; http://ioc.unesco.org/igospartners/) was established in 1998. Its main objective is the definition, development, and implementation of an Integrated Global Observing Strategy. IGOS brings together efforts of a number of international agencies concerned with global environmental issues, research, and observing systems. IGOS theme documents are a primary source of requirements for the development of GEOSS. However, the IGOS Partnership (IGOS-P) has not yet considered many observational needs relating to many aspects of the land, such as sustainable economic development, natural resources management, conservation and biodiversity, ecosystems (functioning, services), biogeochemical cycling, multilateral environmental agreements (development, implementation), mandatory reporting and monitoring. A new IGOS

theme was recently added on Integrated Global Observations for Land (IGOL; Townshend et al., 2007). The main components of the new theme are as follows: land cover and land use, human settlement and population, managed ecosystems, agriculture, pastoralism, forestry, natural ecosystems, conservation, biodiversity, sustainable use, soils, biogeochemical cycles, and elevation. In the context of global remote sensing of human settlements, it is emphasized that satellite data information can improve decision making in a number of application areas, including:

- Spatial modeling of population variables such as population and settlement density (both urban and rural), land use patterns, civil infrastructure, and some types of economic activity.
- Improved modeling of the flow of food, water, energy, disease vectors, and their consequences for natural systems including ecosystem and planetary metabolism.
- The location and density of infrastructure for use in hydrologic modeling, flood prediction, the assessment of land use and land use change, analyzing human impacts on biodiversity, and threats to public health.
- Monitoring, management, and mitigation of natural disasters.
- Urban planning and more effective location decisions and development of support infrastructure.
- Spatial modeling of atmospheric emissions associated with fossil fuel consumption and other anthropogenic activities.

In terms of global urban mapping, IGOL emphasizes the need for coordinated global urban observations with the fundamental focus on reliable and spatially explicit settlement and population databases, transportation infrastructure information, and understanding urban change processes. IGOL is now in the process of being integrated into GEO and once again urges this effort to take on urban monitoring issues.

2.4.3 Global Monitoring for Environment and Security

The objective of this initiative is to "establish by 2008 a European capacity for Global Monitoring for Environment and Security (GMES)" (http://www.gmes.info). GMES, as a joint initiative of the European Commission and the European Space Agency (ESA), aims to support Europe's goals regarding sustainable development and global governance, in support of environmental and security policies, by facilitating and fostering the timely provision of quality data, information, and knowledge. As part of the GMES, an "Urban Services" section (http://www.gmes-urbanservices.info/) has been established. The objectives do not especially refer to global scale urban mapping. GMES priorities in urban mapping are set on local and regional scales to assist urban management and security. The so-called "Fast Track Service" for land monitoring includes a specific European-wide mapping exercise of impervious areas, a process that was started in 2007. Seifert (this volume) provides additional information on these initiatives.

2.4.4 Millennium Ecosystem Assessment

The MEA (http://www.millenniumassessment.org/) is a UN-initiated international work program designed to meet the needs of decision makers and the public for scientific information concerning the consequences of ecosystem change for human well-being and options for responding to those changes. Being tailored at ecosystems, the observation requirements focus on mixed patterns of human use and ecosystems that emphasize on the spatial extent of urban areas. A further focus is on the urbanization processes and on population growth as drivers of ecosystem change on different spatial and temporal scales.

2.4.5 Global Climate Observing Systems Implementation Plan

In support of the UNFCCC, the Global Climate Observing System (GCOS; http://www.wmo.ch/web/gcos/gcoshome.html) has completed an implementation plan in October 2004 (GCOS, 2004) to outline the requirements and actions to provide an appropriate database in the implementation of the UNFCCC objectives and the Kyoto protocols. The focus of this implementation plan is on climate but specifically calls on land cover and changes (and use) on global scales as important terrestrial variables to be derived from Earth observation.

2.4.6 GTOS Coastal Implementation Plan

The GTOS implementation plan on coastal zones (http://www.fao.org/gtos/doc/pub36.pdf) emphasizes the importance of urban areas in this environment because about half of the world population lives within 200 km of the coast. The IGOS Coastal theme already places a priority on urbanization in coastal zones. Coastal GTOS implementation plan specifies several aspects, that is, the rate of change in population, urbanization, and land use in coastal environments. The report discusses "best available global datasets" and their current limitations and prospects including the Department of Energy Landscan Ambient Population, the DMSP Nighttime Data, the global Landsat mosaics, the ESA GLOBCOVER product, and the MODIS land cover/urban product and vegetation continuous field datasets.

2.4.7 UN Global Land Cover Network

The Global Land Cover Network (GLCN, ftp://ftp.fao.org/docrep/fao/004/y3726e/y3726e00.pdf), launched by FAO and UNEP, is an international coordinated effort whose objective is to provide direction, focus, guidance, and standards for harmonization of land cover mapping, and monitoring at national, regional, and global levels. The initiative is based on the recommendations of the Agenda 21 for coordinated, systematic, and harmonized collection and assessment of data on land cover and environmental conditions. GLCN aims at generating essential data needed for sustainable development, environmental protection, food security, and humanitarian programs of the UN, and of other international and national institutions. The major objectives of this initiative are on harmonization and standardization of classification of cover

types, the determination patterns of land cover and its associated change, projections of human response scenarios, support to integrated global and regional modeling, and the global assessment of land cover for international conventions and treaties. The GLCN strategic documents are currently in development and will also address issues of urban mapping and monitoring and related expectations for Earth observations, and standardized mapping using the UN Land Cover Classification System (Di Gregorio, 2005).

2.5 REMARKS AND RECOMMENDATIONS

Urban areas and their dynamics are one of the main drivers of land change on local to global scales. With small and fragmented spatial and spectrally heterogeneous characteristics, their accurate mapping and monitoring has been challenged in the past and certainly has not received as much attention as the global observation of other land types such as forests. A number of satellite remote sensing systems collect data relevant to the global mapping and monitoring of human settlements. Despite a focus on global observations, to data products have to be derived, analyzed, and refined in a multiscale context. Urban phenomena can be observed and show specific characteristics on different levels of spatial and temporal and detail. Linking coarse-scale (250–1000 m spatial resolution), fine-scale (20–50 m spatial resolution), and very fine-scale (1–4 m spatial resolution), and in situ observations should be the central perspective in any related activities. Continuity in Earth observations on all these scales is essential to support such progress. Currently, coarse-scale observations (e.g., MODIS, MERIS, SPOT VEGETATION) and LANDSAT-type observations are widely available. This level of continuity does not exist for the other scales. Ongoing international collaboration is needed to produce consistent global maps of human settlements using multiple sources. A multistage approach could be adopted to reduce the extent of data collection and processing of data from ultrafine spatial resolution systems. For instance, coarse resolution nighttime lights could be used to define the collections plans for higher spatial resolution systems. Key to the value of any effort for global mapping of human settlements is timely product generation and distribution. In general, updates are required on an annual basis with a distribution latency of a year or less. The establishment of a global urban observatory further provides great opportunities to establish successful cases for data integration that is desired in many fields of global Earth observation. Synergy of satellite data from different sensors (DMSP, MODIS, SAR, etc.), linking observations to socioeconomic and demographic information, bridging across and among different scales, and relating empirical measurements, spatial theory, and modeling have been proven to be successful in an urban context. These potentials should be further elaborated on for global scale assessments. Recently there have been some proposals for satellite missions primarily targeted urban monitoring. For example, Nightsat is a concept for a satellite system capable of global observation of the location, extent, and brightness of nighttime lights at a spatial resolution suitable for the delineation of primary features within human settlements (Elvidge et al., 2007).

Recent developments emphasize the need for sustained, harmonized, and validated global Earth observation products of human settlements, that is, by the GEO formed in 2003 aiming to evolve a Global Earth Observation System of Systems

(GEOSS), the European GMES initiative, the GCOS implementation plan calling on land cover, and the requirements advocated by the IGOL. They emphasize a political and strategic mandate. Although these initiatives have long-term goals, they have to start and evolve from an international cooperation and consensus building efforts, both on the strategic level and in implementation activities. It is to be recognized that ongoing international processes on building interoperable spatial data structures and interface specifications such as Infrastructure for Spatial Information in the European Community (www.ec-gis.org/inspire/) and the Open Geospatial Consortium (www.opengeospatial.org) are dealing with a wide range of issues and perhaps would require more detailed consideration of urban monitoring issues in the future.

Given these elaborations, there are several recommendations to the Earth observation community interested in pursuing a global Earth observation survey of urban areas and urban change:

- To learn from the experiences in previous global environmental assessments, a global urban monitoring and assessment effort should be set up as an international process to evolve over time, involve relevant national to global stakeholders and networks active in land cover and urban monitoring, and closely interact and engage with user agencies and policy makers.
- Full advantage should be taken of initiatives such as GEO and IGOL. They have advocated the importance of global urban monitoring and provide documented requirements and expectations for global urban monitoring programs but, so far, have not engaged in dedicated implementation activities.
- Any global and regional urban data products have to be harmonized, accessible, validated, and flexible to provide the best match between observations, data products, and user requirements.
- Consistency of information is essential from global to local scales and requires a common classification scheme for built environments and settlements (see discussions by Jansen, this volume).
- Integration of different satellite data sources is essential for accurate urban mapping on global and regional levels. This relates to different data sources for global observations and more detailed observations to link observations and data among scales.
- Most previous results from global urban change analysis were derived from socioeconomic and demographic data, and remote sensing efforts should be complementary and integrated with these efforts.

Because these efforts have long-term goals, these recommendations may seem ambitious and broad. However, there is a clear opportunity to start such activities in the near future and improve satellite-based observations toward a global urban assessment. Obvious starting points on the technical side are to use existing satellite and nonsatellite data sources and products to make best integrated use of existing information, and to even better address and contribute urban issues to ongoing monitoring initiatives (i.e., MODIS land cover, GLOBCOVER, GMES, etc.). In addition, there is a need to better reflect urban monitoring issues in active international processes (e.g., GEO) that lack current specific urban activities. In this

context, any integrated large-scale urban assessments should perhaps be driven by needs associated with the areas of societal benefits advocated by GEO (see Table 2.1), and the goods and services provided by the urban ecosystem (Constanza and Folke, 1997).

REFERENCES

Beckel, L., Kuehnen, A., Siebert, A., Lichtenegger, J., Gampe, F., and Brisson, P., MegaCities, *ESA Bulletin–European Space Agency*, 110, 81–87, 2002.

Cash, D., and Clark, W., From Science to Policy: Assessing the Assessment Process, John F. Kennedy School of Government, Harvard University Faculty Research Working Papers Series, RWP01-045, 2001, http://ssrn.com/abstract_id=372280.

Cash, D., Clark, W., Alcock, F., Dickson, N., Eckley, N., and Jäger, J., Salience, Credibility, Legitimacy and Boundaries: Linking Research, Assessment and Decision Making, John F. Kennedy School of Government, Harvard University Faculty Research Working Papers Series, RWP02-046, 2002, http://ssrn.com/abstract_id=372280.

Clark, W.C., Mitchell, R.B., and Cash, D.W., Evaluating the influence of global environmental assessments, in Mitchell, R.B., Clark, W.C., Cash, D.W., and Dickson, N.M., eds., *Global Environmental Assessments: Information and Influence*, MIT Press, Cambridge, 2006.

Constanza, R., and Folke, C., Valuing ecosystem services with efficiency, fairness and sustainability as goals, in Daily, G.C., ed., *Nature's Services: Societal Dependence on Natural Ecosystems*, Island Press, Washington, D.C., 49–67, 1997.

Di Gregorio, A., UN Land Cover Classification System (LCCS) — Classification Concepts and User Manual for Software Version 2, 2005.

Elvidge, C.D., Cinzano, P., Petti, D.R., Arvesen, J., Sutton, P., Small, C., Nemani, R., Longcore, T., Rich, C., Safran, J., Weeks, J., and Ebener, S., The nights at mission concept, *International Journal of Remote Sensing*, 28(12), 2645–2670, 2007.

GCOS, Implementation plan for the Global Observing System for Climate in support of the UNFCCC, October 2004, GCOS– 92, WMO Technical Document No. 1219, WMO, Geneva, p. 153, 2004. Available online at: http://www.wmo.ch/web/gcos/gcoshome.html.

GEOSS, The Global Earth Observation System of Systems (GEOSS) 10-Year Implementation Plan and Reference, 2005. Document available online at: http://earthobservations.org.

Grey, W.M.F., Luckman, A.J., and Holland, D., Mapping urban change in the UK using satellite radar interferometry, *Remote Sensing of Environment*, 87(1), 16–22, 2003.

Hafner, J., and Kidder, S.Q., Urban heat island modelling in conjunction with satellite-derived surface/soil parameters, *Journal of Applied Meteorology*, 38(4), 448–465, 1999.

Henderson, F.M., and Xia, Z.G., SAR applications in human settlement detection, population estimation and urban land use pattern analysis: A status report, *IEEE Transactions on Geoscience and Remote Sensing*, 35(1), 79–85, 1997.

Henderson, M., Yeh, E.T., Gong, P., Elvidge, C., and Baugh, K., Validation of urban boundaries derived from global night-time satellite imagery, *International Journal of Remote Sensing*, 24(3), 595–609, 2003.

Herold, M., Global land cover observations, in Group on Earth Observation (GEO), ed., *The Full Picture*, Publication for GEO ministerial summit, Tudor Rose, Cape Town, pp. 235–237, November 2007.

Herold, M., Goldstein, N.C., and Clarke, K.C. The spatio-temporal form of urban growth: Measurement, analysis and modelling, *Remote Sensing of the Environment*, 86, 286–302, 2003.

Herold, M., Hemphill, J., and Clarke, K.C., Remote sensing and urban growth theory. In Weng, Q., and Quattrochi, D., Eds., *Urban Remote Sensing*, pp. 201–220, Taylor & Francis, London, 2007.

Imhoff, M.L., Lawrence, W.T., Elvidge, C.D., Paul, T., Levine, E., and Privalsky, M.V., Using nighttime DMSP/OLS images of city lights to estimate the impact of urban land use on soil resources in the United States, *Remote Sensing of Environment*, 59(1), 105–117, 1997.

Kingdon, J.W., *Agendas, Alternatives, and Public Policies*, Harper Collins, New York, 1995.

Lavalle, C., Demicheli, L., Turchini, M., Casals-Carrasco, P., and Niederhuber, M., Monitoring megacities: The MURBANDY/MOLAND approach, *Development in Practice*, 11(2–3), 350–357, 2001.

Liu, X., Clarke, K.C., and Herold, M., Population density and image texture: A comparison study, *Photogrammetric Engineering and Remote Sensing*, 72(2), 187–196, 2006.

Miller, R.B., and Small, C., Cities from space: Potential applications of remote sensing in urban environmental research and policy, *Environmental Science and Policy*, 6(2), 129–137, 2003.

Mitchell, R.B., Clark, W.C., Cash, D.W., and Dickson, N.M., Eds., *Global Environmental Assessments: Information and Influence*, MIT Press, Cambridge, 2006.

Phinn, S., Stanford, M., Scarth, P., Murray, A.T., and Shyy, P.T., Monitoring the composition of urban environments based on the vegetation–impervious surface–soil (VIS) model by subpixel analysis techniques, *International Journal of Remote Sensing*, 23(10), 4131–4153, 2002.

Schneider, A., Friedl, M.A., Mciver, D.K., et al., Mapping urban areas by fusing multiple sources of coarse resolution remotely sensed data, *Photogrammetric Engineering and Remote Sensing*, 69(12), 1377–1386, 2003.

Seto, K.C., and Kaufmann, R.K., Modelling the drivers of urban land use change in the Pearl River Delta, China: Integrating remote sensing with socioeconomic data, *Land Economics*, 79(1), 106–121, 2003.

Small, C., Global population distribution and urban land use in geophysical parameter space, *Earth Interactions*, 8(8), pp. 1–18, 2003.

Sutherland, W.J., Armstrong-Brown, S., Armsworth, P.R., Brereton, T., Brickland, J., Campbell, C.D., Chamberlain, D.E., Cooke, A.I., Dulvy, N.K., Dusic, N.R., Fitton, M., Freckleton, R.P., Godfray, H.C.J., Grout, N., Harvey, H.J., Hedley, C., Hopkins, J.J., Kift, N.B., Kirby, J., Kunin, W.E., Macdonald, D.W., Marker, B., Naura, M., Neale, A.R., Oliver, T., Osborn, D., Pullin, A.S., Shardlow, M.E.A., Showler, D.A., Smith, P.L., Smithers, R.J., Solandt, J.-L., Spencer, J., Spray, C.J., Thomas, C.D., Thompson, J., Webb, S.E., Yalden, D.W., and Watkinson, A.R., The identification of 100 ecological questions of high policy relevance in the UK, *Journal of Applied Ecology*, 43, 617–627, 2006.

Tatem, A.J., and Hay, S.I., Measuring urbanization pattern and extent for malaria research: A review of remote sensing approaches, *Journal of Urban Health Bulletin of the New York Academy of Medicine*, 81(3), 363–376, 2004.

Trana, H., Uchihamab, D., Ochib, S., and Yasuokab, Y., Assessment with satellite data of the urban heat island effects in Asian mega cities, *International Journal of Applied Earth Observation and Geoinformation*, 8(1), 34–48, 2006.

Townshend, J., and Brady, M., A Revised Strategy for GOFC-GOLD, GOFC-GOLD report 24, GOFC-GOLD report series, 2006, http://www.fao.org/gtos/gofc-gold/series.html.

Townshend, J.R., Latham, J., Arino, O., Balstad, R., Belward, A., Conant, R., Elvidge, C., Feuquay, J., El Hadani, D., Herold, M., Janetos, A., Justice, C.O., Liu J., Loveland, T., Nachtergaele, F., Ojima, D., Maiden, M., Palazzo, F., Schmullius, C., Sessa, R., Singh, A., Tschirley, J., and Yamamoto, H., Integrated Global Observation of Land: An IGOS-P theme, 2007, available at www.fao.org/gtos/igol/.

Voogt, J.A., and Oke, T.R., Thermal remote sensing of urban climates, *Remote Sensing of Environment*, 86(3), 370–384, 2003.

Part II

Urban Characterization over Large Areas

3 A Methodology to Quantify Built-Up Structures from Optical VHR Imagery

Martino Pesaresi and Daniele Ehrlich

CONTENTS

3.1 INTRODUCTION

Describing human settlements by remote sensing data has always been a challenge since the field of Earth observation began more than 50 years ago. General disciplines dealing with human settlement description have often reported difficulties in using available satellite-derived information to describe these settlements. We refer here not only to such disciplines as urban and regional planning, and design and development, but also to sectorial activities related to risk assessment or damage and reconstruction assessment. During these years, the conventional explanation for this

difficulty was mainly attributed to a technological gap — in short, to a lack of spatial resolution in the available civilian satellite data. The fact that broad-scale planning activities (e.g., regional strategic spatial planning) also usually ignored traditional satellite value-added products was omitted in the cited explanation. When noted, this fact was commonly linked to a general lack of "communication," with practitioners or urban planners being unaware of the potentialities of satellite-derived products.

The latest-generation very high resolution (VHR) satellite data are now approaching the spatial resolution of airborne image data (Baltsavias and Gruen, 2003). These data have been profitably used by cartographers and urban planners since airborne photogrammetric technology became available after the Second World War. Contrary to expectations, however, the situation regarding the exploitation of satellite remotely sensed data by decision makers and urban planners has not shown any radical improvement.

Remote sensing specialists are now realizing that the capacity to extract information from satellite data has not kept pace with the improvement in image spatial resolution. VHR data are much more complex in the spatial domain. Geometric increase in the volume of data to be processed and the difficulty in geocoding the data with an absolute spatial accuracy comparable with the pixel size are the two main technical reasons that make VHR data preparation for automatic recognition, including change detection, a difficult task.

In extracting information from VHR satellite imagery, it also appears that the standard model postulating spectral homogeneity of the classes to be extracted is encountering several major difficulties. This is because a greater amount of detail generates increase in internal class spectral variability, and consequently a decrease in discrimination power of any method based on collection and processing of pure spectral image features.

From another viewpoint, the ability to acquire (by visual interpretation) greater amount of details in new-generation satellite data has revealed the inadequacy and the excessive simplification of the traditional method of structuring information extracted from remotely sensed data, say the land use/land cover (LU/LC) paradigm that dominated the remote sensing methodological debate in the past 50 years.

One of the basic concepts presented in this work is that a really effective remote sensing of human settlements needs the harmonic development of three basic areas: remote sensor technology; information extraction methodology; and conceptual tools able to handle the extracted information, say the classification scheme. These three areas should go together; an unbalanced progress involving only the sensor technology, for example, would result in failures on the application of outdated information extraction models. Similarly, progress on sensor technology and information extraction methodology would be ineffective if we maintain the same classification schema tuned for the preceding situation.

This work tries to address these issues applied to the analysis of human settlements by arguing (1) a special status and characteristic of the settlement theme that make difficult the traditional approach of remote sensing, (2) the need of new methodologies for extracting information on settlements from satellite data, and (3) the need of a new paradigm for structuring the extracted geoinformation in more effective data models.

In particular, the special status of the settlement theme is described as *complexity of the use context* of the information about the human settlement, and as *specific physical characteristics* (the spatial heterogeneity of internal materials and mimetism with the surrounding areas) that break the standard remote sensing model postulating spectrally homogenous and distinguishable classes to be recognized.

Because of the specific physical characteristics of the settlement theme, we argue the importance of processing the image structural information in order to improve the effectiveness of the automatic discrimination and analysis of the settlement's elements using satellite data. Because of the specific use content of the information about settlements, we argue the necessity of reducing the rigidity of the conceptual paradigm used for storing and representing the extracted information, say the LU/LC standard classification schema. This is done by modulating the semantic abstraction of the extracted information in three levels, and consequently by avoiding the rapid obsolescence of too abstract or high-level and user-specific semantics. As described in the following paragraphs, these abstraction levels have different matches with possible techniques for image automatic recognition and analysis, and they may have different logical compositional constraints.

3.2 SPECIFICITY OF THE SETTLEMENT THEME

The specificity of the settlement theme is related to a specific complexity of the use context or application field, and to specific physical characteristics described as internal heterogeneity of material and similarity or mimetism with other natural surfaces.

3.2.1 Complexity of the Use Context

Settlements display the highest concentration of human artifacts and functions and are the most valuable part of the territory for human societies. In fact, settlements typically show the maximum concentration of human activity, of manmade structures and objects. Urban areas also show the maximum of stratification of different functions in the same place. Settlements show overlapping economic interests among social groups as well as with and among public authorities. Urban areas also typically show the highest social stratification and differentiation that is often coupled with historical development and identity that define priorities and agendas of different social groups. All these multiple stratifications of interests and functions produce a remarkable multiplicity of point of views, equally valid but not coincident, of the settlement "fact" or geographic physical entity. This situation explains why human settlement is hardly reducible to a unique descriptive scheme, whereas for other type of Earth surfaces, say "forest" or "corn field," such reduction can be eventually more successful. This is because in these other cases, it is easier to reach consensus on a common descriptive scheme defining priorities and semantic hierarchies.

Different functions and priorities also define a multiplicity of possible actions on settlements, as is the case with different planning and management strategies. The required information on settlements can therefore remarkably diverge in terms of scales, semantics, priorities, and timeliness, by varying the social actor, the public

authority, or the given point of view defining a specific "user." We describe this situation as *complexity of the use context* of the information regarding the human settlement. No unique description can be fully effective, but all descriptions have the same or comparable importance.

3.2.2 Physical Characteristics

We can define human settlement as composed by three basic classes of physical elements that are visible in the remotely sensed data: buildings, roads (or moving infrastructures), and remaining open spaces. All these elements contribute to define the built-up pattern, also called urban area, urban fabric, man-made area, settlement surface, and so on.

From the viewpoint of physical composition, the built-up pattern can be defined as the place of heterogeneity. Almost all possible materials and surfaces, including artificial and organic materials, can be reported as belonging to the settlement theme in the same places all over the world. Moreover, in many cases we may observe that several different materials can be used for the same built-up element of the same settlement (i.e., clay tiles, corrugated metal, grass, concrete, plastic, bitumen, stone, for building's roof) and in the same time the identical material for different elements (i.e., the same stones for paved roads and building roofs). The spatial scale of variability of these different materials is typically about a few meters. This situation is described here as *internal spatial heterogeneity* of the Earth surfaces covered by built-up patterns.

Furthermore, because settlements are also often made up of materials present in the surrounding natural areas, it is possible that they will not be distinguishable from the natural or agricultural areas, if we take into account only the characteristics of the materials or the surfaces. Typical examples are unpaved roads and bare soils, but also many roof materials (as clay tiles or stone tile) and again bare soil or rocks. Another typical example is the vegetated open spaces in settlements, as private green surfaces in residential areas, or parks, and other public recreational surfaces present in many settlements. This situation is described here as *mimetism* between the settlement theme and the surrounding areas.

3.3 EXTRACTING INFORMATION ON SETTLEMENTS

3.3.1 Importance of Image Structural Information

It is well known that we can consider any digital image, and consequentially, also satellite data, as composed by two basic families of information or "descriptors": the spectral descriptor and the spatial or structural descriptor. Whereas spectral information reports on the spectral reflectance of the electromagnetic energy for each individual image point (or picture element, pixel), structural information refers to the mutual spatial arrangement of these pixels. Structural information is defined by a given local domain [also called kernel, structuring element (SE), neighborhood, and the like) and an information extraction rule involving in some way the pixels contained in the given local domain. Because it is the spectral information that is the

primary source, structural information has a higher abstraction level: we can say that the structural information is always derived from the primary spectral information contained in the image data.

The standard paradigm for automatic image understanding in remote sensing was based on the following assumptions: (1) the classes to be recognized are made up of the same surfaces, the same surfaces are reflecting the same energy with the same given illumination, then they are spectrally homogeneous; (2) as a corollary, different classes are assumed distant in the space defined by their spectral attributes. Therefore, we can say that the standard automatic image understanding or information extraction paradigm in remote sensing was mainly based on exploitation of image spectral information. Because of the specificity of the human settlement theme (say the internal spatial heterogeneity and the mimetism with the surrounding areas), the standard information extraction paradigm for remote sensing does not give fully satisfactory results. If blindly applied, it may lead to unpredictable results usually strongly depending on local geographic conditions and characteristics of the settlement under study. The situation where the same material with the same illumination conditions (then the same measured spectral reflectance) identify all the same elements of a given built-up pattern and is not present in other types of surfaces of the same data set is more a special case than a general rule. Moreover, the rarity of this special case is directly proportional to the number of satellite scenes, or datasets, it is needed to interpret automatically with the same inferential model (thus directly proportional to the universe of data to be analyzed).

The structural information refers to the mutual spatial arrangement of image pixels in a given local domain. Because of the internal spatial heterogeneity of the settlement theme, different surface materials close together may produce characteristic spatial patterns of spectral reflectance that can be captured by techniques able to handle image structural information. Moreover, by definition built-up structures are extruded from the ground level of at least one floor, and consequently they are often casting shadows with a size detectable by the latest-generation satellite sensors. Shadows in VHR data greatly contribute to the heterogeneity of the detected spectral signal in a given spatial domain, but they may also produce characteristic spatial patterns that can be described by techniques able to handle image structural information. For these reasons, the image structural information has shown to be useful for the description of human settlement.

We may distinguish between two basically different ways of conceptualizing image structural information: one is focused on measuring the repetition of image elements in a given spatial domain (also called image texture), whereas the other is focused on the description of single image structures (also called regions, segments, or objects) by their shape or size characteristics. The application of these two concepts on the analysis of human settlements using remotely sensed data will be discussed in Sections 3.3.2 and 3.3.3, respectively.

3.3.2 About Image Texture

Image texture, defined as a function of the spatial variation in pixel intensities (gray values), is useful in a variety of applications and has been a subject of intense study

by many researchers. In remote sensing, the notion of texture dates back to the pioneering work of Haralick et al. (1973) and Haralick (1979). Numerous different methods of formalizing the concept of "image texture" can be found in the image processing literature; they can be described as geometric, random field, fractal, and signal processing models of texture including Gabor and wavelets filters (Tuceryan and Jain, 1998).

The general interest in the exploitation of image textural information with regard to the discrimination of built-up structures (defined as "urban areas") was already demonstrated by Gong and Howarth (1990 and 1992) and recent contributions by Zhang et al. (2003) and Puissant et al. (2005), merging in a similar manner radiometric and textural information to improve the urban classification. Mynt (2003) demonstrated the use of wavelets for the study of settlement patterns using remotely sensed data.

The usual means of merging spectral and textural information in the same classification scheme assumes Gaussian distribution and/or avoids taking into consideration the possible dominance phenomena due to different data scales and statistical distribution of textural and radiometric values. This standard method of fusing textural and radiometric information in the same classification scheme was criticized by Pesaresi and Bianchin (1996). As an alternative, Pesaresi and Bianchin (1993) and Pesaresi (1994) demonstrate the effectiveness of processing data in two separate chains by exploiting in parallel the radiometric and structural information, and including a knowledge-based final integration step.

In any case, it has been demonstrated that having an input image data set with the necessary spatial resolution approaching the size of built-up structures, the use of radiometric information becomes less relevant and occasionally even adds more noise than discriminatory information. As an alternative approach, Pesaresi and Bianchin (1996) proposed to exploit only morphological and textural information, whereas Pesaresi (2000) demonstrated that textural information alone extracted from panchromatic imageries was adequate for efficiently discriminating between urban and nonurban patterns as well as between different urban patterns.

Lafarge et al. (2005) used textural features as input of a support vector machine–supervised classification procedure for detection of forest fire and urban areas using high-resolution images, whereas De Martino et al. (2004) used spectral and textural features by means of a hierarchical clustering algorithm allowing partially supervised classification. Plaza et al. (2007) presented a joint spatial/spectral classification approach for hyperspectral imagery that is shown to perform effectively in a complex urban environment. In the work of Peijun et al. (2007), urban textural recognition is done by exploiting morphological multiscale characteristics, whereas Zhong and Wang (2007) used image texture derived from multiple conditional Markov random fields model to extract urban areas from monospectral satellite data. In the work of Pesaresi et al. (2008), a simplified "built-up presence index" extracted from images using anisotropic rotation-invariant textural measures is presented and evaluated in a realistic scenario. In the discrimination of built-up patterns, the proposed index shows good accuracy and robustness against seasonal changes, multisensor, multiscene, and data degradation by wavelet-based compression and histogram stretching.

Example: Veneto Region, Italy

Figure 3.1 (left) shows part (7.5 × 24 km) of the result of the automatic extraction of built-up areas using as input a collection of Spot scenes. The test was conducted in 1995 in the frame of a consultancy for the Administration of the Regione Veneto, with the purpose of studying the status of built-up areas in the central area of the region; the derived data set was then presented in a number of international seminars (Pesaresi, 1995), and used in a number of studies at the University of Venice (Munarin and Tosi, 2001). The test was performed by classifying the data recorded by the panchromatic sensor of the Spot satellite, with a spatial resolution of 10 m, which was the maximum spatial resolution offered by satellite remote sensing technology at the time. The dark structures in the image represent built-up structures on the ground with 98% accuracy at a scale 1:25,000.

The data set shown has been chosen only arbitrarily as a historical example. It was the first satellite data set automatically interpreted using an integral texture-based approach. At any rate, the observations reported below are confirmed by several other classification exercises done in the following years in different geographic contexts

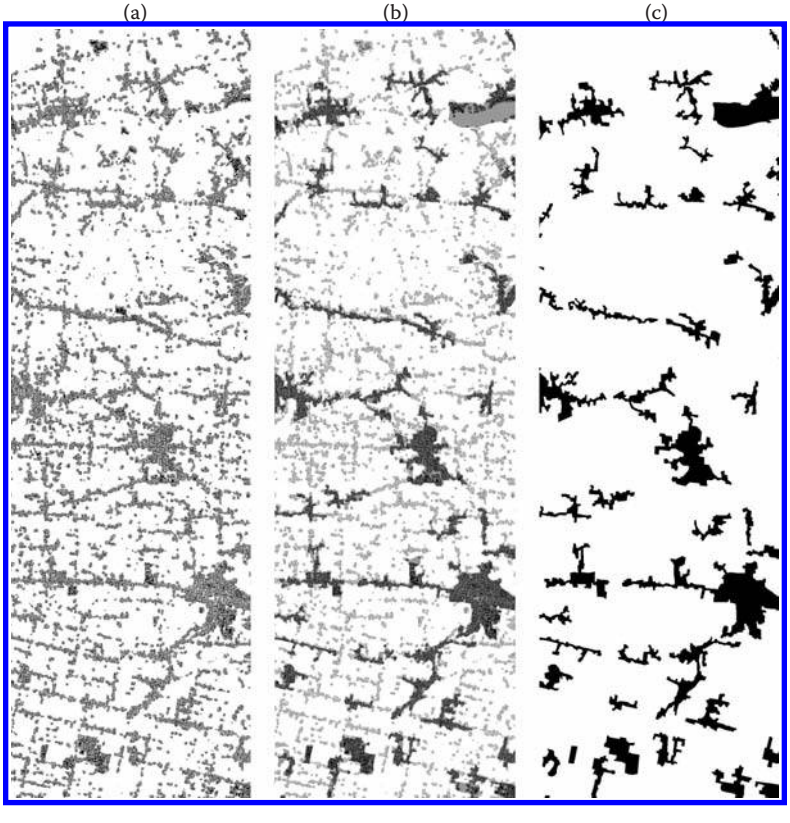

FIGURE 3.1 Veneto Region, Italy: (a) shows the result of the built-up index, an automatic extraction of settlement area from SPOT 4 imagery; (c) shows the result of the visual interpretation; and (b) shows in dark gray the built-up areas mapped by built-up index and visual interpretation and in light gray, as well as the built-up areas missed by visual interpretation.

and using various satellite sensors with similar methodologies. The methodology for extraction of built-up structures was an early version of the one presented in the work of Pesaresi et al. (2008), where more technical details can be found. The discrimination of the built-up structures was based only on image structural information extracted by calculating anisotropic rotation-invariant contrast textural measures from monospectral satellite data. Consequently, it was a clear methodological change with respect to the usual approach based on image spectral information, or trying to merge spectral and structural information in the same classification procedure.

The right panel of Figure 3.1, which shows the same portion of the territory, presents the "urban" classes derived from CORINE LC 1990, a standard product made by visual photointerpretation of satellite data; the middle panel shows a comparison between the two sources.

There are several noteworthy main differences: automatically image-extracted information is reproducing in a more objective manner scattered built-up structures and built-up structures along the road that are sometimes lost in the visually interpreted land cover representation. This occurs not (only) because of different scale of representation or presence of random errors in the visual detection workflow. In fact, not all built-up structures or "urban areas" with the same size are equally lost or retained in the visually interpreted land cover that is defined by a given scale or minimal mapping unit. Assuming the same scale, we can detect that several built-up structures are retained and several are lost with arbitrary choice. Automatically derived information can be more consistent than the visually derived one, because the machine is always producing the same output giving the same signal in input and the same processing procedure.

We can note that the inconsistencies are mainly related to the different cost curbs of the manual and automatic procedures. The visual interpretation cost grows linearly with the number of entities to be detected; consequently, it tends to generate compact and simplified representations of the geographic reality, assuming a finite time/resource available and a priority list putting bigger structures first. The cost of automatic interpretation procedure is instead indifferent to the number of entities to be detected, but only linearly relate to the surface to be analyzed.

Finally, note the dark blob in the upper right corner of the visually interpreted land cover image (Figure 3.1, left) that is instead absent in the texture-derived built-up patterns (Figure 3.1, right). This is an airport that usually belongs to the "artificial surfaces" in the LU/LC classification scheme and then was aggregated into the "urban" class represented in black. In the real world, from the physical point of view, the airport is not only a built-up structure but is also (mostly) a flat open area. The automatic texture-based recognition system is (correctly) detecting only the signal generated by the buildings belonging to the airport area but are ignoring the flat surfaces of the airfield. This is done also if these flat surfaces belong to the abstract concept of "airport" and "artificial surface." Naturally, if we are to use this LU/LC data set of reference for assessing the accuracy of the automatic recognition process, we would take into account the flat airfield area as part of the omission error of the recognition procedure.

From the point of view of image analysis, we can easily agree on the fact that the semantics involved in the notion of "built-up structure" is less abstract than the one involved in the definition of "airport." Similarly, we can say that the basic notion of built-up structure can be found as conceptually belonging to more semantically complex LU/LC classes as "urban areas," "rural villages," "farm nucleus," "isolated dwellings," and so on.

This example depicts well the inverse relationship between the level of abstraction of the classification scheme and the robustness of the automatic recognition procedure based on physical parameters (either spectral or structural) extracted from the remotely sensed data. This example is also useful in recalling the necessity of

harmonic development in the three basic areas of remote sensor technology, information extraction methodology, and conceptual tools able to handle the extracted information, say the classification scheme. All these issues will be addressed in the following paragraphs.

Example: Nairobi City, Kenya

Figure 3.2 compares the basic built-up pattern derived from texture-based automatic satellite image interpretation and the "urban" surface derived from available datasets at the global level. The example is taken from a collection of 50 cities and "urbanized regions" all around the world where the European Commission Joint Research Centre is doing the same comparative exercise focused on the definition of a globally robust methodology for detection of human settlements in remotely sensed data.* The area represented here is about 35 × 35 km, covering part of the city of Nairobi, Kenya, and the region in the north. Figure 3.2(a) shows the radiometric signal recorded by the satellite Spot Panchromatic sensor in 2006, whereas Figure 3.2(b) shows the structural information captured by the texture-derived built-up index as defined by Pesaresi et al. (2008). Note that, although spectral information discriminates mainly between vegetated and not vegetated areas, structural information discriminates mainly between built-up and not built-up areas that are evident at regional level and also with the strong degradation needed for showing the data set in the small space of the page.†

Figures 3.2(c) and 3.2(d) show the same area of Nairobi represented by two available global datasets derived from satellite data and reporting on the presence of "urban" areas on the ground. Figure 3.2c is extracted from the global land cover classification for the year 2000 (GLC2000) produced by JRC using the low-resolution VEGA2000 data set, providing a daily global image from the Vegetation sensor onboard the SPOT4 satellite. The methodology is based on a mixture of supervised and unsupervised automatic classification of the spectral information. Figure 3.2(d) is extracted from the database of "Urban Extent Mask" available from the Global Rural-Urban Mapping Project (GRUMP),‡ produced by the Centre for International Earth Science Information Network (CIESIN) of the Earth Institute at Columbia University. In this case, the potential "urban" areas are discriminated by using the radiometric information recorded by the Operational Linescan System of the U.S. Air Force Defense Meteorological Satellite Program. The inferential model used here assumes a direct relationship between the presence of stable night lights and the presence of human settlement. The "Urban Extent Mask" is then derived by merging satellite-derived urban areas and population census data. Both examples are mainly based on the processing of the radiometric information of satellite sensors. Whereas the first example (GLC2000) is derived from a homogeneous source and an automatic inferential paradigm linking signal reflectance to land cover, the second one (GRUMP) is derived by a more abstract inferential model requiring the signal recorded by the sensor together with other external data sources as the census data. Of course, the probability of inconsistency in the derived information layer is directly proportional to the amount of different sources

* The "Global observatory of human settlement" is part of the institutional activity research of the EC JRC Institute for Protection and Security of the Citizen Information Support for Effective and Rapid External Action 2008 in collaboration with United Nations Habitat and Word Bank.

† Note, for example, the confusion between "urban" and bare soil and desert areas in the lower corners of the sample.

‡ The GRUMP datasets may be accessed through National Aeronautics and Space Administration's Socioeconomic Data and Applications Center, operated by CIESIN, at http://beta.sedac.ciesin.columbia.edu/gpw/.

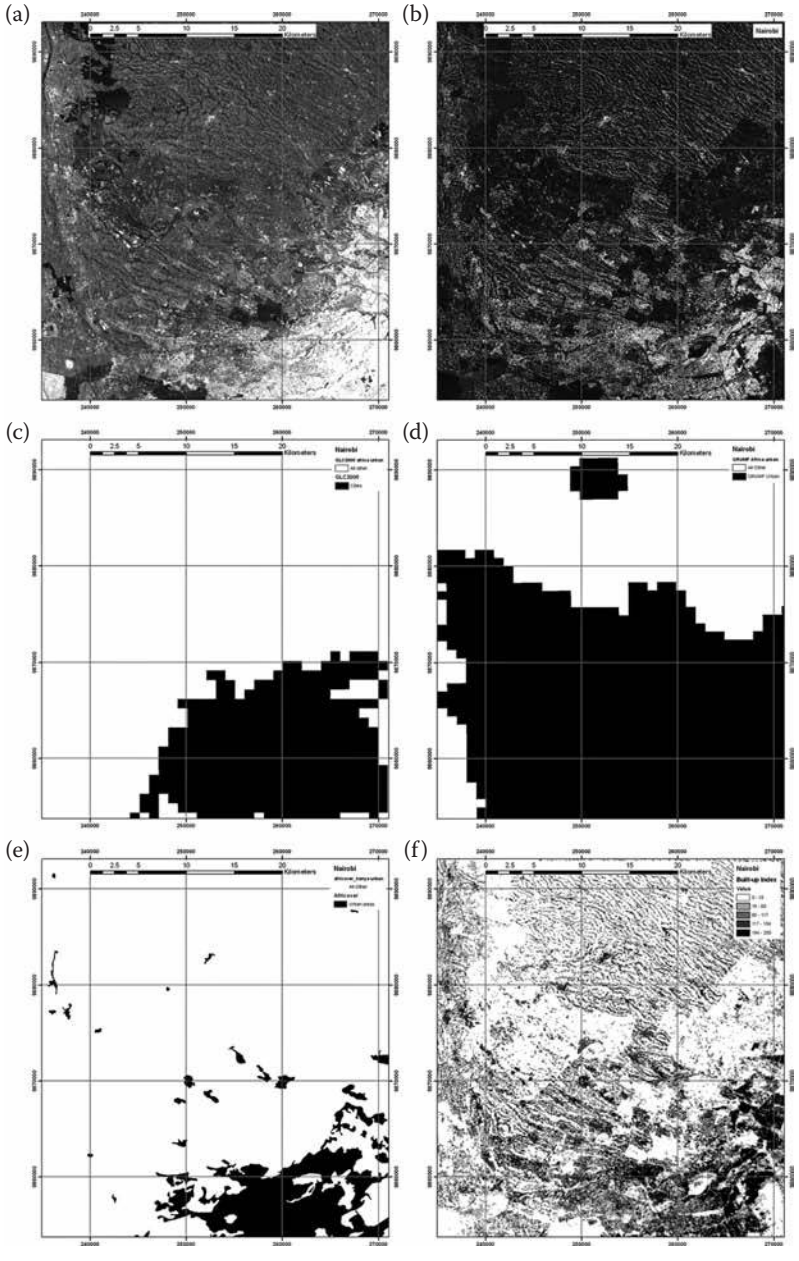

FIGURE 3.2 Nairobi city and the surrounding region of Kenya. Comparison between settlements classified using automatic methodology and those available in satellite-derived information layers at regional and global scales. From top left to bottom right: (a) original data recorded by the panchromatic sensor of SPOT satellite (© SPOT IMAGE); (b) built-up index extracted using image textural information; (c) "urban" class extracted from the GLC2000 land cover; (d) "urban" area in the GRUMP database; (e) "urban areas" class of the AFRICOVER land use/land cover; (f) spatial generalization of the built-up index to 100 meters grid.

required as input in the inferential system, other than the amount of free parameters controlling the recognition paradigm.

Figure 3.2(e) shows the same Nairobi area but as represented by the "urban areas" class extracted from the AFRICOVER land cover database produced by visual photo-interpretation. Figure 3.2(f) represents the same area with a spatial generalization of the texture-derived built-up presence index to 100 m of grid cell. The spatial generalization is done by a simple local average statistic of textural information extracted at the original sensor resolution.

If we compare Figures 3.2(c), 3.2(d), and 3.2(e), we can note how the human-interpreted "urban" land cover (Figure 3.2(e)) can be more spatially precise than the automatically generated satellite land cover. Sharper edges are observable between the "urban" and "not urban" areas, and some small towns are also visible whereas they are omitted in the automatic-generated satellite land cover. In fact, these different representations are derived from satellite datasets having different spatial resolution — they range from hundreds of meters or kilometers of the satellite data used for GLC2000 and GRUMP datasets, respectively, to the 30- or 20-m resolution of the satellite data used for the AFRICOVER data set. However, no regional or global LU/LC derived from 30- or 20-m resolution satellite data with automated methodology and containing reliable information on the human settlement theme was available at the time. This is also attributed to the fact that the standard operational methodology for automatic extraction of information from satellite data, being based only on analysis of spectral information, shows sufficient reliability only when using low spatial resolution image data.

Furthermore, as in the previous example of CORINE LC (Figure 3.1), if we compare the human-interpreted "urban" land cover product (Figure 3.2(e)) and the machine-generated representation of the presence of built-up structures (Figure 3.2(f)), we can observe the advantage of the latter, from the viewpoints of completeness and consistency of the information provided. For example, as a result of the texture-based automatic satellite data analysis, we can realize that a large part of the territory on the north of Nairobi City is actually "covered" by human settlements that were mostly ignored by the available sources derived from satellite data or reported with arbitrary amendments.

Finally, it is important to note that the information about the presence of built-up structures is easily scalable at different levels of spatial generalization. Figure 3.2(e) is now reporting the density of built-up structures detected at the original sensor resolution (2.5 m) in grid cells of 100 m. Of course, the calculation of the same at 1 km or any other cell size is straightforward. This, however, is not true independently from the adopted classification scheme. It can be demonstrated that a more complex or abstract land use or land cover classification scheme would be much more rigid and less easy to scale to different generalization levels. In fact, there is an inverse relation between the level of abstraction of the classification scheme and its scalability to different spatial generalization levels starting from the generalization level used in the production process. This relation will be discussed in the following paragraphs.

3.3.3 About Single Image Structure

With some simplification, we can define an image structure (also called region, segment, or object) as any collection of adjacent (or connected) image pixels sharing a given explicit characteristic. The adjacency (or connectivity) constraint means that in the basic notion of image structure, we cannot avoid to take into account the spatial domain of the image, including the definition of a distance metric.

In computer vision, and then in remote sensing, we usually refer to the process of "image segmentation" as the process of extraction of these image structures from the raw digital image data. Through the segmentation step, it is possible to formalize structural information as a collection of individual image structures (regions) with specific characteristics that can be measured as, for example, statistical distribution of pixel values belonging to the same image structure (region), or area, shape, perimeter of the single image structure (region).

The literature about image segmentation is very important; a recent survey made by Zhang et al. (2008) may give an idea of the available tools and the difficulty of their objective and comparative evaluation. In this chapter, we focus on one specific family of techniques allowing image segmentation, and in particular we will concentrate on the so-called image "mathematical morphology." Mathematical morphology is the name of a collection of operators based on set theory and defined on an abstract structure known as an infinite lattice. These operators were first systematically examined by Matheron and Serra in the 1960s and are an extension of Minkowski's set theory (Serra 1982, 1986). Morphological operators include erosion, dilation, opening, closing, rank filters (including median filters), residual (top hat) transforms, and other derived transforms. These operations can be defined on binary or gray-scale images in any number of dimensions (multispectral data). They can also be defined with Euclidean (isotropic) or non-Euclidean (geodesic) distance metrics (Soille, 2004). The geodesic metric may allow us to introduce the so-called "by reconstruction" morphological operators including the area-based connected operators that recently have been proposed in applications involving remotely sensed data processing (Soille and Pesaresi, 2002).

According to Meyer and Beucher (1990), the standard approach to image segmentation using mathematical morphology is based on the so-called watershed line detection. Watershed segmentation was introduced in image analysis by Beucher and Lantuéjoul (1979) and defined mathematically for the first time by both Meyer (1993) and Najman and Schmitt (1993). Watershed extraction generally means the thinning of a gradient image with a homotopic transformation. It also involves the detection of basins as regions and crest lines as boundaries for these regions. For these reasons, a watershed approach generally leads to finding the structures in an image based on an edge detection strategy.

An alternative to the classical approach for morphological segmentation was introduced by Pesaresi and Benediktsson (2001) and it is based in the so-called morphological profile (MP) and its discrete derivative (DMP). The MP is made by multiscale simplification of the original image using geodesic or "by reconstruction" opening and closing morphological filtering with increasing SE size. The DMP then records for each point of the image the amount of contrast signal that is lost at each simplification (scale) step by opening and closing morphological transforms of increasing size. The idea behind the method is that by looking at the maxima of the multiscale DMP, we can understand for which scale (size) and type of contrast (positive or negative corresponding to opening or closing, respectively) the image structure has been canceled by the morphological filter. Consequently, this information is recorded for each point of the image as per-point specific "morphological characteristic" and the image structures are successively defined as connected components of image points (pixels) sharing the same morphological characteristics.

The advantages of this alternative method of performing image morphological segmentation can be summarized as follows: (1) possibility to handle textured areas, with salient segments of 1–2 pixels impossible to process with edge-based approach, or usually leading to severe oversegmentation effects; (2) fully multiscale approach avoiding the necessity to define one scale parameter, but instead optimizing the image structure recognition inside a given scale range; (3) possibility to handle, in a mathematically consistent manner, a spatial hierarchy of image structures without the necessity of defining their crisp boundaries. The drawbacks are instead mainly related to the more relevant computation efforts that we need for calculation of the multiscale DMP with respect to the traditional watershed segmentation with one scale parameter.

With respect to other image multiscale decomposition techniques such as Laplacian pyramids, Gabor filters, wavelets, and the like, the main advantage of the multiscale DMP is that it allows multiscale image description without losing detail of the edges of the structures. Because of the mathematical proprieties of the morphological operators "by reconstruction," the shape and the maximum detail or resolution of the image structure borders are preserved at all the simplification scales, avoiding the blurring or shape noise effects of the other methods.

In recent years, the DMP concept has been successfully applied in a wide range of computer vision problems; in remote sensing of human settlements, the main applications are related to building detection and change detection in built-up structures (a specific review in the next paragraph) and road detection (Zhu et al., 2005) using latest-generation satellite data.

3.3.3.1 Building Recognition

If we subdivide the elements of the built-up patterns visible in VHR satellite data into three classes as (1) built-up structures, (2) road or other movement infrastructures, and (3) open spaces, it is intuitive to understand that the buildings always belong to the key information needed for settlement analysis.

The automatic detection of buildings using single date optical image data from aerial surveys has been extensively explored by Irvin and McKeown (1989), Shufelt and McKeown (1993), Jaynes et al. (1994), Lin et al. (1995), Shufelt (1999), and Haverkamp (2004). Most approaches are based on a syntactic edge-driven approach, which consists of line detection, parallelogram structure hypotheses extraction, and building polygon verification using knowledge such as geometric structure, shadow, and other information. Methods using single date data are hardly applicable to the available satellite data for two main reasons: (1) they are designed for data input as aerial photograph, with the exception of Haverkamp (2004), with a spatial detail of about 0.2 ms, which is a much finer resolution than that available from current VHR satellite data (1.0 or 0.6 m); and (2) they are built on simple assumptions that fail in many relevant cases. For example, one important assumption considers the building as an isolated rectangular region clearly identifiable on the image. This assumption — valid in most of North America — is instead violated by many relevant settlement patterns including formal cities (e.g., medieval cities both in Europe and North Africa) and informal settlements (slums in Asia, Africa, South America) that are typically an assemblage of adjacent buildings. Similarly, informal

settlements arising in the poorest residential areas of rapidly expanding megacities appear more as "snakes" of continuous built-up structures along roads or cluster around courtyards.

Attempts to overcome these problems can be related to multisensor image fusion techniques (Gamba et al., 2005), or if we miss multisensor or ancillary data input by creating multiscale representation of the image structures using the so-called derivative of the MP or DMP (Pesaresi and Benediktsson, 2001; Benediktsson et al., 2003). In the latter case, the recognition system is based in less rigid geometrical constraints than in the syntactic edge-driven paradigm, and it has been tested with some success using spatial resolution currently available with satellite imagery. The best results in building detection are obtained when optical stereo images are available as well as elevation data (Oriot et al., 1998; Hanson et al., 1997). Unfortunately, image stereo pairs are quite expensive and rarely available in real applicative scenarios.

Pesaresi and Kanellopoulos (1999) first introduced the use of DMP morphologically segmented image for classification using a segment-based or object-based strategy. The approach used a classifier using neural network architecture with different options as input including spectral, morphological, and shape-derived features. The authors showed the superior performance of morphological features. In turn, Benediktsson et al. (2003) directly used the DMP as input of a neural network classifier, skipping the image segmentation step, and demonstrating the relevance of this approach in automatic recognition of an urban scene using Ikonos panchromatic data. Chanussot et al. (2006) used a fuzzy interpretation of the DMP extracted from Ikonos panchromatic images. Plaza et al. (2004) applied morphological transformations on hyperspectral datasets to discriminate between subtle different ground covers in the classification between agricultural and urban areas.

Jin and Davis (2005) demonstrated that structural (including DMP), contextual, and spectral image information can be exploited for automatic building recognition using VHR satellite. By direct comparison, Pagot and Pesaresi (2008) demonstrated that the multitemporal DMP extracted from satellite data was superior to the multispectral data for discrimination of changes on built-up structures. The system was based on supervised classification using a neural network approach.

Example: Kiberia Slum

The very high spatial resolution (VHR) satellite imagery provides information on built-up elements that include buildings, roads, and the open spaces. Figure 3.3 shows an example of automatic analysis of settlement built-up components using automatic image understanding approach.

In the example, we show an area of about 250 × 250 m in the Kibera slum of Nairobi. The data were recorded by the QuickBird satellite using the panchromatic sensor with a resolution of 0.6 m (Figure 3.3(a)). Figure 3.3(b) shows a feature belonging to one layer of the so-called DMP. It is easy to note the correlation between the image feature extracted and the phenomenon at the origin that are the shadows cast by built-up structures. The idea behind the multicriteria approach is that simple image features such as this one can contribute to the automatic understanding of the presence of the entity "building" in the VHR remotely sensed data.

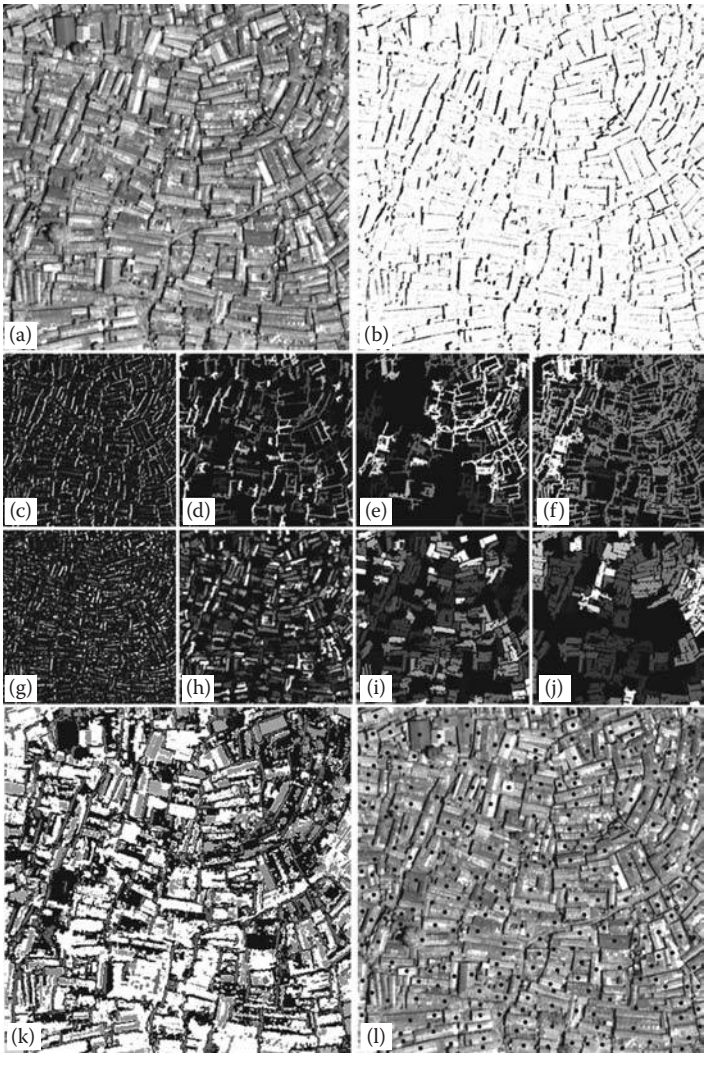

FIGURE 3.3 Kibera settlement in Nairobi, Kenya. Extraction of information related the built-up structures using the mathematical morphology approach: (a) the QuickBird (© DIGITAL GLOBE) satellite at a 0.6m spatial resolution covering an area of 250 × 250 meters; (b) the built-up "shadows" from residual of closing by reconstruction; from (c) to (f) closing derivatives of the morphological profile (DMP) for increasing scale; from (g) to (j) opening derivatives of the morphological profile for increasing scale; (k) segmentation of the image by the "morphological characteristic" or maximum of the DMP; (l) example of automatic enumeration of built-up structures (centroid as black dot in the image) using morphological segmentation.

Figures 3.3(c)–(j) represent four DMP levels extracted using four flat SEs with increasing size. Image decomposition by the DMP profile is able to discriminate different structures present in the image according to the size (increasing from left to right) and to the type of contrast with respect to the adjacent image structures. Figures 3.3(c)–(f) report on

the contrast signal generated by structures darker than the adjacent portion (concavity of the gray level function), whereas Figure 3.3(g)–(j) report on the contrast signal generated by structures brighter than the adjacent (convexity of the gray level function).

The authors feel that the DMP's most important property is its ability to capture image structural information without the necessity of passing through an image segmentation step. In fact, DMP can handle a hierarchy of multiscale image structures having fuzzy spatial definition. In this manner, it can reduce the problem of border error propagation between the scales. Consequently, it improves the robustness of the recognition system. Figure 3.3(k) shows an example of image segmentation based on the morphological characteristics recorded by the multiscale DMP, whereas Figure 3.3l shows the output of an algorithm used for automatic enumeration of the built-up structures in complex settlement patterns such as the one observed in slum areas. The algorithm is automatically inferring the optimal spatial filter to apply to each point of the input image on the basis of the signal recorded in the multiscale DMP decomposition.

Example: Multiscale Image Structures

Figure 3.4 compares radiometric and morphological structural information for the characterization of settlement patterns. Three settlement patterns for Nairobi are taken as examples: Kibera slum (first row), business city center (second row), and a structured residential area (third row). The first column shows the signal as detected by the satellite sensor (QuickBird sensor, panchromatic mode, 0.6 m spatial resolution). The second column shows the radiometric enhancement through histogram stretching of a robust feature ("shadows"). The stretching was done on low radiometric values (linear histogram stretching from 10% to 30% of saturation). The third column shows the size spectrum obtained by decomposition of the "shadows" by closing DMP based on gray-scale morphological transformation with increasing SE. The fourth column shows the anisotropic analysis of the "shadows." This is done by calculating the density of gradient lines for different directions, using morphological opening transforms with a linear rotating SE.

The histogram on the bottom of the figure shows the radiometric frequency histograms for the three settlement patterns. Note that the three subsamples are clearly overlapping: from the point of view of the recorded radiometric signal they are hardly separable. Note also the radiometric cluster appearing as a clear lowest maximum (mode) in the frequency histogram in two of the subsamples. This is clearly associated to the shadowed areas that are some of the most radiometrically evident image structures detectable using VHR data input.

Shadows are related to the volume and height of the built-up structures. Consequently, the size spectrum of the "shadows" detected by the DMP can discriminate the settlement patterns; for example, the evident maxima on the slum shadow DMP are placed at about 3 m in size, whereas the residential area shows an evident maximum at about 8 m. The DMP also captures the heterogeneity of the settlement pattern; this can be appreciated by comparing DMP extracted from the second pattern and the other two. The first and third patterns have only one evident maximum corresponding to built-up structures having homogenous size. The DMP extracted from the second pattern is instead showing heterogeneity of built-up structures translated on the several peaks as detected in the DMP.

Finally, the anisotropic analysis may provide an insight into the building process of the settlement. Usually, more ordered patterns are the result of an urban plan and of an authority that implements it. Spontaneous or "informal" settlement patterns are

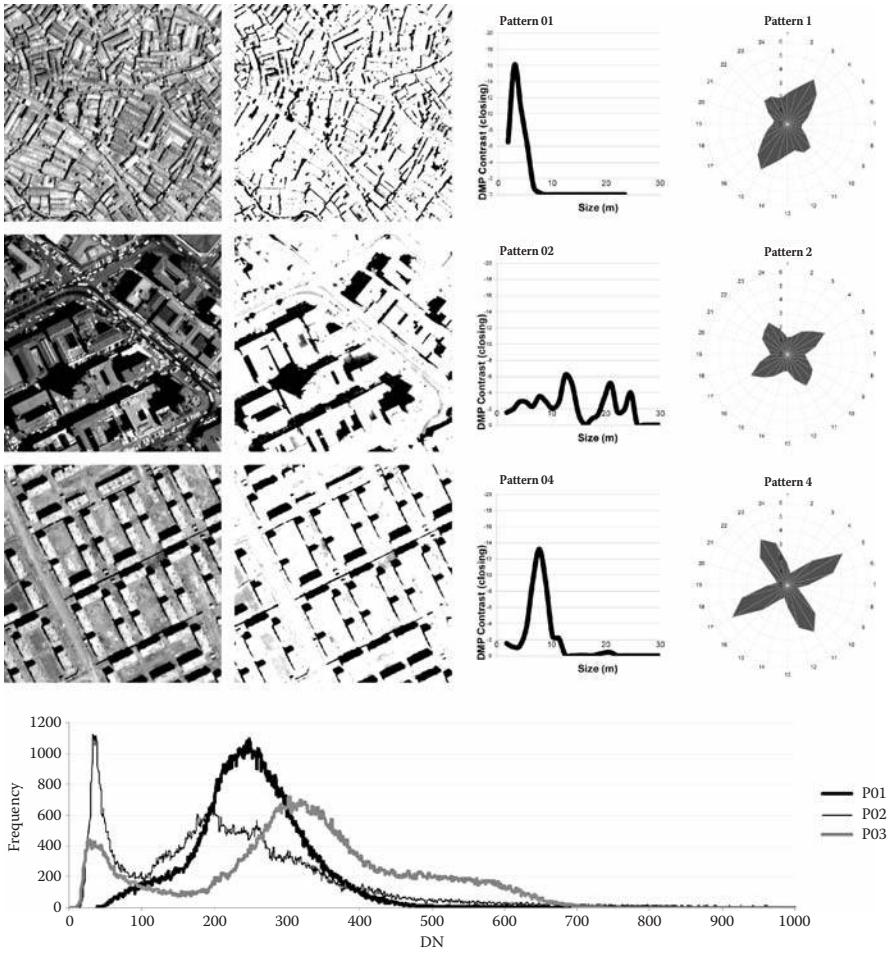

FIGURE 3.4 The figure shows three settlement patterns (rows 1 to 3) over the city of Nairobi as seen from Quickbird imagery (© DigitalGlobe®). Column 1 shows the original images, column 2 the radiometrically enhanced images, column 3 the frequency of image structures at different scales as detected by the DMP based on gray scale morphological transformation, and column 4 the anisotropic analysis of shadows. The bottom histogram shows the radiometric frequencies related to the original images.

more chaotic in nature. The "orderliness" of built-up patterns can thus be measured through the analysis of maxima and the minima DMP measurements as shown in the fourth column.

Again, it is worth noting that the above-mentioned morphological measurements are carried out directly on gray-scale input images. Eventual application to multispectral imageries can be also implemented. The traditional step of image segmentation needed for recognition of crisp mutually exclusive image regions or "objects" is not needed in the proposed approach. According to our experience, this dramatically increases the robustness of the recognition system.

3.4 STRUCTURING THE INFORMATION ON SETTLEMENTS

3.4.1 Standard LU/LC Paradigm

The most widely used conceptual paradigm in satellite remote sensing data analysis is to convert spectral information contained in the image in "land cover" classes. It was the pioneering work of Anderson (1971, 1972) that introduced a classification scheme for medium resolution satellite imagery. A classification based on Landsat TM has been conducted for the United States (Vogelman et al., 1998) as well as for Europe (CORINE, 1994) and Africa (Aficover). Similar land cover classification schemes have been likewise developed for use of coarser resolution satellite imagery to be used in generating global land cover products (IGBP 1992, GLC2000).

Land cover mapping assumes that the surface of the Earth can be grouped into measurable classes of land cover based on the physical properties of the Earth's surface (Comber et al., 2005). Land cover classes include forest, grassland, bare land, water bodies, to mention the most important.

Land cover is often used interchangeably with "land use" — the use of the land — creating some confusion and methodological problems (Fisher et al., 2005) that may have originated from the ambiguity of the definition of land use and land cover proposed by Anderson et al. (1976). Converting remote sensing–derived land cover information — those produced by remote sensing specialists — into land use information needed by planners and decision makers has dominated the methodological debate of remote sensing practitioners.

The ideal geographic entity to be mapped by the standard LU/LC paradigm should be compliant with the following characteristics:

1. It is a homogenous surface (reflecting similar spectral information inside the same surface).
2. It has given geometrical characteristics such as: (a) a size considerably greater than the image pixel size (the satellite image spatial resolution) and (b) a simple shape reducing the number of border pixels with respect to the number of pixels belonging to the entity itself.
3. Logically, it is mutually exclusive with respect to all the other classes.
4. It has a self-evident mode of use that can be deterministically deducted from its physical characteristics.

A typical example of a good entity to be mapped in this paradigm is a modern agricultural field such as corn or soya bean. From the physical point of view, it is typically flat (consequently illuminated in the same way), large with respect to pixel size, has a simple shape, and often reflects homogeneous spectral information. It is mutually exclusive with respect to other classes (if it is corn, it cannot be soya bean) and the deterministic deduction of the land use from the surface type or land cover is working with reasonable results. The physical entity detected as a surface of corn or soya bean is mostly likely "cultivated as" corn or soya bean. It would be difficult or absurd to imagine a different use for the same physical entity (e.g., recreational field for soya bean).

3.4.1.1 Internal Consistency Aspects

Unfortunately, mapping of settlements is not easily accommodated within the LU/LC standard paradigm. All the above-mentioned characteristics needed for effective mapping of geographic entities inside the LU/LC paradigm are violated in different degrees in the case of geographic entities related to human settlements.

As noted earlier in this paper, the specificity of the settlement theme from the physical characteristics viewpoint can be summarized as internal spatial heterogeneity and mimetism with the surrounding areas. In fact, settlements are composed of a large number of physical elements that include vegetation, concrete, stone clay tiles from roofs or straw, which may also be present in other cover classes not belonging to the settlement as natural or agricultural surfaces. Furthermore, typically these different surfaces may have a spatial frequency of change of a few meters. For these reasons, settlements usually violate characteristics (1) and (2) (see list above) relating to the standard LU/LC paradigm. Assuming built-up elements having a size on the order of 10 m, all traditional satellite data up to a resolution of 10 m are, by definition, reporting only mixed-pixel information on surfaces covered by settlement. Because of the heterogeneity of settlement materials, including also spectral variability induced by shadows cast by buildings, this mixture cannot be modeled as a simple linear mix between two surfaces.

Assuming a geographic entity with a size of 500 × 500 m, which is, for example, the minimal mapping unit of 25 ha in the CORINE LC product, the percentage of mixed surface (pixels) over the total is at least of 24% with 30 m of sensor spatial resolution. Assuming a typical minimal built-up element in a settlement, having a size of 10 × 10 m, we need at least 0.5 m resolution in order to have a comparable percentage of mixed pixels (at least 20% in this case). Of course, in reality building's roofs are usually not homogenous because different side slopes are differently illuminated, making an increased number of internal mixed pixels. With 2.4 m resolution, which is the maximum rate possible at the time with a multispectral sensor (the QuickBird satellite), more than 90% of the pixels covering the built-up structure are mixed-border pixels between unknown different materials differently illuminated and partially shadowed.

These simple numbers explain from the physical viewpoint why the standard LU/LC paradigm may be hardly applicable in mapping settlements using satellite remotely sensed data.

Other considerations, however, may make the effort even more difficult. Standard LU/LC classes are mutually exclusive, whereas in general human settlements show stratification of different uses and functions during different times, but also in the same time and place. Although some settlement patterns following a functionalist design segregate different functions in different areas (e.g., residential from commercial areas), many other contemporary settlement patterns show important levels of mixing and stratification of functions in the same place. These patterns may be inherited from earlier historical periods (e.g., medieval centers in many cities of Europe and North Africa), but also show modalities of evolution that are typical of the present.

In developed countries, this is also evident — for example, "commercial stripes" where commercial and residential functions are mixed, or some specialized productive districts where we mix residential and productive surfaces, or scattered rural-

urban areas where scattered agricultural fields are mixed together with residential dwellings. Moreover, because of the increased mechanization of agricultural activities, "rural areas" in several developed countries are mostly inhabited by people engaged in activities not related to agricultural production; in this manner, the typical rural-urban dichotomy that is assumed as self-evident by the LU/LC paradigm is losing explanatory capacity. "Rural areas" may in reality appear inhabited by a population engaged in "urban" activities and/or leading globalized "urban" styles of life.

In developing countries, the mixing of functions is the rule in many important situations. For example, in several slum or informal settlement areas in Asia, it is the rule to have residential, artisanal productive, and commercial functions in the same place, and in numerous cities in Africa we may observe large areas where subsistence agricultural activity is mixed with residential and industrial production and residential function, being part of the same integrated economic model.

These examples show that "mutual exclusivity" assumed by the standard LU/LC paradigm is not universally applicable (it works well in cases where the description of settlements is without risk of excessive reductionism). These exceptions mostly apply in western countries, where functional spatial segregation has been historically applied as rationalist or functionalist planning design strategy. In several other relevant cases at the global level, the implicit risk of applying the LU/LC paradigm is to lose some of the most relevant information needed in the settlement pattern description.

Finally, it should also be mentioned that the deterministic model linking physical appearance, or land cover, with land use has insufficient reliability in describing human settlement patterns. To illustrate our point, we can cite as an example that a rectangular element detected in the satellite image, showing the signal characteristic of a concrete material, can be linked to a variety of different functions: it could be a parking lot, the roof of a swimming pool, the roof of a shopping mall, a museum, an industrial installation, or an apartment block. This is only an example, but anybody who has had an experience in analyzing settlements using remotely sensed image data can agree that often only a direct survey or the collection of additional information coming from external sources can contribute to fill the gap between land cover and land use in the built-up environment. The quantity of external information needed is inversely proportional to the reliability of the deterministic model linking the image-detected land cover to the land use classification.

3.4.1.2 External Adequacy Aspects

The arguments mentioned above show some of the difficulties we have had to face in applying the standard LU/LC paradigm to the description of settlements. It may be noted that these drawbacks can be regarded as both physical (and then operational) and logical inconsistencies between the information to be detected in the image data and the form of representation we use for handling the information itself. Thus, we can say that they are inconsistencies "internal" to the settlement theme and its description.

But there is also another aspect to be considered that we could define as more "external"; this aspect is related to the use of the information extracted from the image data. To explain this concept, we discuss about the suitability or adequacy of

the information structured inside the LU/LC paradigm to be used by decision makers interested in analysis of settlements.

As noted above, part of the specificity of the settlement theme stems from the fact that the information on settlements is immersed inside a complex context of use. The application field is made complex by multiple stratifications of interests and functions that produce a remarkable multiplicity of viewpoints, equally valid but not coincident, of the settlement "reality."

Let us take a very basic LU/LC notion in which "urban area" is contrasted to "agricultural area," "rural area," or "natural area." What is the exact definition of "urban area"? This, of course, is a rhetorical question because many alternative definitions may be found — based on a given spatial density of physical structures as buildings and roads, or density of functions (typically, services and industry), or population density, or market labor specificity, or even the presence of specific cultural heritage or religious sites, or any other arbitrary definition from a traditional perspective. Finally, the definition can even be based on a given specific mix of the above criteria. All these criteria, of course, also involve the application of one or more thresholds in order to define what "urban area" is and what it is not.

It is important to understand that all definitions involving criteria and thresholds may have a specific niche of validity, referring to a specific legitimate ambit of activity of a specific social actor or decision maker. Consequently, the question "What is the correct (or true, valid for all the applications) definition of urban area?" is most probably a wrong one to ask, because it is not solvable and will not likely lead to a useful solution.

It is also worth noting that because of the logical structure of the standard LU/LC classification scheme, the moment we reduce the specific constellation of criteria and thresholds to a given LU/LC class, we lose the primary information. Consequently, in case it is needed to define the same class with other criteria or even slightly different thresholds, this becomes impossible because this information is no longer found in the classification scheme. We can describe this situation as the untranslatability of any given standard LU/LC classification scheme into different semantic user requirements.

The intrinsic complexity of the application domain requires information that is scalable and adaptable to a wide range of possible uses and definitions, different but equally valid, whereas the standard classification scheme requires a unanimous definition of abstract classes that are, by definition, static and untranslatable to other semantic user requirements.

The above situation easily leads to the rapid obsolescence of LU/LC databases and to the proliferation of slightly different but not reducible LU/LC databases over the same areas. This is because the same user may evolve in the detailed definition of the criteria and thresholds. This is also because slightly different users cannot exploit the information contained in the same LU/LC databases since it involves abstract definitions and assumptions that are rigidly defined and usually do not exactly match with their specific needs.

This entire situation can be summarized by establishing an inverse relation between the level of abstraction of any given classification scheme and its adaptability (robustness) to a complex application domain. This is because the more abstract the classification scheme is, the more numerous are the criteria and thresholds

needed for a complete definition, and consequently the more difficult it is to obtain a complete agreement between the different users for all of them. From this point of view, we can say that the level of abstraction in the classification scheme can be directly linked to its fragility.

3.4.2 Modular Abstraction

One important point in our argumentation is that in the case of complex environment, a simple strategy is often the best one. As we have noted earlier, the specificity of the settlement theme and, in particular, the physical characteristics of the built-up environment and the complexity of the application field, make it difficult to recognize and represent this information using traditional conceptual tools.

Let us consider the notion of "built-up structure" that can be defined, for example, as a physical structure with walls and roof, having a minimal size expressed in height and plant surface (e.g., at least one floor or 3 m height, 5 × 5 m of surface in plant), and other similar characteristics. The "built-up pattern" can be consequently defined as a specific composition of elements (buildings, roads, open spaces) measured in a local domain (area) having, for example, a minimal number of built-up structures with a minimal distance in between.

Also, if these notions contain a certain level of abstraction and if alternative definitions can be found,* it is interesting to note that this notion implicates fewer criteria and thresholds, and therefore can be described as semantically simpler or less abstract than the one related to "urban area" discussed in the preceding section (3.4.1.2). Less abstraction means a greater number of slightly different users who may agree on the meaning of the information, and consequently, an increased robustness of the classification scheme and possibility of sharing the related information.

Given the direct relation between fragility of the classification scheme and its abstraction, one way of improving the robustness of the classification scheme could be to revise the standard LU/LC paradigm in a way that more flexibility can be obtained. In particular, we can imagine a classification scheme that does not directly link the uninterpreted image data to the final land use classes, but instead does the same more gradually, by intermediate steps of increasing abstraction of the semantic categories involved.

For example, we can establish a classification scheme sliced in three levels with increasing semantic abstraction: basic or <level 1>, where we distinguish only between built-up and not built-up structures or patterns; intermediate or <level 2>, where we describe the built-up structures or patterns using spectral or spatial (structural) information extracted from imageries; and advanced or <level 3>, where we distinguish between the different modes of use of built-up structures and patterns.

Thus, for example, when a built-up pattern is recognized at <level 1> against a not built-up background, then the compactness, density, and average size of built-up structures is measured at <level 2> together with the presence of vegetated surfaces;

* For example, different constraints on the definition of durable materials for walls and roofs may exclude some slum areas and refugee camps from the "settlement notion."

then at <level 3> these measurements are associated to a specific class of built-up patterns. In other words, at <level 1> we detect the built-up pattern, at <level 2> we describe it for example as a "compact pattern of small buildings with no vegetation," and at <level 3> we associate this to the category of "slum," taking into consideration that we are in a given geographic context of Central Africa. Similar considerations, but at another scale, can be shown relating to the classification of single built-up structures.

In contrast to the standard LU/LC paradigm, in this case we do not try to pass directly from <level 0> of the not-interpreted image data to <level 3> of the "slum" label. As an alternative, we allow the user to choose the right level of abstraction and generality of the classification scheme.

The proposed abstraction modularity of the classification scheme may allow us to understand better the role of automatic recognition procedures and to optimize their tuning. By increasing the semantic level, we may observe a trade-off between automatic and manual recognition capabilities. Although automatic image recognition procedures may play a relevant role with basic semantics such as the one at <level 1>, at <level 2> human experts have to define the set of relevant image measurements that need to be taken into account, and the advanced semantics of <level 3> can only be addressed on a case-to-case basis by human interpreters taking into account a priori knowledge that is site- and application-specific.

The proposed abstraction modularity has an effect on the robustness of the classification scheme and the possibility of sharing information across specific applications and geographic sites. Whereas <level 1> is the most adaptable, <level 2> is partially sharable because eventually it lacks some measurements not included in the proposed set, and <level 3> is only sharable inside the same user requirements and semantics. Often, <level 3> is also site-dependent; for example, the label "slum" or "medieval city center" can be deducted from the same set of measurements if we are dealing with Central Africa or in Europe, respectively. Similarly, there is a relation between abstraction level and possibility of generalizing the information extracted at different scales.

Finally, we can expect that a classification scheme allowing abstraction modularity will be more robust against slight changes in user semantics. Instead of a total collapse in the case of mismatch at the high-level semantics as what happens with the LU/LC standard paradigm, it may accommodate different degrees of mismatching for different abstraction levels, thereby remaining stable at even lower abstraction levels.

3.4.3 Multicriteria Approach, Logics

As shown in earlier sections, structural image information (texture, morphology) is important for the discrimination of different settlement patterns and for the discrimination of settlement components (buildings, roads, open spaces); often, structural information is the primary criterion for a robust discrimination, and is sometimes more important than radiometric criteria.

Of course, structural image information alone cannot solve all the recognition and analysis cases. For example, some areas covered by scattered trees may generate

a texture signal similar to the one generated by built-up structures, if they have similar spatial patterns (average distance and size of structures). Similar considerations may be found concerning areas that contain isolated small rocks scattered with a contrasted background such as vegetation background. In such cases, in order to improve the automatic recognition quality, the merging of spectral and structural information could be necessary.

In general, it is a very rare and fortunate occurrence to find only one criterion extracted from the image data that is able to solve the discrimination problem. This is often solved in a robust manner only by using a multicriteria approach taking into consideration a variety of aspects of the same target.

Moreover, it is very rare for operators to find a stable hard threshold in the decisional space made by the criteria we use for discriminating different targets in the image. Fuzzy logic applied to the multicriteria approach often offers a more stable and modular solution than more complicated analytical approaches. The approach chosen here for the automatic recognition of built-up structures can be defined within a multicriteria methodology as that reported by Eastman et al. (1995), with the adoption of fuzzy logic for the formalization of criteria as described by Yaochu (2003) and Amo et al. (2004). The reason behind the choice is linked to the assumption that a complex problem such as the characterization of built-up structures cannot be solved satisfactorily if addressed by using a too reductive approach, taking into account just one aspect of the problem description and formalization such as spectral, structural, or edge-syntactic chains. The proposed vision is that the complex problems of recognition can be solved with a sufficient degree of robustness and abstraction only if addressed by a multiplicity of viewpoints (Brans, 2002), and the adoption of a fuzzy logic approach also in the sense of improving the link between the verbal description of the recognition paradigm and their formalization, as a tool supporting the modularity and robustness of the overall system.

Examples of the application of the multicriteria approach in remote sensing applications can be found in order to improve the accuracy of multisource forest inventory (Halme and Tomppo, 2001) or within an integrated methodology supporting environmental risk assessment (Chen et al., 2001). Pesaresi et al. (2007) used a fuzzy multicriteria approach for the rapid damage assessment of built-up structures using VHR satellite data. The criteria implemented in the inferential model included textural, morphological, and spectral information. Pesaresi and Pagot (2007) used multitemporal DMP for the study of post-conflict reconstruction in African settlements, using two VHR satellite images taken just after the conflict and a few years later. This approach allowed them to discriminate and to automatically enumerate built-up structures that were destroyed and those that were rebuilt. The discrimination was made possible through the establishment of a knowledge-based system formalized in a fuzzy multicriteria frame. Pesaresi and Pagot (2008) demonstrated the superiority of soft spatial generalization of the image criteria compared to the standard object-based image recognition strategy assuming crisp mutually exclusive image regions.

Finally, in this context, we think it interesting to mention that a recent research area is studying the formal relations between the description of the image structural information via mathematical morphology (MM) and the formalization of

inferential systems based on nondichotomous logic. Bloch (2002) introduced the use of MM for quantitative, semiquantitative, and symbolic setting of spatial relationships between image structures, and later proposed the use of MM for the formalization of belief functions with application to image fusion under imprecision (Bloch, 2008). Hudelot et al. (2008) proposed a fuzzy spatial relation ontology for image interpretation based on MM operators. Meanwhile, Moraes et al. (2002) proposed a fuzzy expert system architecture for image classification using MM operators, and Li (2007) demonstrated the possibility of hierarchical land cover information retrieval in object-oriented remote sensing image databases with native queries also involving MM operators.

3.4.4 Topographic Map as Possible New Paradigm

Figure 3.5 shows three different modalities of representation of the same territory, located north of Nairobi, Kenya. Figure 3.5(a) is a subset extract from the Africover data set, whereas Figure 3.5(b) is a color composition of three criteria extracted by an automatic image processing procedure. The three criteria are (1) presence of built-up pattern recognized using the textural analysis derived by Pesaresi et al. (2008) from panchromatic data, (2) presence of vegetation recognized using the normalized difference vegetation index (NDVI) calculated on multispectral data, and (3) presence of built-up structures calculated from a morphological residual filtering based on connected operators on panchromatic data (area opening top-hat). The used data input was recorded by the Spot 5 satellite platform. The criteria are extracted by a fully automatic knowledge-based processing flow with any free parameter to be tuned manually. They are then standardized by a simple linear rescaling function based on global histogram statistics (min, max linear histogram stretching, with 1% saturation).

In Figure 3.5(a), the classified "urban areas" are shown in red, whereas in Figure 3.5(b) built-up structures in areas with typical built-up pattern are presented in violet (first and third criteria on), green areas are vegetated, and white areas represent bare soil not built-up.

By comparing Figures 3.5(a) and 3.5(b), we may make the same observations described at the beginning of this paper about the consistency and accuracy of the representation of settlements in the two approaches: one linking directly image data to LU/LC classes, and the other linking image data to a classification scheme allowing modular abstraction. In this case, we represent the first semantic level of the classification scheme, containing the minimum possible of abstraction: the recognition of the basic ontology that in this case is composed by built-up structures and vegetation. Of course, starting from this basic level, several other alternative generalizations may be set, for example, defining different thresholds on the local density of built-up structures delineating alternative notions of "settlement" that are functional for selected users. Because of the abstraction modularity of the classification scheme, the information collected at the basic semantic level may be shared also across slightly different applications fields.

Figure 3.5(c) shows the same portion of territory as represented by a standard topographic mapping approach at 1:50,000 scale (© IGN). Figures 3.5(a) and 3.5(c)

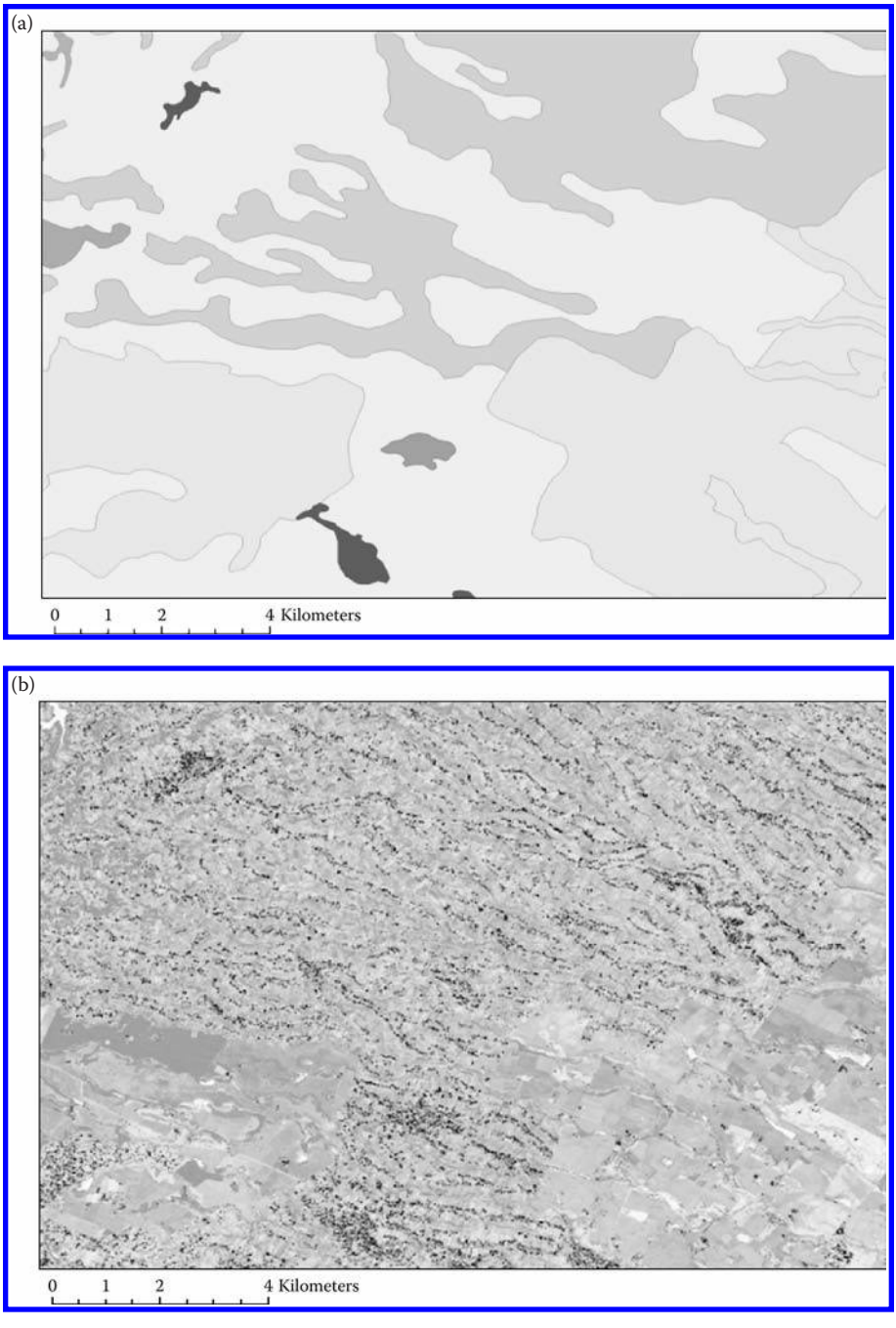

FIGURE 3.5 (See color insert following page 324.) Settlements north of Nairobi, Kenya. Three examples of landscape representations: (a) land cover map produced in the Africover project based on Landsat 5 imagery; (b) built-up index map based on SPOT 5 imagery.

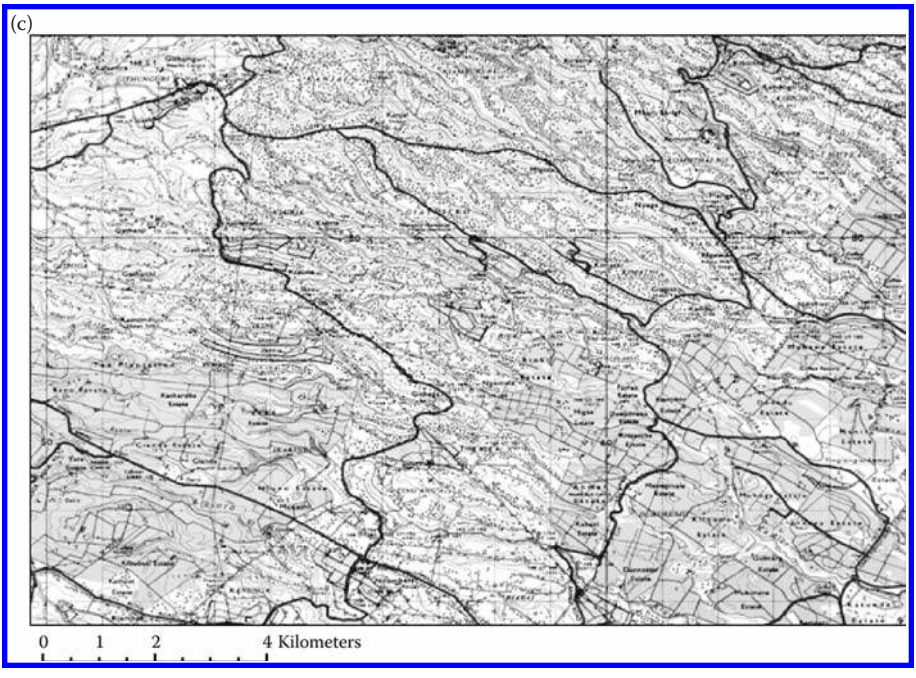

FIGURE 3.5 (Continued) (c) 1: 50.000 scale topographic map.

are abstract representations of the geographic reality, referring to the LU/LC and the topographic model, respectively, whereas Figure 3.5(b) represents a first level of abstraction extracted from the signal recorded by the satellite sensor. In the frame of the arguments presented in this chapter, it is worth observing the degree of similarity between the two mapping paradigms (the LU/LC and the topographic map) from one side and the satellite-derived information from the other side. In particular, concerning the representation of the settlement that is the focus of this paper, we may intuitively remark that the satellite-derived information is much closer to the information provided by the topographic map representation than to the LU/LC model. Anybody trying to measure the accuracy of the built-up structures extracted from satellite data will be much more satisfied by matching Figure 3.5(b) with Figure 3.5(c), than Figure 3.5(b) with Figure 3.5(a).

This homeomorphism between the structure of the satellite-derived information and the topographic map paradigm is important and probably includes part of the solution for finding a more effective method of remote sensing of human settlements using latest-generation satellite sensors. In particular, this alternative paradigm can contribute to define a classification schema, where not only areas but also single structures (or entities, represented as lines or points) may be represented, and where the different entities do not necessarily have to be mutually exclusive as in the LU/LC standard paradigm. The formal characterization of data models allowing topographic map representation has a long history and may be unnoticed by remote sensing experts (Peuquet, 1984), but still manage to produce important developments

toward the definition of more comprehensive classification models, as argued by Forrest (1999).

3.5 CONCLUSIONS

The aim of this chapter is to show that remote sensing data collected by latest-generation sensors can potentially provide information on human settlements with unprecedented detail. Despite this, disciplines such as urban and regional planning, design and development, but also more sectorial activities related to risk assessment or damage and reconstruction assessment are still experiencing difficulties in using satellite-derived information layers.

This paper backs up the theory that a really effective remote sensing of human settlements needs the harmonic development of three basic areas: remote sensor technology; image information extraction methodology; and conceptual tools able to handle the extracted information, say the classification scheme.

Progress made on spatial resolution of the sensor technology alone is not sufficient. If we apply traditional information extraction methodologies based only on spectral image information, we obtain results that are quite suboptimal with respect to the potentialities of satellite data handled. We argue that exploitation of image structural information may dramatically improve the accuracy of detection and discrimination of built-up structures and specific built-up patterns from latest-generation satellite data. In particular, examples on the use of textural and morphological image information are provided.

Still, even if we can use more advanced image information extraction methodologies the problem remains on the adopted classification scheme. The extracted information on human settlements using latest-generation satellite data may be closer to the physical and geographic reality, but the eventual matching with a standard classification scheme will continue to frustrate accuracy expectations. In this context, we argue for the necessity of modifying the standard LU/LC classification scheme and working on a new one that is capable of handling both single structures (geographic entities) and mutually exclusive homogenous areas. Moreover, it is argued that a more flexible classification scheme, which allows for modularity of the abstraction levels of the classes, can contribute to improve the robustness of the automatic recognition and classification against the complexity of the application domain.

REFERENCES

Amo, A., Montero, J., Biging, G., and Cutello, V., Computing, artificial intelligence and information technology — fuzzy classification systems, *European Journal of Operational Research*, 156, 495–507, 2004.

Anderson, J.R., Land use classification schemes used in selected recent geographic applications of remote sensing, *Photogrammetric Engineering and Remote Sensing*, 37, 379–387, 1971.

Anderson, J.R., Hardy, E.E., and Roach, J.T., A land-use classification system for use with remote-sensor data, *United States Geological Survey Circular*, 671, 16 pp., 1972.

Anderson, J.R., Hardy, E.E., Roach, J.T., and Witmer, R.E., Land Use and Land Cover Classification System for use with remote sensor data, *Geological Survey Professional Paper*, 964, 1976. Available online at http://landcover.usgs.gov/pdf/anderson.pdf.

Baltsavias, E.P., and Gruen, A., Resolution convergence: A comparison of aerial photos, LIDAR and IKONOS for monitoring cities, in V. Mesev, ed., *Remotely Sensed Cities*, Taylor & Francis, London, pp. 47–82, 2003.

Benediktsson, J.A., Pesaresi, M., and Arnason, K., Classification and feature extraction for remote sensing images from urban areas based on morphological transformations, *IEEE Transactions on Geosciences and Remote Sensing*, 41(9), 1940–1949, 2003.

Beucher, S., and Lantuéjoul, C., Use of watersheds in contour detection, in: *Proceedings of the International Workshop on Image Processing, Real-time Edge and Motion Detection/ Estimation*, CCETT/IRISA Report no. 132, Rennes, France, 17–21 September 1979, pp. 2.1–2.12, 1979.

Bloch, I., Mathematical morphology and spatial relationships: Quantitative, semi-quantitative and symbolic settings, in: Matsakis, P., and Sztandera, L.M., eds., *Applying Soft Computing in Defining Spatial Relations*, Physica-Verlag, Heidelberg, Germany, pp. 63–98, 2002.

Bloch, I., Defining belief functions using mathematical morphology — application to image fusion under imprecision, *International Journal of Approximate Reasoning*, 48(2), 437–465, 2008.

Brans, P.J., Ethics and decision, *European Journal of Operational Research*, 136, 340–352, 2002.

Chanussot, J., Benediktsson, J.A., and Fauvel, M., Classification of remote sensing images from urban areas using a fuzzy possibilistic model, *IEEE Geoscience and Remote Sensing Letters*, 3, 40–44, 2006.

Chen, K., Blong, R., and Jacobson, C., MCE-RISK: Integrating multicriteria evaluation and GIS for risk decision-making in natural hazards, *Environmental Modelling & Software*, 16, 387–397, 2001.

Comber, A., Fisher, P., and Wadsworth, R., What is land cover? *Environment and Planning B: Planning and Design*, 32, 199–209, 2005.

CORINE, Land Cover Technical Guide, EU, ISBN 92-826-2578-8, 1994. Available at http://reports.eea.europa.eu/COR0-landcover/en.

De Martino, M., Macchiavello, G., and Serpico, S.B., Partially supervised classification of optical high spatial resolution images in urban environment using spectral and textural information, in: *Proceedings, 2004 IEEE International Geosciences and Remote Sensing Symposium*, IGARSS '04. 1, pp. 4896–4897, 2004.

Eastman, J.R., Jin, W., Kyem, P.A.K., and Tolendano, J., Raster procedures for multi-criteria/multi-objective decisions, *Photogrammetric Engineering and Remote Sensing*, 61, 539–547, 1995.

Fisher, P.F., Comber, A.J., and Wadsworth, R.A., Land use and land cover: Contradiction or complement, in: Fisher, P., and Unwin, D., eds., *Re-Presenting GIS*, Wiley, Chichester, pp. 85–98, 2005.

Forrest, D., Geographic information: Its nature, classification, and cartographic representation, *Cartographica: The International Journal for Geographic Information and Geovisualization*, 36(2), 31–53, 1999.

Gamba, P., Dell'Acqua, F., and Dasarathy, B.V., Urban remote sensing using multiple datasets: Past, present, and future, *Information Fusion*, 6, 319–326, 2005.

Gong, P., and Howarth, P.J., The use of structural information for improving land-cover classification accuracies at the rural-urban fringe, *Photogrammetric Engineering and Remote Sensing*, 56, 67–73, 1990.

Gong, P., and Howarth, P.J., Frequency-based contextual classification and grey-level vector reduction for land-use identification, *Photogrammetric Engineering and Remote Sensing*, 58, 423–437, 1992.

Halme, M., and Tomppo, E., Improving the accuracy of multisource forest inventory estimates by reducing plot location error — a multicriteria approach, *Remote Sensing of Environment*, 78, 321–327, 2001.

Hanson, A., Jaynes, C., Riseman, E., and Schultz, H., Building reconstruction from optical and range images, *Proceedings on Computer Vision and Pattern Recognition*, 380–386, 1997.

Haralick, R.M., Statistical and structural approaches to texture, *Proceedings of the IEEE*, 67, 786–804, May 1979.

Haralick, R.M., Shanmugam, K., and Dinstein, I., Texture features for image classification, *IEEE Transactions on Systems, Man and Cybernetics*, 3, 610–621, 1973.

Haverkamp, D., Automatic building extraction from Ikonos imagery, Proceedings of ASPRS 2004 Annual Conference — Mountains of Data, Peak Decisions, 23–28 May 2004, Denver, Colorado, p. 82, 2004.

Hudelot, C., Atif, J., and Bloch, I., Fuzzy spatial relation ontology for image interpretation, *Fuzzy Set and Systems*, 159(15), 1929–1951, 2008.

Irvin, R.B., and Mckeown, M.D., Methods for exploiting the relationship between buildings and their shadows in aerial imagery, *IEEE Transactions on Systems, Man and Cybernetics*, 19(6), 1564–1575, 1989.

Jaynes, C., Stolle, F., and Collins, R., Task driven perceptual organization for extraction of rooftop polygons, Proceedings ARPA Image Understanding Workshop, 1, 359–365, 1994.

Jin, X., and Davis, C.H., Automated building extraction from high-resolution satellite imagery in urban areas using structural, contextual, and spectral information, *EURASIP Journal on Applied Signal Processing*, 2005(1), 2196–2206, 2005.

Lafarge, F., Descombes, X., and Zerubia, J., Textural kernel for SVM classification in remote sensing: Application to forest fire detection and urban area extraction, in: *Proceedings of the IEEE International Conference on Image Processing*, *ICIP 2005*, 3(III), 1096–1099, 2005.

Li, J., Hierarchical land cover information retrieval in object-oriented remote sensing image databases with native queries, in: *Proceedings of the 45th Annual ACM Southeast Regional Conference*, Winston-Salem, North Carolina, March 23–24, 467–472, 2007.

Lin, C., Huertas, A., and Nevatia, R., Detection of buildings from monocular images, in: Gruen, A., Kuebler, O., and Agouris, P., eds., *Automatic Extraction of Man-Made Objects from Aerial and Space Images*, Birkhauser, Basel, pp. 125–134, 1995.

Meyer, F., Integrals, gradients and watershed lines, in: *Proc. Mathematical Morphology and Its Applications to Signal Processing*, Barcelona, Spain, May, pp. 70–75, 1993.

Meyer, F., and Beucher, S., Morphological segmentation, *Journal of Visual Communication and Image Representation*, 1(1), 21–46, 1990.

Mynt, S.W., The use of wavelets for feature extraction of cities from satellite sensor images, in: V. Mesev, ed., *Remotely Sensed Cities*, Taylor & Francis, London, pp. 109–134, 2003.

Moraes, R.M., Banon, G.J.F., and Sandri, S.A., Fuzzy expert systems architecture for image classification using mathematical morphology operators, *International Journal of Informatics and Computer Science*, *Special Issue: Intelligent Information Systems and Applications*, 142(1), 7– 21, 2002.

Munarin, S., and Tosi, C., eds., *Tracce di Città. Esplorazioni di un Territorio Abitato: l'Area Veneta*, Franco Angeli, Milano, 2001.

Najman, L., and Schmitt, M., Definition and some properties of the watershed of a continuous function, in: *Proceedings Mathematical Morphology and Its Applications to Signal Processing*, Barcelona, Spain, May, pp. 75–81, 1993.

Oriot, H., Michel, A., and Goretta, O., Extraction of rectangular roofs on stereoscopic images. An interactive approach, *International Archives of Photogrammetry and Remote Sensing*, XXXII(3), 367–373, 1998.

Pagot, E., and Pesaresi, M., Systematic study of the urban post-conflict change classification performance using spectral and structural features in a support vector machine, *IEEE J-STARS Special Issue on Remote Sensing of Human Settlements: Status and Challenges*, 1(2), 120–128, 2008.

Peijun, L., Hongtao, H., and Jiancong G., Segmentation of high-resolution multispectral image based on extended morphological profiles, in: *Proceedings of IEEE International Geoscience and Remote Sensing Symposium, IGARSS 2007*, pp. 1481–1484, 2007.

Pesaresi, M., A mixed morphological and spectral procedure to improve the accuracy of the built area classification from multisensor satellite data, Proceedings of the ISMM'94 Mathematical Morphology and its Applications to Signal Processing II, 7–9 September, Fontainebleau, France, 1994.

Pesaresi, M., An optimized procedure to built space automatic recognition via Spot HRV panchromatic satellite data processing, in proceedings of ISTAT-EUROSTAT seminar, The impact of remote sensing on the European Statistical Information System, Rome, 27–29 November, 1995.

Pesaresi, M., Texture analysis for urban pattern recognition using fine-resolution panchromatic satellite imagery, *Geographical & Environmental Modeling*, 4(1), 47–67, 2000.

Pesaresi, M., and Benediktsson, J.A., A new approach for the morphological segmentation of high resolution satellite imagery, *IEEE Transactions on Geosciences and Remote Sensing*, 39(2), 309–320, 2001.

Pesaresi, M., and Bianchin, A., Procedure to extract built area, Proceedings of the ITC International Symposium Operationalization of Remote Sensing, Enschede, the Netherlands, 19–23 April, 1993.

Pesaresi, M., and Bianchin, A., Recognizing settlement structure using mathematical morphology and image texture measures, in: Donnay, J.P., and Barnsley, M., *Remote Sensing and Urban Analysis*, Taylor & Francis, London, 1996.

Pesaresi, M., and Kanellopoulos, I., Detection of urban features using morphological based segmentation and very high resolution remotely sensed data, in: Kanellopoulos, I., Wilkinson, G.C., and Moons, T., *Machine Vision and Advanced Image Processing in Remote Sensing*, Springer, Berlin, pp. 271–284, 1999.

Pesaresi, M., and Pagot, E., Post-conflict reconstruction assessment using image morphological profile and fuzzy multicriteria approach on 1-m-resolution satellite data, in: *Proceedings of the Urban Remote Sensing Joint Event*, Paris, 1–8, 2007.

Pesaresi, M., and Pagot, E., Soft versus hard spatial generalization of multi-temporal DMP for settlement post-conflict reconstruction assessment, *IEEE GRSL Special Issue Image Information Mining: Pursuing Automation of Geospatial Intelligence for Environment and Security*, in press.

Pesaresi, M., Gerhardinger, A., and Haag, F., Rapid damage assessment of built-up structures using VHR satellite data in tsunami affected area, *International Journal of Remote Sensing*, 28, 3013–3036, 2007.

Pesaresi, M., Gerhardinger, A., and Kayitakire, F., A robust built-up area presence index by anisotropic rotation-invariant textural measure, *IEEE J-STARS Special Issue on Remote Sensing of Human Settlements: Status and Challenges*, in press.

Peuquet, D.J., A conceptual framework and comparison of spatial data models, *Cartographica: International Journal for Geographic Information and Geovisualization*, 21(4), 66–113, 1984.

Plaza, A., Martinez, P., Perez, R.M., and Plaza, J., A new approach to mixed pixel classification of hyperspectral imagery based on extended morphological profiles, *Pattern Recognition*, 376, 1097–1116, 2004.

Plaza, J., Plaza, A., Gamba, P., and Trianni, G., Efficient multi-band texture analysis for remotely sensed data interpretation in urban areas, in: *Proceedings, Urban Remote Sensing Joint Event*, Paris, 11–13 April, 2007.

Puissant, A., Hirsch, J., and Weber, C., The utility of texture analysis to improve per-pixel classifications for high to very high spatial resolution imagery, *International Journal of Remote Sensing*, 26(4), 733–745, 2005.

Serra, J., *Image Analysis and Mathematical Morphology*, Academic Press, London, pp. 610, 1982.

Serra, J., Introduction to mathematical morphology, *Computer Vision, Graphics and Image Processing,* 35(1), 283–305, 1986.

Shufelt, J.A., Performance evaluation and analysis of monocular building extraction from aerial imagery, *IEEE Transactions on Pattern Analysis and Machine Vision*, 21(4), 311–326, 1999.

Shufelt, J.A., and Mckeown, D.M., Fusion of monocular cues to detect man-made structures in aerial imagery, *Computer Vision, Graphics and Image Processing-Image Understanding*, 57(3), 307–330, 1993.

Soille, P., Geodesic transformations, in: *Morphological Image Analysis: Principles and Applications*, 2nd edition, Springer-Verlag, Berlin, pp. 183–218, 2004.

Soille, P., and Pesaresi, M., Advances in mathematical morphology applied to geoscience and remote sensing, *IEEE Transaction on Geosciences and Remote Sensing*, 40(9), 2042–2055, 2002.

Tuceryan, M., and Jain, A.K., Texture analysis, in: Chen, C.H., Pau, L.F., Wang, P.S.P., eds., *The Handbook of Pattern Recognition and Computer Vision*, 2nd edition, World Scientific Publishing, pp. 207–248, 1998.

Vogelman, J.E., Sohl, T., and Howard, S.M., Regional characterization of land cover using multiple sources of data, *Photogrammetric Engineering and Remote Sensing*, 64, 45–57, 1998.

Yaochu, J., *Advanced Fuzzy Systems Design and Applications*, Physica-Verlag, Heidelberg, 2003.

Zhang, Q., Wang, J., Gong, P., and Shi, P., Urban spatial pattern analysis from SPOT panchromatic imagery using textural analysis, *International Journal of Remote Sensing*, 24(21), 4137–4160, 2003.

Zhang, H., Fritts, J.E., and Goldman, S.A., Image segmentation evaluation: A survey of unsupervised methods, *Computer Vision and Image Understanding*, 110(2), 260–280, 2008.

Zhong, P., and Wang, R., A multiple conditional random fields ensemble model for urban area detection in remote sensing optical images, *IEEE Transactions on Geoscience and Remote Sensing*, 45(12), 3978–3988, 2007.

Zhu, C., Shi, W., Pesaresi, M., Liu, I., Chen, X., and King, B., The recognition of road network from high-resolution satellite remotely sensed data using image morphological characteristics, *International Journal of Remote Sensing*, 26(24), 5493–5508, 2005.

4 The Color of Cities
An Overview of Urban Spectral Diversity

Christopher Small

CONTENTS

4.1 INTRODUCTION

Urban areas are characterized by diversity. Remote sensing provides an efficient way to quantify some aspects of this diversity. In many settings, diversity of land cover may provide a basis for characterizing the urban environment. Similarly, the diversity of urban land cover influences mass and energy fluxes through the urban environment — with direct consequences for the inhabitants. For both of these reasons, it is necessary to understand both the functional diversity of urban land cover and the resulting spectral diversity that is detected by remote sensors. Characterization of spectral properties is essential to remote sensing of any type of land cover, but is especially important in urban environments because the nature of the diversity itself contains valuable information about the structure and function of the land cover within the urban mosaic.

Two of the primary applications of remote sensing to the study of the urban environment are mapping its spatial structure and monitoring its temporal changes. Since at least the early 1970s, visible and infrared (IR) optical satellite imagery has been used to map urban areas and monitor their changes. However, attempts to map urban areas using traditional thematic classification algorithms have met with very limited success. This is primarily a result of the spectral diversity of the urban environment and the fact that this diversity violates the cardinal assumption of spectral homogeneity upon which most classification algorithms are based. This further illustrates why mapping and monitoring urban areas with optical sensors requires knowledge of the variety of land cover spectra that occur within the urban mosaic. In some cases, the mapping objective may be to define the urban area on the basis of its land cover. In other cases, the objective may be to map specific components within the mosaic. In either case, it is necessary to consider the scale and diversity of components within the urban area.

The urban mosaic can be represented, and mapped, in terms of a wide variety of characteristics — both physical and nonphysical. Remote sensing measures physical properties. The most abundant type of remotely sensed observations is the passive optical measurement of reflected sunlight at visible and IR wavelengths (defined below). The focus of this chapter is on the physical properties that can be derived from measurements of reflected sunlight and the wide variety of compositional, structural, and functional characteristics that can be inferred from these physical properties. In this sense, optical remote sensing is analogous to the biophysical phenomenon of vision, and the visible and IR signals detected by the sensor are analogous to color. Color is generally thought of in terms of the sensations it induces in the human eye–brain system but in this chapter, the word color is used more loosely to refer to the visible and IR characteristics of reflected sunlight as measured by sensors. Variations in the color of reflected light convey information about the objects reflecting it. In the current discussion, the word color will be used to include analogous processes occurring in the

near-infrared (NIR) through shortwave infrared (SWIR) regions of the electromagnetic spectrum. The behavior of light in the visible and IR regions of the spectrum can be described effectively by the physics of reflection and absorption in its interaction with matter. The intention of this unconventional usage of color is not to redefine the word but to provide an analog to a familiar, and related, biophysical process. Although this usage is introduced for the benefit of readers not versed in the terminology used in spectroscopy and remote sensing, the analogy is appropriate because the reflection and absorption of light at different visible wavelengths is related to the material properties responsible for what we perceive as color. An excellent overview of these reflection and absorption processes is given by Clark (1999). A comprehensive treatment of the biophysical phenomenon of color is given by Shevell (2003).

4.1.1 Why Color Is Important

Color is important because it is one of our primary sources of information on the world around us. In terms of mapping and monitoring urban environments, color is of particular importance because it has the potential to provide information that would be difficult, or impossible, to obtain otherwise. Specifically, color allows us to map and monitor the urban environment in terms of its physical properties and the processes that influence, or are influenced by, those properties. At present, this potential is largely untapped. However, recent scientific and technological progress has provided a wealth of information on the urban environment and the processes that shape it.

The distinction between visible and IR radiation (light) is based on the sensitivity limits of the human eye–brain system. Other organisms have eye–brain systems with different spectral sensitivities extending into both IR (longer) and ultraviolet (shorter) wavelengths. Our eye–brain system presumably evolved to detect the visible wavelengths (~400 to 700 nm) because the Sun emits most of its energy in this part of the spectrum. However, the NIR (700–1000 nm) and SWIR (1000–2500 nm) IR wavelengths contain more of the characteristic absorption features that make it possible to identify materials that may be indistinguishable at visible wavelengths. These characteristics are discussed in more detail below. Color is particularly useful for mapping and monitoring the Earth's surface because light is provided in abundance by the Sun and efficiently propagated in the form of electromagnetic waves that can be detected remotely — by both eyes and sensors. Optical sensors have been imaging Earth from space since the 1970s, so color (both visible and IR) provides one of our primary sources of information about the spatial distribution, structure, and evolution of cities over a period in which the world's urban population has approximately tripled (United Nations, 2006).

4.1.2 Mapping and Monitoring Urban Land Cover

Mapping of urban land cover (e.g., water, vegetation, soil, impervious surfaces) makes it possible to assess the spatial structure of urban land use (e.g., residential, commercial, industrial) in situations where the relationship between the two is unambiguous. Inferring land use from land cover is not always straightforward, but the mapping

of land cover has numerous direct applications aside from land use determination. Mesoscale weather prediction and climate modeling, surface and subsurface hydrologic modeling, vegetation health, and invasive species monitoring provide a few examples. Applications of remote sensing in the urban environment include both target-specific feature identification and mapping of urban land cover to delineate urban extent. Examples of target-specific feature identification include tasks such as mapping of vegetation abundance and health, monitoring road and infrastructure condition, and mapping spatial extent of pervious and impervious surfaces. In contrast, mapping and monitoring of urban extent rely on differentiating the aggregation of built land covers in the urban mosaic from the land cover types associated with undeveloped areas. Although target-specific tasks can be challenging, they often benefit from relatively unambiguous target definition. In contrast, attempts to map the spatial extent of urban development are often limited by subjective or inconsistent definitions of what is actually urban. This is problematic because different definitions of urban can result in very different estimates of urban extent. Multiple, inconsistent definitions can result in different perceptions which, once engrained within different disciplines, can impede cross-disciplinary collaboration and pose serious obstacles to progress. This conundrum arises naturally from the diversity of urban land use and from the diversity of applications for which a definition is sought. The problem is further compounded by the fact that even agreed-upon definitions may not be expressible in terms of physically measurable quantities. The purpose of this chapter is to provide an overview of some spectral properties of both the individual components and the aggregate of the urban mosaic in order to help determine what can and cannot be quantified with optical remote sensing.

Land cover mapping can take the form of either continuous physical quantities or discrete thematic classes. Optical sensors measure physical quantities resulting from physical processes. The process of transforming a physical quantity to another physical quantity is fundamentally different from the process of transforming a physical quantity to a discrete thematic class — particularly if the thematic class is defined in terms of nonphysical criteria (in whole or in part). Each type of mapping has a wide variety of applications arising from its relative strengths but both depend on color.

Monitoring can be thought of as multitemporal mapping. However, analysis of temporal changes in maps is more complex because it generally involves changes in both the target (land cover) and the imaging conditions (illumination) at the time of each acquisition. Distinguishing between these two types of change can be challenging. However, the distinction is critical because apparent changes can mask actual changes as well as being misinterpreted as a change where none has occurred.

4.1.3 Objectives

The primary objective of this chapter is to provide an overview of some spectral properties of urban land cover and to illustrate some of the strengths and weaknesses of optical remote sensing for both target-specific feature identification and aggregate urban land cover mapping and monitoring. To achieve this, the chapter first compares and contrasts the spectral properties of different materials in the urban mosaic and then provides an overview of their relative abundance within and among

different urban environments. Because of the variety of optical sensors available, and their different capabilities, it is necessary to distinguish between the inherent spectral properties of different materials and those properties that can be resolved with a specific sensor under specific conditions. For this reason, the analysis uses comparisons of different sensors to illustrate their strengths and limitations for detecting spectral properties of different materials and land cover. Similarly, the spectral diversity of urban environments is illustrated by comparisons using different sensors in the same place and the same sensor in different places. The ultimate objective is to help the reader determine what can, and cannot, be measured consistently under different conditions in different settings. Between what can and cannot be measured, there lies a multitude of things that can *sometimes* be measured. The urban remote sensing literature is full of examples of algorithms and methodologies that may be effective in one specific location or circumstance but are not generally robust in other locations or circumstances. The point of the comparisons is both to illustrate confounding sources of variability and to highlight potential consistencies that might be exploited in multiple locations and circumstances. Ultimately, the objective is to determine what can and cannot be resolved consistently. Consistency is key to repeatability.

The presentation in this chapter is directed toward an educated lay audience with basic science background and some willingness to consider the concept of color in both physical terms and in a more abstract mathematical context. The mathematical depiction of color using the concept of a spectral mixing space (explained below) makes it possible to represent a wide variety of colors (both visible and IR) in a physical context that makes spectral diversity easier to understand and greatly facilitates comparison of different urban components and environments at different spatial scales. This chapter is not an attempt to review or summarize the vast literature on urban remote sensing, but rather an attempt to illustrate some spectral characteristics of urban land cover that may be well known to researchers in the remote sensing community but not necessarily discussed in the context presented here.

4.2 WHAT IS COLOR?

4.2.1 Perception and Measurement

Perception is subjective. Measurement should be objective. The human eye–brain system is good at perception. Optical sensors are good at measurement. One of the challenges of remote sensing is to measure what our eye–brain system can perceive in a visual image. This is a challenge because the human eye–brain system can perceive things that are very difficult to measure objectively. Objective measurement is essential to repeatability. Repeatability provides a basis for scientific inference.

The eye–brain system perceives images in terms of both color and texture — as well as spatial context. Traditional image classification algorithms categorize individual picture elements (pixels) on the basis of their color — generally without regard to their texture or spatial context. Analytical approaches that combine color, texture, and spatial context approach the visual interpretive processes of the eye–brain system (e.g., Dana et al., 1999).

One of the strengths of optical sensors is their ability to measure what the human eye–brain system cannot perceive — specifically, IR radiation. This allows us to extend our conception of color to a much wider range of wavelengths that provide considerably more information than the visible spectrum alone. To make use of this information, it is necessary to relate the idea of color to the more general concept of reflectance.

4.2.2 Color and Reflectance

The standard definition of color is a perceived characteristic that is determined by the response of the eye–brain system to light reflected from a target. Reflectance is a physical property of the target that is determined by the interaction between the target material and the electromagnetic radiation (e.g., light) illuminating it. What we perceive as color is determined, in part, by material reflectance properties. It is also determined by illumination (explained below). Reflectance properties are determined by physical interactions (at atomic and molecular scales) that result in absorption of radiation at specific wavelengths and reflection at others. We perceive things as different colors because they absorb and reflect light at different visible wavelengths. Imaging at IR wavelengths makes it possible to distinguish between materials that may be indistinguishable at visible wavelengths. Although sunlight is most energetic at visible wavelengths, there are many more absorption features at IR wavelengths than visible. Distinguishing different target materials and properties from reflectance is a primary objective of optical remote sensing.

The most complete description of an object's color is given by the variations of reflectance as a function of the geometry and wavelength of the radiation illuminating it. Reflectance is a physical property that determines the fraction of incident radiation (light) that is reflected at different wavelengths. The perceived color of an object is a result of both its reflectance properties and its illumination conditions. Changes in illumination can cause changes in the perceived color even without changes in the target's reflectance. Distinguishing between the two is a major challenge in remote sensing. Under controlled conditions, in the laboratory or in the field, reflectance is measured as radiance reflected from the target relative to radiance reflected from a white standard. Under less controlled conditions, from satellite or aircraft, reflectance must be inferred from calibrated radiance measurements. In this chapter, reflectance is depicted spectrally as a function of wavelength and spatially as pixel brightness in either color or grayscale.

4.2.3 Measuring Color

In many ways, the optical sensors discussed here are analogous to digital cameras with superhuman spectral sensitivity. Optical sensors (e.g., digital cameras) measure radiance. Radiance is the amount of electromagnetic energy measured over a specific range of wavelengths. When electromagnetic waves interact with matter, some fraction of the energy is transmitted, absorbed, or reflected at each wavelength. The reflected radiance measured by a sensor is influenced by both the reflectance of the target and the spectral energy distribution of the source that illuminates the target. If

the latter is known, the former can be inferred. Reflectance properties can be inferred from radiance measurements given some knowledge of the incident radiation and the processes that influence it between the source, the target, and the sensor. When radiance is measured in the laboratory or in the field, it can be converted to relative reflectance by normalizing for the incident radiation reflected from a spectrally flat (maximally white) standard such as Spectralon®. Because of the close proximity of the sensor and target, atmospheric interaction with the reflected light is negligible. In the case of radiance measurements collected from aircraft and satellite, the processes of atmospheric scattering and absorption influence both the incident radiation illuminating the target and the fraction of radiance that is reflected from the target and measured by the sensor. These processes must be corrected for — or at least considered — when inferring reflectance properties from radiance measurements. The process of atmospheric correction and radiometric rectification is a major challenge in remote sensing. The examples used in this chapter will compare laboratory/field measurements of relative reflectance with both atmospherically corrected reflectance measured from aircraft and with exoatmospheric (uncorrected) reflectance measured from satellites. The primary differences between direct laboratory/field, aircraft, and satellite measurements are related to the spectral and spatial resolutions of the sensors. The spatial resolution of a sensor determines the size of the smallest object it can image. The spectral resolution of a sensor determines the diversity of colors that it can detect.

In remote sensing, there is a fundamental tradeoff between spatial and spectral resolution. Increasing a sensor's spatial resolution generally comes at a cost of reduced spectral resolution — and vice versa. This is why sensors that collect both panchromatic (total brightness over a wide range of colors) and multispectral (multiple spectral intervals or bands) imagery can resolve smaller objects with the panchromatic band than with the multispectral bands. The loss of spatial detail in the multispectral bands is compensated for by their ability to resolve different colors. Fortunately, many sensors collect multispectral and panchromatic imagery simultaneously so the spatial detail of the panchromatic brightness can be combined with the spectral detail (colors) resolved by the multispectral bands to produce a pan-sharpened color image with the higher spatial resolution of the panchromatic band.

Spatial and spectral resolution together determine the ability of a sensor to discriminate targets from background. Inadequate spatial (or spectral) resolution leads to the phenomenon of aliasing in which some different shapes (or colors) become indistinguishable from each other. In the tradeoff between spatial and spectral resolution, many interpreters favor spatial resolution. However, given sufficient spatial resolution to distinguish a target from its background, incremental increases in spectral resolution can provide information that may be more diagnostic (Gamba and Dell'Acqua, 2007).

4.2.4 Spatial Resolution

The spatial resolution of a sensor determines the size of the smallest object it can image. The spatial resolution is dictated by the angular size of the instantaneous field of view (IFOV) of a single picture element (pixel). A sensor cannot produce a

coherent image of objects smaller than a single pixel — but sensors can detect the spectral contributions of objects smaller than a single pixel. Because the sensor measures a single spatial average of the radiance reflected from all illuminated objects within its IFOV, the reflectance of each of these objects contributes to the aggregate radiance measured by the sensor. This process is referred to as spectral mixing. If the different reflectances that contribute to this aggregate radiance are known, or can be inferred, it is sometimes possible to estimate the relative abundance of the different objects within the IFOV. This is generally referred to as "spectral unmixing" or, occasionally as "subpixel resolution" — although it is really more akin to subpixel detection. The resolving power of an instrument refers specifically to the smallest interval quantity that it can measure. In the case of spectral resolution the interval is a range of wavelengths whereas in the case of spatial resolution it is a distance. This distance determines the pixel size on the target, referred to as the ground instantaneous field of view (GIFOV). A detailed discussion of the importance of spatial resolution to urban remote sensing is given by Jensen and Cowen (1999).

4.2.5 Spectral Resolution

The spectral resolution and dynamic range of a sensor determine how many and which colors it can resolve. Dynamic range refers to the difference between the brightest and darkest targets a sensor can image without saturation. The spectral resolution, or bandwidth, of a sensor's spectral bands determine which parts of the wavelength spectrum it is sensitive to and how small a wavelength interval it can resolve. The ability to measure small wavelength intervals allows a sensor to resolve narrow absorption features (local reflectance minima) resulting from composition and molecular structure.

Imaging sensors can represent reflectance to varying degrees of spectral detail. The prefixes hyper and hypo refer to over- and undersampling in either the spatial or spectral dimensions. Hyperspectral sensors can measure wavelength intervals smaller than the narrowest feature of interest and hence small enough to resolve very narrow absorption features in detail. Broadband multispectral sensors (sometimes referred to as hypospectral) sensors measure a smaller number of broad bands at specific wavelength intervals by integrating radiance across the interval into a single average measurement. Broadband multispectral sensors can detect the presence of some absorption features, but are generally unable to resolve their shape in detail. The importance of absorption features is explained below. A panchromatic sensor that averages over a single wide range of wavelengths is the most hypospectral of sensors because it cannot resolve color at all. In contrast, laboratory and field spectrometers can often resolve hundreds of wavelength intervals as small as 1 nm (=1/1,000,000,000 m) in the visible through SWIR range. This results in an oversampling of most absorption features. Broadband sensors generally image in fewer than 10 bands in this range and average over wavelength intervals from several tens to hundreds of nanometers. This results in undersampling. As might be expected, hyperspectral sensors are more difficult, and expensive, to design, build, and maintain. Until quite recently, satellites carried only broadband sensors. It is therefore

necessary to reconcile the wealth of new hyperspectral information with more abundant broadband information to make best use of the vast historical archive of broadband imagery collected since the 1970s.

4.3 SPECTRAL DIVERSITY OF URBAN MATERIALS

At this point, it is necessary to distinguish between the true spectral diversity and the measurable spectral diversity of the urban environment. The measurable diversity is a subset of the true diversity. The true spectral diversity of an urban environment is not generally known — but can sometimes be inferred from the measurable spectral diversity. However, the measurable spectral diversity depends on both the true spectral diversity and characteristics of the sensor used to measure it — specifically, on the spatial and spectral resolutions of the sensor. Unless stated otherwise, spectral diversity will henceforth refer to measurable spectral diversity.

4.3.1 How Different Sensors See Different Materials

To illustrate the spectral diversity of urban materials, a collection of laboratory and field spectra are compared both by thematic class and as they might be detected by different optical sensors under ideal illumination and viewing conditions. In each case, the bidirectional reflectance spectrum is measured from a specific angle (usually perpendicular if the target is flat), illuminated from a specific direction. However, most materials are not isotropic reflectors so the amplitude and shape of the reflectance spectrum generally varies with viewing and illumination (VI) angles. This variation, represented by the bidirectional reflectance distribution function (BRDF), can be approximated with spectra collected under a range of VI angles — although the procedure is nontrivial in the laboratory (Sandmeier et al., 1998) and must generally be simulated with numerical models at the scale of urban areas (Meister et al., 2001). It is important to remember that each laboratory/field spectrum represents only one of a potentially wide variety of possible reflectance spectra that could be obtained from each sample under different VI conditions. Figure 4.1 shows bidirectional reflectance spectra of several classes of materials that are frequently found in the urban environment. This is an obviously nonrandom collection of materials intended to represent large objects exposed to overhead sensors. It represents a subset of the true diversity of materials within the urban environment at finer scales but depicts the materials composing the largest, most areally abundant targets in the urban environment. In spite of this limitation, the sample does provide a reasonable, although rather conservative, representation of the types of materials that are exposed to remote sensors in most urban environments.

The laboratory and field spectra in Figure 4.1 (left column) were obtained from the U.S. Geological Survery (USGS) Digital Spectral Library — version splib06a (September 2007). A detailed description of the samples, measurements, and instruments is given by Clark et al. (2007). The library is available online at http://speclab.cr.usgs.gov/spectral-lib.html. In this plot, the spectra are divided into thematic classes on the basis of the names of the samples, or in a couple of cases by the most

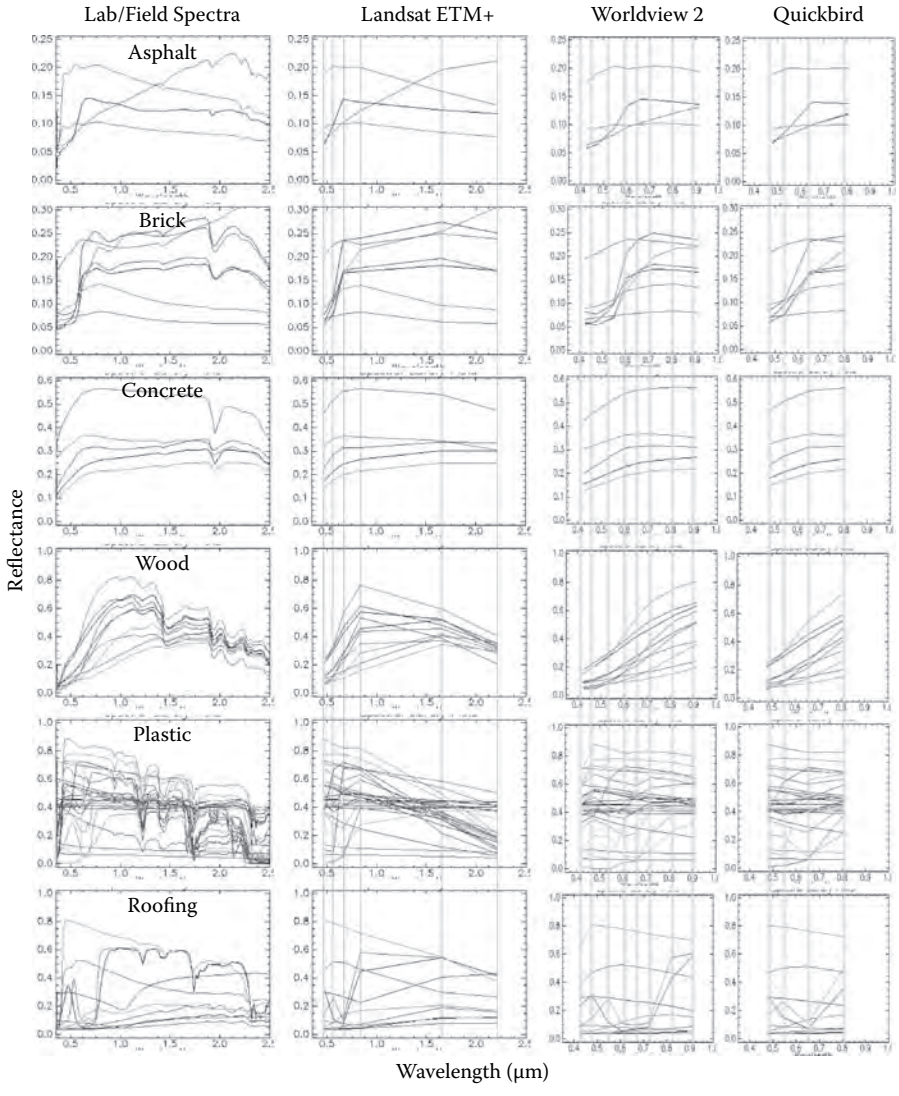

FIGURE 4.1 Spectra of different classes of urban construction materials as resolved by different sensors. Low albedo materials (asphalt and brick) are plotted at an expanded reflectance scale for clarity. Laboratory and Landsat spectra span the full visible-SWIR wavelength range while Worldview and Quickbird span only the visible-NIR range. Spectral variability within each thematic class is comparable to variability among classes Spectra available from ttp://speclab.cr.usgs.gov/spectral-lib.html

appropriate compositional analog. For example, the roofing asphalt and black roof tar spectra are included on the asphalt plot because the composition and spectra are similar. Similarly, a cardboard sample is included with wood and cinder block is included with concrete, along with two samples of dust debris from the World Trade Center collapse site (Clark et al., 2001). Because of the spectral similarity of these recategorized

spectra, the apparent variability of these classes is reduced slightly. In contrast, the Roofing class is a diverse assortment of spectra containing roofing felt, sheet metal, tarp, tarpaper, tin, and vinyl. It is intended to represent a variety of materials frequently used for roofing in informal settlements. All spectra were resampled to 10 nm to reconcile different instrument spectral resolutions to a common set of wavelengths. The decimation to 10 nm results in some slight loss of information but this does not affect the conclusions to be drawn from the comparison. Because these spectra oversample even the narrow absorption features, they are referred to here as hyperspectra — in contrast to the broadband spectra, which generally undersample these features.

The laboratory/field spectra for each class in Figure 4.1 are also compared to the spectra that would be resolved by different satellite sensors. The reflectance spectra for the Landsat, Worldview, and Quickbird sensors were obtained by convolving the spectral response of each instrument with the original laboratory/field spectrum shown in the left column. Landsat depicts the full visible-SWIR spectrum with three visible (red, green, blue) and three IR (one NIR, two SWIR) bands with ~30 m ground resolution. Quickbird images only the visible and near-infrared (VNIR) with three bands in the visible and one in the NIR at ~2.4 m ground resolution. The Worldview 2 sensor, expected to launch in mid 2008, also images the VNIR but with eight bands (three NIR) and an expected 1.8-m ground resolution. The Worldview spectral responses are provisional as of May 2007 (M. Tremblay, personal communication) based on sensor design parameters. Note the spectral scale difference between the VNIR and the visible-SWIR spectra.

The characteristic features of reflectance spectra are the overall albedo (brightness), the specific absorption features, and the slope and curvature of the broad continuum on which the narrower absorption features are superimposed. The laboratory/field hyperspectra capture all of these features over the entire range of visible to SWIR wavelengths. These full-resolution spectra are able to resolve both the depths and the shapes of the different absorption features as well as subtle changes in curvature that result from superposition of multiple absorptions at similar wavelengths. The laboratory/field spectra provide the most complete description of the reflectance characteristics of the materials. The resampled broadband spectra obviously contain far less information. Most notably, the broad spectral bands cannot resolve the depth or shape of the absorption features. They can, however, detect the presence of some broad absorptions in the form of spectral slopes. The narrow band Worldview sensor can also detect some variations in curvature at visible wavelengths. Of these broadband sensors, only the Landsat Enhanced Thematic Mapper (ETM+) sensor can approximate the overall continuum slope or curvature — and only for spectra that do not have large absorptions in any of the wavebands it samples. In this sense, all of the broadband sensors are susceptible to spectral aliasing, whereby the presence of absorptions within specific wavebands can be indistinguishable from continuum or albedo variations. This imposes a fundamental limitation on what can be distinguished with broadband sensors.

4.3.2 Spectral Variability

Both the similarities and differences of the spectra within each thematic class are immediately apparent in the laboratory/field hyperspectra. The absorptions are the most consistent feature in most classes — although every class except concrete has

at least one exception, so even absorptions are not definitive class criteria (for these classes). This persistence of absorptions is physically consistent with the compositional differences that the classes are based on. Continuum shapes vary considerably within most classes (least with wood) and overall albedo varies by at least a factor of 2 in every class. Despite the considerable variability within each class, the spectral differences between classes are readily apparent in the full spectra. Consistencies in these class differences allow for some discrimination among classes, but detailed analyses of spectral separability of classes have found considerable spectral ambiguity even with hyperspectra (Herold et al., 2003, 2004; Heiden et al., 2007). Consistency of spectral shape within a specific class results from the compositional similarity of materials within the class and their common absorption features. A detailed discussion of different urban materials and physical properties is beyond the scope of this chapter but overviews of specific material classes are given by Ben-Dor et al. (2001), Heiden et al. (2001), Herold et al. (2004), Lacherade et al. (2005), and Schiefer et al. (2006).

With the broadband spectra, the variability within each class is more pronounced and the consistencies within the class less so. This is a consequence of the broadband sensors' inability to resolve most of the absorption features apparent in the hyperspectra. In this sense, the spectral degradation resulting from the reduction of spectral resolution is devastating. Although Landsat preserves some consistencies in the slope and curvature of the continuum, the VNIR sensors cannot capture continua. Worldview is able to resolve some significant variations in VNIR curvature but Quickbird is limited to spectral slope and albedo. Unfortunately, spectral slope is highly variable and overall albedo is almost totally useless for discriminating anything more subtle than the brightest of targets.

The hope for broadband spectral discrimination of different materials looks even more grim when we consider that these spectra represent best-case scenarios that could never be obtained with satellites or aircraft. Lighting conditions and illumination geometry cannot be controlled in the field and are rarely as optimal as those used in laboratory conditions. Atmospheric effects are difficult to remove entirely and are almost always based on numerous assumptions about key parameters so their accuracy can rarely be verified retroactively. In addition to these uncertainties, there is the unavoidable issue of spatial scale and spectral mixing (discussed below) that dilutes and perturbs these spectrally pure examples.

The intraclass spectral variability depicts the disparity between the physical composition and the function of each material class. At the same time, the interclass variability depicts the diversity of form represented in the urban mosaic. Taken together, these different types of spectral variability illustrate both the potential utility and the complexity of thematic classification in urban environments. Most urban environments would be expected to contain a wider variety of spectra than the library used in these examples — but the spectral variability present in these examples likely underrepresents actual measurable spectral diversity. This is consistent with the intention of the example because even this underrepresentation of spectral diversity illustrates the difficulty of distinguishing classes of materials with broadband sensors — even under ideal conditions. In addition to compositional variability, thematic classification must contend with measurement variability. These spectra were obtained from known samples under optimal measurement conditions. Spectral ambiguity under these conditions

guarantees spectral ambiguity under less optimal conditions. Variations in VI geometry can have a profound effect on measured reflectance in the urban environment (e.g., Meister, 2001; Schiefer et al., 2006) so the variability in these laboratory/field spectra would only be greater if they were viewed under different VI conditions.

4.3.3 Color Spaces and Spectral Mixing Spaces

Although comparative spectra are useful for illustrating consistencies and differences among different classes of targets, it is difficult to fathom urban spectral diversity by visual comparison of individual reflectance plots. To characterize the spectral diversity of any complex environment, we require a systematic means to represent both the wide variety of spectral shapes as well as their relative abundance. This can be accomplished by transforming the spectra from the geographic space where they originate to a spectral space in which the dimensions are related to the most prominent characteristics of the spectra. The three-dimensional (3-D) color spaces often used to represent visible colors suggest that this may be possible for the greater diversity of visible and IR colors. The familiar red/green/blue and cyan/magenta/yellow color spaces represent the multitude of visible colors as triplets of independent primary colors in which each dimension corresponds to the brightness of a different primary.

The idea of a visible color space can be extended into the IR by adding dimensions to accommodate the wider range of spectral wavelengths. When dimensions correspond to brightnesses of different wavelengths of visible and IR light, the idea of a visible color space can be generalized to a higher dimensional spectral feature space. A spectral feature space is an abstract complement to geographic space. The primary difference is related to the dimensionality. Traditional color spaces approximate visible colors in a 3-D (R, G, B or C, M, Y) space. Adding IR bands increases the dimensionality of the feature space accordingly. Quickbird pixels exist in a 4-D spectral feature space, whereas Landsat pixels occupy a 6-D space. Worldview will hopefully provide us with an 8-D space. Spectra collected by the hyperspectral imaging spectrometers discussed below exist in spectral feature spaces with more than 200 dimensions. The laboratory/field spectra have been down-projected into a 216-dimensional space. However, because of the redundancy that results from band to band correlations, not all spectral dimensions are of equal importance. Plotting the reflectance values of a collection of pixels at one wavelength versus the reflectance at another wavelength (e.g., visible red vs. NIR) results in a 2-D projection (silhouette) of the higher dimensional cloud of points that depicts the collection of pixels in the feature space. A digital camera imaging in three visible bands (red, green, and blue) produces triplets of primary color measurements that can be represented as a 3-D cloud of pixels in a red-green-blue feature space. Projecting higher dimensional spectra into lower dimensional spectral feature spaces provides an alternative means to quantify characteristics that may not be obvious in reflectance plots.

4.3.4 High-Dimensional Clouds

Spectral feature spaces provide a conceptual tool to represent different characteristics of target materials in terms of spectral shape. The shape of a spectrum is determined

by the relationship of each wavelength band to its spectral neighbors. Adjacent bands with similar reflectance values correspond to flat parts of the spectrum, whereas those with different values depict slopes resulting from the continuum or absorption features. Spectral bands with similar values at different brightness levels are, by definition, correlated. In many cases, spectrally adjacent bands are correlated because their bandwidths are too large to resolve reflectance differences between them. Statistically, correlation implies redundancy whereas variance is often considered analogous to information content. Linear transformations (rotations) that minimize covariance or correlation among dimensions are often used to condense information from high dimensional spaces to lower dimensional spaces in a predictable way. Principal component (PC) transformations (Preisendorfer, 1988) and maximum noise fraction transformations (Green et al., 1988; Lee et al., 1990) are commonly used for this purpose. Geometrically, these transformations are analogous to rotations and translations that minimize correlation (redundancy) and reveal variance (information). Statistically, the transformations concentrate as much variance as possible into the smallest number of independent dimensions possible. These concepts have been used to represent high-dimensional rock and mineral spectra in terms of their spectral shapes (Johnson et al., 1983, 1985; Smith et al., 1985). The low-dimensional feature spaces formed from the PCs of the spectra provide a means to represent independent components of spectral shape and to quantify the amount of variance (information) associated with each PC. In this sense, spectral feature spaces with dimensions corresponding to PCs of spectral wavelength bands are analogous to the Hue/Saturation/Brightness space obtained when the rectangular R/G/B or C/M/Y spaces are transformed to a cylindrical coordinate system in which the diagonal gray axis of the R/G/B space becomes the axis of symmetry representing overall brightness and the continuum of red, green, blue, cyan, magenta, and yellow hues are represented by angles about the axis of the cylinder.

Spectral feature spaces offer the additional benefit of representing spectral mixtures in terms of their primary components. When variations in spectral shape result from spectral mixing of targets within an instrument IFOV, the spectral mixing space of the low-order PCs also provides a physically self-consistent means to represent the spectral mixing process (Johnson et al., 1985; Smith et al., 1985). When combined with linear mixture models, this concept provides a basis for inverting mixture models and "unmixing" mixed pixels (Adams et al., 1986, 1993; Smith et al., 1990). When considered in the context of convex geometry, linear spectral mixture models can be cast as linear inverse problems (Boardman, 1989, 1990, 1993; Boardman and Kruse, 1994), thereby allowing the power of geophysical inverse theory (Parker, 1977, 1994) to be brought to bear on them. The power of spectral mixture modeling lies in its ability to translate physical measurements (radiance and reflectance) to physical abundance of the basic components of land cover (abundance of soil, vegetation, water).

When the reflectance spectra of the urban materials are compared with spectra of naturally occurring materials in a spectral feature space their physical characteristics are more apparent. In this chapter the spectral feature space formed from the low order PCs is referred to as a spectral mixing space following Johnson et al. (1985) and Smith et al. (1985). Figure 4.2 shows all 96 (some are occluded) of the anthropogenic material spectra (bright colored points) from Figure 4.1 in comparison to 956 spectra of naturally occurring materials (dark gray points) in a spectral mixing space of the three low order PCs. The supplemental spectra represent a continuum

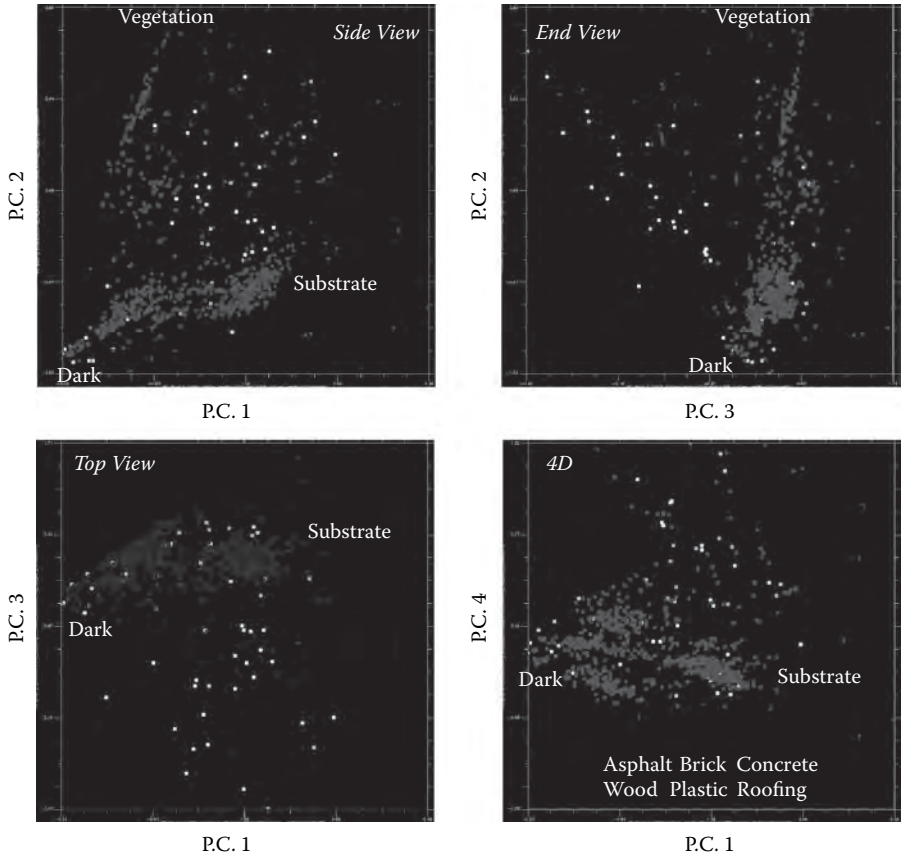

FIGURE 4.2 **(See color insert following page 324.)** Anthropogenic materials in spectral mixing space. Scatterplots of the four primary principal components (P.C.s) of the laboratory spectra in Figure 4.1 show the geometric relationship of the anthropogenic spectra (in color) to vegetation and rock and soil substrates (gray). The latter non-anthropogenic spectra form a sub-planar, triangular distribution resulting from mixtures of bright substrates (e.g., sand) and dense vegetation (e.g., grass) with varying amounts of darker, more absorptive material (e.g., Fe-Mg minerals) or shadow.

of spectral properties found in nature. The supplemental spectra include laboratory and field spectra of sediment and soil substrates from the Ganges-Brahmaputra delta, rock and soil substrates from the Gobi desert, and macroscopic mixtures of grass, soil, and nonphotosynthetic vegetation (NPV) material from the New York metro area. As will be shown below, these three complementary spectral libraries represent the most prominent spectral characteristics of a large variety of natural materials.

4.3.5 Endmembers and Mixtures

When visualizing the orthogonal projections of the first three PCs as in Figure 4.2, the 3-D topology of the mixing space becomes apparent. It takes the form of a partially concave triangular distribution with high albedo substrate, vegetation, and dark

surface (SVD) (absorptive, transmissive, or nonilluminated) targets at the apexes of the triangle. In terms of spectral purity, the spectra residing at the apexes of the triangle are the more spectrally pure endmembers and the spectra on the interior can be represented as spectral mixtures of these endmembers. Binary mixtures occur along the straight edges between the apexes. Binary mixing lines between the dark endmember and other endmembers show the effect of structural microshadow in vegetation and moisture content in the sediment and soil substrates. Because of the very limited number of laboratory/field spectra, the structure of this mixing space is rather sparse. At this point, it is important to distinguish between image endmembers and the true spectral endmembers they are assumed to represent. The image spectra at the corners of the distribution (cloud) are referred to as image endmembers on the basis of the relative difference in their spectral shape. In the case of laboratory spectra, they are known to be spectrally pure. In the case of the image endmembers discussed below, this is not necessarily true.

The locations of the individual spectra within the mixing space represent characteristics of their spectral shape. These characteristics may arise from spectrally distinct mixture components or they may arise from differences in VI geometry. The topology of the mixing space provides a consistent means to quantify the amplitude (albedo), slope and curvature (continuum), and absorption features of the spectra. The primary (low order) PCs represent the overall shape that accounts for most of the variance in the dataset, whereas the more subtle (narrower, lower amplitude) absorption features are represented by the higher order PCs. With low-dimensional sensors such as Landsat ETM+ (6-D) and Ikonos (4-D) or Quickbird (4-D), the primary 3-D mixing space contains almost all of the information in the imagery, but for hyperspectral sensors with tens to hundreds of dimensions the primary 3-D mixing space shows only the broad scale features of the spectra. More subtle distinctions are apparent only in the higher order PCs. The primary mixing space provides a useful geometry for representing spectral diversity and relative abundance of different types of materials — but it conceals a considerable amount of information with hyperspectral sensors. Examples are illustrated in the following section.

The mixing space distributions in Figure 4.2 quantify the spectral variability that is evident in the reflectance plots of Figure 4.1. Most of the anthropogenic spectra lie in or near the triangular plane spanning the SVD endmembers. Most of the plastic spectra lie well outside this plane. This makes physical sense because most of the anthropogenic materials are composed of, and therefore spectrally similar to, the naturally occurring materials in the supplementary spectra (gray). Plastics and a few of the other spectra lie outside this plane because their organic molecular structure produces combinations of absorptions not found in the spectra of the naturally occurring materials. As expected, roofing materials are scattered throughout the space because the class is defined on the basis of function rather than composition.

The commingling of the anthropogenic and nonanthropogenic spectra within the mixing space has important implications for their spectral separability. In the mixing space, spatial proximity implies spectral similarity. The fact that the different material classes do not generally cluster, and are intermingled with each other and with the nonanthropogenic spectra does not bode well for their spectral separability. Most spectral classification algorithms implicitly assume that materials in the

same class will form distinct, separable clusters within the mixing space. Multiple spectral modes (clusters) within the same class can result in spectral commingling that violates this assumption. Some nonparametric algorithms, such as support vector machines (SVMs), are able to accommodate multimodal classes resolvable with hyperspectral data (e.g., Gualtieri and Cromp, 1998; Huang et al., 2002; Foody and Mathur, 2004; Melgani and Bruzzone, 2004) and offer considerable potential for accommodating high-dimensional datasets. SVM classification is particularly well suited to urban hyperspectral imagery because it is robust to the presence of brightness gradients in airborne imagery (van der Linden, 2008). Nonetheless, the spectral similarity suggested by the commingling implies that spectral properties may not be diagnostic of a particular thematic class under certain conditions.

4.3.6 Principal Conclusions and Implications

1. *Urban land cover is characterized by the presence of both anthropogenic materials and naturally occurring materials in forms and combinations that do not occur in nature.* The urban environment also contains an abundance of spectrally distinct anthropogenic materials that do not occur in nature. Many of the materials in the urban environment are compositionally similar to materials found in nature but the form, scale, and geometric arrangement are generally different. Compositional similarity can make different objects spectrally indistinguishable. Variation of form can render compositionally identical materials spectrally distinguishable.
2. *Specific materials, and classes of materials, can be distinguished by combinations of narrow band absorption features superimposed on a spectral continuum shape.* The location, depth, and width of absorption bands may be diagnostic; the shape of the continuum less so. Spectral slope and curvature contain considerably less information — particularly when limited to VNIR wavelengths. Albedo alone is rarely diagnostic.
3. *Hyperspectral resolution is required to detect narrow band absorption features that distinguish different material classes.* Broadband sensors in general cannot resolve these absorptions with sufficient detail to distinguish materials uniquely. Full range (visible-SWIR) broadband sensors can resolve the slope and curvature of the spectral continuum sufficiently to discriminate broad classes of materials. Visible-NIR broadband sensors omit the more informative SWIR wavelengths and are limited to band-limited spectral slope.
4. *Spectral variability within material classes can be comparable to variability between classes.* Spectral variability within classes can result in commingling of different material classes in spectral feature space. When combined with variations in illumination and viewing geometry, this does not bode well for thematic classifications that assume unimodal spectral clustering of material classes. Algorithms that can accommodate multimodal classes (e.g., SVM) are much better suited to classification of urban land cover.
5. *Spectral ambiguity limits discrimination*. Materials with multiple narrowband absorptions throughout the visible to SWIR wavelengths (e.g., wood, plastic) offer the greatest opportunity for spectral discrimination.

Most construction materials do not satisfy this criterion, so uniqueness and spectral separability are important considerations for target identification. However, spectral separability of laboratory/field spectra represents a best-case scenario, free of atmospheric, illumination, and viewing effects. With knowledge of the BRDF of different materials, statistical separability analyses (e.g., Herold et al., 2004) can be combined with simulations of these effects to determine sensitivity of specific targets to spectral masking.

4.4 THE IMPORTANCE OF SCALE

The importance of spatial scale is central to remote sensing of any environment (Woodcock and Strahler, 1987). The information provided by remote sensing depends critically on two related spatial scales. The spatial scale of the sensor GIFOV determines what contributes to the individual radiance measurement associated with each pixel spectrum. The spatial scales of the individual objects (roofs, streets, trees, etc.) in the urban mosaic determine the extent of spectral mixing that occurs within the sensor IFOV that images them. Objects that are much larger than the GIFOV are spatially oversampled and represented as coherent features in the image and pure (compositionally homogeneous) spectra in the mixing space. Objects that are comparable to, or smaller than, the size of the sensor GIFOV are lost within mixed pixels and not spatially or spectrally resolved. However, these otherwise unresolved objects do contribute reflected radiance to the pixel measurement in proportion to their areal abundance. The spectra in the preceding section are effectively scale-independent because they represent spectrally homogeneous samples of specific materials. In urban environments, remote sensors on aircraft and satellites rarely have the opportunity to image spectrally pure pixels because of the spatial commingling of different land cover components at different spatial scales. Scale is particularly important in remote sensing of the urban environment where the objective may be detection of specific objects. Welch (1982) recognized systematic variations in the size of buildings and streets in many urban environments and proposed that a minimum spatial resolution of 5 m is generally required to discriminate individual components.

4.4.1 Characteristic Scales of the Urban Mosaic

The characteristic scale of a collection of objects refers to a spatial scale (or range of scales) that somehow characterizes the overall distribution of scales of all the objects in the collection. In this discussion, scale is equivalent to the size in a particular dimension (generally distance). Knowing the frequency distribution of scales in a collection of objects is important because it determines which objects can be resolved by a sensor of a given spatial resolution — and which cannot. Knowing the true frequency distribution of scales of objects in the urban mosaic is realistic only to a limited extent. One could obtain the distribution by measuring the size of every object in the mosaic — but this could quickly become tedious. Fortunately, a reasonable representation of the characteristic scale of objects resolved in an image can be obtained efficiently from the spatial autocorrelation of the image. Spatial autocorrelation is a statistical measure of scale-dependent spatial similarity. Given sufficiently high spatial resolution imagery of an urban mosaic, it is possible to estimate the characteristic

scale of objects in a finite area (window) of the image from the width of the autocorrelation function. If the window size is larger than most of the objects in the mosaic, but smaller than the image, multiple independent scale estimates can be obtained for different parts of the image. Given a sufficiently large number of estimates, the distribution of these estimates will approximate the true distribution of object scales. Figure 4.3 shows scale distributions obtained from Ikonos 1 m panchromatic imagery for a collection of 14 cities worldwide. For each city, a number of nonoverlapping 100 × 100 m windows were used to calculate area-normalized 2-D spatial autorcorrelation functions from which characteristic scale was estimated as the width of the central peak at 10% of its peak value (Small, 2003). The accuracy and robustness of this estimate can be easily verified by manually measuring dimensions of various objects

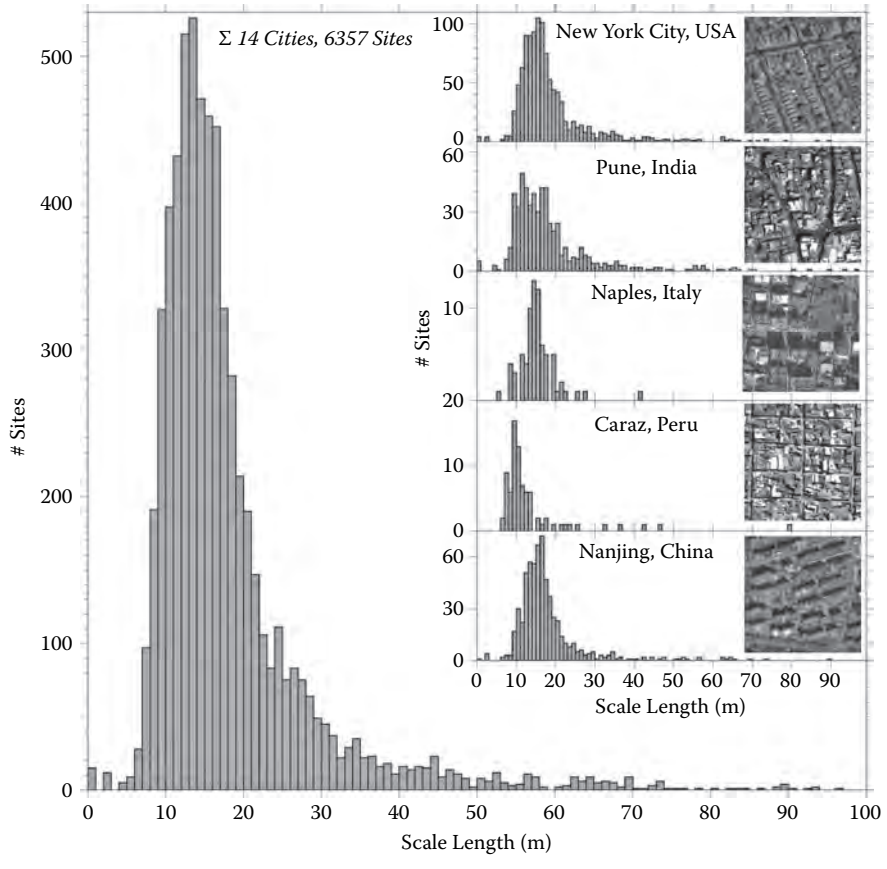

FIGURE 4.3 Spatial scale length distributions for 14 cities worldwide. Scale length estimates of the average size of discrete objects in the urban mosaic. It is estimated using the width of the spatial autocorrelation function derived from 1 m panchromatic imagery collected by the Ikonos sensor. Each estimate is based on a 100 × 100 m site. Each inset example is 200 × 200 m. Modal and median scale lengths are consistently between 10 and 20 m in the 14 cities used in this analysis. Almost all sites in all cities have scale lengths less than the 30 m resolution of the Landsat sensor.

in the images — without the tedium of trying to measure them all directly. There are, of course, caveats associated with these sorts of estimates (e.g., Goodchild, 1986), but they quantify and illustrate what can be observed in the Ikonos imagery.

Characteristic scale distributions for different cities are remarkably consistent. All of the cities have unimodal distributions, with modes significantly larger than the 1 m pixel size but skewed toward finer scales with long tails containing a few coarse scale patches corresponding to larger, spectrally homogeneous objects (e.g., warehouses, athletic fields, water bodies). Some small cities are not large enough to produce a large number of estimates (e.g., Caraz, Peru) but suggest somewhat smaller scales. For most cities, only partial coverage of the entire built area was available — but all the cities contained multiple types of urban land use, so they were functionally and structurally heterogeneous at scales smaller than the image. In spite of the diversity within and among the different cities, overall shapes and modal scales of the distributions are very similar. All 14 city distributions, a total of 6357 scale estimates, indicate that most objects imaged in these cities have spatial scales between 10 and 20 m. This is consistent with the findings of Welch (1982), but suggests that 5 m is the absolute bare minimum spatial resolution necessary to consistently resolve features in this size range. Sampling theory states that the sensor must have a GIFOV of less than half the smallest feature of interest — but in reality finer resolution is generally required because this so-called Nyquist criterion represents the limiting case. Aliasing is still possible above the minimum Nyquist sampling frequency. The paucity of scale estimates smaller than 5 m implies that 1 m is sufficient resolution, but the Ikonos images were not corrected for adjacency effect so the resulting image blur may bias this estimate slightly. The clear implication is that the vast majority of multispectral pixels imaged by moderate resolution (> 10 m) sensors such as Landsat (30 m) and SPOT (20 m) will be spectrally mixed pixels and will rarely image individual components of the mosaic coherently.

4.4.2 Scale, Resolution, and Spectral Mixing

The effect of this spectral mixing can be seen in the mixing spaces of images acquired by different sensors. Figure 4.4 illustrates this effect for three sensors with different spatial and spectral resolutions. The Hyperion sensor is a hyperspectral instrument on the EO-1 satellite measuring 220 spectral bands with 10-nm bandwidth between 357 and 2576 nm. In theory, it has a spectral resolution comparable to the resampled laboratory/field spectra shown in Figures 4.1 and 4.2, but in practice the true spectral resolution is somewhat lower because the noise level of the instrument and imaging process are considerably higher than that of the spectrometers used to collect the laboratory and field spectra. Hyperion's low signal-to-noise (S/N) ratio limits its ability to resolve subtle spectral features (Folkman et al., 2001) but it provides considerably more spectral information than the Landsat ETM+ or Quickbird sensors. The 7.7-km swath width does not allow for synoptic coverage of large cities but can image a wide variety of urban land covers along urban-rural transects. The nominal ground resolution is 30 m so the pixels it images will generally be mixed pixels — but the 10 nm bandwidth provides the hyperspectral resolution necessary to resolve a wide variety of spectrally distinct materials. The spatial and spectral diversity is suggested by the variability of the spectra shown on the sides of the hyperspectral cube in Figure 4.4.

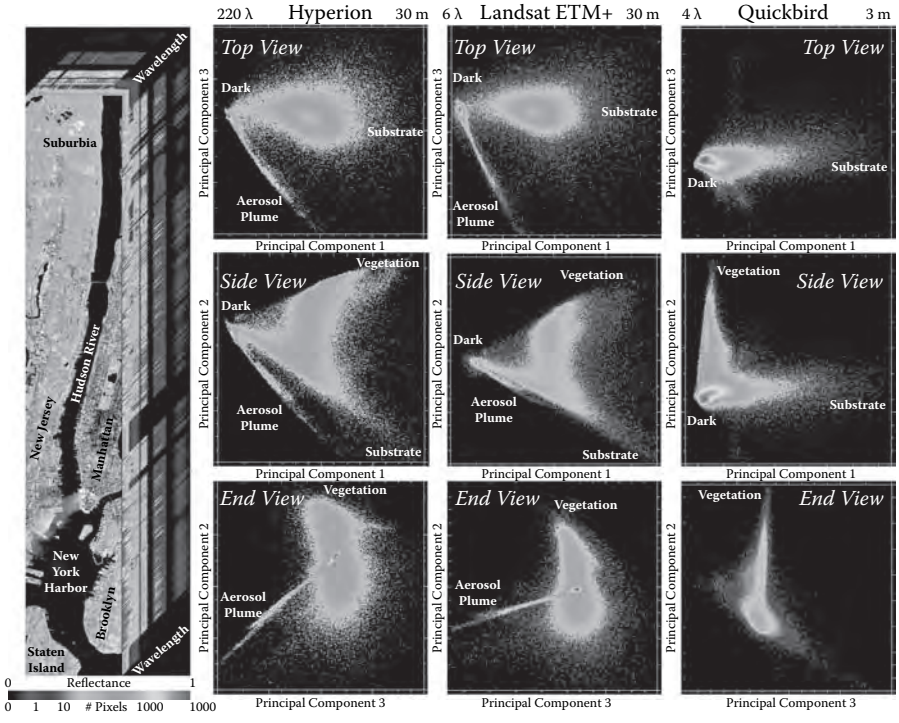

FIGURE 4.4 Spectral mixing spaces at different spatial scales and spectral resolutions. Hyperion hyperspectral cube acquired over New York City on September 12, 2001 shows spatial variability of radiance spectra for both dense urban (right edge) and sparse suburban (top edge) transects. Orthogonal projections of the 3-D mixing spaces of the 30 m Hyperion, 30 m Landsat and 2.8 m Quickbird reveal a similar triangular topology with substrate, vegetation and dark surface endmembers. The Hyperion and Landsat images have the same spatial resolution and were acquired nearly simultaneously under exceptionally clear atmospheric conditions. The Quickbird imagery covers a smaller area east of the Hudson River and was acquired on August 2, 2002 under similar illumination conditions. Aside from a prominent mixing line associated with the aerosol plume, the most significant difference in the mixing spaces results from stronger binary mixing lines in the Quickbird space.

In comparison, the broadband sensors can only approximate the spectrum with a few wide spectral bands. The ETM+ instrument on the Landsat 7 satellite images in six spectral bands over approximately the same spectral range with the same spatial resolution as Hyperion, so a comparison of the two can illustrate the spectral diversity of urban areas at both hyperspectral and hypospectral resolutions — albeit for thoroughly mixed pixels. Figure 4.4 compares spectral mixing spaces for coincident Hyperion and ETM+ images of parts of New York City (NYC) and New Jersey. These mixing spaces are directly analogous to that shown in Figure 4.2 but contain many more spectra. The 2-D projections of the 3-D space show pixel density within the space as color variations in which warmer colors correspond to exponentially greater pixel densities. The ETM+ and Hyperion images were acquired almost simultaneously under

exceptionally clear atmospheric conditions on September 12, 2001. A wide variety of land covers and urban environments are imaged along the transect — as well as the aerosol plume emanating from the collapse site of the World Trade Center at the southern end of Manhattan. For comparison, mixing space diagrams for a Quickbird swath of Manhattan and part of Brooklyn are also shown in Figure 4.4. The Quickbird swath was collected on August 8, 2002, under similar illumination conditions almost one year after the Hyperion and Landsat scenes were collected. The spatial extent of the Quickbird imagery does not include areas west of the Hudson River so it does not image the densely vegetated suburban areas in New Jersey, but is still useful to illustrate the effects of spatial resolution on the observed spectral diversity.

All three sensors represent urban spectral diversity with topologically similar mixing spaces — in the lower dimensions. Of course, Hyperion is capable of imaging a much higher dimensional mixing space than Landsat, and the Landsat space contains SWIR bands not imaged by Quickbird, but the structure of the spaces are consistent with the overall structure of the mixing space in Figure 4.2. All of the spaces show triangular structures with linear binary mixing lines emanating from the dark endmember(s) to the rock and soil substrate and vegetation endmembers. The structure is very similar to that of mixing spaces of diverse compilations of Landsat ETM+ (Small, 2004a, 2005), Ikonos MSI (Small, 2003), and EO-1 Hyperion (unpublished data) imagery from both urban and nonurban environments. Despite the large differences in spatial and spectral resolution of these sensors, analyses of the eigenvalue distributions associated with PCs of the imagery consistently indicate that more than 90% of the variance is associated with the first three dimensions of the mixing space. In each case, linear mixing among the three primary endmembers (rock and soil SVD surfaces) is indicated by the straight or concave edges of mixing space in the two primary dimensions (referred to as "side view" in the figures). Some nonlinear mixing is evident in the third dimension but the entire dimension only accounts for a few percent of the total variance of the image. Even the mixing between the aerosol plume and the underlying water of the Hudson River appears to be strongly linear in the September 12 images. This is not generally the case with normal clouds.

The pixel density variations within the mixing spaces of the images show the relative abundance of different reflectances in the image. The mixing spaces are basically histograms in 3-D and the topology of the distribution reveals the diversity of spectra within it. In comparison with the sparse mixing space constructed from the laboratory/field hyperspectra (Figure 4.2), the mixing spaces from the imagery reveal more structure and illustrate the tendency of the spectral mixing process to produce more continuous gradations among endmembers. The pixel density variations within the spaces show the distribution of different types of reflectance within the urban mosaic. Both Hyperion and Landsat clearly show the spectral effect of compositional variation from the urban core to suburban periphery as a mixing trend extending from moderately bright substrates (e.g., cement) to moderately dense vegetation (suburban trees). This gradation is not seen in the Quickbird mixing space because the imagery does not extend into the greener suburban areas west of the Hudson River. However, the finer spatial resolution (2.8 m) of the Quickbird sensor results in considerably less spectral mixing, so the Quickbird space shows more binary mixing between the dark endmember and the vegetation and substrates but far less between the latter two. This is to be expected because both vegetation and built surfaces have considerable microshadow effects even below the scale

of the 2.8 m Quickbird pixel. The pervasive presence of shadow is responsible for the consistently well-defined binary mixing lines emanating from the dark endmember.

4.4.3 Spectral Mixing and Thematic Classification

As alluded to above, the unavoidable process of spectral mixing has grim implications for thematic classifications that assume spectral homogeneity at pixel scales. The cardinal assumption of spectral thematic classification is that different thematic classes have distinct spectral properties that result in clustering within the spectral mixing space — and that the clusters do not intersect. The continuous variation within the mixing spaces in Figure 4.4 suggests that such clustering only occurs for water at 30 m scales and that the vast majority of pixels fall within a nearly continuous mixing space that is largely spanned by vegetation, rock and soil substrates, and dark surfaces. The dark surface endmember represents a fundamental ambiguity because it can be associated with either heavily absorptive (e.g., tar), transmissive (e.g., water), or nonilluminated (e.g., shadow) targets. This ambiguity further complicates the classification task because shadow is pervasive in almost all environments and varies with illumination conditions. The implication of Figures 4.1 and 4.4 together is that many urban materials are spectrally indistinguishable with broadband sensors — even under ideal conditions — and that the generally unavoidable process of spectral mixing tends to blur the distinction further for all but the largest, most homogeneous, objects in the urban mosaic. Increasing spatial resolution below the characteristic scale of the urban mosaic reduces the frequency of spectral mixing among objects considerably — but highlights the pervasive mixing of illuminated objects with their internal and external shadows. However, without sufficiently high spectral resolution the distinction of many materials cannot be resolved in the VNIR alone. The SWIR waveband contains considerable information related to the vibrational absorptions of many minerals (Clark, 1999) and lignocellulose absorptions in biomass (Roberts et al., 1993).

The combination of spatial and spectral degradation erases the majority of the information contained in the spectral properties of urban land cover. This loss of information, combined with the spectral similarity of many materials in the urban and nonurban environments (apparent in Figures 4.1 and 4.2), suggests the potential for considerable spectral confusion between urban and nonurban mixed pixels in broadband imagery of any scale. This may explain the generally low accuracies that have resulted from numerous attempts to map urban land cover in moderate resolution imagery using statistical classification algorithms designed for more spectrally homogeneous environments. The implications are considered in more detail below.

4.4.4 Spectral Unmixing and Physical Properties

Despite the pessimistic message of the preceding paragraph, moderate resolution broadband imagery such as Landsat ETM+ contain a wealth of spectral information about the urban environment and its constituent components. Even at subpixel scales, these constituents interact with the incident solar radiation and contribute to the aggregate reflected radiance field that the sensors image. In this sense, the mixed pixel contains valuable information about the different reflecting surfaces within its GIFOV. The mixing spaces in Figure 4.5 suggest good news in their form and

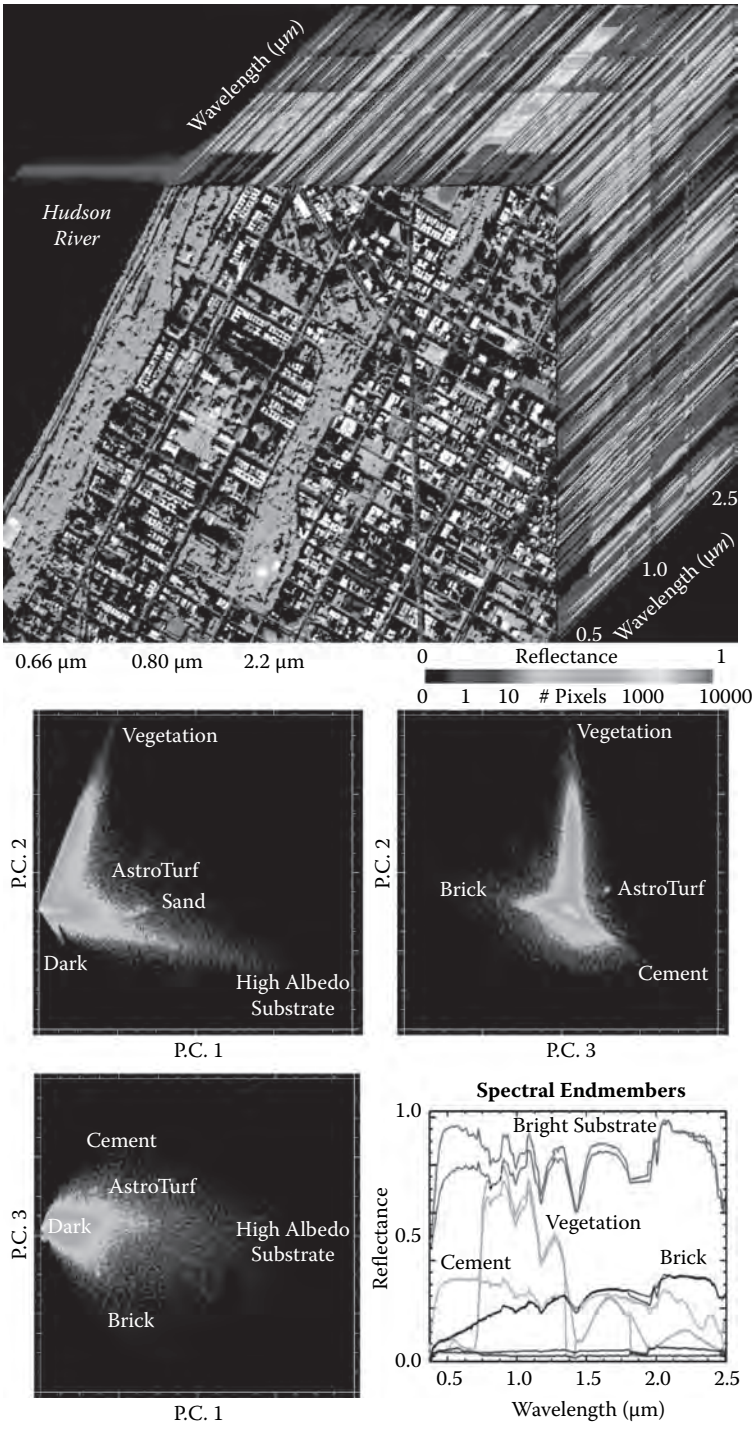

FIGURE 4.5

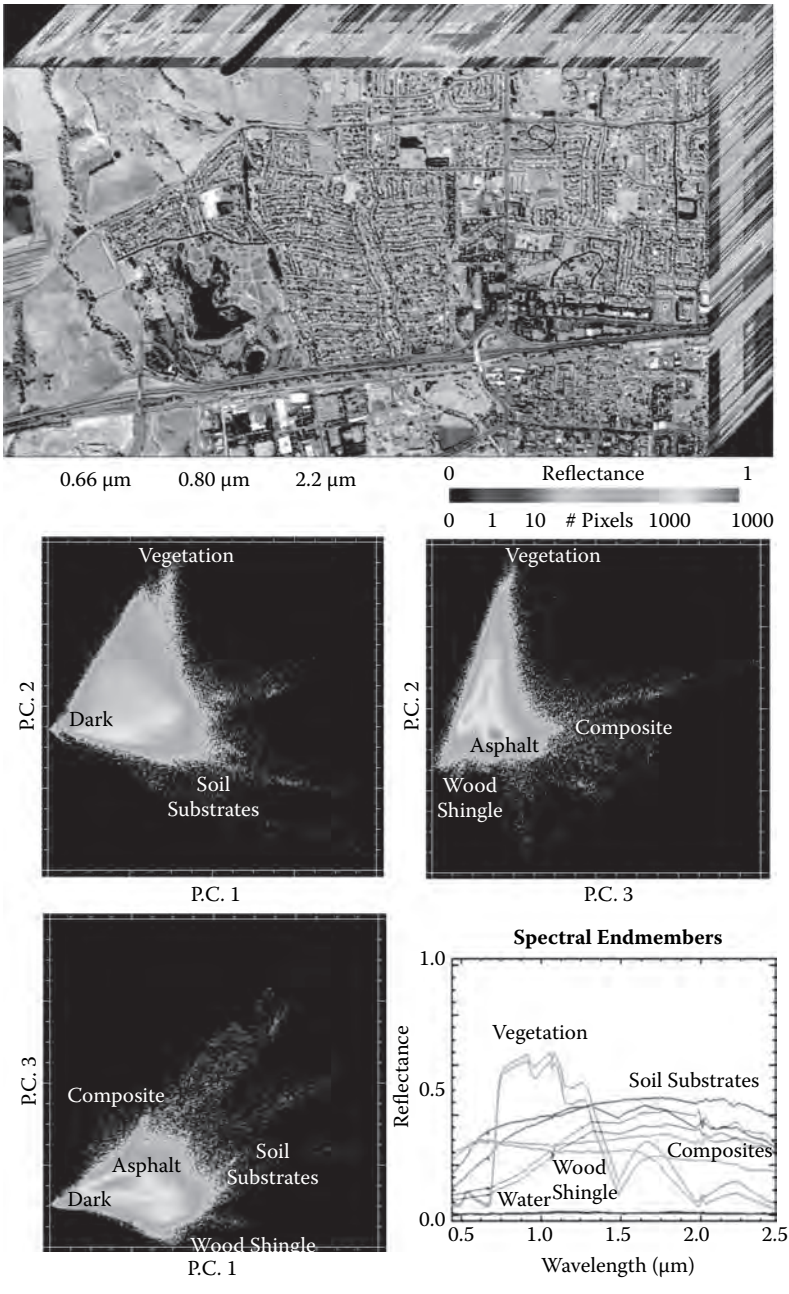

FIGURE 4.5 (Continued) (Opposite) **(See color insert following page 324.)** Hyperspectral urban diversity in New York City and California. AVIRIS hyperspectral cube shows the diversity and scale of urban reflectance in the densely built-up environment of upper Manhattan and in both Goleta and its undeveloped periphery. The "red edge" at 0.7 mm illustrates the abundance of fine scale vegetation in the urban mosaic. Mixing space topology has a skewed pyramid structure with the dark endmember at the apex and prominent mixing lines associated with asphalt and vegetation.

consistency. Straight edges imply linear mixing. As discussed above, the process of spectral mixing can be simulated with linear mixture models (Johnson et al., 1985; Smith et al., 1985) and linear mixture models can be inverted to yield estimates of endmember abundance (e.g., Adams et al., 1986, 1993; Boardman 1989, 1990, 1993; Smith et al., 1990; Gillespie et al., 1990; Settle and Drake, 1993). The consistency of spectral endmembers found in different environments suggests that the endmember fraction maps produced by inversion of linear mixture models may provide a quantitative basis for representing the physical properties of urban areas (e.g., Kressler and Steinnocher, 1996, 2001; Rashed et al., 2001; Small, 1999, 2001, 2002, 2003, 2005; Small and Lu, 2006).

Mapping and monitoring spatial and temporal variations in physical properties within urban environments can provide valuable synoptic information that would be costly, difficult, or even impossible to obtain otherwise. Examples include vegetation health, abundance and distribution, spatial extent of pervious surfaces and hydrologic parameters, as well as numerous inputs to the land surface models that drive climate and weather prediction models. Endmember fraction maps may also provide a basis for thematic mapping of urban land cover. Because the spectral endmembers correspond to the fundamental physical components of land cover (water, soil, vegetation, etc.), thematic classifications based on abundance of endmember fractions may be easier to define and validate than traditional classifications. This is discussed in more detail below.

4.4.5 Principal Conclusions and Implications

1. *Limited spatial resolution and the ubiquitous process of spectral mixing limit the ability of any optical sensor to discriminate specific targets.* Accurate detection requires both spatial and spectral oversampling to avoid aliasing. High spatial resolution hyperspectral (HSRH) imagery has considerable potential because it is capable of oversampling in both spatial and spectral dimensions and because substantial information is preserved in mixed pixels.
2. *The 10- to 20-m characteristic scale of individual objects in the urban mosaic limits the utility of moderate spatial resolution sensors for urban mapping — but this may be a small price to pay for synoptic coverage at urban scales.* Virtually all urban pixels imaged by SPOT, Landsat, and other moderate resolution sensors are mixed pixels but contain valuable information about their constituents. Hyperspectral imagery at the same scale could provide considerably greater detection capability — given sufficiently high S/N ratio anticipated for future ratio sensors such as EnMAP (Kaufmann et al., 2006; Kaufmann, personal communication).
3. *Multiresolution comparisons of moderate and high spatial resolution broadband and hyperspectral imagery reveal consistent mixing space structure.* The primary spectral endmembers corresponding to rock and soil substrates, vegetation, water, and shadow are present in each mixing space. Mixing between the endmembers is predominantly linear.
4. *Low-dimensional spectral mixing spaces provide a robust physical basis for analysis and comparison of diverse environments in terms of the*

fundamental physical components of land cover. Water, vegetation, soil, rocks, ice, and snow are the primary spectral endmembers — distinguishable even in broadband mixing spaces. They also represent the most physically distinctive components of land cover.

5. *Strongly linear mixing at macro scales allows for recovery of valuable information from mixed pixels.* Specifically, the relative abundance of the physical endmembers within each pixel. The physical properties of aggregates of these fundamental endmembers are directly relevant to physical process models in meteorology, hydrology, pedology, and ecology.

The preceding sections have focused on the challenges of measuring and categorizing urban spectral properties at different spatial and spectral scales with different sensors. The following sections discuss urban spectral diversity from the complementary perspectives of variability within the urban mosaic and the variability among different cities.

4.5 INTRAURBAN SPECTRAL DIVERSITY

The preceding sections discussed the spectral diversity of the individual components of the urban mosaic, and the challenges of identifying them with different sensors at different spatial and spectral resolutions. The following sections discuss the geographic diversity of urban spectral properties and what can be inferred from the available information at both local and global scales. In this section, intraurban diversity is considered from the perspective of variability at the scale of the individual object (building, street, tree, etc.) and the variety of spectral responses they produce when combined in different urban environments. In the context of this discussion, spectral diversity refers to the variety of distinct material spectra, whereas spectral variability refers to differences among spectra within an image that is not necessarily diverse. For example, tree canopy spectra may have considerable variability under different illuminations but would not be considered spectrally diverse relative to all spectra found in urban environments.

To represent the diversity of urban form, we consider both the dense urban core and the open urban periphery. This is accomplished by comparing HSRH imagery in both geographic space and spectral mixing space. In terms of spatial and spectral resolution, HSRH provides more complete information in both dimensions because it can image large numbers of individual components of the mosaic in sufficient spectral detail to characterize the variability of their physical properties.

The imagery used for the intraurban comparisons was collected by the National Aeronautics and Space Administration (NASA) Jet Propulsion Laboratory's (JPL) Airborne Visible Infrared Imaging Spectrometer (AVIRIS) sensor. AVIRIS is a state-of-the-art imaging spectrometer designed and built by NASA/JPL to image 224 spectral channels at 10 nm spectral resolution and 1 milliradian spatial resolution with S/N generally greater than 200 and often approaching 1000 (Green et al., 1998). Swath width and GIFOV depend on aircraft altitude but the ability of the Twin Otter aircraft to fly slowly at low altitudes allows for meter scale spatial resolution in some circumstances.

4.5.1 The Dense Urban Core

As an example of a dense urban core, we consider upper Manhattan in NYC. The section of Harlem shown in Figure 4.5(a) consists primarily of multistory (5–20) residential buildings transected by a grid of broad avenues and narrow cross streets. It contains two major commercial corridors, six universities and colleges, several large parks, and numerous vacant lots and public green spaces (e.g., community gardens), and part of the Hudson River. Structurally, it is similar to the urban cores of many large cities worldwide. The area was developed relatively rapidly in the late 19th and early 20th centuries as part of a planned urban expansion, so there may be greater consistency of building materials than in older cities built over longer periods and continuously refurbished. Most of the area imaged in this environment is building roof and broad thoroughfare. Much of the cross street and interbuilding spaces are in shadow or occluded. The considerable variability in building height — relative to building footprint and spacing — results in extensive shadowing and occlusion of small open spaces. At the scale of meters, the surface fractal dimension of this environment is relatively high so considerable shadow is unavoidable.

The area was imaged by the AVIRIS hyperspectral sensor at 10:53 a.m. local time on September 16, 2001 as part of the USGS/NASA/JPL emergency response to the collapse of the World Trade Center on September 11, 2001. The mission was flown as part of an attempt to determine the presence and distribution of carcinogenic asbestiform dust fallout from the cloud of ejecta that resulted from the collapse. A full report on the findings of the USGS/NASA/JPL team is available online at http://pubs.usgs.gov/of/2001/ofr-01-0429/ (accessed on February 26, 2008). At the flight altitude of 3800 m, AVIRIS has a spatial resolution of 4 m and a swath width of ~2.5 km. The radiance imagery was atmospherically corrected and converted to reflectance using the MODTRAN-based FLAASH algorithm (RSI, 2003) with a midlatitude summer atmosphere model. Both urban and maritime aerosol models produced reasonably similar results with spectral polishing (RSI, 2003). The hyperspectral cube and corresponding mixing space are shown in Figure 4.5(a) with the five primary spectral endmembers residing at the corners of the pyramidal 3-D mixing space.

The spectral diversity of the urban core is evident in both the spatial variability of the spectra on the sides of the cube and the structure of the mixing space. The sides of the cube show only the spectra along top (2.5 km) and right (2 km) edges of the image but they reveal considerable spectral diversity from pixel to pixel. The red edge at 700 nm reveals the presence of abundant fine scale vegetation within the mosaic. The characteristic scale of the core is generally in the 10- to 20-m range shown in Figure 4.3, so the 4 m AVIRIS GIFOV slightly oversamples the individual targets in the mosaic. Hence, it has the opportunity to sample spectra from individual objects. This is evident by the fact that individual buildings and streets are clearly resolved in the image. However, the accompanying mixing space in Figure 4.5(a) reveals large numbers of spectrally mixed pixels. The first three dimensions of the mixing space account for 83 + 14 + 1 = 98% of the spectral variance in the image.

The mixing space is dominated by two strongly linear binary mixing lines extending from the dark endmember to the vegetation and high albedo substrate endmembers. These mixing lines are analogous to those seen in the Quickbird mixing space

in Figure 4.4. The binary mixing with the dark endmember indicates that shadow has a very strong influence on the mixing process in this environment. To some extent, New Yorkers' predilection for dark colors, in both clothing and roofing material, contributes to this binary mixing with the dark endmember — but the effect of shadow is pervasive at all scales. Ternary mixing among all three of the primary endmembers does occur but much closer to the dark endmember. The dominance of the mixing space by the two binary mixing lines results from the fact that the brightest of the illuminated targets (vegetation and bright roofs) mix primarily with their adjacent shadows rather than other materials. This is to be expected from the moderate solar elevation (68°) and the pervasive presence of shadows resulting from the highly variable building height and canopy shadow in the forested parks. A third mixing line is also visible in the primary mixing plane corresponding to bright sandy soil in several ballfields. The brightness variations in the soil result from moisture content rather than shadow. Multiple spectra are plotted for each endmember to give some indication of endmember variability. As might be expected, variability is greatest for the high albedo roofing materials because they are generally planar, quasi-specular reflectors (Meister, 2000).

The third dimension of the mixing space reveals two additional spectral endmembers and some degree of nonlinear mixing. The secondary fourth and fifth abundant endmembers correspond to brick tiling and cement roofs. The asphalt on the avenues is darker and therefore difficult to distinguish from the other dark components in the mixing space (shadow, water, roofing tar). At a scale of 4 m, spectrally pure illuminated asphalt is relatively rare in this part of Manhattan because the broad northeast-southwest avenues generally have dense traffic around midday so mixing with vehicle reflectances is hard to avoid. Cross streets have much less traffic but are narrower and rarely receive direct illumination even in midsummer.

Several spectrally distinct clusters can be found even in the low-dimensional mixing space. Different types of metal, cement, and composite roofing are sufficiently homogeneous to form clusters, as does an Astroturf (artificial grass) athletic field and several sandy ballfields. A higher order endmember found in some abundance corresponds to the copper roofs on several of the older large buildings on the Columbia University campus. The campus is located on a topographic ridge so the copper roofs are widely spaced and well illuminated. Because the PC rotation is determined by covariance, spatially abundant materials have a greater influence on the rotation and are more likely to be detected in the low-order dimensions. Clustering of less abundant materials may occur but would be less obvious in the low-order 3-D mixing space.

4.5.2 The Open Urban Periphery

As an example of an open urban periphery, we consider Goleta, CA. Goleta is on the western edge of the Santa Barbara metro area and provides an example of the type of suburban environment on the periphery of many cities. Although the building style and construction materials are not necessarily widely representative, the diversity and scales of land cover are characteristic of many peripheral urban environments and smaller settlements. The area contains mixed-use residential, commercial,

and light industrial development transitioning to agricultural land and undeveloped open space with sparse vegetation and exposed soil. This area is a natural complement to the NYC area because it represents high spectral diversity at multiple scales as the suburban development transitions to undeveloped land cover on the periphery of the built environment. This area has been the focus of very thorough and extensive study by researchers at the University of California Santa Barbara in terms of spectral diversity of several classes of materials under different physical conditions (Herold et al., 2003, 2004, 2006).

The area was imaged by the AVIRIS hyperspectral sensor on June 6, 2000, at ~10:47 a.m. local time. The spatial resolution is 2 m. The image was atmospherically corrected with the MODTRAN radiative transfer code using the approach described by Green et al. (1993) and Roberts et al. (1997) (D. Roberts, personal communication). The 2 × 4 km hyperspectral cube and corresponding mixing space are shown in Figure 4.5(b) along with the five primary spectral endmembers from the corners of the low-dimensional mixing space.

The mixing space is similar to the NYC mixing space in terms of both topology and spectral endmembers. As in the NYC case, the mixing space is strongly two dimensional with 74 + 21 + 3 = 98% of variance in the first three PC with the dark to substrate mixing line on the primary axis (PC 1) and the vegetation mixing line on the secondary axis (PC 2). As in the NYC case, the binary mixing lines from the dark to the substrate and vegetation endmembers are strongly linear. However, in contrast to NYC, shadow is not dominant in this space and the mixtures are more evenly distributed throughout the mixing space. Greater uniformity of surface elevation, in both developed and undeveloped areas, results in far less deep shadow at pixel scales. At 2 m pixel scale, this area has a lower surface fractal dimension than the NYC study area. The area was also imaged under a somewhat higher solar elevation angle of 74° to further reduce shadow effects.

Whereas the two primary dimensions of the mixing space are dominated by vegetation and soil substrate brightness, two secondary endmembers — wood shingle and composite roofing — appear in the third dimension. Several spectrally distinct surfaces also form clusters at the periphery of the mixing space. Composite roofing and wood shingles are present in sufficiently great abundance to form complete mixing continua with the other endmembers. This, combined with the added spectral diversity of the undeveloped periphery and generally greater soil exposure (compared to NYC), results in a more pyramidal mixing space less dominated by the binary shadow mixing lines in the primary mixing plane (PC 1 and PC 2).

Within the interior of the space, three ternary mixing trends are visible. Strong mixing trends between green vegetation, NPV, and asphalt are clearly visible in the PC 3 versus PC 2 (end view) projection in Figure 4.5(b). The limb with higher green vegetation fractions (closer to the vegetation endmember) corresponds to pixels in both the developed and undeveloped areas. At lower vegetation fractions, the mixing trend bifurcates into two limbs with the more asphalt-rich mixtures occurring in the residential areas and the more NPV-rich mixtures occurring in the undeveloped areas — presumably from senescing wild grasses common throughout southern California. The asphalt-rich limb of the mixing line joins another more pure asphalt limb seen in the PC 1 versus PC 3 (top view) projection corresponding

to progressive increase in asphalt albedo along PC 1. This projection actually shows three separate albedo-varying trends with asphalt, soil/NPV, and green vegetation. The trend for vegetation seems to be primarily related to canopy closure and microshadow in the agricultural areas. The soil/NPV trend could result from variations in either soil moisture or microshadow modulating the aggregate albedo of the soil. The albedo variations along the asphalt mixing line are presumably the result of both partial shadow and asphalt weathering. The phenomenon of asphalt weathering, particularly in this study area, has been discussed extensively by Herold et al. (2004, 2006).

4.5.3 Spectral Dimensionality

Given the spectral and spatial oversampling provided by AVIRIS, we can consider the spectral diversity of these two environments in terms of the spectral dimensionality of the two datasets. Estimating the dimensionality of a noisy signal requires discrimination of signal from noise. The effective dimensionality that can be detected by the sensor is limited by the fixed number of bands of the measurements and does not necessarily represent the true dimensionality of the environment imaged. Redundancy between correlated measurements makes estimation of effective dimensionality more difficult. Oversampling guarantees redundancy. The distribution of spectral variance among PCs is often used as an indication of the effective dimensionality of multivariate data (Preisendorfer, 1988). The implicit assumption is that variance implies information, whereas correlation implies redundancy and that decorrelation by rotation provides an efficient means to distinguish information from redundancy. Dimensionality related to the partition of variance can be estimated from the eigenvalues of the covariance matrix if there is a clear distinction between the large eigenvalues representing presumed signal and the small eigenvalues representing presumed noise.

The transformations used to rotate multidimensional data can be determined by different criteria. Most PC transformations derive rotation parameters from the covariance matrix of the data. Some PC transformations use the correlation matrix to reduce the influence of outliers. Mixing spaces can also be rendered using a minimum noise fraction (MNF) transformation (Green et al., 1988; Lee et al., 1990). The MNF transformation is effectively a cascade of PC transformations (Green et al., 1988) designed to accommodate the fact that the noise components of some spectral bands may have larger amplitude than the signal components of other bands (Lee et al., 1990). The MNF transformation used most commonly is the complement to the maximum noise fraction transformation described by Green et al. (1988) but orders the resulting eigenimages by decreasing the S/N ratio rather than increasing S/N ratio as described in the original formulation.

Comparing eigenvalue distributions for different rotations of the HSRH imagery suggests similar spectral dimensionality. The NYC mixing space is strongly two dimensional in terms of variance with 83 + 14 + 1 = 98% of variance in the first three PCs (respectively) and a less high albedo substrate-dominant 58 + 38 + 1 = 97% of variance in the three low-order MNF components. In terms of spectral variance, the Goleta PC mixing space is also basically two dimensional with 74 + 21 + 3 = 98%

of variance in the first three PCs. The MNF transform yielded similar dimension scaling with 65 + 25 + 4 = 94% variance in the three low-order components. In both cases, the PC transforms allocate slightly more variance to the primary 3-D mixing space than do the MNF transforms. The PC transforms also ascribe considerably more variance to the first component than do the MNF transforms — presumably influenced by the high albedo outliers.

Comparing spectral endmembers from the corners of the mixing spaces shows that the primary SVD endmembers are virtually identical for PC and MNF transforms but the secondary endmembers are different in a couple of cases. Rather than cement and brick, the MNF transform of the NYC data shows concrete and copper roofs as secondary endmembers. The MNF transform of the Goleta data produces a less skewed topology with similar endmembers but a tighter, more prominent asphalt mixing line. The secondary endmembers of the NYC and Goleta datasets correspond to different materials (concrete and brick vs. wood shingle and composite) but their spectral shapes have some similarity (SWIR-bright wood and brick; visible-bright cement and composite). The perspective provided by linear transformations depends on the rotation parameters and different transforms use different criteria to obtain these parameters.

Consistency among transformations is generally more meaningful than the differences between them. All of these transformations derive rotation parameters from the data themselves so different datasets generally produce different rotations — sometimes very different. Although this can make intercomparison more difficult, it also lends greater credence to consistencies in the resulting mixing spaces. The PC mixing space and endmembers were used here for consistency with the rest of the examples.

The comparison of mixing spaces derived from different rotations further highlights the persistence of the structure of the mixing space across different urban environments. The secondary endmembers vary, as would be expected, but the SVD endmembers are always present and dominate the topology. The other persistent feature is the relatively continuous distribution of pixels within the mixing space. Clusters do exist but are relatively rare (or hard to detect). The presence of mixing lines extending toward the dark endmember suggests that the internal continuity of the mixing space results not only from spectral mixing within the IFOV but also from continuous variations in illumination and BRDF effects. Extensive study of the BRDF properties of urban materials by Meister and colleagues (Meister et al., 1999; Meister, 2000) highlight the importance of VI geometry in urban environments. Schiefer et al. (2005) and colleagues compared multiple view angle HyMap hyperspectral imagery for Berlin and documented considerable variability in reflectance resulting from brightness gradients as also described by Herold et al. (2006).

It is difficult to overstate the importance of geometry to imaging the urban environment. Roof geometry has been identified as a significant source of variability in both dense urban core environments (Heiden et al., 2001, 2007) as well as more open suburban peripheral environments (Herold et al., 2004). The wide variety of VI geometries in the urban environment effectively blurs the distinction of otherwise spectrally homogeneous materials within the mixing space. A key question for

target discrimination and classification concerns the extent to which these BRDF effects result in spectral similarity of different materials within the mixing space. If the BRDFs of different materials do not intersect in mixing space, they should be spectrally separable — in theory. To the extent that the BRDFs intersect and become spectrally indistinguishable, an unavoidable source of error exists.

4.5.4 Principal Conclusions and Implications

1. *The spectral and spatial oversampling provided by high-resolution hyperspectral imagery has the capacity to distinguish specific materials and classes within the urban mosaic but only if they are actually spectrally distinct.* Many are not.
2. *The spectral mixing space topology of high-resolution hyperspectral data confirms the multiscale persistence of the triangular SVD structure — but does not reveal the true spectral dimensionality.* Covariance-based transformations are biased in favor of representing the most abundant and spectrally distinct classes of spectra — the SVD endmembers. These three fundamental endmembers are complemented by a variety of more exotic but less abundant endmembers that have less influence on the rotation and may be less obvious in the mixing space if they reside nearer the dark apex of the mixing space. The low-order PCs may contain the vast majority of the variance but the remaining few percent may have value far exceeding its variance fraction.
3. *Spectrally distinct materials form clusters in the hyperspectral mixing space — but the clusters are blurred by spectral mixing and by variations in VI geometry.* The minimal clustering observed in the low-dimensional mixing space reveals the broad similarity of many spectral shapes as well as the pervasive influence of the BRDF characteristics of different materials.
4. *Variations in overall brightness resulting from illumination and shadow can account for much of the variance in urban hyperspectral imagery.* Deep shadow is pervasive in urban cores — less so on the periphery.
5. *Higher order endmembers from different urban environments can have similar spectral shapes (slope, curvature) but correspond to compositionally different materials.* The rotations used to render the mixing space are based on variance, not physics. This can result in fundamental ambiguities related to viewing geometry and illumination effects.
6. *The mixing space representation of optical spectra is an important complement to geographic space — but it does not fully lift the curse of dimensionality.* It offers the benefits of being informative, efficient, and repeatable at the cost of data dependency and nonuniqueness.

4.6 INTERURBAN SPECTRAL DIVERSITY

The preceding section examined intraurban spectral diversity at the scale of individual components of the urban mosaic and the differences in their physical composition that give rise to their spectral properties. The combination of high spatial

and spectral resolution provided by AVIRIS illustrates the diversity of spectral responses associated with materials commonly found in urban areas and it shows their relative abundance in different types of urban environments. However, the comparison of two relatively small example locations, no matter how diverse, is not necessarily representative of the spectral diversity of urban areas worldwide. The basic components of urban environments (e.g., buildings, streets, infrastructure) may be the same worldwide but building materials and styles of construction vary widely among cultures and socioeconomic settings. To draw general conclusions about urban spectral characteristics, it is necessary to consider a wider variety of urban environments than NYC and Santa Barbara. Unfortunately, high-resolution hyperspectral imagery is not widely available worldwide — yet.

The Thematic Mapper (TM) and ETM+ sensors carried on the Landsat satellites provide a 25-year archive of multispectral imagery for every city on Earth. Dekameter (10–100 m) resolution broadband sensors, such as those carried by Landsat, Aster, and SPOT, may have sufficient spatial and spectral resolution to distinguish urban land cover from the variety of natural land covers in the nonbuilt environments within which cities are imposed. If so, they could provide an invaluable asset for the study of urban structure and evolution at global scales for a period in which the world's urban population has tripled. Using this resource to map and monitor urban structure and evolution requires a robust, quantitative, repeatable way to distinguish urban from nonurban land cover. This raises the question of which aggregate spectral properties might be generally representative of urban environments worldwide. We can consider this from the perspective of urban spectral diversity in both geographic space and spectral mixing space.

4.6.1 Diversity in Geographic Space

We consider geographic spectral diversity by comparing a pseudorandom collection of 30 cities worldwide. Each city is represented by a 30 × 30 km subscene of multispectral imagery collected by Landsat 7 between 1999 and 2001. In most cases, the dense core and open periphery are completely contained in the image as well as some of the surrounding environments. In a few cases (New York, Phoenix, Sao Paulo, San Francisco), the densely built-up areas are much larger than the image so the location is chosen to illustrate a gradient from dense core through open periphery. In some cases, the city is clearly surrounded by undeveloped land or water but in many cases the urban area is set within a much larger regional metroplex and cannot be meaningfully defined on the basis of its administrative boundary or even population density. The selection of cities is pseudorandom in the sense that it was chosen on the basis of both geographic diversity and availability of cloud-free imagery circa 2002 when the data were compiled. A couple of cities have some cloud cover (Taipei, Santo Domingo), but were included for contrast with other cities in comparable physical or socioeconomic settings.

Identical processing and analyses were applied to each city to facilitate comparison. All of the images are calibrated to exoatmospheric reflectance to remove the effects of seasonal and latitudinal illumination differences. No atmospheric correction is attempted because reliable atmospheric parameters are not generally available

for many (perhaps most) of the cities and validation of the correction would be impractical. In a few cases (Lagos, Santo Domingo, Taipei), strong atmospheric effects are apparent in the image but the majority are relatively clear. The purpose of the comparison is to illustrate similarities and differences in urban spectral properties that are apparent even in the presence of mild atmospheric effects. Twenty-seven of the 30 cities were included in a comparative spectral mixture analysis by Small (2005). Three additional cities (Dhaka, Essen, and Phoenix) were included to increase diversity and facilitate comparison with other more detailed studies of the individual city. The study described by Small (2005) provides a more detailed comparative analysis of the spectral characteristics of each city. The purpose of this comparison is to highlight similarities and differences among the spectral properties of the cities.

Qualitative side-by-side comparison of the cities in geographic space illustrates both interurban and intraurban diversity and suggests that they are comparable in magnitude for most of these cities. Figure 4.6 shows false color composites of 28 of the 30 cities. The blue, green, and red channels of each image correspond to visible (ETM band 2), NIR (4), and SWIR (7) reflectance, respectively. Two cities (Tianjin and Taipei) are omitted to preserve the aspect ratio of the figure but are included in the mixing space analysis and available with the other images at the URL given below. Each image was subjected to the same 1% linear stretch (on the combined histogram) to enhance contrast of the midtones. Identical calibration and enhancement facilitates visual comparison on the basis of color. It is immediately apparent that considerable spectral diversity exists both within and among the different cities. The spectral diversity also spans a wide range of spatial scales. At the scale of the entire 28 image composite viewed simultaneously, only coarse-scale variations are obvious. At the scale of four images viewed simultaneously, a finer, intermediate scale of variation is apparent. Viewed at full resolution of one image pixel per screen pixel, finer-scale variability becomes visible. The full-resolution images in Figure 4.6 are available online at http://www.LDEO.columbia.edu/~small/Urban/Cities. This scale varying heterogeneity is consistent with the high fractal dimension of urban structure and land use (Batty and Longley, 1996) but it precludes the notion of strict self-similarity. The spectral consequences of this scaling are discussed below.

The most clearly identifiable feature in most of the cities is the urban core. It generally appears darker than surrounding areas. Comparative analysis of high spatial resolution imagery indicates that this results from the abundance of shadow in areas with more street canyons and variable building heights (Small, 2003). Although the core is often darker than surrounding areas, it does not show a single consistent hue in the false color composites shown in Figure 4.6. In most of these examples, the hue even varies within the darker areas although it is harder to see without more severe stretching. A comparable variability in hue can also be observed in the somewhat brighter areas surrounding the core in most of these cities.

Discrete urban/nonurban boundaries are not obvious for most of the cities. In many cases, a central core can be identified but in most cases a well-defined edge to the city is not apparent. Numerous sharp transitions in land cover are visible in these images, and many are clearly boundaries between densely and sparsely developed land areas but very few constitute a closed boundary fully separating the city from its surroundings. In many areas, on almost every image, transitions from an urban

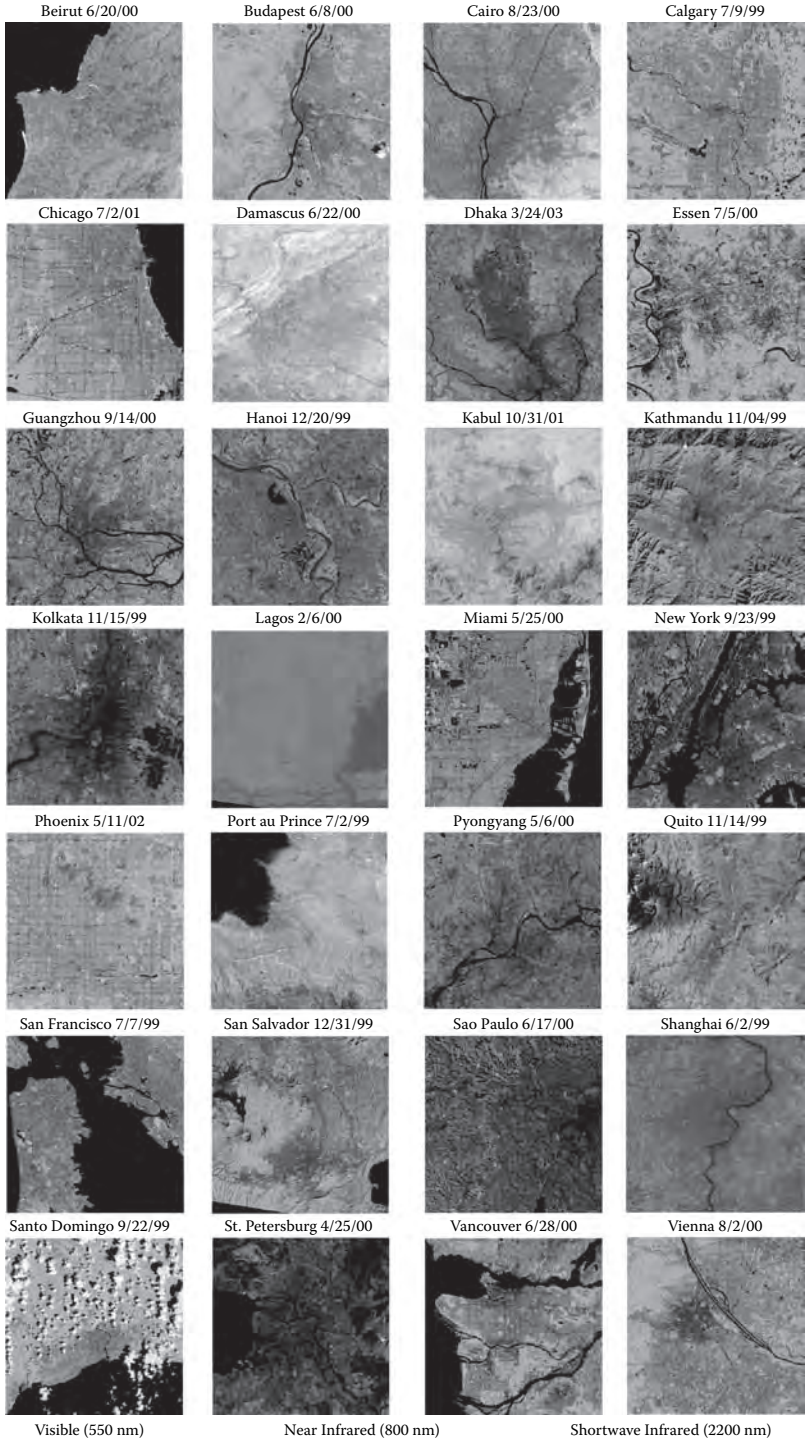

core to undeveloped land cover correspond to spectral gradations. In many cases, the transitions correspond to steep population density gradients (e.g., Guangzhou, NYC, Sao Paulo) but not necessarily to uninhabited densities. Given some ancillary information (e.g., maps), it may be possible to identify spectral transitions associated with specific land cover changes corresponding to population density gradients, but there is no obvious spectral boundary separating urban from nonurban land cover that is consistent in all, or even most, of the cities in Figure 4.6. However, in spite of the inconsistency, an experienced interpreter may feel comfortable distinguishing between anthropogenically modified urban land use and undeveloped land cover in many of these examples — possibly on the basis of image texture. Nonetheless, it is apparent from the spectral diversity that visual interpretation of urban extent would be extremely subjective without clearly defined, measurable criteria and a verifiably repeatable procedure. This is an example of a situation in which human perception is very different from measurement.

4.6.2 Diversity in Spectral Space

Transforming the ETM+ images of these 30 cities from geographic space to spectral mixing space reveals that almost all of these cities have mixing space topologies resembling the ternary SVD topology seen throughout this chapter. A comparative spectral mixture analysis of 28 of these cities showed that all of them have very similar SVD endmembers (Small, 2005) — although the completeness of the triangular topology varies according to relative abundance of spectrally pure vegetation or rock/soil substrate. Specifically, several cities in arid and semiarid environments (Beirut, Cairo, Damascus, Kabul, Phoenix, Quito) have little or no dense natural vegetation and a couple of the cities were imaged when vegetation was largely senescent (Pyongyang, St. Petersburg, Tianjin). In every case, a pronounced mixing line exists between a very consistent dark endmember and a more variable bright substrate endmember. This mixing line is analogous to the gray axis in 3-D color spaces (e.g., RGB, CMY, HSV). The persistence of the SVD topology across different spatial and spectral resolutions for a wide variety of urban areas is analogous to that seen in global mixture analyses of nonurban land cover with Landsat (Small, 2004a). The implication is that urban areas generally contain all three fundamental spectral endmember types in abundance sufficient to approximate global spectral diversity for nonpolar land areas. A direct comparison of the mixing spaces of the global compilation of urban and nonurban ETM+ imagery can illustrate consistent differences (Figure 4.7).

The persistence of the triangular mixing space topology and the SVD spectral endmembers is a fundamental characteristic of urban reflectance. The examples provided here demonstrate its consistency among and within a wide variety of urban environments as measured by several different instruments at different spatial scales. Although conceptually similar to the vegetation–impervious surface–soil (V-I-S)

FIGURE 4.6 (Opposite) **(See color insert following page 324.)** Inter-urban comparison of 28 cities as seen by Landsat 7. Each 30 × 30 km subscene has been calibrated to exo-atmospheric reflectance and enhanced with the same 1% linear stretch so colors are comparable. Full resolution color images available at http://www.LDEO.columbia.edu/~small/Urban

model proposed by Ridd (1995), it is fundamentally different. The V-I-S model represents the *functional* components of urban land cover by their physical properties. The V-I-S components are not equivalent to the SVD endmembers. The SVD endmenbers emerge from analyses of the spectral mixing spaces as illustrated throughout the chapter. In contrast, the V-I-S components are defined on the basis of their functional properties as land cover. They are not equivalent to the spectral endmembers because they are not spectrally distinct. Specifically, impervious surfaces do not represent a single spectral endmember. Imperviousness is not a spectral property but a hydraulic

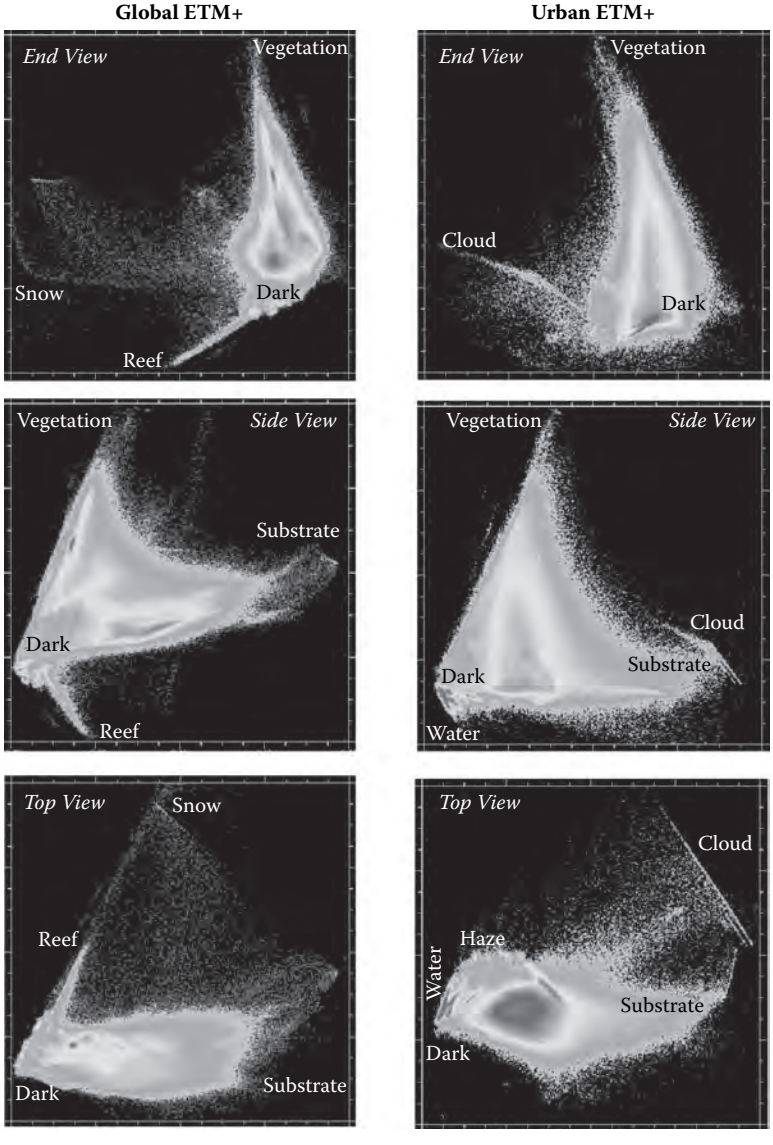

FIGURE 4.7

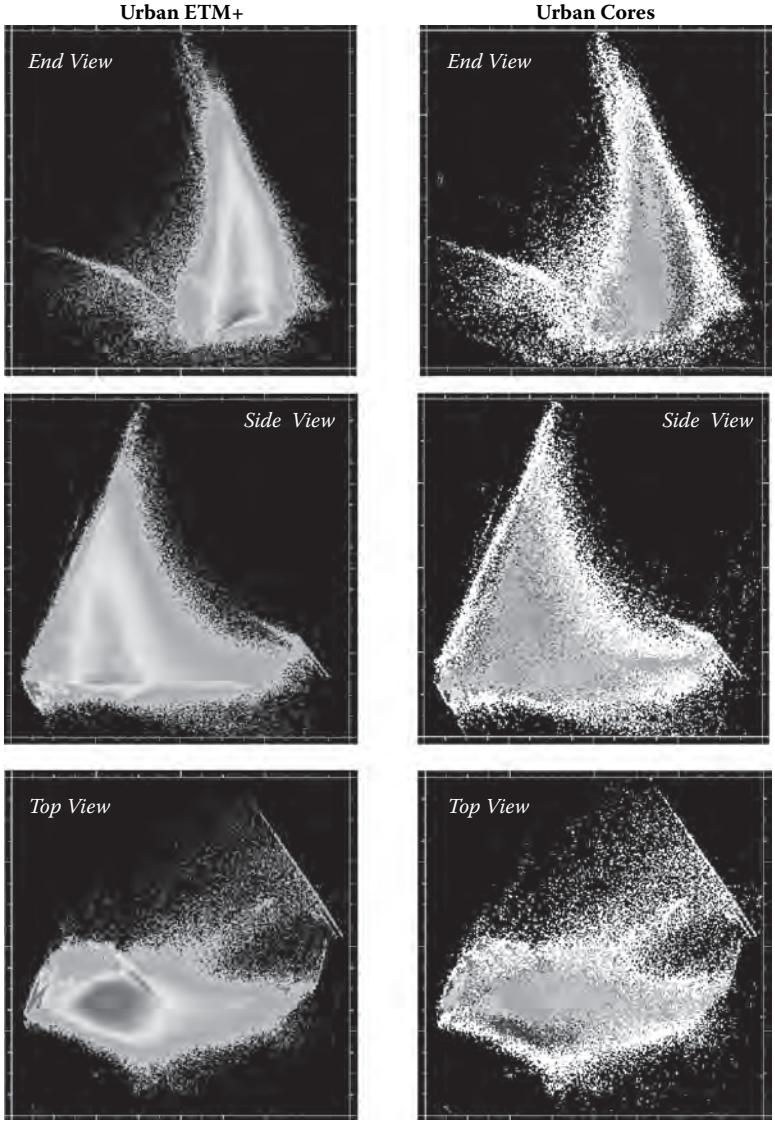

FIGURE 4.7 (Continued) (Opposite) **(See color insert following page 324.)** Comparison of Landsat ETM+ global composite mixing spaces for urban and non-urban environments for 30 cities, and for mixing spaces with 9×9 km cores of each of the 30 cities in the composite. Aside from spurs associated with reefs, ice and snow in the global composite, the topology of the mixing spaces is strikingly similar. The non-urban space has three distinct internal clusters (not including water) along vegetation and substrate mixing lines but the urban space has only one cluster for built-up cores. Note that even the most densely built-up cores together span almost the entire mixing space.

property. As illustrated in Figure 4.1, impervious surfaces have considerable spectral diversity and yet are often spectrally indistinguishable from pervious surfaces. This was explicitly acknowledged by Ridd (1995) when the V-I-S model was proposed,

but is often overlooked in later analyses that attempt to use the V-I-S model as the basis for a spectral mixture model. The V-I-S conceptual model does not provide an adequate basis for a spectral mixture model because there is no single impervious surface that could serve as a spectrally distinct endmember. There are, in fact, a wide variety of impervious surfaces but many of them are spectrally indistinguishable from pervious surfaces. In urban environments there is another ambiguity related to the dark surface endmember. The dark endmember represents an unavoidable ambiguity because it denotes the absence of a reflectance signature. As such, it can represent absorptive, transmissive, or nonilluminated (shadow) surfaces. Unfortunately, a number of impervious surfaces (e.g., roofing tar, tar paper, fresh asphalt) are also largely nonreflective so the misidentification of impervious surface is exacerbated. Although the V-I-S model is a valuable conceptual model for urban land cover, it does not provide a sufficient general basis for a spectral mixture model.

Urban areas do not appear to have a single, consistent spectral signature but rather appear to be characterized by their fine scale spectral heterogeneity. Figure 4.7(a) shows a side-by-side comparison of the global urban and nonurban mixing spaces derived from compilations of ETM+ imagery. The composite mixing spaces are nearly identical in form — although the urban space lacks the mixing lines associated with ice and snow and the spur associated with reefs. Otherwise, the three primary endmembers are consistent and the topology is very similar. The variation of the third dimension (PC 3) with overall brightness (PC 1) reveals the presence of two intermediate albedo endmembers with slightly convex upward continua with opposite spectral slopes similar to the secondary substrate endmembers shown in Figure 6 of Small (2004a). Whereas identification of specific materials from Landsat spectra is speculative at best, the shapes of the continua are consistent with those of high visible reflectance cement and SWIR-bright NPV.

It is interesting that none of the mixing lines or internal clustering of the nonurban global mixing space is present in the urban mixing space. This suggests that the interior of the urban mixing space is more spectrally mixed than that of the nonurban space — although it is not necessarily more spectrally diverse. Spectral heterogeneity and spectral diversity are not equivalent. When comparing these mixing spaces, it is important to remember that the density variations within the space result from the land cover distributions in the 30 subscenes that went into each compilation. The relative abundances of these landcover types in the 30 subscenes do not necessarily represent their global abundance because the subscenes were chosen on the basis of spectral and environmental diversity — not in proportion to global land cover abundance. Nonetheless, the rapid convergence of mixing space topology demonstrated by Small (2004a) suggests that the spectral diversity of the subscenes approaches the true global diversity.

The most obvious differences between the urban and nonurban mixing spaces are related to the internal structure. The nonurban mixing space has a very complex structure with numerous high-pixel density modes and mixing trends connecting them. In contrast, the urban mixing space is dominated by one large mode resembling a broad mixing trend extending from a wide range of dark-substrate mixtures along the gray axis upward to a more restricted range of relatively lush vegetation/shadow mixtures on the dark-vegetation axis. A weak mixing line is visible within this central mode. The top view projection (PC 3 vs. PC 2) shows the mixing line

extending to a strongly convex, nearly circular, edge that extends back toward a multimodal distribution of dark endmembers. The multiple modes of the dark endmember correspond to different water bodies in different cities with different reflectance properties. The mixing trend responsible for the convex appendage on the mixing space is caused by atmospheric scattering and absorption in a few of the images with thick atmospheric haze (Hanoi, Lagos, Calcutta). Most of the subcircular mixing trend is associated with Lagos alone.

The similarity of the global urban and nonurban mixing spaces suggests that the spectral diversity of urban areas — and their immediate surroundings — approaches the global spectral diversity resolved by the ETM+ sensor. This implies that urban areas may contain or be surrounded by a near-global diversity of land covers. However, the centralized clustering shown by the internal structure of the urban mixing space suggests that the cities themselves may occupy a distinct region within the mixing space. A comparison of the overall urban mixing space with 10 × 10 km subsets taken from the center of each urban area indicates that this is not the case. Figure 4.7(b) shows the spectral diversity of these 10 × 10 km urban subsamples (grays) superimposed on the overall mixing space (white). This is shown even more clearly in the color version of the figure available at www.LDEO.columbia.edu/~small/Urban/UrbanMap. Although there is clearly some central tendency to individual urban centers, most of the individual centers span a wider range of spectral diversity than the extent of the core suggests. It appears to be an emergent characteristic of the aggregation of all the cities rather than a characteristic of any one of them.

Another characteristic of many of the cities is a radial vegetation density gradient spanning from the dark core to its periphery. A vegetation abundance gradient is present, to varying degrees, in most of the cities but varies widely in form and magnitude. The appearance of a gradient is enhanced in cities surrounded by dense vegetation in the form of nonurban forest or agriculture (many of them), but can be verified in the spectrally heterogeneous built area with vegetation fraction maps (Small, 2005). To some extent, the vegetation gradient also corresponds to dark fraction diminishing radially outward from the core(s). This could result from increasing distance between buildings allowing more illumination (both direct and scattered) of the street level land cover between buildings casting shadows. In temperate environments, increased open space between buildings is often accompanied by increasing density of trees — both tended and in residual fragments not developed (e.g., riparian corridors and rugged topography). At the peripheries of many cities the abundance of untended herbaceous vegetation in open spaces also results in increased vegetation fraction at the 30-m pixel scale.

4.6.3 Principal Conclusions and Implications

1. Qualitative comparison of 30 diverse cities in Landsat ETM+ imagery suggests that intraurban spectral diversity is comparable to interurban diversity.
2. Urban cores are generally darker than peripheries — but are still spectrally diverse and do not have a consistent reflectance signature. Cores are generally darker because of pervasive shadowing resulting from canyons and building height variations, but low albedo roofing and asphalt paving

contribute by absorption of direct and scattered illumination. Urban canyons are light traps.

3. The urban periphery is generally fractal and gradational making unambiguous identification difficult on the basis of spectral properties alone. Gradational transitions in reflectance between the urban core and periphery are apparent in most cities but are not isotropic or monotonic in all directions. Discrete urban boundaries are rarely discernable at moderate spatial resolutions. This suggests that cities might be more accurately represented as continuous physical entities rather than discrete thematic entities.
4. Comparison of composite Landsat ETM+ spectral mixing spaces shows that urban spectral diversity approaches global spectral diversity in terms of fundamental physical endmembers. The overall topology of the primary mixing space is the same and the primary SVD endmembers are nearly identical but the internal structure is substantially different. Several distinct mixing continua are discernable within the nonurban mixing space. The urban mixing space is dominated by a single central mode confirming the dominance of mixed pixels.
5. The most consistent urban spectral characteristic is heterogeneity — particularly at spatial scales coarser than 20 m. Relative to nonurban land covers, urban spectra are more spatially compositionally heterogeneous at both subpixel and multipixel scales.
6. Pervasive multiscale spectral heterogeneity precludes accurate urban extent mapping on the basis of spectral consistency of specific reflectance signatures. The combination of spectral diversity and heterogeneity results in spectral ambiguity (nonuniqueness), which leads to classification error. Spectral ambiguity is generally unavoidable because cities are composed of materials often spectrally indistinguishable from nonurban land cover. The combination of spectral mixing and spectral heterogeneity further complicates the problem.

4.7 QUESTIONS

The observations discussed above raise several questions relevant to urban mapping and monitoring with optical imagery.

Might aggregate urban land cover have invariant spectral properties?

In spite of the spectral diversity and heterogeneity present at multiple scales, does the aggregate of this diversity have any emergent spectral properties that may be invariant to differences in illumination and view angle? If so, they may be very difficult to discern with broadband imagery but the higher spectral dimensionality provided by hyperspectral imagery may capture them. A comparative multitemporal analysis of even moderate resolution hyperspectral imagery may be able to isolate such properties from a manageably small number of cities.

Can spectral mixing spaces be generalized to higher dimensional parameter spaces to incorporate nonspectral and nonphysical dimensions of urban dynamics?

Increasing availability of geospatial data makes it possible to relate physical and nonphysical parameters to each other on the basis of spatial location. The concepts and analyses used to understand reflectance properties of the urban mosaic could be extended to nonspectral, or even nonphysical dimensions (e.g., Small, 2004b). To some extent, this has been done in different disciplines for many years but not necessarily linked by geographic location. The mathematical and geometric tools used to manage the curse of dimensionality with optical imagery may provide useful approaches to understanding other processes related to the diversity of the urban environment. Might the high-dimensional parameter space provide a basis for linking physical, socioeconomic, and perhaps cultural and historical dimensions of urban evolution and dynamics?

What is urban?

Can urban areas be defined on the basis of physical criteria? If so, which criteria might be detectable in optical imagery and under what conditions? Defining urban environments in terms of physical criteria would facilitate systematic, multiscale global mapping of not only urban extent, but also its physical properties. The benefits of a systematic, multiscale, quantitative depiction of the physical properties of urban environments worldwide could significantly advance our understanding of urban meteorology, hydrology, and ecology. If this mapping could be applied to the vast archive of moderate resolution imagery, it may be possible to conduct quantitative change analyses to extend urban mapping into the time dimension. Applying such an analysis to the 25+-year archive of Landsat imagery could provide a quantitative physical depiction of the process of urban evolution worldwide. However, many important questions about urban dynamics are not related to physical properties, so additional criteria are essential to developing a "universal" mapping of urban areas.

ACKNOWLEDGMENTS

The broad range of observations summarized in this chapter would not have been possible without the multitude of contributions from researchers cited throughout the text. For published research, the author is grateful for the contributions of all the researchers cited in the references. Additional thanks to Patrick Hostert, Sebastian van der Linden, and an anonymous reviewer for helpful comments and criticisms. The author gratefully acknowledges the support of the Palisades Geophysical Institute and the Doherty Foundation. Much of the research described here was funded by the NYC Department of Environmental Protection, U.S. Environmental Protection Agency, the U.S. Department of Agriculture, the National Institutes of Health, NASA, and specifically NASA's Socio-Economic Data and Applications Center. The Goleta AVIRIS data were provided by Martin Herold and Dar Roberts. The NYC AVIRIS data were provided by the AVIRIS team at the NASA Jet Propulsion Laboratory. Satellite data were provided by the USGS, Digital Globe and Space Imaging through the NASA Scientific Data Purchase program, and the University of Maryland Global Land Cover Facility. All analysis was done with ENVI and Matlab software on Apple and Sun computers.

REFERENCES

Adams, J.B., Smith, M.O., et al., Spectral mixture modeling; A new analysis of rock and soil types at the Viking Lander 1 site, *Journal of Geophysical Research*, 91, 8098–8122, 1986.

Adams, J.B., Smith, M.O., et al., Imaging spectroscopy: Interpretation based on spectral mixture analysis, in: Pieters, C.M., and Englert, P., eds., *Remote Geochemical Analysis: Elemental and Mineralogical Composition*, Cambridge University Press**,** New York, pp. 145–166, 1993.

Batty, M., and Longley, P., *Fractal Cities*, Academic Press, London, 1996.

Ben-Dor, E., Levin, N., and Saaroni, H., A spectral based recognition of the urban environment using the visible and near-infrared spectral region (0.4–1.1 μm). A case study over Tel-Aviv, Israel, *International Journal of Remote Sensing*, 22, 2193–2218, 2001.

Boardman, J.W., Inversion of imaging spectrometry data using singular value decomposition, IGARSS '89, 12th Canadian Symposium on Remote Sensing, Vancouver, B.C., 1989.

Boardman, J., Inversion of high spectral resolution data, *SPIE — Imaging Spectroscopy of the Terrestrial Environment*, 1298, 222–233, 1990.

Boardman, J.W., Automating spectral unmixing of AVIRIS data using convex geometry concepts, Fourth Airborne Visible/Infrared Imaging Spectrometer (AVIRIS) Airborne Geoscience Workshop, Jet Propulsion Laboratory, Pasadena, CA, 1993.

Boardman, J.W., and Kruse, F.A., Automated spectral analysis: A geologic example using AVIRIS data, north Grapevine mountains, Nevada, Tenth Thematic Conference on Geologic Remote Sensing, Ann Arbor, MI, Environmental Research Institute of Michigan, 1994.

Clark, R.N., Spectroscopy of rocks and minerals and principles of spectroscopy, in: Rencz, A.N., ed., *Manual of Remote Sensing*, John Wiley & Sons, New York, Chap. 1, pp. 3–58, 1999.

Clark, R.N., Green, R.O., Swayze, G.A., Meeker, G., Sutley, S., Hoefen, T.M., Livo, K.E., Plumlee, G., Pavri, B., Sarture, C., Wilson, S., Hageman, P., Lamothe, P., Vance, J.S., Boardman, J., Brownfield, I., Gent, C., Morath, L.C., Taggart, J., Theodorakos, P.M., and Adams, M., Environmental studies of the World Trade Center area after the September 11, 2001 attack, *U.S. Geological Survey, Open File Report* OFR-01-0429, URL: http://speclab.cr.usgs.gov/wtc/ (accessed in February 2008).

Clark, R.N., Swayze, G.A., Wise, R., Livo, E., Hoefen, T., Kokaly, R., and Sutley, S.J., USGS digital spectral library splib06a, *U.S. Geological Survey, Digital Data Series*, 231, 2007, http://speclab.cr.usgs.gov/spectral-lib.html (accessed in February 2008).

Dana, K.J., Ginneken, B.V., Nayar, S.K., and Koenderink, J.J., Reflectance and texture of real-world surfaces, *ACM Transactions on Graphics*, 18, 1–34, 1999.

Folkman, M., Pearlman, J., Liao, L., and Jarecke, P., EO-1/Hyperion hyperspectral imager design, development, characterization, and calibration, in: *Proceedings of SPIE*, SPIE, 4151, 40–51, 2001.

Foody, G.M., and Mathur, A., A relative evaluation of multiclass image classification by support vector machines, *IEEE Transactions on Geoscience and Remote Sensing*, 42, 1335–1343, 2004.

Gamba, P., and Dell'Acqua, F., Spectral resolution in the context of very high resolution urban remote sensing, in: Weng, Q., and Quattrochi, D., eds., *Urban Remote Sensing*, CRC Press, Boca Raton, pp. 377–391, 2007.

Gillespie, A.R., Smith, M.O., et al., Interpretation of residual images: Spectral mixture analysis of AVIRIS images, Owens Valley, California, Proceedings of the 2nd Airborne Visible/Infrared Imaging Spectrometer (AVIRIS) Workshop, Pasadena, CA, NASA Jet Propulsion Laboratory, 1990.

Goodchild, M., *Spatial Autocorrelation*, Catmog, Geo Books, Norwich, U.K., 1986.

Green, A.A., Berman, M., et al., A transformation for ordering mutispecral data in terms of image quality with implications for noise removal, *IEEE Transactions on Geoscience and Remote Sensing*, 26(1), 65–74, 1988.

Green, R.O., Conel, J.E., and Roberts, D.A., Estimation of aerosol optical depth, pressure elevation, water vapor and calculation of apparent surface reflectance from radiance measured by the airborne visible-infrared imaging spectrometer (AVIRIS) using MODTRAN2, SPIE Conf. 1937, *Imaging Spectrometry of the Terrestrial Environment*, 2–5, 1993.

Green, R.O., Eastwood, M.L., Sarture, C.M., Chrien, T.G., Aronsson, M., Chippendale, B.J., Faust, J.A., Pavri, B.E., Chovit, C.J., Solis, M.S., Olah, M.R., and Williams, O., Imaging spectroscopy and the Airborne Visible Infrared Imaging Spectrometer (AVIRIS), *Remote Sensing of Environment*, 65, 227–248, 1998.

Gualtieri, J.A., and Cromp, R.F., Support vector machines for hyperspectral remote sensing classification, in: Merisko, R.J., ed., *Proceedings SPIE-27th AIPR Workshop Advances in Computer Assisted Recognition*, pp. 221–232, 1998.

Heiden, U., Roessner, S., Segl, K., and Kaufmann, H., Analysis of spectral signatures of urban surfaces for their identification using hyperspectral HyMap data, in *iRemote Sensing and Data Fusion over Urban Areas, IEEE/ISPRS Joint Workshop*, pp. 173-177, IEEE, Rome, Italy, 2001.

Heiden, U., Segl, K., Roessner, S., and Kaufmann, H., Determination of robust spectral features for identification of urban surface materials in hyperspectral remote sensing data, *Remote Sensing of Environment*, 111(4), pp. 537–552, 2007.

Herold, M., Gardner, M.E., and Roberts, D.A., Spectral resolution requirements for mapping urban areas, *IEEE Transactions on Geoscience and Remote Sensing*, 41, 1907–1919, 2003.

Herold, M., Roberts, D.A., Gardner, M.E., and Dennison, P.E., Spectrometry for urban area remote sensing — development and analysis of a spectral library from 350 to 2400 nm, *Remote Sensing of Environment*, 91, 304–319, 2004.

Herold, M., Schiefer, S., Hostert, P., and Roberts, D.A., Applying imaging spectrometry in urban areas, in: Quattrochi, D.A., and Weng, Q.H., eds., *Urban Remote Sensing*, CRC Press, Boca Raton, pp. 137–161, 2006.

Huang, C., Davis, L.S., and Townshend, J.R.G., An assessment of support vector machines for land cover classification, *International Journal of Remote Sensing*, 23, 725–749, 2002.

Jensen, J.R., and Cowen, D.C., Remote sensing of urban suburban infrastructure and socio-economic attributes, *Photogrammetric Engineering and Remote Sensing*, 65, 611–622, 1999.

Johnson, P.E., Smith, M.O., et al., A semiempirical method for analysis of the reflectance spectra for binary mineral mixtures, *Journal of Geophysical Research*, 88, 3557–3561, 1983.

Johnson, P.E., Smith, M.O., et al., Quantitative analysis of planetary reflectance spectra with principal components analysis, *Journal of Geophysical Research*, 90, C805–C810, 1985.

Kaufmann, H., Segl, K., Chabrillat, S., Hofer, S., Stuffler, T., Müller, A., Richter, R., Schreier, G., Haydn, R., and Bach, H., EnMAP — A hyperspectral sensor for environmental mapping and analysis, IEEE International Geoscience and Remote Sensing Symposium — IGARSS 2006, Denver, CO, USA, pp. 1617–1619, 2006.

Kressler, F., and Steinnocher, K., Change detection in urban areas using satellite data and spectral mixture analysis, *International Archives of Photogrammetry and Remote Sensing*, XXXI(B7), 379–383, 1996.

Kressler, F.P., and Steinnocher, K.T., Monitoring urban development using satellite images, in Jürgens, C., ed., *Remote Sensing in Urban Areas* (*Fernerkundung in Urbanen Raumen*), Regensburg, Germany, *Regensburger Geographische Schriften*, 35, pp. 140–147, 2001.

Lacherade, S., Miesch, C., Briottet, X., and Le Men, H., Spectral variability and bidirectional reflectance behaviour of urban materials at a 20 cm spatial resolution in the visible and near-infrared wavelengths. A case study over Toulouse (France), *International Journal of Remote Sensing* (Letter), 26, 3859–3866, 2005.

Lee, J.B., Woodyatt, A.S., and Berman, M., Enhancement of high spectral resolution remote sensing data by a noise-adjusted principal components transform, *IEEE Transactions on Geoscience and Remote Sensing*, 28 (3), 295–304, 1990.

Meister, G., Lucht, W., Rothkirch, A., and Spitzer, H., Large scale multispectral BRDF of an urban area, IEEE International Geoscience and Remote Sensing Symposium, IGARSS '99, Hamburg, vol. II, pp. 821–823, 1999.

Meister, G., Bidirectional Reflectance of Urban Surfaces, PhD thesis, University of Hamburg, II. Institut fur Experimentalphysik, 186 pp., 2000.

Meister, G., Rothkirch, A., Spitzer, H., and Bienlein, J., BRDF field studies for remote sensing of urban areas, *Remote Sensing Reviews*, 19, 37–57, 2000.

Meister, G., Rothkirch, A., Spitzer, H., and Bienlein, J., Large scale bidirectional reflectance model for urban areas, *IEEE Transactions on Geoscience and Remote Sensing,* 39, 1927–1942, 2001.

Melgani, F., and Bruzzone, L., Classification of hyperspectral remote sensing images with support vector machines, *IEEE Transactions on Geoscience and Remote Sensing*, 42, 1778–1790, 2004.

Parker, R.L., Understanding inverse theory, *Annual Reviews of Earth and Planetary Science*, 5, 35–64, 1977.

Parker, R.L., *Geophysical Inverse Theory*, Princeton University Press, Princeton, NJ, 1994.

Preisendorfer, R.W., *Principal Component Analysis in Meteorology and Oceanography*, Elsevier Amsterdam, 1988.

Rashed, T., Weeks, J.R., et al., Revealing the anatomy of cities through spectral mixture analysis of multispectral satellite imagery: A case study of the greater Cairo region, Egypt, *Geocarto International*, 16(4), 5–15, 2001.

Research Systems Inc. (RSI), *ENVI FLAASH User's Guide*, ENVI Version 1.0, November 2001, Research Systems Inc., 58 pp., 2003.

Ridd, M.K., Exploring a V-I-S (vegetation–impervious surface–soil) model for urban ecosystem analysis through remote-sensing — comparative anatomy for cities, *International Journal of Remote Sensing*, 16(12), 2165–2185, 1995.

Roberts, D.A., Smith, M.O., et al., Green vegetation, nonphotosynthetic vegetation and soils in AVIRIS data, *Remote Sensing of Environment*, 44, 255–269, 1993.

Roberts, D.A., Green, R.O., and Adams, J.B., Temporal and spatial patterns in vegetation and atmospheric properties from AVIRIS, *Remote Sensing of Environment*, 62, 223–240, 1997.

Sandmeier, S., Muller, C., Hosgood, B., and Andreoli, G., Sensitivity analysis and quality assessment of laboratory BRDF data, *Remote Sensing of Environment*, 64, 176–191, 1998.

Schiefer, S., Hostert, P., and Damm, A., An analysis of view-angle effects in hyperspectral data of urban areas, in: Moeller, M., and Wentz, E., eds., *Proceedings 3rd International Symposium on Remote Sensing and Data Fusion Over Urban Areas (URBAN 2005*), 14–16 March, 2005, ISPRS, Tempe, USA, 2005.

Schiefer, S., Hostert, P., and Damm, A., Correcting brightness gradients in hyperspectral data from urban areas, *Remote Sensing of Environment*, 101, 25–37, 2006.

Settle, J.J., and Drake, N.A., Linear mixing and the estimation of ground cover proportions, *International Journal of Remote Sensing*, 14 (6), 1159–1177, 1993.

Shevell, S.K., *The Science of Color*, Optical Society of America, 339 pp., 2003.

Small, C., Estimation of urban vegetation abundance by spectral mixture analysis, *International Journal of Remote Sensing*, 21(7), 1334–1350, 2001.

Small, C., Multitemporal analysis of urban reflectance, *Remote Sensing of Environment*, 81, 427–442, 2002.
Small, C., High spatial resolution spectral mixture analysis of urban reflectance, *Remote Sensing of Environment*, 88, 170–186, 2003.
Small, C., The Landsat ETM+ spectral mixing space, *Remote Sensing of Environment*, 93, 1–17, 2004a.
Small, C., Global population distribution and urban land use in geophysical parameter space, *Earth Interactions*, 8, 1–18, 2004b.
Small, C., A global analysis of urban reflectance, *International Journal of Remote Sensing*, 26(4), 661–681, 2005.
Small, C., and Lu, J.W.T., Estimation and vicarious validation of urban vegetation abundance by spectral mixture analysis, *Remote Sensing of Environment*, 100, 441–456, 2006.
Small, C., and Miller, R.B., Digital Cities II: Monitoring the urban environment from space, *Proceedings of the International Symposium on Digital Earth,* Beijing, China, pp. 671–677, 1999.
Smith, M.O., Johnson, P.E., et al., Quantitative determination of mineral types and abundances from reflectance spectra using principal component analysis, *Journal of Geophysical Research*, 90, 792–804, 1985.
Smith, M.O., Ustin, S.L., et al., Vegetation in deserts: I. A regional measure of abundance from multispectral images, *Remote Sensing of Environment*, 31, 1–26, 1990.
United Nations, *World Urbanization Prospects — The 2005 Revision. Executive Summary*, United Nations Population Division, New York, 2006.
van der Linden, S., Investigating the potential of hyperspectral remote sensing data for the analysis of urban imperviousness — a Berlin case study, Dissertation: Humboldt-Universität zu Berlin, Berlin, Germany, 2008.
Welch, R., Spatial resolution requirements for urban studies, *International Journal of Remote Sensing*, 3, 139–146, 1982.
Woodcock, C.E., and Strahler, A.H., The factor of scale in remote-sensing, *Remote Sensing of Environment*, 21, 311–332, 1987.

5 A New Map of Global Urban Extent from MODIS Remote Sensing Data Based on an Urban Ecoregion Approach

Annemarie Schneider, Mark A. Friedl, and David Potere

CONTENTS

5.1 INTRODUCTION

More than 50% of the Earth's population now lives in cities. Cities consume enormous resources, the by-products of urban activity and land use are numerous (Foley et al., 2005), and a variety of recent studies demonstrate that the ecological footprint of many cities is significant and not sustainable (Rees and Wackernagel, 1996; Kareiva et al., 2007). Cities are also emerging as an important source of uncertainty in regional- to global-scale biogeophysical processes in the climate system. For example, the impact of urban areas on atmospheric chemistry and aerosols is both pronounced and well documented (Atkinson, 2000; Arnfield, 2003). Urban land use influences

local to regional climates through urban heat islands (Oke, 1982; Zhou et al., 2004), with concomitant impacts on human health (Patz et al., 2005) and ecosystems (Zhang et al., 2004; Alberti, 2005), and recent evidence has suggested that cities may also significantly affect local precipitation regimes (Kalnay and Cai, 2003; Kaufmann et al., 2007). At larger scales, recent studies have demonstrated that accurate representation of urban land use is both important and poorly captured in current models (Jin et al., 2005; Feddema et al., 2006; Oleson et al., 2008). As the global population grows and societies in developing countries become more urbanized, the environmental impact of cities will become even more pronounced (Mills, 2007; Grimmond, 2007). Accurate and timely information related to the global distribution and nature of urban areas is therefore critical to a wide array of environmental and geophysical research questions related to the effect of humans on the global environment (Sala et al., 2000; Peters-Lidard et al., 2004; Kaye et al., 2006; Pataki et al., 2006).

Despite the acknowledged and growing importance of urban land in local- to global-scale environmental processes, our understanding of urban dynamics has been limited by a lack of reliable and accurate data on the distribution and extent of built-up land at the global scale. The datasets that have emerged to fill this gap (e.g., LandScan, Dobson et al., 2000; Nighttime Lights, Elvidge et al., 1996, 2001, among others) suffer from a number of limitations. In particular, these maps differ by as much as a factor of 5 in their estimate of total urban area (Potere and Schneider, 2007). Furthermore, the majority of these datasets represent population distribution or urban locations, but none represent impervious surface or built-up land.

In this chapter, we present results from recent efforts to produce a new global map of urban land based on a new approach that uses remotely sensed data in association with a global stratification that captures regional variation in the nature and form of urban land use.* This work builds on our past efforts using Moderate Resolution Imaging Spectroradiometer (MODIS) data at 1-km spatial resolution (Schneider et al., 2003, 2005), which is included as part of the MODIS Collection 4 Global Land Cover Product (Friedl et al., 2002) and has been used for applications ranging from environmental modeling (Jin et al., 2005; Mu et al., 2008) to agricultural assessment (Ellis and Ramankutty, 2008) to disease monitoring (Hay et al., 2006). The goal of producing this new map is to address several key deficiencies in the Collection 4 map arising from urban land use in mixed pixels, and confusion between built-up areas, bare ground, and shrublands. To this end, the new global urban land extent data set described in this chapter was produced using newly released Collection 5 MODIS data circa 2001–2002 with increased spatial resolution (463.3 m). As part of this effort, we developed a new strategy based on a typology of "urban ecosystems" designed for this research. Comparison of the MODIS Collection 5 map with other available sources of information on urban land extent indicates good agreement, and more importantly, significant improvement relative to the Collection 4 data set. Using a unique, high-resolution data set that includes 135 cities, we have

* The MODIS map of urban extent at 463.3 m spatial resolution is available at National Aeronautics and Space Administration's Land Processes Distributed Active Archive Center, http://edcdaac.usgs.gov/dataproducts.asp and from the University of Wisconsin's Center for Sustainability and the Global Environment, http://www.sage.wisc.edu.

completed a geographically comprehensive assessment of map quality and accuracy. Our results show that the new Collection 5 data set has a mean overall accuracy of 93% ($\kappa = 0.65$) across the sample, a significant improvement over the Collection 4 map (88%, $\kappa = 0.49$) and other global urban map sources (73–90%, $\kappa = 0.28$–0.49).

5.2 BACKGROUND: GLOBAL MAPPING OF URBAN AREAS

Urban land use is both highly diverse and poorly defined at global scales. For many years, the only available global urban datasets were the Digital Chart of the World (DCW) urban layer (Danko, 1992) based on VMAP0, a collection of digitized navigational charts from the 1950s to the 1970s, and maps derived from the Defense Meteorological Satellite Program's "low light" sensor, or nighttime lights data (Elvidge et al., 1996, 2001). Because of the perceived difficulty of mapping urban areas, most global land cover maps exploited the DCW information [including the Advanced Very High Resolution Radiometer (AVHRR)-based Global Land Cover Characteristics Database (Loveland et al., 2000), the AVHRR Land Cover Map (Hansen et al., 2000), and the MODIS Vegetation Continuous Fields Dataset (DeFries et al., 2000)] despite the outdated, inconsistent nature of the data. During the past decade, however, several teams have created global maps of contemporary urban areas. In part because of the complexity of the label of urban land use, each group has approached this task from a different perspective, using methodologies that draw on a pool of remote sensing imagery, census information, geographic information systems (GIS) data layers, and other global maps.

Our previous efforts to inventory urban land use at a global scale resulted in the first global data set to use daytime multispectral remote sensing data (Schneider et al., 2003, 2005). Our methodology relied on a data fusion approach that combined 1-km MODIS data with additional remote sensing sources. Recently, two new land cover maps with explicit representation of urban areas have been developed using moderate spatial resolution satellite imagery: Global Land Cover 2000, based on Satellite Pour l'Observation de la Terre (SPOT4)-VEGETATION data (Bartholome and Belward, 2005); and GlobCover, developed from Medium Resolution Imaging Spectrometer data (JRC, 2008). Because GLC2000 was a joint effort by 18 regional teams, treatment of urban land is not consistent across regions (Potere and Schneider, 2007; Potere et al., 2008). GlobCover also uses a distributed approach with similar regional inconsistency in urban areas (e.g., urban extent in Eastern Australia covers more ground than all of the urban land in North America).

In parallel with these remote sensing-based efforts, several global datasets have been generated from population-based data on distribution and density and radiance-calibrated nighttime light data, including LandScan (Dobson et al., 2000; Bhaduri et al., 2002) and the Global Rural-Urban Mapping Project (GRUMP; Balk et al., 2006). In addition, two derivative global maps have been produced from LandScan data: the Global Impervious Surface Area Map (IMPSA; Elvidge et al., 2007) and the History Database of the Global Environment (HYDE; Goldewijk 2001, 2005). IMPSA uses LandScan and radiance-calibrated nighttime lights data to model "impervious surface area" globally, whereas HYDE integrates LandScan population density with United Nations (UN) national urban population estimates and assumptions about mean urban

population densities. Despite these efforts and the availability of new datasets, there is still no comprehensive global urban database that offers the detailed information requisite for environmental modeling (e.g., detailed subpixel information on impervious surface, urban vegetation extent and type, etc.). Furthermore, there is significant disagreement across these maps and few of the data sources described above have undergone rigorous validation. The goal of this work is to address some of these limitations by creating a new, accuracy-assessed global data set of urban land use based only on high-quality remote sensing data sources. In addition to the assessment of quality and accuracy undertaken here, we have completed a detailed examination of map differences across all available global urban maps, as outlined in Chapter 13 of this volume.

5.3 METHODS

5.3.1 Supervised Classification of MODIS Data

The classification methodology for this research uses a 1-year time series of data to exploit spectral and temporal differences in land cover types (Strahler et al., 1999; Friedl et al., 2002). The MODIS data inputs are 8-day composites of the seven land bands and the enhanced vegetation index (Huete et al., 2002) for 1 year (February 18, 2001–February 17, 2002) at 463.3 m spatial resolution. All input data are adjusted to a nadir-viewing angle to reduce the effect of varying illumination and viewing geometries (Schaaf et al., 2002). In addition, monthly and yearly minima, maxima, and means for each band are included.

The classification algorithm is trained using 2190 training sites ranging from 1 to 100 km^2 in area, classified according to the International Geosphere-Biosphere 17 class system (Belward and Loveland, 1997). Each site is obtained by manual interpretation of Landsat data, and is assessed for interpretation errors by two or more analysts (Friedl et al., 2002). A set of urban training sites was selected from 182 cities located across the globe using the criteria that a given area must be dominated by urban and built-up areas (specifically, >40% coverage of industrial, commercial, residential, and transportation-related land use).

The specific approach for mapping urban areas globally relies heavily on methods developed for the Collection 4 MODIS urban map at 1-km resolution (Schneider et al., 2003, 2005), with a few key differences. At the core of our previous methodology is a supervised decision tree algorithm (C4.5). For classification problems where large datasets are used and the information content is complex (e.g., nonlinear relations between features and classes) and may contain errors or missing data, decision trees provide an effective and efficient solution (Fayyad and Irani, 1992; Friedl and Brodley, 1997). Decision tree construction involves the recursive partitioning of a set of training data, which is split into increasingly homogeneous subsets based on statistical tests applied to the feature values (here, the satellite data values). Class labels are assigned to each observation based on its assignment at the terminal leaf node; however, a certain amount of "pruning" is also conducted to correct for overfitting of the training data.

To improve classification accuracy, the decision tree algorithm is used in conjunction with a technique called boosting, which improves class discrimination by estimating multiple classifiers while systematically varying the training sample. The

final classification is then produced by an accuracy weighted vote across all of the classifications (Quinlan, 1996). In addition, boosting can also be used to estimate probabilities of class membership for each class at every pixel. These land cover class probabilities — rather than the traditional "hard" class label — are an important component of our methodology. To fully exploit the information content in the probabilities, the classification algorithm is run twice: once with all land cover exemplars (including urban sites) and once with the urban training sites removed. As a result, information from the second classification (without urban sites) produces a reliable estimate of the "second most probable land cover class." These secondary probabilities are then used to modify the original urban probabilities in regions where confusion between classes occurs.

Despite using the same core algorithm, our new approach for the Collection 5 data differs from the Collection 4 methodology in several key ways: (1) no external datasets (population density, nighttime lights, etc.) are used to constrain the classification; (2) postprocessing of the land cover probabilities incorporates information derived from other MODIS-based maps and spectral indices in a data fusion step based on Bayes' rule; (3) postclassification processing is conducted region by region (with region-specific parameters and thresholds), based on a set of *urban ecoregions* designed for this research; and (4) the training database has been expanded and thoroughly updated for application to the Collection 5 MODIS data.

5.3.2 Urban Ecoregionalization

The key element of the new methodology is a global stratification of the Earth's land surface based on the natural, physical, and structural components of urban areas. Although urbanized areas are some of the most complex and heterogeneous landscapes in the world, research within urban studies, urban ecology, and land change science has shown that there is a surprising regularity in city structure, configuration, constituent elements, and vegetation types within geographic regions and by level of economic development (Angel et al., 2005; Schneider and Woodcock, 2008). The approach here exploits these local similarities to approximate regionally homogeneous areas that we term "urban ecoregions" (Figure 5.1, Table 5.1). This typology applies early ideas from Brady et al. (1979) and Pickett et al. (2001) on the physical, cultural, and social elements of cities. We further develop these concepts and apply them for the first time in a spatially explicit format at the global scale.

These urban ecoregions provide a global stratification for efficient data analysis and prioritization of training site selection, and also provide a framework for assessing map quality and accuracy. This stratification can also facilitate future research on urban expansion, urban ecosystem dynamics, and the contribution of urban systems to global environmental change.

To define the urban ecoregions, we start with the terrestrial ecoregions outlined by Olson et al. (2001) to identify broad climatic and biogeographic divisions that influence urban and peri-urban vegetation type and phenology. We then differentiate 16 urban ecoregions based on regional similarities in urban structure, historical development trajectory, level of economic development, vegetation patterns, and agricultural systems (Table 5.1). This step is completed within a GIS using expert

FIGURE 5.1 **(See color insert following page 324.)** The map of urban ecoregions produced for this research to facilitate analysis and processing of the MODIS 463.3 data as well as assessment of the resultant global map of urban extent. The sample 135 cities used for validation purposes are indicated by dots.

TABLE 5.1
Key Features of the 16 Urban Ecoregions

Ecoregion	No.	Geographic Region	Example Areas
Temperate broadleaf, mixed forests	1	North America, Japan, Australia	Eastern United States, Canada
	2	Europe, Japan	Germany, France, Japan
	3	Eastern Asia	Eastern China
Temperate grassland, shrubland	4	North America, South America, Central Asia, Australia	Central U.S., Mexico, Argentina, Australia
	5	Middle East, Central Asia	Turkey, Georgia
Tropical broadleaf forest	6	South America	Brazil, Colombia, Guatemala
	7	Sub-Saharan Africa	Democratic Republic of the Congo
Tropical-subtropical mixed forest	8	South-central, southeast Asia	China, India
Tropical-subtropical savannah, grasslands	9	South America	Southeastern Brazil, Paraguay
	10	Sub-Saharan Africa	Ghana, Kenya, Tanzania, Angola
Tropical-subtropical grasslands	11	South America, southern Africa	Chile, Peru, South Africa
Mediterranean	12	North America, southern Europe, northern Africa	California, Italy, Spain, Portugal
Arid, semi-arid desert	13	Africa, Middle East, Central Asia, Australia	Sahara Desert
Arid, semi-arid steppe, shrubland	14	Central Asia	Western China
Boreal forest, tundra	15	North America, northern Europe, northern Asia	Canada, Russia
Permanent ice, snow	16	North, South Pole	Antarctica

knowledge gathered from urban researchers, practitioners, and an extensive review of the urban studies literature (Schneider, 2005). Additional information was incorporated into our decision criteria from agricultural maps (Ramankutty et al., 2008), economic data (UN, 2005), and maps of geopolitical regions defined by the UN (2007).

Using this stratification, results from the supervised classification were processed on an ecoregion-by-ecoregion basis. For each stratum, classification results were visually assessed against available current data sources on urban areas (Google Earth, etc.). In temperate ecozones dominated by farmland, for example, little post-processing was necessary. In arid and semiarid regions, however, urban areas were often confused with either shrubland or agriculture, and prior information from the land cover probabilities was used to resolve these issues. Accordingly, our regional postprocessing methods included: estimation of posterior probabilities using Bayes' rule in conjunction with prior information derived from the land cover probabilities,

masking of problem areas using thresholded class probabilities (e.g., include urban if $P_{(urban)} > 0.75$), application of the MODIS 463 m water mask, and hand editing (for details, see Schneider et al., 2008a, 2008b).

5.4 RESULTS

5.4.1 Qualitative Assessment

Figure 5.2 illustrates the results of the new MODIS Collection 5 map of urban extent (hereafter the MODIS 463 m map) for the Washington, D.C.–Baltimore urban corridor. For comparison, the same region is shown for a Landsat-based 30 m classification (Figure 5.2(a)), the previously released MODIS-based map at 1 km (Figure 5.2(c)), and two independent datasets, the Nighttime Lights data (Figure 5.2(e)) and the IMPSA map based on Landscan and Nighttime Lights data (Figure 5.2(f)). The pattern of urban land in Washington, D.C. (southwest corner of the image) and Baltimore (northeast corner) is similar across all maps, with two exceptions. First, the results of the MODIS 463 m map provide far more detail on the edge of the city as well as within the urban fabric compared to the other coarse resolution sources. The green areas within Washington, D.C., for example, highlight the improved spatial resolution of the data (these areas correspond to vegetated parks), and the general urban morphology is in good agreement with the high-resolution map (Figure 5.2(a)). Second, the blooming effect of the light emissions (Figure 5.2(e)) masks important ground-based features; this artifact is also discernible in the IMPSA map, primarily in the small towns outside the heart of the city (Figure 5.2(f)). As a result, several small, urbanized clusters in the southernmost part of Figure 5.2(e) and (f) show less spatial detail and a more clumped appearance relative to the MODIS-based results in Figure 5.2(b). A similar loss of detail is apparent in the suburbs southwest of Baltimore: the nighttime lights-based maps characterize these areas as nearly continuous stretches of urban land.

Regionally, our results reveal that previous estimates of urban extent (typically 2–3%) drawn from global maps made from coarse-resolution data (1–2.2 km resolution) may overestimate the true extent of built-up areas. Although still a brushstroke estimate of urban development, the MODIS 463 m map shows that urban land as a percentage of total land area varies from 0.17% in Africa to 0.67% in North America, with most regions near the global average of 0.5% urbanized (e.g., South America, 0.47%; Asia, 0.53%). The exception is the European landmass (1.78% urbanized), a result that is to be expected given the extensive urban morphology in this region.

5.4.2 Quantitative Assessment of City Size

To overcome the challenges associated with assessing accuracy at a global scale, we compare estimates of urban extent at the scale of the city. To do this, estimates

FIGURE 5.2 (Opposite) **(See color insert following page 324.)** A comparison of maps for the Washington D.C.–Baltimore, Maryland conurbation depicting (a) a Landsat-based classification (30 m), (b) the MODIS-based classification (463 m resolution), (c) the prior version of the MODIS-based map (1 km resolution), (d) sub-pixel "urban intensity" from 463 m MODIS data, (e) nighttime lights data, and (f) NOAA's impervious surface area map.

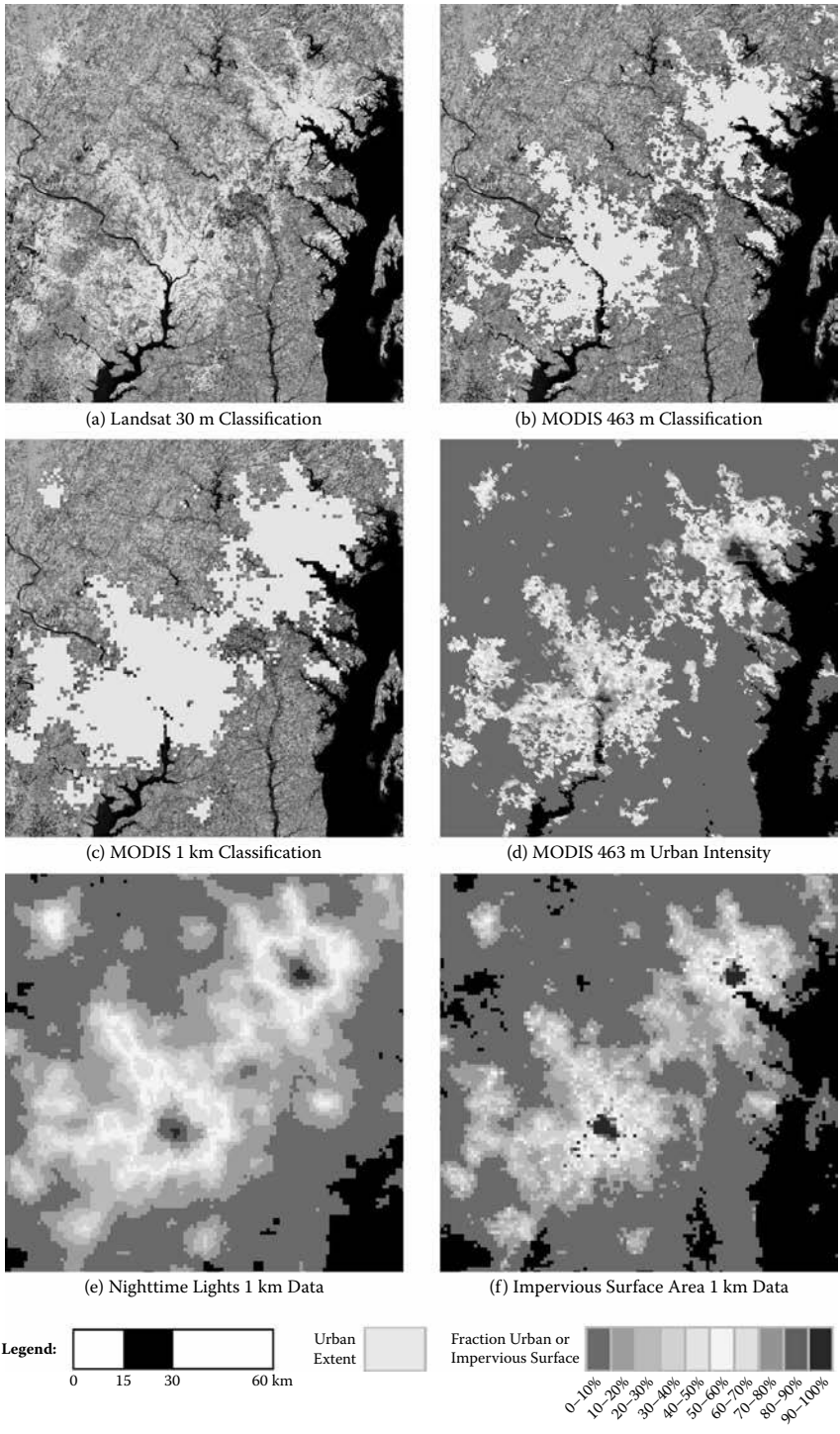

of city size are derived from a global, geographically comprehensive, stratified random sample of 135 Landsat-based classifications (30 m resolution) of urban land (Schneider, 2005; Angel et al., 2005; Schneider and Woodcock, 2008). These 135 maps are independent of the training exemplars used during classification of the MODIS 463 m map, and are assumed to be accurate and valid depictions of on-the-ground urban extent. The cities in the sample range in size from 20 to 5250 km^2, with the extent of each city's study area defined by the municipal boundaries of the city (see Figure 5.1 for the city sample distribution).

Figure 5.3 illustrates how the estimates of urban size (on the *x* axis) compare to estimates obtained from the MODIS 463 m map and the five global urban map sources (on the *y* axis, MODIS 1 km, GLC2000, GlobCover, IMPSA, and GRUMP). The results show that the MODIS 463 m map has the best agreement (Figure 5.2(a)), and the lowest root mean square error (RMSE), 142.6m, when compared against the other sources. Three of the global maps (Figure 5.3(b), (e), (f)) systematically overestimate urban extent across the range of city sizes in the sample (20–5250 km^2). The two remaining maps (Figure 5.3(c) and (d)) have values that cluster around the 1:1 line, but have a high degree of variability and a large number of outliers that reveal how frequently these sources under- or overestimate true city size. The RMSE for these two maps corroborates this finding, with values two to three times higher (288.6 and 344.9, respectively) than the MODIS 463 m map.

Figure 5.3(a) shows that the MODIS 463 m map tends to slightly overestimate city size. Despite the increased detail afforded by a fourfold increase in areal resolution

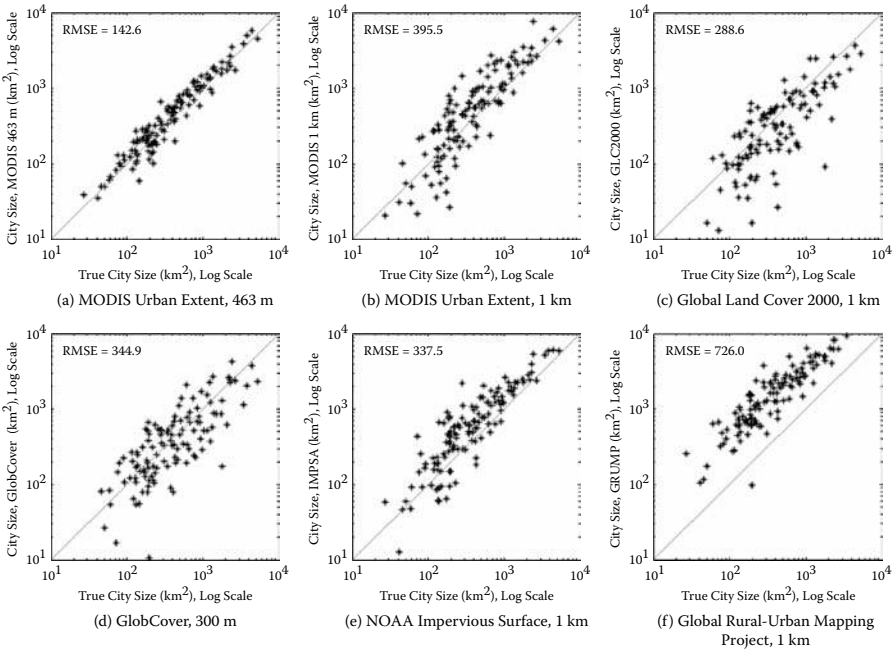

FIGURE 5.3 Scatter plots of the 135 cities in the validation sample, where each plot shows the city size from the high-resolution Landsat-based maps (*x*-axis, assumed to be "truth") against one of the global urban maps (*y*-axis). Note the log scale on both axes.

(from 1 km to 463 m), the pixel size is often too coarse to differentiate distinct urban features (roads, buildings) from agriculture and other land cover types within the pixel. Because of this subpixel heterogeneity, modest overestimation of true areal extent of urban land is expected. The degree of subpixel mixing is explored more fully in Figure 5.5, as well as by Schneider et al. (2008b), who also provide region-specific equations to adjust the MODIS 463 m map areal extent to on-the-ground estimates.

5.4.3 Assessment of Map Agreement at Multiple Spatial Scales

To further assess the quality of the 463 m map, the high-resolution maps were resampled to coarser spatial resolutions (300 m–1 km) and compared to the global maps to estimate the degree of agreement among them. The confusion matrix results are summarized in Figure 5.4, where box plots convey the mean, median, and range of values for Cohen's kappa, and producer's and user's accuracies across the 135-city sample.

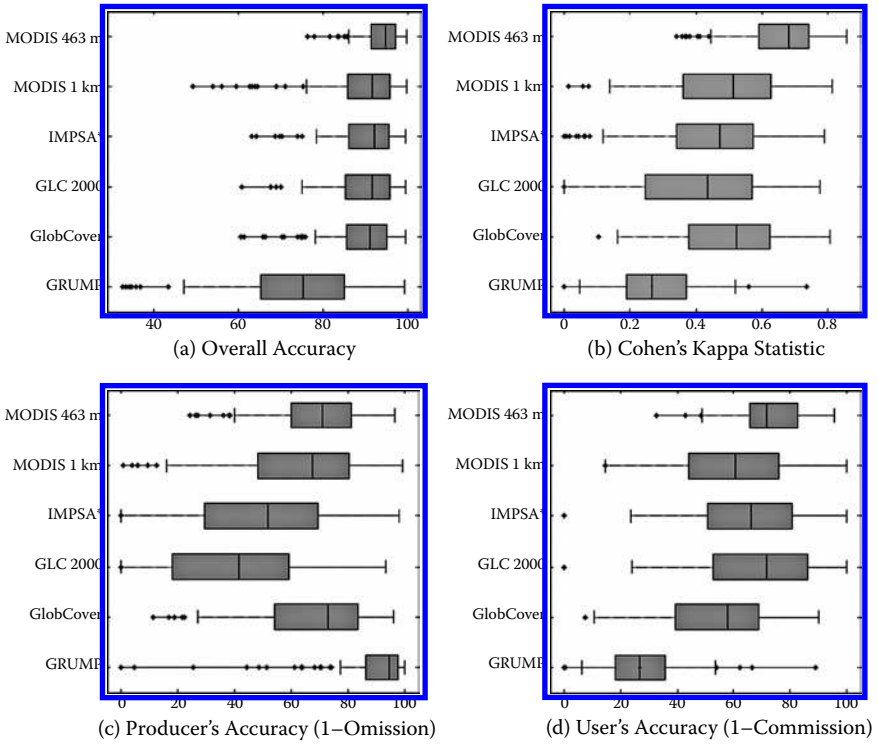

FIGURE 5.4 Box plots of accuracy statistics for the MODIS 463 m map and five additional global urban maps using the 135 city validation sample. The figure shows four measures to assess the accuracy of the global urban maps at the scale of the city: (a) overall accuracy, (b) Cohen's kappa statistic, (c) producer's accuracy (or sensitivity), and (d) user's accuracy (or specificity). The six global urban maps shown along the *y*-axis are the MODIS-based maps of urban extent at 463 m and 1 km spatial resolution, NOAA's impervious surface area map (IMPSA), global land cover 2000 (GLC 2000), the recently released GlobCover map, and CIESIN's Global Rural-Urban Mapping Project (GRUMP).

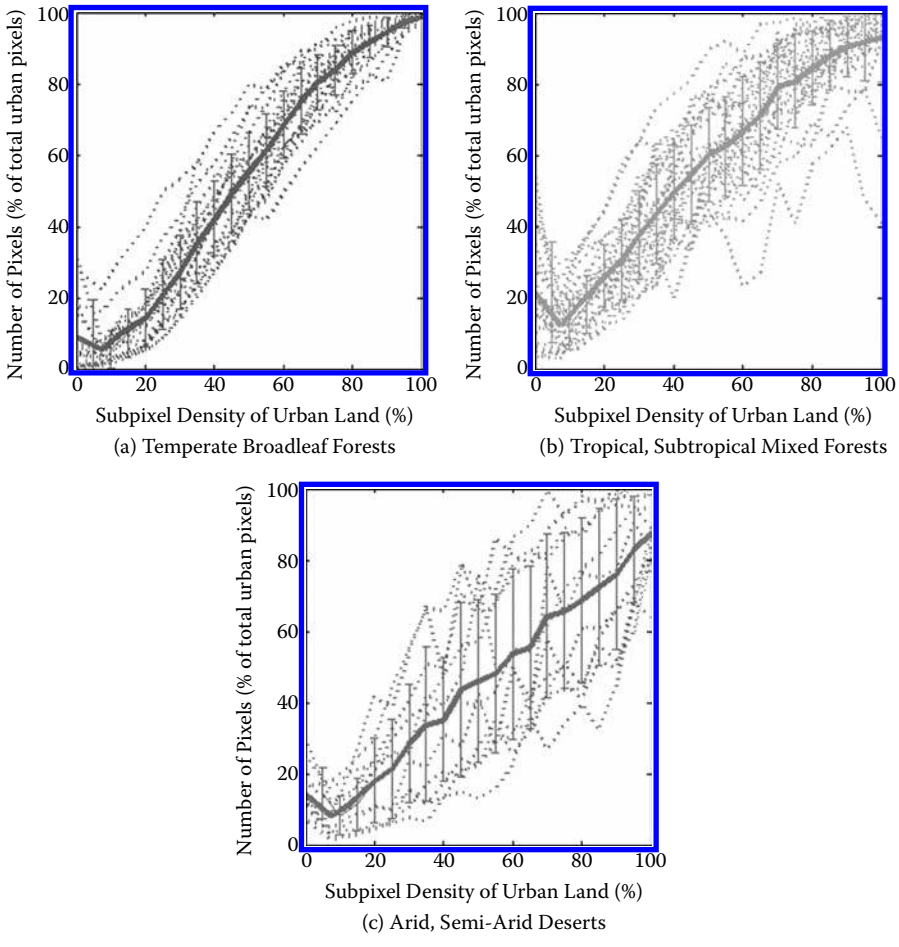

FIGURE 5.5 Plots of urban land densities (i.e., sub-pixel mixing) in the sample of validation cities for three urban ecoregions: (a) temperate broadleaf forests in North America; (b) tropical–subtropical mixed forests in Asia; and (c) arid, semi-arid desert areas. The plots show the distribution of urban land densities that correspond to areas mapped as "urban" in the MODIS 463 m map. Each bin along the *x*-axis contains the number of MODIS urban pixels whose corresponding truth values (derived from the high resolution city maps) fall in a given range (0, 1–5, 6–10, etc.); this value is normalized by the total number of true urban pixels for that bin. This percentage (*y*-axis) is, in effect, the percent of pixels correctly classified for that density range.

The overall accuracy is generally high across all map sources (Figure 5.4(a)), with mean accuracy rates ranging from 73% (GRUMP) to more than 93% (MODIS 463 m map). The MODIS 463 m map has the highest accuracy, the lowest standard deviation (±4.5%, as compared to ±7.2% or greater in the other maps), and the fewest outliers below 75%. Four of the maps — the original MODIS 1 km map, IMPSA, GLC2000, and GlobCover — have mean overall accuracy rates clustered together

in the 90% range (89.0–91.1). Of this group, the MODIS 1 km map displays the most outliers below the mean. This result underscores the degree of improvement provided by the Collection 5 MODIS data and the new region-based methodology. Differences among the maps are also clearly summarized in the kappa statistic: the MODIS 463 m map has the highest mean and median kappa values (0.65), whereas IMPSA, GlobCover, GLC2000, and MODIS 1 km have kappa values ranging from 0.38 to 0.50, and GRUMP has the lowest mean kappa, $\kappa = 0.28$.

The user's and producer's accuracies (bottom row, Figure 5.4) provide additional details about the quality and accuracy of the maps. Producer's accuracy characterizes the error of omission, or the *sensitivity* of the map. Producer's accuracy reveals errors incurred when the classified map effectively misses an area of urban land, or in other words, the map does not label a true built-up area as "urban." Figure 5.4(c) shows the distribution of producer's accuracies across the coarse resolution urban maps. Two of the maps (IMPSA and GLC2000) have mean and median values lower than 50%, which indicates that these datasets are missing developed land in their classifications. This result is somewhat alarming, given that the sample data set only includes cities with substantial populations (more than 200,000) and more than 50 km^2 of urban land. GRUMP, on the other hand, has a producer's accuracy higher than the rest, at nearly 90%. It is important to point out that, although GRUMP does not *miss* many true urban pixels, the map has a large number of erroneously labeled pixels evident from its low overall accuracy and user's accuracy.

User's accuracy, on the other hand, reflects the error of commission, sometimes called map *specificity*. This measure reveals the number of pixels erroneously labeled as urban land. The distribution of user's accuracies (Figure 5.4(d)) mirrors the results of the overall accuracy measure (Figure 5.4(a)): the MODIS 463 m map has the highest user's accuracy (72.9%), with GLC2000 and IMPSA close behind (65.6% and 64.8%, respectively), followed by MODIS 1 km (59.1%), GlobCover (54.2%), and GRUMP (28.1%). In general, the user's accuracies are lower than the producer's accuracies because of difficulties involved in mapping urban land use using moderate resolution data on the edge of cities or in heterogeneous inner city areas relative to high-resolution data. The fact that the MODIS 463 m map has the highest user's accuracy indicates that this map has the fewest pixels across the sample mistakenly labeled urban land, and fewer mislabeled edge pixels due to the increased spatial resolution of the data.

Although overall accuracy is often used as a standard indicator of map quality, the kappa statistic is also widely used for this purpose (Cohen, 1960). Indeed, many contend that kappa provides a better overall measure than simple overall accuracy (Allouche et al., 2006; Foody, 2007). Differences among the maps are clearly summarized in the kappa statistic: the MODIS 463 m map has the highest mean/median kappa values (0.65), whereas IMPSA, GlobCover, GLC2000, and MODIS 1 km have kappa values ranging from 0.50 to 0.38, and GRUMP has the lowest mean kappa of 0.28.

5.4.4 Evaluation of Subpixel Mixing

One final way to evaluate the quality of the MODIS 463 m map is to use the urban ecoregion typology to understand regional trends in how well areas with different densities of urban land are classified. Our goal here is to exploit the high-resolution

city maps to determine the density of urban land at which the MODIS 463 m map labels a pixel as "urban." To derive subpixel urban land densities, the high-resolution city-level maps were resampled and coregistered to the MODIS 463.3 m grid. Using this grid, the percentage of each cell covered by urban land was computed from the high-resolution map. To summarize these results, we compare the number of 463 m urban pixels with the urban density estimated from the high-resolution data, stratified into 20 groups (0%, 1–5%, 6–10%, etc.).

The results for three urban ecoregions are shown in Figure 5.5. Individual cities are shown by dashed lines and the regional mean and standard deviation are shown by the heavy lines and error bars. The number of MODIS urban pixels is normalized by the total number of true urban pixels (from the high-resolution classification) for each density level (or "bin"); this step allows cities of widely different sizes to be compared on the same scale. In this assessment, this normalized value along the *y* axis can be considered the percent of pixels correctly classified for that density range. These plots exemplify three significant patterns. First, each plot displays a distance decay function moving outward from the city center (from the far right of the *x* axis to the left). The MODIS 463 m map does a good job of capturing areas with 70–100% developed land as "urban." For the 70–100% density bins (*x* axis), the values on the *y* axis range from 80% to 100% in Figure 5.5(a), 75–98% in Figure 5.5(b), and 65–90% in Figure 5.5(c). As expected, when subpixel urban land densities drop below 50%, the MODIS 463 m has more varied results with anywhere from 10% to 60% of low-density pixels characterized as urban land. This reflects the definition used to define urban land cover in the training data (i.e., areas with at least 40% developed land).

The second important trend in Figure 5.5 is the difference in the shape of the curve in cities from different regions: the curve shown in Figure 5.5(a) is sigmoidal in form, whereas those in Figure 5.5(b) and (c) are more linear. This result suggests that the map is better at correctly identifying mid-density pixels in temperate ecoregions than in tropical-subtropical or arid-semiarid parts of the world, and echoes the results of the class probabilities from the boosted decision trees, which showed a high level of accuracy before the postprocessing step. In addition, these differences suggest that the urban signal is relatively easy to discern in these regions. The third and final trend is that cities in temperate ecoregions (dashed lines) show less variability about the mean than cities in the other two divisions. It is interesting that the greatest variability in this regard occurs in the midrange density values (roughly 40–80%). However, the results also suggest that — even in regions where it is difficult to map urban land — there is a great deal of consistency in how the MODIS 463 m map depicts densely urban areas (80–100% urban) and low density areas (0–20% urban).

5.5 DISCUSSION AND CONCLUSIONS

Urban areas are an increasingly important part of the global environment, and yet they remain one of the most challenging areas for conducting research. The application of standard measurements and models is particularly difficult given the complex three-dimensional structure of the city; the mixture of surface types with contrasting radiative, thermal, and moisture characteristics; and the complex atmospheric chemistry in these regions. Despite these challenges, researchers and practitioners

are pursuing new frameworks and models that incorporate urban land/land cover change. Because urban and nonurban areas may have different sensitivities to climate change, for instance, it is possible that the true effect of these changes will only be understood if urban areas are explicitly modeled in climate change simulations. It is therefore essential that maps of urban land use not only display the point location of cities or the spatial distribution of population, but also provide up-to-date information regarding the extent, growth, and physical characteristics of urban land.

This paper presents a new, global, moderate resolution map of urban extent circa 2001–2002, with several significant improvements over currently available map sources. The increased spatial resolution and radiometric quality of the MODIS Collection 5 data (463.3 m) has allowed us to map urban land with a fourfold increase in spatial detail. This analysis also presents the first global validation effort performed for any of the currently available global urban maps, and provides important information to the user community on the quality and suitability of this map for a range of environmental science applications. Our assessment shows that the MODIS 463 m map provides the most realistic depiction of global urban land use among the available datasets. Moreover, our research has shown that assessment of accuracy for a small-area class such as urban land should rely on a full suite of measures estimated across local, regional, and global scales. Due to space limitations, this chapter presents only a portion of our analysis (see Schneider et al., 2008b; Potere et al., 2008; and Chapter 13 of this volume).

As part of our approach to monitoring urban areas globally, we have defined a new set of urban ecoregions. This new, spatially explicit map of urban ecoregions is a significant step toward understanding the urban environment on a contextual, regional basis. Because of the consistencies in urban structure, layout, building sizes, materials, vegetation types, and phenology, this new typology can be used to assign or differentiate important parameters of the urban environment (e.g., sensible and latent heat flux, etc.). This provides improvement over parameter assignment based on a single global value. Moreover, the use of urban ecoregions provides a framework for handling a global data set quickly and efficiently by exploiting the seasonal and land cover similarities of each region and developing region-specific methods to handle problematic areas. In this context, our methodology for the MODIS 463 m map incorporates analyst expertise within a fully automated classification algorithm, which we feel is a necessary approach for the successful characterization of a small, heterogeneous, and difficult-to-map class such as urban areas.

Moving forward, the datasets described in this chapter provide a foundation for refined representations of global urban land use. In particular, our ongoing efforts are focused on (1) creating updated maps of urban extent for the period 2002–2007 (corresponding to the years of available Collection 5 data) on a once-per-year or every-other-year basis; (2) creating global maps that provide subpixel estimates of urban land use (preliminary results for this type of "urban intensity" map are shown in Figure 5.1(d)) that correspond to percent impervious surface; and (3) rounding out the suite of land surface characteristics for urban areas by producing maps of the type and percent coverage of vegetation within urbanized areas. In addition, we hope to build on these results to create a globally consistent, validated map of land cover change in and around cities. Information on the rates and patterns of growth in urban areas has important implications for models and studies that require information related to the role of humans in the global environment.

ACKNOWLEDGMENTS

The authors wish to thank Solly Angel and Dan Civco for generous use of their datasets, Scott Macomber and Damien Sulla-Menashe for technical assistance and support, and Mutlu Ozdogan for comments on an earlier draft of this paper. This work was supported by NASA grant NNX08AE61A.

REFERENCES

Alberti, M., The effects of urban patterns on ecosystem function, *International Regional Science Review*, 28, 168–192, 2005.

Allouche, O., Tsoar, A., and Kadmon, R., Assessing the accuracy of species distribution models: Prevalence, kappa and the true skill statistic (TSS), *Journal of Applied Ecology*, 43, 1223–1232, 2006.

Angel, S., Sheppard, S.C., and Civco, D.L., *The Dynamics of Global Urban Expansion*, World Bank, Washington, D.C., 2005. http://www.williams.edu/Economics/UrbanGrowth/WorkingPapers.htm (last accessed May 1, 2008).

Arnfield, A.J., Two decades of urban climate research: A review of turbulence, exchanges of energy and water, and the urban heat island, *International Journal of Climatology*, 23, 1–29, 2003.

Atkinson, R., Atmospheric chemistry of VOCs and NO_x, *Atmospheric Environment*, 34, 2063–2101, 2000.

Balk, D.L., Deichmann, U., Yetman, G., Pozzi, F., Hay, S.I., and Nelson, A., Determining global population distribution: Methods, applications and data, *Advances in Parasitology*, 62, 119–156, 2006.

Bartholome, E., and Belward, A.S., GLC2000: A new approach to global land cover mapping from Earth observation data, *International Journal of Remote Sensing*, 26, 1959–1977, 2005.

Belward, A.S., and Loveland, T., The IGBP-DIS global 1-km land cover data set, DISCover: First results, *International Journal of Remote Sensing*, 18, 3291–3295, 1997.

Bhaduri, B., Bright, E., Coleman, P., and Dobson, J., LandScan: Locating people is what matters, *Geoinfomatics*, 5, 34–37, 2002.

Brady, R.F., Tobias, T., Eagles, P.F.J., Ohrner, R., Micak, J., Veale, B., and Dorney, R.S., A typology for the urban ecosystem and its relationship to larger biogeographical landscape units, *Urban Ecology*, 4, 11–28, 1979.

Cohen, J., A coefficient of agreement for nominal scales, educational and psychological measurement, *Educational and Psychological Measurement*, 20, 37–46, 1960.

Danko, D.M., The Digital Chart of the World Project, *Photogrammetric Engineering and Remote Sensing*, 58, 1125–1128, 1992.

DeFries, R.S., Hansen, M.C., Townshend, J.R.G., Janetos, A.C., and Loveland, T.R., A new global 1-km dataset of percentage tree cover derived from remote sensing, *Global Change Biology*, 6, 247–254, 2000.

Dobson, J.E., Bright, E.A., Coleman, P.R., Durfee, R.C., and Worley, B.A., Landscan: A global population database for estimating populations at risk, *Photogrammetric Engineering and Remote Sensing*, 66, 849–857, 2000.

Ellis, E., and Ramankutty, N., Putting people in the map: Anthropogenic biomes of the world, *Frontiers in Ecology and the Environment*, 6, 2008, doi:10.1890/070062.

Elvidge, C.D., Baugh, K.E., Kihn, E.A., and Davis, E.R., Mapping city lights with nighttime data from the DMSP operational linescan system, *Photogrammetric Engineering and Remote Sensing*, 63, 727–734, 1996.

Elvidge, C., Imhoff, M.L., Baugh, K.E., Hobson, V.R., Nelson, I., Safran, J., Dietz, J.B., and Tuttle, B.T., Nighttime lights of the world: 1994–95, *ISPRS Journal of Photogrammetry and Remote Sensing*, 56, 81–99, 2001.

Elvidge, C., Tuttle, B.T., Sutton, P.C., Baugh, K.E., Howard, A.T., Milesi, C., Bhaduri, B.L., and Nemani, R., Global distribution and density of constructed impervious surfaces, *Sensors*, 7, 1962–1979, 2007.

Fayyad, U.M., and Irani, K.B., On the handling of continuous-valued attributes in decision tree generation, *Machine Learning*, 8, 87–102, 1992.

Feddema, J.J., Oleson, K., and Bonan, G., Developing a global database for the CLM urban model, in *Proceedings of the American Meteorological Society Sixth Symposium on the Urban Environment*, 28 January–2 February, 2006.

Foley, J.A., DeFries, R., Asner, G., Barford, C., Bonan, G., Carpenter, S., Chapin, F., Coe, M., Daily, G., Gibbs, H., Helkowski, J., Holloway, T., Howard, E., Kucharik, C., Monfreda, C., Patz, J., Prentice, I., Ramankutty, N., and Snyder, P., Global consequences of land use, *Science*, 309, 570–574, 2005.

Friedl, M.A., and Brodley, C.E., Decision tree classification of land cover from remotely sensed data, *Remote Sensing of Environment*, 61, 399–409, 1997.

Friedl, M., McIver, D., Hodges, J., Zhang, X., Muchoney, D., Strahler, A., Woodcock, C., Gopal, S., Schneider, A., Cooper, A., Baccini, A., Gao, F., and Schaaf, C., Global land cover mapping from MODIS: Algorithms and early results, *Remote Sensing of Environment,* 83, 287–302, 2002.

Foody, G.M., Map comparison in GIS, *Progress in Physical Geography*, 31, 439–445, 2007.

Goldewijk, K., Estimating global land use change over the past 300 years: The HYDE database, *Global Biogeochemical Cycles*, 15, 417–434**,** 2001.

Goldewijk, K., Three centuries of global population growth: A spatially referenced population density database for 1700–2000, *Population and Environment*, 26, 343–367**,** 2005.

Grimmond, S., Urbanization and global environmental change: Local effects of urban warming, *Geographical Journal*, 173, 83–88, 2007.

Hansen, M.C., Defries, R.S., Townsend, R.G., and Sohlberg, R., Global land cover classification at 1 km spatial resolution using a classification tree approach, *International Journal of Remote Sensing*, 21, 1331–1364, 2000.

Hay, S.I., Tatem, A.J., Graham, A., Goetz, S.J., and Rogers, D.J., Global environmental data for mapping infectious disease distribution, *Advances in Parasitology*, 62, 37–77, 2006.

Huete, A., Didan, K., Miura, T., Rodriguez, E.P., Gao, X., and Ferriera, L.G., Overview of the radiometric and biophysical performance of the MODIS vegetation indices, *Remote Sensing of Environment*, 83, 195–213, 2002.

Jin, M.L., Dickinson, R.E., and Zhang, D.L., The footprint of urban areas on global climate as characterized by MODIS, *Journal of Climate*, 18, 1551–1565, 2005.

Joint Research Center (JRC), European Space Agency, The GlobCover Portal, 2008. Available at: http://ionia1.esrin.esa.int (last accessed May 1, 2008).

Kalnay, E., and Cai, M., Impact of urbanization and land-use change on climate, *Nature*, 423, 528–531, 2003.

Kareiva, P., Watts, S., McDonald, R., and Boucher, T., Domesticated nature: Shaping landscapes and ecosystems for human welfare, *Science*, 316, 1866–1869, 2007.

Kaufmann, R., Seto, K.C., Schneider, A., and Zhou, L., Climate response to rapid urban growth: Evidence of a human-induced precipitation deficit, *Journal of Climate*, 20, 2290–2306, 2007.

Kaye, J.P., Groffman, P.M., Grimm, N., Baker, L.A., and Pouyat, R.V., A distinct urban biogeochemistry? *Trends in Ecology and Evolution*, 21, 192–199, 2006.

Loveland, T.R., Reed, B.C., Brown, J.F., Ohlen, D.O., Zhu, J., Yang, L., and Merchant, J.W., Development of a global land cover characteristics database and IGBP DISCover from 1-km AVHRR data, *International Journal of Remote Sensing*, 21, 1303–1330, 2000.

Mills, G., Cities as agents of global change, *International Journal of Climatology*, 27, 1849–1857, 2007.

Mu, Q., Zhao, M., Running, S.W., et al., Contribution of increasing CO_2 and climate change to the carbon cycle in China's ecosystems, *Journal of Geophysical Research-Biogeosciences*, 113, G1, G01018, 2008.

Oke, T.R., The energetic basis of the urban heat island, *Quarterly Journal of the Royal Meteorological Society*, 108, 1–24, 1982.

Oleson, K.W., Bonan, G.B., Feddema, J., and Vertenstein, J., An urban parameterization for a global climate model: 2. Sensitivity to input parameters and the simulated urban heat island in offline simulations, *Journal of Applied Meteorology and Climatology*, 2008.

Olson, D., Dinerstein, M.E., Wikramanayake, E., Burgess, N., Powell, G., Underwood, E., D'Amico, J., Itoua, I., Strand, H., Morrison, J., Loucks, C., Allnutt, T., Ricketts, T., Kura, Y., Lamoreux, J., Wettengel, W., Hedao, P., and Kassem, K., Terrestrial ecoregions of the world: A new map of life on Earth, *BioScience*, 51, 933–938, 2001.

Pataki, D.E., Alig, R.J., Fung, A.S., Golubiewski, N.E., Kennedy, C.A., McPherson, E.G., Nowak, D.J., Pouyat, R.V., and Romero Lankao, P., Urban ecosystems and the North American carbon cycle, *Global Change Biology*, 12, 2092–2102, 2006.

Patz, J.A., Campbell-Lendrum, D., Holloway, T., and Foley, J.A., Impact of regional climate change on human health, *Nature*, 438, 310–317, 2005, doi:10:1038.

Peters-Lidard, C.D., Kumar, S., Tian, Y., Eastman, J.L., and Houser, P., Global urban-scale land atmosphere modeling with the land information system, in: *Symposium on Planning, Nowcasting, and Forecasting in the Urban Zone*, 84th American Meteorological Society Annual Meeting, 11–15 January, Seattle, WA, USA, 2004.

Pickett, S.T.A., Cadenasso, M.L., Grove, J.M., Nilon, C.H., Pouyat, R.V., Zipperer, W.C., and Costanza, R., Urban ecological systems: Linking terrestrial ecological, physical, and socioeconomic components of metropolitan areas, *Annual Review of Ecology and Systematics*, 32, 127–157, 2001.

Potere, D., and Schneider, A., A critical look at representations of urban areas in global maps, *GeoJournal*, 69, 55–80, 2007.

Potere, D., Schneider, A., Civco, D., and Angel, S., Comparative analysis of global urban maps: Assessment of accuracy and recommendations for use, in preparation.

Quinlan, J.R., Bagging, boosting, and C4.5, in: *Proceedings of the 13th National Conference on Artificial Intelligence (AAAI-96)*, 4–8 August, Portland, OR, AAAI Press, pp. 725–730, 1996.

Ramankutty, N., Evan, A.T., Monfreda, C., and Foley, J.A., Farming the planet: 1. Geographic distribution of global agricultural lands in the year 2000, *Global Biogeochemical Cycles*, 22, GB1003, 2008.

Rees, W., and Wackernagel, M., Urban ecological footprints: Why cities cannot be sustainable, and why they are a key to sustainability, *Environmental Impact Assessment Review*, 16, 223–248, 1996.

Sala, O.E., Chapin, F.S., Armesto, J.J., et al., Biodiversity — global biodiversity scenarios for the year 2100, *Science*, 287, 1770–1774, 2000.

Schaaf, C.B., Gao, F., Strahler, A.H., Lucht, W., Li, X., Tsang, T., Strugnell, N., Zhang, X., Jin, Y., Muller, J., Lewis, P., Barnsley, M., Hobson, P., Disney, M., Roberts, G., Dunderdale, M., Doll, C., d'Entremont, R., Hu, B., Liang, S., Privette, J.L., and Roy, D., First operational BRDF, albedo nadir reflectance products from MODIS, *Remote Sensing of the Environment*, 83, 135–148, 2002.

Schneider, A., Urban growth as a component of global change, Ph.D. dissertation, Boston University, Boston, MA, 2005.

Schneider, A., and Woodcock, C.E., Compact, dispersed, fragmented, extensive? A comparison of urban expansion in twenty-five global cities using remotely sensed data, pattern metrics and census information, *Urban Studies*, 45, 659–692, 2008.

Schneider, A., Friedl, M.A., Mciver, D.K., and Woodcock, C.E., Mapping urban areas by fusing multiple sources of coarse resolution remotely sensed data, *Photogrammetric Engineering and Remote Sensing*, 69, 1377–1386, 2003.

Schneider, A., Friedl, M.A., and Woodcock, C.E., Mapping urban areas by fusing multiple sources of coarse resolution remotely sensed data: Global results, in: *Proceedings of the 5th International Symposium of Remote Sensing of Urban Areas*, 14–16 March, Tempe, AZ, 2005.

Schneider, A., Friedl, M.A., and Potere, D., A new map of global urban extent from MODIS data, *Geophysical Research Letters*, 2008a, in review.

Schneider, A., Friedl, M.A., and Potere, D., Monitoring spatial and temporal patterns of global urbanization: A data fusion approach using MODIS 500m and a new set of urban ecoregions, *Remote Sensing of Environment*, 2008b, in review.

Strahler, A.H., Muchoney, D., Borak, J., Gao, F., Friedl, M.A., Gopal, S., Hodges, J.C.F., Lambin, E., McIver, D.K., Moody, A., Schaaf, C.B., and Woodcock, C.E., MODIS Land Cover/Land Cover Change Algorithm Theoretical Basis Document, Version 5.0, Department of Geography, Boston University, Boston, MA, 1999. Available at: http://geography.bu.edu/landcover/index.html (last accessed May 1, 2008).

UN Population Division, United Nations World Urbanization Prospects — the 2005 Revision, 2005. Available at: http://esa.un.org/unup (last accessed May 1, 2008).

UN Statistics Division, Standard Country or Area Codes for Statistical Use, 2007. Available at: http://unstats.un.org/unsd/methods/m49/m49.htm (last accessed May 1, 2008).

Zhang, X.Y., Friedl, M.A., Schaaf, C.B., Strahler, A., and Schneider, A., The footprint of urban climates on vegetation phenology, *Geophysical Research Letters*, 31, L12209, 2004.

Zhou, L.M., Dickinson, R.E., Tian, Y.H., Fang, J.Y., Li, Q.X., Kaufmann, R.K., Tucker, C.J., and Myneni, R.B., Evidence for a significant urbanization effect on climate in China, *Proceedings of the National Academy of Sciences*, 101, 9540–9544, 2004.

Part III

Mapping and Monitoring Projects and Research

6 Global Urban Mapping Based on Nighttime Lights

Christopher D. Elvidge, Paul C. Sutton, Benjamin T. Tuttle, Tilottama Ghosh, and Kimberly E. Baugh

CONTENTS

6.1 INTRODUCTION

Urban places may be broadly defined as settlements where most people live and work. Human beings worldwide tend to cluster in spatially limited habitats occupying less than 5% of the world's land area. The density of infrastructure — or "urbanness" — can be viewed as a continuum ranging from wilderness at one extreme to central business districts at the other extreme (Weeks, 2004). Because of their key role in sustaining human civilization and their impact on the environment, there is substantial interest in global mapping of human settlements and updating such maps on a routine basis.

Satellite sensors provide one of the few globally consistent and repeatable sources of observations. In the environmental sciences, satellite data have proven crucial for global mapping and global assessment of processes such as deforestation. Fewer applications for satellite data have been developed in the social and economic sciences. In part, this can be attributed to the fact that most Earth observation satellite sensors are optimized for observation of natural phenomena (e.g., the movement of clouds and the characteristics of the land and sea surface) that are not directly related to socioeconomic measures such as population density, living conditions, and economic activity. The physical structures of urban areas produce distinctive spatial and spectral signatures that are recorded by many types of remotely sensed data.

However, no satellite sensor has been designed and flown specifically for mapping and monitoring urban areas.

With moderate (10–50 m) resolution imagery, it is possible to map the extent of urbanized land and delineate basic urban classes such as commercial/industrial, residential, and open areas such as parks with reasonable accuracy. With high spatial resolution imagery (~1 m), it is possible to outline individual buildings and with stereo imagery estimate the volumes of individual structures.

To date, an openly accessible global urban map has not been produced from moderate- or high-resolution satellite imagery. Although it is possible to collect a sufficient quantity of cloud-free moderate resolution imagery for such a map in a single year, the generation of an urban map from sources such as Landsat is complicated by the lack of a uniform spectral or spatial signature for urban areas (Small, 2005). Collection and processing difficulties combine to frustrate the production of a global urban map from high spatial resolution satellite imagery. As a consequence, the present state of global urban mapping is much more modest, with most products simply attempting to depict the outline of the developed area at or near 1-km resolution.

Among the data sources regarded as most promising for global urban mapping are the observations of nighttime lights. The widespread use of such lighting is a relatively recent phenomenon, tracing its roots back to the electric light bulb commercialized by Thomas Edison in the early 1880s. Artificial lighting has emerged as one of the hallmarks of modern development and provides a unique attribute for identifying the presence of development or human activity that can be sensed remotely. Although there are some cultural variations in the quantity and quality of lighting in various countries, there is a remarkable level of similarity in lighting technology around the world. Thus, the remote sensing of artificial lighting is viewed as an accurate, economical, and unambiguous way to map the global distribution and density of developed areas.

The only satellite sensor currently collecting global low-light imaging data suitable for mapping urban lighting is the U.S. Air Force Defense Meteorological Satellite Program (DMSP) Operational Linescan System (OLS). The DMSP OLS was designed to collect global cloud imagery using a pair of broad spectral bands placed in the visible and thermal. The DMSP satellites are flown in polar orbits and each collects 14 orbits per day. With a 3000-km swath width, each OLS is capable of collecting a complete set of images of the Earth twice a day. At night, the visible band signal is intensified with a photomultiplier tube (PMT) to enable the detection of moonlit clouds. The boost in gain enables the detection of lights present at the Earth's surface. Most of the lights are from human settlements (cities and towns) and fires, which are ephemeral. Gas flares are also detected and can easily be identified when they are offshore or in isolated areas not impacted by urban lighting.

The DMSP-OLS has a number of favorable characteristics for global urban mapping including the potential for nightly global coverage and a manageable data volume. Over the years, a number of researchers have attempted to use DMSP-OLS nighttime lights as a representation of the urban geographic footprint (Doll et al., 2000; Ebener et al., 2005; Elvidge et al., 1997, 1999, 2004; Foster, 1983; Gallo et al.,

1995, 2004; Imhoff et al., 1997; Lo, 2002; Sutton and Costanza, 2002; Sutton, 2003; Sutton et al., 2007; Welch, 1980). These studies revealed that the OLS-derived lighting features are substantially larger than the lighting sources present on the ground and that local economic conditions impact the detection and brightness of satellite observed lighting. Both of these effects detract from the value of the data in mapping urban footprints. On the other hand, it is possible that nighttime lights depict the spatial patterns of global resource consumption and economic activity more clearly than any other available satellite data source. In this chapter, we examine three types of global urban product types developed based on DMSP-OLS nighttime lights and discuss possible improvements in the remote sensing of nocturnal lighting.

6.2 DENSITY OF CONSTRUCTED SURFACES

Human beings around the world build, use, and maintain constructed impervious surfaces for shelter, transportation, and commerce. Constructed surfaces include roads, buildings, sidewalks, driveways, and parking lots. Collectively, these represent one of the primary anthropogenic modifications of the environment. Expansion in population numbers and economies combined with the popular use of automobiles has led to the sprawl of development and a wide proliferation of constructed impervious surfaces. It is anticipated that the worldwide pattern of sprawl development will continue in the coming decades in response to both population growth and improvement in living standards.

Constructed impervious surfaces can be viewed as hydrological and ecological disturbances. However, constructed surfaces are different from most other types of disturbances in that recovery is arrested through the use of materials that are resistant to decay and are actively maintained. The same characteristics that make impervious surfaces ideal for use in construction produce a series of effects on the environment (Schueler, 1994). Impervious surfaces alter sensible and latent heat fluxes, causing urban heat islands (Changnon, 1992). In heavily vegetated areas, the proliferation of impervious surface area (ISA) reduces the sequestration of carbon from the atmosphere (Milesi et al., 2003). ISA alters the character of watersheds by increasing the frequency and magnitude of surface runoff pulses (Booth, 1991). Watershed effects of ISA begin to be detectable once 10% of the surface is covered by impervious surfaces, altering the shape of stream channels, raising water temperatures, and sweeping urban pollutants into aquatic environments (Beach, 2002; Carlson, 2007). Hydrologic consequences of ISA include increased flooding, reductions in ground water recharge, and reductions in surface water quality.

Spatial grids depicting the density of constructed surfaces are typically in units of percent cover and are widely used in hydrologic modeling and flood prediction. These grids are distinctly different from traditional urban land use products that report classes such as commercial/industrial, high-density residential, and low-density residential. For applications such a hydrologic modeling, land use data are not nearly as useful as constructed surface density grids.

There are three primary remote sensing approaches to estimating the density of constructed surfaces (Slonecker et al., 2001; Weng, 2007). The first approach is to

map constructed areas using high spatial resolution imagery (Goetz et al., 2003; Yang et al., 2003; Slonecker, and Tilley, 2004). Typically, ISA products derived from high spatial resolution imagery cover small areas and to date, there has not been a standardization of methods that would facilitate the merger of products generated by diverse organizations. The second approach is to use moderate spatial resolution multispectral data (e.g., Landsat) to estimate the density of ISA. Such a product was recently produced by the U.S. Geological Survey using Landsat 7 data from the early 2000s (Yang et al., 2003; Crane et al., 2005). This product has 30-m resolution and a combination of spectral and spatial methods to estimate the density of ISA. A subsample of high spatial resolution imagery was used to establish the methodology and to provide an accuracy assessment. The third approach is to use indicators to estimate the density of ISA. As an example, Stankowski (1972) proposed the estimation of ISA based on population density. Another indirect method is the estimation of ISA based on coverage coefficients developed for standard land cover classes, such as low-density residential, high-density residential, commercial/industrial (Jennings et al., 2004).

We have used nighttime lights to estimate the density of constructed surfaces. Elvidge et al. (2004) pioneered this approach, producing a 1-km^2 grid of constructed surface densities for the conterminous USA using nighttime lights, street, and road density (from the U.S. Census Bureau), and three urban land cover classes from the early 1990s (Vogelmann et al., 2001). Subsequently, Elvidge et al. (2007a) produced a global density grid of constructed surfaces using nighttime lights and population count from the U.S. Department of Energy Landscan data (Dobson et al., 2000; Bhaduri et al., 2002). These data products are available at http://www.ngdc.noaa.gov/dmsp/download_global_isa.html.

The 20 leading countries in terms of total ISA are shown in Table 6.1. Also listed is the quantity of ISA per person in square meters. At the bottom of the table, we list the total ISA for all countries and the average amount of ISA found per person worldwide. Clearly, the countries that measure high on total ISA are either large in areal extent and/or total population, or have high levels of economic development.

The countries with particularly high values of ISA per person according to our estimation are almost universally affluent (United States, Canada, Norway, Sweden, Finland, Spain, France, Bahrain, Brunei, Qatar, and the United Arab Emirates). With the exception of Brunei, these countries cluster in the northern hemisphere (Figure 6.1). It is interesting to note that Japan and Mexico both score at lower identical levels (114 m^2 of ISA per person). Japan's moderate level of ISA (relative to their GDP per capita) can be attributed to the topographic and agricultural constraints on development present in that country.

The total ISA of the world is estimated to be 579,703 km^2. This is nearly the same size as the country of Kenya (584,659 km^2), and larger than Spain (505,735 km^2) or France (546,962 km^2). The country with the most ISA is China (87,182 km^2), followed closely by the United States (83,881 km^2) and India (81,221 km^2). China's and India's ISA footprints are population-driven, whereas the United States ISA footprint is more driven by affluence. Explorations of ISA per capita show generally expected patterns in that countries with high population densities (e.g., "big denominators") show lower levels of ISA per capita. The global average of

TABLE 6.1
Top 20 Countries in Terms of Constructed Surface Area

Country	Constructed Surface Area (km^2)	Population (Landscan 2004)	Constructed Surface Area per Person (m^2)
China	87,182	1,292,548,864	67.4
United States	83,881	282,575,328	296.8
India	81,221	1,058,349,824	76.7
Brazil	17,766	177,885,936	99.9
Russia	17,135	138,947,840	123.3
Indonesia	16,490	230,000,208	71.7
Japan	13,990	122,192,928	114.5
Mexico	11,854	103,608,488	114.4
Canada	11,295	32,022,750	352.7
Pakistan	10,666	150,465,168	70.9
France	9537	59,497,124	160.3
Bangladesh	8878	140,275,504	63.3
Germany	8500	82,406,312	103.1
Italy	8294	56,528,760	146.7
Nigeria	7668	125,118,728	61.3
United Kingdom	7576	58,926,004	128.6
Spain	7037	39,481,976	178.2
Iran	6949	66,604,152	104.3
Vietnam	5981	81,249,416	73.6
Egypt	5745	75,240,640	76.4
Total Worldwide	579,703	6,245,732,591	93

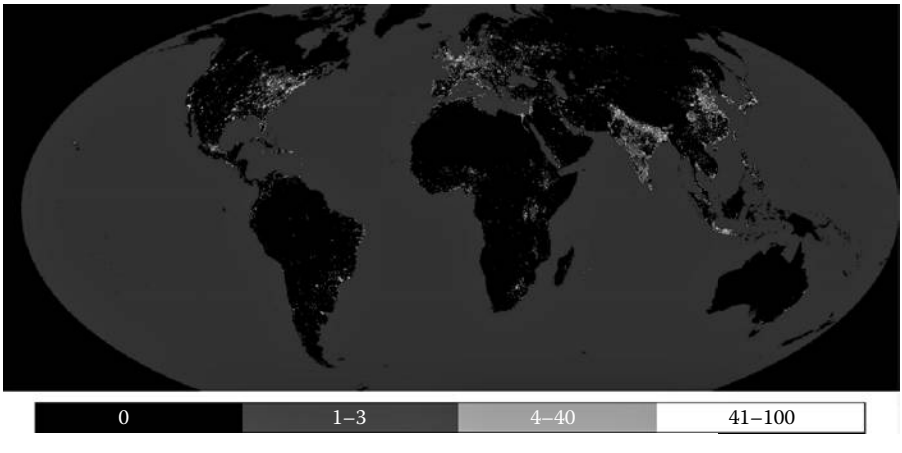

FIGURE 6.1 Global distribution and density of constructed surfaces modeled from DMSP nighttime light and LandScan population count.

ISA per capita was estimated to be 93 m^2 per person. Examinations of ISA at the watershed level support ideas that there are both economic and demographic forces contributing to changes in the hydrologic and ecologic functioning of watersheds around the world.

The estimate of ISA is derived solely from the brightness of satellite observed nighttime lights and population count. Both of the input sources (nighttime lights and population count) are produced as 30 arc second grids (~1 km^2 resolution) and could potentially be updated on an annual basis. These two data sources are complementary in that the nighttime lights are generally brightest in the commercial and industrial areas — which are generally not well defined in the population count data. In areas where no lighting is detected the ISA estimate is based solely on population count. In the absence of detected lighting, the population count at which 100% ISA is reached is slightly more than 11,000 persons/km^2. At this density, each person is directly associated with 91 m^2 of ISA, nearly the global average of 93 m^2 per person.

As the world economy and population expands it can be projected with confidence that the constructed surfaces of the Earth will expand significantly. For the moment, this product stands as the only global ISA grid. We offer it as a pathfinder, recognizing that the mapping of constructed surface at both the global and local scale will continue to improve over time.

6.3 GLOBAL POVERTY MAP

During our work with nighttime lights and the Landscan population count data, we had the occasion to overlay the two datasets as a color composite image. In this image, it is possible to see areas devoid of satellite detected lighting in the densely populated belts of poverty in China, India, and across Africa. Using Europe and the United States as visual reference, it is also possible to see regions where the satellite-detected lighting is dim relative to the population numbers. We developed the notion of using the quantity of lighting per person as an indicator of poverty levels. The concept is that in prosperous regions of the world there is no shortage in lighting. The quantity of lighting per person declines as poverty rates increase. Our assumption is that the satellite will be unable to detect lighting in the areas with the most extreme poverty levels.

Poverty has emerged as one of the chronic dilemmas facing civilization during the 21st century. Based on data from the World Development Indicators (World Bank, 2006), approximately 42% or 2.6 billion people live in poverty. Poverty is the general term describing living conditions that are detrimental to health, comfort, and economic development. There are different forms of poverty, such as inadequate supply or quality of food, water, sanitation, housing, clothing, schools, and medical services. In locations where poverty levels are high, there is typically a convergence of inadequacies across several of these areas. Widely noted consequences of poverty include higher infant mortality, shorter life spans, and lower literacy rates. Poverty is also closely associated with environmental degradation (Snel, 2004). The United Nations Millennium Development Goals includes a 50% reduction in extreme poverty by the end of 2015. Economic analyses (Sachs, 2005) indicate that eliminating poverty is a realistic objective.

The primary source for statistics on global poverty is the World Bank, which has collected and distributed national-level data on poverty levels since 1990. Their methods are based on the analysis of household surveys conducted in almost 100 countries. Survey questions cover sources of income, consumption, expenditures, and numbers of individuals making up the household. Most surveys are conducted by government employees. Two styles of poverty data are produced — national poverty line data and international poverty line data. Individual countries establish their own poverty line for the national data. Differing standards in defining poverty make pooling the national poverty line data problematic. More recently, purchasing power parity has been introduced into the formulation of international poverty line data, which is specified in terms of the number of individuals living on either $1 or $2 per day (Figure 6.2).

There are a number of problems recognized with the World Bank poverty line data: not all countries conduct the surveys, the currently available data were derived from surveys spanning 1988 through 2004, and the survey repeat cycle is uncertain. The intercomparability of the estimates is uncertain due to difficulties in reconciling consumption and income data, plus discrepancies in the purchasing power parity estimates for individual countries (Karshenas, 2004). It is also possible for governments to influence the outcome of the surveys, because they design the questions, select the areas for survey, and conduct the interviews. The use of the $1 and $2 per day standards for the international poverty line data is not applicable to prosperous countries such as the United States, where 12% of the population is listed in poverty (De Navas-Walt et al., 2005).

Poverty maps have emerged as important tools for targeting aid and development resources (Sachs, 2000; Sachs et al., 2001; Henninger and Snel, 2002; CIESIN, 2006). Poverty maps traditionally depict a single measure or index value for an entire administrative unit, such as country or state. Spatially disaggregated global maps of the numbers of individuals living in poverty, based on a consistent definition of the poverty line would be extremely useful for targeting of efforts to reduce poverty (Hentschel and Lanjouw, 1998). Part of the value of spatially disaggregated data is that they can be aggregated to multiple levels: national, state, substate, or

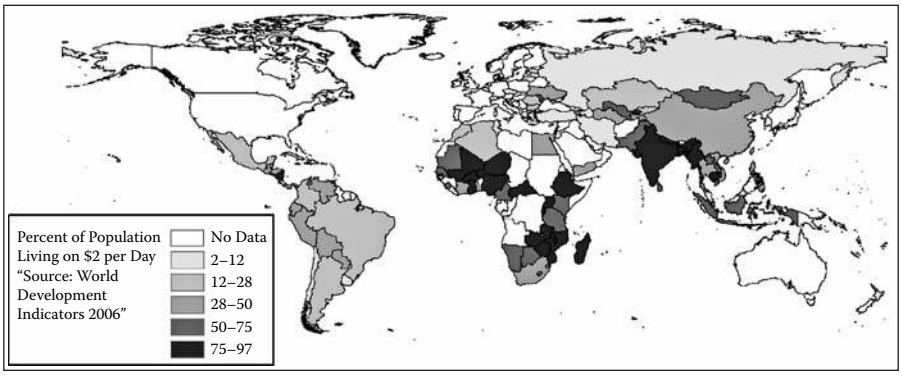

FIGURE 6.2 Map of poverty levels for countries reporting international poverty line data (percent of population living on $2 per day or less) from the World Development Indicators 2006. Note that a number of countries have no data reported and that the $2 per day poverty line is not applicable to developed countries.

municipal. If spatially disaggregated poverty maps could be updated on an annual or semiannual basis, they could be used to track the effectiveness of poverty reduction efforts in specific localities and the consequences of natural disasters, epidemics, or conflicts.

Two spatially disaggregated data sources have been combined to form a global poverty index (PI): LandScan population counts and DMSP nighttime lights. We defined a PI as the LandScan 2004 population count divided by the average visible band digital number from the lights (Figure 6.3). In areas where population is present but no lights were detected, the full population count is passed to the index.

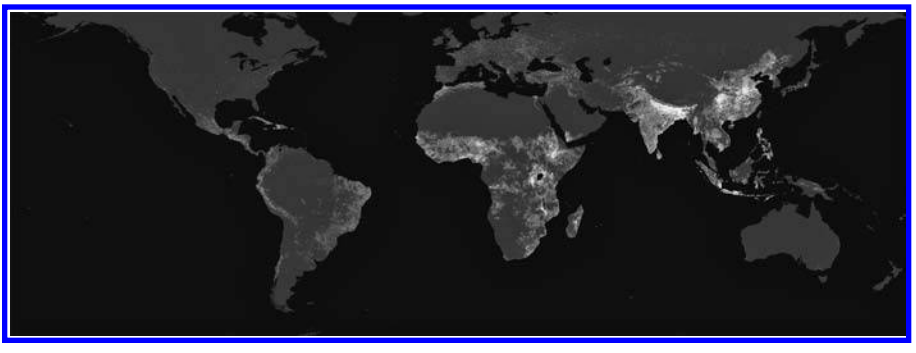

FIGURE 6.3 Poverty index calculated by dividing the LandScan 2004 population count by the average digital number of the DMSP satellite F15 nighttime lights from 2003.

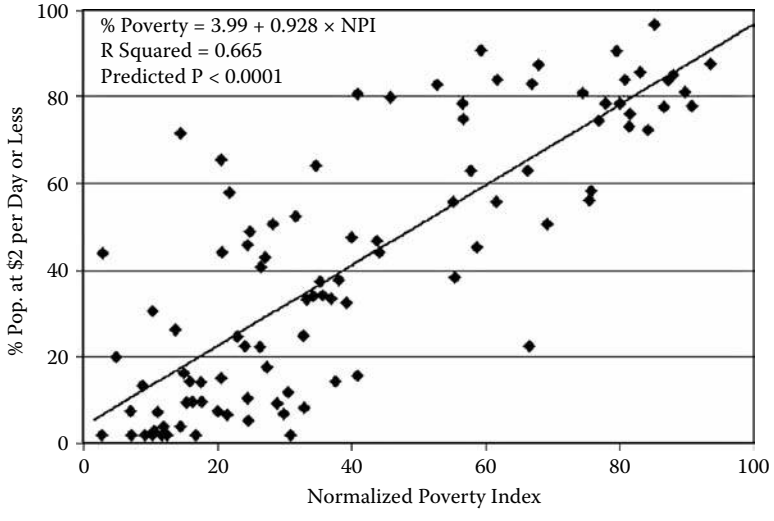

FIGURE 6.4 Calibration of the Normalized Poverty Index (NPI) for estimation of poverty levels.

A calibration for estimating the number of people living in poverty was developed based on the World Development Indicators 2006 national level estimates for the percentage of people living on $2 or less per day. To establish the calibration, the sum of the PI values was extracted for each country. This sum was then divided by the total population count and multiplied by 100.0 to form a normalized poverty index (NPI). The NPI was then regressed to the percentage of the population living on $2 per day or less (Figure 6.4).

The calibration from Figure 6.4 was applied to the NPI grid to estimate the poverty level in each grid cell and then multiplied by the LandScan population grid to yield an estimate of the poverty count. The gridded product is available at http://www.ngdc.noaa.gov/dmsp/download_poverty.html. The calibration was also applied to national level NPI and LandScan population counts to yield spatially aggregated poverty estimates. This was done for 232 countries to generate national poverty levels and poverty counts, which are available in spreadsheet form at the Web site. Among the 80 countries having populations greater than 10 million, those having poverty rate estimates greater than 80% are Ethiopia, Burkina Faso, Madagascar, Cambodia, Uganda, Tanzania, and Niger. Those having estimated poverty rates less than 10% include Taiwan, South Korea, Egypt, Saudi Arabia, Japan, Belgium, Netherlands, Italy, United Kingdom, and the United States.

The procedure used to generate the national level poverty estimates was then applied at subnational level for 2543 administrative units having LandScan population values above zero. These results are presented graphically in Figure 6.5. Many of the patterns present within individual countries match expected results, with lower poverty levels in the more prosperous areas. For instance, coastal China has lower poverty rates than the interior area, northeastern India has higher poverty rates than western and southern India, and the prosperous Sao Paulo region has lower poverty rates than other parts of Brazil. The effects of lighting from gas flares, which reduce the poverty estimates, can be observed in coastal Nigeria. A comparison of the estimated poverty rates in the United States versus measured rates reported for 2004 by De Navas-Walt et al. (2005) revealed an RMSE of 4.22%.

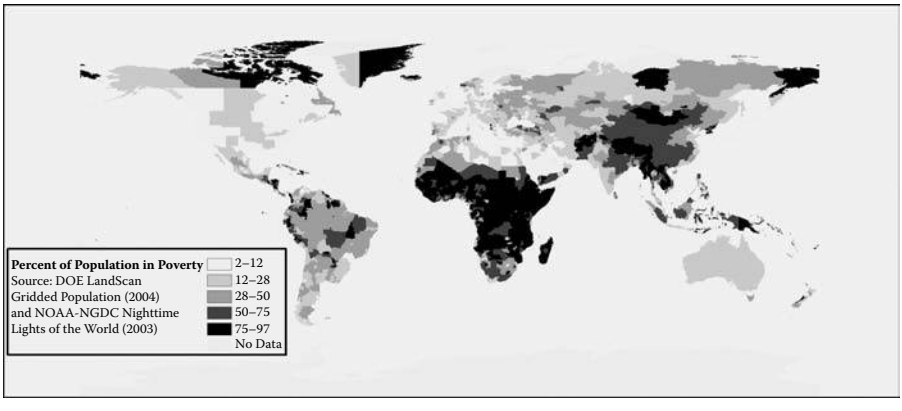

FIGURE 6.5 **(See color insert following page 324.)** Map of poverty levels for 2,543 subnational administrative units estimated based on the satellite data–derived poverty index.

6.4 ESTIMATION OF ECOLOGICAL FOOTPRINTS

We have explored the potential of using satellite-based estimates of a constructed area as a spatially disaggregated proxy for the human ecological footprint. Recently, the National Geophysical Data Center produced the first global grid of constructed area densities based on satellite-derived nighttime lights and population count data (Elvidge et al., 2007a). We have preliminary evidence (presented below) that spatial variation in the density of constructed area strongly correlates with the spatial variation in human ecological footprints.

The ecological footprint is a well-established resource accounting tool that estimates how much biologically productive land and water area an individual or a geographically defined population uses to produce the resources it consumes and to absorb the wastes it generates based on prevailing technology and resource management practices (Wackernagel and Rees, 1996). Ecological footprint calculations have emerged as a valuable means to communicate and understand human impacts on the natural systems upon which we depend. They are also useful in modeling the longer-term impacts of human consumption — both on natural systems and society.

One of the principles in calculating ecological footprints is that populations utilize widely distributed resources. This is a key consideration for urban populations because the land used to generate their food, fiber, and wood are widely distributed and could be halfway around the world. Similarly, the absorption of CO_2 produced by fossil fuel is widely distributed. Another principle used in the calculation of ecological footprints is that it is not necessary to pinpoint the location that produces the resources used by a population. Based on this consumption, the quantity of land or water surface required to generate that quantity of resource is calculated in terms of a normalized standard for biological productivity.

The Ecological Footprint's widely used normalized standard measurement unit is global hectares (GHA), defined as a biologically productive hectare with world average productivity. Kitzes et al. (2007) estimate that in 2003 the Earth made available 11.2 billion GHA while maintaining humanity's consumption depended on 14.1 billion GHA. Thus, humanity's resource consumption in 2003 was rated at 25% more than the Earth was able to produce in the same year. Another way to look at this number is that it took the Earth 15 months to produce the resources used by humanity in a 12-month period. When consumption exceeds production, the difference between the two numbers is made up by liquidating the Earth's ecological stores and the accumulation of waste products such as CO_2 in the atmosphere. These results and the ecological implications appeared in a recent report issued by WWF International (2006).

While a growing number of organizations are producing estimates of ecological footprints, the Global Footprint Network (GFN) has emerged as the premier organization in establishing and updating the standards used and produces the most widely cited national and global ecological footprint estimates. The GFN assembles data from a wide range of sources to produce National Footprint Accounts, which record the resources consumed, CO_2 emissions, and calculations of the land and water areas that need to produce the resources and absorb the CO_2. The data sources and modeling continue to evolve under the auspices of a standards

committee. Their most recent report (Ecological Footprint Standards 2006) is available at http://www.footprintstandards.org/. Each year, national footprint accounts are updated to track the consumption of crop products, fibers, livestock, fish, timber, fuel wood, and CO_2 produced. From these values, the model calculates the GHA utilization. The surface cover types that are tracked by national footprint accounts include cropland, grazing land, fishing grounds, forest, built-up land, and "carbon land." Land cover extents are drawn from multiple sources including CORINE, Global Agro-Ecological Zones, GLC 2000, and World Conservation Monitoring Center. Of these cover types, built-up land area estimates may be the least reliable data set, and weakest for global comparison (Kitzes et al., 2007).

By dividing the constructed area by population count, it is possible to produce a disaggregated grid estimating the constructed area per person. By aggregating these values, it is possible to estimate the constructed area per person at a variety of levels — including national and subnational administrative units. Figure 6.6 shows the national level constructed area per person (in square meters) versus the ecological footprint per person (in GHA) for 149 countries (from the GFN). For constructed area per person values in the 30- to 60-m^2 range, the ecological footprint is set at about 1 GHA. Beyond 60 m^2, the ecological footprint increases along with the constructed area per person values in a largely linear manner.

The constructed area data may be used to improve either the quality or the spatial resolution of ecological footprints: (1) by using the quantity of built-up land as an input into the National Footprint Account estimation models. The satellite derived constructed area data can be used as the input for built-up lands. (2) As Figure 6.6 shows, it is possible to estimate national level ecological footprints based on the constructed area per person metric. This relationship can be used to estimate and evaluate the ecological footprints for the 80+ countries and small islands (e.g., Brunei, Oman, Seychelles, Aruba) not covered by the GFN estimates, and (3) the subnational estimation of ecological footprints can also be made by working from the highly refined national level estimates and the disaggregated constructed area/person grid.

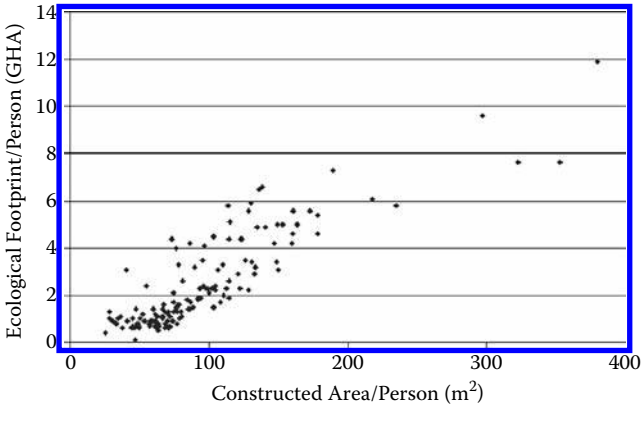

FIGURE 6.6 Constructed area per person versus ecological footprint per person for 149 countries.

6.5 CONCLUSION

Global urban mapping has, in most cases, been constrained to simple delineations of urban or developed areas. In this chapter, we have presented concepts for three types of global maps that characterize the density, living conditions, and resource consumption levels within human settlements on spatially disaggregated grids.

The estimate of ISA has been derived solely from the brightness of satellite-observed nighttime lights and the population count has been derived from the Landscan population grid. The ISA per capita revealed that countries with high population densities such as China and India had lower levels of ISA per capita.

A global map of poverty levels has been produced using a combination of four types of satellite data [DMSP lights, moderate resolution imaging spectroradiometer (MODIS) land cover, shuttle radar topography mission (SRTM) topography, and controlled image base (CIB)]. The MODIS, SRTM, and CIB data were used as inputs (along with census data) into a global population grid. DMSP lights were used as a measure of economic activity. The PI used to estimate poverty levels is calculated by dividing population count by the brightness of the nighttime lights. A calibration was developed using national-level poverty levels reported by the World Development Indicators 2006. The resulting estimate for the number of people living in poverty is 2.3 billion, consistent with the 2.6 billion estimated by the World Bank (2006).

The third style of global urban mapping that we have explored is focused on resource consumption. Although the OLS is remarkable for its detection of dim lighting, it is clear that the quality of global urban mapping products could be improved through the detection of even dimmer lighting with improvements in spatial resolution. The full suite of shortcomings of the OLS data for urban mapping include: (1) coarse spatial resolution (2.7-km ground sample distance), (2) lack of onboard calibration, (3) lack of systematic recording of in-flight gain changes, (4) limited dynamic range, (5) 6-bit quantization, (6) signal saturation in urban centers resulting from standard operation at the high gain setting, (7) lack of a thermal band suitable for fire detection, (8) limited data recording and download capabilities (most OLS data are averaged on-board to enable download of global coverage), (9) lack of a well-characterized point spread function (PSF), (10) lack of a well-characterized field of view, and (11) lack of multiple spectral bands for discriminating lighting types.

Several of the observational shortcomings of the OLS will be addressed by the low-light imaging data that will be acquired with the Visible/Infrared Imaging Radiometer Suite (VIIRS), which will fly on the National Polar Orbiting Environmental Satellite System (NPOESS) in the next decade. The VIIRS low-light imaging sensor will continue to acquire nightly global data, but will have onboard calibration and at higher spatial resolution (0.8 km) than the OLS. Thus, it can be expected that poverty assessments made with VIIRS data will be of higher quality than those that can be achieved with the OLS. The VIIRS, however, is not designed with the objective of sensing nighttime lights. Rather, it has the objective of nighttime visible band imaging of moonlit clouds — the same mission objective of the OLS low-light imaging. The VIIRS low-light imaging spatial resolution will be too coarse to permit the observation of key nighttime lighting features within human settlements. Also, the spectral band to be used for the low-light imaging is not tailored for nighttime lighting.

In total, OLS lighting was not detected for 1.68 billion people. Although the OLS is remarkable for its detection of dim lighting, it is clear that the quality of the PI could be improved through the detection of even dimmer lighting. The VIIRS instrument is designed to match the detection limits achieved by the OLS. In addition, both OLS and VIIRS will only acquire low-light imaging data in a single broad visible/near-infrared band. There is spectral information on the type of lighting, and changes in the type of lighting could be quite useful for improving the quality of poverty estimates. The final area where a substantial improvement in low-light imaging could be envisioned is in spatial resolution. On the basis of recent simulations made with high spatial resolution airborne camera imagery of nighttime lights, nighttime photography from the International Space Station and ground-based spectral measurements, Elvidge et al. (2007b, 2007c) developed the Nightsat mission concept. To be effective in delineating primary nighttime lighting patterns, Nightsat low-light imaging data should not exceed 50- to 100-m spatial resolution and achieve minimal detectable radiances in the range of 2.5×10^{-8} W cm^{-2} sr^{-1} μm^{-1}. Although panchromatic low-light imaging data would be useful, multispectral low-lighting imaging data acquired with three to five spectral bands would enable more quantitative applications and enable the detection of lighting type conversions.

Cloud and fire screening of the low-light imaging data would be accomplished using simultaneously acquired thermal band data. The thermal band data could come from VIIRS if Nightsat were flown on an NPOESS satellite. The system would use a combination of methods to produce radiance-calibrated data. Geolocation accuracy would be 50 m, comparable to that of Landsat. The system objective would be to collect a sufficient quantity of imagery to construct annual global cloud-free composites of nighttime lights. A near-Sun-synchronous polar orbit, with an early evening overpass, would provide temporal consistency important for change detection (Elvidge et al., 2007b, 2007c).

Nightsat system would enable a wide range of social, economic, and biological applications where there is currently a dearth of systematically collected, unbiased, global data. Nightsat data would provide important constraints and inputs for the spatial modeling of human population growth and distribution, land use, rates of development, anthropogenic emissions to the atmosphere, and independent estimation of economic indices. In addition, Nightsat data would be used to model and understand human impacts on the environment such as the proliferation of impervious surface area, nonpoint sources of aquatic pollution, habitat fragmentation, and the direct effects of nocturnal lighting on night environment, human health, security, and the visibility of stars. Moderate-resolution low-light imaging sensor data would be an important complement to the mapping capacity of moderate resolution daytime imaging sensors such as Aster and Landsat because it would provide an unambiguous indication of the presence of development and growth in development. Nightsat data would also be useful for calibrating and validating coarser resolution low-light imaging data acquired with the OLS and VIIRS sensors (Elvidge et al., 2007b, 2007c).

Although urban areas occupy only a small fraction of the Earth's surface, urbanization has risen to become one of the driving forces altering the Earth environment. Urban areas are the focal points for the consumption of food, water, and energy. They are likewise the focal points for both air and water pollution. Most of the agricultural,

fisheries, and resource exploitation activities constituting the balance of human impacts on the environment are driven by the consumption occurring in urban areas. The widespread use of impervious construction materials results in vastly increased surface runoff, which alters the stream flow and biodiversity. Urban areas tend to be built on flat, low-lying areas, often replacing wetlands. Although urban areas cover only a small percentage of the Earth's surface, their influence is enormous.

In the coming decades, urbanization will have a profound effect on the biological, chemical, and climate systems of our planet, both at local and at global scales. Urban areas are the largest sources of anthropogenic greenhouse gas emissions, and major sources of aerosols and water pollution. Urban expansion results in losses of agricultural lands and the fragmentation of wildlife habitats. Urban areas will expand dramatically as human population numbers are expected to double in the next 60–70 years. The increased urban demands for energy, food, and water will tax natural systems.

In no small measure, the activities concentrated in urban areas will determine the future habitability of our planet as a home for humankind and other species. There are legitimate questions regarding the sustainability of the current pattern of urbanization in the face of anticipated population and economic growth. Over time, urban areas may evolve to become more compact, energy-efficient, and less polluting, exerting a smaller footprint on the environment. In the interim, remotely sensed data provide one of the best sources of information on how urban areas are changing through time and how they affect the environment.

REFERENCES

Beach, D., Coastal sprawl: The effects of urban design on aquatic ecosystems of the United States, Pew Oceans Commission, Arlington, VA, USA, 2002.

Bhaduri, B., Bright, E., Coleman, P., and Dobson, J., LandScan: Locating people is what matters, *Geoinformatics*, 5, 34–37, 2002.

Booth, D., Urbanization and the natural drainage system — impacts, solutions, and prognoses, *Northwest Environmental Journal*, 7, 93–118, 1991.

Carlson, T.N., Impervious surface area and its effect on water abundance and water quality, in: Weng, Q., ed., *Remote Sensing of Impervious Surfaces*, CRC Press/Taylor and Francis Group, Florida, 2007.

Changnon, S.A., Inadvertent weather modification in urban areas: Lessons for global climate change, *Bulletin of the American Meteorological Society*, 73, 619–627, 1992.

CIESIN (Center for International Earth Science Information Network), *Where the Poor Are: An Atlas of Poverty*, Columbia University, Palisades, NY, 2006.

Crane, M., Xian, G., and McMahon, C., Estimation of sub-pixel impervious surfaces using Landsat and ASTER imagery for assessing urban growth, in: Moeller, M., and Wentz, E., eds., *Proceedings from ISPRS Joint Conference 2005: 3rd International Symposium Remote Sensing and Data Fusion Over Urban Areas (URBAN 2005)*, *5th International Symposium Remote Sensing of Urban Areas (URS 2005)*, XXXV1, 8/W27, Tempe, AZ, 2005.

De Navas-Walt, C., Proctor, B.D., and Lee, C.H., *Income, Poverty, and Health Insurance Coverage in the United States: 2004*, U.S. Census Bureau, Current Population Reports, P60-229, Government Printing Office, Washington, D.C., 2005.

Dobson, J., Bright, E.A., Coleman, P.R., Durfee, R.C., and Worley, B.A., LandScan: A global population database for estimating populations at risk, *Photogrammetric Engineering and Remote Sensing*, 66, 849–857, 2000.

Doll, C.N.H., Muller, J. P., and Elvidge, C.D., Night-time imagery as a tool for global mapping of socioeconomic parameters and greenhouse gas emissions, *Ambio*, 29(3), 157–162, 2000.

Ebener, S., Murray, C., Tandon, A., and Elvidge, C., From wealth to health: Modeling the distribution of income per capita at the sub-national level using night-time light imagery, *International Journal of Health Geographics*, 4(5), 1–17, 2005.

Elvidge, C.D., Baugh, K.E., Kihn, E.A., Koehl, H.W., Davis, E.R., and Davis, C.W., Relation between satellite observed visible near-infrared emissions, population, economic activity and power consumption, *International Journal of Remote Sensing*, 18, 1373–1379, 1997.

Elvidge, C.D., Baugh, K.E., Dietz, J.B., Bland, T., Sutton, P.C., and Kroehl, H.W., Radiance calibration of DMSP-OLS low-light imaging data of human settlements, *Remote Sensing of Environment*, 68, 77–88, 1999.

Elvidge, C.D., Milesi, C., Dietz, J.B., Tuttle, B.T., Sutton, P.C., Nemani, R., and Vogelmann, J.E., U.S. constructed area approaches the size of Ohio, *EOS Transactions, American Geophysical Union*, 85(24), 233, pp., 2004.

Elvidge, C.D., Tuttle, B.T., Sutton, P.C., Baugh, K.E., Howard, A.T., Milesi, C., Bhaduri, B., and Nemani, R., Global distribution and density of constructed impervious surfaces, *Sensors*, 7, 1962–1979, 2007a.

Elvidge, C.D., Cinzano, P., Pettit, D.R., Aversen, J., Sutton, P.C., Small, C., Nemani, R., Longcore, T., Rich, C., Safran, J., Weeks, J., and Ebener, S., The Nighsat mission concept, *International Journal of Remote Sensing*, 28(2), 2645–2670, 2007b.

Elvidge, C.D., Safran, J., Tuttle, B., Sutton, P., Cinzano, P., Pettit, D., Arvesen, J., and Small, C., Potential for global mapping of development via a Nightsat mission, *GeoJournal*, 69, 45–53, 2007c.

Foster, J.L., Observations of the earth using nighttime visible imagery, *International Journal of Remote Sensing*, 4, 785–791, 1983.

Gallo, K.P., Tarpley, J.D., McNab, A.L., and Karl, T.R., Assessment of urban heat islands: A satellite perspective, *Atmospheric Research*, 37, 37–43, 1995.

Gallo, K.P., Elvidge, C.D., Yang, L., and Reed, B.C., Trends in night-time city lights and vegetation indices associated with urbanization within the conterminous USA, *International Journal of Remote Sensing*, 25(10), 2003–2007, 2004.

Goetz, S.J., Wright, R.K., Smith, A.J., Zinecker, E., and Schaub, E., IKONOS imagery for resource management: Tree cover, impervious surfaces, and riparian buffer analysis in the mid-Atlantic region, *Remote Sensing of Environment*, 88, 195–208, 2003.

Henninger, N., and Snel, M., *Where Are the Poor: Experiences with the Development and Use of Poverty Maps*, World Resources Institute, Washington, D.C., 2002.

Hentschel, J., and Lanjouw, P., Using disaggregated poverty maps to plan sectoral investments, PremNotes No. 5, World Bank, Washington, D.C., 1998.

Imhoff, M., Lawrence, W.T., Elvidge, C.D., Paul, T., Levine, E., Privalsky, M., and Brown, V., Using nighttime DMSP/OLS images of city lights to estimate the impact of urban land use on soil resources in the United States, *Remote Sensing of Environment*, 59, 105–117, 1997.

Jennings, D., Jarniagin, S.T., and Ebert, D.W., A modeling approach for estimating watershed impervious surface area from National Land Cover Data 92, *Photogrammetric Engineering and Remote Sensing*, 70(11), 1295–1307, 2004.

Karshenas, M., Global Poverty Estimates and the Millennium Goals: Towards a Unified Framework, International Labour Office, Employment Strategy Papers, 5, 2004.

Kitzes, J., Peller, A., Goldfinger, S., and Wackernagel, M., Current methods for calculating national ecological footprint accounts, *Science for Environment & Sustainable Society*, 4(1), 1–9, 2007.

Lo, C.P., Urban indicators of China from radiance calibrated digital DMSP-OLS nighttime images, *Annals of the Association of American Geographers*, 92(2), 225–240, 2002.

Milesi, C., Elvidge, C.D., Nemani, R.R., and Running, S.W., Assessing the impact of urban land development on net primary productivity in the Southeastern United States, *Remote Sensing of Environment*, 86, 401–410, 2003.

Sachs, J.D., A new map of the world, *Economist Magazine*, 24, 81–83, 2000.

Sachs, J.D., *The End of Poverty: Economic Possibilities of Our Time*, Penguin Group, New York, 2005.

Sachs, J.D., Mellinger, A.D., and Gallup, J.L., The geography of poverty and wealth, *Scientific American*, 284(3), 70–75, 200l.

Schueler, T.R., The importance of imperviousness, *Watershed Protection Techniques*, 1(3), 100–111, 1994.

Slonecker, E.T., and Tilley, J.S., An evaluation of the individual components and accuracies associated with the determination of impervious area, *GIScience and Remote Sensing*, 41(2), 125–144, 2004.

Slonecker, E.T., Jennings, D.B., and Garofalo, D., Remote sensing of impervious surfaces: A review, *Remote Sensing Reviews*, 20(3), 227–255, 2001.

Small, C., Pozzi, F., and Elvidge, C.D., Spatial analysis of global urban extent from DMSP-OLS night lights, *Remote Sensing of Environment*, 96, 277–291, 2005.

Snel, M., Poverty-conservation mapping applications, 3rd IUCN World Conservation Congress, Bangkok, 2004.

Stankowski, S.J., Population density as an indirect indicator of urban and suburban land-surface modification, *USGS Professional Paper 800-B*, 219–224, 1972.

Sutton, P.C., An empirical environmental sustainability index derived solely from nighttime satellite imagery and ecosystem service evaluation, *Population and Environment*, 24(4), 293–311, 2003.

Sutton, P.C., and Costanza, R., Global estimates of market and non-market values derived from nighttime satellite imagery, land cover, and ecosystem service evaluation, *Ecological Economics*, 41, 509–527, 2002.

Sutton, P.C., Elvidge, C.D., and Ghosh, T., Estimation of gross domestic product at sub-national scales using nighttime satellite imagery, *International Journal of Ecological Economics and Statistics*, 8(S07), 5–21, 2007.

Vogelmann, J.E., Howard, S.M., Yang, L., Larson, C.R., Wylie, B.K., and Van Driel, N., Completion of the 1990s National Land Cover Data set for the conterminous United States from Landsat Thematic Mapper data and ancillary data sources, *Photogrammetric Engineering and Remote Sensing*, 67, 650–662, 2001.

Wackernagel, M., and Rees, W., *Our Ecological Footprint: Reducing Human Impact on the Earth*, New Society Publishers, Gabriola Island, BC, Canada, 1996.

Weeks, J.R., Using remote sensing and geographic information systems to identify the underlying properties of urban environments, in: Champion, T., and Hugo, G., eds., *New Forms of Urbanization: Conceptualizing and Measuring Human Settlement in the Twenty-first Century*, Ashgate Publishing Limited, London, 2004.

Welch, R., Monitoring urban population and energy utilization patterns from satellite data, *Remote Sensing of Environment*, 9, 1–9, 1980.

Weng, Q., Remote sensing of impervious surfaces: An overview, in: Weng, Q., ed., *Remote Sensing of Impervious Surfaces*, CRC Press/Taylor and Francis Group, Florida, 2007.

World Bank, *World Development Indicator*, World Bank, Washington, D.C., 2006.

World Wildlife Fund International (WWF), Global Footprint Network, Zoological Society of London, *Living Planet Report 2006*, WWF, Gland, Switzerland, 2006.

Yang, L., Huang, C., Homer, C.G., Wylie, B.K., and Crane, M.J., An approach for mapping large-area impervious surfaces: Synergistic use of Landsat-7 ETM+ and high spatial resolution imagery, *Canadian Journal of Remote Sensing*, 29, 230–240, 2003.

7 More Than a Name
Why Is Global Urban Population Mapping a GRUMPy Proposition?

Deborah Balk

CONTENTS

7.1 INTRODUCTION

Although significant progress has been made recently to assess the distribution of human population with respect to physiographic features — coastline, rivers, elevation (Small and Cohen, 2004) — these estimates cannot distinguish urban from rural areas. Considerable unmet need for global delineation of urban areas, as well as unmet need for spatial estimates of urban population (Montgomery et al., 2003), led to the design of the Global Rural-Urban Mapping Project (affectionately known as GRUMP).

GRUMP has produced the only known global database aimed at understanding patterns of urbanization that systematically incorporates spatial and demographic data. Efforts to understand urbanization at a global scale have a long history within the United Nations Population Division (see, for example, World Urbanization Prospects, UN 2006), yet a spatial orientation is well beyond its historical or current purview. Concomitantly, in the past 20 years, there have been major improvements in the spatial delineation of what could potentially pass as urban proxies: boundaries through geospatial technologies and the detection of built-up areas or other urban forms through remote sensing technologies.

The unique features and methods of the GRUMP databases are described below. Before doing so, however, it is important to understand that a project such as GRUMP required institutional commitments and maturity of several types in order to succeed. The future of urban population mapping remains uncertain for the research and policy communities most directly affected.

7.2 INSTITUTIONAL CONSIDERATIONS

GRUMP was conceived by a group of like-minded researchers attempting to better understand the distribution of human population with a particular interest in being able to disentangle urban settlements from more diffuse and sparse patterns of rural settlement largely for the study of human–environmental interactions at global and regional scales.* Although there were methodological and data contributions from multiple project partners, GRUMP was primarily implemented by a single organization—the Center for International Earth Science Information Network (CIESIN), at Columbia University.

CIESIN was in a unique position to implement the project for the following reasons. The various data inputs for this project are vast: they include spatial data on administrative subnational units at the finest resolution available, with associated populated counts; place name, geographic coordinates, and population estimates; and spatial boundaries indicating which areas are urban. Many of these inputs — such as administrative boundary data and population counts reported by administrative units —are generally the purview of national statistical offices (often different units within them). Yet, no single international organization collects, standardizes, and disseminates such data. The World Health Organization leads the Secondary Administrative Level Boundary project (http://www.who.int/whosis/database/gis/salb/salb_home.htm), which makes administrative boundary data publicly available, but the level of data in that collection is too coarse for the study of urban areas, and those data do not include population, nor is the collection global in extent at this point. To complicate matters, finely resolved administrative boundary data are often proprietary or costly to purchase. Population data at these finer levels are usually available freely from national statistical offices but they may not be joined to the spatial data. Thus, university-based efforts, such as those led by Columbia University's CIESIN since the early 1990s, to collect, clean, and render population estimates of a freely distributable transformed grid — the Gridded Population of the World (GPW) data set—fill a critical role (Balk and Yetman, 2004). Furthermore, the investments in GPW's underlying data and methods (Tobler et al., 1997) provide a critical backbone on which GRUMP was developed. Replication of the GPW input data holdings beyond those held by CIESIN alone would have made the GRUMP investment prohibitively expensive in time and other costs.

International bodies — which have made a considerable mark in establishing standards for undertaking national census and collecting geospatial data (UN, 2008) — may not have the flexibility to modify their current mandates to fulfill

* Individuals are identified at http://sedac.ciesin.columbia.edu/gpw/credits.jsp, and a fuller history of the project is at: http://sedac.ciesin.columbia.edu/gpw/history.jsp.

the role of data collector, repository, and disseminator of global subnational demographic data. One may wonder why the UN Statistics Division, which maintains *The Demographic Yearbook*, could not take on such a role. Although the Statistics Division receives reports or data from national statistical offices, its mandate does not cover subnational data or geospatial data. Furthermore, even though this arm of the UN maintains working relationships with national statistical offices, the end product of the *Demographic Yearbook* has been widely criticized by user (Montgomery et al., 2003). For example, it reports country- and city-level statistics without conducting sufficient analysis on the quality of those data. In contrast, the United Nations Population Division goes to great length to assess data quality and uses a variety of well-established democratic techniques to correctly estimate and forecast population. Even for its estimates of urban population, however, the Population Division's emphasis is on cities of 750,000 persons or more, and ignores the spatial dimension. Beyond international agencies, some efforts of international networks address spatial data. One such network is the Global Spatial Data Infrastructure Association, which pays no particular attention to demographic data.

Universities are not necessarily bound by the same constraints that international and national agencies face. For example, the UN complies with certain political realities of its institution: it does not recognize Taiwan as a separate national authority from that of the People's Republic of China. In contrast, universities (apart from those in China) are free to do so. A national agency such as the United States Census Bureau also produces fine-grained estimates of its own population as well as national-level population trends for all other countries, but it does not see subnational estimation of foreign nations as within its domain.

International agencies often have a global scope that single universities or consortia thereof do not. Yet international bureaucracies have become rigid, whereas universities (and governmental or international agency contracts to them) offer greater flexibility for constructing new methods. A retrospective examination makes it clear that the development of GRUMP would have been far easier had there been a ready-made set of input datasets supplied by international agencies — leaving only the integration and methodological development to universities. Who will carry the torch in future decades is unclear, but one hopes that an increasing awareness of the importance of spatial data to studies of urbanization (Montgomery, 2008) will lead to more informed decisions — if not a complete reevaluation and overhaul — in the institutions participating in data standards, collection, dissemination, and so forth.

7.3 THE GOLD STANDARD FOR GLOBAL EXTENT URBAN DATA

When a group of researchers or planners sets out to address an issue, it usually does so with a specific set of questions in mind, rather than the construction of new data for data's sake. The GRUMP project was no different; yet, because GRUMP was undertaken at an institution that also produces and disseminates global datasets it quickly became apparent that the need for, and usage of, a global-scale georeferenced urban population data set was potentially tremendous. Several basic features

emerged to set a "gold standard" — an implicitly recognized set of standards of excellence — as required to understand urbanization in a spatial context, at a global scale. These include (1) time-varying population characteristics coupled with time-varying urban boundaries; (2) estimates should be comparable not only in time, but also by location (irrespective of the level of economic development, topography, and so forth)*; (3) urban contours should be identifiable at the extent of an urban area as well as within urban areas.

There is no single definition of what makes an area "urban." The appendix of the United Nations World Urbanization Prospects (UN, 2006) identifies how each country defines "urban." Criteria include a variety of population size or population density thresholds associated with administrative areas, economic activity characteristics of administrative areas, capitol cities, and combinations thereof, sometimes with additional criteria such as contiguity specification. Specifications that are associated with the degree of "built-up" area as detectable from vegetated areas are more readily adopted by the physical sciences (Small, 2005) and planning communities, but no single consensus on "built-up" or method for identification yet exists.

When defining the population characteristics of an urban area, at minimum, a count of persons living in each urban area is necessary. Yet, far more information is a desirable option to ascertain demographic composition, trends, and change (Montgomery et al., 2003). Demographic forecasts require demographic rates (fertility and mortality), age, and life expectancy are the basics for demographic forecasting, although new methods hold promise for using different data streams and factors than found in the traditional cohort component forecasting (Montgomery and Balk, forthcoming). A full understanding of the demography of urban change also requires information on migration. Demographic censuses are typically held once per decade, and in some places, intercensal estimates are made in the mid-period. Yet, if migration — or residential mobility — is frequent, say on the order of more than once per year neither current censuses nor standard demographic surveys, such as the Demographic and Health Surveys (http://measuredhs.com) and Multiple Indicator Cluster Surveys (www.childinfo.org), can measure it accurately. Socioeconomic characteristics are also relevant. It would be important to know if rich or poor groups (or ethnic groups, or many other characteristics) are growing at different rates or are highly concentrated or distributed.

Defining the urban extent characteristics requires some means of systematic identification of an urban area's boundaries or physical "footprint." Some national statistical offices supply boundary data files for urban areas (even to distinguish the city proper from outlying areas) but most do not. When the administrative unit is fine enough, and nested hierarchical relationships between administrative units are known, these data may be called "building blocks" (Champion and Hugo, 2004) and would likely suffice as a means for constructing urban contours. In the absence of these building blocks, remote sensing technologies have provided several possible

* This is not a call for a population-based criteria for urbanization but rather use of some built-environmental characteristic typically associated with urban areas in contrast to rural areas. There may be more than one applicable standard, and any standard even of the built environment should take care to incorporate differences in that environment that occur both naturally and due to anthropogenic factors.

proxies to delineate urban footprints, some of which are discussed elsewhere in this volume. Indeed, much work has been done using optical imagery to detect urban changes in particular localities. Here, my comments will be limited to efforts that are global in extent.

High-resolution imagery has not been used at a global scale. Moderate-resolution imagery that detects land cover (e.g., Landsat, Spot Vegetation) has been used to determine urban areas as the presence of "mixed pixels" localities (such as reflectants from trees, buildings, roads, water, and grass). These have been used in the development of global databases such as the Global Landcover 2000 data set (http://www-tem.jrc.it/glc2000/). Optical data of this type — even with trained classifiers and clear guidelines — have been subjectively classified, opening it up to analyst interpretation. Furthermore, clouds remain a concern for any frequently repeated views. The most commonly used moderate-resolution data to indicate urban areas at a global scale are the nighttime lights data (Elvidge et al., 1997a, 1997b). These data do not indicate either built-up area or the heterogeneous pixels from vegetation imagery, but rather stable sources of light produced by electricity and permanent fires. Although several "lights" datasets exist, only the 1994–1995 stable city lights data product was cleaned to remove oil and gas flares and other anomalies. By all accounts, this data set can be seen as a proxy for urban areas. Nevertheless, it may be subject to bias associated with levels of economic activity — i.e., poor cities may indeed exist but their extent may be spatially underrepresented as compared to wealthier cities of equal geographic size. Recent work indicates that the built-up areas can be more sharply identified with radar data (Nghiem et al., 2008) than with optical data, and shows some promise for making at least crude intraurban distinctions of the built-up areas. As this recent work is based on case studies, however, the prospects for global assessment are unknown. The gold standard areal extents would be able to detect change in the true built-up area over time, as well as changes within urban areas (sometimes referred to as in-fill; see Angel et al., 2005).

Both population and spatial extents estimates for urban areas are necessary elements for a linked database, yet they are not sufficient. There must be a means for linking these data sources. Although data may be matched spatially an exact spatial match can occur only if the boundaries are identical between data streams. This is very unlikely to happen. Urban areas detected through satellites never have place names associated with them. Administrative areas may have names, but these are not necessarily the same as urban places (they may have higher- or lower-order units). Population must then also be assigned to these extents, again ideally with corresponding names. If more than one spatial data set is to be used, all boundaries must be accounted for so that resulting products do not truncate observations where boundaries do not match. The issue of linkages is difficult enough at the scale of a city, but likely to be more complex when identifying areas within a city. Obviously, no global work has attempted to link demographic characteristics within urban areas; however, several case studies, notably by Weeks and colleagues (2004, 2005, 2007), have attempted this to generate fertility contours within a city.

This gold standard is not met by GRUMP or any other approach, such as that using sampling (Angel et al., 2005), nor by creating modeled population surfaces (e.g., LandScan), that do not indicate urban areas in a systematic way (Dobson et al., 2000). Although each of these as well as other approaches offer something

significant to the questions they were constructed to answer, and to the discourse at large, GRUMP comes closest to meeting the gold standard, and lays the foundation for meeting the gold standard in the foreseeable future.

7.4 GRUMP AND THE GOLD STANDARD

GRUMP measures population with associated spatial extents. Population is estimated for more than one target year (1990, 1995, and 2000) so that the estimates can be integrated with other single-year data ranging the same decadal span (i.e., so that 1990 environmental data can be matched with 1990 population data, not with year 2000 population data). The database is not designed to be used to determine change over time, in spatial terms, or to measure implicitly spatial concepts — such as change in population density over time.* This is because the extents are measured at only one point — 1994–1995 — using the nighttime lights "stable city light" data set. No demographic characteristics other than population counts are estimated. Place and administrative names are also identified. Subcity population distributions are detected in many localities, but not all. No attempt is made to classify them as inner city, suburban, and so forth. How GRUMP meets or fails the gold standard is elaborated on, in turn.

One shortcoming of using the nighttime lights (even the stable city lights data, which surely have fewer "false positives," or locations detected through the lights that are, in fact, not cities) is known as the lights overglow or a "blooming effect" (Elvidge et al., 2004). This overestimation of the true extents of urban areas is believed to be dependent on the intrinsic characteristics of the sensor. The extent to which the blooming effect is associated with the economic status of locations is unclear. Furthermore, the lights cannot detect less-electrified regions of the world, and thus some settlements, in particular those that are small or poor (i.e., without electricity), go unmeasured. The former leads to an overestimation of the size of some urban areas, whereas the latter two concerns lead to detection of fewer urban areas. These shortcomings aside, the lights appear to detect settlements as small as a few thousand persons in South America, for example. Unlike other approaches to urban detection, the limitations with the use of these lights are well known at this point, and acknowledged by the data producers. Furthermore, the lights make an extremely important contribution to establishing a gold standard for urban detection. Future lights datasets may be used to provide a time series of detectable footprints. Future research can help identify the potential bias associated with using a measure of light rather than built-up areas; and new methods may be used to overcome any resulting bias as well as the limitations associated with the overglow.

* National-level estimates of population in 1990 and 2000 match those of the United Nations, so change over time at that level will be consistent with estimates from the UN. However, estimates of change over time that are subnational in nature, particularly at the resolution of the GRUMP data, are not intended. With modification to the GRUMP methodology to incorporate subnational growth, improved estimates could be generated to permit assessment of change in subnational population over time. Yet this is secondary, as change in areal extents and, therefore population density over time, would remain problematic so long as only a single set of nighttime lights were used. The primary reason constraining spatiotemporal comparisons is the use of a single, mid-period, footprint to detect urban extents.

GRUMP has no means for assigning intraurban contours of the built-up area. In some instances (particularly for populous cities), as described below, the population grid associated with the GRUMP databases produces estimates of population at a subcity level. One could argue that defining the urban footprints as is accomplished in GRUMP should precede that of understanding the intraurban contours, because it is necessary to first establish the boundaries in which the intra-urban contours nest. In this sense, GRUMP is a first step in this direction. Furthermore, future versions of night-lights data hold promise for making distinctions of light areas within a contiguous light.

No other demographic indicators apart from population counts and density are produced from GRUMP.

7.5 GRUMP

Details for the GRUMP methodology are found elsewhere (see Balk et al., 2005) and are summarized here.* The GRUMP project produces three basic types of data products: a data set of human settlement points, an urban extent mask, and an urban population grid (CIESIN, 2004a, 2004b, 2004c). The latter two datasets may be combined to produce urban population estimates associated with urban footprints. Figure 7.1 shows the population points. Figure 7.2 shows the process by which the points are allocated to the urban footprints: as in the case of Cali (which has 12 settlement points within and one additional point within the margin of error of the extent boundary), the population of the points is summed to the urban extent. Figure 7.3

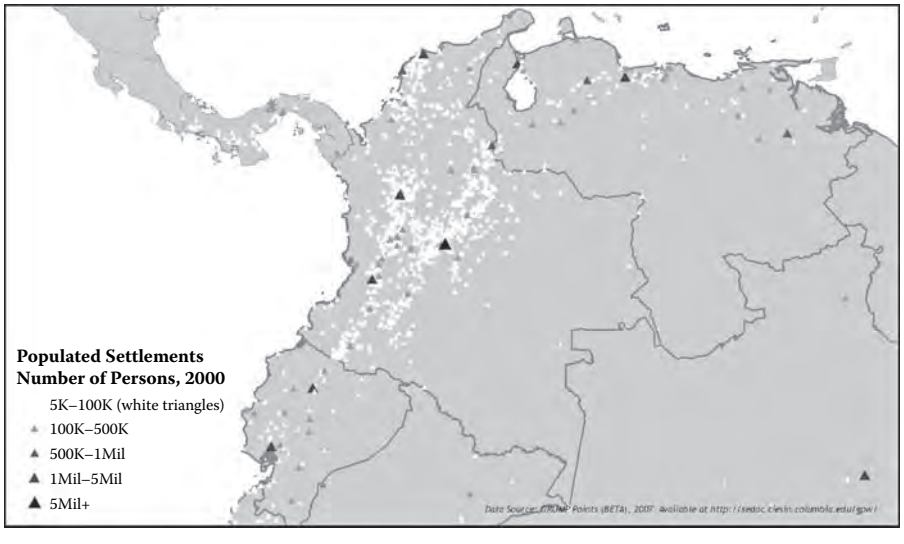

FIGURE 7.1 GRUMP settlement points by population size, 2000, in Colombia and surrounding countries.

* A revised write-up of the GRUMP methods has been drafted, and expected to be available by fall 2008.

FIGURE 7.2 GRUMP inputs: administrative units along with urban extents and settlement points, Cali, Colombia, and surrounding areas.

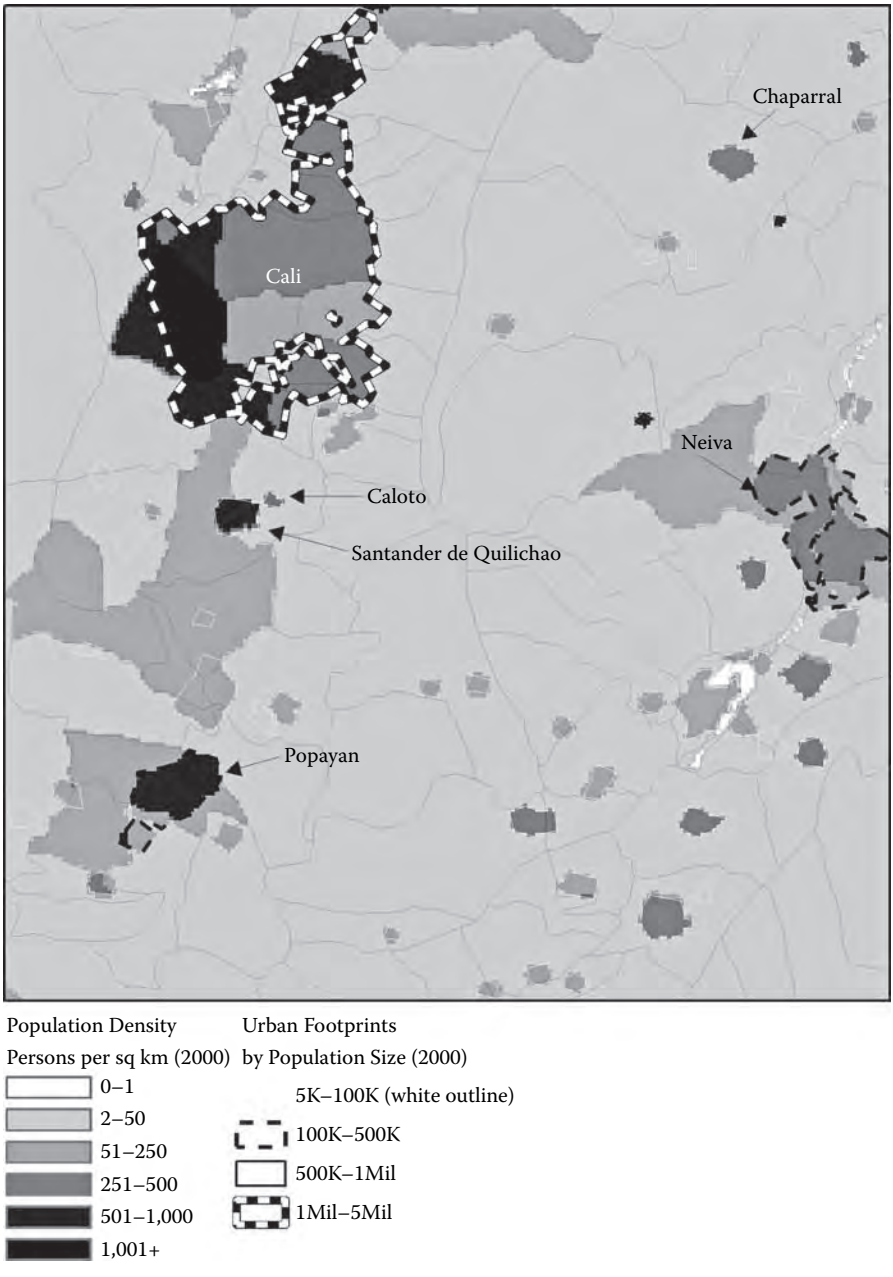

FIGURE 7.3 GRUMP outputs: population distribution and urban extents, Cali, Colombia, and surrounding areas.

shows how population is reallocated when accounting for administrative area totals. The third database renders the right panel of Figure 7.2 as a population grid (not shown). Greater detail on these steps follows.

Unlike the population estimates associated with administrative boundaries that have been the backbone of national censuses and significant international technical assistance, population estimation of urban places has received little scrutiny or investment by the global community. The settlement points database (Figure 7.1) is constructed by culling national statistical office and publicly available databases with estimates of populated places: names, population, and geographic coordinates. In many instances, three different data sources were required for a given place. (Source information for each datum is retained in the disseminated GRUMP settlements point database.) When it was evident how the population estimate associated with each point was classified — city proper, agglomeration, etc. — such classifications were noted.

Next, the settlement points were spatially joined with the settlement extents and the population assigned, or summed, if more than one point was found, as in the case of Cali (Figure 7.2).* The name of the most populous place within the buffer was assigned to the polygon. For points without polygons, areal extents for urban areas were estimated based on a relationship between population size and areal extents for the points with known parameters. (This relationship is derived from a logarithmic regression that predicts the expected geographic size of a place, given its population size, given a minimum number of observations, or by combining data in regional groupings supplied by the UN Statistics Division.). Based on these estimated area values, a circular urban area centered on the known points was created. The resulting polygons were then added to the existing lights-based ones to create a complete urban extent coverage for each country.

The penultimate step was to generate a 30-arc second population distribution raster data set. To create it, we modeled population by applying a mass-conserving algorithm that reallocates people into urban areas, within each administrative unit. This uses data inputs from two vector sources: (1) administrative polygons, containing the total population for each administrative unit (as indicated in Figure 7.2), and (2) urban areas, containing the urban population for each area resulting from the urban extent coverage (i.e., the sum of points for each extent, as shown in Figure 7.2). The algorithm works on a country-by-country basis and accounts for the following information: the area and population of each urban extent, the area and population of each administrative unit, the size of the intersected areas where the urban and administrative areas overlap, and the UN national estimates for the percentage of the population in urban and rural areas. The goal of the algorithm is to reallocate, or adjust, the total population in each administrative unit into rural and urban. It follows a "do-no-harm" principle. The algorithm is set so that the least amount of reallocation takes place, yet is applied when it is necessary to make sure that the population of the urban extents (as estimated by the settlement points) does not exceed

* A 3-km buffer distance was used to assign points to polygons as this is in keeping with the margin of error inherent in the light measurement (Elvidge et al., 2004).

that from the administrative area data. It takes the settlement points as summarized to the urban footprints as the starting point, and adjusts to ensure that no population estimate exceeds the maximum of the administrative areas that intersect it. A second set of constraints is imposed to ensure balance in urban and rural population densities — that is, reallocation cannot produce population estimates of a given urban area that would result in urban population densities that are less than rural densities (on average). UN (2006) national-level rural/urban percentage estimates and those from the countries are used as guidelines. When the number of administrative units for a given urban extent was high relative to the size of the urban area (e.g., dozens or more of suburban units within a medium- to large-size city), the reallocation algorithm was not used. Those areas were gridded directly and then the population values were assigned to the urban extents, strictly on spatial overlays, in the final step.*

When there is only one urban area per administrative unit or when the urban area (even if subdivided into many smaller subunits) lies wholly within the administrative unit, the adjustment in population is trivial. GRUMP was designed in part to estimate population in urban areas where no estimates exist. It is not intended as a "good data" model. The reallocation becomes increasingly complex, however, when there is more than one urban area, when urban areas overlap more than one administrative area (e.g., Cali), and when large urban areas contain more than one administrative area as shown in Figure 7.2.

The resulting map is shown in Figure 7.3, with a close-up view of Cali, Colombia, showing the data after running the algorithm. Where urban areas are present in a given administrative unit, the density of the administrative unit decreases after the algorithm has been used because people are reallocated into their respective urban areas.

The final GRUMP database is an urban mask with attributes, such as the name, population, and land area, as shown for selected cities in Colombia in Table 7.1. Although the administrative data in Colombia are relatively good, the size of the units is such that the reallocation in general works well, especially for medium and small cities. Figure 7.3 shows some cases of relatively large administrative units with one or two cities where GRUMP has assigned people to urban areas, decreasing the density of the remaining administrative unit (e.g., Santander de Quilichao and Caloto). For example, Caloto is a small town (about 5000 persons) that is not reported in most city lists. Yet here it is identifiable, given a population estimate and location close to the nearest large city (Santander de Quilichao). Chapparal, a city of nearly 200,000 persons (in 2000), is differentiated from the rest of the administrative area in which it falls. This is GRUMP working as designed. In the case of Cali, where the urban areas identified by the lights expand over several administrative units, the estimated population of the greater Cali area is larger than estimates based on the administrative area for Cali proper than one might find in other sources (such

* This has the effect of rendering population estimates for the units that border the city (on both sides of the border) as an average. The GRUMP algorithm, in these instances, tends to produce a "donut" effect and this was not employed.

TABLE 7.1
Estimates of Population Size and Density, and Land Area for All Selected Urban Areas Near Cali, Columbia

	Estimates Derived from GRUMP		
Urban Area Name	Population (2000), in 000s	Land Area (ca. 1995), in km^2	Population Density (persons per km^2)
Cali	3020	2515	1201
Neiva	264	558	474
Chapparal	197	62	446
Santander de Quilichao	40	69	585
Popayan	27	259	761
Caloto	5	10	499

as www.citypopulation.de). Neiva, a much smaller city than Cali, similarly expands across more than one administrative area. Once again, this is GRUMP working as it should.*

GRUMP estimates may differ from other published estimates for a number of reasons. In some instances, GRUMP will attribute peri-urban population to an urban agglomeration, perhaps by increasing the population. In other instances, it will reduce the population of a given area, if the input data referred to an administrative area (such as large metropolitan counties) that contains urban and rural areas. An example of such is shown in Figure 7.4 and Table 7.2 for Beijing.† Although the UN Population Division comes up with estimate B for the population of Beijing, as does the GRUMP project, the Chinese government reports many different estimates, none of which is fully interpretable without an accompanying map of this type. The urban portions of Beijing county are not spatially delineated as urban without GRUMP. GRUMP assigns an urban population estimate for each of these localities. Thus, any given urban area needs to be assessed with nearby localities from which the lights — the footprint in GRUMP — may have been spatially separated.

7.6 CONCLUDING REMARKS

Each of the three basic data products from GRUMP makes a contribution: the human settlement points data attempts to resolve the classification type of locality, attaches geographic coordinates to named, populated places, and includes settlements of much

* In Figure 7.2, it is apparent that some urban extents have no settlement points and in Figure 7.3 that they have no population reallocated to them. (That is, their population would not differ per pixel from that in the surrounding area.) This is because no named settlement with population was found for those locations. As is evident from the map, these localities are smaller than those with known settlements.

† A variation of this figure appears in the work of Montgomery and Balk (forthcoming) and Montgomery (2008, Figure 1, p. 761), and was developed with insight from S. Henning of the United Nations and K.W. Chan of the University of Washington (Chan and Hu, 2003; Chan, 2007).

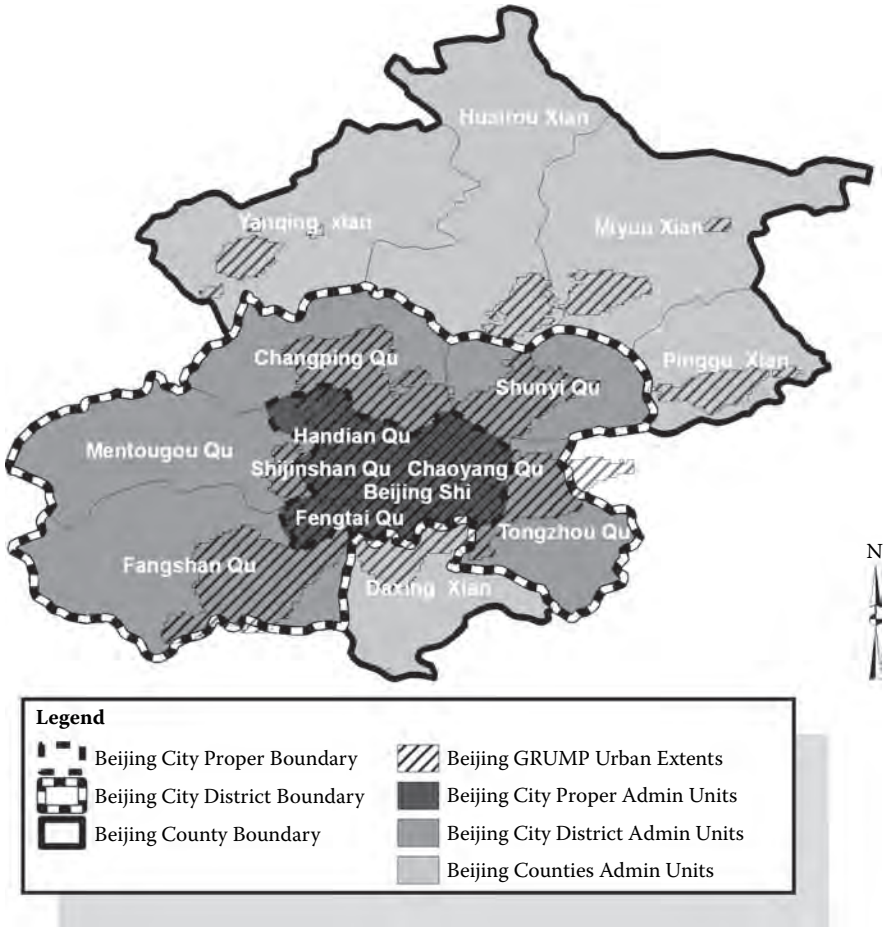

FIGURE 7.4 The administrative boundaries of Beijing, China, with GRUMP urban extents overlaid.

smaller sizes than other compendia. That said, the settlement points database relies on inputs that have had only a fraction of the level of global investments in technical assistance and standards that have been made in administrative boundary data. When coupling points with urban extents, it becomes apparent that settlement point data in the future will require much greater scrutiny and transparency.*

The urban extent mask (described here as having population size and names associated with it) is more and less than the lights data on which it is based. It is more because it "verifies" that each and every light has at least one corresponding

* It is possible that very finely resolved administrative data, if at the subcity level, would provide a suitable alternative, but those data — despite the increasing availability and quality of georeferenced administrative data — do not seem imminent at the scale of city any time soon.

TABLE 7.2
Various Population Estimates of Beijing, Corresponding to Different Administrative Criteria (Corresponding to Boundaries Shown in Figure 7.4)

Administration Division Type and Name		Population			
		Total	Urban	Rural	% Urban
City proper	Beijing Shi	2,114,586	2,114,586	–	100%
City proper	Chaoyang Qu	2,289,756	2,289,756	–	100%
City proper	Fengtai Qu	1,369,480	1,369,480	–	100%
City proper	Shijinshan Qu	489,439	489,439	–	100%
City proper	Handian Qu	2,240,124	2,240,124	–	100%
Subtotal A		*8,503,385*	*8,503,385*		
City district	Mentougou Qu	266,591	187,616,	78,975	70%
City district	Fangshan Qu	814,367	379,882	434,485	47%
City district	Tongzhou Qu	673,952	346,645	327,307	51%
City district	Shunyi Qu	636,479	207,341	429,138	33%
City district	Changping Qu	614,821	251,792	363,029	41%
Subtotal B		*11,509,595*			
Subtotal C			*9,876,661*		
Beijing county	Daxing Xian	671,444	188,109	483,335	28%
Beijing county	Pinggu Xian	396,701	119,053	277,648	30%
Beijing county	Huairou Xian	296,002	116,900	179,102	39%
Beijing county	Miyun Xian	420,019	128,999	291,020	31%
Beijing county	Yanqing Xian	275,433	92,742	182,691	34%
Subtotal D		*13,569,194*			
Subtotal E			*10,522,464*		

populated place that falls inside of it. It can be argued that it is a more complete rendering of places because it also renders settlement points that were undetected by the light (as may be common in poorly lit parts of the world, and for small urban extents). That said, lights with no corresponding populated places, were dropped.* These lights may include other forms of settlement — such as industrial location — which may be important. Future work should further evaluate the night-time lights with this concern in mind. Whether the population associated with these urban extents is superior to the underlying input data depends in part on the quality of the GRUMP population grid (discussed below). That said, the extents alone could and have already been used in any number of applications that distinguish urban from rural land areas both in conjunction with and apart from the population estimation

* CIESIN intends to include in the final GRUMP data products two versions of the urban extent mask: one to include all verified extents, and one that also includes all other lights. The estimated population counts for the light type of urban extent — that could derive from a spatial overlay of the population surface with the mask — would almost certainly produce estimates of population that are too low, and should be used with caution.

(e.g., McGrahanan et al., 2005, 2007, which include additional maps of GRUMP inputs and outputs).

The GRUMP population grid makes an important contribution for refining the estimates of population distribution beyond what can be accomplished using administrative boundary data alone, but without using a variety of biophysical parameters to model population: the model uses only one additional type of data for the reallocation — urban extents. In countries where they are of very good quality — finely resolved administrative data at the level of the city — GRUMP as a reallocation method is not necessary. (Even when the administrative data are of high resolution, a common means to identify urban contours in a consistent way — such as the use of the lights-based "footprints" — is still necessary.) Yet, where administrative data are of poor to average quality, and the lights are detectable, GRUMP performs moderately well — the final extent databases identifies more than 25,000 urban agglomerations globally. When used in conjunction with maps, it is evident why urban population estimates associated with GRUMP differ from those given by a variety of sources — including those that rely heavily on (sometimes geographically large and coarse) administrative area representations of urban areas. Where both the administrative data and the lights (or its substitutes) are poor, GRUMP just does not have much to work with. As is generally the case, there are no perfect substitutes for good data.

GRUMP is just a starting point to think about how to systematically identify population and urban areas, both in time and space. There is no obvious global "truth" — that is, a known benchmark with which to compare these estimates. The other existing estimates of urban population do not correspond to space. As seen here, the spatial dimension changes those estimates. Over time, GRUMP and kindred approaches will be improved, reworked, and, hopefully, keep active a dialogue for future efforts for a community of urban scholars and planners.

ACKNOWLEDGMENTS

The data described in this chapter were developed at the CIESIN, at Columbia University, where I was research scientist through September 2006 (and am now adjunct), primarily with funding from the NASA-funded data Center, the Socioeconomic Data and Applications Center, which provided much of the data presented herein. See http://sedac.ciesin.columbia.edu/gpw for a complete list of project partners and sponsors. Thanks to Sanders Korenman for comments and to Karen von Muehldorfer for comments and assistance with preparation of Table 7.1 and Figure 7.3, and to Valentina Mara and Leila Forouzan for assistance with Figure 7.4. All views represented herein are mine alone and do not represent those of my colleagues at Columbia or the GRUMP project.

REFERENCES

Angel, S., Sheppard, S.C., and Civco, D.L., *The Dynamics of Global Urban Expansion*, World Bank Transport and Urban Development Department, Washington, D.C., 2005.

Balk, D., Pozzi, F., Yetman, G., Deichmann, U., and Nelson, A., The distribution of people and the dimension of place: Methodologies to improve the global estimation of urban extents, Paper presented at the International Society for Photogrammetry and Remote Sensing Proceedings of the Urban Remote Sensing Conference, March 14–16, Tempe, AZ, 2005.

Balk, D., and Yetman, G., The Global Distribution of Population: Evaluating the gains in resolution refinement." Working paper Center for International Earth Science Information Network (CIESIN), 2004. Available at: http://sedac.ciesin.columbia.edu/gpw/docs/gpw3_documentation_final.pdf (accessed February 1, 2008).

Champion, T., and Hugo, G., ed., *New Forms of Urbanization: Beyond the Urban–Rural Dichotomy*, Ashgate Publishing Limited, Aldershot, 2004.

Chan, K.W., and Hu, Y., Urbanization in China in the 1990s: New definition, different series, and revised trends, *China Review*, 3(2), 49–71, 2003.

Chan, K.W., Misconceptions and complexities in the study of China's cities: Definitions, statistics, and implications, *Eurasian Geography and Economics*, 48(4), 383–412, 2007.

Dobson, J.E., Bright, E.A., Coleman, P.R., Durfee, R.C., and Worley, B.A., LandScan: Global population database for estimating populations at risk, *Photogrammetric Engineering and Remote Sensing*, 66(7), 849–857, 2000.

Elvidge, C.D., Baugh, K.E., Kihn, E.A., Kroehl, H.W., and Davis, E.R., Mapping city lights with nighttime data from the DMSP Operational Linescan System, *Photogrammetric Engineering and Remote Sensing*, 63(6), 727–734, 1997a.

Elvidge, C.D., Baugh, K.E., Hobson, V.R., Kihn, E.A., Kroehl, H.W., Davis, E.R., and Cocero, D., Satellite inventory of human settlements using nocturnal radiation emissions: A contribution for the global toolchest, *Global Change Biology*, 3(5), 387–395, 1997b.

Elvidge, C.D., Safran, J., Nelson, I.L., Tuttle, B.T., Hobson, V.R., Baugh, K.E., Dietz, J.B., and Erwin, E.H., Area and position accuracy of DMSP nighttime lights data, in: Lunetta, R.S., and Lyon, J.G., eds., *Remote Sensing and GIS Accuracy Assessment*, Chap. 20, CRC Press, Boca Raton, FL, pp. 281–292, 2004.

Center for International Earth Science Information Network (CIESIN), Columbia University, International Food Policy Research Institute (IFPRI), The World Bank and Centro Internacional de Agricultura Tropical (CIAT), Settlement Points, 2004a. Available at: http://sedac.ciesin.columbia.edu/gpw (accessed February 1, 2008).

Center for International Earth Science Information Network (CIESIN), Columbia University, IFPRI, World Bank, and CIAT, Global Rural-Urban Mapping Project (GRUMP): Urban Extents, 2004b. Available at: http://sedac.ciesin.columbia.edu/gpw (accessed February 1, 2008).

Center for International Earth Science Information Network (CIESIN), Columbia University, IFPRI, World Bank, and CIAT, Global Rural-Urban Mapping Project (GRUMP): Gridded Population of the World, version 3, with Urban Reallocation (GPW-UR), 2004c. Available at: http://sedac.ciesin.columbia.edu/gpw (accessed February 1, 2008).

McGrahanan, G., Marcotullio, P., Bai, X., Balk, D., Braga, T., Douglas, I., Elmqvist, T., Rees, W., Satterthwaite, D., Songsore, J., and Zlotnik, H., Urban systems, in: *Ecosystems and Human Well-Being: Current State and Trends, Findings of the Condition and Trends Working Group*, Chap. 27, Island Press, Chicago, pp. pp. 795–826, 2005.

McGrahanan, G., Balk, D., and Anderson, B., The rising tide: Assessing the risks of climate change and human settlements in low elevation coastal zones, *Environment and Urbanization*, 19(1), 17–37, 2007.

Montgomery, M.R., The urban transformation of the developing world, *Science*, 319(5864), 761–764, 2008.

Montgomery, M.R., Stren, R., Cohen, B., and Reed, H.E., eds., *Cities Transformed: Demographic Change and its Implication in the Developing World*, National Academy Press, Washington, D.C., 2003.

Montgomery, M.R., and Balk, D., The urban transition in developing countries: Demography meets geography, in: Birch, E., and Wachter, S., eds., *Global Urbanization in the 21st Century*, University of Pennsylvania Press, Philadelphia, forthcoming.

Nghiem, S.V., Balk, D., Rodriguez, E., Neumann, G., Sorichetta, A., Small, C., and Elvidge, C.D., Observations of urban and suburban environments with global satellite scatterometer data, *ISPRS Journal of Photogrammetry and Remote Sensing*, forthcoming.

Small, C., and Cohen, J., Continental physiography, climate and the global distribution of human population, *Current Anthropology*, 45(2), 269–277, 2004.

Small, C., Global analysis of urban reflectance, *International Journal of Remote Sensing*, 26(4), 661–681, 2005.

Tobler, W., Deichmann, U., Gottsegen, J., and Maloy, K., World Population in a grid of spherical quadrilaterals, *International Journal of Population Geography*, 3(3), 203–225, 1997.

United Nations, *World Urbanization Prospects: The 2005 Revision*, United Nations, New York, 2006.

United Nations, *Principles and Recommendations for National Censuses of Population and Housing Revision 2*, United Nations Department of Economic and Social Affairs, New York, 2008.

Weeks, J.R., Using remote sensing and geographic information systems to identify the underlying properties of urban environments, in: Champion, T., and Hugo, G., eds., *New Forms of Urbanization: Conceptualizing and Measuring Human Settlement in the Twenty-First Century*, Chap. 17, Ashgate Publishing Limited, London, pp. 325–346, 2004.

Weeks, J.R., Larson, D., and Fugate, D., Patterns of urban land use as assessed by satellite imagery: An application to Cairo, Egypt, in: Entwisle, B., Rindfuss, R., and Stern, P., eds., *Population, Land Use, and Environment*, Chap. 11, National Academy Press, Washington, D.C., pp. 265–286, 2005.

Weeks, J.R., Hill, A.G., Stow, D., Getis, A., and Fugate, D., Can you spot a neighborhood from the air? Defining neighborhood structure in Accra, Ghana, *GeoJournal*, 69(1–2), 9–22, 2007.

8 The Africover and PMUR Datasets and the Challenge of Human Settlement Mapping in Africa

John Latham, Barbara Huddleston, Renato Cumani, Antonio Martucci, Ilaria Rosati, Mirella Salvatore, Babikar Fadl El Seed El Sidding Adam, and Nihad El Nogoumy

CONTENTS

8.1 DEFINING HUMAN SETTLEMENTS

According to the United Nations Population Division, because of national differences in the characteristics that distinguish urban from rural areas, there is no internationally agreed consensus on how the dividing lines between urban, suburban, and rural settlements should be demarcated (UN, 1998). Sometimes the administrative boundaries of human settlements such as cities, towns, and villages are available and are used to distinguish urban from rural — the populations within these administrative units being classified as urban, and the populations outside of them being classified as rural. Sometimes qualitative terminology with no precise meaning is used, for example, "urban centers," "major cities," "administrative centers," or "municipalities." Local inhabitants know the settlements to which these terms refer, but they are not otherwise defined.

When definitions are based on quantitative thresholds, the minimum population for a place to be considered urban varies greatly. For instance, in several countries in Latin America and West Africa, the threshold is a population of 2000, whereas in Iceland it is 200 and in countries such as Italy and Benin it runs to 10,000. Alternatively, the definition of an urban population can be very complex, involving the socioeconomic characteristics of the population or community (UN, 2004). For example, in countries that are still largely agricultural, the presence or absence of agriculture as the dominant form of economic activity may be used as the basis for distinguishing rural from urban space.

The term "human settlement" implies the presence of both structures and people in a bounded area. When a technically consistent method for mapping human settlements is applied, it will reveal the presence of settlements in some countries that are not classified as "urban" according to national usage. Some mapmakers refer to the bounded area of any human settlement as "urban area," whereas others use the term to refer only to mapped human settlements that have been determined by one method or another to correspond to national usage. Therefore, extreme caution should be exercised when comparing urban extents generated by different mapping methods [Food Agriculture Organization (FAO), 2005].

8.2 DIFFERING APPROACHES TO MAPPING HUMAN SETTLEMENTS

The utility of one approach versus another for mapping human settlements depends on the intended purpose. For associating population counts with urban extents, approaches that bound the urban areas appear appropriate. For land use planning in and around expanding urban areas, approaches that seek to distinguish different land use classes within an urban area and its periphery are likely to prove more valuable.

For some purposes, it is sufficient to know the geographic locations and areal extents of bounded human settlements and the number of people inhabiting each such settled area. However, the area within and around any human settlement is actually a complex landscape of natural features, artificial surfaces, and structures,

and it is this landscape in its entirety, and the way it changes through time, that is of interest for urban planning.

Highly detailed local maps of land cover and land use patterns in and around human settlements are used by managers of cities, towns, or municipalities who wish to have visual representations of the features of the territories that they administer, and the options they have for managing development of settled areas in the face of rapid population growth and changing patterns of economic activity. The value of global mapping of human settlements is that it establishes methods and standards that can aid this effort, and provides the basis for comparative research that may shed additional light on issues and options for national policy makers as well as for decentralized planners and managers.

Areas with land cover resulting from human activities may be described in terms of use, for example, settlement or agriculture, or in terms of cover, for example, impervious surface or vegetation. Changes in land use patterns, the condition of structures, and the presence of services that require linear constructions (roads, railways, power grids, communications lines) or built-up objects (schools, hospitals, markets) are all features of settled areas that can be studied with the use of human settlement maps that depict the entire landscape. Mapping can show where these services are currently available in relation to settlement size and built-up area, and can suggest the most efficient routes for expanding water and sanitation networks. Other examples of urban planning issues that can be addressed by analyzing the characteristics of the urban landscape include analysis of runoff patterns and peak flow characteristics of water as an input to planning drainage systems, and planning the construction of tarmac roads in hilly terrain so as to avoid soil erosion resulting from inadequate provision for discharge of excess water (FAO, 2008).

Remote sensing is the science of acquiring, processing, and interpreting images obtained from instrumentation aboard Earth-orbiting satellites. In a map derived from the interpretation of remote sensing imagery, each feature detected on the Earth's surface is represented by its spectral signature, and these unique spectral characteristics provide the basis for interpretation, characterization, and classification of the feature being mapped. When converting satellite imagery into grids of interpreted features, the occurrence of each feature in each cell of the grid is calculated and expressed as a percentage share of the total surface area of the cell. A grid that combines information about more than one feature provides the first averaging of spectral reflectance of the phenomena being monitored, proportional to the pixel resolution of the sensor.

Two of the most commonly used indicators of human settlement derived from remotely sensed images are nighttime lights (e.g., reflections from city lights that are visible when the sun is down) and artificial surfaces (e.g., reflections from artificial, manmade constructions that cover the land and are mostly impervious surfaces such as concrete, metal, wood, or thatch). Nighttime lights have been widely used to establish the boundaries and extents of urban areas. Aggregating pixels containing high percentages of artificial surfaces can also generate areal extents for urban areas. However, if the original data are not highly aggregated, and a large number of land cover/land

use classes are retained for analysis, the urban landscape emerges. Box 8.1 provides a brief summary of similarities and differences between commonly used methods for mapping human settlements, using nighttime lights and/or artificial surfaces.

Box 8.1 Mapping Human Settlements — Similarities and Differences between Commonly Used Methods

A. Early efforts to map human settlements
   1. Populated Places layer of Digital Charts of the World (DCW) and its refinements.
      The DCW populated places layer contains polygons that have been digitized from paper maps, and point data for a large number of human settlements for which the geographic coordinates are known
      (ESRI; see also Danko, 1992).
   2. Nighttime Lights of the World
      Four types of lights are distinguished on the basis of location, brightness/persistence, and visual appearance, and four different datasets are available as a result: human settlements (cities, towns, villages, and industrial sites), gas flares, fires, and heavily lit fishing boats.
      (US NOAA; see also Imhoff et al., 1997)

B. Use of DCW polygons and Nighttime Lights by other recent mapping efforts
   1. The built-up area class in the Global Land Cover Characteristics database (GLCC)
      GLCC was developed by the United States Geological Survey (USGS), the University of Nebraska–Lincoln, and the European Commission's Joint Research Centre (JRC) on a continent-by-continent basis, based on Advanced Very High Resolution Radiometer (AVHRR) data for the year from April 1992 to March 1993, with a nominal 1-km resolution. It was originally released to the public in 1997 and has subsequently been updated based on feedback from users. Its built-up area layer is not derived from the imagery, but instead is based on DCW and its refinements.
      (US Geological survey GLCC dataset)
   2. Treatment of built-up area by LandScan™
      The original LandScan™ Global Population Database was made public in 1998 and updates have been released annually since 2000, as part of the Oak Ridge National Laboratory Global Population Project for estimating ambient populations at risk. LandScan apportions census counts to each cell in a 30 arc-second grid, based on likelihood coefficients that are, in turn, based on proximity to roads, slope, land cover, nighttime lights, and other information.

The GLCC classification system was used as the starting point for developing a LandScan Land Cover Database as an input for running its population distribution model. For urban area, however, the GLCC built-up area class was replaced with two new, greatly improved urban classes, namely,

(i) A developed urban class composed of GLCCs built-up area cells from DCW plus all cells included in the Census Bureau's P-95 circles, and

(ii) A partly developed class representing suburban areas, small towns, and scattered industries, airports, and other lit objects, and containing all cells with a frequency value of 90% or greater from Nighttime Lights of the World.

In 2002 global AVHRR land cover data were replaced with MODerate resolution Imaging Spectroradiometer (MODIS) land cover data. Extensive use has been made of Controlled Image Base imagery for verification and validation, for refining urban built-up areas, and for adding thousands of smaller villages and populated places.

(Bright, 2002; see also Dobson et al., 2000)

3. Urban extents generated by the Global Rural Urban Mapping Project (GRUMP)

   To prepare its urban/rural population grid Colombia University's research team at the Center for International Earth Science Information Network (CIESIN) created two intermediate products

   (i) A human settlements database of about 55,000 settlement points with an estimated population of 1000 or more, and for which population counts and geographic coordinates were obtained from official sources, Gazetteers, and the DCW populated places layer.

   (ii) An urban extent database of more than 21,000 settled areas for which the physical extents have been derived from the Nighttime Lights data set for the period 1994–1995, the 1992 DCW Populated Places layer and cities shown in Australia's Tactical Pilotage Charts, IPFRI.

   (CIESIN, IFPRI, World Bank, and CIAT, 2004)

4. Urban area derived from MODIS 1-km data for 2002

   In the Boston University (BU)-MODIS approach, a team of BU scientists generated a global map of urban area in 2002, based on the fusion of multiple data sources. The primary source was the remotely sensed 1-km data from MODIS — a key instrument aboard the Terra AM and Aqua PM satellites of the U.S. National Aeronautics and Space Administration's Earth Observing System. Due to similarities in the spectral signatures of built-up area and barren area at the 1-km resolution of the 2002 data, classifications based on MODIS alone resulted in confusion between these two land cover classes. Therefore, two ancillary sources were also used

to generate the urban area map, namely, the Nighttime Lights data and the population density data from CIESIN's Gridded Population of the World (GPW) — a database that allocates population counts to the lowest level administrative units for which CIESIN was able to obtain official boundaries and census data, and distributes population counts evenly across all grid cells in any given administrative unit.

(Schneider et al., 2003; USGS Archive Center)

5. Urban and rural settlement grids in FAO's Poverty Mapping Urban Rural (PMUR) database

   To derive a rural population distribution grid appropriate for global analysis of poverty and environment linkages in rural areas, FAO chose to use LandScan rather than GPW as its base data source, because the population densities in LandScan take land cover into account. In order to differentiate the global distribution of rural and urban populations, FAO developed and applied an urban mask, using Nighttime Lights of the World 2000 to identify the location and extent of urban areas, and applying UN urban population data for each country for the year 2000 as a threshold that the aggregate population of identified urban areas was not allowed to exceed. A rural settlements class was also created, including smaller settled areas that did not meet the urban class criteria and all other pixels in the grid having a population density greater than 2000 per km^2.

   (FAO, 2005, 2006; GEONetwork)

6. Global Land Cover 2000 (GLC2000)

   The Global Vegetation Monitoring Unit (GVM) of the JRC of the European Commission, in collaboration with more than 30 research teams, developed a global land cover product for the year 2000 (GLC2000) by applying the Land Cover Classification System (LCCS), developed by FAO and UNEP as part of the Africover project, to vegetation data from the SPOT satellite, at 1-km resolution. The LCCS allows local and regional vegetation types to be defined at any desired detail by adding further attributes foreseen in the LCCS. For GLC2000, each of the 19 defined regions was mapped by local experts, which guaranteed an accurate classification, based on local knowledge. The global legend consists of a limited number of land cover classes, derived by the aggregation of the regional and subregional classes provided by the GLC2000 partners.

   For urban area, documentation for Africa and South America regions indicates that nighttime lights were used as a seeding layer to locate the presence of large urban areas in the SPOT vegetation data set. The procedure involved creating a mask from the stable lights data to extract the corresponding areas from the

SPOT classes. Visual interpretation was used to retain those classes related to urban areas.
(EC/JRC/GVM; see also EC/JRC, 2002, 2003a, 2003b)

7. GlobCover
GlobCover is an initiative of the European Space Agency (ESA), in partnership with JRC, EEA, FAO, UNEP, Global Observation of Forest Cover and of Land Dynamics, and IGBP (International Geosphere–Biosphere Program). The GlobCover project aims at producing a global land cover map at a resolution of 300 meters, using input observations from the MERIS sensor on board ESA's ENVISAT environmental satellite. The Land Cover Classification is derived by an automatic and regionally tuned classification of a time series of the MERIS Full Resolution Composites, using the 22 global land cover classes of the LCCS. Class labels are assigned by cross-referencing the classification with a database of regional land cover maps and a set of decision rules. For many land cover classes, this new product updates and improves upon GLC2000, because of the finer spatial resolution. However, as regards the urban area class, the cross-referencing procedure produces an urban layer in GlobCover similar to GLC2000.
(Arino et al., 2007; see also ESA GlobCover Project)

C. Recent advances in urban mapping methods

1. History Database of the Global Environment (HYDE)
This database attributes historical population data from 1700 to 2000 to subnational administrative units, using a new global map of administrative boundaries at the subnational level developed at the National Institute for Public Health and the Environment (RIVM) in the Netherlands. The map comprises 222 countries, divided into 3441 administrative units. Where possible, historical population data were collected at the ISO3166-2 level or converted to match that level. Important sources for the subnational population data were the Populstat database (Lahmeyer, 2004) and the World Gazetteer (2004). Urban data are captured only where a mapped subnational administrative unit is an urban district. For a complete description of the methodology, see Goldewijk (2005).
(Netherlands Environmental Assessment Agency; see also Lahmeyer, 2004; World Gazetteer, 2004; Goldewijk, 2005)
2. Global Impervious Surface Area Map
Similar to the PMUR, this map uses nighttime lights data and population distribution data from LandScan to model the global distribution of impervious surface areas. It was produced by NGDC's Earth Observation Group as a contribution to the quantification of

the human impact on the terrestrial carbon dynamics. However, it shares many of the characteristics of other global maps of urban area, based on nighttime lights.
(Elvidge et al., 2007; US NGDC, 2007)

3. Urban area derived from MODIS 500m data for 2005
According to preliminary documentation, a new urban map based on 500m MODIS data for 2005 will soon be released that uses remotely sensed data in association with a global stratification of "urban ecoregions" without reliance on external datasets to constrain the classification. The datasets are expected to provide a foundation for refined representations of global urban land use.
(See Schneider et al., Chapter 5 of this book)

Detailed descriptions of Nighttime Lights, GRUMP, and BU-MODIS approach are discussed in Chapters 2.3, 2.4, and 3.1.

8.3 THE AFRICOVER METHOD FOR DETERMINING LOCATIONS AND EXTENTS OF HUMAN SETTLEMENTS AND MAPPING URBAN LANDSCAPES

The overall goal of the Africover initiative is to develop a digital goeoreferenced database on land cover and baseline geographic data for the whole Africa. The first Africover project was operational from 1995 to 2002, with financing from the Italian Cooperation. It developed the FAO-United Nations Environment Programme (UNEP) Land Cover Classification System (LCCS) and implemented the Eastern African module (FAO-Africover, 2003a).

8.3.1 Structure of the FAO-UNEP LCCS Developed by the Africover Project

The LCCS developed by the Africover project is the only universally applicable classification system for land cover that is in operational use at present. It enables a comparison of land cover classes regardless of data source, economic sector, or country. Work began in 1993, when UNEP and FAO organized a meeting to catalyze coordinated action toward harmonization of data collection and management, and to take a first step toward an internationally agreed reference base for land cover and land use, as called for by Chapter 12 of Agenda 21. At about the same time, funding for the Africover initiative was coming on stream from the Italian Cooperation to map land cover, initially for Eastern Africa and the Riparian Nile, and eventually for the whole of Africa, and a land cover reference system for operational use was needed. Thus, the Eastern Africa module of the Africover Program took on the task of developing an LCCS that could be used

not only by the project, but also as a more general reference system to assist users worldwide in harmonizing their interpretations of land cover from satellite imagery.

After the release of the original version of the FAO-UNEP LCCS in 2000, the concepts and system software have undergone two further revisions and the approach is now being promoted globally through the Global Land Cover Network (GLCN), which seeks to perpetuate the uptake of LCCS standards on a global basis. Today, it is establishing norms that all countries and regions can adhere to, without sacrificing the specificity needed to address local concerns.

An *a priori* classification system achieves standardization by requiring that all the classes have to be defined in advance. Although standardization of land cover classes was an objective of the Africover project, putting in place a complete a priori system for consistent description of land cover occurring anywhere in the world would have required creating an enormous number of predefined classes. Therefore, the project introduced an innovative approach for developing an LCCS that enhances the standardization process but minimizes the problem of dealing with a very large amount of predefined classes (FAO and UNEP, 2005).

The new innovative approach means that instead of predefining the classes, it predefines the classification criteria that uniquely identify the classes. The concept is based on the presumption that any land cover class, regardless of its type and geographic location, can be defined by a set of preselected independent diagnostic attributes, the classifiers. The number of classifiers used determines the detail with which the land cover is classified. Thus, a larger number of classifiers is needed when more detailed classification (description) of land cover is required.

All classifiers are coded, and each land cover class is defined by the string of codes for the classifiers used. Each class is also given a standardized descriptive name and a unique numerical code for use in geographical information systems.

The heterogeneity of land cover does not allow the same set of classifiers to be used in defining all land cover types. Therefore, these classifiers are tailored to fit eight major land cover groups. This has greatly reduced the number of classifiers needed for the precise definition of any land cover class, and thus significantly simplified the classification procedure. However, it required designing the LCCS implementation in two phases.

The dichotomous classification phase consists of three classification levels, which define eight major land cover classes in the third level, as shown in Table 8.1. The classification criteria used in the dichotomous phase are the presence of vegetation, edaphic condition, and artificiality of land cover. In the modular-hierarchical classification phase, the selection of classifiers and their hierarchical arrangement are tailored to each of the eight major land cover classes of the dichotomous classification phase. Thus, eight different classifier sets are used in this phase. The user is not obliged to use all classifiers. Depending on the required level of land cover information, the classification can be stopped at any time and the corresponding land cover class determined.

Table 8.1 Dichotomous Classification Phase of the LCCS

First Level	Second Level	Third Level
Primarily vegetated	Terrestrial	Managed terrestrial areas
		Natural and seminatural terrestrial vegetation
	Aquatic or regularly flooded	Cultivated aquatic areas
		Natural and seminatural aquatic vegetation
Primarily nonvegetated	Terrestrial	Artificial surfaces
		Bare land
	Aquatic or regularly flooded	Artificial water bodies
		Natural water bodies
		Snow and ice

Land cover classification based on preselected sets of classifiers can be further extended when a more detailed description of land cover is required, by applying two other sets of optional classification attributes, which provide additional description of land cover characteristics, but are not used to define the class. These are environmental attributes, such as climate, landform, altitude, soils, lithology, and erosion, and specific technical attributes, for example, the description of crop types in managed terrestrial areas, floristic aspects of natural and seminatural terrestrial and aquatic vegetation, salinity of artificial and natural water bodies, and so forth.

In July 2008, the International Organization for Standardization (ISO) distributed a proposed Draft International Standard for an LCCS (ISO 19144-2) for review and comment. The purpose of the ISO 19144-2 standard is to define a common reference structure for the comparison and integration of data for any generic LCCS. Following the FAO-UNEP approach, the ISO draft defines a Land Cover Meta Language (LCML) that provides a general framework of rules from which more exclusive conditions can be derived to create specific classification systems. It is a language based on physiognomy and stratification of both biotic and abiotic materials. The system may be used to specify any land cover feature anywhere in the world, using a set of independent diagnostic criteria that allow correlation with existing classifications and legends. Moreover, any national or multinational LCCS can be described in terms of the LCML (ISO, 2008).

8.3.2 Definition of the Built-Up Urban Area Land Cover Class in the FAO-UNEP LCCS

The FAO-UNEP LCCS classifies all artificial surfaces as belonging to a land cover class called built-up area. This class includes:

1. Linear built-up area
   - Roads

- Railways
- Communication lines, power lines, and pipelines

2. Nonlinear built-up area
   - Urban (populated) area
   - Industrial and other areas related to trade, manufacturing, distribution, and commerce, including built-up objects*

3. Non-built-up area
   - Waste dump deposits
   - Extraction sites

In the FAO-UNEP LCCS, urban areas are nonlinear built-up areas covered by artificial, often impervious structures adjacent to or connected by streets. This land cover class represents centers of human population. It usually occurs in combination with industrial and/or other built-up area and urban vegetated area. The density of urban area is based on the occurrence of impervious surfaces compared to permeable surfaces, and may be high, medium, or low (FAO and UNEP, 2005).

8.3.3 The Africover Method of Land Cover Interpretation

The Africover project applied the FAO-UNEP LCCS to develop detailed land cover grids for each of the 10 countries included in the East Africa module (Burundi, Democratic Republic of Congo, Egypt, Eritrea, Kenya, Rwanda, Somalia, Sudan, Tanzania, and Uganda).† An important aspect of the methodology is that land cover is mainly derived from visual interpretation of high-resolution satellite images (all Landsat in origin) that have been digitally enhanced, using techniques such as geometric rectification, principal component analysis, and contour stretching. In the East Africa module, national photo interpreters were recruited to implement the methodology.

In the first step, they selected and georectified the satellite imagery and collected ancillary data on the different aspects influencing land cover in their countries. This became the basis for the development of a virtual legend of land cover classes, based on the FAO-UNEP LCCS, which was used to start the interpretation. The second step consisted of preliminary photo interpretation of the satellite images. This involved:

- Marking on the false-color image the boundaries of areas or aerial photographs to be used for identifying land cover classes.
- Iterative extrapolation of the identified classes to all parts of the image expressing similar characteristics (color, structure, and texture.).

* Standardized FAO-UNEP LCCS list of built-up objects includes the following: aerodrome; airport; breeding center; cemetery; commercial area (shopping, warehousing, wholesaling, retailing); cultural, entertainment, and recreation area; heavy industrial area; historical site; hospital premises; light industrial area; military facilities; port area; power generation plant; refugee camp; religious site; school premises; sewage treatment plant; sports and leisure facilities; station(including depots); transportation facilities — bus area; transportation facilities — car park; urban playgrounds with structures; water treatment facilities; other.

† A technical description of the methodology may be downloaded from the Africover website (FAO-Africover, 2003b).

After the preliminary interpretation, those areas that had not been definitively delineated or where there were still outstanding doubts were identified and divided into two groups:

- Areas where ground truth surveys were the only solution.
- Areas where it was considered sufficient to study aerial photographs.

Because their spectral signature is close to that of bare areas, urban areas were considered as features that are hard to interpret, so validating the accuracy of visual interpretations was considered especially important for this land cover class.

As well as conducting ground truth surveys to provide a conclusive answer to any unresolved questions of interpretation, they were also used to provide a general check on the quality of the results of the photo interpretation. The final interpretation involved statistical analysis of the field data, locating the actual GPS points, reviewing the checked classes, extrapolating the results onto the interpretation sheets, introducing needed corrections, and aligning the interpretation with the edges of the images. This edge matching had to assure that coding and polygons were seamless in the full land cover interpretation coverage.

After completing the final interpretation, the following checks were made to assure its quality:

- Homogeneity of the interpretation per scene and between the different ones.
- Consistency of the interpretations of the different interpretation teams.
- Consistency of codification of the various units in comparison with the false-color images.
- Ensuring that only a single code has been assigned to each unit (closed polygon).
- Ensuring that adjacent polygons have different codes.
- The size limit of the smallest units, according to the Variable Minimal Mappable Area, assuring the level of detail of the interpretation.

Finally, the results of the Africover land cover interpretation had to be digitized for incorporation into the Eastern Africa database and for production of thematic maps at varying scales and with different levels of generalization.

8.4 COMPARISON OF URBAN AREA EXTENTS FROM POVERTY MAPPING URBAN RURAL DATABASE AND AFRICOVER

The method used to generate the Poverty Mapping Urban Rural (PMUR) database method described in Box 8.1 establishes boundaries for urban extents, but does not distinguish between different types of land cover that occur within the urban areas. In the initial step, nighttime lights data were used to establish the location and extents of urban area. To compensate for overestimation of the actual extents of urban areas in heavily lit areas, PMUR used UN urban population data to create a threshold. In countries where application of the threshold excluded pixels with population density greater than 2000 per km2, PMUR classified these pixels as rural settlements (FAO, 2005).

By contrast, as discussed above, the built-up urban area class generated by Africover relies on the visual interpretation of the spectral signature of artificial surfaces. Although it is labor-intensive and relatively costly, the LCCS approach used by Africover produces a richly detailed output that is not matched by any other human settlement mapping method currently in use.*

The PMUR method establishes boundaries for urban extents that do not distinguish between different types of land cover that occur within the urban areas, whereas the Africover method distinguishes built-up urban (populated) area from other types of urban area. Consequently, it is to be expected that the extents generated by aggregating only the built-up urban area class from Africover will be smaller than the urban area extents generated by PMUR; data for the year 2000 show this to be the case (Table 8.2).

Nevertheless, although the extent of settled area generated by PMUR is much greater than that generated by Africover, both methods place human settlements in approximately the same locations. Comparison of the distribution of urban area obtained by PMUR and that obtained by Africover for the Nile delta region show a nontrivial correspondence. Results of the chi-square test confirming this are reported in Box 8.2.

Table 8.2 Settled Area Extents for 10 Eastern African Countries, 2000

Country Name	Urban Area from PMUR Extent (km^2)	Settled Rural Area from PMUR Extent (km^2)	Built-Up Urban Area from Africover Extent (km^2)
Burundi	309	141	101
Congo, Democratic Republic of	5203	21	2450
Egypt	3332	6346	2451
Eritrea	297	144	146
Kenya	5601	890	613
Rwanda	293	328	79
Somalia	182	63	133
Sudan	17,144	–	3500
Tanzania, United Republic of	9325	–	2844
Uganda	1822	626	394

The correspondence is depicted visually in Figures 8.1 and 8.2. Figure 8.1 shows urban and rural extents in the Nile Delta obtained by PMUR. In this figure, bounded urban areas are shown in black, and pixels with population density of more than 2000 per km^2, denoting rural settlements, are shown in red. The remainder of the map image, colored green, is classified simply as rural area.

* Although not yet released at the time of writing, preliminary documentation for the new MODIS 500-m urban map indicates the interest of the authors in eventually mapping the type and percent coverage of vegetation within urbanized areas, but so far, the focus of the work has been on refining the mapping of urban extents, not on refining the characterization of urban landscapes.

BOX 8.2 Chi-Square Test of Degree of Independence of Urban Area Generated by PMUR and by Africover in the Nile Delta

Test values where:
$\chi^2 = 371.5603$
Threshold = 6.64
$p = 0.01$
df = 1 (degree of freedom)

	PMUR	Africover	Total
Observed Frequencies			
Africover	796	72	868
PMUR	721	649	1370
	1517	721	2238
Expected Frequencies			
Africover	588	280	868
PMUR	929	441	1370
	1517	721	2238

RESULTS

Chi-square (observed value)	369.773
Chi-square (critical value)	6.635
df	1
p-value	< 0.0001
alpha	0.01

Chi square distribution

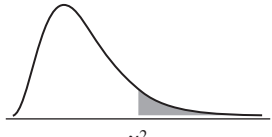

INTERPRETATION

As the computed *p*-value is lower than the significance level (alpha = 0.01), one should reject the null hypothesis that the rows and the columns of the table are independent, and accept the alternative hypothesis that there is a link between the rows and the columns of the table. The risk to reject the null hypothesis, while true, is lower than 0.01%. This shows that there is a statistically significant relationship between the number and location of urban areas mapped by PMUR and those mapped by Africover in the Nile Delta.

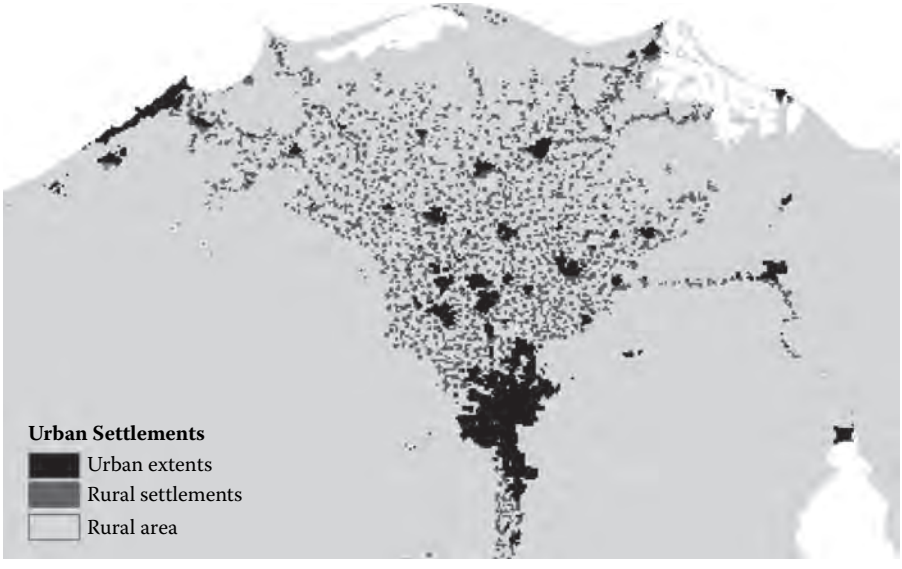

FIGURE 8.1 **(See color insert following page 324.)** Urban extents and rural settlements in the Nile Delta (FAO-PMUR), 2000.

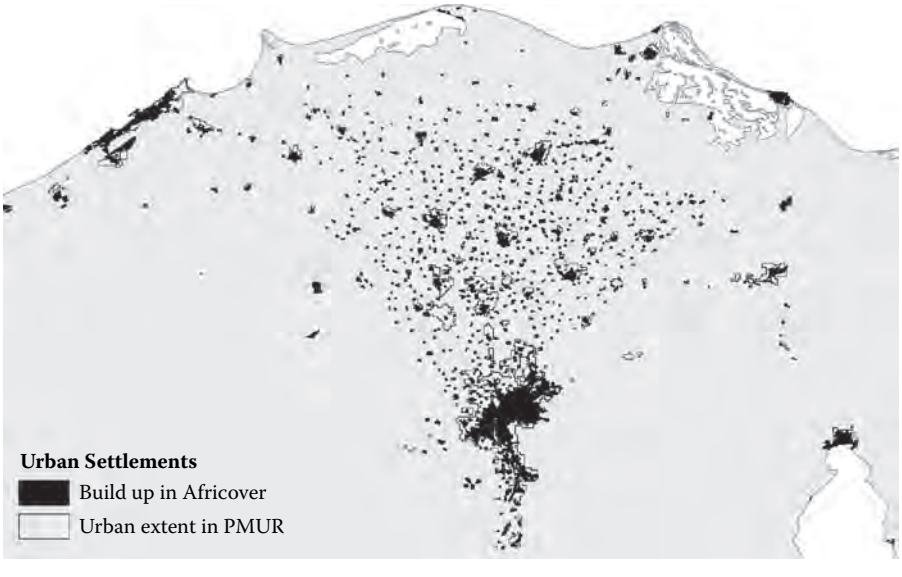

FIGURE 8.2 **(See color insert following page 324.)** Overlay of built-up area from Africover on urban extents from PMUR in the Nile Delta, 2000.

In Figure 8.2, the built-up urban area land cover class from Africover for the Nile Delta (shown in black) is overlaid on the bounded urban area extents from PMUR (shown in yellow). This figure shows very clearly how Africover produces smaller

extents for large metropolises, but picks up and classifies as urban many of the locations classified as rural settlements by PMUR.

8.5 USE OF AFRICOVER GRIDS TO DETECT LAND COVER CHANGE IN AND AROUND HUMAN SETTLEMENTS: SOME EXAMPLES FROM EASTERN AFRICA

For some types of land-cover change analysis, a high level of detail is desirable. In other instances, it is more revealing to report results for only a few highly aggregated classes. The hierarchical classification method used by Africover permits the user to aggregate land cover classes according to need. Illustrations of both disaggregated and aggregated approaches for detecting land cover change in the Nile Delta, and examples of an aggregated land cover change analysis for a study area encompassing the Egyptian city of El Mahala El Kobra and for ten capital cities in Eastern Africa are given below.

8.5.1 Nile Delta

An FAO-led pilot project undertaken under the auspices of the Global Terrestrial Observing System and the GLCN has been working to define a robust methodology to analyze and assess land cover changes in delta areas that would be applicable worldwide. Initial results for the Nile Delta are reported by Latham (2006). The study carried out a photo interpretation of satellite imagery for four periods — 1972 (Landsat MSS), 1984 (Landsat TM), and 1997 and 2000 (Landsat ETM) — using the Africover methodology and 68 land cover classes defined on the basis of the FAO-UNEP LCCS. The 1997 interpretation already prepared by the Africover project was used as a baseline, allowing about 70% of time saving in the interpretation phase.

Figure 8.3 shows the continuous land cover image for the 68 different land cover classes generated by the Africover approach for the Nile Delta in the year 2000. As the number of classes is very large, the same color is assigned to more than one land cover class in the map image. Therefore, for an accurate interpretation of the map, it is necessary to use the unique LCCS code assigned to each polygon, and not the colors. The legends for Figures 8.4 and 8.5 contain the codes used in the illustrative examples presented below.

The utility of the map is in the small-area detail. In the two examples that follow, significant changes in land use patterns have occurred in areas that are not classified as urban, but that are almost certainly affecting the dynamics of growth and development in the nearby towns and cities.

Figure 8.4 illustrates human capacity to transform inhospitable environments into habitable settled areas. In 1972, the area shown in the zoom was covered mainly with sparse low forbs (herbaceous nonwoody plants) on waterlogged soil with salt crust (4FRLW-Z), adjacent to a natural lake at the top (8WP) and combined with natural lakes in the lower half (4FRLW/8WP). Rain-fed herbaceous crops were grown on small fields on bare, deep stony soil only in a small area in the lower right-hand corner of the zoom (6ST1D/HR14). Bare rock with a thin sand

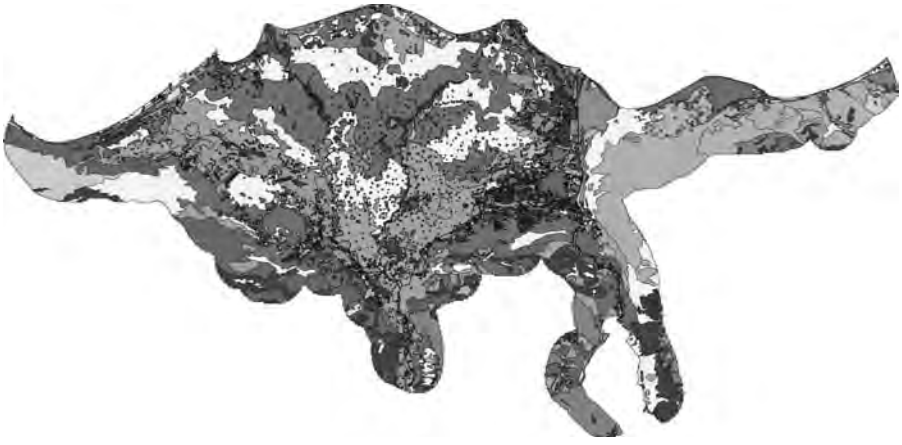

FIGURE 8.3 Continuous land cover in the Nile Delta, 2000.

layer covered most of the upper part of the top left-hand quadrant (6RL), with a belt of waterlogged soil (4FRLW-Z) surrounding a built-up urban area on loose and shifting sand in the far corner (5U/6L). By 2000, the waterlogged area had been converted into artificial lakes and reservoirs (7WP) and fish ponds (7WP-Y), the area planted to rain-fed herbaceous crops on small fields on bare, deep stony soil had expanded, the bare rock and waterlogged soil in the upper part of the top left-hand quadrant had given way to rain-fed tree crops on small fields, and the urban area had been stabilized and was no longer sitting on loose, shifting sand (5U). These transformations represent not only change but also improvement, both for the environment and for the economic utility of the natural resource base of the area.

In 1972, the area shown in the zoom for Figure 8.5 was covered mainly with bare, deep stony soil (6ST1D) and bare rock with a thin sand layer (6RL), with a small amount of bare, shallow stony soil (6ST1H). By 2000, the bare, shallow stony soil was covered with small fields on which an irrigated herbaceous crop and an additional herbaceous crop were being cultivated (6ST1H/HR3HQ57); a small portion of the bare rock with thin sand layer and a large portion of the bare, deep stony soil had been converted to a combination of an irrigated and an additional herbaceous crop on small fields and an irrigated tree crop on medium fields (HD3HQ57/TM57V). In some patches of the larger area there are no tree crops, and the area is covered entirely with irrigated and additional herbaceous crops on small fields. Not shown in the zoom but appearing as a green patch in the larger image just to the left of the zoom in the second row of Figure 8.5, a built-up urban area appears (5U), illustrating how the expansion of human settlements and the expansion of cultivated area have gone hand in hand throughout much of the deltaic zone.

Some types of analysis, however, do not require such a high level of detail. Therefore, the hierarchical classification method used by Africover also permits the user to aggregate land cover classes according to need. Figure 8.6 shows a four-class aggregation that has been created for the Nile Delta to investigate broad trends in land

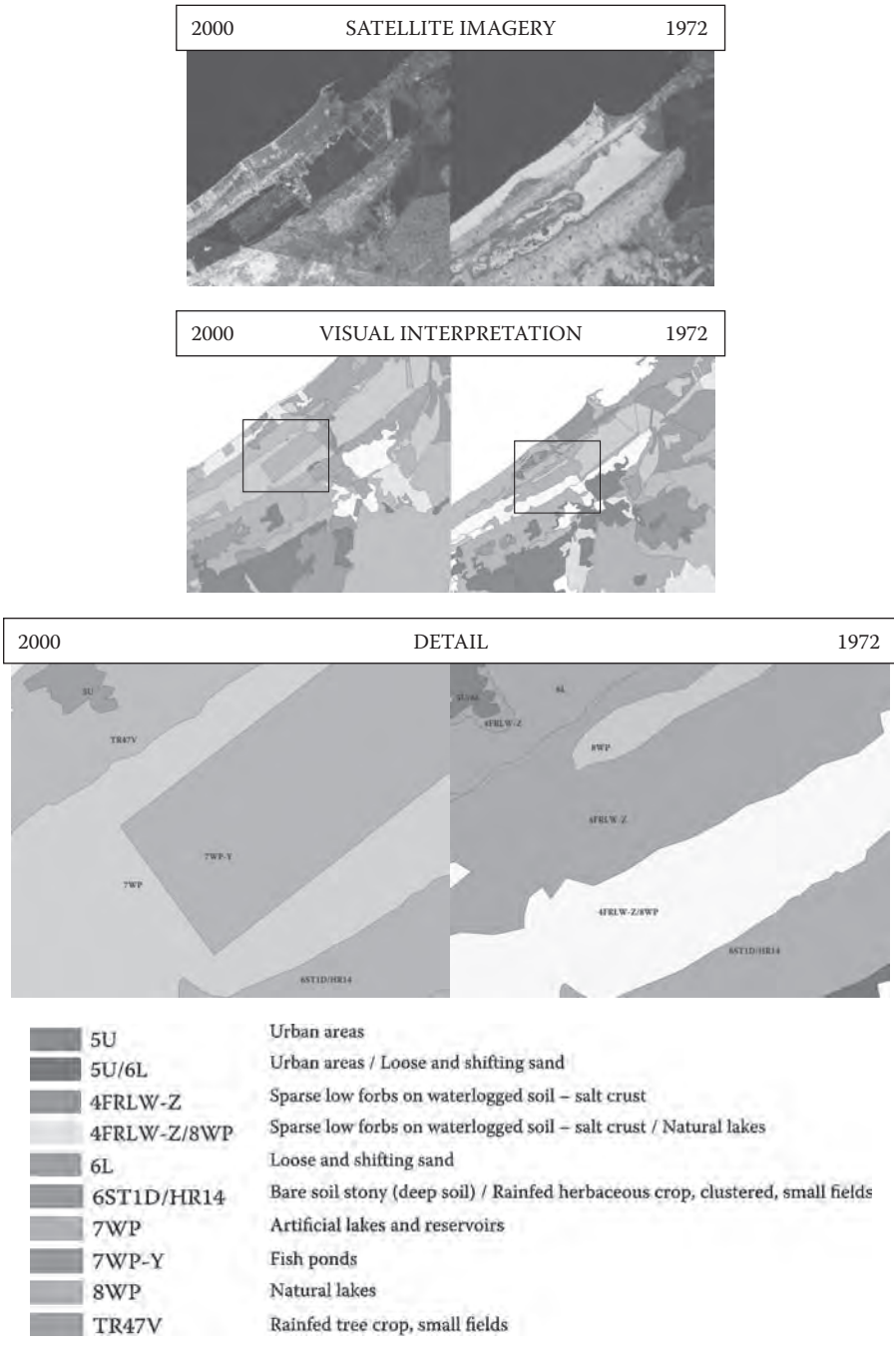

FIGURE 8.4 **(See color insert following page 324.)** Transformation around the Nile Delta lagoon, changes from 1972 to 2000.

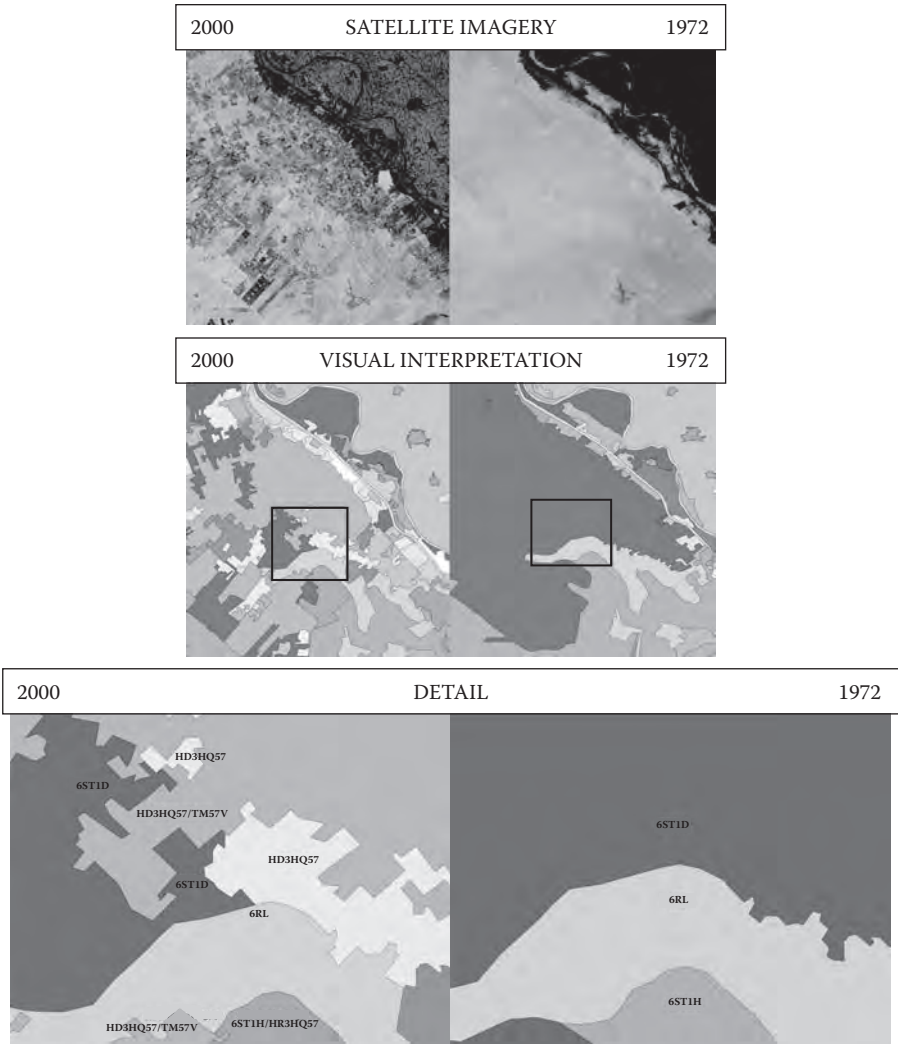

FIGURE 8.5 **(See color insert following page 324.)** Land reclamation in the Nile Delta, changes from 1972 to 2000.

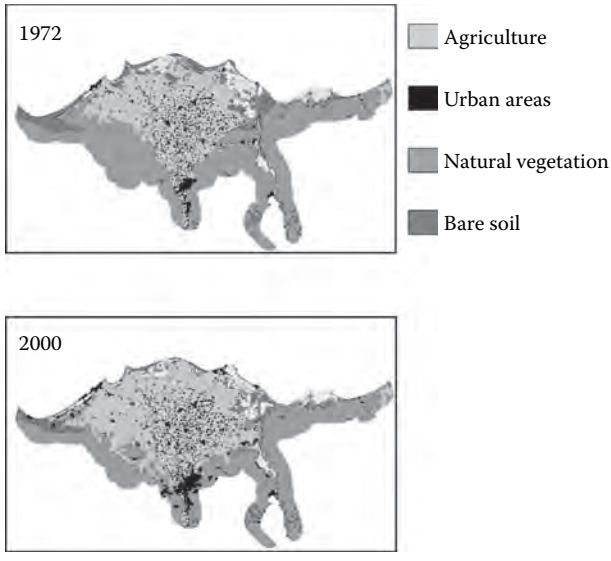

FIGURE 8.6 **(See color insert following page 324.)** Land cover change in the Nile Delta from 1972 to 2000, Africover aggregations.

use patterns for the entire area. The figure illustrates the extent to which both urban area and agricultural area in the Nile Delta have expanded over the past 30 years, mostly through a process of land reclamation where the soil was previously barren.

Statistical results of the assessment of changes in land cover in the delta over the 30-year period show that urban area increased from 2.0% to 3.4% of the total deltaic area of approximately 55,000 km2, and agriculture increased from 33% to 45% (Figure 8.7). Compensating reductions came from bare soil, which dropped from 50% to 39% of total area, from natural vegetation, which dropped from 10% to 7%, and from natural water, which dropped from 4.3% to 3.5%. Artificial water, on the other hand, increased from 0.5% to 2%. This was due to a decrease in the size of a natural lagoon and an increase in the practice of aquaculture and agriculture around the lagoon — a typical transformation of agricultural activity in an urban periphery where natural water bodies occur.

8.5.2 City of El Mahala El Kobra, Egypt

Results from the standard approach being developed for analysis of land cover change in and around urban areas in Africover countries and the Egyptian city of El Mahala El Kobra are presented in this section (see Adam, 2006, for detailed description of the approach). For each settlement to be analyzed, an arbitrary study area will be defined that encompasses the named city and its environs, and a land cover change detection map for the study area will be generated. Figure 8.8 shows the change detection map for El Mahala El Kobra for the period 1984–2002, whereas Figure 8.9 depicts the growth in built-up urban area and compensating area reduction for other land cover classes in each study area. Underlying statistical data (Table 8.3) indicate that vegetated area decreased by 11.2%, with about half of the loss

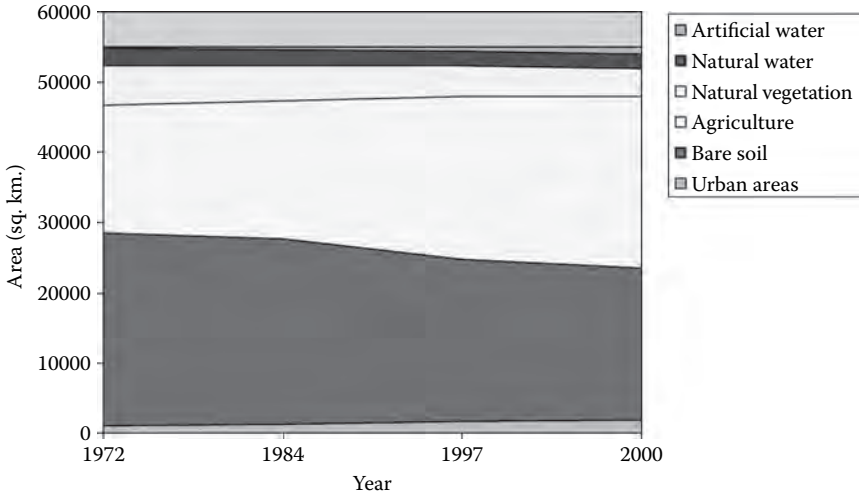

FIGURE 8.7 Graphic representation of land cover change in the Nile Delta from 1972 to 2000.

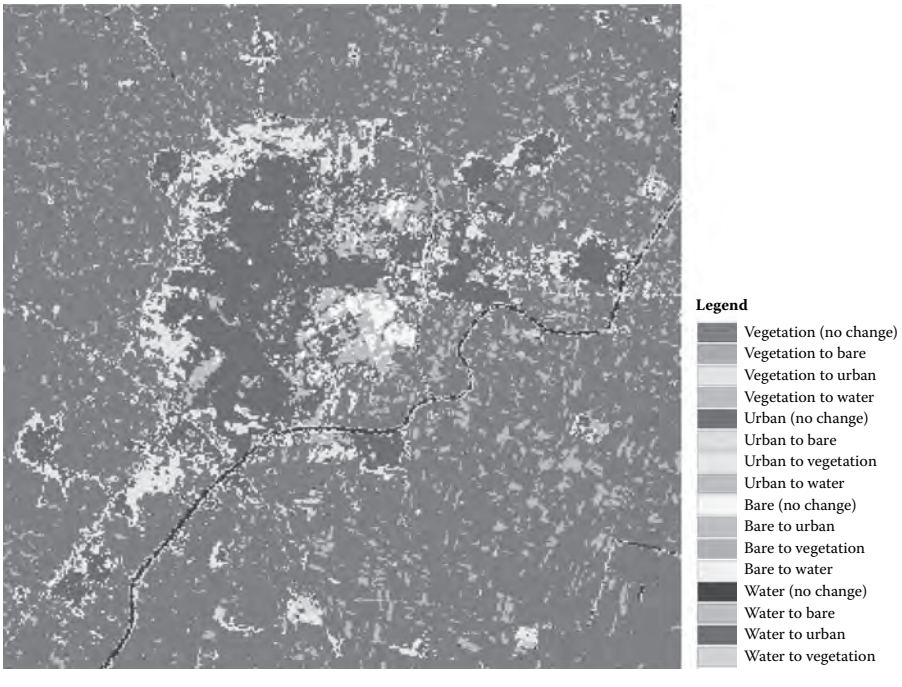

FIGURE 8.8 **(See color insert following page 324.)** Land cover change in the Egyptian city of El Mahala El Kobra from 1984 to 2002, Africover aggregations.

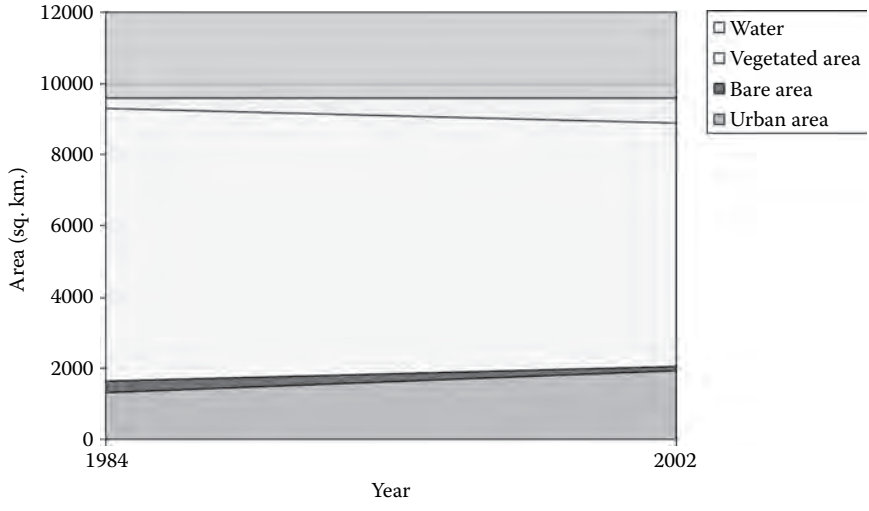

FIGURE 8.9 Graphic representation of land cover change in the Egyptian city of El Mahala El Kobra from 1984 to 2002.

going into irrigated area (shown as water on the map) and the other half into urban area. On the other hand, 60% of the area classified as water in 1984 was reclaimed for agriculture during the period under review. Urban area increased by nearly 45%, with about two-thirds of the increase coming from vegetated area and one-third from bare area.

Table 8.3 Land Cover Change in and around El Mahala El Kobra, 1984–2002

	Bare Area	Urban Area	Vegetated Area	Water
1984 area (km^2)	300.54	1323.07	7680.64	250.91
2002 area (km^2)	121.70	1912.85	6824.11	696.50
Gain/loss (km^2)	−178.84	589.78	−856.53	445.59
Percent change (%)	−59.5	44.6	−11.2	177.6

8.5.3 Capital Cities of Eastern and Northern Africa

The standard approach has also been applied to develop a comparative analysis of land cover change for selected capital cities and their environments in Northern and Eastern Africa, from the mid-1980s to around 2000. Whereas the Africover method generates vector images, the data reported in Table 8.4 come from a digital interpretation of the satellite imagery. Urban areas increased in the peripheries of all capital cities for which comparative data was available. However, the data show significant differences in the rate of increase, ranging from 9% for Asmara to 74% for

Table 8.4 Growth in Urban Area from 1985 to 2002 in and around 10 Capital Cities of Eastern and Northern Africa

	Urban Population, 1985–2005		Observation Dates		Urban Extents in Study Areas			
	Average Annual Growth Rate						Rate of Change (%)	
Country	(%)	Capital City	Base Year	Recent Year	Base Year Extent (km²)	Recent Year Extent (km²)	Entire Period	Annual
Burundi	5.50	Bujumbura	1986	2002	14	57	74	19
Egypt	2.00	Cairo	1984	2000	401	794	49	6
Eritrea	3.25	Asmara	1984	2000	20	22	9	1
Ethiopia	4.50	Addis Ababa	1986	2002	112	142	21	2
Kenya	4.00	Nairobi	1987	2002	77	200	62	11
Libya	2.25	Tripoli	1989	2001	122	198	38	5
Malawi	5.75	Lilongwe	1990	2001	32	59	45	8
Somalia	2.50	Mogadishu	1986	2000	43	56	22	2
Sudan	5.25	Khartoum	1987	2000	84	211	60	12
Uganda	5.25	Kampala	1986	2001	119	245	61	7

Bujumbura over the total observation period, and from 1% to 19% annually. Eastern and Northern African capitals with urban area growth rates in excess of 40% over the 15-year period include Bujumbura, Nairobi, Khartoum, Kampala, Cairo, and Lilongwe. In Bujumbura, Cairo, and Nairobi the rate of expansion in urban area is three times higher than the average annual growth rate in national urban population, and in Khartoum it is twice as high (see UN Population Division, 2007, for urban population growth rates). Data such as these indicate where the most important magnets for urban in-migration in the Eastern and Northern Africa sub-regions are located and can help policy makers prioritize investments in urban infrastructure accordingly.

8.6 CONCLUDING REMARKS

Unlike the statistical or modeling approaches typical of other methods that have been developed to map human settlements on a global scale, the visual interpretation approach developed by the Africover project (outlined above) is a labor-intensive interpretation method best suited for classification work at national or subnational scales. Software has since been developed that permits several of the steps in the interpretation process to be automatically performed. Nevertheless, validation by the human eye remains essential, particularly for the detection of artificial surfaces, which have a spectral signature very similar to that of bare areas.

Global mapping using this method will require building up a set of compatible national and regional products that can eventually constitute the tiles of a harmonized global map. A new GlobCover map is currently under production from medium resolution imaging spectrometer (MERIS) data at a resolution of 300 m, by the European Space Agency in collaboration with European Commission-Joint Research Centre, FAO, and UNEP, among others. It is expected to make further methodological advances in the application of this approach.

In the FAO-UNEP LCCS, built-up urban area is considered to represent centers of population, irrespective of size. When boundaries are imposed where concentrations of urban built-up area are found, it is possible to estimate urban area extents and associate population counts for each known center of population with its mapped location and extent. As discussed above, it is also possible to investigate relationships between the built-up area that has been detected, and other features of the urban landscape represented by other land cover classes. It is this latter aspect of human settlement mapping, based on LCCS, that makes the approach attractive for planners.

A particularly interesting finding from the set of cases that were presented is that expansion of urban area is often accompanied by expansion rather than reduction in agricultural area in the urban periphery. An increase in the presence of artificial water bodies has also been observed in the Nile Delta. Besides conversion of bare or open area to built-up area, loss of natural vegetation and tree cover are also common. The degree to which this pattern of change is or is not common to all expanding urban areas merits further study, as do underlying reasons for observed patterns of change and their environmental consequences.

Human beings tend to cluster in spatially limited habitats. Today, more than half of the world's population lives in urban areas, which occupy, in aggregate, less than 5% of the world's land area. Sprawl on the urban fringe and exurban development are two of the more conspicuous signs of urban change, but structural change permeates urban areas through continuous processes of intensification of use, decay, and development, and aging urban infrastructures are undergoing continuous replacement and change. Thus, urban areas are in a constant state of flux that reflects both growing urban populations and the evolution of urbanizing technologies.

According to the forthcoming Land Theme Report of the Integrated Global Observing Strategy (IGOS) (Townshend et al., 2008), "global remote sensing of human settlements can significantly improve decision making in a number of application areas, including:

- Spatial modeling of population variables such as population and settlement density (both urban and rural), land use patterns, civil infrastructure, and some types of economic activity;
- Improved modeling of the flow of food, water, energy, and disease vectors, and their consequences for natural systems, including ecosystem and planetary metabolism;
- The location and density of infrastructure for use in hydrologic modeling, flood prediction, the assessment of land use and land use change, analysis of human impacts on biodiversity, and threats to public heath;
- Monitoring, management, and mitigation of natural disasters;
- Urban planning and more effective location decisions and development of support infrastructure; and
- Spatial modeling of atmospheric emissions associated with fossil fuel consumption and other anthropogenic activities."

The report identifies a suite of remotely sensed product types that would make these applications possible and challenges the international community to make the generation of these products a priority for future work on human settlement mapping.

REFERENCES

Adam, B.F.S.S., An assessment of the physical growth of greater Khartoum, Sudan, using remote sensing and GIS techniques, Ile-Ife Nigeria, African Regional Centre for Space Science and Technology Education in English (ARCSSTEE), PMB 019 OAU, 2006.

Arino, O., Leroy, M., Ranera, F., Gross, D., Bicheron, P., Nino, F., Brockman, C., DeFourny, P., Vancutsem, C., Achard, F., Durieux, L., Bourg, L., Latham, J., Di Gregorio, A., Witt, R., Herold, M., Sambale, J., Plummer, S., Weber, J.-L., Goryl, P., and Houghton, N., GlobCover — A Global Land Cover Service with MERIS, 2007. Available online at: http://www.dup.esrin.esa.int/files/project/131-176-131-25_2007510152516.pdf.

Bright, E.A., LandScan Global Population 1998 Database Documentation, 2002. Available online at: http://www.ornl.gov/sci/landscan/landscan Common/landscan_doc.html.

Center for International Earth Science Information Network (CIESIN), Columbia University; International Food Policy Research Institute (IFRPI), the World Bank, and Centro Internacional de Agricultura Tropical (CIAT), Global Rural-Urban Mapping Project (GRUMP): Gridded Population of the World, version 3, with Urban Reallocation (GPW-UR), Palisades, NY, USA, 2004. Available online at: http://beta.sedac.ciesin.columbia.edu/gpw/global.jsp.

Danko, D.M., The Digital Chart of the World project, *Photogrammetric Engineering and Remote Sensing*, 58, 1125–1128, 1992.

Dobson, J.E., Bright, E.A., Coleman, P.R., Durfee, R.C., and Worley, B.A., LandScan: A global population database for estimating populations at risk, *Photogrammetric Engineering and Remote Sensing*, 66(7), 849–857, 2000.

Elvidge, C., Tuttle, B.T., Sutton, P.C., Baugh, K.E., Howard, A.T., Milesi, C., Bhaduri, B.L., and Nemani, R., Global distribution and density of constructed impervious surfaces, *Sensors*, 7, 1962–1979, 2007.

Environmental Systems Research Institute, Inc. (ESRI), Digital Chart of the World (DCW), Available online at www.maproom.psu.edu/dcw/.

European Commission (EC), Joint Research Centre (JRC), Global Vegetation Monitoring Unit (GVM), Global Land Cover 2000. Available online at: http://www-gem.jrc.it/glc2000/defaultglc2000.htm.

EC/JRC, A vegetation map of South America, by Eva, H.D., de Miranda, E.E., Di Bella, C.M., Gond, V., Huber, O., Sgrenzaroli, M., Jones, S., Coutinho, A., Dorado, A., Guimarães, M., Elvidge, C., Achard, F., Belward, A.S., Bartholomé, E., Baraldi, A., De Grandi, G., Vogt, P., Fritz, S., and Hartley, A., 2002. Available online at http://www-gem.jrc.it/glc2000/Products/southamer/ GLC2000_Downloads/final_report_v2.pdf.

EC/JRC, A land cover map of Africa, by Mayaux, P., Bartholomé, E., Massart, M., Van Cutsem, C., Cabral, A., Nonguierma, A., Diallo, O., Pretorius, C., Thompson, M., Cherlet, M., Pekel, J.-F., Defourny, P., Vasconcelos, M., Di Gregorio, A., Fritz, S., De Grandi, G., Elvidge, C., Vogt, P., and Belward, A., EUR 20665 EN, et al., 2003a. Available online at: http://www-gem.jrc.it/glc2000/ Products/africa/GLC2000_africa3.pdf.

EC/JRC, The GLC2000 land-cover classification, by Stibig, H.J., in: Bartholmé, E., ed., Global Land Cover 2000 "final results" workshop, Ispra, 24–26 March 2003, Ispra, Italy, 2003b. Available online at: http://www-tem.jrc.it/PDF_publis/2003/Bartholome_ GLCfinal_2003.pdf.

European Space Agency (ESA) GlobCover Project, Ionia GlobCover Portal. Available at: http://ionia1.esrin.esa.int/index.asp.

FAO, Mapping global urban and rural population distributions, by Salvatore, M., Pozzi, F., Ataman, E., Huddleston, B., and Bloise, M.; and Annex: Estimates of future global population distribution to 2015, by Balk, D., Brickman, M., Anderson, B., Pozzi, F., and Yetman, G., Environment and Natural Resources Working Paper No. 24, Rome, 2005.

FAO, Food Insecurity, Poverty and Environment Global GIS Database: DVD and Atlas for the Year 2000, by Ataman, E., Salvatore, M., Huddleston, B., Zanetti, M., Bloise, M., Dooley, J.E., Ascione, M., van Velthuizen, H., Fisher, G., and Nachtergaele, F.O., Environment and Natural Resource Working Paper No. 26, Rome, 2006. The PMUR database at high resolution (30arc-second) can be found in the DVD included in the publication at the following path: Archive\30arc_seconds\PMUR. Also available at (GeoNetwork): http://www.fao.org/geonetwork/srv/en/main.home under the title Rural Population Distribution (persons per pixel), 2000 (High Resolution Layer) (FGGD).

FAO, Land Cover Classification System (LCCS), Conceptual Basis and Registration of Classifiers: Proposed Draft Standard ISO, 2008.

FAO-Africover, The Africover initiative, the Eastern Africa module, other Africover modules, and Africover goes global: the Global Land Cover Network program (GLVN), 2003a. Available online at: http://www.africover.org/.

FAO-Africover, The Africover methodology, 2003b. Available online at: http://www.africover.org/africover_methodology.htm.

FAO and UNEP, *Land Cover Classification System: Classification Concepts and User Manual, Software Version 2*, revised by Di Gregorio, A., based on the original software version 1 prepared by Di Gregorio, A., and Jansen, L.I.M., Environment and Natural Resources Series No. 8, FAO, Rome, 2005.

Goldewijk, K., Three centuries of global population growth: A spatial referenced population (density) database for 1700–2000, *Population and Environment*, 26(5), 343–367, 2005.

Imhoff, M.L., Lawrence, W.T., Stutzer, D.C., and Elvidge, C.D., A technique for using composite DMSP/OLS "city lights" satellite data to map urban area, *Remote Sensing of Environment*, 61(3), 361–370, 1997.

International Organization for Standardization (ISO), Geographic Information — Classification Systems — Part 2: Land Cover Classification System (LCCS) — Proposed Draft International Standard, ISO 19144-2 CD, 2008.

Lahmeyer, J., Populstat database: Growth of the population per country in a historical perspective, including their administrative divisions and principal towns, 2004. Available online at: http://www.populstat.info/.

Latham, J., GTOS Nile Delta Land Cover Change Analysis, Pilot project report, June 2006. Available online at: www.fao.org/gtos.

Netherlands Environmental Assessment Agency, HYDE Basic Driving Factors: Population. Available online at: http://www.mnp.nl/en/themasites/hyde/basicdrivingfactors/population/index.html.

Schneider, A., Friedl, M.A., McIver, D.K., and Woodcock, C.E., Mapping urban areas by fusing multiple sources of coarse resolution remotely-sensed data, *Photogrammetric Engineering & Remote Sensing*, 69(12), 1377–1386, 2003.

Townshend, J.R., Latham, J., Arino, O., Balstad, R., Belward, A., Conant, R., Elvidge, C., Feuquay, J., El Hadani, D., Herold, M., Janetos, A., Justice, C.O., Liu Jiyuan, Loveland, T., Nachtergaele, F., Ojima, D., Maiden, M., Palazzo, F., Schmullius, C., Sessa, R., Singh, A., Tschirley, J., and Yamamoto, H., Integrated Global Observations of the Land: an IGOS-P Theme, IGOL Report No. 8, 2008.

United Nations, Principles and Recommendations for Population and Housing Censuses, Revision 1, Series M, No. 67, Rev. 1 (United Nations publication, Sales No. E.98. XVII.8), 1998.

United Nations, World Urbanization Prospects, the 2003 Revision, United Nations Publication sales No. E.04.XIII.6, 2004.

United Nations Population Division, World Urbanization Prospects, the 2007 Revision Population Database. Available online at: http://esa.un.unup.

United States National Aeronautics and Space Administration (NASA), Global Land Cover Facility (Terra-MODIS). Available online at: www.landcover.org.

United States Geological Survey (USGS), Global Land Cover Characteristics (GLCC) dataset, Available online at http://edcdaac.usgs.gov/glcc/glcc.asp.

USGS, Land Processes Distributed Active Archive Center: MODIS/Terra Land Cover Type 96-Day L3 Global 1 km ISN Grid. Available online at: http://edcdaac.usgs.gov/modis/mod12q1.asp.

United States National Geophysical Data Center (NGDC), News of the Month Archive, January 2007. Available online at: http://www.ngdc.noaa.gov/nndc/struts/results?eq_0=2007/01&op_3=eq&v_3=N&t=102750&s=3&d=10,6,11m.

United States National Oceanic and Atmospheric Administration (NOAA), Database of Nighttime Lights of the World. Available at http://dmsp.ngdc.noaa.gov/html/download_world_ change_pair.html.

World Gazetteer, 2004, Most recent update available online at: http://www.world-gazetteer.com/.

9 The Urban Environmental Monitoring/100 Cities Project

Legacy of the First Phase and Next Steps

Elizabeth A. Wentz, William L. Stefanov, Maik Netzband, Matthias S. Möller, and Anthony J. Brazel

CONTENTS

9.1 INTRODUCTION

The Urban Environmental Monitoring (UEM) project, now known as the 100 Cities Project (http://hundredcities.asu.edu/index.html), at Arizona State University (ASU) is a baseline effort to collect and analyze remotely sensed data for 100 urban centers worldwide. Our overarching goal is to use remote sensing technology to better understand the consequences of rapid urbanization through advanced biophysical measurements, classification methods, and modeling, which can then be used to inform public policy and planning.

Urbanization represents one of the most significant alterations that humankind has made to the surface of the Earth. In the early 20th century, there were less than 20 cities in the world with populations exceeding 1 million; today, there are more than 400. The consequences of urbanization include the transformation of land surfaces from undisturbed natural environments to land that supports different forms

of human activity, including agriculture, residential, commercial, industrial, and infrastructure such as roads and other types of transportation. Each of these land transformations has impacted, to varying degrees, the local climatology, hydrology, geology, and biota that predate human settlement. It is essential that we document, to the best of our ability, the nature of land transformations and the consequences to the existing environment.

The focus in the UEM project since its inception has been on *rapid* urbanization. Rapid urbanization is occurring in hundreds of cities worldwide as population increases and people migrate from rural communities to urban centers in search of employment and a better quality of life. The unintended consequences of rapid urbanization have the potential to cause serious harm to the environment, to human life, and to the resulting built environment because rapid development constrains and rushes decision making. Such rapid decision making can result in poor planning, ineffective policies, and decisions that harm the environment and the quality of human life. Slower, more thought-out, decision making could result in more favorable outcomes. The harm to the environment includes poor air quality, soil erosion, polluted rivers and aquifers, and loss of wildlife habitat. Human life is then threatened because of increased potential for disease spreading, human conflict, environmental hazards, and diminished quality of life. The built environment is potentially threatened when cities are built in areas that can be impacted by events such as hurricanes, tsunamis, Earthquakes, fires, and landslides. Our goals include assessing the threat of such events on cities and the people living there.

Remote sensing is now a proven technology to support research to better understand rapid urbanization. Using remote sensing to document and analyze rapid urbanization can facilitate planning and new policies to better protect the natural environment, human life, and built structures. A large majority of urban remote sensing studies involve measuring the extent of urbanization and monitoring the rate of urban growth (Howarth and Boasson, 1983; Imhoff et al., 1997; Ridd and Liu, 1998; Zhang and Foody, 1998; Sutton, 2003; Weber and Puissant, 2003). Along with documenting the extent of urbanization, other researchers have used remotely sensed imagery to quantify the physical characteristics of growth such as urban shape, density, and morphology (Herold et al., 2003; Rashed et al., 2003; Small, 2003; Stefanov and Netzband, 2005, 2009; Seto et al., 2007); to classify land use/land cover (LU/LC) in urban areas (Howarth and Boasson, 1983; Martin et al., 1988; Stefanov et al., 2001b; Schneider et al., 2003; Schöpfer and Moeller, 2006); to infer population density (Welch, 1980; Li and Weng, 2005; Pozzi and Small, 2005); to assess the ramifications of urbanization such as air quality, urban heat islands (UHIs), hydrology, energy use, local fauna (Roth et al., 1989; Lo et al., 1997; Arthur-Hartranft et al., 2003;Voogt and Oke, 2003; Weng, 2003; Gillies et al., 2003; Hammer et al., 2003; Hawkins et al., 2004; Stefanov et al., 2004; Kato and Yamaguchi, 2005; Nichol, 2005; Harlan et al., 2006; Jenerette et al., 2007); and to identify specific urban features such as buildings, industrial complexes, and automobiles (Dell'Acqua and Gamba, 2001; Bian, 2003; Song and Civco, 2004; Dell'Acqua et al., 2006; Gamba et al., 2006). These studies demonstrate the magnitude and diverse possibilities of the technology.

9.2 PROJECT HISTORY AND ORGANIZATIONAL OVERVIEW OF UEM

The UEM project (http://hundredcities.asu.edu/index.html) was initially conceived in the early 1990s as a focus of data collection and analysis for Japan's Advanced Spaceborne Thermal Emission and Reflection Radiometer (ASTER) sensor, planned for launch aboard the National Aeronautics Space Administration (NASA) Terra satellite in mid-1999 (Abrams, 2000). The original goal was to collect daytime and nighttime ASTER data over 100 urban centers twice per year to capture seasonal variations and to provide baseline observations of the physical state of each city. The urban centers were initially selected based on population growth and potential vulnerability to natural hazards. Primary characterization of each urban center was to be accomplished by land cover classification using a modified expert system approach developed for Phoenix, AZ (Stefanov et al., 2001b, 2007) — the "home city" of the UEM project. This global baseline data set would then be used for comparison and change detection during the duration of the Terra mission (nominally, 6 years; Ramsey et al., 1999; Stefanov et al., 2001a; Ramsey, 2003). Led by Dr. Philip Christensen, the 100 cities were submitted as part of the original ASTER Science Team Acquisition Request, and supported by NASA. An up-to-date list of the Science Team is listed on the project website (http://hundredcities.asu.edu/index.html). Although the launch of Terra was achieved in 1999, usable ASTER data for urban centers only became available in 2000.

The ASTER is a request-driven instrument, and the UEM is only one among several data acquisition requests. Unforeseen difficulties with the ASTER data acquisition scheduling algorithm — urban targets had low priority due to their relatively small size — resulted in incomplete coverage and sampling of the original 100 cities. As such, the original goal of establishing baseline data for all 100 cities became impractical. Despite the scheduling difficulties, a large number of high-quality scenes were acquired, with initial comparisons focusing on urban texture and spatial metric analysis to explore observable groupings or types of cities based on remotely sensed measurements of urban form.

A recompetition of the ASTER Science Team was required by NASA in 2003, and this was used by the UEM team as an opportunity to focus the project goals and objectives in response to the data collection difficulties described above. Perhaps the single greatest change to the project was focus on a subset of intensive study cities, rather than the broad view on the "100 city" approach. This was done to balance science goals with the practical realities of data collection and analysis, and to establish a firmer theoretical framework for the project. To that end, a suite of cities from within the 100-city set were selected on the basis of exposure to natural hazards (e.g., Earthquakes, volcanoes, and hurricanes), regional geography, climate, and population. Potential for urban growth and current urban population (based on United Nations data circa 2000) were also factors (Figure 9.1), and the reframed project now reflects a significant component of urban ecological research — particularly in terms of urban climate (discussed below). Eight cities were ultimately selected for intensive study — Chiang Mai, Thailand; Berlin, Germany; Canberra, Australia; Delhi, India; Lima, Peru; Manila, Philippines; Mexico City, Mexico; and Phoenix, Arizona, USA.

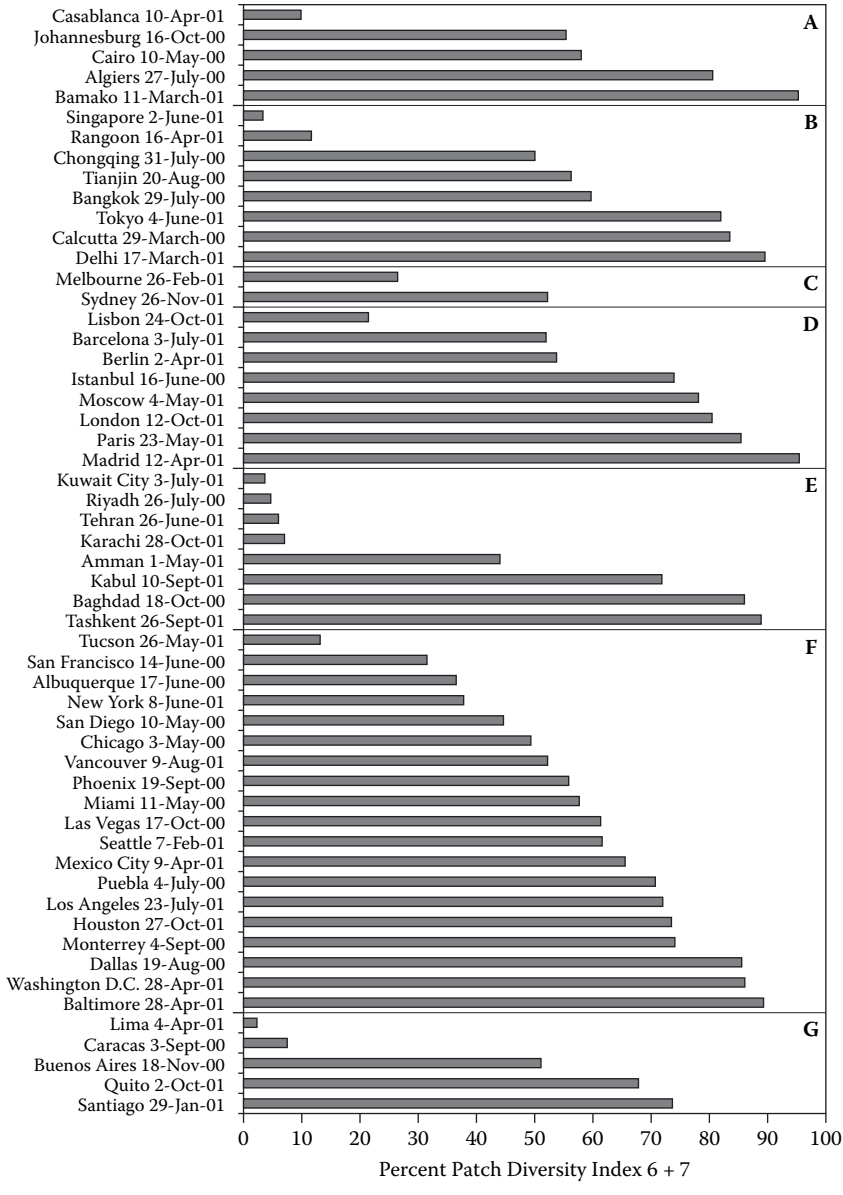

FIGURE 9.1 Fragmentation analysis using patch diversity metric for 55 urban centers. Patch diversity index results are in raster format; "6+7" indicates the two highest-value classes of the index used for percentage calculation. ASTER data acquisition time is indicated for each city. A: Africa; B: Asia; C: Australia; D: Europe; E: Middle East; F: North America; G: South America. (From Netzband and Stefanov (2003). Used with permission.)

Of the eight intensive study cities, the majority of work to date has been focused on Phoenix, AZ, USA; Delhi, India (Wentz et al., 2008); Berlin, Germany (Hostert, 2007); and Chiang Mai, Thailand (Lebel et al., 2007). The Phoenix metropolitan area

was used as a test bed for more in-depth analysis of the spatial structure of the city, and the relation of that structure to biophysical parameters of ecological interest measured by the Moderate Resolution Imaging Spectroradiometer (MODIS) (Stefanov and Netzband, 2005, 2009). This work also carried on the multisensor philosophy of the UEM project, as the MODIS sensors onboard the NASA Terra and Aqua platforms collect a high temporal frequency multispectral data set that is of great potential use for monitoring of urban biophysical parameters (Schneider et al., 2003).

9.3 CONTRIBUTIONS TO URBAN REMOTE SENSING

Scientists associated with the UEM (the names are listed at http://hundredcities.asu.edu/index.html) project have made several contributions to the field of urban remote sensing. From a technical and methodological perspective, we have developed and evaluated new methods for classifying LU/LC and we have utilized spatial metrics on our data to better understand urban land use patterns. Our second contribution to urban remote sensing is through applying our datasets to better understand the consequences of urbanization, including habitat structure and productivity and the UHI. In this section, we describe in more detail the findings of these investigations.

9.3.1 Classification Approaches for Diverse Urban Areas

With 100 or more cities to classify, one important objective was to establish a methodology for LU/LC classification that was portable to multiple urban centers. The expert system approach, established for the baseline urban center in Phoenix, USA, was established as the model system. The expert system approach was selected over other methods because of its high level of accuracy as well as its ability to distinguish multiple urban classes. We also investigated the portability of using an object-based approach to land use classification.

The initial experiment to test the portability of the Phoenix expert system is reported by Wentz et al. (2008). They applied the Phoenix expert system approach to Delhi, India, with mixed success. Aspects of the transfer that were easily adapted were the selection of ancillary data needed by the expert system. Land use, derived from aerial photography (Phoenix) and paper maps (Delhi), was essential to establish the customized rules in the expert system. Some of the ancillary data (e.g., water rights) were specific to the Phoenix area and therefore not used in the Delhi study. The most challenging aspect of transferring the expert system rules from one area to another was to identify a similar set of land use classes. The two cities have different urban structures with strikingly different dominant LU/LC types. The different urban structure resulted in a very different set of classes and therefore a unique set of expert system rules.

Using a modified and more portable form of the expert system classification developed for Phoenix by Stefanov et al. (2001b), Stefanov and Netzband (2005) compared MODIS Normalized Difference Vegetation Index (NDVI) data at spatial scales of 250, 500, and 1000 m/pixel to a suite of gridded spatial metrics (class area, mean patch size, edge density, and interspersion/juxtaposition index) derived from land cover classification of ASTER data. In a related study, Stefanov and Netzband (2009) used the same land cover classification of ASTER data to investigate potential

correlations between 1000 m/pixel MODIS albedo, fraction of photosynthetically active radiation, leaf area index, and land surface temperature with gridded spatial metric patterns. The results of both studies suggest that clear control of biophysical variables by urban spatial structure is not visible in MODIS; however, some control of vegetation-related parameters by spatial structure is indicated.

Most urban areas are composed of similar features such as streets, buildings, parks, and gardens. These represent "objects" in the urban environment and therefore make the object-based classification approach an obvious alternative to the classical pixel-based approach. With the classical pixel-based multivariate statistical approach, these urban features cannot be extracted as entities; instead, each object is represented as a clump of aggregated pixels. Aggregated pixels classified as "building" may be directly located in the center of "street," which is an incorrect classification. In addition to the spectral information, the object-based image analysis (OBIA) also considers shape, neighborhood relations, and context information for a classification, and consequently the OBIA approach often leads to results with increased classification accuracy for urban areas.

OBIA in a computer environment follows a three-step principle: segmentation, class rule set development and establishing of a cognition network (the netted rule sets), and finally the iterative classification process (Blaschke and Hay, 2001; Blaschke et al., 2004). In a first step, a multiresolution segmentation is calculated for the area of interest. The resulting segments reflect image areas with homogeneous gray values. Objects are represented as segments; however, urban objects have different sizes — consequently, image segments have to be calculated on several hierarchical levels varying in size and shape. On a low level, for example, small objects such as buildings, garages, etc., can be represented in segments, depending on the spatial image resolution. On a higher level, streets can be segmented with different segmentation parameters, because streets differ significantly in shape and size from buildings. All segment levels are linked to each other in a parent-child relation — parents know their children and vice versa. Due to the hierarchical structure and the linkage of all segmentation levels, we can distinguish between streets and buildings with a strict classification rule: "building may never be part of street."

The rule set definition is part of the second step in the OBIA classification process, where objects have to be described with their individual ontologies. Those may contain multispectral properties, surface texture, neighborhood relations (both horizontal and vertical), and object-specific shape parameters. The rule sets may be linked and connected, and they will finally build a cognition network. Based on the cognition network, a classification run is performed and the result is checked for its semantic accuracy. However, the first classification result will not be satisfactory for some classes and the rule sets for those have to be fine-tuned with their parameters in an iterative self-improving cycle until the classification output has reached an acceptable accuracy level.

An advantage of the OBIA classification approach is the transferability of segmentation parameters and classification rule sets with the entire cognition network from one area of interest to another area. Those areas should consist of almost the same objects to classify, and the location should be in a similar natural environment. It is also advantageous to use the same type of image data. As part of the US National Science Foundation-funded Agricultural Landscapes in Transition project (http://sustainability.asu.edu/agtrans/), in

tight cooperation with the UEM project, a transferability test for segmentation parameters and rule sets was performed for Phoenix, AZ, and Las Vegas, NV (Schöpfer and Moeller, 2006). Segmentation, classification rule sets, and cognition network were initially developed for the Phoenix area and later transferred and adapted to Las Vegas. ASTER multispectral (bands 1–3) 15 m/pixel resolution image data were used for both classifications. The image datasets were acquired on April 1, 2005 (Phoenix), and May 1, 2005 (Las Vegas), to guarantee a similar vegetation phenology.

The Phoenix image data were segmented on three levels, and a cognition network with rule sets based on the class schema of the 100 Cities Project expert classification system (Figure 9.2) was developed. Using the eCognition software environment, this classification resulted in overall accuracies of: 84.24% ($K\text{^} = 0.8268$) for Phoenix and 83.33% ($K\text{^} = 0.8148$) for Las Vegas, both verified with high-resolution images.

The valuable outcome of this method is the "blind" transfer of classification rules to areas with a similar natural environment. The next step would be the development of robust rule sets and reliable cognition networks for nonarid environments and the application to urban areas located in these regions. Once these standardized algorithms have been established and positively tested, this move would significantly reduce the classification efforts and costs. These schemas can be developed first for one sensor image product, for example, ASTER, and can be extended (with more detailed classes, for example) to fit to additional remote sensing sensor products with finer spatial resolution.

Spatial texture analysis was used to investigate and classify the spatial structure of 13 urban centers as a component of an expert classification system by Stefanov et al. (2001a). The results of this study suggested that urban centers could be characterized as centralized (i.e., Baltimore, MD), decentralized (i.e., Phoenix, AZ), and intermediate (i.e., Riyadh, Saudi Arabia), using ASTER 15 m/pixel visible to near-infrared data. A more sophisticated analysis of urban form and environmental fragmentation using spatial metrics was presented by

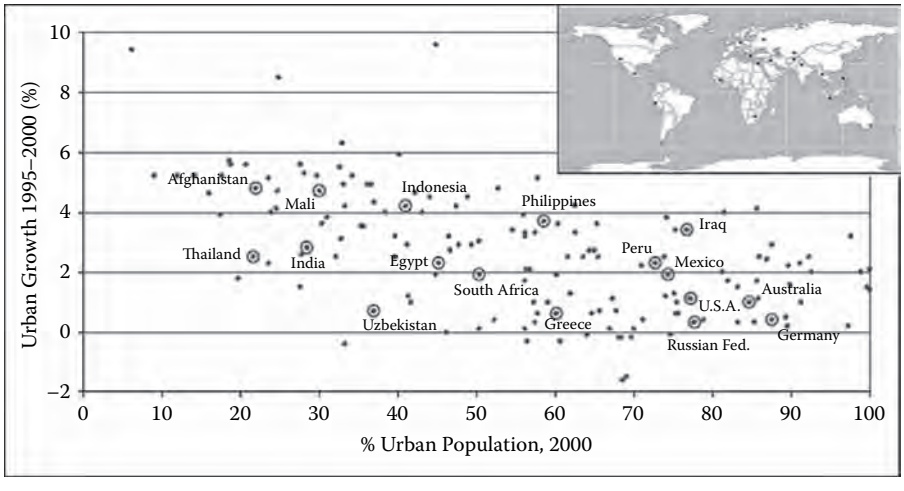

FIGURE 9.2 Geographic distribution of initially selected "intensive study" cities (circled) on the basis of urban growth and population trends, circa 2000.

Netzband and Stefanov (2003). This study used a simplified expert system to classify land cover into eight generalized classes (Water, Bare Soil/Low Vegetation, Moderate Vegetation, High Vegetation, Low Density Urban, Moderate Density Urban, and High Density Urban) for comparison of urban centers. The land cover classifications were then used for gridded analysis of a suite of spatial metrics for a subset of 10 cities. Metrics used were class area, patch density, edge density, area weighted mean shape index, and interspersion/juxtaposition index; see McGarigal and Marks (1994) for definition of the different metrics. In addition, 55 cities were selected for regional fragmentation analysis using a patch diversity metric (Forman, 1995). Although the results of both the regional fragmentation analysis and the metric suite analysis indicated interesting trends many variables such as scale dependence (Wu et al., 2000), classification scheme, and seasonality required further sensitivity analysis.

9.3.2 Better Understanding of Urban Ecosystems

There are many unanswered questions on the consequences of rapid urbanization on urban ecosystems: How have the biodiversity and the population density of plants and animals been affected? Do plants and animals indigenous to the area maintain dominance? What is the spatial distribution of plants and animals? How have the home range and the movement patterns of animals changed? LU/LC classifications can be incorporated into local and regional ecosystem models to assess the effects of urban change on carbon cycling and source/sink relationships. Empirical studies have demonstrated that the variations of landscape elements (e.g., natural vegetation remnant patches, parks, golf courses, agricultural fields, urban blocks) may significantly influence ecosystem processes, such as net primary productivity, energy flux, watershed discharge characteristics, and nutrient cycling (Lowrance et al., 1985; McDonnell and Pickett, 1990; Risser, 1990; Knapp et al., 1993; McDonnell et al., 1997). To detect the changes in landscape pattern and the ecological consequences (e.g., C source-sink dynamics) at the regional scale or above, it is imperative to integrate remote sensing, field work, and ecosystem modeling. There are several contributions in these areas resulting from the UEM project.

Scientists associated with the UEM project have participated in research associated with urban climatology, including mesoscale atmospheric modeling and measurement and analysis of the UHI. One component of this work has been to integrate classified remotely sensed imagery, such as LU/LC, into mesoscale meteorological models, such as the MM5 (Grossman-Clarke et al., 2005). Previous implementations of the MM5 used only a single "urban" class for atmospheric forecasting purposes. The more detailed LU/LC classification system, which contained 12 urban classes, improved the modeling of the boundary layer and improved the ability of the MM5 to simulate temperature ranges in the Phoenix area (Grossman-Clarke et al., 2005). In a second study in urban climatology, researchers have measured the extent and impact of UHI on the local climatology and on the residents living there. Urban remote sensing is proving to be an effective tool to measure the spatial extent and intensity of the effect of urban development on local temperatures (Voogt and Oke, 2003; Stefanov et al., 2004; Hartz et al., 2006a, 2006b; Jenerette et al., 2007; Stefanov and Brazel,

2007). This is especially true in UHI analysis with acquisition of nighttime ASTER imagery — taken at times of the maximum heat island development in the diurnal cycle (Hartz et al., 2006a). This increased temperature in cities is contributing to heat stress in the residents living there. To investigate this effect in Phoenix, Harlan et al. (2006) made use of a human comfort simulation model (after Brown and Gillispie, 1995; Heisler and Wang, 2002; and Hartz et al., 2006b) to estimate a temperature comfort measure based on local climate conditions, and found that lower-income neighborhoods were more likely to have a higher heat stress indicator, suggesting that policies associated with UHI mitigation should target these vulnerable neighborhoods.

Satellite remote sensing data provide universal coverage, but typically provide little biotic resolution with respect to the scale of individual flora and fauna. This means that remote sensing information can only be linked to meaningful biodiversity indicators through spatial parameters such as land use and land cover and the related habitat structure. Perhaps, the highest contribution of remote sensing methodology to urban ecological remote sensing is in monitoring the highly heterogeneous and fragmented land use and land cover as well as change in both, including information on biophysical attributes, vegetation structure, and habitat fragmentation, which are essential determinants of species distributions. Remotely sensed data are of particular use for monitoring biodiversity in the urban mosaic of artificial and natural surfaces due to the relatively high temporal resolution (compared to ground survey campaigns) for change detection of ongoing and fast land use changes.

To focus analysis on the monitoring of the actual LU/LC and its current and potential changes, we will continue to generate products such as vegetation indices (NDVI, SAVI, EVI) and day/night surface kinetic temperature maps using the ASTER database for selected city sites. These data, combined with multispectral and object-oriented LU/LC classifications, will be used for analysis of landscape structure change applying spatial metrics. Performing cross-site temporal comparisons of change-related landscape structure and associated biophysical responses will be undertaken to improve our understanding of how urban systems respond to such changes. This line of research will also provide insight into vulnerability and resilience of various ecosystem types to human impact, which will help address the question of consequences of change for human civilization from the perspective of biodiversity and ecosystem services.

9.4 CONCLUSIONS AND FUTURE OBJECTIVES

In recent years, urban remote sensing has proven to be a useful tool for cross-scale urban planning and urban ecological research as described above. The UEM/100 Cities Project, (http://hundredcities.asu.edu/index.html) at ASU has been successful as a baseline effort to collect and analyze remotely sensed data for urban centers worldwide. Although the focus of the project has only touched on all 100 cities, our aim is to grow to meet that goal. The 100 Cities Project continues to grow our team of researchers and practitioners at ASU and at other institutions around the world to share datasets and participate in collaborative, interdisciplinary research. We seek to create meaningful partnerships with cities internationally. As we build our partnerships, we can then develop a model of how to approach cities and address

their problems with urban remote sensing. Our self-conception is that the 100 Cities Project shall serve as an open platform designed to bring policymakers and researchers together to apply urban remote sensing to the problems of urbanization, the environment, and sustainability. We intend to operationalize this ambitious goal by making urban remote sensing products and processes useful and available to **cities** for planning and policy making through outreach and partnerships. Currently, datasets are accessible by contacting our project director. Furthermore, our academic experience allows us to utilize mapping and modeling results of our remote sensing research to advance the understanding of urban development trajectories and urban "futures." Finally, we aim to develop an international network of urban data providers, researchers, and end users to rapidly disseminate and archive data, analytical approaches, and results.

A major question that continues to be posed and refined is how to grow the 100 Cities Project into an integrated interdisciplinary physical and social science tool with a focus on urban sustainability. One can observe that social science studies are attracted to remote sensing data due to the objective measurement of biophysical characteristics on a local (e.g., urban studies), regional (forest cover changes, urban to peri-urban demographic development), or even on a global scale. However, there is no correspondence in nature or landscape units to grids or even small-scale administrative units. Hence, studies concentrating on the challenge of world urbanization still claim an unmet need for linked spatial biophysical and sociodemographic information. Rindfuss and Stern (1998) discuss the gap between social science and remote sensing research as well as the potential benefits in bridging that gap.

There are examples on how to bridge this gap. A workshop at the International Human Dimensions Programme (IHDP) Open Meeting 2008 jointly organized by the 100 Cities Project and the IHDP core project on Urbanization and Global Environmental Change (http://www.ugec.org/tiki-index.php) seeks to understand how urban remote sensing can best be utilized by both researchers and practitioners in urban models, planning, and policy formulation. Two major questions posed in the workshop were: "What is the potential of urban remote sensing for an integrated interdisciplinary physical and social science with a focus on urban sustainability?" and "How can urban remote sensing fill the gaps in scientific information best for the needs of such an integrated discipline?" More efforts such as this will allow for continued growth of 100 Cities partnerships.

REFERENCES

Abrams, M., The advanced spaceborne thermal emission and reflection radiometer (ASTER): Data products for the high spatial resolution imager on NASA's Terra platform, *International Journal of Remote Sensing*, 21(5), 847– 859, 2000.

Arthur-Hartranft, S.T., Carlson, N.T., and Clarke, K.C., Satellite and ground-based microclimate and hydrologic analyses coupled with a regional urban growth model, *Remote Sensing of Environment*, 86, 385–400, 2003.

Bian, L., Retrieving urban objects using a wavelet transform approach, *Photogrammetric Engineering and Remote Sensing*, 69(2), 133–141, 2003.

Blaschke, T., and Hay, G., Object-oriented image analysis and scale-space: Theory and methods for modeling and evaluating multi-scale landscape structure, *International Archives of Photogrammetry and Remote Sensing*, 34(4/W5), 22–29, 2001.

Blaschke, T., Burnett, C., and Pekkarinen, A., New contextual approaches using image segmentation for object-based classification, in: De Meer, F., and de Jong, S., eds., *Remote Sensing Image Analysis: Including the Spatial Domain*, Kluwer Academic Publishers, Dordrecht, pp. 211–236, 2004.

Brown, R.D., and Gillespie, T.J., *Microclimatic Landscape Design: Creating Thermal Comfort and Energy Efficiency*, John Wiley, New York, 1995.

Dell'Acqua, F., and Gamba, P., Detection of urban structures in SAR images by robust fuzzy clustering algorithms: The example of street tracking, *IEEE Transaction on Geoscience and Remote Sensing*, 39(10), 2287–2297, 2001.

Dell'Acqua, F., Gamba, P., and Trianni, G., Semi-automatic choice of scale-dependent features for satellite SAR image classification, *Pattern Recognition Letters*, 27(4), 244–251**,** 2006.

Forman, R.T.T., *Landscape Mosaics*, Cambridge University Press, Cambridge, 632 pp., 1995.

Gamba, P., Dell'Acqua, F., Lisini, G., and Cisotta, F., Improving building footprints in InSAR data by comparison with a lidar DSM, *Photogrammetric Engineering and Remote Sensing,* 72(1), 63–70, 2006.

Gillies, R.R., Box, J.B., Symanzik, J., and Rodemaker, E.J., Effects of urbanization on the aquatic fauna of the Line Creek watershed, Atlanta — a satellite perspective, *Remote Sensing of Environment*, 86(3), 411–422, 2003.

Grossman-Clarke, S., Zehnder, J.A., Stefanov, W.L., Liu, Y., and Zoldak, M.A., Urban modifications in a mesoscale meteorological model and the effects on near-surface variables in an arid metropolitan region, *Journal of Applied Meteorology*, 44, 1281–1297, 2005.

Hammer, A., Heinemann, D., Hoyer, C., Kuhlemann, R., Lorenz, E., Muller, R., and Beyer, H.G., Solar energy assessment using remote sensing technologies, *Remote Sensing of Environment*, 86(3), 423–432, 2003.

Harlan, S.L., Brazel, A.J., Prashad, L., Stefanov, W.L., and Larsen, L., Neighborhood microclimates and vulnerability to heat stress, *Social Science and Medicine*, 63, 2847–2863, 2006.

Hartz, D.A., Prashad, L., Hedquist, B.C., Golden, J., and Brazel, A., Linking satellite images and hand-held infrared thermography to observed neighborhood climate conditions, *Remote Sensing of Environment*, 104, 190–200, 2006a.

Hartz, D.A., Brazel, A.J., and Heisler, G., A case study in resort climatology of Phoenix, Arizona, USA, *International Journal of Biometeorology*, 51, 73–83, 2006b.

Hawkins, T.W., Brazel, A.J., Stefanov, W.L., Bigler, W., and Safell, E.M., The role of rural variability in urban heat island determination for Phoenix, Arizona, *Journal of Applied Meteorology*, 43(3), 476–486, 2004.

Heisler, G.M., and Wang, Y., Applications of a human thermal comfort model, in: Preprints of Fourth Symposium on the Urban Environment, 20–24 May 2002, American Meteorological Society, Norfolk, VA, pp. 70–71, 2002.

Herold, M., Goldstein, N.C., and Clarke, K.C., The spatiotemporal form of urban growth: Measurement, analysis and modeling, *Remote Sensing of Environment*, 86(3), 286–302, 2003.

Hostert, P., Advances in urban remote sensing: Examples from Berlin (Germany), in: Netzband, M., Stefanov, W.L., and Redman, C., eds., *Applied Remote Sensing for Urban Planning, Governance, and Sustainability*, Springer, Berlin, 37–51, 2007.

Howarth, P.J., and Boasson, E., Landsat digital enhancements for change detection in urban environments, *Remote Sensing of Environment*, 13, 149–160, 1983.

Imhoff, M.L., Lawrence, W.T., Stutzer, D.C., and Elvidge, C.D., A technique for using composite DMSP/OLS "City Lights" satellite data to map urban area, *Remote Sensing of Environment*, 61(3), 361–370, 1997.

Jenerette, G.D., Harlan, S.L., Brazel, A., Jones, N., Larsen, L., and Stefanov, W.L., Regional relationships between surface temperature, vegetation, and human settlement in a rapidly urbanizing ecosystem, *Landscape Ecology*, 22, 353–365, 2007.

Kato, S., and Yamaguchi, Y., Analysis of urban heat-island effect using ASTER and ETM+ data: Separation of anthropogenic heat discharge and natural heat radiation from sensible heat flux, *Remote Sensing of Environment*, 99, 44–54, 2005.

Knapp, A.K., Fahnestock, J.T., Hamburg, S.P., Statland, L.B., Seastead, T.R., and Schimel, D.S., Landscape patterns in soil-plant water relations and primary production in tallgrass prairie, *Ecology*, 74, 549–560, 1993.

Lebel, L., Thaitakoo, D., Sangawongse, S., and Huaisai, D., Views of Chiang Mai: The contributions of remote-sensing to urban governance and sustainability, in: Netzband, M., Stefanov, W.L., and Redman, C., eds., *Applied Remote Sensing for Urban Planning, Governance, and Sustainability*, Springer, Berlin, 221–247, 2007.

Li, G. ., and Weng, Q.H., Using Landsat ETM plus imagery to measure population density in Indianapolis, Indiana, USA, *Photogrammetric Engineering and Remote Sensing,* 71(8), 947–958, 2005.

Lo, C.P., Quattrochi, D.A., and Luvall, J.C., Application of high-resolution thermal infrared remote sensing and GIS to assess the urban heat island effect, *International Journal of Remote Sensing*, 18(2), 287–304, 1997.

Lowrance, R., Leonard, R., and Sheridan, J., Managing riparian ecosystems to control non-point pollution, *Journal of Soil and Water Conservation*, 55, 87–91, 1985.

Martin, L.R.G., Howarth, P.J., and Holder, G., Multispectral classification of land use at the rural-urban fringe using SPOT data, *Canadian Journal of Remote Sensing*, 14(2), 72–79, 1988.

McDonnell, M.J., and Pickett, S.T.A., Ecosystem structure and function along urban-rural gradients: An unexploited opportunity for ecology, *Ecology* 71(4), 1232–1237, 1990.

McDonnell, M.J., Pickett, S.T.A., Pouyat, R.V., Parmelee, R.W., Carreiro, M.M., Groffman, P.M., Bohlen, P., Zipperer, W.C., and Medley, K., Ecosystem processes along an urban-to-rural gradient, *Urban Ecosystems*, 1, 21–36, 1997.

McGarigal, K., and Marks, B.J., *FRAGSTATS: Spatial Pattern Analysis Program for Quantifying Landscape Structure*, Oregon State University, Corvallis, 1994.

Netzband, M., and Stefanov, W.L., Assessment of urban spatial variation using ASTER data, *International Archives of the Photogrammetry, Remote Sensing, and Spatial Information Sciences*, 34 (7/W9), 138–143, 2003.

Nichol, J., Remote sensing of urban heat islands by day and night, *Photogrammetric Engineering and Remote Sensing*, 71(5), 613–621, 2005.

Pozzi, F., and Small, C., Analysis of urban land cover and population density in the United States, *Photogrammetric Engineering and Remote Sensing*, 71(6), 719–726, 2005.

Ramsey, M.S., Mapping the city landscape from space: The advanced spaceborne thermal emission and reflectance radiometer (ASTER) urban environmental monitoring program, in: Heiken, G., Fakundiny, R., and Sutter, J., eds., *Earth Science in the City: A Reader*, American Geophysical Union, Washington, D.C., 337– 361, 2003.

Ramsey, M.S., Stefanov, W.L., and Christensen, P.R., Monitoring world-wide urban land cover changes using ASTER: Preliminary results from the Phoenix, AZ LTER site, Proceedings of the 13th international conference, Applied Geological Remote Sensing, vol. 2, Vancouver, British Columbia, Canada, ERIM International, 1999.

Rashed, T., Weeks, J.R., Roberts, D., Rogan, J., and Powell, R., Measuring the physical composition of urban morphology using multiple endmember spectral mixture models, *Photogrammetric Engineering and Remote Sensing*, 69(9), 1011–1020, 2003.

Ridd, M.K., and Liu, J., A comparison of four algorithms for change detection in an urban environment, *Remote Sensing of Environment*, 63, 95–100, 1998.

Rindfuss, R.R., and Stern, P.C., Linking remote sensing and social science: The need and the challenges, in: Livermand, D., Moran, E.F., Rindfuss, R.R., and Stern, P.C., eds., *People and Pixels. Linking Remote Sensing and Social Sciences*, National Academy Press, pp. 1–27, 1998.

Risser, P.G., Landscape pattern and its effects on energy and nutrient distribution, in: Zonneveld, I.S., and Forman, R.T.T., eds., *Changing Landscapes: An Ecological Perspective*, Springer-Verlag, New York, 1990.

Roth, M., Oke, T.R., and Emery, W.J., Satellite-derived urban heat islands from three coastal cities and the utilization of such data in urban climatology, *International Journal of Remote Sensing*, 10(11), 1699–1720, 1989.

Schneider, A., McIver, D.K., Friedl, M.A., and Woodcock, C.E., Mapping urban areas by fusing coarse resolution remotely sensed data, *Photogrammetric Engineering and Remote Sensing*, 69, 1377–1386, 2003.

Schöpfer, E., and Moeller, M.S., Comparing metropolitan areas — a transferable object-based image analysis approach, *Photogrammetrie, Fernerkundung, Geoinformation*, 4, 277–286, 2006.

Seto, K.C., Fragkias, M., and Schneider, A., 20 years after reforms: Challenges to planning and development in China's city-regions and opportunities for remote sensing, in: Netzband, M., Stefanov, W.L., and Redman, C., eds., *Applied Remote Sensing for Urban Planning, Governance, and Sustainability*, Springer, Berlin, 249–269, 2007.

Shochat, E., Stefanov, W.L., Whitehouse, M.E.A., and Faeth, S.H., Urbanization and spider diversity: Influence of human modification of habitat structure and productivity, *Ecological Applications*, 14, 268–280, 2004.

Small, C., High spatial resolution spectral mixture analysis of urban reflectance, *Remote Sensing of Environment*, 88, 170– 186, 2003.

Song, M.J., and Civco, D., Road extraction using SVM and image segmentation, *Photogrammetric Engineering and Remote Sensing*, 70(12), 1365–1371, 2004.

Stefanov, W.L., and Brazel, A.J., Challenges in characterizing and mitigating urban heat islands — a role for integrated approaches including remote sensing, in: Netzband, M., Stefanov, W.L., and Redman, C., eds., *Applied Remote Sensing for Urban Planning, Governance and Sustainability*, Springer, Berlin, 117–135, 2007.

Stefanov, W.L., and Netzband, M., Assessment of ASTER land cover and MODIS NDVI data at multiple scales for ecological characterization of an arid urban center, *Remote Sensing of Environment*, 99, 31–43, 2005.

Stefanov, W.L., and Netzband, M., Characterization and monitoring of urban/peri-urban ecological function and landscape structure using satellite data, in: Rashed, T., and Jürgens, C., eds., *Remote Sensing of Urban and Suburban Areas*, Springer, 2009, in press.

Stefanov, W.L., Christensen, P.R., and Ramsey, M.S., Remote sensing of urban ecology at regional and global scales: Results from the central Arizona–Phoenix LTER site and ASTER Urban Environmental Monitoring Program, *Regensburger Geographische Schriften*, 35, 313– 321, 2001a.

Stefanov, W.L., Ramsey, M.S., and Christensen, P.R., Monitoring urban land cover change: An expert system approach to land cover classification of semiarid to arid urban centers, *Remote Sensing of Environment*, 77(2), 173–185, 2001b.

Stefanov, W.L., Robinson, J.A., and Spraggins, S.A., Vegetation measurements from digital astronaut photography, *International Archives of the Photogrammetry, Remote Sensing, and Spatial Information Sciences*, 34(7/W9), 185–189, 2003.

Stefanov, W.L., Netzband, M., Möller, M.S., Redman, C.L., and Marks, C., Phoenix, Arizona, USA: Applications of remote sensing in a rapidly urbanizing desert region, in: Netzband, M., Stefanov, W.L., and Redman, C., eds., *Applied Remote Sensing for Urban Planning, Governance and Sustainability*, Springer, Berlin, 137–164, 2007.

Stefanov, W.L., Prashad, L., Eisinger, C., Brazel, A., and Harlan, S., Investigations of human modification of landscape and climate in the Phoenix, Arizona metropolitan area using MASTER data, *International Archives of the Photogrammetry, Remote Sensing, and Spatial Information Sciences*, 35(B7), 1339–1347, 2004.

Sutton, P.C., A scale-adjusted measure of "Urban sprawl" using nighttime satellite imagery, *Remote Sensing of Environment*, 86(3), 353–369, 2003.

Voogt, J.A., and Oke, T.R., Thermal remote sensing of urban climates, *Remote Sensing of Environment*, 86(3), pp. 370–384, 2003.

Weber, C., and Puissant, A., Urbanization pressure and modeling of urban growth: Example of the Tunis metropolitan area, *Remote Sensing of Environment*, 86, 341–352, 2003.

Welch, R., Monitoring urban population and energy utilization patterns from satellite data, *Remote Sensing of Environment*, 9, 1–9, 1980.

Weng, Q.H., Fractal analysis of satellite-detected urban heat island effect, *Photogrammetric Engineering and Remote Sensing*, 69(5), 555–566, 2003.

Wentz, E.A., Nelson, D., Rahman, A., Stefanov, W.L., and Roy, S.S., Expert system classification of urban land use/cover for Delhi, India, *International Journal of Remote Sensing*, 29(15), 4405–4427, 2008.

Wu, J., Jelinski, D.E., Luck, M., and Tueller, P.T., Multiscale analysis of landscape heterogeneity: Scale variance and pattern metrics, *Geographic Information Sciences*, 6, 6–19, 2000.

Zhang, J., and Foody, G.M., A fuzzy classification of sub-urban land cover from remotely sensed imagery, *International Journal of Remote Sensing*, 19(14), 2721–2738, 1998.

10 Megacities
Hints for Risk Management Using EO Data

Hannes Taubenböck, Achim Roth, and Stefan Dech

CONTENTS

10.1 INTRODUCTION

Over the past 50 years, the world has faced dramatic growth of its urban population. The percentage of urban inhabitants exceeded the rural population for the first time in 2007. Furthermore, the trends imply that almost all the expected world population growth until 2030 will be absorbed by urban areas (United Nations, 2003). From 1975 up to the present, the number of so-called megacities increased from 4 to 22, mostly in less developed regions (Münchner Rück, 2005). In general, the term "megacity" describes the world's largest agglomerations. Quantitatively, megacities are defined as megalopolises with more than 10 million inhabitants (United Nations, 2003; Mertins, 1992). Qualitatively, megacities are characterized by high and dense population concentration, and a high density of industries, and social, technical, and transportation infrastructure. They show extreme, uncontrolled urban sprawl, high traffic pressure, ecologic overload, concentration of assets

and power, high spatiotemporal dynamics, and the coexistence of socioeconomic disparities (Kötter, 2004; Kraas and Coy, 2003). In these megacities, in particular, the enormous dimension of quantitative growth, the high concentration of people, infrastructure, and economic power, but also the synchronism, complexity, and interaction of diverse urban processes, imply nonassessable risks. Thus, megacities can be both victims and producers of risks.

Table 10.1 displays the temporal population development of the 10 largest megacities since 1900. The largest megacity today has about 5.5 times the population of the largest megacity in 1900, and there is also an unbroken trend of urban sprawl visible. A clear shift in the top 10 megacities from developed countries, which more or less remain static, to developing countries, which show explosive urban growth, is observable.

Such explosive growth causes uncontrolled and unplanned urbanization. This makes megacities particularly prone to supply crises, social disorganization, and political conflicts. In addition to the structural exposure of such megacities, the location of many cities in areas prone to natural hazards adds to the risks.

The UN (2004) determined that the risk to a particular system has two factors. One factor is the "hazard" itself, which is a potentially damaging physical event, phenomenon, or human activity that is characterized by its location, intensity, frequency, and probability. The second factor is "vulnerability," which denotes the relationship between the severity of hazard and the degree of damage caused. Thus, risk results from a future interplay of a hazard and the various components defining vulnerability. This general conceptualization as a theoretical framework for risk management is used to approach the difficult and complex task of progressing from identifying risks to decision making. The two components defining risk — vulnerability and hazard — are used as an outline in the study to identify the potential contributions of multisensoral remote sensing data to this framework before, during, and after a disastrous event.

In recent years, satellite systems and image analysis techniques have developed to an extent where civil and commercial Earth observation (EO) instruments can contribute significantly in supporting the management of major technical and natural disasters as well as humanitarian crisis situations (Voigt et al., 2007; Taubenböck et al., 2008a). Even before an expected disastrous event, explosive urban sprawl and inner-urban dynamic transformations in megacities challenge the need for up-to-date and area-wide information on the urban environment. Remotely sensed imagery from satellites has become an important tool providing information on the current urban situation useful for assessing the vulnerability of urban areas and grasping damage distribution due to natural disasters (Yamazaki, 2001). The platform and sensors used for remote sensing must be selected by taking into account the area to be covered, the urgency, desired image resolution, weather, and time conditions. The most important data sources for monitoring urban areas are medium to very high resolution optical systems and synthetic aperture radar (SAR) systems.

The heterogeneity and small-scale structure of urban morphology requires geometric resolution that enables differentiation of objects necessary for analyzing spatial patterns of vulnerability and risk. Very high optical resolution satellite data

TABLE 10.1
Population Development of Megacities Since 1900

1900		1950		1975		2000		2015	
London	6.5	New York	12.3	Tokyo	26.6	Tokyo	34.5	Tokyo	35.5
New York	5.5	Tokyo	11.2	New York	15.9	Mexico City	18.1	Mumbai	21.9
Tokyo	5.2	London	8.4	Mexico City	10.7	New York	17.8	Mexico City	21.6
Paris	4.0	Shanghai	6.1	Osaka-Kobe	9.8	Sao Paulo	17.1	Sao Paulo	20.6
Berlin	2.4	Paris	5.4	Sao Paulo	9.6	Mumbai	16.1	New York	19.9
Chicago	1.9	Moscow	5.4	Los Angeles	8.9	Shanghai	13.2	Delhi	18.6
Wien	1.6	Buenos Aires	5.1	Buenos Aires	8.7	Kolkata	13.1	Shanghai	17.2
Kolkata	1.5	Chicago	5.0	Paris	8.6	Delhi	12.4	Kolkata	17.0
St. Petersburg	1.4	Kolkata	4.5	Kolkata	7.9	Buenos Aires	11.8	Dhaka	16.8
Philadelphia	1.4	Beijing	4.3	Moscow	7.6	Los Angeles	11.8	Jakarta	16.8

Source: Bronger, 1996; United Nations 2005; Spreitzhöfer, 2007.

from Ikonos, Quickbird, or SPOT feature a geometric resolution ranging from 60 cm to 2.5 m, which is feasible for urban environments. In terms of temporal analysis, optical sensors such as Landsat (since 1972), SPOT (1986), and IRS (1988) enable the monitoring and detection of changes with reduced spatial resolution. In addition to optical systems, SAR antennas operate almost independently of meteorological conditions and solar illumination. There are, at present, several SAR sensors in space offering a broad and global observation of the planet (e.g., ERS-2, RadarSat, Envisat, TerraSAR-X, and the space shuttle) (Jordan, 1997) in different frequencies, polarizations, and geometric resolutions. Even aerial acquisitions (Gamba, Houshmand, and Saccani, 2000) are possible due to the full-time imaging potential of radar. Interferometric SAR has been applied widely to derive digital elevation models (DEMs) (Rabus et al., 2003) and to study ground displacements (Rosen et al., 2000). In particular, the Shuttle Radar Topography Mission (SRTM) of the year 2000 (Farr et al., 2007; Marschalk et al., 2004) supports urban analysis with area-wide DEMs. Furthermore, new radar satellites such as TerraSAR-X, CosmoSkyMed, and Advanced Land Observing Satellite (ALOS) enable the extraction and analysis of urban structures based on geometric resolutions up to 1 m (Roth et al., 2005; Esch et al., 2005; Esch, 2006).

Utilizing multisource remotely sensed data, geospatial information, maps, and thematic analysis can be produced in various scales to support risk and disaster management before, during, and after an event. This study addresses the following specific questions regarding risk management using remotely sensed data in megacities:

- How can risk management be conceptualized?
- What are the capabilities and limitations of remote sensing to contribute to risk assessment and support risk management?
- What are future perspectives regarding megacities and remote sensing?

10.2 RISKS IN MEGACITIES

10.2.1 Hazards

Hazards can be either natural (e.g., such as Earthquakes, volcanic eruptions, landslides, storms, floods, droughts, heat waves, snowfall, frost, avalanches, and global sea level rise) or man-made (e.g., water and soil pollution, accidents, fire, industrial explosions, sinking land levels, diseases and epidemics, socioeconomic crises, civil riots and terror attacks, nuclear accidents, war, and germ or nuclear warfare) (Kraas and Coy, 2003). (Natural) hazards are defined as the probability of a disastrous event occurring within a certain period at a certain place. They are a phenomenon of a certain intensity having a destructive impact on the affected environment (UNESCO, 1973).

Many megacities are located in areas exposed to natural disasters. Examples are the Earthquake-prone megacities of Istanbul, Los Angeles, Mexico City, and Tokyo; landslide hazards that threaten Caracas, Hong Kong, Rio de Janeiro, and

Manila; floods in Mumbai, Dhaka, Kolkata, Seoul, and Bangkok; tropical storms over Shanghai and Taipeh; tsunamis inundating Jakarta, Mumbai, and Tokyo; and volcanic eruptions near Mexico City (Mitchell, 1999). Sole consideration of the hazard only reveals an incomplete view of risks, with Birkmann (2006) stressing the need for a paradigm shift from the quantification and analysis of the hazard to the identification, assessment, and ranking of vulnerabilities.

10.2.2 Vulnerability, Risk, and Their Management

Risk is imaginary, and thus implies uncertainty. Risk management deals with prognoses about future events. To be suitably prepared, access to substantial, up-to-date, and area-wide information is mandatory. Risk is the interaction of a hazard and the vulnerability of a system. Vulnerability is a complex interaction of various aspects concerning a specific hazard. The UN (2004) defines vulnerability as the condition determined by physical, economic, social, environmental factors, or processes that increases the susceptibility of a community to the impact of hazards (Figure 10.1). Thus, indicators contributing to the vulnerability concept describe the exposure and the susceptibility as stressors of the system, with the coping capacity as the potential of the system to decrease the impact of the hazard (White et al., 2005).

The general outline of the risk framework is defined using abstract terms. To make them measurable, they are resolved down to quantifiable, clearly comparable, and utilizable indicators to support decision making. As an example, the physical sphere represents one aspect that can be specified in measurable indicators, such as number of buildings, built-up density, structural vulnerability, or accessibility, among many others. Their combination simulates the holistic idea of the risk framework. Thus, the indicators can either stress the system (exposure, susceptibility) or counter vulnerability (coping capacity).

The risk framework specifies the various hazards and types of vulnerability, but does not address issues of temporal progress. The timeline of risk (Wisner, 2004; DKKV, 2002) supports decision making in all phases. In the predisaster phase, substantial, up-to-date, and area-wide information is the foundation for identifying risks and their spatial pattern. The first step is assessing the weaknesses of a system (here, urban) in order to systematically implement preventive measures. In the disaster phase, required information supports the decision maker in assessing the situation by estimating the location, dimension, and spatial pattern of the impact. In the postdisaster phase, knowledge about the impact makes it possible to organize the reaction and rehabilitation processes. Figure 10.1 shows the theoretical conceptualization of the risk framework with respect to the timeline. The resulting indicators frame the basis to support decision making with substantial, objectively measurable, up-to-date, and area-wide information.

In the following, the risk framework and its timeline present the guideline to identify the capabilities of remote sensing in urban areas to provide decision makers with an information basis.

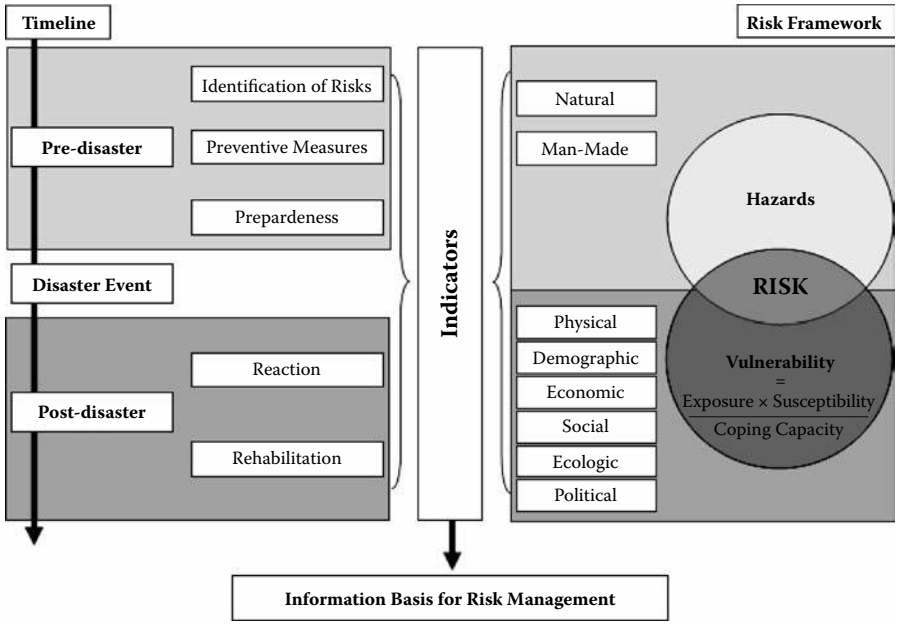

FIGURE 10.1 Risk framework in dependency of timeline of potential disasters.

10.3 CONTRIBUTIONS OF REMOTE SENSING TO RISK MANAGEMENT IN MEGACITIES

Problems associated with hazard identification, risk assessment, and developing mitigation solutions are inherently spatial in nature. Remote sensing provides various data sources appropriate for analyzing different aspects (indicators) of the holistic risk framework spatially with respect to its timeline. Well-founded decisions are a prerequisite for the formulation of successful mitigation, response, preparedness, and recovery strategies. To a large extent, however, successful strategies depend on the availability of accurate information presented in an appropriate and timely manner. Information is also important because it increases the transparency and accountability of the decision-making process and can therefore contribute to good governance (Montoya, 2003). In the following, possible contributions of remote sensing in the predisaster phase for assessing vulnerability and risk, in the disaster phase to support coordination, and eventually in the postdisaster phase to support rehabilitation measures are shown for a selection of the world's megacities.

10.3.1 Predisaster Phase

The identification of risks is essential in the predisaster phase to enable sustainable development and preventive measures finally leading to preparedness. As presented in Figure 10.1, risk is the interaction between two components: the hazard and the vulnerability of a system. Remote sensing contributes spatial information on both.

10.3.1.1 Hazards

Radar technology, in particular, is well suited for monitoring and assessing the hazard side of the risk framework. Differential SAR (DiffSAR) interferometry allows, in principle, the measurement of very small movements of the ground and can cover large areas. Using the permanent scatterers (PS) technique (Ferreti et al., 2001), several procedures have been developed in recent years; these include the Small BAseline Subset (SBAS) technique (Berardino et al., 2002, 2004), Coherent Point Target Analysis (Mora et al., 2003), Interferometric Point Target Analysis (Wegmüller et al., 2005), and the Spatio-Temporal Unwrapping Network (Kampes and Adam, 2005). Examples for applications are monitoring the deformation of volcanoes (Lu et al., 1997; Berardino et al., 2002), land subsidence (Crosetto et al., 2003; Hoffmann et al., 2001), crustal movements (Colesanti et al., 2003; Tobita et al., 2006), and the use of DiffSAR interferometry to monitor and model large slope instability (Berardino et al., 2003; Xia et al., 2004). By default, coherent scatterers mainly appear in urban areas, making this technique an important tool for assessing natural and man-made hazards in an urban environment.

Interferograms can also be used to produce DEMs (Rabus et al., 2003). The height information in combination with the orientation of the slopes using a DEM based on SRTM data can be used to support the modeling of affected areas in the case of a tsunami wave hitting an urban coastline.

By using a DEM based on SRTM data, various contributions to assess the spatial distribution of potentially endangered areas are possible. The location of urbanized areas has a great influence on their vulnerability and exposure. Orographic information or distance to expected sources of natural hazards allows a first assessment of a spatial pattern of vulnerability. The utilization of a DEM enables the integration of orographic surface information when assessing high risk zones such as flood- or tsunami-prone areas based on height information, or landslide prone slopes derived from the terrain's steepness.

Figure 10.2 displays an SRTM-based DEM of the megacity Rio de Janeiro, Brazil. In the example, the hilly coastal urban landscape prone to landslides is visualized. The result projects the spatial distribution of the steepness of slopes, which serves as an indicator to identify areas at high risk for landslides. Areas classified as having steep slopes overlapping with Landsat imagery showing urban sprawl help users to identify areas with steep, landslide-prone slopes, indicate high risks, and thus give a first spatial pattern of the hazard side of risk.

10.3.1.2 Vulnerability

10.3.1.2.1 Physical Sphere

As mentioned above, one major influencing factor is the growing urbanization around megacities. As cities expand, spontaneous and informal settlements tend to alter typical environmental peri-urban areas, such as agricultural and natural spaces. Correct analysis of these changes and settlement characteristics is needed to establish planning procedures and, in particular, to assess and monitor disaster prevention (Lavalle et al., 2001). Medium-resolution satellite data such as Landsat cover large areas of megacities and, because they are available from 1972 onward, enable consistent monitoring of urban sprawl dimensions and directions. With its field of

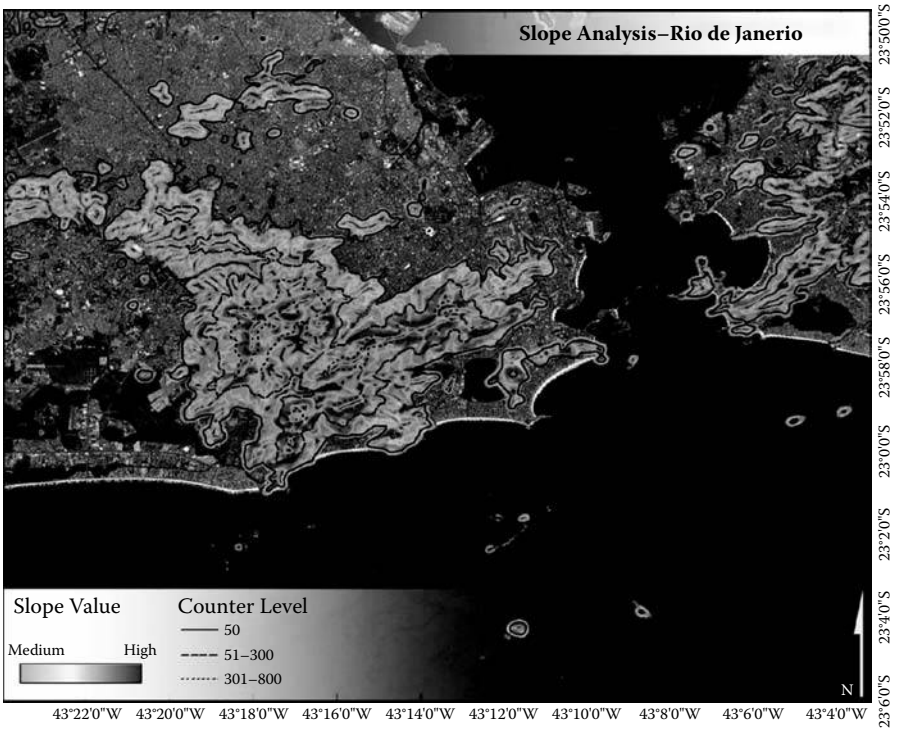

FIGURE 10.2 **(See color insert following page 324.)** Overlapping of the DEM and Landsat data indicating areas of high landslide risk based on steepness of slopes in the megacity Rio de Janeiro, Brazil.

view of 185 km, this satellite is able to survey the large metropolitan areas of the study sites. Measurements of both areal coverage and spatial distribution are needed to adequately describe the morphology of an urban area (Schweitzer and Steinbrink, 1998). The chosen level of description with Landsat data features geometric resolutions from 79 m (Multispectral Scanner) to 15 m (Enhanced Thematic Mapper) not flooded with microscopic detail, but incorporating specific features of the urban system. On the other hand, requirements for the differentiation of classes are limited to the classification of built-up versus non-built-up areas. Also, the accuracy of classification is limited because of the coarse geometric resolution and therefore many "mixed-pixels" with information on various thematic classes must be accommodated. This limited differentiation and accuracy nevertheless enables monitoring and detection of the correct dimension of spatial and temporal changes, urban sprawl, and the spatial direction of urban development.

Multidate satellite data are used for analyzing spatial urbanization. A hierarchical object-oriented classification algorithm is used to derive a land cover classification. The segment-based algorithm utilizes spectral signatures of the scene, and arithmetic operations to derive indices such as Normalized Difference Vegetation Index and Soil Adjusted Vegetation Index to enable differentiation of four classes — sealed

areas, vegetation, water, and bare soil. In addition, the use of a principal component analysis and shape information from the segmentation approach supports the fuzzy-based classification algorithm. The accuracy has been checked by a 200-sample point visual comparison for each class. With respect to the limitation of the geometric capability of Landsat data, the overall accuracy was 92%. Postclassification comparison was found to be the most accurate procedure and had the advantage of indicating the nature of the changes (Mas, 1999). A comparative analysis of independently produced spectral classifications for times t_1 and t_2 (Singh, 1989) was therefore carried out to monitor and analyze the explosive changes in the metropolitan areas of the megacity Mumbai, India.

The example in Figure 10.3 shows the enormous urban sprawl of the megacity Mumbai in India since 1973. The available satellite data from the Landsat series enables monitoring almost 30 years of urban development, identifying axial directions of growth, the development of peripheral satellite towns, and decreasing redensification processes in the urban center. The urbanized areas almost quadrupled between 1973 and 2001. An artificial raster is used to analyze built-up density, or, as displayed in Figures 10.3 and 10.4, the urbanization rates with spatial reference. Decreasing redensification in the urban center and relocation of urban sprawl to the edges of the urban core, forming axial development lines to satellite towns, can be quantified.

By using change detection, the pace of development and its spatial distribution, urbanization directions, or absolute values can be measured. As an example, the built-up density for Mumbai is displayed, showing only a moderate redensification processes over time in zone 1 (urban center), whereas explosive urbanization is relocating to peripheral zones (zones 2–4). However, urbanization per se does not imply high vulnerability. Combining this result with the terrain information (Figure 10.2) presented above allows a first linkage of hazard and vulnerability components.

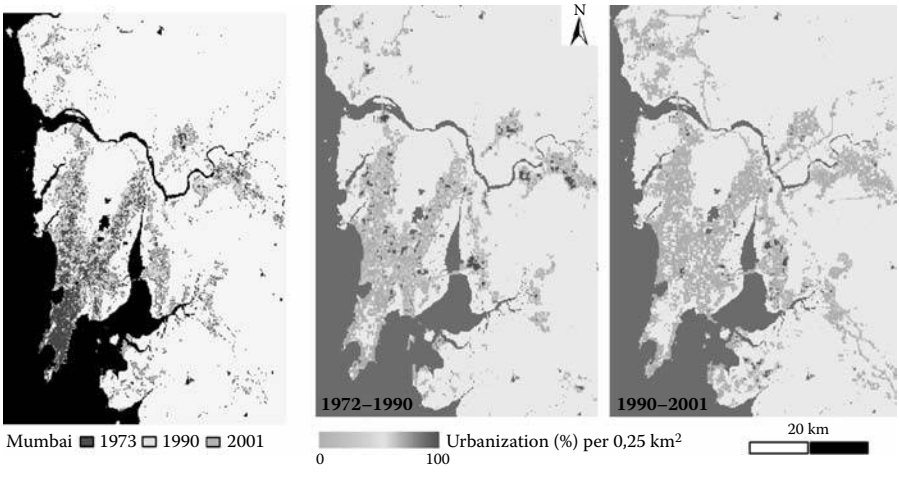

FIGURE 10.3 (See color insert following page 324.) Change detection and urbanization rates in the megacity Mumbai, India.

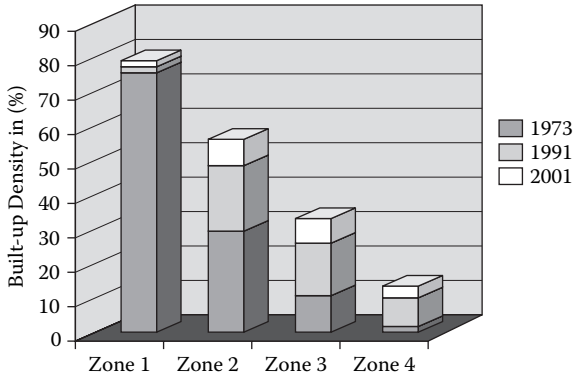

FIGURE 10.4 Quantification of urban sprawl with spatial reference in Mumbai, India.

Although Landsat data enable temporal and spatial analyses for the large extents of megacities at medium resolution, very small-scale, heterogeneous, and variable urban morphology is not detectable. Very high resolution satellite data enable mapping in the required detail of small-scale urban objects such as buildings, streets, and their characteristics (e.g., structural alignment or density). Thus, the assessment improves from an overview analysis to coverage of the heterogeneous, small-scale, and detailed structures of urban morphology. The high spatial variability and small-scale transitions in the urban morphology result in patterns of varying urban vulnerability. The basic product for analyzing vulnerability and risks is a thematic urban land cover classification basically showing "what" is "where" in the complex urban landscapes of megacities. In recent literature, many diverse approaches address novel techniques for the classification of high-resolution optical remote sensing images. De Martinao et al. (2003) use gray-level co-occurrence matrix texture features to incorporate the spatial context for classification, whereas Bruzzone and Carlin (2006) present a supervised multilevel context-based system to analyze the spatial patterns in high-resolution satellite data, and a subsequent classifier based on support vector machines. Fauvel et al. (2006) propose a technique called decision fusing, which combines several individual classifiers. Gamba et al. (2007) use edge extraction to exploit object boundaries in segmentation processes for enhanced object extraction. Meher et al. (2007) present a wavelet feature–based classification method analyzing the spatial and spectral characteristics of a pixel along with its neighbors. To utilize the full geometric capabilities for classification in very high resolution satellite data such as Ikonos (1 m), Quickbird (0.61 cm), or from 2008 on Worldview I and II (50 cm), object-oriented approaches are suitable (Barr et al., 2004; Shackelford and Davis, 2003; Van Der Sande et al., 2003).

Here, an object-oriented, hierarchical, multilevel top-down classification approach (Taubenböck and Roth, 2007) implemented in Definiens Developer software was developed. The approach uses not only spectral, but also shape, textural, hierarchical, and contextual information to achieve high classification probabilities. The multilevel approach uses a fuzzy-based decision-fusion of the various types of information provided to extract detached houses, main street infrastructure, vegetation areas, bare

soil, and water areas. The fixed framework eases transferability for any optical very high resolution sensor with few adjustments on the specific spectral characteristics of the data or regional structural particularities. The approach has been applied to various datasets (Quickbird and Ikonos) (Taubenböck and Roth, 2007) and megacities (Istanbul, Mexico City, Hyderabad) (Taubenböck et al., 2007b), taking about 5 days on an average PC to produce the results for one scene. The corresponding accuracy assessment provided an overall average accuracy of this automated procedure of more than 84% correctly classified houses. In comparison to the automated approach, a different study used manual digitalization of the urban objects in one Ikonos scene to extract 80,000 existing buildings (for Padang, Indonesia), taking 6 months to complete, but improving the accuracy to 96% (Taubenböck et al., 2008b).

The result of the implemented object-oriented approach, as an example, displays a highly dense built-up area in the center of the megacity Mexico City, Mexico. Here, the algorithm was tested on Quickbird data. It clearly shows the extracted street network, the coexistence of small residential buildings in block alignment with large, commercially used buildings as well as vegetated areas and bare soil (Figure 10.5).

Vulnerability and risk show a diverse spatial pattern based on various influencing indicators. Analysis of land cover classification contributes to a structural analysis of urban morphology. The built-up density distribution reflects the quantity of potentially affected structures. The small-scale built-up density distribution is spatially highly variable and does not follow any theoretical rules. Changeovers are calculated based on the data themselves and not on predetermined borders such as the street network. A moving window approach scanning the neighborhood of each house pixel has been implemented. Using this highly variable density distribution, Savitzky-Golay filtering fits a polynomial to the data surrounding each data point (density value). The derived polynomial function is used to detect built-up density borders. By using a curve sketching approach, the surrounding density values of each point in the urban landscape are analyzed. The changeovers are reflected in inflexion points (Taubenböck et al., 2006). The spatially built-up density distribution

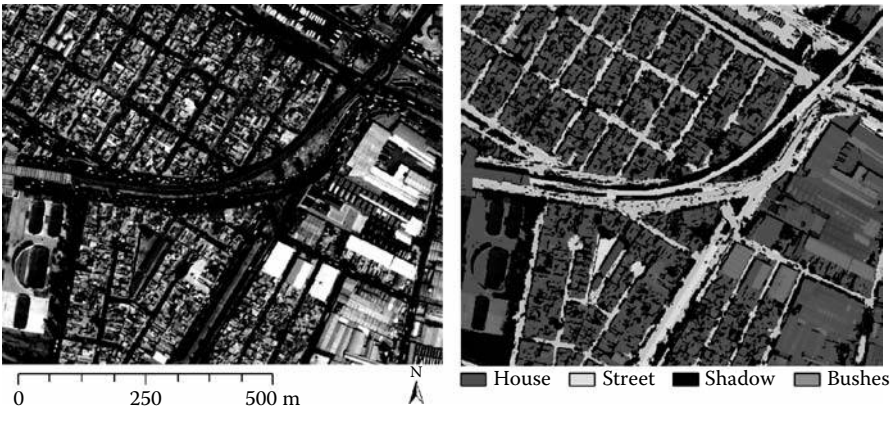

FIGURE 10.5 **(See color insert following page 324.)** Land cover classification of the dense urban structures of Mexico City, Mexico, based on Quickbird data.

is shown in Figure 10.6(a), characterizing the urban morphologic structure of a district of the megacity Istanbul, Turkey.

The identification of open spaces and their location and dimension provides information on potentially safe and sheltered areas. In addition, the main street network extracted from the land cover classification supports the assessment of accessibility. Thus, indicators describing the coping capacity of the urban system are used to analyze bottlenecks and identify necessary preventive measures. Figure 10.6(b) shows the calculation of distance functions to open spaces and the main street network to assess the accessibility of areas within the urban environment.

A further parameter to structure the urban morphology is building height. A cost-intensive new technology is Laser Altimeter (LIDAR) for highly detailed profiles of 3-D elevations of the Earth's surface (Gamba and Houshmand, 2000); stereo images can also be used. If such datasets are unavailable, an indirect method using single-look high-resolution satellite data can be used to assess building heights. Using the classified shadow length from the land–cover classification, the corresponding building heights can be recalculated based on the sensor azimuth angle and the sun elevation. By adding an interpolation methodology for buildings showing incomplete shadows, building heights have been assessed with 94.1% accuracy for three height classes: 1–3 floors, 4–7 floors, and higher than 7 floors (Taubenböck, 2008).

As a further physical indicator to classify structures using satellite data, the properties of building roofs were successfully used in the megacity Istanbul. The

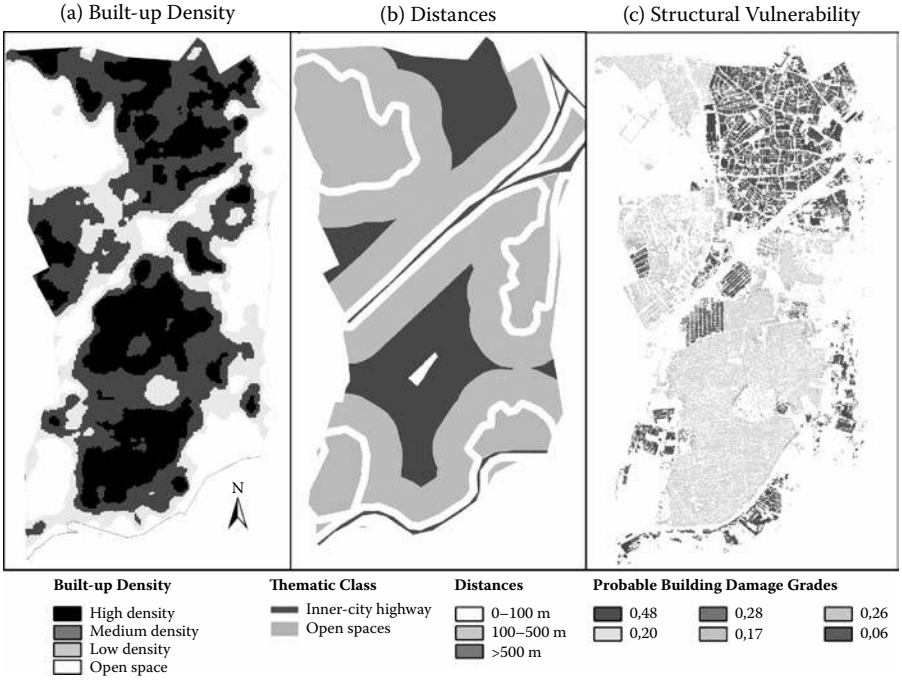

FIGURE 10.6 **(See color insert following page 324.)** Indicators contributing to a holistic concept of risk and vulnerability.

layer "houses" taken from the thematic urban classification was used for further analysis. The fundamental idea behind differentiation of the two different roof types is the coexistence of a sun facing side and a side turned away from the sun for the case of a pitched roof. The spectral difference is in this case used to derive the presence of gabled roofs, whereas the missing spectral difference is used to classify flat roofs. In combination with the average building sizes of an area, usage (residential or commercial) is indirectly reflected in the physical structures. In addition, the temporal analysis of Landsat data presented above enables on a lower resolution the detection of development areas, in general, and thus a coarse estimation of building ages.

As an example of interdisciplinary value adding for remote sensing products, the synergistic usage of the derived structural building characteristics from high-resolution satellite data and methods of civil engineering is presented (Münich et al., 2006). The assessment of the expected damage to buildings in case of an Earthquake impact is based on the classification of buildings using physical parameters derived from remote sensing and the so-called capacity spectrum method from civil engineering. The capacity spectrum method has three main steps: In the first step, the seismological impact is calculated, which is displayed by the response spectrum. In the second, the physical characteristics of various building types show their global load capacity as a result of the specific strength and deformation characteristics of the different components of the structure. In the third step, the correlation between the expected deformation and the probability of an expected damage grade is derived. Damage functions link the seismic impact and the expected damage of the structure.

Figure 10.6(c) shows the calculated probability of damage grades for Zeytinburnu, Istanbul. It shows high structural vulnerability in the northeast of the district, identifying high-risk areas in case of an Earthquake.

Results show the broad capabilities of remote sensing data and methods for supplying up-to-date and area-wide physical information on the urban environment to support the assessment of hazards and vulnerability, and thus risk. The physical urban patterns reflect the spatial nature of risk and vulnerability patterns.

10.3.1.2.2 Demographic Sphere

Furthermore, knowledge of the physical structure of urban morphology can be used to indirectly derive further parameters crucial for risk management. The basic idea behind inferring the population distribution is based on a correlation between the structural characteristics of the urban environment and its population. The hypothesis is based on the assumption that populations living in areas showing nearly similar housing conditions will have homogeneous social and demographic characteristics (Baudot, 2000; Wlodarczyk, 2005). The distribution of a known total population following the structural characteristics of an urban morphology is determined by assuming a dependency between numerical and spatial units. Here, homogeneous urban zones are reflected by areas of similar urban morphology characteristics such as built-up density, building heights, the floor area of buildings, and land use. This information is used to correlate the static urban morphology to dynamic population distribution.

Thus, a top-down distribution method has been implemented to estimate the daytime population based on the floor areas in the various zones. The information on land use has been used to estimate a relocation of population distribution during nighttime (Figure 10.7). A spatial shift from commercially used areas to areas classified as residential has been mapped (Taubenböck et al., 2007a). The result is a local distribution of the generalized total population information based on the spatial unit of a whole district. The benefit appears in the significant spatial differences of population densities within the district. Thus, the total population is resolved into smaller units, resulting in a spatial coexistence of maximum extremes from open spaces with no inhabitants to more than 60,000 inhabitants per km^2 in high-density residential built-up areas with buildings containing more than seven floors. This provides more specific and systematic knowledge for city planners, economists, ecologists, and resource managers to support sustainable development and to understand the chronology of urban dynamics.

FIGURE 10.7 **(See color insert following page 324.)** Nighttime population estimation.

The analysis of our example — Istanbul's Zeytinburnu district — shows basically higher daytime than nighttime population. From this observation, it follows that commuters working in the large commercial areas increase the daytime population significantly compared to the permanent residents. This is expressed by a large difference between nighttime and daytime populations in the commercial areas. Moreover, in the residential areas an immense increase of population during the day can be observed. This suggests predominantly mixed use, with business areas on the ground floors. An accuracy assessment has been carried out based on a comparison to population data within a 500 × 500 m raster in Zeytinburnu (Erdik, 2002). The results support the hypothesis that population distribution correlates directly with the structural characteristics of the urban environment. The absolute values in the corresponding test raster are consistently of the same dimension. This shows the capabilities of remote sensing to distribute demographic input parameters based on an analysis of urban structural characteristics (Taubenböck et al., 2007b). Although remote sensing cannot accurately map cadastral data, it can provide a fast assessment of the correct dimension of a population based on a correspondence to the dynamic development in an urban area.

This precise knowledge allows an analysis of population flows, carrying capacities, localization of spatial and temporal population patterns, catchments areas, and necessary supply and disposal units, as well as an assessment potential to quantify potential emergency measures. In short, the methodologies provide up-to-date data and correctly dimensioned information for decision makers managing highly dynamic urban areas.

10.3.1.2.3 Socioeconomic, Ecological, and Political Sphere

As discussed above, the capabilities of remote sensing are predominantly linked to direct derivations from image information. The indirect correlation of structural characteristics directly derived from satellite data with population information or structural vulnerability showed synergistic effects to achieve value-added products.

A further step is the analysis — if socioeconomic indicators are reflected in the physical urban morphology. The possibility of deriving parameters such as built-up density, building sizes, building height, location, or land use enables a semantic classification of urban structure types. As an example, an unstructured, organic, high-density built-up area in a peripheral location, with low (residential) buildings, and maybe with rusted roofs, allows the derivation of a semantic class, that is, a slum. Thus, socioeconomic parameters such as high unemployment rate, low income, or low education levels can be assumed. Future research is intended to identify socioeconomic parameters that are, in fact, reflected in physical urban morphology. In addition, direct methods can be used to assess economic indicators such as the measurement of rudimentary or nonexisting infrastructure (transportation).

Figure 10.8 shows the differences between a slum typically featuring the above-mentioned physical parameters and a structured, planned area of detached medium-sized buildings, with a high vegetation fraction and good infrastructural connections. Thus, for the latter, a difference in socioeconomic indicators for the

FIGURE 10.8 Comparison of physical urban morphology to correlate to socioeconomic parameters in the megacity Cairo, Egypt (source: Google Earth).

population living there is reflected by the physical urban morphology. Figure 10.8 visualizes the urban morphology discrepancy using the example of the megacity Cairo in Egypt.

In the ecologic sphere of the vulnerability outline, direct information can be derived from satellite data. The above presented urban sprawl, urban expansion in ecologically fragile areas, and vegetation fraction contribute indicators on ecologic stress by an urban system. Eventually, the collation of the various aspects of vulnerability and hazards enables a substantial information system to be provided aiming at educating, raising awareness, and thereby also influencing the political thought processes. Apart from scientific studies, an established information system is therefore the basis for managing and governing risks with political support.

10.3.2 Disaster Phase

10.3.2.1 Ad Hoc Coordination and Rapid Mapping

The substantial information basis generated before an expected disastrous event enables ad hoc coordination during the disaster. A first step suggests the calculation of expected damage grades for the actual scenario. Thus, a first assessment of affected structures and affected people enables localization of focus areas and the diagnosis of the dimension of the impact. Using this information basis, the coordination of a fast reaction can be supported and accomplished.

In a further step, the needed shelter areas can be spatially identified by analyzing their best location with respect to affected areas. Accessibility to those areas can be assessed using an analysis of the street network and distance functions in combination with a structural damage assessment. That ad hoc analysis is the foundation for ad hoc coordination and reaction measures during or very shortly after a disastrous event, based on spatial information surveyed before the event and used to assess the situation. But, the capabilities of remote sensing enable in addition the analysis of satellite data recorded shortly after the event to obtain current information on de facto impacts.

Accurate and spatially precise information on the damage caused is of vital importance for rescue and relief operations and to mobilize resources for repair and recovery (Pesaresi et al., 2007; Saito and Spence, 2004). Fast acquisition of satellite data from the affected area enables a measurement of the actual damage caused by the impact. In case of a disaster on a large scale, the International Charter of Space and Major Disasters (http://www.disasterscharter.org) provides satellite data from different sensors. It focuses on the preprocessing of satellite data, a value-adding step, and visualization of the results. Critical elements are hereby the availability of essential datasets, the processing time, the quality of information extraction, and the usefulness of the products for the end users (Allenbach et al., 2005; Buehler, 2007).

Voigt et al. (2007) showed many examples of rapid mapping products based on multisource satellite data. The applications they presented pertained to tsunami impact, forest fire mapping, Earthquake damage assessment, and landslide mapping. Assessment of the dimension and its spatial distribution is elementary information for fast and coordinated relief measures.

The example in Figure 10.9 shows a product produced by the DLR-ZKI (Center for Satellite Based Crisis Information) to support the spatial extension of flooding as a basis for supporting, managing, and coordinating relief activities. Up-to-date acquisitions of satellite data show the dimension and location of flooded areas of the megacity Dhaka, Bangladesh, during the monsoon, and provide critical information for coordinating and directing rescue and recovery operations.

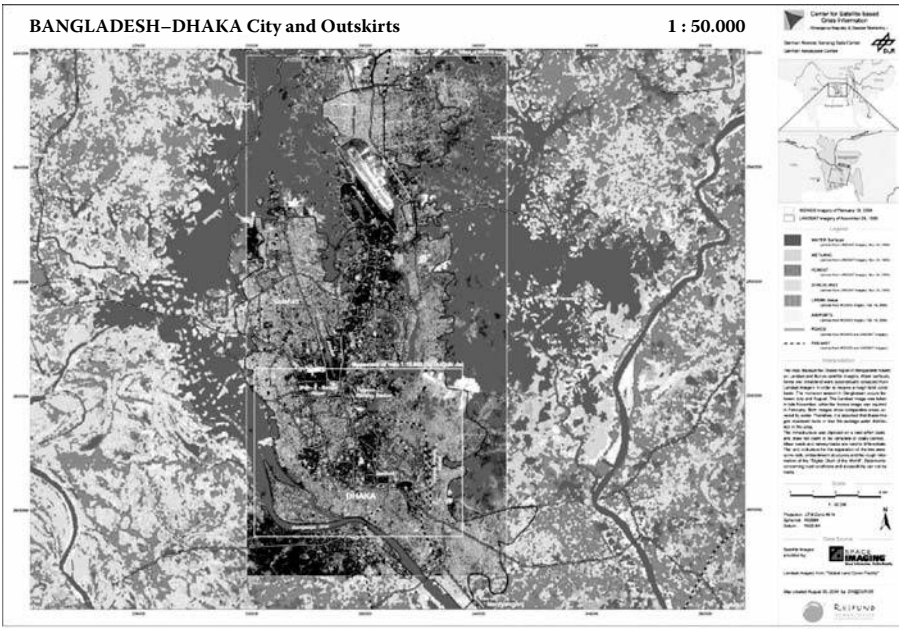

FIGURE 10.9 **(See color insert following page 324.)** Flooding of the megacity Dhaka, Bangladesh. Rapid mapping product produced at DLR-ZKI to derive up-to-date spatial information for relief operations. (Image from the Center for Satellite-Based Crisis Information. With permission.)

10.3.3 Postdisaster Phase

The dimension and dynamics of megacities make achieving an area-wide and consistent information basis a difficult task. Remote sensing supports an assessment of the impact by answering questions such as "where," "what," and "how many." Postdisaster change detection provides information on the degree of damage caused, and in consequence the amount of probably affected people and their spatial distribution.

Remote sensing data and methodologies are increasingly valuable as postdisaster damage assessment tools. Recent studies demonstrated that physical damage in urban environments can be identified using various datasets. Change detection in the aftermath of disastrous events using very high resolution optical satellite data enables the measurement of changes and thus, detection of structural damage and assessing its extent (Al-Khudhairy et al., 2005; Saito et al., 2004; Bitelli et al., 2004; Voigt et al., 2007).

In addition, radar technology supports weather-independent postdisaster damage detection. SAR systems illuminate the Earth's surface and record the intensity and the phase information of the backscattered signals. The radar return is strongly influenced by topography and the geometry of the surface structure — in particular, the small-structured and heterogeneous urban morphology entails effects such as foreshortening and layover, shadow, and double bounce (Ulaby, 2006). Nevertheless, changes in the urban structure such as the collapse of buildings affect the backscattering process. By using the coherence and intensity information from the backscattering process, changes in multidate imagery can be detected. As an example, texture analyses of the intensity images were used for damage assessment purposes (Bignami et al., 2004). Gamba et al. (2000) extracted and characterized building structures starting from the three-dimensional terrain elevation data provided by interferometric SAR measurements. Interferometric coherence is a very sensitive measure for mapping damages that occurred during a disastrous event. Hoffmann (2007) defines a coherence change index to interpret damage quantitatively. In addition, Huyck et al. (2002) combined SAR and LIDAR technology to assess changes.

The prerequisite for SAR interferometry is a coherent backscattering process for the different observation dates. The degree of similarity of these reflections can be estimated from the SAR data themselves and is provided as the interferometric SAR coherence. Of course, collapse of buildings reduces coherence. To separate damage from other decorrelation effects, pre- and coseismic coherence images were analyzed. Figure 10.10 shows an example of the effects of the magnitude 6.6 Earthquake that occurred in the city of Bam, southeastern Iran, in 2003. Five SAR scenes acquired by the Envisat-ASAR instrument were used to derive coherence changes. The color bar indicates changes in coherence after the Earthquake event. White means no changes, dark blue indicates change to a higher coherence, and areas in brown show where significant decorrelation took place. This decorrelation was mainly caused by the collapse of buildings. The results have been projected on administrative districts in Bam.

New high-resolution radar sensors on satellites such as TerraSAR-X, Cosmo SkyMed, or Radarsat-2 are initiating a new era of satellite-based applications and will enable more highly detailed and accurate mapping of damage. Figure 10.11 shows a comparison of Envisat-ASAR data featuring a 30-m spatial resolution to the spotlight imagery of TerraSAR-X featuring 1-m spatial resolution for the urban

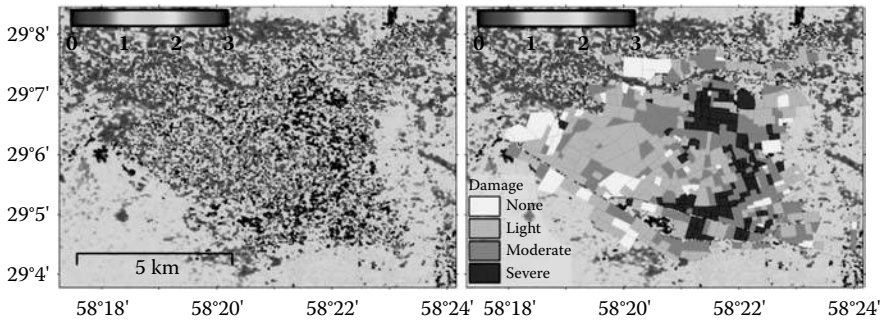

FIGURE 10.10 **(See color insert following page 324.)** Mapping damage from an earthquake in an urban environment using interferometric coherence.

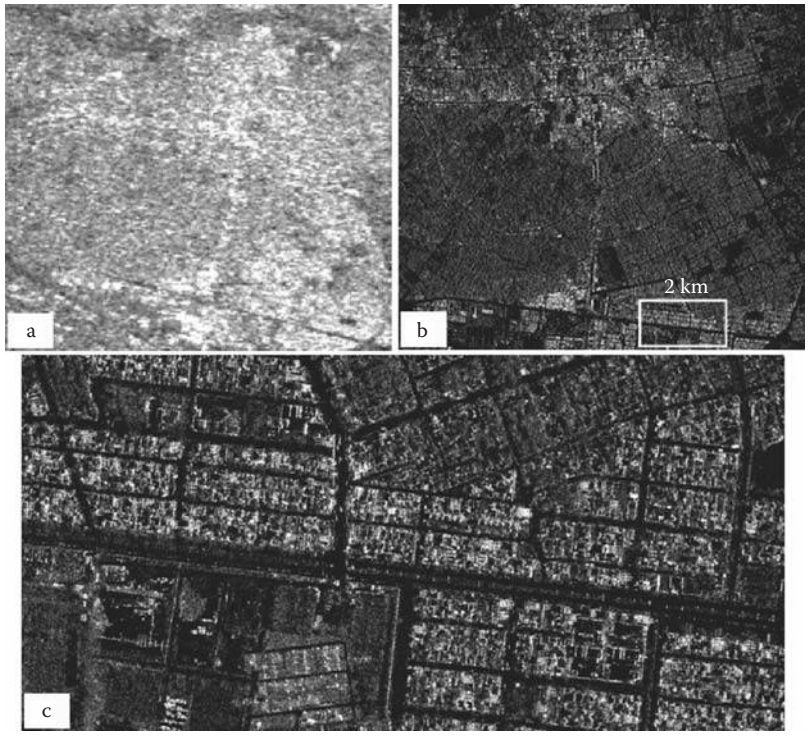

FIGURE 10.11 Comparison of intensity imagery of (a) Envisat and (b), (c) TerraSAR-X.

area of Bam, Iran. Nowadays, structural pattern and objects of the small-scale and heterogeneous urban environment are clearly detectable and provide a great degree of detail for damage detection and assessments.

Since both SAR and optical images provide information for building detection, it is promising to synergistically use both types in the context previously described. By using methods of data fusion (Gamba et al., 2005; Hellwich et al., 2000; Tupin and

Roux, 2003), improvement in the detection of building damage has been achieved (Stramondo et al., 2006, 2007).

10.4 CONCLUSION

The study presents the capabilities of remote sensing by using a theoretical risk framework as an outline. Following this outline, how various indicators derived from remote sensing data contribute to risk and disaster management before, during, and after an event is discussed. The resulting data products are presented using the example of selected megacities of the world. In particular, this study aims to address several questions regarding risk management in megacities. How can risk management be conceptualized? What are the capabilities and limitations of remote sensing that contribute in assessing risk and supporting risk management? What are the future perspectives regarding megacities and remote sensing?

Risk management can only be as good as the information provided. The presented risk framework aims at a theoretical conceptualization of the complex influencing components and temporal phases of a potential disastrous event. Systematization of the abstract terms describing vulnerability and hazards, and thus risks, suggests measurable indicators. Advantages of this conceptual approach result in indicators that are quantifiable, that show spatial reference, and are understandable. Indicators from a physical, demographic, social, economic, ecological, or political perspective contributing to a holistic concept make risk management and decision making a complex task.

Explosively growing megacities around the globe struggle with current data availability. The capabilities of remote sensing are manifold, considering the various types of available satellite data, and providing up-to-date and area-wide data promptly is a basic strength of remote sensing. In any case, the predominant potential lies in up-to-date physical coverage of complex urban morphology. Mapping spatially variable urban structures reflects patterns of urban vulnerabilities and risks. Physical parameters such as hazard-prone areas based on surface or structural characteristics such as distances to safe areas or building stability reflect vulnerability. The methods presented in this work are transferable and their quality and diversity for mapping and analyzing urban environments from various perspectives is high. By using physical urban structures, value-added products that correlate ancillary datasets can be assessed. Capabilities to indirectly correlate physical structures with the dynamic distribution of population are presented. Indirect derivation of parameters correlating with physical urban morphology successfully shows population distribution and enables a structural vulnerability assessment. Furthermore, important socioeconomic parameters such as poverty or education level show potential for being mapped from a study of urban structures. Ideas to correlate socioeconomic parameters with urban structures such as slums or high-income structured urban areas are indicated. In conclusion, multisource remote sensing data can be used to provide up-to-date, area-wide, quantitative, reproducible, understandable indicators with spatial reference. However, limitations of remote sensing are reflected in the difficulty of deriving detailed demographic information, socioeconomic indicators, or political aspects within the holistic risk framework. The approach does not provide the accuracy of cadastral

datasets, but does enable an assessment of the dimension and location of damage in a quality suitable for decision making.

Future perspectives for risk management in megacities based on EO data provide manifold directions for improvements. New sensors such as optical systems on Rapid Eye (http://www.rapideye.de/), WorldView I and II (http://www.geoeye.com/), radar technology on TerraSAR-X and Tandem-X (http://www.dlr.de/tsx/start_ge.htm) and ALOS, as well as hyperspectral satellite sensors such as EnMap (http://www.enmap.org/) will make possible improved temporal, spectral, and spatial coverage of the Earth's surface.

To utilize the large amount of expected data, methodologies have to be further improved to derive the necessary information in time. An important step toward using the holistic risk framework is integrating and correlating multiple data types and sources. Examples in this paper show the interdisciplinary approach of combining results from remote sensing and civil engineering as well as demographic information. A classification of physical urban morphology and its correlation with further socioeconomic parameters is indicated.

Finally, the large information basis that can be derived from multisource remote sensing data increases not only public perception and awareness, it also leads to influencing political decision making, potentially leading to funding for crisis and risk management institutions that can identify hazards, warn of risks, raise awareness, mitigate damage, and coordinate relief activities.

ACKNOWLEDGMENT

The authors would like to thank Ursula Marschalk, Tobias Ullmann, and Susan Giegerich from DLR-DFD for their support. Furthermore, we would like to thank Christian Münich and Lothar Stempniewski as well as Jochen Zschau from the Center for Disaster Management for their cooperation.

REFERENCES

Al-Khudhairy, D.H.A., Caravaggi, I., and Glada, S., Structural damage assessments from Ikonos data using change detection, object-oriented segmentation, and classification techniques, *Photogrammetric Engineering and Remote Sensing*, 71(7), pp. 825–837, 2005.

Allenbach, B., Andreoli, R., Battiston, S., Bestault, C., Clandillon, S., Fellah, K., Henry, J.-B., Meyer, C., Saus, H., Tholay, N., Yesou, H., and de Fraipont, P., Rapid EO disaster mapping service: Added value, feedback and perspectives after 4 years of charter actions, *IEEE International Geoscience and Remote Sensing Symposium,* 1155–1158, 2007.

Barr, S.L., Barnsley, M.J., and Steel, A., On the separability of urban land-use categories in fine spatial scale land-cover data using structural pattern recognition, *Environment and Planning B: Planing and Design*, 32, pp. 397–418, 2004.

Baudot, Y., Geographical analysis of the population of fast-growing cities in the third world, in: Donnay, J., Barnsley, M., and Longley, P., eds., *Remote Sensing and Urban Analysis*, Taylor and Francis, London, 229–246, 2000.

Berardino, P., Fornaro, G., Lanari, R., and Sansosti, E., A new algorithm for surface deformation monitoring based on small baseline differential SAR interferograms, *IEEE Transactions on Geoscience and Remote Sensing*, 40(11), pp. 2375–2383, 2002.

Berardino, P., Costantini, M., Franceschetti, G., Iodice, A., Pietranera, L., and Rizzo, V., Use of differential SAR interferometry in monitoring and modelling large slope instability at Maratea (Basilicata, Italy), *Engineering Geology*, 68(1–2), 31–51, 2003.

Berardino, P., Sansosti, E., Lanari, R., and Pepe, A., On the extension of the SBAS algorithm for the generation of ERS/Envisat deformation time-series, in: *Proceedings of the IGARSS 2004*, Anchorage, AK, 2004, ISBN 0-7803-8742-2.

Bignami, C., Chini, M., Pierdicca, N., and Stramondo, S., Comparing and combining the capability of detecting earthquake damages in urban areas using SAR and optical data, in: *Proceedings of the IGARSS '04*, 2004, ISBN: 0-7803-8742-2.

Birkmann, J., Measuring vulnerability to promote disaster-resilient societies: Conceptual frameworks and definitions, in: Birkmann, J., ed., *Measuring Vulnerability to Natural Hazards — Towards Disaster Resilient Societies*, United Nations University, New York, pp. 9–54, 2006.

Bitelli, G., Camassi, R., Gusella, L., and Mognol, A., Image change detection on urban area: The earthquake case, *Proceedings of International Society for Photogrammetry and Remote Sensing*, 2004.

Bronger, D., Megastädte, *Geographische Rundschau*, 48, 74–81, 1996.

Bruzzone, L., and Carlin, L., A multilevel context-based system for classification of very high spatial resolution images, *IEEE Transactions on Geoscience and Remote Sensing*, 44(9), 2587–2600, 2006.

Buehler, Y.A., and Kellenberger, T.W., Development of processing chains for rapid mapping with satellite data, in: Li, J., Zlatanova, S., and Fabbri, A.G., eds., *Geomatics Solutions for Disaster Management*, *Lecture Notes in Geoinformation and Cartography*, pp. 49–60, Springer, Berlin, 2007.

Colesanti, C., Ferreti, A., Prati, C., and Rocca, F., Monitoring landslides and tectonic motions with permanent scatterers technique, *Engineering Geology*, 69(1–2), 3–14, 2003.

Crosetto, M., Castillo, M., and Arbiol, R., Urban subsidence monitoring using radar interferometry: Algorithms and validation, *Photogrammetric Engineering and Remote Sensing*, 69(7), 775–783, 2003.

De Martinao, M., Causa, F., and Serpico, S.B., Classification of optical high resolution images in urban environment using spectral and textural information, *Proceedings of IGARSS*, 1, 467–469, 2003.

Deutsches Komitee Katastrophenvorsorge e.V. (DKKV), Lessons learned — Hochwasservorsorge in Deutschland: Kurzfassung für die Versicherungswirtschaft, 2002. Available at http://www.dkkv.org/DE/publications/schriftenreihe.asp?h=5.

Erdik, M., Earthquake risk assessment for Istanbul metropolitan area, The American Red Cross–Turkish Red Crescent, Department of Earthquake Engineering, Bogazici University Istanbul, 352 pp., 2002.

Esch, T., Automatisierte Analyse von Siedlungsflächen auf der Basis Höchstauflösender Radardaten, Bayerische Julius-Maximilian Universität, Ph.D. thesis, 202 pp., 2006.

Esch, T., Roth, A., and Dech, S.W., Robust approach towards an automated detection of built-up areas from high resolution radar imagery, in: Proceedings of the ISPRS WG VII/1 Human Settlement and Impact Analysis, 3rd International Symposium on Remote Sensing and Data Fusion over Urban Areas (URBAN 2005) and 5th International Symposium on Remote Sensing on Urban Areas (URS 2005), Tempe, AZ, USA, CD-ROM, 2005.

Farr, T., Rosen, P., Caro, E., Crippen, R., Duren, R., Hensley, S., Kobrick, M., Paller, M., Rodriguez, E., Roth, L., Seal, D., Shaffer, S., Shimada, J., Umland, J., Werner, M., Oskin, M., Burbank, D., and Alsdorf, D., The shuttle radar topography mission, *Reviews of Geophysics*, 45(RG2004), 33, 2007.

Fauvel, M., Chanussot, J., and Benediktsson, J.A., Decision fusion for the classification of urban remote sensing images, *IEEE Transactions on Geoscience and Remote Sensing*, 44(10), 2828–2837, 2006.

Ferreti, A., Prati, C., and Rocca, F., Permanent scatterers in SAR interferometry, *IEEE Transactions on Geoscience and Remote Sensing*, 39(1), 8–20, 2001.

Gamba, P., and Houshmand, B., Digital surface models and building extraction: A comparison of IFSAR and LIDAR data, *IEEE Transactions on International Geoscience and Remote Sensing*, 66(7), 1959–1967, 2000.

Gamba, P., Houshmand, B., and Saccani, M., Detection and extraction of buildings from interferometric SAR data, *Geoscience and Remote Sensing, IEEE Transactions*, 38(1), 611–617, 2000.

Gamba, P., Dell'Acqua, F., and Dasarathy, B.V., Urban remote sensing using multiple datasets: Past, present, and future, *Information Fusion*, 6, 319–326, 2005.

Gamba, P., Dell'Acqua, F., Lisini, G., and Trianni, G., Improved VHR urban area mapping exploiting object boundaries, *IEEE Transactions on Geoscience and Remote Sensing*, 45(8), 2676–2682, 2007.

Google Earth, http://earth.google.com/intl/de/download-earth.html.

Hellwich, O., Günzl, M., and Wiedemann, C., Fusion of optical imagery and SAR/INSAR data for object extraction, *International Archives of Photogrammetry and Remote Sensing*, XXXIII(Part B3/1), 389–396, 2000.

Hoffmann, J., Mapping damage during the Bam (Iran) earthquake using interferometric coherence, *International Journal of Remote Sensing*, 28(6), 1199–1216, 2007.

Hoffmann, J., Zebker, H.A., Galloway, D.L., and Amelung, F., Seasonal subsidence and rebound in Las Vegas, Nevada, observed by synthetic aperture radar interferometry, *Water Resources Research*, 37(6), 1551–1566, 2001.

Huyck, C.K., Eguchi, R.T., and Houshmand, B., Advanced technologies for loss estimation: Bare-earth algorithms for use with SAR and LIDAR digital elevation models, Technical Report MCEER-02-0004, Multidisciplinary Center for Earthquake Engineering Research, University of Buffalo, 2002.

Jordan, R., Shuttle radar topography mission system functional requirements document, Technical Report, JPL D-14293, 1997.

Kampes, B.M., and Adam, N., The STUN algorithm for persistent scatterer interferometry, Fringe 2005 Workshop, Frascati (Italy), 2005. Available at http://earth.esa.int/fringe2005/proceedings/papers/58_kampes.pdf.

Kötter, T., Risks and opportunities of urbanisation and megacities, *FIG Working Week*, Athens, Griechenland, S. 9, 2004.

Kraas, F., and Coy, M., Probleme der Urbanisierung in den Entwicklungsländern, *Petermanns Geographische Mitteilungen*, 147(1), 32–41, 2003.

Lavalle, C., Demicheli, L., Turchini, M., and Casals, P., Monitoring megacities: The MURBANDY/MOLAND approach, *Development in Practice*, 11(2–3), 350–357, 2001.

Lu, Z., Fatland, R., Wyss, M., Li, S., Eichelberger, J., Dean, K., and Freymueller, J., Deformation of New Trident volcano measured by ERS-1 SAR interferometry, Katmai National Park, Alaska, *Geophysical Research Letters*, 24(6), 695–698, 1997.

Marschalk, U., Roth, A., Eineder, M., and Suchandt, S., Comparison of DEMs derived from SRTM / X– and C-band, in: *Proceedings of the IGARSS 2004*, Anchorage, USA, 2004.

Mas, J.-F., Monitoring land-cover changes: A comparison of change detection techniques, *International Journal of Remote Sensing*, 20(1), 139–152, 1999.

Meher, S.K., Shankar, B.U., and Ghosh, A., Wavelet-feature-based classifiers for multispectral remote-sensing images, *IEEE Transactions on Geoscience and Remote Sensing*, 45(6), 1881–1886, 2007.

Mertins, G., Urbanisierung, Metropolisierung und Megacities. Ursachen der Stadtexplosion in der Dritten Welt, in: *Deutsche Gesellschaft für die Vereinten Nationen* (Hrsg.): *Mega-Städte — Zeitbombe mit Globalen Folgen*?, Bonn, pp. 7–21, 1992.

Mitchell, J., Megacities and natural disasters: A comparative analysis, *GeoJournal*, 49, 137–142, 1999.

Montoya, L., Geo-data acquisition through mobile GIS and digital video: An urban disaster management perspective, *Environmental Modelling & Software*, 18(10), 869–876, 2003.

Mora, O., Mallorqui, J., and Broquetas, A., Linear and nonlinear terrain deformation maps from a reduced set of interferometric SAR images, *IEEE Transactions on Geoscience and Remote Sensing*, 41(10), 2243–2253, 2003.

Münich, J.C., Taubenböck, H., Stempniewski, L., Dech, S., and Roth, A., Remote sensing and engineering: An interdisciplinary approach to assess vulnerability in urban areas, in: First European Conference on Earthquake Engineering and Seismology, Genf, Schweiz, Paper no. 1412, 2006.

Münchner Rück, Megastädte — Megarisiken. Trends und Herausforderungen für Versicherung und Risikomanagement, 2005. Available at: www.munichre.com/publications/302-04270_de.pdf.

Pelling, M., *The Vulnerability of Cities — Natural Disasters and Social Resilience*, Earthscan Publications Ltd., London, p. 212, 2003.

Pesaresi, M., Gerhardinger, A., and Haag, F., Rapid damage assessment of built-up structures using VHR satellite data in tsunami-affected areas, *International Journal of Remote Sensing*, 28(13–14), 3013–3036, 2007.

Rabus, B., Eineder, M., Roth, A., and Bamler, R., The shuttle radar topography mission (SRTM) — a new class of digital elevation models acquired by spaceborne radar, *ISPRS Journal of Photogrammetry and Remote Sensing*, 57, 241–262, 2003.

Rosen, P.A., Hensley, S., Joughin, I.R., Li, K.F., Madsen, S.N., Rodriguez, E., and Goldstein, R.M., Synthetic aperture radar interferometry, *Proceedings of the IEEE*, 88, 333–382, 2000.

Roth, A., Hoffmann, J., and Esch, T., TerraSAR-X: How can high resolution SAR data support the observation of urban areas?, in: *Proceedings of URBAN 2005 & URS 2005*, March 14–16, Tempe, AZ, USA, CD-ROM, 2005.

Saito, K., and Spence, R., Rapid damage mapping to support post-disaster recovery, in: *WCEE: 13th World Conference on Earthquake Engineering, Conference Proceedings*, 2004.

Saito, K., Spence, R., Going, C., and Markus, M., Using high-resolution satellite images for post-earthquake building damage assessment: A study following the 26 January 2001 Gujarat Earthquake, *Earthquake Spectra*, 20(1), 145–169, 2004.

Schweitzer, F., and Steinbrink, J., Estimation of mega-city growth, *Applied Geography*, 18/1, 69–82, 1998.

Shackelford, A.K., and Davis, C.H., A combined fuzzy-pixel based and object-based approach for classification of high resolution multi-spectral data over urban areas, *IEEE Transactions on Geoscience and Remote Sensing*, 41(10), 2354–2363, 2003.

Singh, A., Digital change detection techniques using remotely-sensed data, *International Journal of Remote Sensing*, 6, 989–1003, 1989.

Spreitzhöfer, G., Megacities: Zwischen (Sub)urbanisierung und Globalisierung, in: Online Akademie — Friedrich Ebert Stiftung, pp. 1–21, 2007. Available at: http://library.fes.de/pdf-files/akademie/online/50340.pdf.

Stramondo, S., Bignami, C., Chini, M., Pierdicca, N., and Tertulliani, A., Satellite radar and optical remote sensing for earthquake damage detection: Results from different case studies, *International Journal of Remote Sensing*, 27(20), 4433–4447, 2006.

Stramondo, S., Bignami, C., Pierdicca, N., and Chini, M., SAR and optical remote sensing for urban damage detection and mapping: Case studies, Urban Remote Sensing Joint Event, Paris, France, S. 7, 2007.

Taubenböck, H., Post, J., Roth, A., Zosseder, K., Strunz, G., and Dech, S., A conceptual vulnerability and risk framework as outline to identify capabilities of remote sensing, *Natural Hazards and Earth System Sciences*, 8(3), pp. 409–420, 2008a. Available at: http://www.nat-hazards-earth-syst-sci.net/8/409/2008/nhess-8-409-2008.html.

Taubenböck, H., Post, J., Kiefl, R., Roth, A., Ismail, F., Strunz, G., and Dech, S., Risk and vulnerability assessment to tsunami hazard using very high resolution satellite data, in: Jürgens, C., ed., *Proceedings of the EARSeL Joint Workshop: Remote Sensing: New Challenges of High Resolution*, Bochum, Germany, pp. 77–86, 2008b.

Taubenböck, H., Vulnerabilitätsabschätzung der Megacity Istanbul mit Methoden der Fernerkundung, PhD thesis, University of Würzburg, p. 178, in press.

Taubenböck, H., and Roth, A., A transferable and stable classification approach in various urban areas and various high resolution sensors, Urban Remote Sensing Joint Event, Paris, France, S. 7, 2007.

Taubenböck, H., Roth, A., and Dech, S., Linking structural urban characteristics derived from high resolution satellite data to population distribution, in: Coors, Rumor, Fendel, and Zlatanova, eds., *Urban and Regional Data Management*, Taylor & Francis Group, London, pp. 35–45, 2007a.

Taubenböck, H., Pengler, I., Schwaiger, B., Cypra, S., Hiete, M., and Roth, A., A multi-scale urban analysis of the Hyderabad Metropolitan area using remote sensing and GIS, in: Urban Remote Sensing Joint Event, Paris, France, S. 6, 2007b.

Taubenböck, H., Habermeyer, M., Roth, A., and Dech, S., Automated allocation of highly-structured urban areas in homogeneous zones from remote sensing data by Savitzky-Golay filtering and curve sketching, *IEEE Geoscience and Remote Sensing Letters*, 3(4), 532–536, 2006.

Tobita, M., Suito, H., Imakiire, T., Kato, M., Fujiwara, S., and Murakami, M., Outline of vertical displacement of the 2004 and 2005 Sumatra earthquakes revealed by satellite radar imagery, *Earth Planets Space*, 58, e1–e4, 2006.

Tupin, F., and Roux, M., Detection of building outlines based on the fusion of SAR and optical features, *ISPRS Journal of Photogrammetry and Remote Sensing*, 58(1–2), 71–82, 2003.

Voigt, S., Kemper, T., Riedlinger, T., Kiefl, R., Scholte, K., and Mehl, H., Satellite image analysis for disaster and crisis-management support, *IEEE Transactions on Geoscience and Remote Sensing*, 45(6), 1520–1528, 2007.

Ulaby, F.T., *Fundamentals of Applied Electromagnetics*, 5th edition, Prentice-Hall, Upper Saddle River, NJ, 1997, 407 pp., 2006.

UNESCO, *Annual Summary of Information on Natural Disasters*, UNESCO, Paris, 1973.

United Nations, *World Urbanization Prospects — The 2003 Revision*, UN, New York, 2003.

United Nations, *World Urbanization Prospects — The 2005 Revision*, UN, New York, 2005.

United Nations/ISDR (International Strategy for Disaster Reduction), *Living with Risk: A Global Review of Disaster Reduction Initiatives*, United Nations International Strategy for Disaster Reduction, UN Publications, Geneva, Switzerland, 2004.

Van Der Sande, C.J., De Jong, S.M., and De Roo, A.P.J., A segmentation and classification approach of IKONOS-2 imagery for land-cover mapping to assist flood risk and flood damage assessment, *International Journal of Applied Earth Observation and Geoinformation*, 4, 217–229, 2003.

Wegmüller, U., Werner, C., Strozzi, T., and Wiesmann, A., ERS-ASAR integration in the interferometric point target analysis, Fringe 2005 Workshop, Frascati (Italy), 2005. Available at: http://earth.esa.int/workshops/fringe05/proceedings/papers/196_wegmuller.pdf.

White, P., Pelling, M., Sen, K., Seddon, D., Russell, S., and Few, R., Disaster risk reduction. A development concern, DFID, 2005.

Wisner, B., Blaikie, T., Cannon, T., and Davis, I., *At Risk: Natural Hazards, People's Vulnerability and Disasters*, Routledge, London, 2004.

Wlodarczyk, D., Structural analysis of urban space in residential areas, in: *Methodologies in Housing Research*, Urban International Press, Newcastle upon Tyne, 2005.

Xia, Y., Kaufmann, H., Guo, X.F., Landslide monitoring in the Three Gorges area using D-InSAR and corner reflectors, *Photogrammetric Engineering and Remote Sensing*, 70(10), 1167–1172, 2004.

Yamazaki, F., Applications of remote sensing and GIS for damage assessment, in: Swets, Zeitlinger, eds., 8th International Conference on Structural Safety and Reliability, 2001.

11 Improving Urban Monitoring toward a European Urban Atlas

Frank M. Seifert

CONTENTS

11.1 BACKGROUND

Throughout the world, and particularly in Europe, processes related to urbanization, development of transport infrastructures, industrial constructions, and other built-up areas have a significant impact on the environment, and are often modifying the landscape at an unsustainable pace. In the past two decades, several steps have been taken that aim toward achieving a better quality of life in an urban environment. This chapter reviews the milestones and efforts within Europe to derive urban information and monitor urban areas, heavily drawing from remote sensing data, which have been instrumental in the implementation of a European Urban Atlas.

In 1990, the European Commission (EC) issued a green paper on urban environment (Green Paper on the Urban Environment, 1990) addressing the main problems in urban areas and the need to monitor their environmental conditions. This document covered the environmental effects of urban growth not only in Europe, but also in other parts of the world. For environmental management and sustainable development, accurate and comprehensive spatial data are critical. The lack of appropriate data is a major hindrance for policy makers and the scientific community. In the light

of sustainable development, comparable information is essential, which requires a collective effort from various players.

The Earth Summit held in Rio de Janeiro in 1992 (United Nations Conference on Environment and Development, 1992) brought human beings into the center of concerns for sustainable development, with the view that humans are entitled to a healthy and productive life in harmony with nature. Subsequent efforts included conferences such as Aalborg 1994, in which Local Agenda 21 — a global action plan for sustainable development establishing the link between city and environment — was formulated. The related Lisbon action plan in 1996 went further and led to the Vienna Urban Forum in 1998, where a framework for action toward a sustainable urban development in the European Union (EU) was established. In May 1999, the European Spatial Development Perspective (ESDP) was adopted by the ministers of the member states responsible for regional planning. Its aim is to improve the coordination of national policies in this field. It is based on three key principles: the development of a balanced and polycentric urban system and a fresh relationship between cities and the countryside; the assurance of equal access to knowledge infrastructures; and sustainable development — the intelligent management and conservation of nature and cultural assets.

11.2 URBAN AUDIT

In 1999, the EC issued the terms of reference for an Urban Audit pilot project (http://www.urbanaudit.org/) with the following objectives: to enable an assessment of the state of individual European cities and to provide access to comparative data. A main goal of the Urban Audit is to allow city authorities to compare their city directly with other cities in Europe, because such comparisons can facilitate the exchange of experience and improve the quality of European and local urban policies. Furthermore, the gathered information should inform EU member states and the EC of the quality of life in European cities. Between 1997 and 2000, 58 cities participated and gathered indicators of the Urban Audit in five fields: socioeconomic aspects, participation in civic life, education and training, environment, and culture and leisure. The successful pilot project led to an implementation of the Urban Audit under the responsibility of the Directorate General (DG) for Regional Policy at the EC, in cooperation with the Statistical Office of the European Communities (EUROSTAT) and the national statistical offices. The first full-scale European Audit took place in 2003 and 2004 with 258 participating cities (State of the European Cities Report, 2007). The following round of the Urban Audit collected information on living conditions in 357 large- and medium-sized cities in Europe from May 2006 to September 2007 (Figure 11.1).

The Urban Audit contains data for almost 500 variables and indicators across domains such as demography, social and economic aspects, civic involvement, training and education, environment, travel and transport, information society, and culture and recreation.

The Urban Audit works in three different spatial levels: the city, the larger urban zone, and the subcity district.

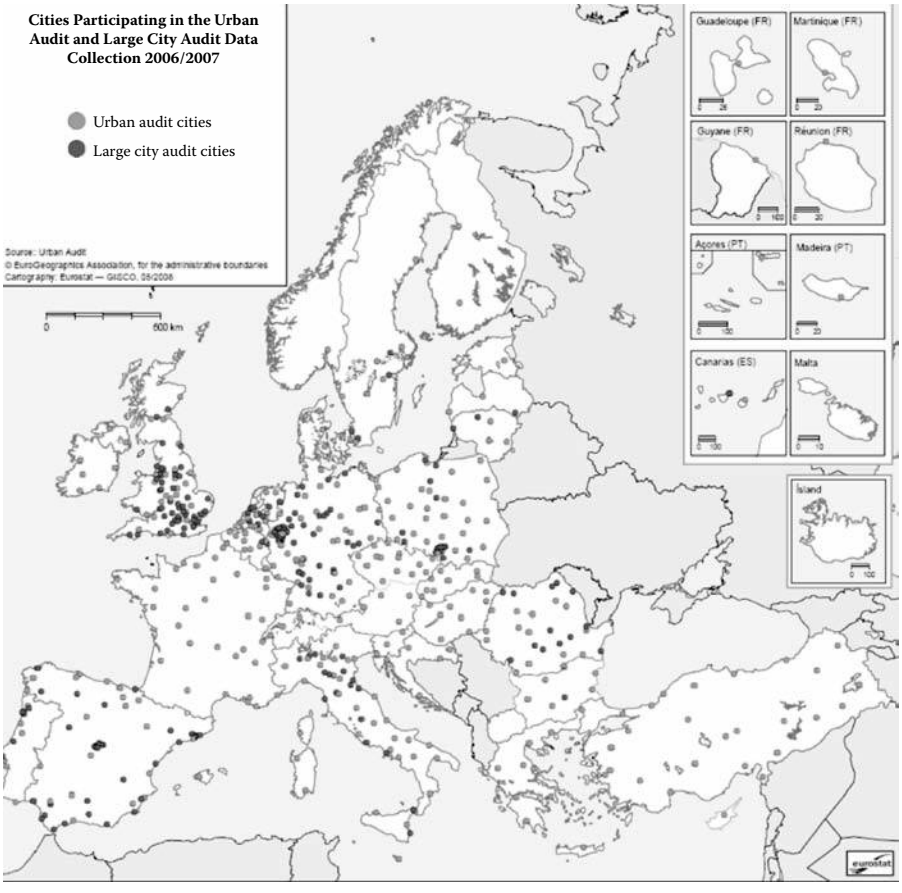

FIGURE 11.1 **(See color insert following page 324.)** Cities participating in the Urban Audit, 2006–2007. (Courtesy of Urban Audit.)

- The most important is the city level, where political boundaries are used mostly to ensure that this level is directly relevant to policy makers and politicians.
- The larger urban zone allows a comparison between the city and its surroundings. The goal is to have an area from which a significant share of the resident population commutes into the city, a concept known as the "functional urban region." To ensure good data availability, the Urban Audit works with administrative boundaries that approximate the functional urban region.
- The subcity districts are taken from a division of Urban Audit cities to analyze their disparities. To ensure that these districts can be compared, they had to comply with strict population thresholds: minimum of 5000 inhabitants and maximum of 40,000 inhabitants.

An Urban Audit Perception Survey to measure the local perceptions of quality of life in a subset of 75 European cities was conducted in 2006 to complement the data from the main Urban Audit. The most diverging opinions of the residents were expressed on employment opportunities, housing costs, safety, cleanliness of cities, public transport, air pollution, integration of immigrants, and overall satisfaction with the quality of life of their city.

Urban Audit's most recent update is based on data from 2006 to 2007, whereas the next one is foreseen in 2011. A new strategy is under discussion for Urban Audit to conduct a full audit every 5 years, supported by a yearly update of the main parameters.

11.3 MURBANDY/MOLAND

In parallel to the statistically oriented Urban Audit, the spatial dimension of urban dynamics has been followed by Monitoring Urban Dynamics (MURBANDY)/Monitoring Land Use/Cover Dynamics (MOLAND). MURBANDY was initiated in 1998 with the objective of monitoring the developments in urban areas and identifying trends at the European scale. It specifically addresses issues mentioned in the ESDP that are related to urban and regional development and those linked to sustainable land use management, and its further implementation including the establishment of the European Spatial Planning Observation Network (ESPON; http://www.espon.eu). The main aim of the MOLAND project (http://moland.jrc.it), which is coordinated by the Institute for Environment and Sustainability of the EC's Joint Research Centre, is to provide up-to-date, standardized, comparable information on the past, current, and likely future land use development in Europe. The work comprised the computation of indicators and the assessment of the impact of anthropogenic stress factors with a focus on expanding settlements, transport and tourism in and around urban areas, and along development corridors (Towards an Urban Atlas: EEA/JRC report, 2002). MOLAND also directly addresses several environmental topics at the European level, such as the actions on sustainable urban development and related communications, the initiatives on Environmental Impact Assessment and on Strategic Environmental Assessment. Relevant services of the EC in the Directorate General for Regional Policy (DG REGIO), Environment (DG ENV), Energy and Transport (DG TREN), EUROSTAT, and the European Environment Agency (EEA) received technical support, in terms of consultancy, provision of products, and contributions to policy work. To date, the MOLAND database has covered several urban areas (in Europe and outside), transport corridors, and extended regions (see Figure 11.2).

MOLAND supports main EU policy areas such as:

- The 6th EC Environment Action Programme's Thematic Strategy on the Urban Environment, for DG ENV (Thematic Strategy on the Urban Environment, 2006)
- Indicators for sustainable urban and regional development, for DG ENV, EUROSTAT, and the EEA

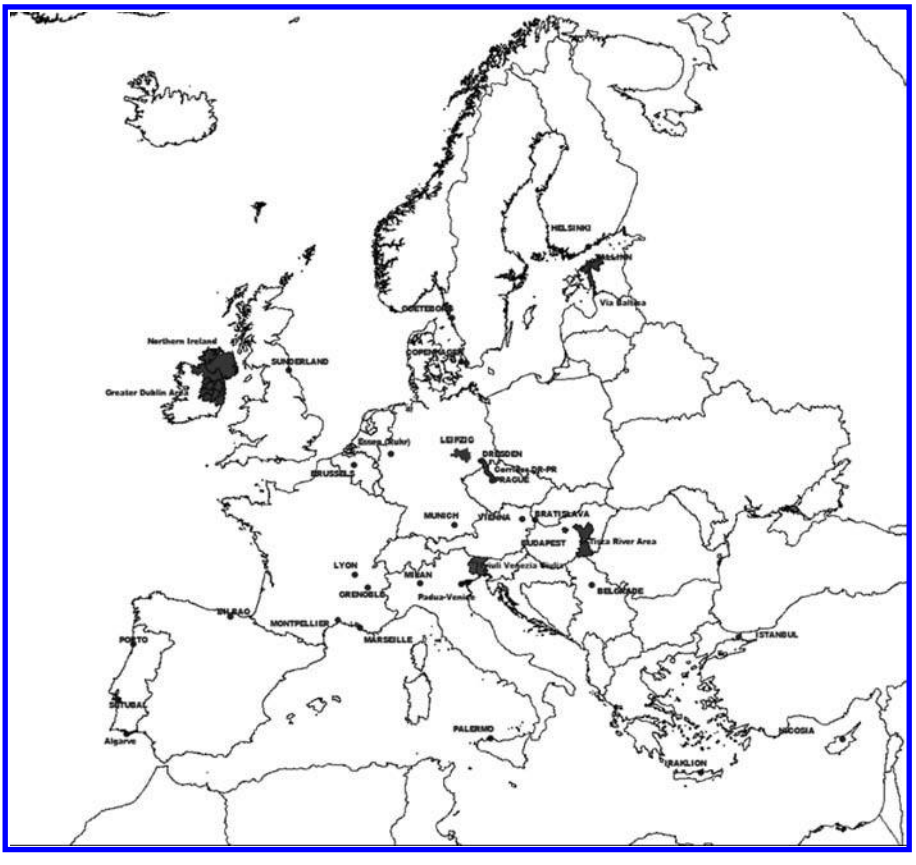

FIGURE 11.2 MOLAND coverage in Europe. (From JRC-MOLAND project, © European Communities, 1995–2008. With permission.)

- ESDP and ESPON for DG REGIO
- Impacts of the Structural and Cohesion Funds, for DG ENV
- Strategic Environmental Assessment of the Trans-European Transport Networks for DG TREN.

MOLAND has served well on research and demonstration level, but was not taken up for an operational implementation on a larger European scale. In the future, MOLAND is expected to continue the development of indicators, whereas mapping is transferred under Global Monitoring for Environment and Security (GMES) services. A current focus is the further development and use of spatial dynamic models for simulating future urban and regional development (including transport), where simulation of urban growth and related sprawl is becoming more important in a regional context based on policy and zoning regulations (Urban Sprawl Report 2006, EEA, 2006). A further line of action is monitoring sustainability and adaptation to natural hazards such as floods, droughts, desertification, and forest fires, and prevision of related vulnerabilities. MOLAND

contributes to the development of an integrated methodology for the assessment of current and future natural risks in combination with high-resolution regional climate scenarios and hydrological and geophysical models.

11.4 GLOBAL MONITORING FOR ENVIRONMENT AND SECURITY

GMES (http://www.gmes.info/) is an EU-led initiative to secure Europe with an autonomous and operational information system in support of the environment and security policies. The initiative is set up jointly by the EC and the European Space Agency (ESA; http://www.esa.int). It is driven by the need to improve the monitoring of the European and global environment in view of pursuing the sustainable management of our resources and the security of the citizen. GMES was formed in Baveno, Italy, in 1998 with the formulation of "Global Monitoring for Environmental Security: a Manifesto for a New European Initiative" by mainly representatives of space agencies and scientists. The Baveno Manifesto demonstrated the need for global information services and expressed an ambitious vision for Europe to tackle environmental issues with its advanced technological and scientific capabilities. It calls for a long-term commitment to the development of space-based environmental monitoring services for Europe. In 2001, both ESA and the EC obtained approval for some €100 million each to initiate GMES services and build up a sustainable user community. In 2005, the roles of the two organizations in GMES were clarified further, where ESA's task is to define the technical specification and to implement the space component, and EC's function is to identify and develop services relying on both in situ and remote sensing data, and to define and set up a sustainable governance structure (Liebig, et al., 2007).

11.5 GMES SERVICE ELEMENT

Under the ESA GMES Service Element (GSE; http://www.esa.int/gmes), 10 service portfolios were developed, where each responds to user needs in a specific sector of environmental or security policy. One of the thematic areas ESA addressed in this framework is the monitoring of urban areas, covering issues related to urban agglomeration such as urban sprawl, modeling and forecast in urban planning, changes in urban land use, environmental monitoring, to name a few. During GSE's first stage — the consolidation phase (2003–2005) — the GMES Urban Services project (GUS; http://www.gmes-urbanservices.info) conducted a policy-foundations analysis documenting the underlying drivers of the demand for information in the urban policy sector and identifying products and services that could be offered over decades. The objective of the GUS project was to consolidate a portfolio of products derived from satellite data and other sources in close cooperation with a selection of users (cities, regional authorities, and DG REGIO on the European level) and demonstrate the associated services.

On the city level, the national and European policies force municipalities to ensure environmentally friendly and economically sound management of local resources. The GUS project demonstrated the potential of geospatial information

from remote sensing imagery to support local authorities in the required planning, monitoring, and control of urban development as well as in the implementation of environmental policies at the urban level. The products and services are designed to exploit this information from remote sensing data in a reliable, consistent, and cost-efficient manner.

On the Pan-European regional level, the related policies require sustainable environmental management as well as infrastructure planning and development. Standardized geospatial information, which is comparable between all European regions, is a necessary source for profound decision-making processes by implementation agencies at European, national, or regional levels. The developed products and services consider these needs by standardized and transferable modules of local products as well as special regional products and lower scale.

To encourage a more sustainable development in urban conglomerations well as the urban fringe, and to evaluate the compliance and success of planning measures, detailed knowledge of urban land use is essential for monitoring and analyzing changes on a geolocated basis. The GUS products, oriented to serve the strategic urban planning needs all over Europe, are clustered into four categories:

- Land use, including change detection and modeling tools for urban planners and regional authorities
- Urban Development Control: short-term hot spot monitoring for urban planning and discipline enforcement
- Environment Quality: noise, sealing, thermography, and risk mapping
- Regional Products: basic land use and sealing maps for monitoring of soil consumption.

Urban Atlas falls in the first category of the GUS portfolio, which contains the core products land use and land use change, where a generalized workflow and a standardized output is applicable for all European municipalities. The classes and legend are an evolution of the MOLAND concept taking into account the use of high-resolution remote sensing data, enabling a more automatic classification and an independence from additional information such as socioeconomic data. Figure 11.3 shows an example of a satellite image and derived map of Erfurt, Germany. The core products are extended to highly customized products and services by the local service providers. These local variations ensure that the individual needs of municipalities with different socioeconomic environment and with unique geographic characteristics can be met.

With these services, the authorities responsible for urban planning on local, regional, European, and global levels could receive up-to-date and homogeneous information allowing them to respond to political and market (economic, social, technological, and environmental) drivers.

In the second stage of GSE — the implementation phase (2005–2008) — land-oriented services consolidated by earlier projects such as SAGE (Service for the Provision of Advanced Geo-Information on Environmental Pressure and State), GUS, and Coastwatch were joined in the GSE Land project (http://www.gmes-gseland.info)

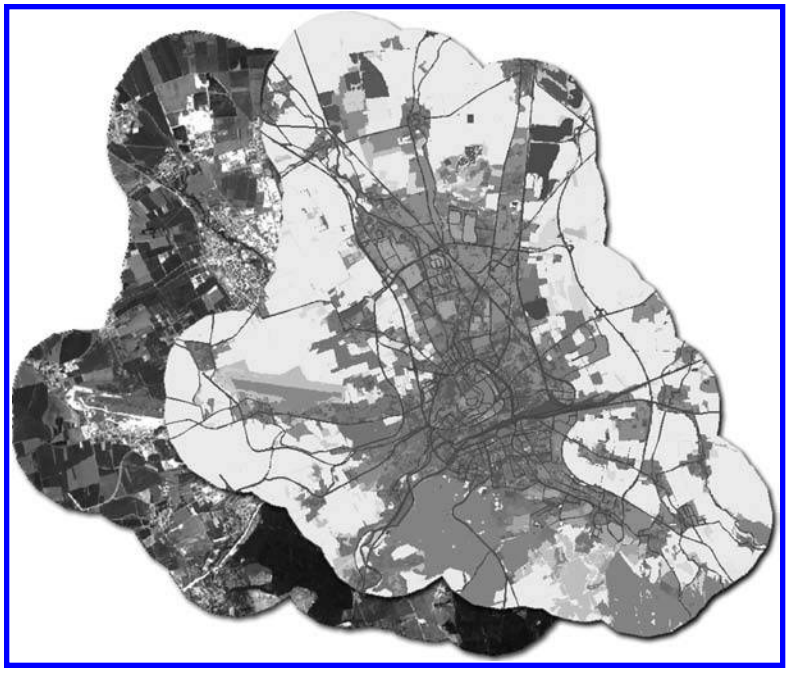

FIGURE 11.3 **(See color insert following page 324.)** Satellite image and derived land use map from city of Erfurt, Germany. (Courtesy of GUS, H.G. Geo Data Solutions.)

to demonstrate their implementation on a larger scale and to work toward their sustainability. Notwithstanding the progress that has been made in growing user engagement and support for the individual services during the GSE service consolidation phase, it is recognized that none of these services can be considered fully sustainable. To achieve sustainability, all services must ultimately satisfy three critical requirements. They must become:

- Available — readily accessible to users when needed, now and in the future;
- Reliable — consistently meeting user-defined quality and standards;
- Affordable — where benefits justify the costs.

GSE Land tackles these sustainability criteria for four end-to-end service lines, that is, European Urban Atlas, impervious areas and sealing levels, inland water quality and irrigation/agricultural water consumption, and an intermediate multipurpose land cover service on the European scale. Furthermore, user feedback emphasizes the need for improved validation of the services to increase acceptance.

Within GSE Land, the Urban Atlas line has concentrated on the consolidation of the European product mainly for the use of DG REGIO as its main objective before further value adding toward the specific needs of local administrations and municipalities. This took into account the announcement of the EC Fast Track Services (FTS) on Land, Marine, and Emergency in 2005, in which Urban Atlas was identified as the local component of the Land Monitoring Core Service (LMCS). The establishment of the Implementation Group of the LMCS (LMCS Strategic Implementation Plan, 2007) facilitated the interaction between the GSE Land project and the EC and provided an interface toward several European users.

GSE Land uses semiautomated processing chains for the generation of the up-to-date urban land cover/land use information. SPOT 5 satellite images serve as basic input data together with topographic maps and a road network. Subsequently, image analysis results are controlled and manually improved with the help of supplementary information provided by city authorities. In recent years Google™ Earth has been increasingly used as an additional interpretation aid and to better identify the nature of objects, but not to delineate them. Aerial photography samples are used by an independent external validation team to validate the accuracy (GSE Land Service Validation Protocol, 2008). The basic urban land use information is enhanced by urban indicators such as the degree of sealing, that is, the different levels of impervious areas, based on Normalized Difference Vegetation Index and supplementary data for detailed and accurate up-to-date sealing mapping. Through this approach, the products are embedded and linked to the European sealing layer from EEA.

11.6 URBAN ATLAS

11.6.1 Nomenclature and Product Specification

The European Urban Atlas provides very high resolution hot spot mapping of urban functional areas collected repeatedly and homogenously over larger European

cities. This land use and land cover database on cities' territorial evolution allows users to link spatial information with other parameters such as social economical statistics to produce indicators in the assessment of sustainable development of cities for urban administrations, regional and European institutions, and the European citizen.

The Urban Atlas nomenclature is based on the work done in MOLAND and its adaptation in GUS and GSE Land. It has been discussed and developed with DG REGIO and designed to fit their requirements. It encompasses 22 urban classes in four hierarchical levels and four nonurban classes listed in Table 11.1. The minimum mapping unit for all classes is 0.25 ha.

The derived product features summarized in Table 11.2 reflect the need to work at the European level with a limited input data set (EO data, street network, and topographic maps) and for all cities independent of additional local datasets.

11.6.2 Urban Atlas Validation

A major effort was placed on the qualification of the Urban Atlas service. The exercise was planned as a qualification of service providers on this service, but it served as well in identifying problems in harmonization and common understanding of the specification and in reassessing the quality assurance procedure. Two 10 × 10 km test sites in Bremen, Germany (representing a larger central European city), and Badajoz, Spain (as a smaller Mediterranean city), were selected for the benchmark approach. Ten service providers took the challenge to deliver, within 4 weeks, their classification based on the same standard input data:

- SPOT 5 satellite images with 2.5 m resolution (multispectral, pan-sharpened)
- Extract of the TeleAtlas database for the respective area with road information and points of interest
- Topographic map (1:25,000)
- Mapping guidelines for GSE Land product M1.1 — Urban Atlas (Urban Atlas Mapping Guide, 2008)

A point sampling with approximately 800 points was chosen for the validation approach. For urban and nonurban parts of the pilot area, different sampling grids were designed, taking into account that a 90% confidence interval of the accuracy assessments should be reached. A reference interpretation for each city was produced by a team of five experts, who first individually interpreted the sampling points based on the standard data set and higher resolution data and then agreed on a common reference. The validation results were obtained by overlaying the service provider data with the results of the expert validation in a GIS system, that is, for each point the class code of the reference interpretation was compared to the class code attribute by the service provider at the same location. The mapping, that is, object delineation and interpretation, was done at the most detailed level of the nomenclature.

TABLE 11.1
Urban Atlas Nomenclature

Urban Atlas No.	Vector Data Code	Nomenclature
1		Artificial surfaces
1.1		Urban fabric
1.1.1		Continuous urban fabric
1.1.1.1	11110	Residential continuous dense urban fabric
1.1.1.2	11120	Informal continuous dense settlement
1.1.2		Discontinuous urban fabric
1.1.2.1	11210	Residential discontinuous dense urban fabric (sealing layer: 50–80%)
1.1.2.2	11220	Residential discontinuous medium dense urban fabric (sealing layer: 30–50%)
1.1.2.3	11230	Residential discontinuous sparse urban fabric (sealing layer: 10–30%)
1.1.2.4	11240	Informal discontinuous residential structures
1.1.3		Special urban fabric features
1.1.3.1	11310	Residential urban blocks
1.1.3.2	11320	Isolated urban fabric
1.2		Industrial, commercial, and transport units
1.2.1		Industrial, commercial, public, and private units
1.2.1.1	12110	Industrial areas
1.2.1.2	12120	Commercial areas
1.2.1.3	12130	Public, military, and private services not related to the transport system
1.2.1.4	12140	Inland artificial infrastructure related to water
1.2.2		Road and rail network and associated land
1.2.2.1	12210	Fast transit roads and associated land
1.2.2.2	12220	Other roads and associated land
1.2.2.3	12230	Railways and associated land
1.2.3	12300	Port areas
1.2.4	12400	Airports
1.3		Mine, dump, and construction sites
1.3.1	13100	Mineral extraction and dump sites
1.3.3	13300	Construction sites
1.3.4	13400	Land without current use
1.4		Artificial nonagricultural vegetated areas
1.4.1	14100	Green urban areas
1.4.2	14200	Sports and leisure facilities
2	20000	Agricultural areas
3	30000	Forests and seminatural areas
4	40000	Wetlands
5	50000	Water

TABLE 11.2
Urban Atlas Product Features

Urban Atlas	• Digital thematic map with thematic classes based on CORINE LC nomenclature and GUS legend
Input data sources	• Earth Observation (EO) Data with 2.5 m or less spatial resolution multispectral or pan-sharpened (multispectral merged with panchromatic) data. The multispectral data includes near-infrared band • Topographic maps at a scale of 1:50,000 or more detailed • COTS navigation data for the road network • Areas of interest for Urban Atlas mapping as determined by DG REGIO. • Sealing layer based on FTS specifications for degree of sealing for level 3 classes 111 and 112 and level 4 classes (1.1.2.1, 1.1.2.2, 1.1.2.3, 1.1.2.4) • All input data should be described by metadata
Ancillary data optional for all classes	• COTS navigation data: points of interest, land use, land cover, water areas • Google™ Earth as interpretation help, but not for delineation • Local city maps
Ancillary data required for certain classes	• Local zoning data (e.g., cadastral data) • Field check (on-site visit) • Very high resolution imagery (better than 1 m ground resolution, e.g., aerial photographs)
Geometric resolution (scale)	1:10.000; minimum mapping unit = 0.25 ha
Geographic projection	As per user request, but uniform within project area.
Reference system	As per user request, but uniform within project area.
Positional accuracy	±5 m
Thematic accuracy	• Minimum overall accuracy for level 1 class 1 "artificial surfaces": 80% • Minimum overall accuracy (all classes): 85 % • Methodology for quality control has to be defined
Update frequency	3–5 years
Base data topicality	To be determined
Delivery format	Topological correct GIS file Single part features
Data type	Vector

Figure 11.4 shows one of the 10 classifications of Badajoz, whereas Figure 11.5 shows the divergence image of Badajoz, which brings into evidence the level of agreement between the service providers. The colors show the level of agreement for the individual mapping elements between the 10 service providers, in which 10 — the highest score (in dark green) — means that all 10 service providers have interpreted the object in the same way (same class code). On the other extreme, 0 (red) means that all service providers have labeled this particular object differently.

The exercise showed that the product specifications were still ambiguous and need improvement. Second, it highlighted a certain subjectivity in the mapping of land use classes. The accuracy assessment showed that the accuracy requirement of 80% for urban points could hardly be reached at the most detailed level. The aggregation to level 3, which is in line with DG REGIO, and the integration of the soil sealing degree from the precursor FTS soil sealing layer will lead to less uncertainty and improved accuracy values. After considering these findings, the specifications and mapping guidelines for the Urban Atlas were updated and resulted in the revised nomenclature already presented in Table 11.1.

FIGURE 11.4 **(See color insert following page 324.)** Badajoz, Spain, example of Urban Atlas classification. (Courtesy of GSE Land.)

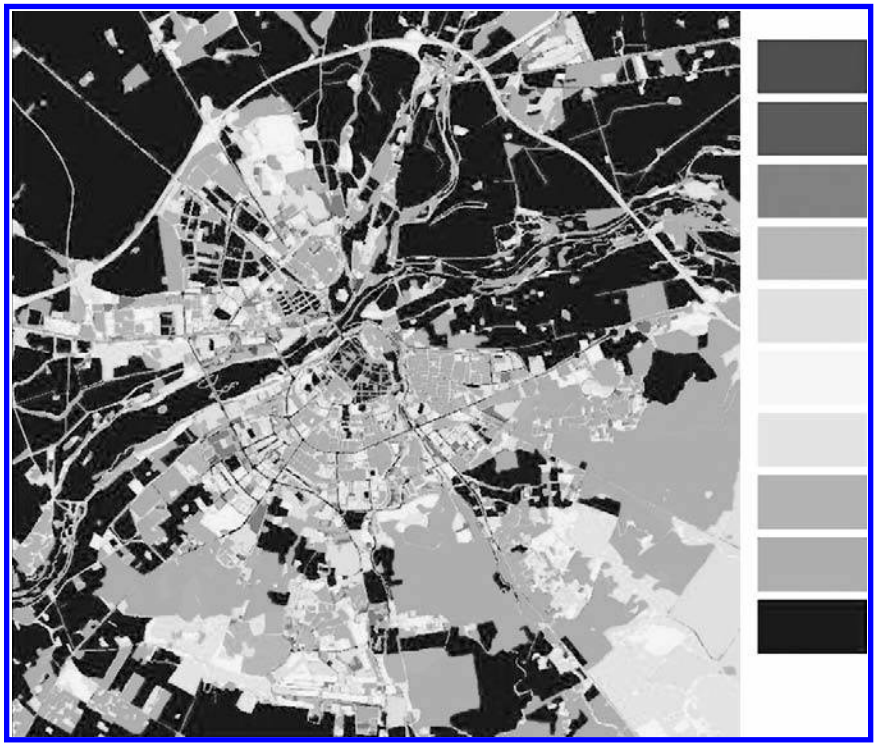

FIGURE 11.5 **(See color insert following page 324.)** Badajoz divergence image — from red for no agreement to green for total agreement among the 10 service providers. (Courtesy of ETC-Lusi.)

11.6.3 Urban Atlas Applications

Many downstream applications and information services can be based on Urban Atlas, for which a few examples are presented here. Information on urban green is vital for planning, design, and maintenance of the urban environment. An inventory of urban green is essential for a proper green management within the urban zone. Figure 11.6 shows an urban green map of Poperinge in Belgium.

"Green urban area" and "public open area" are indicators of Urban Audit and MOLAND. Figure 11.7 shows these indicators for the city of Madrid, extracted from the Urban Atlas and local population statistics.

Land use classifications can be combined with other data such as population statistics to visualize and upgrade regional population data. Figure 11.8 shows a rescaled inhabitant density and quantity map with an increased spatial resolution of the region of Ieper in Belgium.

Detailed soil sealing maps provide an assessment of land consumption with its corresponding sealing intensity, and can also be used for monitoring the land take trends over a certain period. This product helps in identifying conflicts in land use and supports sustainable and harmonized solutions. For Munich, Germany, two processing levels of soil sealing maps are shown; the pixel-based product (Figure 11.9),

FIGURE 11.6 **(See color insert following page 324.)** Urban green map for the city of Poperinge, Belgium. (Courtesy of GUS – Eurosense.)

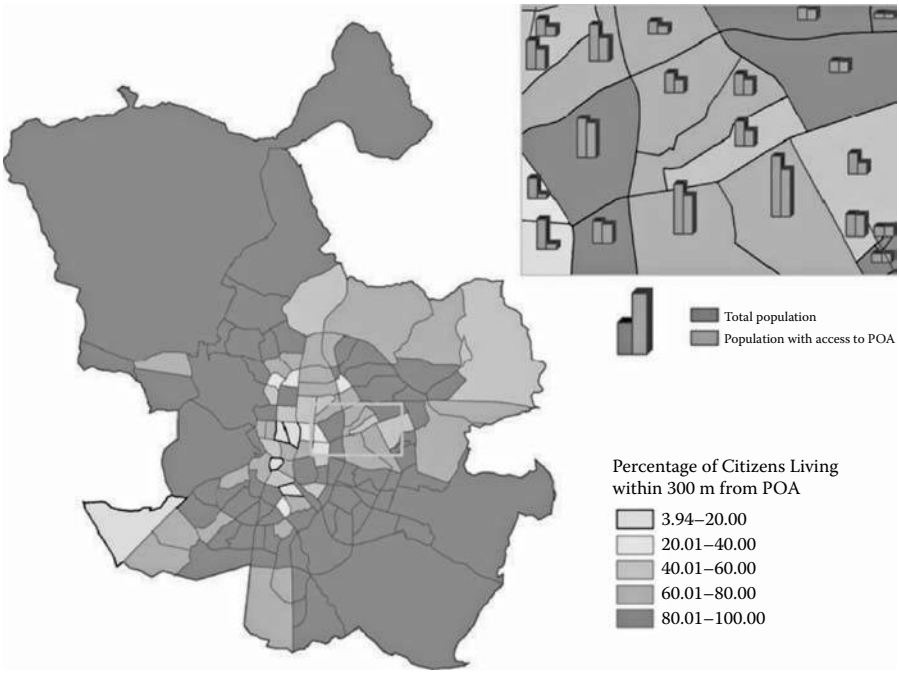

FIGURE 11.7 Urban audit indicators "green urban area" and "public open areas" for Madrid, Spain. (Courtesy of Indra Espacio.)

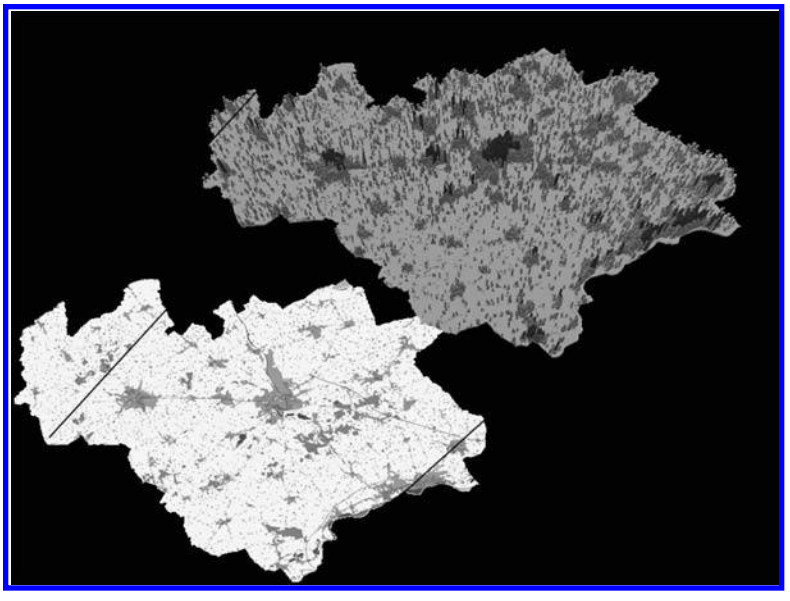

FIGURE 11.8 Land use and derived population estimation for the region of Ieper, Belgium. (Courtesy of GUS – Eurosense.)

FIGURE 11.9 **(See color insert following page 324.)** Pixel-based soil sealing map of Munich, Germany. (Courtesy of GSE Land – H.G. Geodata Solutions.)

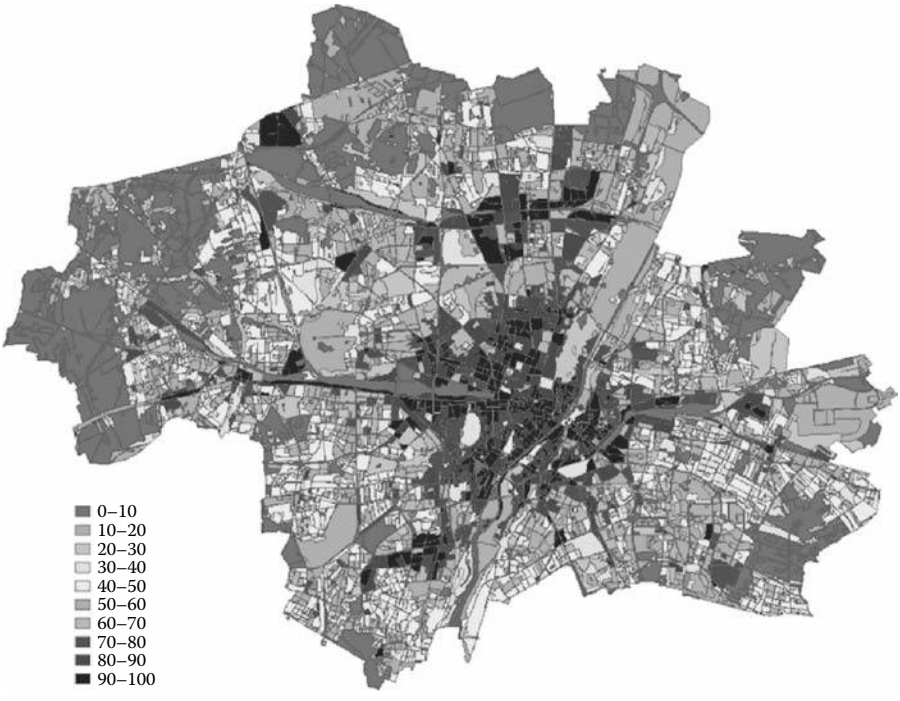

FIGURE 11.10 (See color insert following page 324.) Object-based soil sealing map of Munich, Germany. (Courtesy of GSE Land – H.G. Geodata Solutions.)

which is similar to the EEA FTS sealing layer, can be further treated toward the higher-level object-based product (Figure 11.10).

11.7 OUTLOOK

In the framework of the European GMES LMCS portfolio, the local component Urban Atlas foresees the production of the top 500 urban areas in Europe in support of the Urban Audit. This mapping database will provide for the first time homogeneous and up-to-date spatial information on urban environments, allowing for a comparison of different cities all across Europe. The first step is a call of DG Enterprise and Industry on behalf of DG REGIO for an Urban Atlas mapping of priority cities issued in May 2008. Within the next few years, there will be a special focus on implementing and developing more tools in order to reach a higher degree of automation also in the direction of change mapping. Assuming a successful run of the current implementation, it is likely that there will be a regular update of all major European urban conglomerations using the specified Urban Atlas methodology in the same timeframe as the Urban Audit. For cities outside of Europe, the methodology could be adapted, enabling worldwide comparison of urban settlements.

ACKNOWLEDGMENT

The author wishes to thank all contributors to the projects that paved the way to a European Urban Atlas, such as MOLAND, Urban Audit, GMES Urban Services, and GSE Land, which provided figures and examples for this chapter. Thanks for all the comments and suggestions improving the quality of this review.

REFERENCES

Green Paper on the Urban Environment — Communication from the Commission to the Council and Parliament, COM(90), 218, 1990.

GSE Land Service Validation Protocol, 2008. Available online at: http://www.gse-land.info.

Liebig, V., Aschbacher, J., Briggs, S., et al., GMES — Global Monitoring for Environment and Security: The second European flagship in space, *ESA Bulletin*, 130, May 2007.

LMCS Strategic Implementation Plan, 2007. Available online at: http://www.gmes.info.

Report of the United Nations Conference on Environment and Development A/CONF.151/26, Vol. I, Rio de Janeiro, June 1992.

State of European Cities Report, DG REGIO, 2007.

Thematic Strategy on the Urban Environment, Communication from the Commission to the Council and Parliament COM(2005) 718, 2006.

Towards an Urban Atlas, EEA/JRC Report, 2002.

Urban Atlas Mapping Guide, GSE Land, 2008. Available online at: http://www.gse-land.info.

Urban Sprawl Report 2006, EEA, 2006.

Part IV

Critical Issues and Avenues for Future Research

12 Semantic Characterization of Human Settlement Areas
Critical Issues to be Considered

Louisa J.M. Jansen

CONTENTS

12.1 INTRODUCTION

Currently, approximately half of the world population lives in urban areas and this is anticipated to exceed 60% by 2030, with 90% of projected urbanization occurring in low-income countries (UN, 2004). The rapid and uncontrolled development of human settlement areas has many potentially detrimental effects, including the loss of valuable agricultural and ecologically sensitive lands, enhanced energy consumption, and greenhouse gas emissions from increasing private and public

vehicle use (Guindon et al., 2004). Timely information on changes in human settlement type, distribution, location, and size, and the probable effects of changes is therefore needed, as well as information on social, demographic, and economic parameters.

Human settlement areas are among the most complex structures created by human societies. Growth and dynamism are two of the elements that characterize such areas (Barredo et al., 2003). Urbanization processes are a basic element in the dynamics of human societies. Through the changes in the spatial distribution of population and resources, these processes reflect the links and relationships between urban and rural areas, economic factors, and social classes and groups (Bonifazi and Heins, 2003). Growth management and sustainable development are widely considered essential to maintain the quality of life in metropolitan landscapes (Daniels, 1999; van der Valk, 2002).

Urbanization as land *cover*, in the form of built-up or paved-over areas, occupies less then 2% of the Earth's surface (Gruebler, 1994). Changes in the spatial extent of human settlement areas per se, therefore, do not appear to be central in global change dynamics. However, although the areas may be small, urbanization leads to transformations of urban-rural linkages, the so-called urban "ecological footprint" (Lambin et al., 2001). These urban-rural transformation processes are a causative factor of the current renewed interest in the complex dynamics of urban systems. Current international thinking on urban policy in multilateral institutions (e.g., World Bank and United Nations) emphasizes a strong role for municipal local governments. UN Habitat argues that decentralization will increase economic efficiency and political accountability, and hence help reduce urban poverty (Devas, 2004; UN Habitat, 2005). A sustainable balance between the influences of present and proposed human activities and the sensitivities of the urban and rural environment needs to be found.

For human settlement characterization, the interest lies in the land use and not the land *cover* category (Guindon et al., 2004), in contrast to Herold et al. (2006), who consider land cover of prime importance. Many scientists, working in disciplines that are not related to remote sensing, view land use as the elemental variable driving many processes, as observed by Comber et al. (2007). One should note that in several languages there is no equivalent term for "land cover" (in some, such as French or Italian, it is closer to "soil cover"), whereas there are similar terms for "land use" (*landgebruik* in Dutch and *Landnutzung* in German).

Human settlement areas are characterized by a complex pattern of land use. Within the study of spatial decision making, several land-use allocation factors have been identified as determinants of urban activities (Barredo et al., 2003): (1) environmental characteristics, that is, constraints for urban growth; (2) local-scale neighborhood characteristics (e.g., present and past land use patterns and their dynamics); (3) spatial characteristics of the cities (e.g., distance to the city center, accessibility, flows or transport networks); (4) urban and regional planning policies (e.g., land use (zoning) — plans that regulate the legal aspects of occupation of land uses in space and time); and (5) factors related to individual preferences, level of economic development, socioeconomic and political systems, that is, related to human decision-making processes.

Such factors can be built into existing models and underlying theories. For instance, the differential urbanization model links the processes of urbanization/concentration, polarization reversal, and counterurbanization across the development continuum within developed and developing countries [e.g., Botswana (Gwebu, 2006), Italy (Bonifazi and Heins, 2003)], mainly using migration statistics to understand the processes. Both sociodemographic and environmental factors are used by Henry et al. (2003) to explain migration processes. Linear extrapolation of a trend combined with land use suitability based on physical properties, operational policies, relations to nearby land use functions, and expert judgment can be used to simulate the future (Schotten et al., 2001). Multiagent modeling at the household level is used to understand patterns (Loibl et al., 2007) or to represent the behavior of the different actors (Ettema et al., 2007). Hybrid models including cellular automata and dynamic spatial simulation modeling have been developed to understand spatial dynamics at different levels (Engelen et al., 2007; Piyathamrongchai and Batty, 2007). The impact of temporal dynamics on urban growth has been studied by using modified Markov random field and probabilistic cellular automata (Liu and Andersson, 2004). The Conversion of Land Use and its Effects (CLUE) modeling framework is a tool to better understand the processes that determine the spatial pattern of land use (Verburg et al., 2002; Verburg and Overmars, 2007).

Such modeling efforts are limited in the link between human settlement patterns and change processes resulting from planning, policy, and decision making. Few models, such as the Land Use Scanner and Environment Explorer, include policy-related parameters (Pontius et al., 2008). This link is necessary if one wants to understand the "why" and "how" of human settlement developments. Spatial *pattern* refers to the spatially explicit changes in human settlement areas, whereas *process* refers to the underlying drivers and proximate causes that explain these changes (Geist and Lambin, 2001; Overmars, 2006).

The international scientific community is also interested in human settlement areas. The Global Land Project (GLP), a multidisciplinary project of the International Geosphere-Biosphere Programme (IGBP) and the International Human Dimensions Programme on Global Environmental Change, aims "to measure, model and understand the coupled human-environmental system" and asks specifically for characterization of human settlement areas (GLP, 2005, p. 54).

If human settlement areas are to be characterized in a consistent manner, then it should be clear to the data producer (the generator of datasets), the distributor (the subsequent distribution of datasets), and user (in the end the user of datasets) that the primary aim is not the *static mapping* of the areas to know their location and extent, that is, land *cover*, but that the primary aim is change analysis, monitoring, and modeling to predict future land use developments under existing spatial plans and policies, and to compare alternative planning and policy scenarios in terms of their effects on future land use development. Thus, considering that for policy and decision making the national and municipal levels are important, the latter aims are also the key levels for characterization and, subsequently, for data collection.

In recent years, the semantic contents of environmental change data have been receiving increasing attention. Measuring semantic similarity of categories, either

before or after data collection or between existing datasets, is an emerging area of research (Ahlqvist, 2005). There are various initiatives dealing with the changing context of access to spatial data (e.g., Spatial Data Infrastructures such as the European Union INSPIRE project), and there is recognition that spatial data integration is an essential step in environmental change monitoring and modeling and initiatives that aim to respond to environmental change (Comber et al., 2005a). Data users are becoming increasingly interested in understanding the wider meaning of data, that is, the concepts adopted and categorizations used. However, current metadata standards convey very little about the semantic contents of class sets (Comber et al., 2005b; Schuurman and Leszczynski, 2006). Similarly, remotely sensed data–derived products report technical aspects of the data (e.g., scale, spatial resolution, positional and thematic accuracy) but the semantic aspects are often largely ignored (Comber et al., 2005c).

This chapter will first explore the semantic aspects of land use and land cover categorization (Section 12.2), followed by an analysis of the influence of semantics on change analysis, monitoring, and modeling (Section 12.3), and a discussion of the semantic differences between land use and land cover (Section 12.4). The chapter next takes a side step in order to highlight some aspects of characterization using remote sensing as a tool, as that is particularly appropriate in the context of this book (Section 12.5). The main theme will be continued in the examination of ways to include semantics in metadata standards (Section 12.6) and approaches for semantic characterization, that is, standardization and harmonization, are analyzed (Section 12.7). Suggestions are made for the way forward (Section 12.8).

12.2 SEMANTIC ASPECTS OF CATEGORIZATION

Because different applications have different worldviews and semantics, interoperability can be primarily understood as a semantic modeling problem (Bishr et al., 1999). The variation in the semantic content of data expressed as differences in categorization has received limited attention until recently (Feng and Flewelling, 2004). Comber et al. (2004a) report that differences in semantic concepts are often *the* major barrier to data integration. Achieving semantic interoperability in order to use existing datasets at a satisfactory level has therefore become a key issue.

Categorization produces datasets comprising classes that have different semantic contents (e.g., class labels and class definitions). Categorization, or classification, is defined as "the ordering or arrangement of objects into groups or sets on the basis of relationships. These relationships can be based upon observable or inferred properties" (Sokal, 1974). An earlier definition by Shapiro (1959) viewed categorization as "the sorting of a set of phenomena composed of generally-alike units into classes or kinds, each class or kind consisting of members having definable characteristics in common." Sokal's definition clearly underlines the issue of relationships, whereas Shapiro's definition uses the word "phenomena" instead of "objects." The term "phenomenon" would better suit land use than the term "object." However, Sokal's definition will be adhered to here, as it is the most widely applied definition.

Classes are the results of a categorization process and they serve as the tangible vehicles for communication of meaning (Ahlqvist, 2008). Anyone using classes of a certain categorization will have to interpret these classes and may therefore introduce bias (Jansen et al., 2008). Clear definition of all elements that make up a categorization is therefore crucial. The primary aim of categorization is often to create order for the communication of knowledge, but often includes ambiguity in both concepts and definitions.

Categorizations embody a worldview. Data collected with a specific categorization are intended for a certain purpose and this leads to a particular or prevalent view. From the analysis of semantic information and used definitions, one can deduce something about this view and the intent of the data producers. In the land cover domain, for instance, the class definitions of "Continuous urban fabric" and "Discontinuous urban fabric" in the CORINE Land Cover (CLC) categorization (CEC, 1999; Bossard et al., 2000) is described by taking a map view, or two-dimensional view, and only the word "structure" in the definition implies a third dimension. In the Land Cover Classification System (LCCS) (FAO, 2005), that the category name "Artificial surfaces and associated areas" is described by the parameter "Surface aspect" says enough. Both CLC and LCCS take a *map* view rather than a *geographic entity* view.

Definitions are the main, and usually the only, descriptions of category terms, because other elements that could contribute to the semantic definition of categories (e.g., the parameters or criteria used) are often missing. Definitions expressed in natural language associated by subtype/supertype relationships are called *terminological ontologies* (Sowa, 2000). Almost all land use and land cover categorizations to date are terminological ontologies. Ontology is an explicit specification of a conceptualization to represent shared knowledge (Gruebler, 1994; Ahlqvist, 2008). Semantic information can be determined from the definitions of the ontology, and the representation of categories can be enriched with semantic properties (e.g., purpose, time, location, etc.) and relations (e.g., "is-a," "is-a-part-of," "associated-with," etc.) in order to reveal similarities and heterogeneities (Kavouras et al., 2005). Subsequently, (dis)similarities can be visualized (e.g., Kavouras et al., 2005; Ahlqvist, 2007). With the progress in computer and information sciences, there seems to be a real need to improve existing categorization concepts and the operational use of such categorizations, in particular when comparing different categorizations in change analysis, monitoring, or modeling efforts.

12.3 INFLUENCE OF SEMANTICS ON CHANGE ANALYSIS, MONITORING, AND MODELING

In change analysis, monitoring and modeling the semantics often form a problem due to the limited description of how exactly class labels should be understood (Comber et al., 2004a) and expert opinions differ (Comber et al., 2005a). Moreover, datasets from the same area but from different times often need to be integrated in a geodatabase while at the same time each is based on a (slightly) different categorization (Comber et al., 2004b). Similarity in terms does not necessarily imply equivalent category terms.

If one looks at change analysis and monitoring from the semantic perspective, then one can observe that it is often performed in a rather straightforward manner by constructing a change matrix for spatially explicit evaluation of changes. This approach is based on *standard set* theory in which the crisp class A has either changed in another crisp class or crisp class A remained unchanged. Changes of crisp class A into crisp class B or into crisp class C are treated in an identical manner, although one change type may relate to a *conversion* and the other to a *modification*. A conversion means large semantic differences between classes (e.g., change from pasture into residential area), whereas modification means small semantic differences (e.g., change from low-density residential area into a high-density residential area). A more detailed approach has been used in the EU PHARE Land Use Policy project in Albania, where not only changes were identified as either conversions between land use categories or modifications within a land use category, but the categorization hierarchy was also used to distinguish for each type of modification three levels of intensity (Jansen et al., 2007).

Another approach to change analysis uses *probabilistic reasoning* (Haenni, 2005) instead of standard set theory, although this approach considers the classes still as being crisp and unambiguous. A more sophisticated approach is to consider the notion of vagueness in the categorization system using *fuzzy set* theory. The notion of category semantics and category similarity metrics (e.g., overlap and distance) is concerned with the vagueness inherent in category definitions and semantic relations between categories (Ahlqvist, 2007), thereby overcoming the traditional limitations on the exhaustiveness and mutually exclusivity of classes (Rocchini and Ricotta, 2007).

The interpretation of a change matrix under the assumption of fuzzy categories will differ from the standard one, where diagonal elements hold instances of "no change" and off diagonal elements hold instances of category gains and losses (Fisher et al., 2006; Pontius and Cheuk, 2006). The diagonal can no longer be treated as holding instances of "no change" and the use of category semantics and category similarity metrics should be considered. Ahlqvist (2007) provides an interesting example of such an approach in which not only a spatially explicit evaluation of changes is given, but also a nuanced assessment on changes of heterogeneous class types.

Much of the integration of knowledge on land use change takes place through (spatial) models that aim at explaining the causes, locations, consequences, and trajectories of land use change (Verburg and Veldkamp, 2005). Models, like categorizations, simplify the complexity of the reality. The two main sets of drivers (social and biophysical) each seem to play a prevalent role at a specific scale: social drivers are associated with finer-scale spatial patterns and biophysical drivers with coarser-scale spatial patterns. As a result, two complementary modeling approaches are advocated: from pattern-to-process (top-down) and from process-to-pattern (bottom-up) (Walsh et al., 1999; Laney, 2004; Castella et al., 2007; Castella and Verburg, 2007; Overmars et al., 2007). The above also means that land use and land cover operate at different scales, a cause that affects their interoperability. Modeling efforts in which pattern and process in human settlement areas are linked are limited. Even more limited are research efforts in which the influence of semantics on modeling outcomes is examined. Much more research should be undertaken in this area.

12.4 SEMANTIC DIFFERENCES BETWEEN LAND USE AND LAND COVER CLASS AND DATASETS

The ambiguity and heterogeneities of land use terminology were already signaled in the 1950s (Mitchell and Rapkin, 1954, cited in Guttenberg, 2002). Land use is defined as "the type of human activity taking place at or near the surface" (Cihlar and Jansen, 2001), whereas land cover is defined as "the observed (bio)physical cover on the Earth's surface" (Di Gregorio and Jansen, 2000).

Although land use and land cover are often amalgamated in class and datasets, there are three major *semantic* differences that affect their interoperability (Brown and Duh, 2004):

- The *category definitions* of land cover and land use are different. In land use terminology, an "undeveloped forest" is a clear-cut area that continues to be used for forestry (Lund, 1999), whereas in land cover terminology the term "forest" would not be used for an area without trees.
- Land cover and land use have different *geometric expressions*. The consequence is that a categorization cross-walk approach to semantic interoperability without defining interrelations between categorization schemes and without redefining spatial objects, such as proposed and implemented for alternative vegetation/land cover classifications by the IGBP (Loveland et al., 2000), is likely to be an inadequate solution for the proper translation between land use and land cover. As Cihlar and Jansen (2001) pointed out, the spatial objects might need to change in addition to the class definitions.
- Land cover and land use have different *spatial rules* to assign attributes to land use/land cover features because land-use class definitions tend to integrate information about activities taking place within a spatial unit (e.g., cadastral parcel or zone), whereas land cover class definitions assess the static and in situ conditions. Thus, the entities of a land cover data set (e.g., polygons) usually show more spatial variation than those of a spatially explicit land use data set (assuming both datasets are compiled based on sources of the same level of detail).

Cihlar and Jansen (2001) pointed out the complexity of the relationships between land use and land cover class and datasets. They developed a framework for analysis of the land cover/land use relationships, arguing that these relationships should always be considered from a spatial and semantically consistency viewpoint at a certain point in time, because the relationship may change over time in the domain of interest and vary between different domains of interest. Thus, there are no preset relationships between land cover and land use that could form a basis for building linkages between a priori *categorization systems*, that is, categorization systems comprising sets of predefined classes (e.g., CLC and LCCS). It is clear that class and datasets in which land use and land cover are amalgamated further complicate matters.

From the semantic differences listed above and the fact that land use and land cover operate at different scales (Section 12.3), it should be clear that attempts to

link land use to land cover categorization "to base a common system for land-use classification on existing land-cover standards to ensure full compatibility" and "land-cover and land-use transitions have to be interoperable" (Herold et al., 2006, p. 162) are conceptually wrong from the spatial, temporal, and semantic perspectives.

12.5 REMOTE SENSING AND CLASSIFICATION

Another reason for the renewed interest in the complex dynamics of urban systems may be the increasing availability of (very) high spatial resolution satellite sensor data. Satellite images give a physical description of the Earth's surface (e.g., materials, surface roughness, and structure) related to land cover. Land use needs to be inferred from image characteristics or through the incorporation of ancillary information. Figure 12.1 gives an example of the hierarchical ordering of urban surface cover types that can be detected with remote sensing with a map view (see Section 12.2).

The term "classification" as used in remote sensing means something different from the categorization discussed in previous paragraphs. The term "categorization" embodies two meanings (Duhamel, 1998): (1) *establishment of groupings* of all objects in a given field (according to Sokal's definition); and (2) using the established groupings in order to decide the *membership status* of other objects. The second meaning is used in remote sensing where the imagery is used for the identification process of objects.

Research themes evident today in human settlement remote sensing can be divided into: (1) improving techniques for classifying images or (2) understanding the human settlement environment with interpreted scenes (Wentz et al., 2006). The

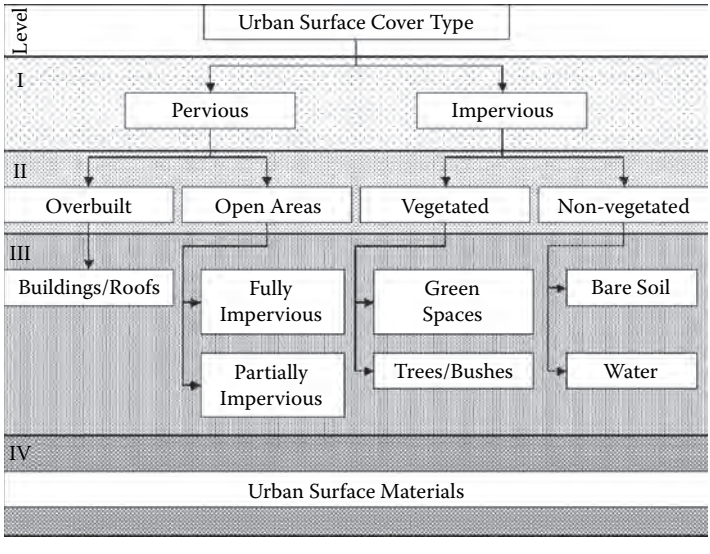

FIGURE 12.1 Hierarchical ordering of urban surface cover types. (Adapted from Roessner et al., 2001).

first is dealt with in numerous publications (e.g., Herold et al., 2004; Jacquin et al., 2007; Heiden et al., 2007, to cite a few). The relationship between human settlement land uses and spectral responses recorded in such images is very complex and indirect, excluding the use of traditional remote sensing classification approaches. Land use *functions* may be distinguished on the basis of the differences in spatial distribution and pattern of land cover *forms* using advanced software with object-oriented fuzzy-rule (fuzzy logic) classification techniques (Bauer and Steinnocher, 2001). The philosophy behind such software is that important semantic information necessary to interpret an image accurately is not represented in single pixels, but in meaningful image objects and their mutual relationships. However, in both research themes the understanding of the spatial patterns and the underlying processes and the role of semantics in such analyses is absent.

Human settlement characterization is fundamentally different from remotely sensed based classification. The parameters used in the latter do not (necessarily) coincide with the first. Characterization with remote sensing, that is, a tool, is dependent on the type of image used, its spectral and spatial characteristics. Tool dependence is *against* the principles of categorization (Duhamel, 1998; Di Gregorio and Jansen, 2000; EC, 2001; Jansen, 2006). Furthermore, if remote sensing is used to detect land use based on land cover, then the relationships between human settlement land cover and land use need to be established for the area of interest, and where the relationship is not consistent in either space or time ancillary data need to be used to establish this relationship (Cihlar and Jansen, 2001). In a time-series analysis, this means that the land cover/land use relationship needs to be established for each moment in time. This is not a trivial matter in an environment as dynamic as human settlements.

Although the contribution of remote sensing to the characterization of urban settlement areas may be limited, it is a useful contribution. Taking into account that human settlement areas cover only 2% of the Earth's surface, intensive urban "field" survey campaigns for verification and validation of remotely sensed derived interpretations do not involve travel over large distances and difficult terrain, such as are generally encountered by rural field survey campaigns. Collection of especially land use–related information on the ground should therefore not be a major obstacle to enrich land cover interpretations.

12.6 SEMANTICS AND METADATA

Data are collected for an intended purpose and this leads to a particular or prevalent view (Section 12.2). Related to this view is the meaning of the data. The latter may be obvious to the data producer, but it is rarely as clear to the distributor and data users unless they were part of the data collection process. Access to data through Spatial Data Infrastructures initiatives implies that countless potential users may be reached. However, in almost all cases to date, the metadata do not provoke users to consider the wider meaning of the data (Comber et al., 2004a).

Recognition of semantic heterogeneity is the basis for creating sound data linkages between multiple datasets that are needed for planning, policy, and decision making. Metadata are an existing means for conveying ontological information about the

semantic contents of data. Currently, however, fields to express semantic information are lacking and only information of the technical and geometric domain is included. Schuurman and Leszczynski (2006) present an example of how ontological information can be linked with metadata as a means of providing deep meaning and context to both semantic and numeric metadata. Current ontology research in geographic information science has focused on data structuring and modeling. Implementation of these schemes demands restructuring of existing relational database models. An alternative is to extend current metadata schemes (e.g., ISO 19115) to include context-based and tacit information about semantic attributes. Such ontology-based extended metadata permits data selection and interoperability decisions that are ultimately more justifiable.

The current trend is to incorporate ontological context at the model level in geographic information science. The development of ontology-based metadata, as described above, is very much a different issue. It is pragmatic, however, in that it presents a means for incorporating use context with data in a manner that is accessible, requires little reengineering, and is intuitively understood by geographic information system users (Schuurman and Leszczynski, 2006).

12.7 APPROACHES FOR SEMANTIC CHARACTERIZATION: STANDARDIZATION AND HARMONIZATION

Semantic interoperability goes beyond attempts to homogenize differences through standards (Harvey et al., 1999). Although standards in themselves are useful, because they provide a "common language," they usually lag behind activity and therefore cannot represent the depth of knowledge held within a community (Comber et al., 2005b). Standards also change over time, so they are not so "standard" as their name seems to suggest. Table 12.1 shows, for instance, differences between the third and fourth revisions in the main categories of the International Standard Classification of all Economic Activities (ISIC) (UN, 1989, 2006). Such changes do not only affect the class set but also the data set behind it, and thus may mean difficulties when trying to establish correspondence between categories and classes as this is no longer of the type one-to-one. To give some examples of changes:

- The third revision category of "A. Agriculture, hunting, and forestry" is no longer compatible with the fourth revision category "A. Agriculture, forestry, and fishing" even when one would include "B. Fisheries," because the latter is not fully compatible with "A-03 Fishing and aquaculture."
- The category "E. Electricity, gas, and water supply" (third revision) has been extended to "D. Electricity, gas, steam, and air conditioning supply" (fourth revision) and water supply has its own class "E. Water supply; sewerage, waste management, and remediation activities."

Adoption of a standard implies adoption of a particular worldview embodied in the data. This becomes a critical issue because a world in which several worldviews coexist seems not only a much more flexible approach suited to the intended purpose of data collection, but also one that makes the world richer (Jansen et al., 2008).

TABLE 12.1
Main Categories of ISIC — Third Revision and Draft for the Fourth Revision

International Standard Classification of All Economic Activities

Code	Third Revision (UN, 1989)	Code	Fourth Revision (Draft) (UN, 2006)
A	Agriculture, hunting, and forestry	A	Agriculture, forestry, and fishing
	A-01 Agriculture, hunting, and related service activities		A-01 Crop and animal production, hunting, and related service activities
	A-02 Forestry, logging, and related service activities		A-02 Forestry and logging
			A-03 Fishing and aquaculture
B	Fisheries	B	Mining and Quarrying
C	Mining and quarrying	C	Manufacturing
D	Manufacturing	D	Electricity, gas, steam, and air conditioning supply
E	Electricity, gas, and water supply	E	Water supply; sewerage, waste management, and remediation activities
F	Construction	F	Construction
G	Wholesale and retail trade	G	Wholesale and retail trade; repair of motor vehicles and motorcycles
H	Hotels and restaurants	H	Transportation and storage
I	Transport, storage, and communication	I	Accommodation and food service activities
J	Financial intermediation	J	Information and communication
K	Real estate, renting, and business activities	K	Financial and insurance activities
L	Public administration and defense	L	Real estate activities
M	Education	M	Professional, scientific, and technical activities
N	Health and social work	N	Administrative and support service activities
O	Other community, social, and personal service activities	O	Public administration and defense; compulsory social security
P	Private households with employed persons	P	Education
Q	Extraterritorial organizations and bodies	Q	Human health and social work activities
		R	Arts, entertainment, and recreation
		S	Other service activities
		T	Activities of households as employers; undifferentiated goods- and services-producing activities of households for own use
		U	Activities of extraterritorial organizations and bodies

Do we need to standardize the characterization of human settlement areas, or is "Should we invest in better ways to harmonize?" the key question to be raised? Standardization takes categorization one step further in that it fixes a categorization (Ahlqvist, 2008). Standardization defined as "the use of a single standard basis for classification of a specific subject" (McConnell and Moran, 2001) assumes that the advances in knowledge, technological developments, and changing policy objectives would not have an impact on the existing systematic categorization framework. Lessons from the past impart the message that this may be an unrealistic expectation, so data standardization seems to be only partly feasible (Jansen et al., 2008). As Cihlar and Jansen (2001), Comber et al. (2005b, 2007), and Ahlqvist (2008) point out, manifold ways to conceptualize and communicate knowledge exist according to the perspective of (groups of) experts, professions, etc., so that there are necessarily many-to-many relationships between classes and thus inherent ambiguity in any categorization. Categorizations and standardizations contribute to communication of knowledge and in making joint progress in that, knowledge by facilitating communication. However, they can only make such contributions by being *dynamic* in nature. The latter means that no formalization of categorization should be sought.

Harmonization of categorization systems defined as "the intercomparison of data collected or organized using different classifications dealing with the same subject matter" (McConnell and Moran, 2001) seems a more realistic avenue for future applications as the emphasis is shifting from *static* mapping toward more *dynamic* monitoring and modeling (Lambin et al., 2000; McConnell and Moran, 2001; Dolman et al., 2003).

12.8 THE WAY FORWARD

Semantics should contribute not just to the *static* mapping of areas to know the location and extent, but especially to the *dynamics* of changes. Concentrating too much on "mapping" is limiting oneself to a type of snapshot of a specific moment in time with a specific categorization. Understanding the dynamics of changes requests much more of semantics than mapping.

If human settlement areas are to be characterized semantically in a consistent manner, it should be clear that communication between the generator of datasets, the data distributor, and in the end the user of datasets is crucial. One should be able to retrieve the meaning of the semantics used and the context in which they are used. Categorizations could be improved by taking a parameterized approach in which the class labels are accompanied by a clear and unambiguous description and the parameters used in the definition of classes are *explicitly* mentioned and well defined. But there is also a need for rich narratives that further specify and clarify what is included in a term, a class, or categorization. Such parameterized categorizations would contribute to the harmonization of semantics. At present, there is often no explicit recognition of semantic differences in cases where two or more different categorizations are involved. Extended metadata, comprising information on semantics, would also be a major improvement.

Land use and land cover are closely linked, however they are not identical and should not be amalgamated in categorizations. The temporal, spatial, and semantic

perspectives of land use and land cover are different and attempts to link them in categorization should be abandoned.

The way forward is the development of systematic approaches for data harmonization that also provide quantitative measures for the harmonization results both at individual class level as between two categorizations. The latter is not the subject of this paper (see Jansen et al., 2008), but the capability to measure and compare similarity between categorizations and classes within a categorization system or between categorization systems is becoming increasingly important, not only as part of a categorization or interpretation process, but especially in change analysis, monitoring, and modeling. The harmonization of semantics is only one aspect of data harmonization, sitting alongside the adopted data concepts, the spatial, temporal, and data quality aspects. Data harmonization will allow the continued use of different categorizations, each with its own worldview and particular purpose. These different categorizations enrich the understanding of our environment by taking different perspectives.

More information on the semantics of land use and land cover categorizations is needed to enable us to make better and informed use of existing class and datasets. However, the interoperability between land use and land cover will not be enhanced with such information although the insight into the limitations of such interoperability will become more apparent.

ACKNOWLEDGMENTS

The author would like to gratefully acknowledge Geoff Groom, National Environmental Research Institute, Denmark, for his constructive comments on the manuscript.

REFERENCES

Ahlqvist, O., Using semantic similarity metrics to uncover category and land-cover change, in: Rodríguez, M.A., Cruz, I.F., Egenhofer, M.J., and Levashkin, S., eds., *Geospatial Semantics (GeoS) First International Congress*, 29–30 November 2005, Mexico City, Mexico, Springer, Berlin, 107–119, 2005.

Ahlqvist, O., Extending post-classification change detection using semantic similarity metrics to overcome class heterogeneity: A study of 1992 and 2001 US National Land-Cover database changes, *Remote Sensing of Environment*, 112(3): 1226–1241, 2008.

Ahlqvist, O., In search for classification that supports the dynamics of science: The FAO Land-Cover Classification System and proposed modifications, *Environment and Planning B*, 35, 169–186, 2008.

Barredo, J.I., Kasanko, M., McCormick, N., and Lavalle, C., Modelling dynamic spatial processes: Simulation of urban future scenarios through cellular automata, *Landscape & Urban Planning*, 64, 145–160, 2003.

Bauer, T., and Steinnocher, K., Per parcel land-use classification in urban areas applying a rule-based technique, *GeoBIT/GIS*, 6, 24–27, 2001.

Bishr, Y.A., Pundt, H., Kuhn, W., and Radwan, M., Probing the concept of information communities — a first step toward semantic interoperability, in: Goodchild, M., Egenhofer, M., Fegeas, R., and Kottman, C., eds., *Interoperating Geographic Information Systems*, Kluwer Academic Publishers, Dordrecht, pp. 55–69, 1999.

Bonifazi, C., and Heins, F., Testing the differential urbanisation model for Italy, *Tijdschrift voor Economische en Sociale Geografie*, 94, 23–37, 2003.

Bossard, M., Feranec, J., and Otahel, J., CORINE Land Cover Technical Guide — Addendum 2000. Technical Report 40, European Environment Agency, Copenhagen, 105 pp., 2000.

Brown, D.G., and Duh, J.-D., Spatial simulation for translating from land use to land cover, *International Journal of Geographic Information Science*, 18(1), 35–60, 2004.

Castella, J.-C., and Verburg, P.H., Combination of process-oriented and pattern-oriented models of land-use change in a mountain area of Vietnam, *Ecological Modelling*, 202, 410–420, 2007.

Castella, J.-C., Kam, S.P., Quang, D.D., Verburg, P.H., and Hoanh, C.T., Combining top-down and bottom-up modelling approaches of land-use/cover change to support public policies: Application to sustainable management of natural resources in northern Vietnam, *Land-Use Policy*, 24, 531–545, 2007.

CEC [Commission of the European Communities], CORINE Land Cover, Brussels, 1999.

Cihlar, J., and Jansen, L.J.M., From land cover to land use: A methodology for efficient land-use mapping over large areas, *Professional Geographer*, 52(2), 275–289, 2001.

Comber, A.J., Fisher, P.F., and Wadsworth, R.A., Assessment of a semantic statistical approach to detecting land-cover change using inconsistent datasets, *Photogrammetric Engineering & Remote Sensing*, 70(8), 931–938, 2004a.

Comber, A.J., Fisher, P.F., and Wadsworth, R.A., Integrating land-cover data with different ontologies: Identifying change from inconsistency, *International Journal of Geographical Information Science*, 18(7), 691–708, 2004b.

Comber, A., Fisher, P., and Wadsworth, R., Comparing statistical and semantic approaches for identifying change from land-cover datasets, *Journal of Environmental Management*, 77, 47–55, 2005a.

Comber, A., Fisher, P., and Wadsworth, R., What is land cover? *Environment and Planning B: Planning & Design*, 23, 199–209, 2005b.

Comber, A., Fisher, P., and Wadsworth, R., You know what land cover is but does anyone else? An investigation into semantic and ontological confusion, *International Journal of Remote Sensing*, 26(1), 223–228, 2005c.

Comber, A.J., Fisher, P.F., and Wadsworth, R.A., Land cover: To standardise or not to standardise? Comment on 'Evolving standards in land-cover characterisation' by Herold et al., *Journal of Land-Use Science*, 2(4), 283–287, 2007.

Daniels, T., *When City and Country Collide: Managing Growth in the Metropolitan Fringe*, Island Press, Washington, D.C., 1999.

Devas, N., *Urban Governance, Voice and Poverty in the Developing World*, Earthscan, London, 240 pp., 2004.

Di Gregorio, A., and Jansen, L.J.M., *Land-Cover Classification System (LCCS): Classification Concepts and User Manual*, FAO/UNEP/Cooperazione Italiana, Rome, 177 pp. (with CD-ROM), 2000.

Dolman, A.J., Verhagen, A., and Rovers, C.A., eds., *Global Environmental Change and Land Use*, Kluwer Academic Publishers, Dordrecht, 2003.

Duhamel, C., First approximation for a land-use classification. CESD-Communautaire, Luxembourg, FAO commissioned study, 1998.

EC [European Commission], Manual of concepts on land-cover and land-use information systems. EUROSTAT Theme 5 Agriculture and Fisheries — Methods and nomenclatures, Office for Official Publications of the European Commission, Luxembourg, 106 pp., 2001.

Engelen, G., Lavalle, C., Barredo, J.I., van der Meulen, M., and White, R., The MOLAND modelling framework for urban and regional land-use dynamics, in: Koomen, E., Bakema, A., Stillwell, J., and Scholten, H., eds., *Modelling Land-Use Change — Progress and Applications*, *GeoJournal Library*, Vol. 90, Springer, Berlin, pp. 297–319, 2007.

Ettema, D., de Jong, K., Timmermans, H., and Bakema, A., PUMA: Multi-agent modelling of urban systems, in: Koomen, E., Bakema, A., Stillwell, J., and Scholten, H., eds., *Modelling Land-Use Change — Progress and Applications*, *GeoJournal Library*, Vol. 90, Springer, Berlin, pp. 237–258, 2007.

FAO [Food and Agriculture Organization of the United Nations], *Land-Cover Classification System — Classification Concepts and User Manual*. Software version 2, Environment and Natural Resources Series 8, Rome, 190 pp., 2005.

Feng, C.-C., and Flewelling, D.M., Assessment of semantic similarity between land-use/land-cover classification systems, *Computers, Environment & Urban Systems*, 28, 229–246, 2004.

Fisher, P., Arnot, C., Wadsworth, R., and Wellens, J., Detecting change in vague interpretations of landscapes, *Ecological Informatics*, 1(2), 163–178, 2006.

Geist, H.J., and Lambin, E.F., What drives tropical deforestation? A meta-analysis of proximate and underlying causes of deforestation based on sub-national case study evidence, LUCC Report Series No. 4, Land-Use and Land-Cover Change (LUCC) programme element of the International Geosphere-Biosphere Programme (IGBP) and International Human Dimensions Programme on Global Change (IHDP), Louvain-la-Neuve, 2001.

GLP [Global Land Project], Global land project, in: Ojima, D., Moran, E., McConnell, W., Stafford Smith, M., Laumann, G., Morais, J., and Young, B., eds., *Science Plan and Implementation Strategy*, IGBP Report 53/IHDP Report 19, IGBP Secretariat, Stockholm, 64 pp., 2005.

Gruebler, A., Technology, in: Meyer, W.B., and Turner, B.L., II, eds., *Changes in Land Use and Land Cover: A Global Perspective*, University of Cambridge Press, Cambridge, pp. 287–328, 1994.

Guindon, B., Zhang, Y., and Dillabaugh, C., LANDSAT urban mapping based on a combined spectral-spatial methodology, *Remote Sensing of Environment*, 92, 218–232, 2004.

Guttenberg, A., Multidimensional land-use classification and how it evolved: Reflections on a methodological innovation in urban planning, *Journal of Planning History*, 1(4), 311–324, 2002.

Gwebu, T.D., Towards a theoretical exploration of the differential urbanisation model in Sub-Saharan Africa: The Botswana case, *Tijdschrift voor Economische en Sociale Geografie*, 97, pp. 418–433, 2006.

Haenni, R., Towards a unifying theory of logical and probabilistic reasoning, 4th International Symposium on Imprecise Probabilities and Their Applications (ECSQARU'05), Pittsburgh, PA, 2005.

Harvey, F., Kuhn, W., Pundt, H., Bishr, Y., and Riedemann, C., Semantic interoperability: A central issue for sharing geographic information, *Annals of Regional Science*, 33, 213–232, 1999.

Heiden, U., Segl, K., Roessner, S., and Kaufmann, H., Determination of robust spectral features for identification of urban surface materials in hyperspectral remote sensing data, *Remote Sensing of Environment*, 111, 537–552, 2007.

Henry, S., Boyle, P., and Lambin, E.F., Modelling inter-provincial migration in Burkina Faso, West Africa: The role of socio-demographic and environmental factors, *Applied Geography*, 23, 115–136, 2003.

Herold, M., Roberts, D.A., Gardner, M.E., and Dennison, P.E., Spectrometry for urban area remote sensing — development and analysis of a spectral library from 350 to 2400 nm, *Remote Sensing of Environment*, 91, 304–319, 2004.

Herold, M., Latham, J.S., Di Gregorio, A., and Schmullius, C.C., Evolving standards in land-cover characterisation, *Journal of Land-Use Science*, 1(2–4), 157–168, 2006.

Jacquin, A., Misakova, L., and Gay, M., A hybrid object-based classification approach for mapping urban sprawl in peri-urban environment, *Landscape & Urban Planning*, 84(2): 152–165, 2008.

Jansen, L.J.M., Harmonisation of land-use class sets to facilitate compatibility and comparability of data across space and time, *Journal of Land-Use Science*, 1(2–4), 127–156, 2006.

Jansen, L.J.M., Carrai, G., and Petri, M., Land-use change dynamics at cadastral parcel level in Albania: An object-oriented geo-database approach to analyse spatial developments in a period of transition (1991–2003), in: Koomen, E., Bakema, A., Stillwell, J., and Scholten, H., eds., *Modelling Land-Use Change — Progress and Applications*, *GeoJournal Library*, Vol. 90, Springer, Berlin, pp. 25–44, 2007.

Jansen, L.J.M., Groom, G., and Carrai, G., Land-cover harmonisation and semantic similarity: Some methodological issues, *Journal of Land-Use Science*, 3(2–3), 131–160, 2008.

Kavouras, M., Kokla, M., and Tomai, E., Comparing categories among geographic ontologies, *Computers & Geosciences*, 31, 145–154, 2005.

Lambin, E.F., Rounsevell, M.D.A., and Geist, H.J., Are agricultural land-use models able to predict changes in land-use intensity? *Agriculture, Ecosystems & Environment*, 82, 321–331, 2000.

Lambin, E.F., Turner, B.L., Geist, H.J., Agbola, S.B., Angelsen, A., Bruce, J.W., Coomes, O.T., Dirzo, R., Fischer, G., Folke, C., George, P.S., Homewood, K., Imbernon, J., Leemans, R., Li, X., Moran, E.F., Mortimore, M., Ramakrishnan, P.S., Richards, J.F., Skånes, H., Steffen, W., Stone, G.D., Svedin, U., Veldkamp, T.A., Vogel, C., and Xu, J., The causes of land-use and land-cover change: Moving beyond the myths, *Global Environmental Change*, 11, 261–269, 2001.

Laney, R.M., A process-led approach to modelling land change in agricultural landscapes: A case study from Madagascar, *Agriculture, Ecosystems & Environment*, 101, 135–153, 2004.

Liu, X., and Andersson, C., Assessing the impact of temporal dynamics on land-use change modelling, *Computers, Environment & Urban Systems*, 28, 107–124, 2004.

Loibl, W., Toetzer, T., Koestl, M., and Steinnocher, K., Simulation of polycentric urban growth dynamics through agents. Model concept, application, results and validation, in: Koomen, E., Bakema, A., Stillwell, J., and Scholten, H., eds., *Modelling Land-Use Change — Progress and Applications*, *GeoJournal Library*, Vol. 90, Springer, Berlin, pp. 219–235, 2007.

Loveland, T.R., Reed, B.C., Brown, J.F., Ohlen, D.O., Zhu, Z., Yang, L., and Merchant, J.W., Development of a global land-cover characteristics database and IGBP DISCover from 1 km AVHRR data, *International Journal of Remote Sensing*, 21(6–7), 1303–1330, 2000.

Lund, H.G., A 'forest' by any other name…, *Environmental Science & Policy*, 2, 125–133, 1999.

McConnell, W.J., and Moran, E.F., eds., Meeting in the middle: The challenge of meso-level integration, An international workshop on the harmonisation of land-use and land-cover classification, LUCC Report Series No. 5, Anthropological Center for Training and Research on Global Environmental Change, Indiana University and LUCC International Project Office, Louvain-la-Neuve, 2001.

Mitchell, R.B., and Rapkin, C., *Urban Traffic — A Function of Land Use*, Columbia University Press, New York, 1954.

Overmars, K.P., Linking process and pattern of land-use change. Illustrated with a case study in San Mariano, Isabela, Philippines, Ph.D. thesis, University of Leiden, 165 pp. 2006.

Overmars, K.P., Verburg, P.H., and Veldkamp, A., Comparison of a deductive and an inductive approach to specify land suitability in a spatially explicit land-use model, *Land-Use Policy*, 24, 584–599, 2007.

Piyathamrongchai, K., and Batty, M., Integrating cellular automata and regional dynamics using GIS — the Dynamic Settlement Simulation Model (DSSM), in: Koomen, E., Bakema, A., Stillwell, J., and Scholten, H., eds., *Modelling Land-Use Change — Progress and Applications*, *GeoJournal Library*, Vol. 90, Springer, Berlin, pp. 259–277, 2007.

Pontius, R.G., and Cheuk, M.L., A generalized cross-tabulation matrix to compare soft-classified maps at multiple resolutions, *International Journal of Geographical Information Science*, 20(1), 1–30, 2006.

Pontius, R.G., Boersma, W., Castella, J.-C., Clarke, K., de Nijs, T., Dietzel, C., Duan, Z., Fotsing, E., Goldstein, N., Kok, K., Koomen, E., Lippitt, C.D., McConnell, W., Sood, A.M., Pijanowski, B., Pithadia, S., Sweeney, S., Trung, T.N., Veldkamp, A., and Verburg, P.H., Comparing the input, output and validation maps for several models of land change, *Annals of Regional science*, 42, 11–47, 2008.

Rocchini, D., and Ricotta, C., Are landscapes as crisp as we may think? *Ecological Modelling*, 204(3–4), 535–539, 2007.

Roessner, S., Segl, K., Heiden, U., and Kaufmann, H., Automated differentiation of urban surfaces based on airborne hyperspectral imagery, *IEEE Transactions on Geoscience and Remote Sensing*, 39(7), 1525–1532, 2001.

Schotten, K., Goetgeluk, R., Hilferink, M., Rietveld, P., and Scholten, H., Residential construction, land use and the environment: Simulations for The Netherlands using a GIS-based land-use model, *Environmental Modelling & Assessment*, 6, 133–143, 2001.

Schuurman, N., and Leszczynski, A., Ontology-based metadata, *Transaction in GIS*, 10(5), 709–726, 2006.

Shapiro, I.D., Urban land-use classification, *Land Economics*, 35(2), pp. 149–155, 1959.

Sokal, R., Classification: Purposes, principles, progress, prospects, *Science*, 185(4157), 1115–1123, 1974.

Sowa, J.F., *Knowledge Representation: Logical, Philosophical and Computational Foundations*, Brooks Cole Publishing Co., Pacific Grove, CA, 594 pp., 2000.

UN [United Nations], International standard classification of all economic activities (ISIC), Third revision, United Nations Statistics Division, Statistical Classifications Section, New York, 1989.

UN, World urbanisation prospects, 2004 revision, UN, New York, 2004.

UN, International standard classification of all economic activities (ISIC), Fourth revision (draft), United Nations Statistics Division, Statistical Classifications Section, New York, 2006.

UN Habitat, UN-Habitat annual report 2005, Responding to the challenges of an urbanizing world, 2005. Available at www.unhabitat.org.

van der Valk, A., The Dutch planning experience, *Landscape & Urban Planning*, 58, 201–210, 2002.

Verburg, P.H., and Veldkamp, A., Spatial modelling to explore land-use dynamics — editorial, *International Journal of Geographical Information Science*, 19(2), 99–102, 2005.

Verburg, P.H., Soepboer, W., Limpiada, R., Espaldon, M.V.O., Sharifa, M., and Veldkamp, A., Land-use change modelling at the regional scale: The CLUE-s model, *Journal of Environmental Management*, 30, 391–405, 2002.

Verburg, P.H., and Overmars, K.P., Dynamic simulation of land-use change trajectories with the CLUE-s model, in: Koomen, E., Bakema, A., Stillwell, J., and Scholten, H., eds., *Modelling Land-Use Change — Progress and Applications*, *GeoJournal Library*, Vol. 90, Springer, Berlin, pp. 321–335, 2007.

Walsh, S.J., Evans, T.P., Welsh, W.F., Entwisle, B., and Rindfuss, R.R., Scale-dependent relationships between population and environment in northeastern Thailand, *Photogrammetric Engineering & Remote Sensing*, 65(1), 97–105, 1999.

Wentz, E.A., Stefanov, W.L., Gries, C., and Hope, D., Land-use and land-cover mapping from diverse data sources for an arid urban environment, *Computers, Environment & Urban Systems*, 30, 320–346, 2006.

examples of such algorithms. These algorithms are increasingly used in projecting current urbanization trends into the future. In general, these forecasting algorithms capture the growth of a city by learning how the city had grown based on satellite sensor images. It is thus important that growth patterns be correctly mapped both in space and time to provide a reliable basis for forecasting.

16.4 CURRENT METHODS FOR HIGH TEMPORAL RESOLUTION DATA ANALYSIS

The remote sensing literature is rich with change detection methods (Singh, 1989; Lu et al. 2004). These techniques include image regression, image subtraction, postclassification comparison, multidate principal components analysis, multidate tasseled cap transformation, change vector analysis, and neural networks (Fung, 1990; Lambin and Strahler, 1994; Collins and Woodcock, 1994; Gopal and Woodcock, 1996; Dai and Khorram, 1999). Numerous methods have been developed because of the variation in the types of study areas, the types of land cover changes being mapped, and the temporal and spatial resolution of the data. In turn, the variation in applications, study areas, and data constraints means that there is no such thing as a "best" technique.

Most change detection studies evaluate change between two periods (Howarth and Boasson, 1983; Green et al., 1994; Kwarteng and Chavez, 1998; Mas, 1999). Although studies that use more than two dates of imagery exist (Jensen et al., 1995; Pax Lenney et al., 1996; Collins and Woodcock, 1996), most do not use consecutive dates, nor do they extract annual estimates of land use or land cover. Furthermore, analyses that use more than two images are largely limited to AVHRR data (Eastman and Fulk, 1993; Barbosa et al., 1999; Lambin, 1996). Few methods have been developed or adapted for high temporal resolution data. A survey of the literature reveals that there are fewer than one dozen studies where the algorithm was developed for the purpose of high temporal frequency mapping (Kaufmann and Seto, 2001; Pan and Zhao, 2007; Xu et al., 2007).

The success of pixelwise change detection method is, first of all, a function of the quality of the registration (Townshend et al., 1992; Dai and Khorram, 1998). Coregistration of very long time series is difficult and can be an impediment to even the best multitemporal method. One cannot expect high accuracy of the results if the geographical location of pixels across the images is not reliable.

16.4.1 Postprocessing of Classified Images

The simplest change detection method classifies each image independently; changes are then identified by comparing the classified images. This is by far the least complex and most widely used change detection method. Although each map taken individually may be accurate, there is no guarantee that the time series will be well classified. The problem lies in the compounding of the errors across time. The time series accuracy is approximately the product of accuracy associated with each individually classified map (Singh, 1989). For example, a series of seven classified maps, each with an overall accuracy of 80%, may have a time series accuracy of 0.87, or

20% under the assumption of uncorrelated classification errors across time or space. Thus, a good single time classification on each map is no guarantee of an accurate time series.

16.4.2 Classification of Trajectories

A second change detection method consists of analyzing the stacked images concurrently and classifying the class trajectories (Singh, 1989). For example, instead of classifying a pixel as urban or agriculture, all the possible transitions between those classes (urban to urban, urban to agriculture, agriculture to urban, and agriculture to agriculture) are considered. The drawback of this method is that all pixel trajectories in time must be exhaustively stated before the classification. Furthermore, it requires having training data representing all these transitions. This technique is efficient and generates good accuracy when the time series is relatively short and contains few possible transitions. However, a long time series or the inclusion of just a few additional land cover classes can generate far too many possibilities to be manageable.

16.4.3 Econometrics Time Series

A third method models every pixel as a time series, where the time of change is estimated. For example, Kaufmann and Seto (2001) use time series econometrics to detect dates of change with better results than when the changes are obtained from postprocessing independently classified images. The method is efficient in finding the date of change on long time series but does not address which land cover types were involved in the changes.

16.4.4 The Cascade Approach

The cascade approach features a good balance between ease of use and performance in classifying long time series (Swain, 1978). It consists of sequentially classifying the land cover classes, usually in a chronological order. Past classifications are used to condition future classifications. The link between land cover at different times is parameterized with transition probabilities. The main drawback of doing the classification chronologically is that the accuracy will decrease as the time series increases. Moreover, if the first pixel is not well classified, the remaining portion of the time series, being conditioned to that misclassified pixel, is also likely to be misclassified.

Instead of a classical chronological classification, one can start by classifying the image that contains the most information relative to other images in the series. By first identifying this image, rather than the first image in the series, these high confidence classifications can be used to better classify the data in other periods where classification is more uncertain (Boucher et al., 2006). The image with the best information can be found with some information content metrics such as entropy. Thus, adding images with high information content to a time series can increase the mapping accuracy by constraining the images carrying less information.

The integration of satellite sensor data at different times is done with transition probabilities. The transition probability between land cover A and land cover B is the probability that a pixel will change from A to B within a defined period. The probability that no change occurred is the transition probability between land cover A and A or B and B. If there are L land cover types, then there are L^2 transition probabilities. It is misleading to assume that the transition probabilities are extra information that is not needed with the previous techniques; in fact, it can be shown that postprocessing independently classified images is equivalent of setting the transition probability from A to B to the global proportion of B. Not explicitly choosing a set of transition probabilities is simply equivalent to choosing an implicit, and likely incorrect, set of transition probabilities. Bruzzone and Serpico (1997) provide a technique for estimating these transition probabilities.

The cascade approach is the most scalable method for long time series. The algorithm complexity increases approximately linearly with the length of the time series. Furthermore, it does not require radiometric corrections or that the ground truth be colocated as required by the trajectory methods. It does, however, require the additional effort of obtaining the transition probability for any land cover to change into any other land cover in one time step. Ideally, each remote sensing image should have been taken at regular intervals, say every year in December. The transition probability matrix must be adjusted if the images are distributed irregularly in time.

A more rigorous approach would be to jointly classify all the dates through an iterative method such as expectation-maximization; such an iterative approach would be prohibitively and computationally costly for long time series and large images.

16.4.5 Issues of Spatial Resolution

The techniques discussed above assumed that the images have the same spatial resolution. This may not always be the case. For example, combining Landsat MSS with Landsat Thematic Mapper imagery has the additional challenges of integrating images with different radiometric and spatial resolution. Newer sensors provide spatial resolution that is finer than existing sensors. Combining images from sensors with different spatial resolution pose additional challenges that will be increasingly relevant if we wish to take advantage of the available information. At this point, one can either adjust the spatial scale of the images by upscaling or downscaling so that they will share the same spatial resolution.

16.5 ACCURACY ASSESSMENT OF HIGH TEMPORAL RESOLUTION TIME SERIES

A classified map is only useful if associated with an accuracy assessment. Moreover, that accuracy assessment must target the mapping objectives. Most change detection studies address issues of accuracy, but few address the issue of accuracy through time. In addition to cross-sectional accuracy, such as the confusion matrix and the kappa coefficient, the classification of land covers over time must also be accurate. The temporal component becomes as important as the spatial component when it is necessary to

know both when and where changes have occurred. Classifying a time series of remote sensing images differs from classifying each image independently. Independently classifying each image provides an accurate mapping of the urban area at each time, that is, cross-sectional accuracy. It may provide reasonable estimates of the rates of overall growth between two periods. It will not, however, provide an accurate temporal pattern of growth, that is, where, when, and how the changes occurred. The reader is referred to Biging et al. (1999) for a perspective on accuracy for change detection.

Ideally, a time series of georeferenced ground truth data would exist for each pixel in the training data set. Having enough of these fully known time series greatly eases the validation of the temporal mapping. Take the example of mapping five land covers (e.g., water, vegetation, agriculture, urban, and transition) over 8 years, from 1988 to 1996, in the Pearl River Delta, China. Figure 16.2 shows the accuracy of the time series as a function of its length; the accuracy assessment is performed on more than 2000 known time series with a fivefold cross-validation. The solid and the dashed lines are obtained with the cascade approach, whereas the gray line is obtained by classifying each image independently. Two measures of accuracy are displayed; the first one is the accuracy in mapping change. In this case, a time series is considered to be well classified if the dates of change have been correctly identified. The land covers involved in the change are not considered at this point. A second accuracy metric, also shown in Figure 16.2 (right), considers a time series well classified only if all the land cover types have been correctly identified for all points in time. This measures the *type* of land cover change — change from what to what land cover classes — as well as *when* the change occurred. This is a more stringent accuracy metric, but it is also more relevant when linking changes in land covers with socioeconomic policies.

As the length of the time series increases, the accuracy generally decreases. The rate of decrease is higher when the images are independently classified (shown by the gray line) than when the cascade approach is used (shown by the solid and dashed lines). For the cascade approach, accuracy is also a function of the sequencing. For instance, classifying the most informed pixels first (solid line) delivers a higher accuracy than doing a chronological classification (dashed line). Using temporal

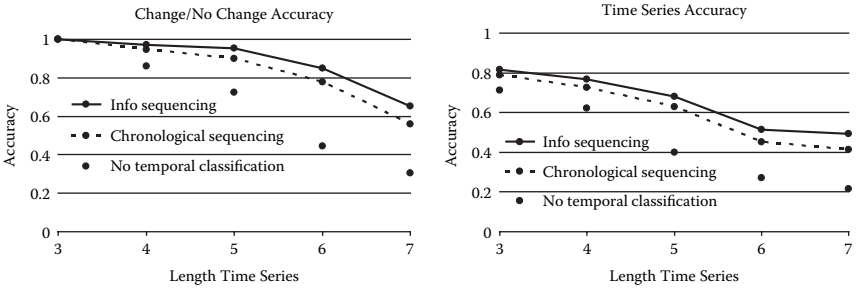

FIGURE 16.2 Computed accuracy for increasing length of time series for five land covers with a cascade approach with information-based sequencing (solid line), a chronological approach, and independently classified images (gray lines). Left: change/no change accuracy. Right: full time-series accuracy.

information — in this case, transition probabilities — increases the accuracy of a long time series.

For a given length of a time series, a useful accuracy indicator is the percentage of time series containing at least *n* consecutive pixels that are correctly classified. Consider the examples in Figure 16.2 with a time series length of seven. The first point in Figure 16.3 shows the percentage of time series that have at least two consecutive times, out of the seven, that are well classified. That same accuracy is computed for a consecutive sequence of three, four, up to seven, which yields the same values as in Figure 16.2.

In the most difficult case, where the ground truth data are not georeferenced through time, the validation of the time series becomes more difficult because there are no data to compare the classification over time. In that case, one cannot obtain a precise accuracy number. The issue of how to assess time series accuracy for long time series and high temporal frequency data will require significant research, especially as the satellite record continues to lengthen. New metrics, albeit imperfect, will be required that describes time series accuracy. One alternative is to search and count how many impossible or very unlikely transitions, based from expert knowledge, have been mapped (Liu and Zhou, 2004). For example, if it is impossible for an urban land cover to change into a forest within 2 years, one can then scan the classified maps searching for such a transition. If some are found, it is indicative of some of the errors contained in the map. Tabulating such impossible transitions would give the user a broad idea about its accuracy in mapping change patterns.

16.6 CONCLUSION

As the physical size and number of cities continue to grow, their impacts on the environment will also increase. The questions and challenges generated by these fast-growing cities required high-temporal resolution time series, and algorithms can

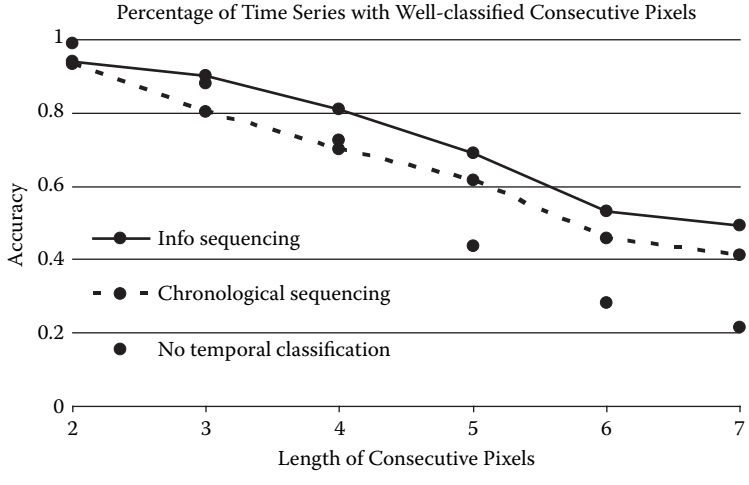

FIGURE 16.3 Percentage of time series with at least *n* consecutive years that are well-classified. The number of consecutive dates *n* is set to vary between 2 and 7.

efficiently process these images. Learning what influenced the growth patterns and linking urban growth with sociopolitical or economic events is essential in developing policies that will lead to more sustainable built places.

New methods for classifying and assessing these long time series are needed to reduce the time and effort required in generating these high-temporal resolution images. Most of the development about multitemporal mapping focuses on classifying only two or three images when, in fact, many more are needed to link urban growth with social and economics policies.

REFERENCES

Barbosa, P.M., Gregoire, J.-M., and Pereira, J.M.C., An algorithm for extracting burned areas from time series of AVHRR GAC data applied at a continental scale, *Remote Sensing of Environment*, 69, 253–263, 1999.

Batty, M., The size, scale, and shape of cities, *Science*, 319, 769–771, 2008.

Beauregard, R., Theorizing the global-local connection, in: Knox, P.L., and Taylor, P.J., eds., *World Cities in a World System*, Cambridge University Press, Cambridge, pp. 232–248, 1995.

Beaverstock, J.V., Smith, R.G., Taylor, P.J., Walker, D.R.F., and Lorimer, H., Globalization and world cities: Some measurement methodologies, *Applied Geography*, 20, 43–63, 2000.

Biging, G.S., Chrisman, N.R., Colby, D.R., Congalton, R.G., Dobson, J.E., Fergurson, R.L., Goodchild, M.F., Jensen, J.R., and Mace, T.H., in: Khorram, S., ed., *Accuracy Assessment of Remote Sensing-Detected Change Detection*, American Society for Photogrammetry and Remote Sensing, 1999.

Boucher, A., Seto, K.C., and Journel, A.G., A novel method for mapping land cover changes; Integrating space and time with geostatistics, *IEEE Transactions on Geosciences and Remote Sensing*, 44, 3427–3435, 2006.

Bruzzone, L., and Serpico, S.B., An iterative technique for the detection of land-cover transitions in multitemporal remote-sensing images, *IEEE Transactions on Geosciences and Remote Sensing*, 35, 858–867, 1997.

Clarke, K.C., Hoppen, S., and Gaydos, L., A self-modifying cellular automaton model of historical urbanization in the San Francisco Bay area, *Environment and Planning B: Planning and Design*, 24, 247–261, 1997.

Collins, J.B., and Woodcock, C.E., Change detection using the Gramm-Schmidt transformation applied to mapping forest mortality, *Remote Sensing of Environment*, 50, 267–279, 1994.

Collins, J.B., and Woodcock, C.E., An assessment of several linear change detection techniques for mapping forest mortality using multitemporal Landsat TM data, *Remote Sensing of Environment*, 56, 66–77, 1996.

Dai, X.L., and Khorram, S., The effects of image misregistration on the accuracy of remotely sensed change detection, *IEEE Transactions on Geosciences and Remote Sensing*, 36, 1566–1577, 1998.

Dai, X.L., and Khorram, S., Remotely sensed change detection based on artificial neural networks, *Photogrammetric Engineering and Remote Sensing*, 65, 1187–1194, 1999.

Eastman, R.J., and Fulk, M., Long sequence time series evaluation using standardized principal components, *Photogrammetric Engineering and Remote Sensing*, 59, 1307–1312, 1993.

Fragkias, M., and Seto, K.C., Modeling urban growth in data-sparse environments: A new approach, *Environment and Planning B*, 34, 858–883, 2007.

Fung, T., An assessment of TM imagery for land-cover change detection, *IEEE Transactions on Geoscience and Remote Sensing*, 28, 681–684, 1990.

Gopal, S., and Woodcock, C.E., Remote sensing of forest change using artificial neural networks, *IEEE Transactions on Geoscience and Remote Sensing*, 34, 398–404, 1996.

Green, K., Kempka, D., and Lackey, L., Using remote sensing to detect and monitor land-cover and land-use change, *Photogrammetric Engineering and Remote Sensing*, 60, 331–337, 1994.

Homewood, K., Lambin, E.F., Coast, E., Kariuki, A., Kikula, I., Kivalia, J., Said, M., Serneels, S., and Thompson, M., Long-term changes in Serengeti-Mara wildebeest and land cover: Pastoralism, population, or policies? *Proceedings of the National Academy of Sciences*, 98, 12544–12549, 2001.

Howarth, P.J., and Boasson, E., Landsat digital enhancements for change detection in urban environments, *Remote Sensing of Environment*, 13, 149–160, 1983.

Jabareen, Y.R., Sustainable urban forms: Their typologies, models, and concepts, *Journal of Planning Education and Research*, 26, 38–52, 2006.

Jensen, J.R., Rutchey, K., Koch, M.S., and Narumalani, S., Inland wetland change detection in the everglades water conservation area 2A using a time series of normalized remotely sensed data, *Photogrammetric Engineering and Remote Sensing*, 51, 199–209, 1995.

Kaufmann, R.K., and Seto, K.C., Change detection, accuracy and bias in a sequential analysis of Landsat imagery in the Pearl River Delta, China: Econometric techniques, *Agriculture, Ecosystem Environment*, 85, 95–105, 2001.

Knox, P.L., The restless urban landscape: Economic and sociocultural change and the transformation of metropolitan Washington, D.C., *Annals of the Association of American Geographers*, 81, 181–209, 1991.

Kwarteng, A.Y., and Chavez, P.S., Jr., Change detection study of Kuwait City and environs using multi-temporal Landsat Thematic Mapper data, *International Journal of Remote Sensing*, 19, 1651–1662, 1998.

Lambin, E.F., Change detection at multiple temporal scales: Seasonal and annual variations in landscape variables, *Photogrammetric Engineering and Remote Sensing*, 62, 931–938, 1996.

Lambin, E.F., Rounsevell, M., and Geist, H., Are agricultural land-use models able to predict changes in land use intensity? *Agriculture, Ecosystems & Environment*, 82, 321–331, 2000.

Lambin, E.F., and Strahler, A.H., Change-vector analysis in multitemporal space: A tool to detect and categorize land-cover change processes using high temporal-resolution satellite data, *Remote Sensing of Environment*, 48, 231–244, 1994.

Landis, J., and Zhang, M., The second generation of the California Urban Futures Model: Part 1. Model logic and theory, *Environment and Planning B: Planning and Design*, 25, 657–666, 1998.

Liu, H., and Zhou, Q., Accuracy analysis of remote sensing change detection by rule-based rationality evaluation with post-classification comparison, *International Journal of Remote Sensing*, 25, 1037–1050, 2004.

Lo, C.P., and Faber, B.J., Integration of Landsat Thematic Mapper and census data for quality of life assessment, *Remote Sensing of Environment*, 62, 143–157, 1997.

Lu, D., Mausel, P., Brondízio, E., and Moran, E., Change detection techniques, *International Journal of Remote Sensing*, 25, 2365–2407, 2004.

Lunetta, R.S., Johnson, D.M., Lyon, J.G., and Crotwell, J., Impacts of imagery temporal frequency on land-cover change detection monitoring, *Remote Sensing of the Environment*, 89, 444–454, 2004.

Makse, H.A., Havlin, S., and Stanley, H.E., Modeling urban growth patterns, *Nature*, 377, 608–612, 1995.

Marcotullio, P.J., Asian urban sustainability in the era of globalization, *Habitat International*, 25, pp. 577–598, 2001.

Mas, J.-F., Monitoring land-cover changes: A comparison of change detection techniques, *International Journal of Remote Sensing*, 20, 139–152, 1999.

Nagendra, H., Munroe, D.K., and Southworth, J., From pattern to process: Landscape fragmentation and the analysis of land use/land cover change, *Agriculture, Ecosystems, and Environment*, 101, 111–115, 2004.

Pan, X., and Zhao, Q., Measurement of urbanization process and the paddy soil loss in Yixing city, China between 1949 and 2000, *CATENA*, 69, 65–73, 2007.

Pax Lenney, M., Woodcock, C.E., and Collins, J.B., The status of agricultural lands in Egypt: The use of multitemporal NDVI features derived from Landsat TM, *Remote Sensing of Environment*, 56, 8–20, 1996.

Reid, R.S., Kruska, R.L., Muthul, N., Taye, A., Wotton, S., Wilson, C. J., and Mulatu, W., Land-use and land-cover dynamics in response to changes in climatic, biological and socio-political forces: The case of southwestern Ethiopia, *Landscape Ecology*, 15, 339–355, 2000.

Schneider, A., and Woodcock, C., Compact, dispersed, fragmented, extensive? A comparison of urban growth in twenty-five global cities using remote sensing data, pattern metrics, and census information, *Urban Studies*, 45, 659–692, 2008.

Schneider, A., Seto, K.C., and Webster, D., Urban growth in Chengdu, western China: Application of remote sensing to assess planning and policy outcomes, *Environment and Planning B*, 32, 323–345, 2005.

Seto, K.C., and Kaufmann, R.K., Using logit models to classify land cover and land-cover change from Landsat Thematic Mapper, *International Journal of Remote Sensing*, 26, 563–577, 2005.

Singh, A., Digital change detection techniques using remotely-sensed data, *International Journal of Remote Sensing*, 10, 989–1003, 1989.

Swain, P.H., Bayesian classification in a time-varying environment, *IEEE Transactions on Systems, Man, and Cybernetics*, 8, 879–883, 1978.

Townshend, J.R.G., Justice, C.O., Gurney, C., and McManus, J., The impact of misregistration on change detection, *IEEE Transactions on Geoscience and Remote Sensing*, 30, 1054–1060, 1992.

Wang, Y.Q., and Zhang, X.S., A dynamic modeling approach to simulating socioeconomic effects on landscape changes, *Ecological Economics*, 140, 141–162, 2001.

Xu, C., Liu, M., Zhang, C., An, S., Yu, W., and Chen, J.M., The spatiotemporal dynamics of rapid urban growth in the Nanjing metropolitan region of China, *Landscape Ecology*, 22, 925–937, 2007.

13 Comparison of Global Urban Maps

David Potere and Annemarie Schneider

CONTENTS

13.1 INTRODUCTION

Before 2000, if one asked the question, "How much of the Earth is urban, and where are these urban places located?" the only global map available was a digitized mosaic of maps and charts from the 1960s through the 1990s [Digital Chart of the World (DCW) or Vector Map Level Zero; Danko, 1992]. That landscape has changed. International research groups from both government and academia have produced eight global-scale urban maps and at least two global-scale urban-related maps; three of these maps were released in early 2008. These new maps have been made possible by the availability of global coarse-resolution (250 m–2 km) daytime and nighttime satellite remote sensing observations, the worldwide collection of census results and other urban-related map layers that are in a geographic information system (GIS) format, and increases in computational power and the effectiveness of semiautomated mapping techniques. The new methods and data sources offer, for the first time, a planetary perspective on the spatial extent and distribution of urban

land. Because this synoptic perspective is quite new and the community of map users is diverse and expanding, it is important that we step back from the limited perspective of individual mapping efforts and strengthen our understanding of the similarities and differences among the suite of available global urban maps. The aim of this chapter is to conduct that comparison by using a wide array of map agreement measures across a range of spatial resolutions and geographic regions, providing those who use these maps with the diagnostic tools to determine the map or set of maps most suited to their application.

We begin this chapter by briefly summarizing the methodologies and underlying source data for each of the eight existing global urban maps (Section 13.2). In part because of the complexity of the label "urban," there is a great deal of heterogeneity in the approaches used by each research group. Next, we bring these maps into focus by creating a common analysis environment and exploring each of the maps at three scales: at the level of the city, the continental region, and the globe (Section 13.3). We find evidence for a surprisingly high degree of difference across all world regions and map resolutions. For example, these maps vary by an order of magnitude in their estimates of the total extent of urban land, from 0.3 to 3.5 million km^2 (Figure 13.1). In the following section, we explore the structure underlying these bulk differences by making all of the 28 possible intermap comparisons (Section 13.4). We use three different approaches to measuring map agreement: (1) pixel-by-pixel comparisons, (2) national-level comparisons of urban extent, and (3) multiresolution comparisons of urban extent based on a global system of hexagonal cells. The intermap differences that we uncover in Sections 13.3 and 13.4 point toward the need for a common urban taxonomy and a global map assessment based on medium- and high-resolution validation data. In the final analytical section of this chapter, we present some early results from an evaluation of the eight coarse-resolution global urban maps against high-resolution Google Earth (GE) imagery and a set of 120 medium-resolution city maps based on Landsat imagery (Section 13.5). We conclude with a summary of our findings thus far, and a brief sketch of the road ahead (Section 13.6).

13.2 METHODOLOGIES BEHIND GLOBAL URBAN MAPPING EFFORTS

Since 1990, there have been several attempts to estimate the total urban extent of the Earth using national- and regional-scale tabular methods. The basic approach is to combine urban population estimates from census data with regional estimates of urban population density. Applying this technique to country-level urban population estimates from the United Nations (UN) and urban density estimates from unnamed sources, Douglas (1994) arrived at a global figure of 2.47 million km^2 of urban land circa 1985. Grübler (1990) used similar global values on urban populations in combination with a small collection of city-scale studies on the built environment to estimate a global total of 1.3 million km^2 for urban area circa 1990. Angel et al. (2005) used satellite imagery and census data to calculate regional urban population densities, and combined these densities with a global dataset of city populations circa 2000 to arrive at an estimate of approximately 400,000 km^2 for urban land within cities of 100,000 people or more.

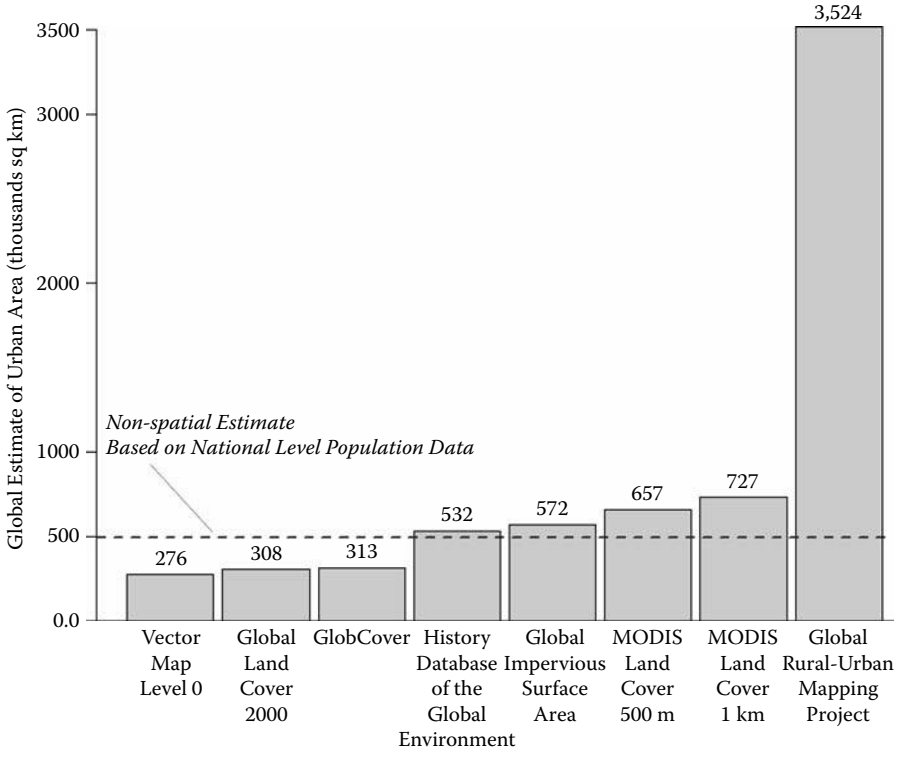

FIGURE 13.1 Global extents for eight spatially explicit estimates of urban area (thousands of km^2): Vector Map Level Zero, Global Land Cover 2000 v1.1, GlobCover, History Database of the Global Environment v3, Nighttime Lights–based Global Impervious Surface Area beta product, Moderate Resolution Imaging Spectroradiometer (MODIS) 500 m Urban Land Cover v5 2001, MODIS 1 km Urban Land Cover v4 2001, and Columbia University's Global Rural-Urban Mapping Project version alpha. Above each bar is the estimate of global extent in thousands of km^2. The dotted line is an estimate of urban area based on national-level urban statistics (UN Population Division 2005) and regional-level urban population densities for the year 2000 (Angel et al. (2005). Note the order of magnitude difference for these are 8 totals. (From Potere, D. and Schneider, A. *GeoJournal*, 69: 55–80, 2007. With permission.)

The first attempt to build a global land cover map based on satellite observations began with the Global Land Cover Characteristics (GLCC) database, a joint effort between the United States Geological Survey (USGS) and the European Joint Research Center (JRC), based on one year (1992–1993) of observations from the National Aeronautics and Space Administration (NASA) Advanced Very High Resolution Radiometer (AVHRR) instrument (Loveland et al., 2000). Because the vegetation indices used by GLCC are not particularly well suited to classifying nonvegetated areas, the GLCC group chose not to map urban areas (Loveland et al., 2000). Instead, GLCC rasterized the urban polygons from the DCW, which is a public-release version of the Vector Map Level Zero (Danko, 1992). The same approach was used by the University of Maryland (UMD) group in their global AVHRR-based

land cover map (Hansen et al., 2000a). Both the GLCC and the UMD maps are not included here; instead, we include VMAP level 0, which is the common data source underlying their urban classes.

Table 13.1 describes the eight global urban maps and two urban-related maps included in this chapter, together with the acronyms that will be used from this point forward. They are arranged in order of increasing global urban extent (from left to right in Figure 13.1 and top to bottom in Table 13.1), with the two urban-related maps listed in the last two rows. Each of these maps approaches urban land from a unique perspective (Table 13.2), using methodologies that draw on a sometimes-overlapping pool of remote sensing imagery, ground-based census results and GIS data layers, and other global maps. Three of these maps — Vector Map Level Zero (VMAP0), Global Landcover 2000 (GLC00), and GlobCover (GLOBC) — are general multiclass land cover maps that include an urban class. Three are binary (presence/absence) maps devoted entirely to urban land: Moderate Resolution Imaging Spectroradiometer (MODIS) Urban Land Cover 1 km (MOD1K), MODIS 500 m (MOD500), and Global Rural-Urban Mapping Project (GRUMP).* Two maps, Global Impervious Surface Area Map (IMPSA) and History Database of the Global Environment (HYDE3), characterize urban land as a continuous variable: the fraction of impervious surface and the fraction of urban land, respectively. The remaining two maps, LandScan 2005 (LSCAN) and Nighttime Lights (LITES), measure continuous variables closely associated with urban land: the ambient human population (defined as the population of a given area averaged over a 24-hour period) and the intensity of stable nighttime illumination, respectively. The majority of the maps are conducted at approximately 1-km spatial resolution, with the exception of HYDE3 (approximately 10 km), MOD500 (approximately 500 m), and GLOBC (approximately 300 m).

These maps are beset by the problem of a consistent operational definition of urban areas. Places that can be described as urban include: densely settled city cores, tree-covered suburbs, slum neighborhoods, and the "urban villages" of sub-Saharan Africa. There is no generally accepted set of criteria for creating a binary urban-rural classification. This challenge is not unique to the land cover mapping community; the UN Population Division faces the same problem in their national-level census estimates of urban populations. In a review of the UN's statistics on urban populations, Utzinger and Keiser (2006) point out that 228 member nations use at least 10 categories of urban population classification, drawing on various combinations of population size and density, administrative boundaries, and economic activities. The map legends used by our eight global urban maps reveal the same lack of consensus and precision regarding a definition of the urban land category — for example, VMAP0 uses the term "built-up," GLC00 and GLOBC make use of "artificial surfaces and associated areas," MOD1K and MOD500 use "urban and built-up," and GRUMP uses "urban extent." Although not reflected in these simple legends, each of the eight global urban maps model urban areas based on a complex matrix of attributes, including: (1) remotely sensed daytime

* Although both MODIS land cover maps include 17 land cover classes, the urban class is created in a wholly independent process from the other 16 land cover categories (Schneider et al., 2003, 2005, forthcoming).

TABLE 13.1
The Eight Global Urban Maps Examined in this Research in Order of Increasing Global Urban Extent, and the Two Urban-Related Maps (Last Two Codes)

Code	Map/Paper	Producer	Specifications/Source
VMAP0	Vector Map Level Zero (Danko, 1992)	US National Geospatial-Intelligence Agency (US)	Land cover and map features, vector, 1:1,000,000 scale, geographic projection, (http://geoengine.nga.mil/)
GLC00	Global Land Cover 2000 v1.1 (Bartholome and Belward, 2005)	European Commission Joint Research Center (EC-JRC)	Land cover, 22 classes, raster, 32″ arc-seconds (~1 km), geographic projection, (http://www-gvm.jrc.it/glc2000/)
HYDE3	History Database of the Global Environment v3 (Goldewijk, 2005)	Netherlands Environmental Assessment Agency	Global fraction of urban land, raster, 5′ arc-minutes (~10 km), geographic projection, *http://www.mnp.nl/hyde/*
IMPSA	Global Impervious Surface Area (2000–2001) (Elvidge et al., 2007)	Earth Observation Group, US National Geophysical Data Center (NGDC) (US NOAA)	Global fraction of urban land, raster, 30″ arc-seconds (~1 km), geographic projection, (http://www.ngdc.noaa.gov/dmsp/)
MOD500	MODIS Urban Land Cover 500 m (2001v5) (Schneider et al., forthcoming)	University of Wisconsin and Boston University (US NASA)	Global urban land, Raster, ~500 m resolution sinusoidal projection (http://www.sage.wisc.edu)
MOD1K	MODIS Urban Land Cover 1 km (2001v4) (Schneider et al., 2003, 2005)	Boston University Department of Geography (US NASA)	Global urban land, raster, ~1 km resolution, sinusoidal projection (http://www-modis.bu.edu/landcover/)
GLOBC	GlobCover	EC-JRC	Land cover, 22 classes raster, 10″ arc-seconds (~300 m), geographic projection (http://ionia1.esrin.esa.int/)
GRUMP	Global Rural-Urban Mapping Project, alpha	Earth Institute at Columbia University (US-UN)	Urban/rural map, raster, 30″ arc-seconds (~1 km), geographic projection, (http://sedac.ciesin.columbia.edu/gpw/)
LITES	DMSP-OLS Nighttime Lights v2 (2001, F15 sat.)	NGDC (US NOAA)	Nighttime illumination intensity, raster, 30″ arc-seconds (~1 km), geographic projection, (http://www.ngdc.noaa.gov/dmsp/)
LSCAN	LandScan 2005	US Oak Ridge National Laboratory (US DOE)	Ambient human population, raster, 30″ arc-seconds (~1 km), geographic projection, (http://www.ornl.gov/sci/landscan/)

Abbreviations: DOE, Department of Energy; DMSP-OLS, Defense Meteorological Satellite Program-Operational Line Scanner; EC, European Commission; MODIS, Moderate Resolution Imaging Spectroradiometer; NASA, National Aeronautics and Space Administration; NOAA, National Oceanographic and Atmospheric Administration; UN, United Nations.

TABLE 13.2
Major Inputs Used to Produce the Eight Global Urban Maps and LandScan

	Primarily image-based				Combination				Map-based
	MOD500	MOD1K	GLOBC	GLC00	IMPSA	LSCAN	HYDE3	GRUMP	VMAP0
Imagery									
High Res.						Various[a]			
Medium Res.	Landsat	Landsat		Landsat	Landsat[b]	GeoCover[c]			
Coarse Res.	MODIS 500m, '01	MODIS 1km, '01	MERIS 300m, '05	SPOT4-VGT 2001					
Night Lights		1996-97		1994-95	2000-01[d]			1994-95	
Census & Maps									
Census						US[e]	UN[f]	UN[f]	
Maps / Charts	X	X	X			X		X	X
City Gazetters						X		X	X
Road Vectors			X			X			
Global Maps									
VMAP				level 0		level 1[g]	level 0	level 0	
MOD1K						X			
GLC-2000			X				X		
LandScan					2004		2005		

[a] various commercial and government high resolution satellites.
[b] Landsat impervious surface maps from the National Land Cover Dataset.
[c] GeoCover's 30 meter land cover product, based on circa-1990, 2000 Landsat.
[d] Radiance-calibrated Nighttime Lights product.
[e] US Census Bureau, International Programs Center.
[f] UN Population Division (2005), Urban Population Estimates.
[g] VMAP level 0 is global in extent and at 1:1,000,000 scale, VMAP level 1 products are 1:250,000 regional maps.

Note: The four leftmost columns are primarily based on expert and semiautomated classification of satellite imagery, the rightmost column relies on paper maps and charts, and the middle columns use a combination of both. LITES is not listed for the sake of brevity, and is based entirely on nighttime lights data.

observation of impervious surfaces,* (2) remotely sensed nighttime observation of artificial illumination, and (3) map layers characterizing the built environment or census data. Only one of these attributes is central to the urban models of every global urban map: impervious surface area or built environment. The built environment is visible in the daytime satellite imagery that underlies the VMAP0, GLC00, GLOBC, IMPSA, MOD500, MOD1K, and LSCAN maps. Although GRUMP and HYDE3 do not directly include daytime imagery in their models, they rely heavily on maps that do (VMAP0, GLC00, and LSCAN). For the remainder of this chapter, the term "urban" refers the human built environment or impervious surface. For the six binary raster

* Impervious surfaces reduce the penetration of rainwater into the soil to levels below that of undisturbed land. Examples of impervious surfaces can involve many forms of human disturbance, including: paved and dirt roads, parking lots, buildings, airport runways, etc. Ridd (1995) provides an excellent introduction to impervious surface from the perspective of remote sensing.

maps considered here, the "urban" label means that a pixel is more than 50% impervious surface. For the two continuous maps, the actual amount of impervious surface area is described by the "percent-urban" label. Table 13.2 lays out the complex relationships between the global maps and their input data, and serves as a reference point for a more detailed discussion of their methodologies.

VMAP0 (Table 13.2, rightmost column), is the earliest global map that includes an urban class. It is a GIS product created by the United States through digitizing a large collection of roughly 1:1,000,000 scale maps and navigational charts starting in the 1960s. The DCW map was based on the 1992 version of VMAP0 (Danko, 1992). The urban polygons of VMAP0 often trace the outer edge of urban areas, without delineating interior patches of nonurban land. These urban polygons are not labeled with the date of the underlying map from which they were extracted, and are sometimes poorly geolocated. Because VMAP0 was designed to support the needs of the US government, it also contains a higher level of detail within regions of national interest to the United States (e.g., Russia). Nevertheless, because VMAP0 is a global dataset and a conservative estimate of urban land area, it is used as part of the input stream for GLC00, GRUMP, and HYDE3. LSCAN relies on higher resolution VMAP products (levels 1 and 2), which are at scales of 1:250,000 and are based on more recent imagery.

The four columns on the left side of Table 13.2 describe maps that draw on a full year of multispectral coarse-resolution daytime satellite imagery. MOD500 and MOD1K are derived from the supervised classification of bimonthly data spanning the year 2001 from the MODIS instrument aboard NASA's *Terra* and *Aqua* platforms (Schneider et al., 2003, 2005, forthcoming). MOD500 is based on newly released 463-m resolution nadir bidirectional reflectance factor-adjusted data (NBARs), and MOD1K is based on the 927-m resolution NBARs data (Schaaf et al., 2002). Both MOD1K and MOD500 use manual interpretation of medium-resolution (30 m) Landsat imagery and other ancillary datasets to construct training sites for supervised classifications. GLC00 is also built using 1 year of 1-km resolution data from 2001, but GLC00 draws from the Satellite Pour l'Observation de la Terre (SPOT4) VEGETATION instrument. The GLC00 map was completed by 18 separate production regions, each relying primarily on unsupervised classification methods (Bartholome and Belward, 2005). The GLOBC map relies on 300-m resolution data spanning May 2005–April 2006 from the Medium Resolution Imaging Spectrometer (MERIS) instrument aboard the ENVISAT platform. In general, the GLOBC methodology exploits unsupervised approaches similar to those of GLC00. The exception for GLOBC is Australia, where it appears that the road network and other map layers were included during processing. Over several large regions and countries, GLOBC has relied on the earlier GLC00 map for the urban class, including: South America, much of Western Asia, much of Africa, and all of India and Japan. The MOD1K and GLC00 maps incorporate LITES data to constrain their classifications (1996–1997 and 1994–1995 LITES, respectively), whereas MOD500 is the first global map to rely entirely on daytime multispectral MODIS observations.

The remaining maps in the center columns of Table 13.2 use a combination of remote sensing and ground-based inputs. GRUMP integrates VMAP0, thresholded 1994–1995 LITES, census data, and a variety of ancillary GIS datasets such as city gazetteers (Center for International Earth Science Information Network, 2004). IMPSA models impervious surface area globally by using LSCAN 2004

and radiance-calibrated LITES 2000–2001 data (Elvidge et al., 2007). The IMPSA model was trained using a medium-resolution Landsat map of impervious surface area for the United States produced by the USGS as part of the National Land Cover Data set project (Vogelmann, 2001; Yang et al., 2003). HYDE3 combines LSCAN 2005 population density with 2003 UN national urban population estimates, city gazetteers, and assumptions about mean urban population densities to estimate the fraction of urban land cover (Goldewijk, 2001, 2005).

One additional global land cover map that also contains a representation of urban areas is GeoCover Land Cover (LC). GeoCover LC is a supervised land cover classification of the GeoCover image archive, a near-global collection of circa 1990 and 2000 Landsat imagery (Tucker et al., 2004). Although the underlying 30-m resolution imagery is freely available (Global Land Cover Facility, 2007), the land cover classification is a commercial product produced under NASA contract. GeoCover LC includes a class for "urban/built-up, developed areas greater than 60 m wide," which was produced by digitizing urbanized areas visible in the Landsat imagery. GeoCover LC serves as an input into the LandScan product stream, but is not included in this analysis because it is not a truly global dataset* and its prohibitive cost makes widespread use impractical.

The two other products included in this study, LITES and LSCAN, map urban-related variables. LSCAN models the ambient human population using GeoCover LC, MOD1K, VMAP level 1 and above, GIS census products, Landsat data, and high-resolution imagery (1–5 m). Although LSCAN was originally conceived during work related to LITES (Sutton et al., 1997; Dobson et al., 2000), the current LSCAN versions do not rely on LITES data (Bhaduri et al., 2002). LSCAN is an ongoing project, and each year the LSCAN team releases a new global map based on the latest census estimates from the International Programs Center at the US Census Bureau and new urban imagery and map layers.

The LITES map is created by the Earth Observation Group at the National Geophysical Data Center (NGDC) using data from the Defense Meteorological Satellite Program's Operational Line Scanner (DMSP-OLS), a nighttime imaging satellite that has a primary mission of monitoring cloud cover by moonlight. NGDC models the average illumination intensity of human settlements and activities for all cloud-free observations within a given year by compositing many individual images at 2.2-km resolution, later resampled to 1 km (Elvidge et al., 2001; NGDC, 2007). The DMSP-OLS instrument applies a variable gain during flight, and the gain settings are only monitored on a select number of orbits. Because of these variable gain settings, it is not possible to convert standard LITES composites into radiance values. However, the NGDC group also produces a smaller number of radiance-calibrated composites using fixed-gain imagery (Elvidge et al., 2007). Whether the composites are radiance-calibrated, thus far, the relationship between LITES and urban areas appears to be complex and context-dependent (Imhoff et al., 1997; Henderson et al., 2003;

* GeoCover LC is often obscured by clouds in the tropics, uses other datasets for coverage of the United States, and has no land cover data for regions above 60°N, over most of Europe (except for a land–water mask), all of Australia and New Zealand, and much of Central Asia.

Schneider et al., 2003; Small et al., 2005), which is why the IMPSA team draws on LSCAN as well as LITES data for their urban model.

13.3 PORTRAITS OF THE GLOBAL URBAN MAPS ACROSS SCALES — FROM CITIES TO CONTINENTS

13.3.1 Map Preparation

Not all of the global urban maps share a common geospatial model (see Table 13.1, rightmost column). For our analytical environment, we selected a geographic projection, 30″ arc-second raster (approximately 0.86 km^2 cells at the equator), and the WGS-84 datum. LITES, LSCAN, GRUMP, and IMPSA required no modification. HYDE3 was downsampled to 30″ arc-second cells from 5 arc-minute cells (approximately 9.27 km wide at the equator). The MODIS LC group provided a geographic reprojection of their native sinusoidal 1 km and 500 m products. For the 500 m MODIS product and the 300 m GLOBCOVER map, we aligned the 15″ arc-second and 10″ arc-second grids (respectively) with the common 30″ arc-second grid. Although GLC00 is in a geographic projection, the pixel size was resampled from 32.14″ arc-seconds to 30″ arc-seconds. Finally, the VMAP0 product is in a vector format, and was converted to raster. All of the modified products were checked against their native counterparts at various stages, and biases were determined to be negligible throughout the map preparation process.

To make comparisons across maps at continental, subcontinental (regional), and national scales, we needed a coarse-resolution map of international boundaries. Unfortunately, few options exist at 1-km spatial resolution with a consistent land and water boundary. We opted to use the international boundary grid produced and distributed by the LSCAN program, as it is at 30″ arc-second resolution and is updated annually. To account for significant differences in how each map delineated land and water, we created custom international border and land-water boundary files for each product. In this step, land pixels from each map that fell outside of the LSCAN land-water mask were retained as land and assigned to the country of their nearest land neighbor in the LSCAN country boundary file. This procedure prevents the land water mask from eliminating some of the coastal areas within several of the maps, which can result in serious underestimation of urban land.

We then cross-walked the LSCAN country names (derived from the US Census Bureau) to their counterparts in the system used by the UN Statistics Division and the International Organization for Standardization (UN Statistics Division, 2007). These UN country codes are accompanied by a 20-region scheme for delineating world regions. The regional scheme used throughout the rest of this analysis is a slightly modified version of this UN regional scheme (Figure 13.2). These modifications include: (1) reassignment of Sudan from the Northern Africa region to the West Africa region in order to maintain Sudan's traditional association with the super-region of sub-Saharan Africa; (2) combining the Australia and New Zealand region with the North America region on the basis of demographic and economic similarities (e.g., moderate levels of projected population growth and in-migration); (3) merging Japan with the Western Europe region due to Japan's similarly high levels of

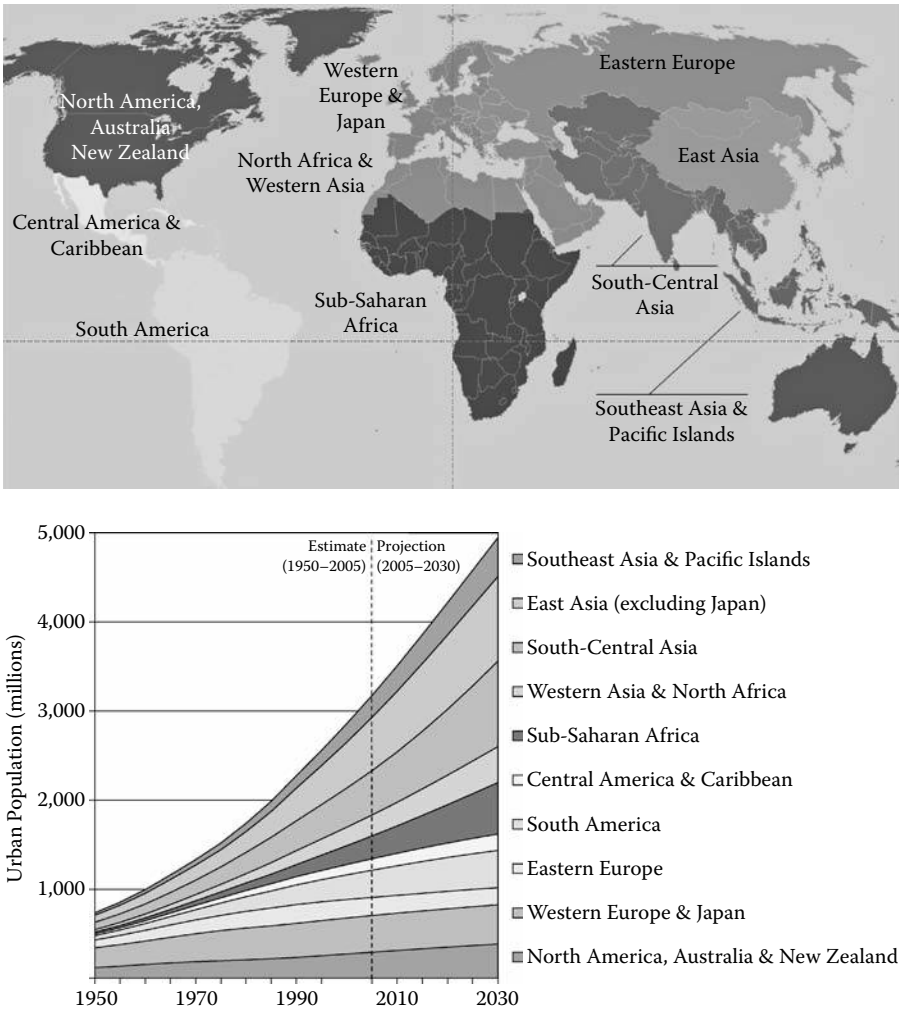

FIGURE 13.2 (a) Map of the ten regions used in this study (modified from the UN regional scheme). The grayscale in this map match the legend in Figures 13.5, 13.8, and 13.10. Figure 13.2(b) tracks the UN Population Division estimates for urban populations by region from 1950–2030 (UN Population Division 2005). (From Potere, D. and Schneider, A. *GeoJournal*, 69: 55–80, 2007. With permission.)

contemporary urbanization and projected population decline; and (4) combining the remaining UN regions into 10 superregions, the majority of which are related to the nine-region scheme used by the UN Human Settlement Programme (UN-HABITAT; Angel et al., 2005). Figure 13.2 depicts these 10 regions and describes the UN's urban population projections for each region through 2030.

The global GLC-2000 v1.1 map indicates that virtually no urban areas are present in southern China. To correct for these and other urban omissions, we relied on recently updated regional GLC maps. These updates are still based on circa 2000

imagery, but represent refinements in the regional protocols by the GLC2000 production regions for Europe and Asia. By including these improved regional maps, the GLC00 map used in this analysis contains 9% (28,000 km^2) more urban area than the original global map (v 1.1). The following regions received additional urban area: Southern Europe (9000 km^2), Northern Europe (6800 km^2), East Asia (4700 km^2), Southeast Asia (4500 km^2), and South Central Asia (2300 km^2).*

13.3.2 City-Scale Descriptions

Figure 13.3 depicts the eight urban maps and two urban-related maps for Beijing and Tianjin, China (top row); Mumbai, India (second row); Paris, France (third row); Moscow, Russia (fourth row); and Cairo, Egypt (bottom row). The first two columns are for the urban-related maps: Nighttime Lights for 1 year spanning 2000–2001 and LandScan 2005. The global urban maps begin with the third column (from left to right): VMAP0, GLC00, GLOBC, HYDE3, IMPSA, MOD500, MOD1K, and GRUMP. Although only HYDE3 and IMPSA map urban land as a continuous variable (fraction of a pixel classified as urban), for the purpose of facilitating comparison in these visualizations we create continuous variables for the binary (urban/rural) maps by aggregating these binary maps from 30″ arc-seconds pixels to 1.5′ arc-minute cells (approximately 3-km resolution at the equator). Each new 1.5′ arc-minute cell is shaded from zero percent urban (blue) to fully urban (red) using a linear scale. The same legend is used for IMPSA and HYDE3, but those pixels remain at their native resolution (30″ arc-seconds and 5′ arc-minutes, respectively). All of the city subsets are approximately 150 × 150 km and oriented north up.

Even a quick glance at the VMAP0 column confirms the often dated nature of this map, particularly in countries of the developing world; significant urban expansion has occurred in all of these cities since the charts and maps that underlie VMAP0 were digitized. In the GLC00 column, the heterogeneous impact of the distributed mapping strategy is apparent; the Europe mapping team clearly enforced a different standard for the urban classification of the Paris metropolitan area than the China team did for Beijing and Tianjin. The close relationship between the GLOBC and GLC00 research teams is evident in Mumbai, where GLOBC relied completely on the GLC00 map. The important role of both LITES and LSCAN is clear when one considers the shape of IMPSA's Cairo map, which includes both the distinctive fan shape of the Nile delta and the urban core of the city center. The two MODIS maps are quite similar to IMPSA in overall form, but are somewhat more expansive. Comparing GRUMP to LITES reveals the important role of the thresholded nighttime lights data in the GRUMP mapping process. Note that several urban clusters in the LITES imagery for both Beijing-Tianjin and Cairo do not appear in GRUMP because the LITES imagery in Figure 13.3 is for 2000–2001, whereas GRUMP relied on 1994–1995 LITES. GRUMP's use of buffers surrounding gazetteer city points is also noticeable in the cluster of circular urban patches in the lower left corner of the GRUMP Beijing map. Overall, these examples from

* MOD1K also includes a small region of urban omission, just visible as a thin stripe over southern Europe in Figure 13.7(g), which was not corrected.

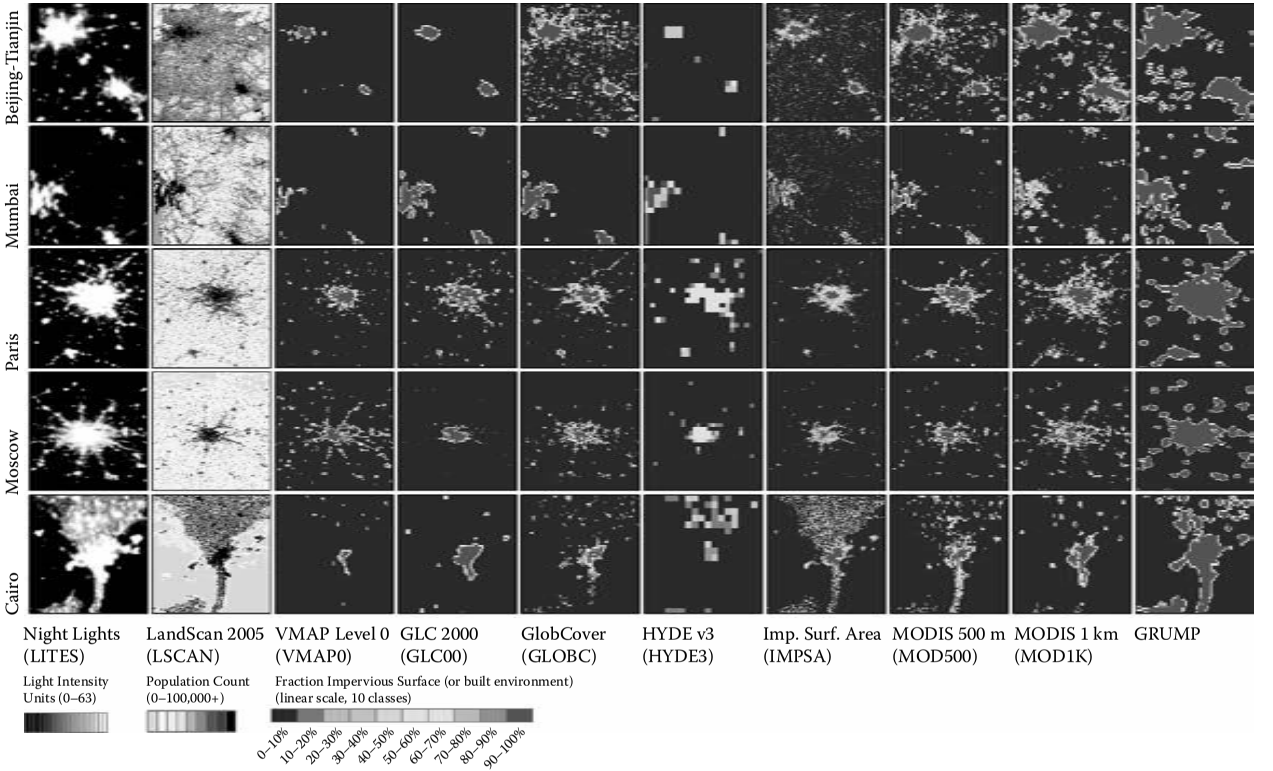

FIGURE 13.3 **(See color insert following page 324.)** The eight global urban maps and two urban-related maps for Beijing–Tianjin, China; Mumbai, India; Paris, France; Moscow, Russia; and Cairo, Egypt. Each subset is approximately 150 × 150 km. LITES, LSCAN and IMPSA are at 30" arc-second resolution, HYDE3 is at 5' arc-minutes, and the remaining maps have been aggregated from 30" arc-seconds to 1.5' arc-minutes for display and comparison, effectively converting their legends from binary (urban/rural) to continuous (percentage urban). (From Potere, D. and Schneider, A. *GeoJournal*, 69: 55–80, 2007. With permission.)

Figure 13.3 demonstrate the diversity of the eight global urban maps, and the challenges of intermap comparison.

We continue this city-level comparison by examining the size distribution of urban "patches," where patches are defined as contiguous areas of urban pixels (Figure 13.4).* This analysis provides information on the effective minimum mapping unit used in each map, as well as some indication of whether urban area is distributed in large clusters (e.g., extensive cities such as Chicago), or in a large number of small-sized patches (e.g., small towns and villages, 1–2 km^2 in size). The absolute number of urban patches varies widely across datasets (in descending order): MOD500 (140,000), GLOBC (88,000), MOD1K (54,000), VMAP0 (32,000), GLC00 (22,000), GRUMP (21,000), and HYDE3 (17,000). The number of patches is influenced by the resolution at which each map is produced; the two maps conducted at resolutions finer than 30″ arc-seconds (GLOBC and MOD500) have higher numbers of patches than the rest, whereas HYDE3 (5′ arc-minutes resolution) naturally has the fewest patches. IMPSA is not included here or in Figure 13.4 because of the difficulty in delineating individual patches from a continuous (percent impervious surface) 1-km resolution map.

The most striking feature of Figure 13.4 is the strong log-linear decay of patch size from 2 to 1000 km^2 for all seven maps. Although this trend is consistent with the long-recognized rank-size rules observed for city sizes at the national scale, it is interesting how marked the trend is among global maps that are based on such

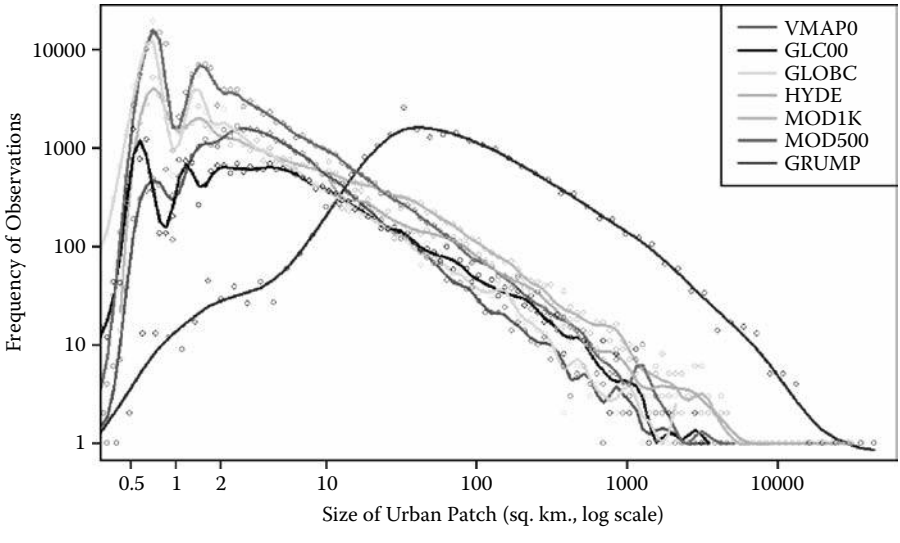

FIGURE 13.4 (See color insert following page 324.) The frequency of urban patch sizes (log-log scale) for each map (excluding IMPSA). Observations are indicated with hollow circles and the solid line is a fitted spline. HYDE3 is plotted starting at 10 km^2 because of the coarse resolution of HYDE3 pixels (5' arc-minutes). (From Potere, D. and Schneider, A. *GeoJournal*, 69: 55–80, 2007. With permission.)

* Patches were described by using a rooks-case rule for adjacency.

a diverse set of methods. On the far left of Figure 13.4 (smallest patch sizes), the double peaks for the four imagery-based distributions correspond to patches that contain only one or two pixels (GLC00, GLOBC, MOD1K, MOD500). Because the geographic projection used for map comparison is not equal-area, single pixels in each map vary in size from 0.86 km^2 at the equator to 0.42 km^2 at the southern tip of Greenland. The overall shape of the GRUMP distribution is quite distinct, and it reflects the larger size of most GRUMP patches relative to all other global urban maps. Yet, for the majority of city sizes, GRUMP adheres to the pattern of roughly log-linear decay.

13.3.3 Regional-Scale Descriptions

Figure 13.5 and Table 13.3 present the total areal extent of urban land for each of the eight urban maps at the scale of world regions. The thickness of each horizontal bar in Figure 13.5 is scaled to reflect the relative amount of urban land within each of the eight maps. These horizontal bars are divided into colored sections representing the relative distribution of urban land within each of the 10 world regions (the 10-color scheme is the same as in Figure 13.2). Because both axes are scaled proportionately, it is possible to make direct comparisons between segments and across both rows and columns. The most obvious feature of Figure 13.5 and Table 13.3 is the previously noted order-of-magnitude difference in total urban area, revealed by the pronounced differences in the thickness of the eight horizontal bars.

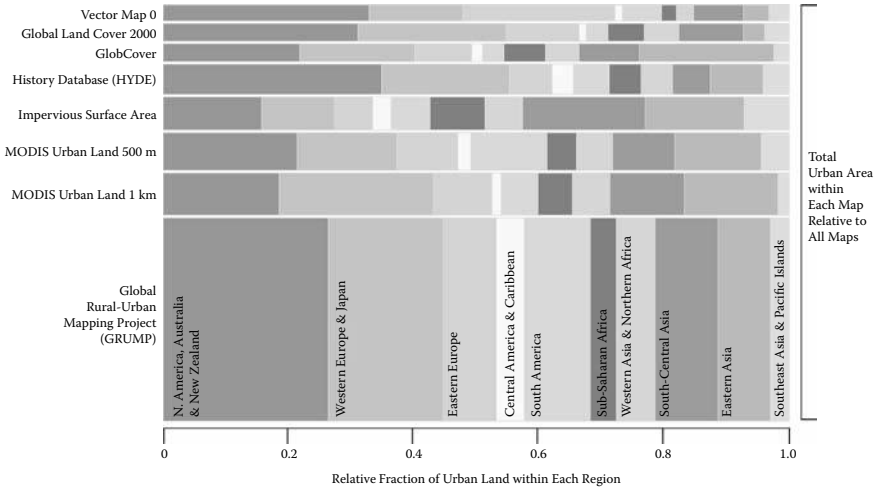

FIGURE 13.5 **(See color insert following page 324.)** The distribution of urban land per continental region for eight global urban maps. The thickness of the horizontal bars reflects the relative amount of urban land within each of the eight maps. These horizontal bars are divided into sections representing the relative distribution of urban land area within each of the ten regions. (From Potere, D. and Schneider, A. *GeoJournal*, 69: 55–80, 2007. With permission.)

TABLE 13.3
Areal Extent of Each of the Eight Global Urban Maps (in km²) for Each of the 10 Regions[a] and Select Countries

Region	VMAP0	GLC00	GLOBC	HYDE3	IMPSA	MOD500	MOD1K	GRUMP
North America, Australia & N. Zealand	***91,123***	***95,982***	***68,409***	***186,303***	***89,963***	***140,506***	***134,764***	***933,537***
USA	79,607	80,482	26,434	161,041	75,488	121,200	117,504	755,881
Canada	4,201	6,054	6,021	12,400	11,300	8,704	7,895	132,472
Australia & New Zealand	7,315	9,446	35,954	12,845	3,161	10,602	9,366	45,027
Western Europe & Japan	***41,327***	***72,761***	***57,602***	***108,435***	***66,469***	***105,449***	***178,887***	***641,608***
Western Europe	15,789	27,372	18,726	56,509	20,855	47,855	53,386	180,709
Northern Europe	16,083	27,413	13,855	18,788	13,157	12,585	21,829	159,799
Southern Europe	4,102	16,133	23,183	19,625	19,250	25,460	50,127	196,262
Japan	5,352	1,842	1,838	13,513	13,207	19,548	53,545	104,839
Eastern Europe	***67,056***	***35,937***	***28,232***	***35,796***	***34,540***	***63,494***	***68,487***	***301,596***
Russia	40,760	15,044	15,374	16,321	20,073	26,504	37,731	188,346
Eastern Europe (excluding Russia)	26,296	20,893	12,858	19,475	14,467	36,990	30,757	113,250
Central America & Caribbean	***3,466***	***3,468***	***5,322***	***17,802***	***17,581***	***13,099***	***10,274***	***154,951***
Central America	2,534	2,309	4,146	12,254	14,245	8,896	8,863	122,462
Caribbean	933	1,159	1,176	5,548	3,335	4,203	1,411	32,490
South America	***17,074***	***10,731***	***10,801***	***30,499***	***35,382***	***82,242***	***42,876***	***374,942***
Brazil	10,113	5,025	5,007	17,021	17,938	39,989	19,254	189,286
South America (excluding Brazil)	6,962	5,706	5,794	13,478	17,445	42,253	23,622	185,655
Sub-Saharan Africa	***6,828***	***17,937***	***20,458***	***27,201***	***49,788***	***31,053***	***39,621***	***144,996***
East Africa	1,585	3,286	4,835	6,181	17,887	5,006	10,136	32,310
West Africa (plus Sudan)	1,483	5,378	6,879	10,448	20,430	12,788	15,468	45,967
Southern Africa	2,459	7,883	7,775	7,717	4,965	8,486	10,482	49,977
Middle Africa	1,301	1,390	970	2,856	6,506	4,772	3,535	16,741
Western Asia & North Africa	***7,433***	***16,905***	***17,285***	***27,114***	***34,492***	***37,782***	***44,039***	***222,113***
West Asia	5,732	6,108	6,684	20,396	21,527	27,347	29,393	145,247
Northern Africa (excluding Sudan)	1,701	10,797	10,601	6,717	12,966	10,435	14,645	76,866
South Central Asia	***22,026***	***31,680***	***29,690***	***32,327***	***112,296***	***64,973***	***86,298***	***350,383***
India	8,160	21,288	20,904	17,020	76,244	31,334	30,857	204,676
South Central Asia (excluding India)	13,866	10,392	8,786	15,307	36,052	33,639	55,440	145,708
East Asia	***11,063***	***10,788***	***67,562***	***44,634***	***90,059***	***90,966***	***109,100***	***297,692***
China	9,579	10,012	65,263	39,547	82,301	81,120	88,977	261,920
East Asia (excluding Japan & China)	1,484	776	2,299	5,087	7,758	9,846	20,123	35,772
Southeast Asia & Pacific Islands	***8,981***	***11,819***	***7,416***	***21,874***	***40,933***	***29,197***	***12,597***	***102,290***
Southeast Asia	8,866	11,714	7,308	21,560	40,252	28,911	12,522	97,440
Melanesia	97	102	104	216	553	285	71	3,454
Micronesia	4	3	4	40	68	0	4	688
Polynesia	13	0	0	58	60	0	0	707
Total (sq. km)	***276,377***	***308,007***	***312,779***	***531,985***	***571,504***	***658,760***	***726,943***	***3,524,109***

[a] Modified from the UN regional designations.

[b] The North American total includes Greenland, Bermuda, and St. Pierre and Miquelon.

The pattern of regional banding within each map (measured on the horizontal axis) reveals large differences at the scale of world regions. The results for VMAP0 reflect the Cold War legacy of this data source, as shown in the wide bands for Eastern Europe (light green bar, third from left). The US agencies responsible for VMAP0 likely focused more mapping efforts on this region, causing VMAP0's relative amount of Russian urban land to be far above that of any other map (Table 13.3). Aside from differences in the relative importance of South Central and East Asia, GLC00 and HYDE3 have very similar regional banding patterns. GLOBC has by far the widest East Asian (salmon) band, nearly the same width as North America, Australia, and New Zealand (Figure 13.5). It is surprising to note that GLOBC attributes more urban land to Australia than to the entire

United States (Table 13.3). Overall, IMPSA's regional bands are the most distinct from the rest; in relative terms, IMPSA has the least amount of urban area in the North America, Australia, and New Zealand region (dark green), and the most in Asia (red, salmon, and gray). This difference can be explained by IMPSA's reliance on LSCAN; because LSCAN tracks population density, it favors the two demographic billionaires of India and China. The most significant difference between the new 500 m MODIS map and the older 1-km MODIS map is the reduction in the urban area of Western Europe, and the increase in the urban area of South America. The regional distribution of urban area (but not the absolute amount of urban area) for GRUMP is nearly identical to the distribution of urban land derived by applying Angel et al.'s (2005) urban population densities to UN regional urban population estimates for 2000. This seems to indicate that the GRUMP team normalized their urban area totals to UN urban population estimates (at least at the regional level).

13.3.4 Global-Scale Descriptions

Figure 13.1 presents the total urban extent of the eight maps at the global scale. As noted earlier, the urban extents vary by an order of magnitude, from 0.3 to 3.5 million km^2. For scale, the difference in the GRUMP and VMAP0 totals is approximately equal to the land surface area of India. It is a challenge to move beyond the plots of Figures 13.1 and 13.5 and to display global 30″ arc-second resolution maps with sufficient detail for a meaningful comparison; at a reasonable resolution of 300 dots per inch, the 40,000 × 20,000 raster (column × row) would be roughly 3.4 × 1.7 m in size. Even at this resolution, the urban class would be difficult to discern because urban areas occupy at most 1–3% of the Earth's 140 million km^2 of land. One way to deal with these issues is through the use of Geodesic Discrete Global Grids (DGGs) (Sahr et al., 2003). DGGs are a class of equal area, uniformly distributed partitions of the Earth's surface. The hexagonal partitions provide a scheme for assessing the urban area of a given map that is independent of arbitrarily defined political boundaries or world regions, constant in cell size (unlike the varying raster cell sizes of a geographic projection), and constant in cell shape (unlike the deformed parallelograms of the sinusoidal projection). Despite these clear advantages, DGGs have only recently been used for map comparisons (Potere and Schneider, 2007). By computing the square root of the facet area, we can also derive a rough estimate of effective spatial resolution of the DGGs across different hexagonal sizes (Small and Cohen, 2004). For illustration, in Figure 13.6 we use five resolutions of DGGs with hexagonal cell sizes ranging from 800 to 70,000 km^2 (29- to 264-km resolution).

By aggregating the 30″ arc-second pixels of our global urban maps up to the 51-km resolution DGG facets (yellow facets in Figure 13.6(b)), we have created a series of maps that provide a comparative view of urban areas at a global scale (Figures 13.7(a–h)). In all of these maps, royal blue areas represent completely urban-free facets. Of the eight maps, IMPSA (Figure 13.7(d)) has by far the fewest facets that are completely free of urban land, whereas GLC00 (Figure 13.7(b)) has the most. From these global-scale visualizations, regional trends are apparent: VMAP0 (Figure 13.7(a)) portrays Eastern

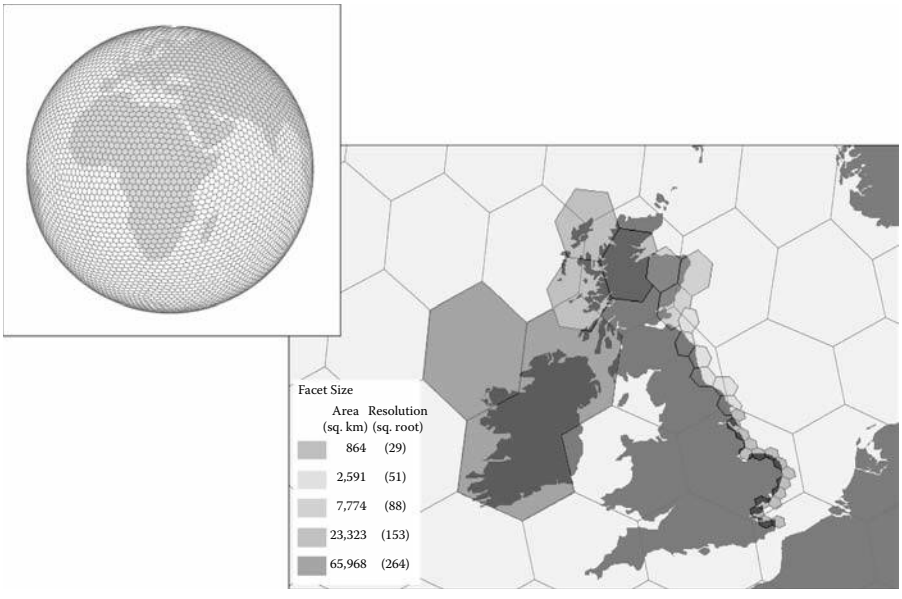

FIGURE 13.6 (See color insert following page 324.) Five levels of a discrete global grid (DGG) system with hexagonal facets for the globe (upper left) and over the United Kingdom (lower right). The DGG displayed for the globe is at the coarsest facet size of 70,000 km^2 (purple facets in the lower right). The map legend also shows the effective spatial resolution for each facet size, estimated by the square root of the facet area. (From Potere, D. and Schneider, A. *GeoJournal*, 69: 55–80, 2007. With permission.)

Europe as a more extensive urban network than Western Europe, GLC00 depicts a world in which Europe and the Eastern United States are the only urban-dominated regions and Africa is almost completely urban-free, GLOBC is unique in depicting Australia as an urban system on par with Western Europe or North America, HYDE3 has the most uniform view of the distribution of urban land, and IMPSA portrays a massive portion of the world's surface area as very low-fraction urban (the light blue regions of the IMPSA map (Figure 13.7(e)) represent DGG facets that are less than 0.05% urban).

In Figure 13.7(i), the amount of urban area for each grid cell is averaged across all eight maps. The total extent of this mean urban map is 864,000 km^2. Because GRUMP's urban area is more extensive than any of the other five maps, GRUMP has strongly influenced this mean urban map, as is evident in a comparison of Figures 13.7(h) and (i). In the mean map, the largest blocks of intensely urban areas include the Eastern United States, Western Europe, India, Eastern China, and Japan, and to a lesser degree the southeastern coast of South America. The largest contiguous urban-free areas across all eight maps are the Sahara desert, interior Australia, Siberia, Mongolia, Northern Canada and Greenland, the Rhub al Khali of Saudi Arabia, and to a lesser degree the tropical rainforests of South America and the Kalahari Desert of Southern Africa.

13.4 INTERMAP COMPARISONS

13.4.1 Previous Comparative Studies

Urbanized areas make up a small portion of the Earth's total land area, and the urban class is rare when compared to land cover types such as forest, grassland,

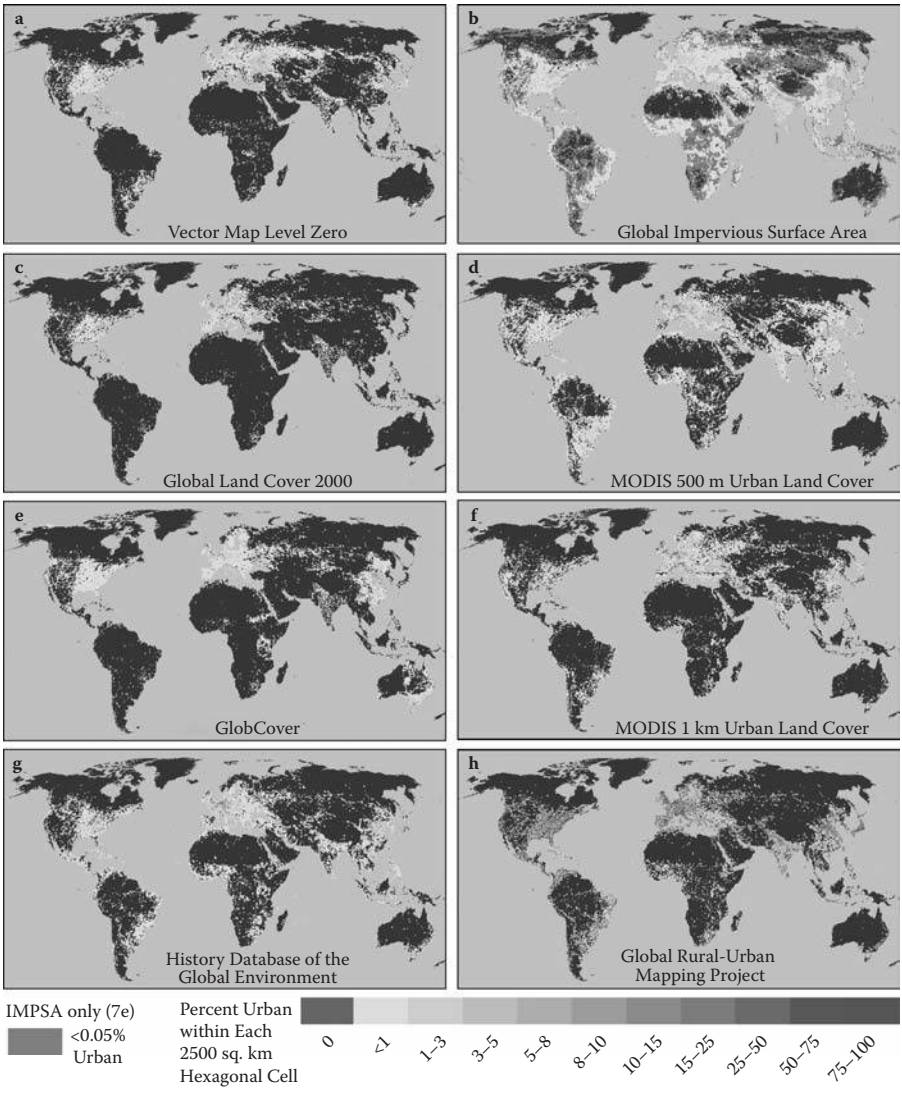

FIGURE 13.7 **(See color insert following page 324.)** Depiction of the percentage of urban land per facet for all eight global urban maps, aggregated to a discrete global grid with hexagonal facets 2,591 km^2 in area (effective resolution of 51 km); (i) shows the amount of urban area for each grid cell averaged across all eight maps. Dark blue indicates absence of urban land. (From Potere, D. and Schneider, A. *GeoJournal*, 69: 55–80, 2007. With permission.)

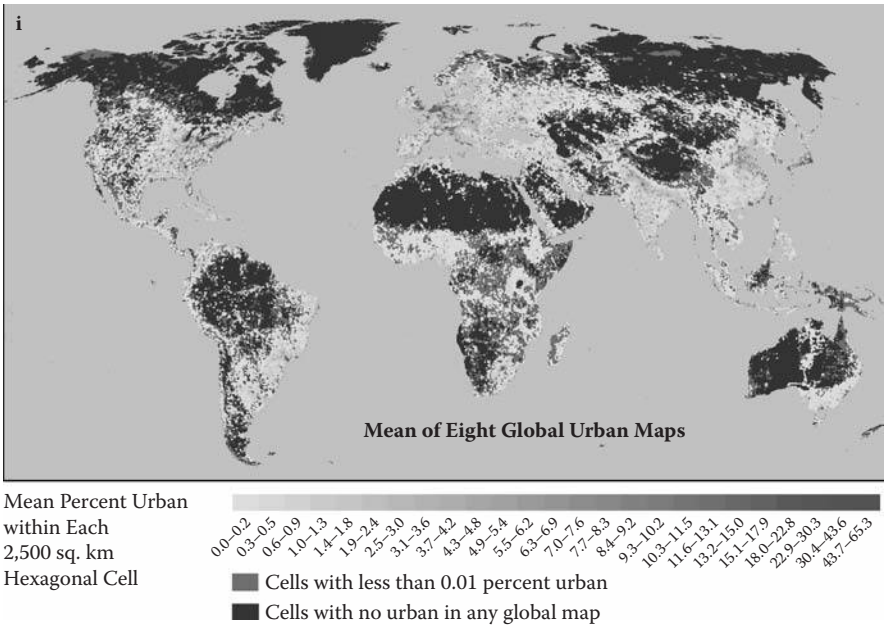

FIGURE 13.7 (continued)

and savanna. This minority status has led to scant urban-specific analysis in comparisons of global land cover products. This study, together with a companion article (Potere and Schneider, 2007), is the first systematic global comparison focused on urban maps. Although there has been a recent increase in the number of global-scale land cover comparison projects, these assessments have either failed to include the urban class, considered only areal extent, included only a subset of currently available urban maps, or inadvertently compared multiple maps whose urban layer is actually derived directly from VMAP0 (Hansen and Reed, 2000b; Giri et al., 2005; See and Fritz, 2006; Jung et al., 2006; McCallum et al., 2006; Mayaux et al., 2006).

At regional and city scales, there have been a number of comparative studies that include some of the urban maps considered here. Schneider et al. (2003) compared VMAP0, LITES, and the MODIS-derived urban map for cities in North America, uncovering variable amounts of underestimation of urban land by VMAP0 and systematic overestimation of urban land by the 1994–1995 nighttime lights data (thresholded) when compared against more recent medium-resolution maps of urban land derived from Landsat imagery. Tatem et al. (2005) compared a map of urban areas in Kenya to five global scale urban maps, and unsurprisingly reported that a medium-resolution Kenya map based on Landsat and Radarsat imagery is of higher accuracy than the coarse-resolution global maps. Finally, Small et al. (2005) assessed thresholded 1994–1995 and 2000 LITES data against Landsat-based maps for a global sample of 17 cities, confirming that no single LITES threshold is suitable for mapping urban land.

13.4.2 Per-Pixel Comparison

Contingency tables, sometimes referred to as confusion matrices, are a common way to begin intermap comparisons (Table 13.4). These tables are produced by overlaying a set of maps and estimating the areas of agreement and disagreement pixel by pixel. We constructed contingency matrices for all eight global urban maps (Table 13.5). Each entry describes the fraction of map A (shown in the rows) also present in map B (shown in the columns). For example, although VMAP0 is a part of the input data streams for both GLC00 and GRUMP (Table 13.2), only 41% and 76% of this map agrees with GLC00 and GRUMP, respectively. Some portion of this could be due to differences in georegistration; relative to the other global maps, GLC00 appears to be shifted 1′30″ eastward and 30″ arc-seconds southward over parts of North America, Central America, and the

TABLE 13.4
A Typical Contingency Table for a Two-Class Map Comparison
n* = *a* + *b* + *c* + *d

		Validation Data	
		Presence	**Absence**
Data under review	Presence	*a*	*b*
	Absence	*c*	*d*

Note: For the map comparisons in Section 13.4, there is no distinction between "data under review" and "validation data," because the contingency table is used to compare two maps. In the assessment of Section 13.5, "data under review" is the global urban map in question and "validation data" is the medium-resolution Landsat map.

TABLE 13.5
Summary of the Contingency Tables for Each of the 28 Pairwise Map Comparisons

	VMAP0	GLC00	GLOBC	HYDE3	IMPSA	MOD500	MOD1K	GRUMP
VMAP0	1	0.41	0.28	0.37	0.26	0.57	0.54	0.76
GLC00	0.37	1	0.47	0.40	0.27	0.55	0.60	0.89
GLOBC	0.25	0.47	1	0.29	0.24	0.49	0.52	0.72
HYDE3	0.19	0.23	0.17	1	0.18	0.34	0.38	0.74
IMPSA	0.12	0.15	0.13	0.17	1	0.25	0.26	0.46
MOD500	0.24	0.26	0.24	0.28	0.22	1	0.51	0.75
MOD1K	0.21	0.26	0.22	0.28	0.20	0.45	1	0.80
GRUMP	0.06	0.08	0.06	0.11	0.07	0.14	0.16	1

Note: Each entry represents the percent of Map A (shown in the rows) that is also present in Map B (shown in the columns).

Caribbean relative to all of the other urban maps. It is not possible to correct for this shift because the georegistration problem appears to be nonconstant within the northwest hemisphere. Similar registration problems are not apparent for GLC00 in any other region of the world (or for any other urban map examined in this chapter). A more methodical evaluation of georegistration is beyond the scope of this study.

The GLC00 example highlights one of the fundamental problems of conducting a global map comparison at the pixel level: a shift of a single pixel can significantly reduce map agreement. We address some of these concerns with our multiscale comparison in Section 13.4.4. Another issue that arises when interpreting these simple contingency tables is the order-of-magnitude variance in total map area (Figure 13.1). For instance, 60% of GLC00 agrees with MODIS, whereas only 26% of MODIS agrees with GLC00. This is not surprising when one considers that MODIS is 2.4 times the size of GLC00. Even if every MODIS pixel were in agreement with GLC00, this would only represent 42% of MODIS urban land.

There are several statistics based on contingency tables that have long been used to confront the challenges of assessing map agreement against random chance and for maps of varying extent (Congalton and Green, 1999). There remains considerable debate in both the remote sensing and the spatial ecology literatures concerning the selection of optimal map agreement measures (Fielding and Bell, 1997; Manel et al., 2001; McPherson et al., 2004; Allouche et al., 2006; Lobo et al., 2007; Liu et al., 2007; Foody, 2006, 2007), yet there is broad consensus that statistics based on the entire contingency table are welcome improvements on the basic accuracy, sensitivity, and specificity measures (top three rows, Table 13.6). In our comparison, we follow the recommendations of Foody (2006, 2007) and rely on several agreement measures across a wide range of spatial scales. We choose Cohen's kappa (Congalton and Green, 1999), the normalized mutual information (NMI) coefficient (Forbes, 1995), and the true skill statistic (TSS) (Allouche et al., 2006) for their consideration of both omission and commission errors, their reliance on the entire contingency table, and their robustness with respect to changes in the extent of the maps under review (bottom three rows, Table 13.6).

Cohen's kappa statistic (κ) is designed to measure the strength of agreement, taking into account the potential for chance agreement (Cohen, 1960; Monserud and Leemans, 1992; Goldewijk and Ramankutty, 2004). Landis and Koch (1977) suggest that Cohen's κ values of 0.00–0.20 can be considered "slight" agreement, values of 0.21–0.40 as "fair," and 0.41–0.60 as "moderate" agreement; however, they caution that these are only intended as useful benchmarks. In Table 13.7, we report global-scale kappa values for the 28 map pairs. The overall impression is that these maps are quite distinct on the per-pixel level, as shown by the relatively low level of agreement among all of the map pairs ($\bar{\kappa} = 0.26$). The strongest agreement is between the two map pairs created by related research groups: MOD1K and MOD500 ($\kappa = 0.48$), and GLC00 and GLOBC ($\kappa = 0.47$). The next strongest agreements are between GLC00 and VMAP0, and GLC00 and the two MODIS maps. This result is also expected, considering that VMAP is an input into the

TABLE 13.6
Six-Map Agreement Measures Used in This Chapter

Measure	Formula
Overall Map Accuracy (OMA)	$\frac{a+d}{n}$
Specificity (1 – Commission)	$\frac{d}{b+d}$
Sensitivity (1 – Omission)	$\frac{a}{a+c}$
Cohen's Kappa	$\frac{\left(\frac{a+d}{n}\right) - \frac{(a+b)(a+c)+(c+d)(d+b)}{n^2}}{1 - \frac{(a+b)(a+c)+(c+d)(d+b)}{n^2}}$
Normalized Mutual Information	$1 - \frac{-aln(a) - bln(b) - cln(c) - dln(d) + (a+b)ln(a+b) + (c+d)ln(c+d)}{nln(n) - ((a+c)ln(a+c) + (b+d)ln(b+d)}$
True Skill Statistic	sensitivity + specificity – 1, or $\frac{ad-bc}{(a+c)(b+d)}$

Note: Each measure is based on the elements of the contingency table from Table 13.4. The top three are traditional measures that suffer from biases due to variation in overall map extent. The bottom three measures are more robust. Cohen's kappa has the longest history of use for map accuracy assessment.

TABLE 13.7
Cohen's Kappa (κ) Statistic[a] for Each Combination of the Eight Maps

	VMAP0	GLC00	GLOBC	HYDE3	IMPSA	MOD500	MOD1K	GRUMP
VMAP0	1							
GLC00	0.39	1						
GLOBC	0.26	0.47	1					
HYDE3	0.25	0.29	0.21	1				
IMPSA	0.16	0.19	0.17	0.17	1			
MOD500	0.34	0.35	0.32	0.30	0.23	1		
MOD1K	0.30	0.36	0.31	0.31	0.22	0.48	1	
GRUMP	0.11	0.14	0.11	0.19	0.12	0.23	0.27	1

[a] A measure of overall map agreement.

[b] Kappa approaches 1.0 as maps approach perfect agreement. Kappa is designed to adjust for the amount of agreement that one could expect due to chance alone.

GLC00 product and that MOD1K and GLC00 are both derived primarily from coarse-resolution daytime imagery.

To understand how map agreement varies in space, we conducted these same per-pixel comparisons at a regional scale. We began by creating contingency tables and associated map agreement statistics for all of the intermap comparisons (28 pairs) for each of the 10 world regions. We use box plots in Figure 13.8 to display the median and quantiles of these 28 agreement measures for each region (color-coded to correspond to Figure 13.2). We report Cohen's kappa, NMI, and TSS measures, where complete agreement is 1.0 for each measure. The dominant trend in Figure 13.8 is that of decreasing overall agreement as one moves from the affluent regions of North America and Europe (green bars on left) and toward the developing countries of Asia (red, salmon, and gray bars on right). This does not imply that the maps are any less accurate in these lesser developed regions, merely that there is less intermap agreement. Across all three agreement metrics, the overall pattern points toward three superregions: relatively high agreement in the North America, Australia, and New Zealand region (also including Western Europe in the TSS measure), relatively low levels of agreement in most of Asia (South Central Asia, East Asia, and Southeast Asia and the Pacific Islands), and medium levels of agreement for the remaining regions (Eastern Europe, Central and South America and the Caribbean, Africa, and Western Asia). This trend aligns well with our more complete understanding of cities of the developed world, and the relative challenges of describing the complex and rapidly changing cities of the developing world.

13.4.3 Country-Level Comparison

By comparing the total extent of urban area within each country, we can approach the issue of map agreement without some of the limitations of pixel-by-pixel comparisons. Large area aggregations using national borders also reduce the importance of any persistent georegistration problems. We first present our country-level results by ranking the 10 countries with the largest urban extents for each of the eight global urban maps (Table 13.8). There is considerable variation in these rank lists, with only United States, India, Russia, and China appearing in all of the top 10 lists. For three maps, IMPSA, MOD500, and GRUMP, the five countries with the largest mapped urban extents also have the five largest urban populations according to the UN Population Division. For IMPSA, this correlation extends further; IMPSA's top 10 rankings closely mirror their order by urban population. This is not surprising considering the important role that demographic attributes play in the methodologies of IMPSA and GRUMP.

We estimate the relationships between the country-level urban extents of each map pair by using Kendall's tau (τ), which provides a quantitative assessment of the correlation among the urban area rankings for all 223 countries within the global datasets (Kendall, 1938) (Table 13.9). The overall impression from this measure is one of far greater agreement than that of the per-pixel comparisons (Tables 13.5 and 7), with $\overline{\tau} = 0.73$ and a range of 0.64–0.86 (top eight rows, Table 13.9). This country-level analysis reveals that international comparisons of the *relative* areal extent of

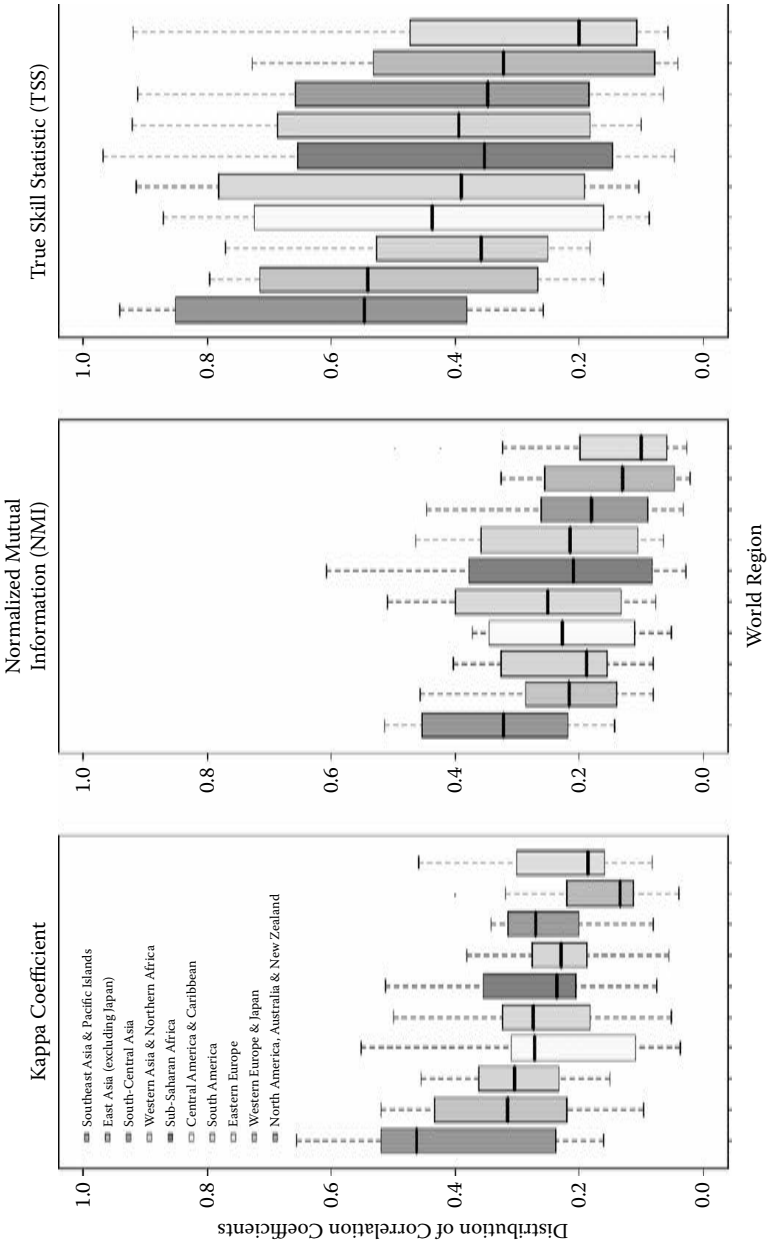

FIGURE 13.8 **(See color insert following page 324.)** Regional box-plots for Cohen's Kappa, Normalized Mutual Information (NMI) and the True Skill Statistic (TSS) from contingency tables for all 28 inter-map comparisons, grouped by world region. All measures approach one when the maps are in complete agreement. (From Potere, D. and Schneider, A. *GeoJournal*, 69: 55–80, 2007. With permission.)

TABLE 13.8
Ranks for the 10 Countries with the Most Urban Area within Each of the Eight Global Urban Maps

	China (2)	India (4)	USA (1)	Brazil (9)	Russia (10)	Indonesia	Japan (3)	Mexico	Germany (5)	UK (7)	Pakistan	France (6)	Iran	Italy (8)	Ukraine	Argentina	Spain	Canada	South Africa	Australia
VMAP0	6	8	1	5	2		10		7	4					3					9
GLC00	6	2	1		4				5	3		10		8					9	7
GLOBC	1	4	3		5				8	7				6			10		9	2
HYDE3	2	6	1	5	7		8		3			4						9		10
IMPSA	1	2	3	5	4	6	7	9			10							8		
MOD500	2	4	1	3	5		7		6			10		9		8				
MOD1K	2	5	1	10	4		3		9			8	7	6						
GRUMP	2	3	1	4	5		7	8				9		10				6		

Note: The countries are ordered left to right according to their rank in the UN's estimate of the total urban population for the year 2000 (UN Statistics Division 2008). In parenthesis is the country-rank for the top ten highest per capita gross domestic products (purchasing power parity) in the year 2000 (World Bank 2008).

TABLE 13.9
Rank Correlation Matrix (Kendall's tau, τ) for a Sample of 223 Countries

	VMAP0	GLC00	GLOBC	HYDE3	IMPSA	MOD500	MOD1K	GRUMP	Population	GDP
VMAP0	1									
GLC00	0.69	1								
GLOBC	0.64	0.86	1							
HYDE3	0.74	0.69	0.65	1						
IMPSA	0.69	0.65	0.65	0.78	1					
MOD500	0.79	0.69	0.67	0.78	0.75	1				
MOD1K	0.75	0.72	0.70	0.78	0.76	0.81	1			
GRUMP	0.76	0.71	0.67	0.81	0.77	0.79	0.79	1		
Population	0.72	0.66	0.64	0.78	0.85	0.77	0.75	0.76	1	
GDP	0.69	0.68	0.65	0.77	0.71	0.69	0.71	0.78	0.74	1

Note: Kendall's tau is estimated for each map pair, and for national urban populations in 2000 (UN Statistics Division, 2008) and national GDP (purchasing power parity) estimated by the World Bank for 2000 (UN Statistics Division, 2008). The mean tau for the 28 intermap comparisons (top eight rows) is 0.73 (±0.06 standard deviation). For the correlations involving population and GDP, the mean correlation is 0.71 (bottom two rows). For GDP, reliable purchasing power parity data was available for only 169 countries, for the other correlation estimates all 228 countries were included. All correlations are highly significant. The GLOBC–GLC00, MOD500–MOD1K, and GRUMP–HYDE3 pairs have the highest intermap tau values (>0.80). At the national level, GDP is most highly correlated with GRUMP (0.78) and urban population with IMPSA (0.85).

urban land are far less sensitive to the selection of a particular global urban map than the per-pixel results imply. Of course, the large *absolute* differences between these maps remain important across all aggregation scales. The map pairs with the highest correlations are either produced by closely related research teams (GLC00–GLOBC, $\tau = 0.86$; MOD1K–MOD500, $\tau = 0.81$) or both rely on similar demographic data (HYDE3–GRUMP, $\tau = 0.81$).

In Table 13.9, we also explore the eight maps' correlation with urban population for the year 2000 (UN Statistics Division, 2008) and gross domestic product (GDP) (purchasing power parity) for 2000 (World Bank estimate).* There are many potential pathways through which a wealthier and more numerous urban population could increase the amount of urban land in a given country. Although it is not possible to determine the direction of causality, Table 13.9 certainly reveals a strong positive correlation; the $\bar{\tau} = 0.71$ for pairs involving either population or GDP (all correlations are highly significant). GRUMP has the highest correlation with GDP ($\tau = 0.78$), which is not surprising when one considers the important role that thresholded LITES data plays in the GRUMP methodology and the strong association between GDP and nighttime illumination (Welch, 1980; Sutton and Costanza, 2002; Doll et al., 2006). IMPSA has the highest correlation with population ($\tau = 0.85$), which again makes sense when one considers that LSCAN plays an important role in the IMPSA methodology and LSCAN is heavily influenced by demographic data.

13.4.4 Multiresolution Hexagonal Comparison

As mentioned previously, any comparison of the spatial pattern of urban land in these eight global urban maps is made more challenging by the rarity of the urban class, the very large differences in estimates of the total urban area for each map, and the potential problems of georegistration. Although using national borders can help alleviate these problems, the distribution of country sizes varies widely and it is not possible to explore subnational intermap differences with this approach. Here, we again turn to DGGs to create a global equal-area partitioning system with minimal shape distortion over the entire Earth's surface. For each hexagonal DGG facet, we estimate the percentage of urban coverage for each of the eight global maps. Because the resulting aggregation is continuous, we can test for linear correlation. We carry out these tests in Figure 13.9 for each map combination (28 pairs) across all five DGG resolutions (29 to 264 km). We restrict our regressions to hexagonal facets that contain urban land in at least one map. Although this multiresolution global map comparison is similar to the methods used by Goldewijk and Ramankutty (2004) and Greyner et al. (2006), both studies used a series of traditional rectangular raster grids in a geographic projection. Although the raster approach is more straightforward than DGGs, the drawback is that the size and shape of individual cells varies widely with latitude. This effect creates nonuniform sampling, with sparser sampling in tropical versus temperate regions.

* Purchasing power parity GDP data was available only for 169 countries; $n = 228$ for all other correlations.

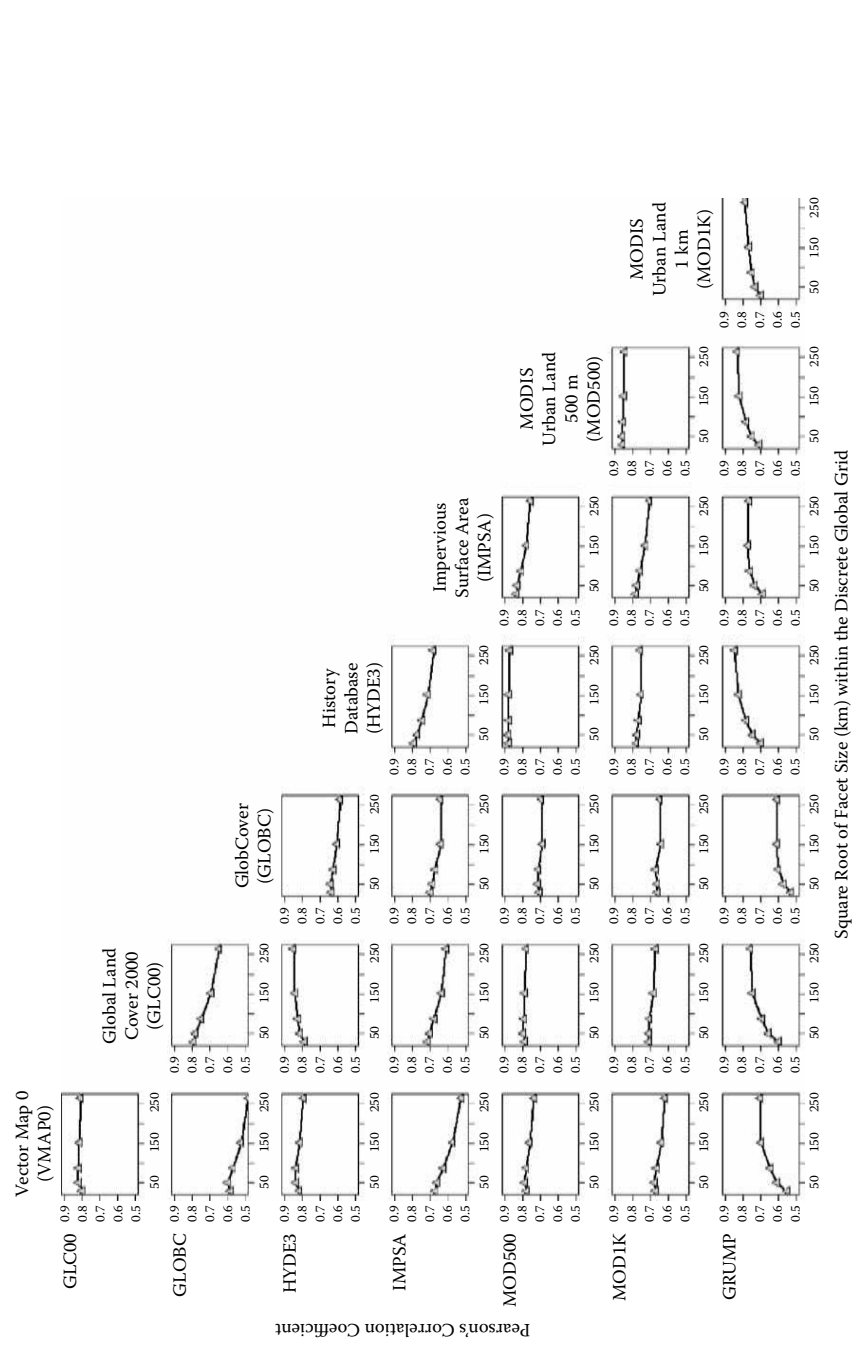

FIGURE 13.9 The global correlations in percent urban area between all 15 pairwise map combinations for five levels of discrete global grid (DGG) aggregation (i.e., hexagonal facets approximately 29, 51, 88, 153, and 264 km across).

The highest overall intermap correlation curves are for the closely related MOD500-MOD1K maps and for MOD500-HYDE3, a correlation that is more difficult to explain. The correlations among the VMAP0-GLC00-HYDE3 group (upper left of Figure 13.9) are also quite high (at or about 0.8 for all resolutions). This result is understandable considering that VMAP0 was an important input for GLC00 (in some regions, the sole input), and that HYDE3 was the only map to draw on both GLC00 and VMAP0. The lowest overall correlation curve is for VMAP0-GLOBC ($r \leq 0.6$ for all resolutions). In general, GLOBC has the lowest correlation curves of any of the maps; GLOBC is involved in 6 of the 11 curves where $r \leq 0.7$. When one compares IMPSA and MOD1K with either VMAP0 or GLC00, the resulting correlation curves are also quite low ($r \leq 0.7$). Considering that neither MOD1K nor IMPSA drew on VMAP0, and given the aforementioned similarity between VMAP0 and GLC00, these low correlations are also to be expected.

The slopes of the correlation curves are more difficult to interpret, but may be related to the size distribution and density of urban patches within each urban map and their relationship to the various hexagonal facet sizes. The 28 curves in Figure 13.9 can be divided into three categories: 12 cases of flat curves (no significant change in correlation with change in hexagon grid cell resolution), 8 cases of upward sloping curves (increasing correlation with coarser hexagon grid cell resolution), and 8 cases of downward sloping curves (decreasing correlation with coarser hexagon grid cell resolution). All but one of the flat, resolution-independent curves involve MOD1K (four cases) or MOD500 (three cases). The downward sloping curves are more evenly divided, but IMPSA (six cases) and VMAP (five cases) are most frequently involved. Interestingly, nearly all of the positive-sloped curves (seven of eight cases) involve GRUMP. This result is likely tied to the unique size distribution of the GRUMP urban patches relative to all of the other maps (Figure 13.4). At the finest DGG resolution of 29 km, each facet contains roughly 900 km^2 of land. GRUMP has by far the most urban patches that are of sufficient size to saturate these facets, potentially reducing intermap correlations at this finest hexagon grid cell resolution. This effect gradually fades as the pixel sizes become large relative to the mean urban patch size of GRUMP (resolutions above 150 km).

The DGG aggregates are also an effective tool for uncovering regional patterns in the intermap correlations. The box plots of Figure 13.10 chart the distributions (median, interquartile range, and outliers) of the Pearson correlations for the 28 global urban map pairs across all five DGG resolutions and all 10 world regions. Each region has five box plots showing correlations from the finest to the coarsest DGG (29 to 264 km, left to right). The colors correspond to the world regional scheme used throughout this analysis (Figure 13.2). From Figure 13.10, it is clear that the North America, Australia, and New Zealand region (far left) has by far the strongest intermap correlations ($\bar{r} = 0.83$), indicating the highest agreement in terms of the intraregional distribution of urban land. By comparison, the Asian regions (four regions, far right) have the lowest intermap correlations ($\bar{r} = 0.66$), and the remaining regions are intermediate ($\bar{r} = 0.79$, red horizontal bars in Figure 13.10).*

* When single maps are held out of the box plots from Figure 13.10, the same overall regional pattern persists. The one exception is GLOBC; when GLOBC is held out, the mean North American correlation increases to 0.91, and the other regions remain relatively unchanged.

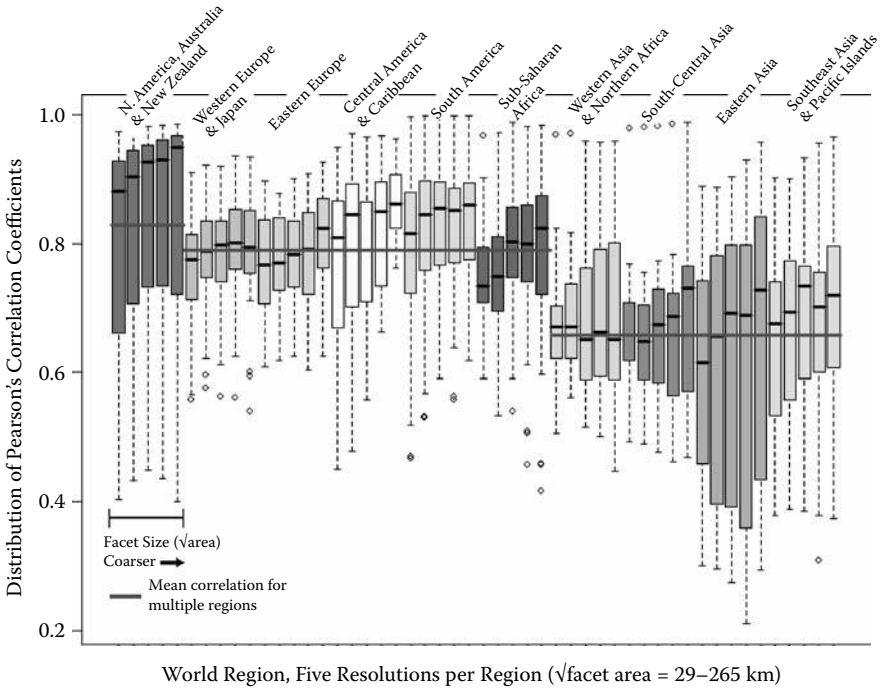

FIGURE 13.10 These box-plots capture the 28 pair-wise Pearson correlations between global maps at five resolutions for each of ten world regions. For instance, the five left-most box-plots represent the inter-map correlations for the North America, Australia, and New Zealand region at five discrete global grid (DGG) resolutions (finest to coarsest, 29–264 km, left to right). For this region, the median inter-map correlation (black horizontal bars) improves as the hexagonal grid resolution becomes coarser. Each of the long horizontal bars represents a mean correlation for a group of regions: the top bar ($\bar{r} = 0.83$) is for North America, Australia, and New Zealand, the middle bar ($\bar{r} = 0.79$) is for Europe and Japan, South and Central America, and Sub-Saharan Africa, and the bottom bar ($\bar{r} = 0.66$) is for Western Asia and North Africa, South Central Asia, East Asia, and Southeast Asia and Pacific Islands. (From Potere, D. and Schneider, A. *GeoJournal*, 69: 55–80, 2007. With permission.)

The eight maps have the most dispersed distribution of correlations in the East Asia region (salmon color, including China). Most of the variance in this region is caused by very low intermap correlations for all the comparisons that include VMAP0 or GLC00 ($\bar{r} = 0.36$ and $\bar{r} = 0.44$, respectively) relative to the other six maps ($\bar{r} > 0.60$). As previously discussed, this result is an artifact of GLC00's significant urban omissions over East Asia. VMAP0's underestimation is likely tied to China's exceptionally rapid urban expansion over the past 20 years, and the older dates of many of the maps used to create VMAP0.

13.5 MAP ASSESSMENT

To characterize what each global map means when it classifies an area as urban, the *comparative* and *descriptive* studies described in Section 13.3 and 13.4 are not

sufficient. A global *assessment* of these maps is the subject of ongoing research (Potere, in preparation). Such an assessment should leverage both medium- and high-resolution imagery to better characterize the accuracy of the coarse-resolution global urban maps. We are in the first stages of conducting such an assessment, using a combination of high-resolution imagery from GE and a large collection of medium-resolution Landsat city maps from the Angel et al. (2005) and Schneider and Woodcock (2008) assessments of global urban expansion (Figure 13.11). The cities listed by Angel et al. (2005) are a global stratified random sample from the roughly 4000 cities with populations greater than 100,000 (where the stratification was conducted with respect to city population size, GDP, and geographic region).*

As an initial step, we verified the centroids of all of the Angel et al. (2005) city maps using the high-resolution imagery of GE; all were correctly mapped. We then overlaid the Landsat and coarse-resolution maps in search of cities from within the sample that were omitted in the eight global urban maps. Table 13.10 presents a summary of the omitted cities by region, where we consider any city with less than 5 km^2 of urban extent in a given map as omitted by that map. Similarly, there are eight Asian cities of more than 1 million people that were omitted in at

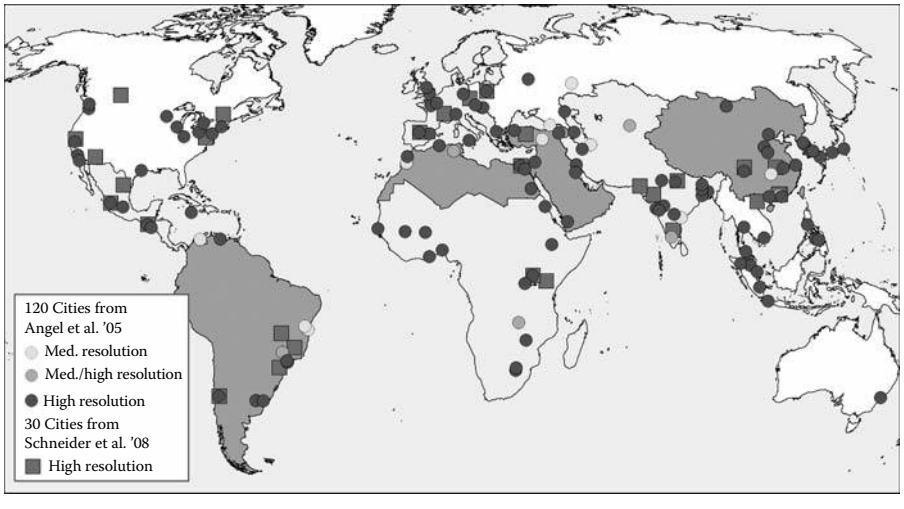

FIGURE 13.11 (See color insert following page 324.) A global sample of 120 cities with populations greater than 100,000 from Angel et al. (2005) and 30 world cities from Schneider and Woodcock (2008). The Schneider and Woodcock cities are blue boxes, all of which are covered by high-resolution imagery from the Google Earth (GE) archive. The circles represent Angel et al. cities, and the color indicates the resolution of GE imagery available for that city as of March 2008, where "high" is QuickBird, Spot 5, or aerial photography, and "medium" is Landsat GeoCover. (From Potere, D. and Schneider, A. *GeoJournal*, 69: 55–80, 2007. With permission.)

* Angel et al. (2005) created a universe of cities of 100,000 people or more in support of their sampling plan. Data from their report, "Dynamics of Global Urban Expansion," can be found at the Center for Land Use Education and Research (CLEAR), http://clear.uconn.edu (last accessed March 1, 2008). In stratifying by region, Angel et al. employed the same nine world regions used by the UN-HABITAT.

TABLE 13.10
Omitted Cities from a 120-City Sample of Cities Greater than 100,000 in Size

City Name (Population 2000, x1000)		VMAP0	GLC00	GLOBC	HYDE3	IMPSA	MOD500	MOD1K	GRUMP	Regional Omission Rates
Zhengshou, China	(2,070)		0							East Asia (56%) (9/16)
Yulin, China	(1,558)	<5	0							
Leshan, China	(1,373)	<5								
Yiyang, China	(1,343)		0						<5	
Ulan Bator, Mongolia	(738)									
Changzhi, China	(594)		0							
Anging, China	(566)		0							
Chinju, Korea	(287)		0	0						
Chonan, Korea	(114)		<5	<5						
Baku, Azerbaijan	(1,936)		<5	<5						W. Asia (63%) (5/8)
Sanaa, Yemen	(1,653)		<5	<5						
Yerevan, Armenia	(1,407)		0	0						
Malata, Turkey	(437)		0	0						
Zugdidi, Georgia	(105)		<5	<5						
Gorgan, Iran	(189)		0	0						SC Asia (6%) (1/16)
Cebu, Philippines	(719)							<5		SE Asia (8%) (1/12)
Vallendupar, Columbia	(274)		0	0						Latin Am. (19%) (3/16)
Ilheus, Brazil	(162)	0								
Jequie, Brazil	(130)	0	<5	<5						
Banjul, Gambia	(399)	<5								SS Africa (17%) (2/12)
Kigali, Rwanda	(351)	<5	0							
Port Sudan, Sudan	(384)	<5	0						<5	N. Africa (25%) (2/8)
Tebessa, Algeria	(163)	<5								
Fukuoka, Japan	(1,341)		<5	<5						ODC + Europe (3%) (1/32)
Total Omissions		**8**	**18**	**11**	**0**	**0**	**0**	**1**	**2**	
Omission Rate (120 cities)		**7%**	**15%**	**9%**	**0%**	**0%**	**0%**	**1%**	**2%**	
		VMAP0	GLC00	GLOBC	HYDE3	IMPSA	MOD500	MOD1K	GRUMP	

Abbreviations: ODC, Other Developed Countries; SS Africa: Sub-Saharan Africa; SC Asia, South Central Asia.

Note: Cities that were completely omitted from a global urban map are marked by a "0," and cities that were mapped with less than 5 km^2 of urban land are denoted by a "< 5." To estimate omission rates, any city mapped as 5 km^2 or less was considered an omission. The rightmost entries track regional omission rates (across all maps). The bottom row tracks omission totals and rates for each map (across all regions). The numbers in parenthesis to the right of the city names is the population (in thousands) in the year 2000. The regional scheme is from Angel et al. (2005).

least one of the global urban maps. Overall, GLC00, GLOBC, and VMAP0 have by far the highest omission rates from our sample (15%, 9%, and 7%, respectively). MOD500, IMPSA, and HYDE3 have no omissions, and GRUMP and MOD1K have 1–2% omission rates. By region, Asia has the most cities omitted by at least one map (West Asia 63% of sample, East Asia 56%, Southeast Asia 8%, South central Asia 6%), followed by Africa (North Africa 25%, sub-Saharan Africa 17%), and Latin America (19%). Only one city from Europe and the Other Developed Countries (ODC) region was omitted; Fukuoka, Japan, with a population of 1.3 million people was omitted by both GLC00 and GLOBC. Only three of the

maps, MOD500, IMPSA, and HYDE3, manage to map all 120 cities of the sample (i.e., 0% omission rate); this result is the same if the threshold for considering a city as omitted is increased from 5 to 10 km^2.

This strategy of searching for omission errors by seeking out large urban centers is a logical first step in assessing any global urban map. Essentially, we are evaluating whether such maps can at least reproduce the information contained in city gazetteers, which list the position and population of major cities worldwide. The complement to this approach is to search for urban commission errors in regions of the world that are least likely to contain developed land or a human presence. In addition to checking desert environments (as discussed in connection with Figure 13.7 above), we can also check protected areas (conservation lands). The World Database on Protected Areas (WDPA) from the UN World Conservation Monitoring Center provides a global-scale portrait of lands that are least likely to be occupied by urban settlement (WDPA, 2006). We are in the process of overlying the WDPA map atop the eight global urban maps to identify potential urban commission errors (areas incorrectly labeled as urban). The added benefit of an approach that draws upon WDPA is that it will provide the conservation community with an assessment of the degree of land degradation within existing protected areas, an attribute of considerable concern (Rouget et al., 2006). More than 90% of our cities and much of their peri-urban hinterlands are present within the high-resolution GE archive, making GE a potential accelerator of searches for these omission and commission errors. Preliminary research on the geospatial accuracy of the high-resolution GE archive indicates that it is sufficiently accurate for use in assessing these global maps (Potere, in preparation).

Thus far, we have described point-based assessment procedures, where we search for urban omission and commission errors within a sample of point locations. A second line of assessment involves estimation of map agreement statistics between medium-resolution (30 m) Landsat-based city maps and each of the eight global maps. For each of the cities in the samples of Angel et al. (2005) and Schneider and Woodcock (2008), we downsample the coarse-resolution global urban maps to 30 m, overlay them atop the Landsat validation maps, create contingency tables, and process these contingency tables to produce the six measures of map agreement from Table 13.4b for each city-map combination. Figure 13.12 contains box plots for the distribution of agreement measures, using the 120 city maps of Angel et al. (2005) as validation data; as before, values approaching 1.0 indicate higher agreement. For the most robust measures of overall agreement (kappa, NMI, and TSS), the MODIS-based maps (MOD500 and MOD1K) appear to be in significantly stronger agreement with the Landsat validation data than the other six maps. The asterisks adjacent to HYDE3 and IMPSA indicate that we used thresholded versions of these continuous maps, where all pixels with more than 50% impervious surface were labeled as urban. A more complete analysis is ongoing, which will explore the accuracy distributions associated with a wide range of thresholds for HYDE3 and IMPSA.

Because the bottom row measures in Figure 13.12 (sensitivity, specificity, and overall map accuracy) are influenced by the overall extent of the maps in question, it is important to interpret them together; in this respect, they are unlike the

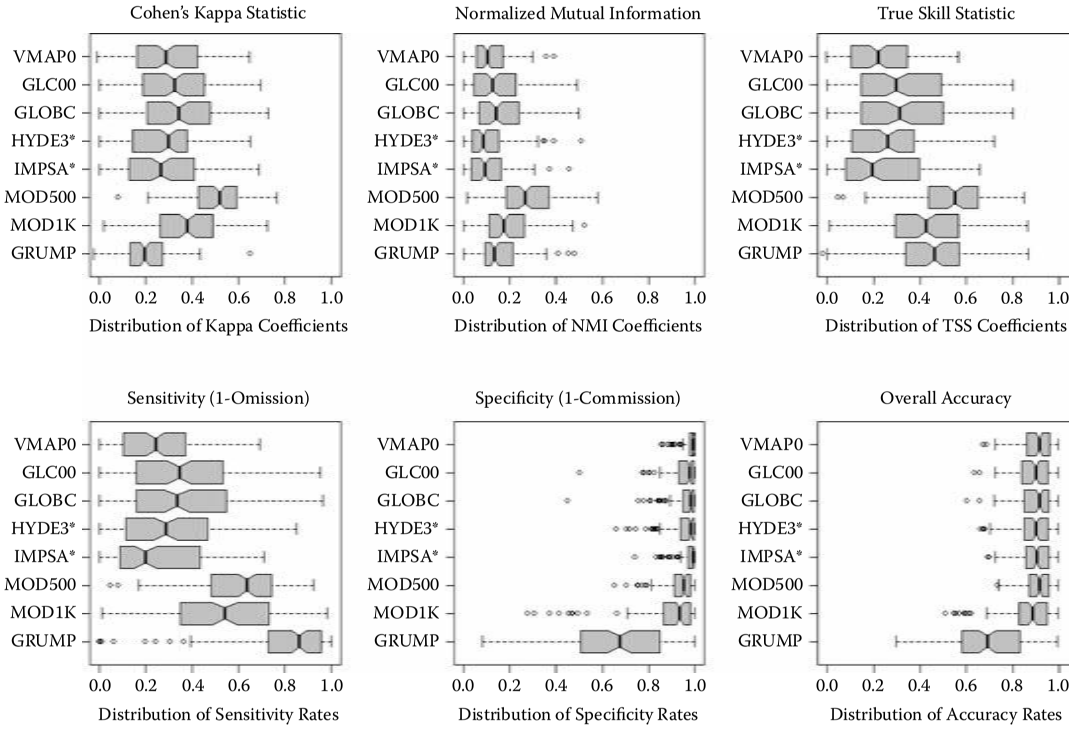

FIGURE 13.12 Map agreement statistics for the eight global urban maps. We constructed contingency tables for each of the 120 cities in the Angel et al. (2005) *Dynamics of the Global Urban Expansion* report. The box-plots depict the map accuracy measures for each map and each of the 120 cities. The top row plots overall map agreement statistics that consider both omission and commission errors and are adjusted to take into consideration chance agreement (kappa) and variations in the overall extent of the maps (NMI and TSS). The bottom row plots traditional map accuracy statistics (sensitivity, specificity, and accuracy). The asterisks adjacent to HYDE3 and IMPSA indicate that a thresholded version of those maps was used, where the majority urban pixels (≥ 50% impervious surface) were labeled as urban and all others as non-urban. (From Potere, D. and Schneider, A. *GeoJournal*, 69: 55–80, 2007. With permission.)

overall measures of agreement from the top row (kappa, MNI, TSS), which can be considered alone. For instance, in part because GRUMP is by far the most extensive map, it has very high sensitivity, indicating that it rarely omits urban pixels; however, GRUMP also has quite low specificity, meaning that it often makes commission errors. These commission errors draw down the overall accuracy of GRUMP. Because the global urban maps are arranged from least extensive to most extensive (top to bottom, Figure 13.12), a trend is apparent where those maps with higher overall extent (i.e., MOD500, MOD1K, and GRUMP) have higher sensitivity than those maps with lower overall extent (i.e., VMAP0, GLC00, and GLOBC). An inverse trend is apparent with regard to specificity. Although sensitivity, specificity, and overall accuracy can sometimes provide important information, this trade-off between omission and commission errors is one of the principal reasons behind measures from the top row of Figure 13.12, which consider all aspects of the contingency table.

This map assessment should be taken only as a useful first glimpse into the accuracy of global urban maps. The assessment is ongoing, and we are working to address limitations with regard to the adequacy of the validation sample, geolocation errors, and temporal mismatch. With regard to the former, our sample is biased in that we omit cities of less than 100,000 persons; this omission is worrisome considering that 26% of the global urban population may live in these areas.* We are working to increase the number of cities by including those from a recent assessment of urban expansion (Schneider and Woodcock, 2008) and using imagery from GE. The GE imagery may also be beneficial in providing us with a source of validation data to improve our accuracy assessments for the medium-resolution city maps, allowing us to weight the distributions in Figure 13.12 by the accuracies of the underlying Landsat-based validation maps.† The map agreement measures may also be sensitive to small geolocation errors that are not evident on gross inspection; only by testing accuracy with small shifts to the underlying validation data can we eliminate these potential biases. Finally, there are temporal concerns for both the global urban maps and the validation data; many of the input data for the global urban maps span the late 1990s to 2005, the Landsat validation maps range from 1997 to 2003, whereas the GE imagery rarely indicates the image acquisition date. Because urbanization is rapid in some regions of the world (e.g., China and parts of Southeast Asia), a difference of only a few years can bias estimates of omission and commission error rates. In our current work, we are attempting to balance these concerns to present a robust analysis of the eight global urban maps across spatial and temporal resolutions.

* The total population in the Angel et al. (2005) universe of cities of 100,000 persons or more for the year 2000 was 2.12 billion, and the UN Population Division estimate for the total urban population (regardless of city size) in 2000 was 2.86 billion — a 26% difference.

† Although the original Angel et al. assessment indicates an 89.2% overall map accuracy for their Landsat maps, this assessment was confined to 10% of the maps. Ongoing research indicates that GE high-resolution imagery is of sufficient spatial accuracy to be of use in assessing medium-resolution Landsat imagery (Potere, in preparation).

13.6 DISCUSSION AND CONCLUSIONS

As both recipients of ecosystem services and modifiers of ecosystem processes, humanity is an important part of the biosphere. To better understand the role humans play in ongoing global change processes, there is a need for a global, accuracy-assessed, moderate-resolution, and regularly updated map of contemporary human settlement. Global urban maps can make an important contribution here, by accounting for the residences of more than half of the human population. To meet this need, eight international groups from government and academia have created global maps that can be used to describe contemporary urban areas (Vector Map Level Zero, Global Landcover 2000, GlobCover, HYDE3, Global Impervious Surface Area, MODIS Urban Land Cover 1 km, MODIS Urban Land Cover 500 m, and GRUMP). Such maps are of significant interest to a wide range of users, including regional and national planners, disaster management specialists, humanitarian and development aid coordinators, epidemiologists and public health officials, demographers, economists, conservation biologists, climatologists, and urban ecologists (Potere and Schneider, 2007).

Despite the considerable resources allocated to the task of creating global urban maps, this chapter has revealed that the eight maps differ by as much as an order of magnitude in their estimates of the total areal extent of the Earth's urban land (0.27–3.52 million km^2). Differences in these eight maps persist at the scale of urban patches, countries, and world regions. To better visualize these maps and to conduct a quantitative map comparison, we used a hexagonal system of DGGs. An analysis of the spatial distribution of urban land based on these DGGs across a wide range of spatial resolutions (29–264 km) has revealed that intermap correlations are highest in North America ($\overline{r}$ = 0.83), lowest in Asia ($\overline{r}$ = 0.66), and intermediate in Europe, South and Central America, and sub-Saharan Africa ($\overline{r}$ = 0.79). It seems that large intermap differences are driven by a combination of several factors, including differences in the timing of map construction, differences in map resolution and class enumeration, and fundamental differences in each group's approach to urban land. Scale and resolution are of concern because many of these maps combine coarse-resolution inputs with binary classifications (urban/nonurban classes). Because urban land does not occur in neat 30″ arc-second square blocks, there are considerable problems inherent in any attempt to infer total areal extent from coarse-resolution binary classifications (Latifovic and Olthof, 2004; Ozdogan and Woodcock, 2006).

Of the aforementioned sources of intermap variance, perhaps the most important is a fundamental divergence in each group's approach to defining and modeling urban land. The problem of creating a meaningful and workable characterization of "urban" is not trivial. In the absence of a clear set of definitions, each group constructs an implicit model of urban extent that can be inferred from their methodologies. The eight global urban maps that emerge are sensitive to many attributes commonly associated with urban areas, including high population density, extensive built environment, nighttime illumination, and proximity to transportation infrastructure. The degree to which any one of these attributes contributes to an urban classification is likely regionally dependent and is not specified by any of the makers

of these maps. We can do better if progress can be made toward synchronizing legends and negotiating a common set of multifaceted urban definitions that draw on both the demographic and the physical dimensions of urbanization.

The only way to truly understand the source and impact of the large intermap differences is to conduct a global map accuracy assessment. In Section 13.5, we report initial findings from an ongoing assessment, which indicate that the MODIS-based maps are in stronger agreement with the assessment data than the other six global urban maps. We also find that only three maps avoid omitting any of the 120 assessment cities (MODIS Urban Land Cover 500 m, HYDE3, and Global Impervious Surface Area). This assessment is a first step toward building a better understanding of the global urban fabric. Future assessments based on larger sets of validation data will allow us to make more meaningful statements about regional map accuracy, georegistration, and the underlying models of urban extent implicit within each global urban map. In the longer term, an improved understanding of each map's strengths and weaknesses in both space and time will facilitate the construction of a suite of composite urban maps that are tailored to particular user groups. We could address the specific needs of users by first devising a group-specific definition of urban areas (either ordinal or categorical), and next fusing components of existing global urban maps and urban-related maps that best meet the requirements of those definitions.

The human built environment is complex, and no single binary definition of the urban/rural divide is likely to satisfy the demands of a growing user community. With more than two billion new urban residents due to arrive within the next quarter century, there can be little doubt that a new series of urban maps is on the way. Whether those maps are more successful at capturing the complexities of urban areas depends on how effectively we engage the multidisciplinary community of map users and map producers to resolve the fundamental issue of urban taxonomy and agree on a common map assessment regime.

REFERENCES

Allouche, O., Tsoar, A., and Kadmon, R., Assessing the accuracy of species distribution models: Prevalence, kappa, and the true skill statistic (TSS), *Journal of Applied Ecology*, 43, 1223–1232, 2006.

Angel, S., Sheppard, S.C., and Civco, D.L., *The Dynamics of Global Urban Expansion*, World Bank, Washington, D.C., 2005. Available at: http://www.williams.edu/Economics/UrbanGrowth/WorkingPapers.htm (accessed April 15, 2007).

Bartholome, E., and Belward, A.S., GLC2000: A new approach to global land cover mapping from Earth observation data, *International Journal of Remote Sensing*, 26, pp. 1959–1977, 2005.

Bhaduri, B., Bright, E., Coleman, P., and Dobson, J., LandScan: Locating people is what matters, *Geoinfomatics*, 5, 34–37, 2002.

Center for International Earth Science Information Network, Global Rural-Urban Mapping Project (GRUMP), Alpha Version: Urban Extents. Socioeconomic Data and Applications Center (SEDAC), Columbia University, Palisades, NY, 2004. Available at: http://sedac.ciesin.columbia.edu/gpw (accessed April 15, 2007).

Cohen, J., A coefficient of agreement for nominal scales, educational and psychological measurement, *Educational and Psychological Measurement*, 20, 37–46, 1960.

Congalton, R.G., and Green, K., *Assessing the Accuracy of Remotely Sensed Data: Principles and Practices*, CRC Press, New York, 1999.

Danko, D.M., The Digital Chart of the World Project, *Photogrammetric Engineering and Remote Sensing*, 58, pp. 1125–1128, 1992.

Dobson, J.E., Bright, E.A., Coleman, P.R., Durfee, R.C., and Worley, B.A., Landscan: A global population database for estimating populations at risk, *Photogrammetric Engineering and Remote Sensing*, 66, 849–857, 2000.

Doll, C.N.H., Muller, J.P., and Morley, J.G., Mapping regional economic activity from nighttime light satellite imagery, *Ecological Economics*, 57, 75–92, 2006.

Douglas, I., Human settlements, in Meyer, W.B., and Turner, B.L., II, eds., *Changes in Land Use and Land Cover: A Global Perspective*, Cambridge University Press, Cambridge, 1994.

Elvidge, C., Imhoff, M.L., Baugh, K.E., Hobson, V.R., Nelson, I., Safran, J., Dietz, J.B., and Tuttle, B.T., Nighttime lights of the world: 1994–95, *ISPRS Journal of Photogrammetry and Remote Sensing*, 56, 81–99, 2001.

Elvidge, C., Tuttle, B.T., Sutton, P.C., Baugh, K.E., Howard, A.T., Milesi, C., Bhaduri, B.L., and Nemani, R., Global distribution and density of constructed impervious surfaces, *Sensors*, 7, 1962–1979, 2007.

Fielding, A.H., and Bell, J.F., A review of methods for the assessment of prediction errors in conservation presence/absence models, *Environmental Conservation*, 24, 38–49, 1997.

Foody, G.M., What is the difference between two maps? A remote senser's view, *Journal of Geographical Systems*, 8, 119–130, 2006.

Foody, G.M., Map comparison in GIS, *Progress in Physical Geography*, 31, 439–445, 2007.

Forbes, A.D., Classification algorithm evaluation: Five performance measures based on confusion matrices, *Journal of Clinical Monitoring*, 11, 189–206, 1995.

Giri, C., Zhu, Z.L., and Reed, B., A comparative analysis of the Global Land Cover 2000 and MODIS land cover datasets, *Remote Sensing of the Environment*, 94, pp. 123–132, 2005.

Global Land Cover Facility, 2007. Available at: http://glcf.umiacs.umd.edu (accessed February 20, 2007).

Goldewijk, K., Estimating global land use change over the past 300 years: The HYDE database, *Global Biogeochemical Cycles*, 15, 417–434**,** 2001.

Goldewijk, K., Three centuries of global population growth: A spatially referenced population density database for 1700–2000, *Population and Environment*, 26, 343–367**,** 2005.

Goldewijk, K., and Ramankutty, N., Land cover change over the last three centuries due to human activities: The availability of new global datasets, *GeoJournal*, 61, 335–344**,** 2004.

Greyner, R., Orme, C., Jackson, S., Thomas, G. Davies, R., Davies, T., Jones, K., Olson, V., Ridgely, R., Rasmussen, P., Ding, T., Bennett, P., Blackburn, T., Gaston, K., Gittleman, J., and Owens, I., Global distribution and conservation of rare and threatened vertebrates, *Nature*, 444, 93–96, 2006.

Grübler, A., Technology, in: Meyer, W.B., and Turner, B.L., II., eds., *Changes in Land Use and Land Cover: A Global Perspective*, Cambridge University Press, Cambridge, 1990.

Hansen, M.C., Defries, R.S., Townsend, R.G., and Sohlberg, R., Global land cover classification at 1 km spatial resolution using a classification tree approach, *International Journal of Remote Sensing*, 21, 1331–1364, 2000a.

Hansen, M.C., and Reed, B., A comparison of the IGBP DISCover and University of Maryland 1 km global land cover products*, International Journal of Remote Sensing*, 21, 1365–1373, 2000b.

Henderson, M., Yeh, E.T., Gong, P., Elvidge, C., and Baugh, K., Validation of urban boundaries derived from global night-time satellite imagery, *International Journal of Remote Sensing*, 24, 595–609, 2003.

Imhoff, M.L., Lawrence, W.T., Stutzer, D.C., and Elvidge, C.D., A technique for using composite DMSP/OLS "City Lights" satellite data to accurately map urban areas, *Remote Sensing of Environment*, 61, 361–370, 1997.

Jung, M., Henkel, K., Herold, M., and Churkina, G., Exploiting synergies of global land cover products for carbon cycle modeling, *Remote Sensing of Environment*, 101, 534–553, 2006.

Kendall, M., A new measure of rank correlation, *Biometrika*, 30, 81–89, 1938.

Landis, J.R., and Koch, G.G., The measurement of observer agreement for categorical data, *Biometrics*, 33, 169–174, 1977.

Latifovic, R., and Olthof, I., Accuracy assessment using sub-pixel fractional error matrices of global land cover products derived from satellite data, *Remote Sensing of Environment*, 90, 153–165, 2004.

Liu, C., Frazier, P., and Kumar, L., Comparative assessment of the measures of thematic classification accuracy, *Remote Sensing of the Environment*, 107, 606–616, 2007.

Lobo, J.M., Jimenez-Valverde, A., and Real, R., AUC: A misleading measure of the performance of predictive distribution models, *Global Ecology and Biogeography*, 17, 145–151, 2007.

Loveland, T.R., Reed, B.C., Brown, J.F., Ohlen, D.O., Zhu, J., Yang, L., and Merchant, J.W., Development of a Global Land Cover Characteristics database and IGBP DISCover from 1-km AVHRR data, *International Journal of Remote Sensing*, 21, 1303–1330, 2000.

Manel, S., Williams, H.C., and Ormerod, S.J., Evaluating presence-absence models in ecology: The need to account for prevalence, *Journal of Applied Ecology*, 38, 921–931, 2001.

Mayaux, P., Eva, H., Gallego, J., Strahler, A.H., Herold, M., Agrawal, S., Naumov, S., Miranda, E., Bella, C., Ordoyne, C., Kopin, Y., and Roy, P., Validation of the Global Land Cover 2000 map, *IEEE Transactions on Geoscience and Remote Sensing*, 44, 1728–1739, 2006.

McCallum, I., Obersteiner, M., Nilsson, S., and Shvidenko, A., A spatial comparison of four satellite derived 1 km global land cover datasets, *International Journal of Applied Earth Observation and Geoinformation*, 8, 246–255, 2006.

McPherson, J.M., Jetz, W., and Rogers, D.J., The effects of species' range sizes on the accuracy of distribution models: Ecological phenomenon or statistical artefact? J*ournal of Applied Ecology*, 41, 811–823, 2004.

Monserud, R., and Leemans, R., Comparing global vegetation maps with the kappa statistic, *Ecological Modeling*, 62, 275–293, 1992.

National Geophysical Data Center, 2007. Available at: http://www.ngdc.noaa.gov/dmsp/sensors/ols.html.

Ozdogan, M., and Woodcock, C.E., Resolution dependent errors in remote sensing of cultivated areas, *Remote Sensing of the Environment*, 103, 203–217, 2006.

Potere, D., and Schneider, A., A critical look at representations of urban areas in global maps, *GeoJournal*, 69, 55–80, 2007.

Potere, D., The geodetic accuracy of Google Earth's high resolution imagery archive, in preparation.

Ridd, M.K., Exploring a V-I-S (vegetation–impervious surface–soil) model for urban ecosystem analysis through remote sensing — comparative anatomy for cities, *International Journal of Remote Sensing*, 16, 2165–2185, 1995.

Rouget, M., Cowling, R.M., Vlok, J., Thompson, M., and Balmford, A., Getting the biodiversity intactness index right: The importance of habitat degradation data, *Global Change Biology*, 12, 2032–2036, 2006.

Sahr, K., White, D., and Kimerling, A., Geodesic Discrete Global Grid Systems, *Cartography and Geographic Information Science*, 30, 121–134, 2003.

Schaaf, C.B., Gao, F., Strahler, A.H., Lucht, W., Li, X., Tsang, T., Strugnell, N., Zhang, X., Jin, Y., Muller, J., Lewis, P., Barnsley, M., Hobson, P., Disney, M., Roberts, G., Dunderdale, M., Doll, C., d'Entremont, R., Hu, B., Liang, S., Privette, J.L., and Roy, D., First operational BRDF, albedo nadir reflectance products from MODIS, *Remote Sensing of the Environment*, 83, 135–148, 2002.

Schneider, A., Friedl, M.A., Mciver, D.K., and Woodcock, C.E., Mapping urban areas by fusing multiple sources of coarse resolution remotely sensed data, *Photogrammetric Engineering and Remote Sensing*, 69, 1377–1386, 2003.

Schneider, A., Friedl, M.A., and Woodcock, C.E., Mapping urban areas by fusing multiple sources of coarse resolution remotely sensed data: Global results, in: *Proceedings of the 5th International Symposium of Remote Sensing of Urban Areas,* 14–16 March, Tempe, AZ, 2005.

Schneider, A., and Woodcock, C.E., Compact, dispersed, fragmented, extensive? A comparison of urban expansion in twenty-five global cities using remotely sensed data, pattern metrics and census information, *Urban Studies*, 45, 659–692, 2008.

Schneider, A., Friedl, M.A., and Potere, D., Monitoring the extent and intensity of urban areas globally using MODIS 500 m resolution satellite imagery, *Geoscience and Remote Sensing Symposium, IEEE International*, 5, 346–349, 2008.

See, L.M., and Fritz, S., A method to compare and improve land cover datasets: Application to the GLC-2000 and MODIS land cover products, *IEEE Transactions in Geoscience and Remote Sensing*, 44, 1740–1746, 2006.

Small, C., and Cohen, J.E., Continental physiography, climate, and the global distribution of human population, *Current Anthropology*, 45(2), 269–277, 2004.

Small, C., Pozzi, F., and Elvidge, C.D., Spatial analysis of global urban extent from DMSP-OLS night lights, *Remote Sensing of the Environment*, 96, 277–291, 2005.

Sutton, P., Roberts, D., Elvidge, C., and Meij, H., A comparison of night-time satellite imagery and population density for the continental United States, *Photogrammetric Engineering and Remote Sensing*, 63, 1303–1313, 1997.

Sutton, P.C., and Costanza, R., Global estimates of market and non-market values derived from nighttime satellite imagery, land cover, and ecosystem service valuation, *Ecological Economics*, 41, 509–527, 2002.

Tatem, A.J., Noor, A.M., and Hay, S.I., Assessing the accuracy of satellite derived global and national urban maps in Kenya, *Remote Sensing of the Environment*, 96, 87–97, 2005.

Tucker, C.J., Grant, D.M., and Dykstra, J.D., NASA's global orthorectified Landsat data set, *Photogrammetric Engineering and Remote Sensing*, 70, 313–322, 2004.

UN Population Division, *United Nations World Urbanization Prospects — The 2005 Revision*, 2005. Available at: http://esa.un.org/unup (accessed April 15, 2007).

UN Statistics Division, Standard Country or Area Codes for Statistical Use, 2007. Available at: http://unstats.un.org/unsd/methods/m49/m49.htm (accessed March 1, 2008).

UN Statistics Division, United Nations Common Database, 2008. Available at: http://unstats.un.org/unsd/cdb/cdb_help/cdb_quick_start.asp (accessed March 1, 2008).

Utzinger, J., and Keiser, J., Urbanization and tropical health — then and now, *Annals of Tropical Medicine and Parasitology*, 100, 517–533, 2006.

Vogelmann, J.E., Howard, S.M., Yang, L., Larson, C.R., Wylie, B.K., and Van Driel, N., Completion of the 1990s National Land Cover Data set for the coterminous United States from Landsat Thematic Mapper data and ancillary data sources, *Photogrammetric Engineering and Remote Sensing*, 67, 650–662, 2001.

Welch, R., Monitoring urban population and energy utilization patterns from satellite data, *Remote Sensing of the Environment*, 9, 1–9, 1980.

World Database of Protected Areas Consortium, World Database on Protected Areas, 2006. Available at: http://sea.unep-wcmc.org/wdbpa (accessed March 1, 2008).

World Bank, World Development Indicators, 2008. Available at: http://web.worldbank.org (accessed February 20, 2008).

Yang, L., Huange, C., Homer, C., Wylie, B., and Coan, M., An approach for mapping large-are impervious surfaces: Synergistic use of Landsat 7 ETM+ and high spatial resolution imagery, *Canadian Journal of Remote Sensing*, 29, 230–240, 2003.

14 The Role of SAR Sensors

Fabio Dell'Acqua

CONTENTS

14.1 INTRODUCTION

Urban areas represent a very complex environment in terms of shape and number of different materials and patterns found in the widest "urban" land cover class.

Remote sensors to be used for the analysis of the urban environment are subject to strict requirements with respect to spectral and spatial resolution, as well as to their capability to handle the third dimension.

Synthetic aperture radar (SAR) sensors seem to possess all the necessary features to qualify as a suitable candidate, including the three-dimensional (3-D) capabilities granted by the interferometric version of SAR (InSAR). The SAR community has indeed been gaining increasing importance in the urban remote sensing scenario, as testified by a scanning of the papers presented in the various editions of the URBAN conference.

In this chapter, the use of SAR in the urban environment is briefly recalled from an historical perspective, then some current, important fields of application are outlined in the following subchapters. Finally, several conclusions are drawn.

14.1.1 Historical Evolution and Scenario

SAR sensors have been long reputed as unsuitable for precise characterization of the urban environment, and even today very high resolution (VHR) optical data are considered somehow mandatory for efficient and reliable land use mapping. Besides the very first works on SEASAT images, the seminal papers in applying SAR sensors to urban environments appeared in 1990. Later, a more extensive introduction

of SAR sensors into remote sensing techniques over urban areas was to appear. This was represented by a special issue of the *IEEE Transactions on Geoscience and Remote Sensing* in 1997. Henderson and Xia's (1997) review of those articles showed that much remained to be done in the direction of a better automatization of the analysis process. From that point on, many papers appeared that mainly exploited the possibility of capturing the geometrical features that are peculiar to man-made structures. For instance, textural features have been widely considered, because they allow evaluation of spatial correlations between urban objects. As for the future, recent reviews of SAR urban remote sensing, proposed in three special sessions — two in EUSAR '06 (EUSAR, 2006) and one in IGARSS '06 (IGARSS, 2006) — show a big stress on high-resolution (HR) SAR data, possibly in conjunction with optical data, and the use of interferometric information for 3-D analysis of the urban environment.

Unfortunately, satellite SAR sensors have achieved only recently very fine spatial resolution. At the time of writing, TerraSAR-X images have just seen the start of their distribution, whereas those of RADARSAT-2 and COSMO/SkyMed have not been distributed yet, with the exception of a few sample images under the form of "fine quick-looks," which are of little use for research purposes. Therefore, another very active line of research today is the use of available, low-resolution (LR) satellite SAR data for mapping the structure of urban areas. The huge amount of past SAR imagery carries a wealth of information about the evolution of urban areas still to be fully exploited. Moreover, enlarging the research view from urban areas in a strict sense to "human settlements" opens a whole new panorama of applications and possibilities. The arguments against using former SAR data for these applications are related to the insufficient spatial resolution of data and the unstructured character of most human settlements. Both problems deserve attention, but recent approaches have shown that they can be eased by means of more precise spatial pattern analysis of SAR data and data fusion.

The most important advantage of SAR over optical images is related to the complex nature of the radar signal. By exploiting this feature, it is possible not only to improve knowledge about the backscattering properties of the urban material thanks to the information carried by the phase of the signal, but also to extract 3-D information by means of the so-called InSAR (Gens and Van Genderen, 1996). SAR interferometry has a number of different applications in urban areas, ranging from subsidence monitoring (Ferretti et al., 2000) to the characterization of 3-D builtscape (Gamba et al., 2000). A comparison of airborne and satellite systems for 3-D urban analysis (Gamba and Houshmand, 2002) has shown that C-band and X-band data have very similar responses from man-made structures but show differences in vegetated areas, which may be useful for mapping purposes and for discrimination of these two land uses in 3-D maps. Moreover, SAR coherence has been widely considered in urban areas because of their peculiarity of containing many strong and long-lasting backscatterers. As a result, in urban areas the typical coherence is usually much higher than in agricultural fields and forestry (Usai and Klees, 1999), unless some dramatic change in the observed objects takes place. Thus, coherence has been used to map human settlements (Dammert et al., 1999), to assess damage after

Earthquakes (Yonezawa and Takeuchi, 2001) and for change detection (Dierking and Skriver, 2002).

Long sequences of SAR data are also useful for urban area monitoring. The permanent scatterers technique (Ferretti et al., 2000) allows users to sense tiny, slow vertical motion for elevated objects naturally including urban and other man-made structures. This technique is widely used for monitoring of subsidence movements and is naturally of considerable interest for analyzing factors of risk (deformation, collapse, sinking) connected to slow vertical motion of the terrain underlying urban areas. Several-year-long sequences can correct for disturbing factors causing decorrelation (De Zan and Rocca, 2005) and provide extremely precise measurements. Long sequences fused with geographic information systems are also useful, as shown by Gamba et al. (2008), in improving the accuracy of classification in urban areas, especially with respect to urban sprawl monitoring.

Finally, polarimetry is becoming increasingly important for new SAR systems, because the availability of multiple polarization allows users to discriminate among the various backscattering mechanisms that take place in urban areas. As a consequence, different building structures may be recognized (Dong et al., 1997). Polarimetric interferometry is also starting to provide 3-D information from a single polarimetric sensor, further enhancing our ability to reconstruct building information using radar data.

The new generation of satellite sensors, featuring a level of resolution comparable with that of VHR optical satellites but offering coherent backscattering evaluation as a bonus, will enable a detailed analysis of urban areas, and polarimetric capabilities will push further the analysis capabilities by providing more means to distinguish different building patterns and urban land cover classes.

In the following sections, we will show several examples of how SAR data can be fruitfully used for detection, delineation, and in-depth analysis of human settlements.

14.2 High-Resolution Observation of Human Settlements

The use of SAR systems to observe human settlements is a recent addition to the technical literature in Earth observation. Long after SAR was introduced, the possibility of using such sensors for urban area observation was first proposed in a systematic fashion by Henderson and Xia (1997) and in other papers in the special issue. Since then, a number of papers have appeared that invoked HR SAR as a requirement for an in-depth analysis of urban areas.

Nowadays, the successful launch of low Earth orbit satellites, such as the German TerraSAR-X (Roth, 2003) and the Italian COSMO/SkyMed (Impagnatiello et al., 1998), is about to open a new possibility to researchers, whereas Radarsat-1 (Weydahl et al., 2003) fine mode and ALOS PALSAR (Rosenqvist et al., 2004) data provide an intermediate step towards fine-resolution observation of human settlements.

When one moves from ERS (European Remote Sensing)-like spatial resolutions (30 m) to about 7 m, which is the common value for the two latter instruments, a number of new issues arise. First of all, human settlements reveal their nonhomogeneity, and even different parts of the same objects tend to act — and appear — as separate-response scatterers. This adds to the traditional unreliability of pixel

digital numbers (DNs) in a coherent radar image, and as a result no approach based on pixel-by-pixel analysis is capable of suitably handling this variety of possible responses within the same land cover class. Segmentation approaches are more likely to succeed (Lombardo et al., 2003) and can be based either on statistical (Macrì Pellizzeri et al., 2003) or spatial (Dell'Acqua and Gamba, 2003) analysis. The latter approach has a more immediate meaning and is directly related to the spatial structure of the settlement, which is one of the basic indicators of its usefulness. It has been shown that formal and informal settlements differ by the "order-versus-disorder" appearance in remotely sensed images (Niebergall et al., 2007), and different land uses can be discriminated even using coarser data (Dell'Acqua and Gamba, 2006), with a feasible scale-adaptive approach. In the following subsections, two representative examples of urban observation derived from HR SAR data are discussed.

14.2.1 Extraction of Single Buildings

Although satellite HR SAR data still have a limited availability, HR airborne SAR has allowed developing techniques, which prepare the ground for the exploitation of future satellite data. Three-dimensional building recognition (Thiele et al., 2007) is a typical application, which becomes feasible when such data are available instead of traditional LR satellite data.

SAR and InSAR data have been exploited in city cores with high-rise buildings (Gamba et al., 2000), rural areas, and industrial plants (Simonetto et al., 2005). These techniques still show limits, especially when compared with the expensive LIDAR data (Stilla et al., 2003).

A first reason for the nonfavorable situation of SAR is obviously its side-looking nature, which results in phenomena such as foreshortening, layover, occlusion, total reflection, and multibounce scattering. All these phenomena are found also in natural scenes, but are made far more dramatic by the typical features of the urban environment, rich of smooth (with respect to wavelength), planar patches often at right angles with each other (resulting in corner-cube-like reflection) or parallel to each other (resulting in several bounces of the incident electromagnetic wave).

Depending on the viewing direction, acquisition of large parts of an urban scene can be plagued with these phenomena (Dong et al., 1997); regions of radar shadow (e.g., cast behind buildings) coincide with noisy InSAR elevation data. One may get around such obstacles by acquiring SAR data from different vantage points and fusing interpretation results (Soergel et al., 2005).

14.2.2 Information Fusion with LIDAR Data

Another sensor especially useful in urban areas is LIDAR (light detection and ranging). Its use has gained support, thanks to its suitability for precise 3-D mapping of urban areas, where precision is required in characterization of building footprint location and delineation, height, and in recognition of fine details. LIDAR systems exploit the light reflected by the Earth surface illuminated by a laser source to form a 3-D model of the surfaces seen by the sensor.

InSAR and LIDAR data are both interesting for urban area characterization, and their combination is even more so. SAR data can be easily acquired on a much wider area and at a lower cost per square kilometer than LIDAR data, thanks to spaceborne systems; on the other hand, LIDAR data are less subject to distortions, due to the nadir-looking nature of the sensor, and feature finer ground spatial sampling.

An interesting way to combine LIDAR and InSAR data is to use LIDAR to reduce artifacts in InSAR 3-D characterization of buildings inside an urban area. Comparison between the data in a small portion of the SAR data where LIDAR information is available may suggest a correction procedure, which can be extended to the whole radar image. A possible algorithm, described in more detail by Gamba et al. (2006a), is recalled here as an example of how some of the most undesirable features of InSAR data in urban areas may be overcome through data fusion.

Whenever a SAR instrument images an elevated object, such as a building, a displacement of each building footprint in SAR data toward the sensor takes place, due to the side-looking nature of the radar, together with 2-D and 3-D distortion of the same footprint due to layover and/or shadowing effects. One could exemplify all these problems via a nonlinear transformation that translates the original footprint into a displaced and deformed one. This transformation is a function of the radar illumination angle θ, the structure orientation φ, and height h, and the terrain slope. This nonlinear transformation may be reduced to a planar transformation in areas where the buildings share roughly the same features. In this situation, jointly applying a footprint shift and a stretching step would be enough to restore the original footprints. The processing chain in the above-mentioned work (Gamba et al., 2006a), basically a procedure of data fusion between InSAR and LIDAR data, is composed of the following steps:

1. Extraction of the Digital Terrain Model (DTM) and the building footprints;
2. Shifting of the buildings to correct side-looking effects;
3. Reduction of the area mismatch due to layover/shadowing by means of a geometrical correction of InSAR footprints;
4. Improvement of the InSAR 3-D building shapes by masking the height values using the relocated and geometrically corrected footprints.

By applying this technique, the overall InSAR builtscape in the urban area improves, and further regularization algorithms may be applied to extract the 3-D shape of each building.

14.3 LR SAR OBSERVATION OF HUMAN SETTLEMENTS

14.3.1 Damage Assessment with LR SAR

When dealing with a single SAR image, the sheer number of different backscattering measurement results in HR images and places the conveyed amount of information above that of any LR SAR image. However, the situation may change when a large number of LR images are considered, because a set of such images can also

lead to very interesting results, especially if the phase/interferometric information is exploited. Let us consider a particular change detection problem for which the latter condition is especially relevant, that is, Earthquake damage assessment in LR SAR data.

Two main research approaches have been explored in this field: one is to consider the decorrelation due to the change in orientation of strong scatterers (Usai and Klees, 1999), and the other tries to detect backscatter intensity changes due to the geometric deformation of damaged buildings.

Damage assessment using coherence was proposed by Yonezawa and Takeuchi (2001), who compared interferometric coherence and intensity correlation. The proposed approach relied on interferometric processing; although this option is somewhat "delicate" in that, for example, multisensor SAR interferometry is often impossible, and phase information is highly dependent on the acquisition geometry, damage mapping through coherence may allow more precise discrimination among different damage levels, due to the highest sensitivity of coherence to geometric changes.

A more robust approach to damage assessment is to use SAR intensity data, explored and discussed by Matsuoka and Yamazaki (2004). Indeed, the authors showed that intensity measures are more reliable, and through a suitable choice of a discriminating function, it is possible to map the affected and unaffected areas with higher reliability. The presence of speckle noise suggested to apply a despeckling filtering step, and not to consider intensity at the pixel level, but rather in terms of its statistics computed over a suitably sized neighborhood of the location under test.

Unfortunately, some form of degradation in terms of spatial resolution is to be expected when processing SAR images, because of the necessity of having to deal with the problem of speckle noise through some form of averaging or statistical feature extraction over local neighborhoods. Naturally, this is a more remarkable handicap for LR SAR, as geometrical clues in HR SAR remain detectable not withstanding speckle, whereas radiometric analysis more suitable for LR SAR is more heavily impaired by this phenomenon.

Although most papers share the conclusion that LR SAR data may be useful for damage mapping, an accurate damage-mapping tool is still far from being fully developed. However, two points are worth stressing for multitemporal SAR data analysis in this field. Coherence and intensity are two different, not so tightly related, sources of information; moreover, the same measures only allow damage mapping at a scale comparable with the window used for their computation.

Intensity and coherence are jointly considered, and show how their combination may provide better results, as in the work of Gamba et al. (2007), by also incorporating the awareness of spatial relations among nearby backscattering areas on the ground, because these relations are necessary to correctly perform the damage assessment task.

14.3.2 Low Resolution, Object Scales, and Urban Area Mapping

The scales of urban features may be very different, and even for classification purposes they depend on the level of land cover/land use that one is seeking to discriminate

(Woodcock and Strahler, 1987). It is thus of paramount importance to find the best combination of datasets, feature manipulation techniques, and interpretation/classification procedures for a given scale of interest. SAR data provide information about scatterers in an area and this information is also important to discriminate among different parts of the same urban areas by recognizing different scattering patterns. This approach was proposed by Dell'Acqua and Gamba (2003), who analyzed single date and multitemporal ERS data to detect the city center, residential areas, and the outer sparsely built zones. The idea is based on the use of co-occurrence matrix texture measures. A similar method was proposed by Dekker (2001), using other textures for the same purpose.

Key references in the issue of scales in remote sensing images are Quattrochi and Goodchild (1997) and Marceau and Hay (1999). In particular, Marceau and Hay (1999) introduce an interesting connection between remote sensing and geographical entities. It is shown that the issue of scales in remotely sensed images may be seen as a modifiable area-unit problem. In this framework, the proposed methods may be reduced to optimal spatial zoning systems, approaches based on geographical entities, algorithms based on spatial statistics, and procedures for analyzing relationships among results, variables, and scales. More recently, the same problems have been addressed by Atkinson and Aplin (2004), who showed that a single scale is an excessive simplification when characterizing objects in a remotely sensed image. Further investigation in the same field, that is, the possibility of using different textures and/or different scales to improve the classification results in urban area mapping, is proposed by Dell'Acqua and Gamba (2006).

An accurate texture-based discrimination of land use/land cover classes needs, for instance, the computation of multiscale textural features for a wide range of parameters of the co-occurrence algorithm.

In the cited paper, a technique is proposed to reduce the full multiscale feature set to the most suitable subset for a classification using a fuzzy ARTMAP neural network. This is done by analyzing the relevance of each feature for this particular classifier via the Histogram Distance Index, which is a measure of the separation between the various features performed through a joint evaluation of their histograms. The procedure is validated on the urban test site of Pavia, for which the authors own a very accurate ground truth map, and the results appear encouraging, showing that characterization of an urban environment can be improved by using multiscale textural features extracted from satellite SAR data.

A big issue of urban mapping — again, related to scale — which is still to be solved satisfactorily, is connected with the precise, accurate location of the urban area boundaries. Conflicting requirements push, on one hand, for the consideration of smaller classification units in order to achieve a better resolution in the classification map, whereas, on the other hand, reliability of local statistics and texture measures pull toward larger computation windows. This has to be addressed for LR data if, for example, historical urban mapping is the objective, as scaling down spatial resolution of the data means zero availability of historical data, except for a few sites where airborne acquisition has been previously conducted.

14.4 CONCLUSIONS AND FUTURE PERSPECTIVE

In this chapter, a number of aspects concerning the exploitation of SAR data in the analysis of urban areas have been discussed, and some concrete examples of SAR data processing over urban areas have been presented, considering both HR and LR data.

The trends that may be inferred from a scanning of the literature —including, in a broad sense, plans of various space agencies — and from our personal experience, are exposed in the following few points, from sensor-oriented to processing-oriented:

1. Improvement of the sensor resolution. This is a specific aspect of a general trend, independent of the particular application at hand. The interesting consequence is an increasing availability of spatially detailed measurements: this will increasingly expand the use of satellite (In-)SAR data into sectors that used to be restricted to airborne sensors, such as modeling of single buildings, or — more, generally — 3-D information extraction, with the bonus of repeatability.
2. Improvement of acquisition frequency and, above all, of effective data delivery time. Constellations of satellites seem to be the new standard for future systems, because placing more alike satellites means not only reducing the time required to deliver an image, but also improving the overall reliability (the ability to deliver an image at all) — although, for time-critical applications such as disaster alerting and monitoring, even in the best cases one still has to wait long (not less than 72 hours in realistic estimates) to receive the data on his/her desk. On top of it all, there's still the processing time to add to the time lapse between the moment a disaster occurs and the time the first results are made available. Paradoxically, with the advancement in automatic processing techniques — and in processing speed — the time required to deliver images is projected to become the most limiting factor in emergency applications.
3. Fusion of HR SAR and HR optical data, to make each type of data fill in the other's gaps. For example, severe geometric distortions in radar data may be eased where near-nadir HR optical data are available, faithfully reproducing the shape of the objects. Conversely, height information may be more easily extracted from radar shadows than from nadir HR optical data.
4. Recovery of historical archives to study long-term evolution of urban areas. The series of ERS and ERS-like instruments (currently, ENVISAT ASAR) have been in operation since 1991 and noncontinuous, earlier acquisitions are also available thanks to, for example, Shuttle radar missions. This means that by using suitable, ad hoc land cover classification techniques, an approximate and roughly time-seamless "urban map" could be extracted from LR SAR data covering nearly 20 years of urban evolution in any selected location on Earth. An advantage of such an approach with respect to worldwide nighttime light map — besides finer resolution and all-weather capability — is that urban areas impose a clearer mark on radar data than on nighttime light map; for example, public illumination level depends strongly

on the wealth of the country/city at hand, whereas the presence of geometric features favorable to strong radar backscatter phenomena is practically guaranteed in any case, regardless of the different building criteria in different countries.

As a final remark, we may conclude that SAR sensors may cover a large set of information needs regarding urban areas, both in terms of static, one-shot acquisition and in terms of monitoring the evolution of phenomena, and the forthcoming refinement of spatial and (maybe even more important) time resolution will open up a whole new world of possibilities in this sense. The scientific community is expected to contribute to the improvement of information extraction procedures even earlier than the actual availability of such products, relying on simulated and airborne data.

REFERENCES

Atkinson, P.M., and Aplin, P., Spatial variation in land cover and choice of spatial resolution for remote sensing, *International Journal of Remote Sensing*, 25(18), 3687–3702, 2004.

Dammert, P.B.G., Askne, J.I.H., and Kuhlmann, S., Unsupervised segmentation of multitemporal interferometric SAR images, *IEEE Transactions on Geoscience and Remote Sensing*, 37(5), 2259–2271, 1999.

Dekker, R.J., Texture analysis of urban areas in ERS SAR imagery for map updating, in: 1st IEEE/ISPRS Joint Workshop on Data Fusion and Remote Sensing over Urban Areas, 8–9 November, Rome, Italy, pp. 226–230, 2001.

Dell'Acqua, F., and Gamba, P., Texture-based characterization of urban environments on satellite SAR images, *IEEE Transactions on Geoscience and Remote Sensing*, 41(1), 153–159, 2003.

Dell'Acqua, F., and Gamba, P., Discriminating urban environments using multiscale texture and multiple SAR images, *International Journal of Remote Sensing*, 27(18), 3797–3812, 2006.

De Zan, F., and Rocca, F., Coherent processing of long series of SAR images, *Proceedings of the 2005 IEEE International Geoscience and Remote Sensing Symposium*, 3, 1987–1990, 2005.

Dierking, W., and Skriver, H., Change detection for thematic mapping by means of airborne multitemporal polarimetric SAR imagery, *IEEE Transactions on Geoscience and Remote Sensing*, 40(3), 618–635, 2002.

Dong, Y., Forster, B., and Ticehurst, C., Radar backscatter analysis for urban environments, *International Journal of Remote Sensing*, 18(6), 1351–1364, 1997.

European SAR Conference (EUSAR06), 16–18 May, Dresden, Germany, 2006.

Ferretti, A., Prati, C., and Rocca, F., Permanent scatterers in SAR interferometry, *IEEE Transactions on Geoscience and Remote Sensing*, 38, 2202–2212, 2000.

Gamba, P., and Houshmand, B., A comparison of C and X-Band InSAR data for 3D characterization of an urban area, *IEEE Aerospace and Electronic Systems Magazine*, 17(6), 9–15, 2002.

Gamba P., Houshmand, B., and Saccani, M., Detection and extraction of buildings from interferometric SAR data, *IEEE Transactions on Geoscience and Remote Sensing*, 38(1), 611–617, 2000.

Gamba, P., Dell'Acqua, F., Lisini, G., and Cisotta, F., Improving building footprints in InSAR data by comparison with LIDAR DSM, *Photogrammetric Engineering & Remote Sensing*, 72(1), 63–70, 2006a.

Gamba, P., Dell'Acqua, F., and Trianni, G., Semi-automatic choice of scale-dependent features for satellite SAR image classification, *Pattern Recognition Letters*, 27(4), 244–251, 2006b.

Gamba, P., Dell'Acqua, F., and Trianni, G., Rapid damage detection in the bam area using multitemporal SAR and exploiting ancillary data, *IEEE Transactions on Geoscience and Remote Sensing*, 45(6), 1582–1589, 2007.

Gamba, P., Dell'Acqua, F., and Trianni, G., Hypertemporal SAR sequences for monitoring land cover dynamics, *Proceedings of the 2008 IEEE Radar Conference, Rome, Italy,* 1–5, 2008.

Gens, R., and Van Genderen, J.L., SAR interferometry: Issues, techniques, applications, *International Journal of Remote Sensing*, 17(10), 1803–1836, 1996.

Henderson, F.M., and Xia, Z.-G., SAR applications in human settlement detection, population estimation and urban land use pattern analysis: A status report, *IEEE Transactions on Geoscience and Remote Sensing*, 35(1), 79–85, 1997.

IEEE Geoscience and Remote Sensing (IGARSS '06), 31 July–4 August, Denver (USA), 2006.

Impagnatiello, F., Bertoni, R., and Caltagirone, F., The SkyMed/COSMO system: SAR payload characteristics, *Proceedings of IGARSS'98*, 2, 689–691, 6–10 July 1998, Seattle, WA.

Lombardo, P., Sciotti, M., Pellizzeri, T.M., and Meloni, M., Optimum model-based segmentation techniques for multifrequency polarimetric SAR images of urban areas, *IEEE Transactions on Geoscience and Remote Sensing*, 41(9), Part 1, 1959–1975, 2003.

Macrì Pellizzeri, T., Gamba, P., Lombardo, P., and Dell'Acqua, F., Multitemporal/multiband SAR classification of urban areas using spatial analysis: Statistical versus neural kernel-based approach, *IEEE Transactions on Geoscience and Remote Sensing*, 41(10), Part 1, 2338–2353, 2003.

Marceau, D.J., and Hay, G.J., Remote sensing contributions to the scale issue, *Canadian Journal of Remote Sensing*, 25, 357–366, 1999.

Matsuoka, M., and Yamazaki, F., Use of satellite SAR intensity imagery for detecting building areas damaged due to earthquakes, *Earthquake Spectra*, 20(3), 975–994, 2004.

Niebergall, S., Loew, A., and Mauser, W., Object-oriented analysis of very-high-resolution Quick Bird data for mega city research in Delhi/India, Proceedings of 2007 Urban Remote Sensing Joint Event, unformatted CD-ROM, 11–13 April 2007, Paris (France).

Quattrochi, D.A., and Goodchild, M.F., eds., *Scale in Remote Sensing and GIS*, CRC Press, New York, 1997.

Rosenqvist, A., Shimada, M., Watanabe, M., Tadono, T., and Yamauchi, K., Implementation of systematic data observation strategies for ALOS PALSAR, PRISM and AVNIR-2, *Proceedings of IGARSS'04*, vol. 7, pp. 4527–4530, Sept. 2004, Anchorage, AK.

Roth, A., TerraSAR-X: A new perspective for scientific use of high resolution spaceborne SAR data, Proc. of 2nd GRSS/ISPRS Joint Workshop on Remote Sensing and Data Fusion over Urban Areas, pp. 4–7, 22–23 May 2003, Berlin (Germany).

Simonetto, E., Oriot, H., and Garello, R., Rectangular building extraction from stereoscopic airborne radar images, *IEEE Transactions on Geoscience and Remote Sensing*, 43(10), 2386–2395, 2005.

Soergel, U., Schulz, K., Thoennessen, U., and Stilla, U., Integration of 3D data in SAR mission planning and image interpretation in urban areas, *Information Fusion*, 6(4), 301–310, 2005.

Stilla, U., Soergel, U., and Thoennessen, U., Potential and limits of InSAR data for building reconstruction in built up-areas, *ISPRS Photogrammetric Engineering & Remote Sensing*, 58(1–2), 113–123, 2003.

Thiele, A., Cadario, E., Schulz, K., Thönnessen, U., and Soergel, U., Building recognition from multi-aspect high-resolution InSAR data in urban areas, *IEEE Transactions on Geoscience and Remote Sensing*, 45(11), 3583–3593, 2007.

Usai, S., and Klees, R., SAR interferometry on a very long time scale: A study of the interferometric characteristics of man-made features, *IEEE Transactions on Geoscience and Remote Sensing*, 37(4), 2118–2123, 1999.

Weydahl, D.J., Bretar, F., and Bjerke, P., Comparing RADARSAT-1 and IKONOS satellite images for urban features detection, Proceedings of 2nd GRSS/ISPRS Joint Workshop on Remote Sensing and Data Fusion over Urban Areas, pp. 305–308, 22–23 May 2003, Berlin (Germany).

Woodcock, C.E., and Strahler, A.H., The scale factor in remote sensing, *Remote Sensing of Environment*, 21, 311–332, 1987.

Yonezawa, C., and Takeuchi, S., Decorrelation of SAR data by urban damages caused by the 1995 Hyogoken-Nambu earthquake, *International Journal of Remote Sensing*, 22(8), 1585–1600, 2001.

15 Future EO Sensors of Relevance — Integrated Perspective for Global Urban Monitoring

Manfred Ehlers

CONTENTS

15.1 INTRODUCTION

In its report entitled "State of the World Cities 2006/2007" (United Nations, 2006), the United Nations predicted that the number of urban dwellers worldwide will rise to almost 5 billion by 2030, or 62% of the estimated global population of 8.1 billion. Cities and urban areas will have to expand to accommodate such increases in population, resulting in a variety of social and environmental problems. The corresponding and rapid development and changes in cities and urban areas make timely, accurate, and low-cost spatial information necessary for formulating and monitoring social, economic, and environmental issues that arise in response to increasing population pressures. The synoptic view and the repeatability afforded by Earth observation (EO) sensors offer great potential for the collection of information over urban areas (Small, 2001).

The launch of the first EO satellites more than 35 years ago brought about a major paradigm shift from the use of film-based to digital data, and more recent technological advancements have included the developments of high spatial and spectral resolution sensors and of multisensor systems. These are accompanied by other advances: (1) improvement in computer speed and graphics capability which, according to Moore's law, doubles every 18–24 months (Moore, 1965); (2) developments in Global Positioning System (GPS) and inertial navigation system (INS) technology, which enable operators to fix the position and attitude of sensors more accurately; (3) improvements in communications and spatial data infrastructure, which enable efficient handling and distribution of enormous volumes of data; and (4) new software enabling faster and more reliable information extraction. These developments have allowed considerably more data from a greater range of sensors to be collected, and have significantly advanced the potential applications of EO data (Ehlers, 2004a).

Of special importance for urban applications is the spatial resolution required to capture fine details from complex urban environment composed of typically small features. The spatial resolution of 0.5–5 m suggested as the required resolution for accurate urban feature extraction (Welch, 1982; Konecny et al., 1982; Cowen and Jensen, 1998) was first achieved by spaceborne platforms in 1999 with the launch of the first commercial very high resolution (VHR) EO satellite by Space Imaging (now part of GeoEye) with 1-m (panchromatic) and 4-m (multispectral) image channels. An ever-increasing number of satellites with similar or even better spatial resolution have been launched or is being planned for the near future. These satellites are being developed and launched not only by the longtime industrialized countries, but also by newly industrialized and emerging nations. This chapter tries to look at these developments from a global application perspective.

15.2 TAXONOMY OF REMOTE SENSING SYSTEMS

In general, remote sensing (RS) can be broadly defined as the art, science, and technology of obtaining reliable information about physical objects and the environment, through the process of recording, measuring, and interpreting imagery and digital representation of energy patterns derived from noncontact sensors (Colwell, 1997). Over the past years, discussions have largely centered on the spatial resolution of new RS systems. However, as important as this parameter is, a number of parameters are also being used to characterize and classify RS systems.

RS has come a long way from its aerial photography and image interpretation origins. Electromagnetic wavelengths used by RS systems have been extended from the visible light to the near-infrared, thermal infrared, and the microwave domains. Remotely sensed information is recorded by digital sensors onboard satellite platforms. Sensors can passively record emitted or reflected radiation from the Earth's surface, as in the case of optical systems, or act as their own energy source in an active mode, as in Radar and LIDAR (light detection and ranging) systems. Optical images can be acquired as panchromatic (1 band), multispectral, or even hyperspectral data depending on the type of sensor used. One might also discuss the question of remoteness and look at the recording platform for sensor differentiation. Remotely sensed information is recorded by digital sensors onboard satellites as well

as airborne platforms. For ground truthing, ground-based (stationary) RS platforms (e.g., boomtrucks) are used for measurements that still qualify as RS. Which way is chosen to categorize an RS system depends mainly on the application range and the background of the scientists involved. In the absence of standard rules governing the classification of sensors based on the above parameters, Ehlers (2004a) used the classification scheme shown in Table 15.1 to propose a taxonomy for RS systems.

15.3 VERY/ULTRA HIGH RESOLUTION SATELLITE SENSORS

The advent of commercial satellite programs with very and ultra high resolution (i.e., 1 m and better) has opened new application fields for space-based RS. Satellite data offer the potential for large-scale applications such as urban planning and environmental monitoring at the highest level of detail (Ehlers et al., 2008). Spatial resolutions of 0.50–1.00 m (panchromatic) and 2.50–4.00 m (multispectral) from spaceborne sensors have begun to challenge aerial photography as a cost-effective data acquisition alternative.

Companies such as Digital Globe (http://www.digitalglobe.com/) or GeoEye (http://www.geoeye.com/) promise extremely fast processing. Data are typically delivered within days of recording (or even hours, if downloading via Internet is possible). Tiltable cameras and satellites offer short revisit periods of 2–3 days, making near-continuous data acquisition possible, and across-track as well as along-track stereo capabilities. Launched in September 1999, the Ikonos II was the first commercial VHR satellite in orbit (see Table 15.2). Figures 15.1 and 15.2 show the level of details provided by the panchromatic Ikonos and QuickBird sensors. The potential of these sensors for urban application is demonstrated by the resolution of clearly discernible individual buildings in these images.

TABLE 15.1
Taxonomy of Remote Sensing Systems (after Ehlers 2004a)

Recording platform	Satellite/Shuttle		Aircraft/Balloon		Stationary	
Recording mode	Passive (visible, near-infrared, thermal infrared, thermal microwave)				Active (laser, radar)	
Recording medium	Analog (film camera, video)				Digital (Whiskbroom, line array, 2-D charge-coupled camera (CCD))	
Spectral coverage	Visible/ultraviolet		Reflected infrared		Thermal infrared	Microwave
Spectral resolution	Panchromatic 1 band		Multispectral 2–20 bands		Hyperspectral 20–250 bands	Ultraspectral >250 bands
Radiometric resolution	Low (<6 bit)		Medium (6–8 bit)		High (8–12 bit)	Very high (>12 bit)
Spatial ground resolution	Very low >250 m	Low 50–250 m		Medium 10–50 m	High 4–10 m	Very high 1–4 m	Ultra high <1 m

TABLE 15.2
Current Satellite Systems of Very High and Ultra High Spatial Resolution (Sample Selection)

Company	GeoEye (Space Imaging) US		Digital Globe US		KARI (Korean Aerospace Research Institute)		Imagesat Israel
System	Ikonos II launch 9/1999		QuickBird 2 launch 11/2001		KOMPSAT 2 launch 7/2006		EROS B launch 4/2006
Modus	Pan 11 bit	Multispectral 11 bit	Pan 11 bit	Multispectral 11 bit	Pan 10 bit	Multispectral 10 bit	Pan10 bit
Geometric resolution	1 m	4 m	0.61 m	2.44 m	1 m	4 m	0.7 m
Spectral resolution (nm)	525–929	445–516 (b) 506–595 (g) 632–698 (r) 767–853 (nir)	450–900	450–520 (b) 520–600 (g) 630–690 (r) 760–900 (nir)	500–900	450–520 (b) 520–600 (g) 630–690 (r) 760–900 (nir)	500–900
Scale for applications				1:2500–1:25,000			
Swath width	11 km		16.5 km		15 km		7 km
Image scene size	11 × 11 km^2		16.5 × 16.5 km^2 strip: 16.5 × 165 km^2		15 × 15 km^2		7 × 7 km^2 vector scene: 7 × 70 km^2
Orbit height	681 km		450 km		685 km		500 km
Inclination	98.1 sun synchronous		97.2 sun synchronous		98.1 sun synchronous		97.3 sun synchronous

FIGURE 15.1 Ikonos image with a spatial resolution of 1 m. (Image courtesy of GeoEye.)

New VHR satellites that were launched in 2007 or will be launched in 2008 include the first Radar sensor with a spatial resolution of 1 m. Currently, the highest spatial resolution provided by spaceborne sensors is Digital Globe's Worldview 1 (panchromatic only) with about 50 cm resolution (Table 15.3). Although GeoEye-1, launched in early 2008, will produce panchromatic images with a nominal resolution of 41 cm, the general public will only be able to purchase images with a degraded resolution of 50 cm. Although GeoEye-1's spectral characteristics resemble those of QuickBird and Ikonos, Digital Globe's WorldView 2 (to be launched no later than 2008) will offer four additional bands for coastal monitoring (coastal and yellow) as well as a red edge and a second near-infrared band. In 2007, Infoterra (http://www.infoterra.de/) and Germany's Aerospace Center, DLR, launched the world's first 1-m resolution Radar satellite TerraSAR-X, which offers day and night as well as bad-weather EO capabilities. Another interesting development is the Rapideye five-satellite constellation, which is scheduled for a simultaneous launch in 2008 (http://www.rapideye.de/). At slightly coarser than VHR spatial resolution (6.5 m), the constellation's multispectral sensors will provide large-area coverage on a daily basis, weather permitting. It must be noted that this overview provides only a few selected examples; for a complete description of VHR and HR space sensors, see Ehlers et al. (2009).

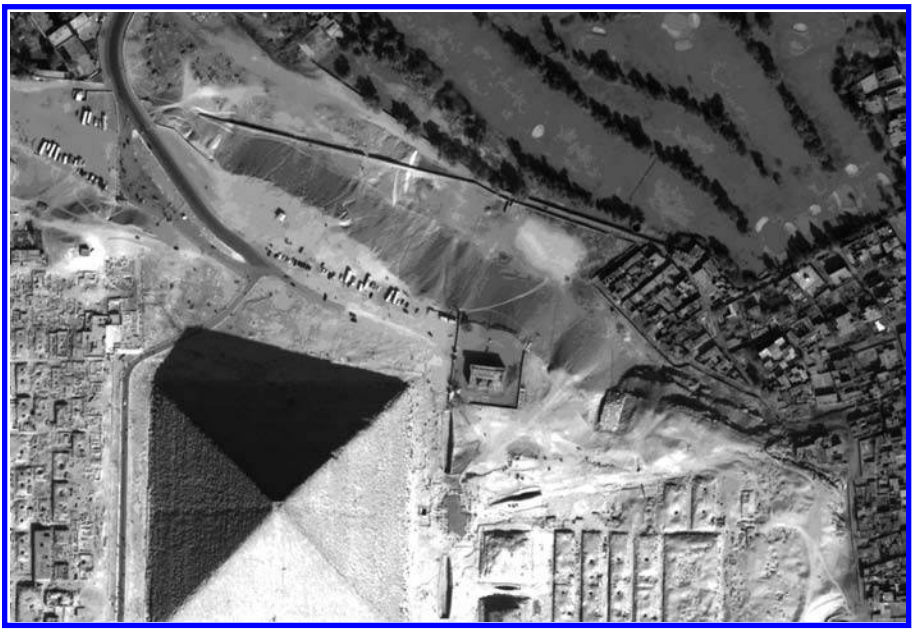

FIGURE 15.2 QuickBird image with a spatial resolution of 0.7 m. (Image from DigitalGlobe®. With permission.)

15.4 DIGITAL AIRBORNE SENSORS

After a long period of development, the emergence of operational digital camera systems has challenged aerial frame cameras as EO data source for large-scale mapping. Advanced technologies such as GPS-coupled navigation systems and advanced digital sensor technologies have overcome the strongest deficiency of aircraft scanners: the lack of geometric stability. In response, public and private research has concentrated on the development of digital line array or matrix scanners that serve as successors to the "classical" aerial cameras. Companies such as Leica Geosystems, Intergraph's Z/I, and Microsoft's Vexcel are providing the first commercial systems for these types of sensors; research centers such as DLR fly their own prototypes. Such systems have to establish their market somewhere between the satellite image user seeking higher resolution and the air photo user seeking digital input and GIS compatibility. Consequently, airborne scanner systems have to offer stereo capability and multispectral recording.

Two different technologies are being used to accomplish an airborne digital recording system. Z/I Imaging and Vexcel make use of two-dimensional (2-D) arrays and a set of coupled nadir-looking lenses to emulate a standard frame camera's central perspective (Dörstel, 2003; Leberl and Gruber, 2003). Leica Geosystems and the DLR use triplet scanner technology with 1-D line arrays arranged in fore-, nadir-, and aft-looking modes (Fricker et al., 2000; Hoffmann and Lehmann, 2000). The advantage of a 2-D matrix camera is that all standard photogrammetric techniques can be used in a digital environment and that forward motion compensation (FMC)

TABLE 15.3
Selected VHR Satellite Systems 2007–2008

Company	GeoEye US		Digital Globe US	Digital Globe US		Infoterra Germany l
System	GEOEYE-1 launch early 2008		WorldView 1 launch 9/2007	WorldView 2 launch late 2008		TerraSAR-X (Radar) launch 6/2007
Modus	Pan 11 bit	Multispectral 11 bit	Pan 11 bit	Pan 11 bit	Multispectral 11 bit	X-band 16 bit
Geometric resolution	0.41 m	1.65 m	0.51 m	0.46 m	1.84m	1 m (spot mode)
Spectral resolution (nm)	450–900	450–520 (b) 520–600 (g) 625–695 (r) 760–900 (nir)	400–900	450–800	450–510 (b) 510–580 (g) 630–690 (r) 770–895 (nir1) 400–450 (coastal) 585–625 (yellow) 705–745 (red edge) 860–1040 (nir2)	9.62 GHz (3 cm)
Scale for applications	1:1500–1:15,000					
Swath width	15.2 km		17.6 km	16.4 km		5–10 km
Image scene size	15×15 km^2		17.6×17.6 km^2 up to 60×100 km^2	16.4×16.4 km^2 up to 96×110 km^2		5×10 km^2
Orbit height	684 km		496 km	770 km		512 km
Inclination	sun synchronous		sun synchronous	sun synchronous		97.4 sun synchronous

can be achieved through time delayed integration. The advantage of a stereo triplet solution is that photogrammetric preprocessing [i.e., digital surface model (DSM) and orthoimage generation] is performed before the user receives the data, alleviating the user's need to run sophisticated software. The image data are provided in the required coordinate system and can be easily integrated into an existing GIS database. Which of the two approaches is more suitable will largely depend on the user demands and the price-performance ratios of the respective systems. Table 15.4 presents four selected ultrahigh resolution airborne digital camera systems.

The advantages of digital cameras are widely understood: no film, no photo processing, no scanning, better radiometric quality through direct sensing, "non-aging" storage, and direct integration into GIS and image processing systems. The disadvantages of digital scanners, most notably its geometric distortions and monoscopic imaging mode, are overcome due to the stereo capabilities of the new sensors and the use of integrated INS and differential GPS technology during image acquisition.

15.5 POTENTIAL FOR URBAN MONITORING

In a highlight article for *Photogrammetric Engineering and Remote Sensing*, Nichol et al. (2007) outlined a set of requirements for EO sensors to be used for urban planning and management. They identified four application areas: (1) environmental monitoring, (2) land use/land cover (LU/LC) mapping, (3) planning, and (4) geotechnical monitoring. In the following, we will address the first three topics as they are more closely aligned with the scope of this chapter.

15.5.1 Environmental Monitoring

EO sensors have been used to study the magnitude and extent of urban heat islands using thermal RS data (Streutker, 2003; Voogt and Oke, 2003; Nichol, 2005). Most thermal images, however, are not collected at the most suitable times for analysis of heat islands, which are best observed at night or even require a day- and a nighttime temperature recording. Despite this, thermal images from satellites have been used with some success for analysis of urban climates and can indicate heat mitigation measures such as appropriate building geometry, materials, green spaces, and air flow corridors (Quattrochi et al., 2000; Nichol and Wong, 2007). However, the spatial resolution of the only thermal sensors with assured continuity (ASTER with 90 m and MODIS with 1000 m) are too low for sufficient microclimatic application. In addition, the resolution discrepancy is too great to permit fusion with high-resolution (HR) or VHR sensors. As there exist no plans for launching a thermal sensor in the near future with a higher resolution, there will be no satellite missions suitable for urban microclimate analyses (Nichol et al., 2007).

15.5.2 LU/LC Change

LU/LC changes address not only the analysis of the urban areas but also the surrounding regions as LU/LC changes there can impact the urban climate and environment. Continuity of data acquisition for LU/LC change monitoring is essential

TABLE 15.4
Digital Airborne Camera Sensors (after Watson and Ehlers, 2006)

Company	DLR	Leica Geosystems	Vexcel Corp.	Z/I Imaging
Sensor	HRSC-AX	ADS 40	UltraCam-D	DMC
Sensor type	Triplet stereo	Triplet stereo	2-D CCD Camera w. FMC	2-D CCD Camera w. FMC
Year of introduction	2000	2000	2003	2002
Focal length	151 mm	62.7 mm	100 mm (28 mm multispectral)	120 mm (25 mm multispectral)
Total field of view	29°	62.5°	55 × 37°	74 × 44°
Number of CCD lines	9	12	7500 (pan) 2672 (ms)	8000 (pan) 2000 (ms)
Sensors per CCD line	12,172	12 × 12,000 (pan and ms)	11,500 (pan) 4008 (ms)	13,500 (pan) 3000 (ms)
Sensor size	6.5 µm	6.5 µm	9 µm	12 µm
Radiometric resolution	12 bit	12 bit	14 bit	12 bit
Spectral resolution in nm	520–760 (pan) 450–510 (blue) 530–576 (green) 642–682 (red) 770–814 (nir)	465–680 (pan) 428–492 (blue) 533–587 (green) 608–662 (red) 833–887 (nir)	4 bands: blue, green, red, infrared 1 band pan	400–850 (pan) 400–580 (blue) 500–650 (green) 590–675 (red) 675–850 (nir)
Read-out frequency	1640 lines/s	800 lines/s	0.75 images/s	0.5 images/s
Largest appl. scale	1:500		1:150	
Stabilization	Z/I T-AS platform	LH platforms	Not specified	Z/I T-AS platform
Data recording	Sony high-speed data recorder	MM40 mass memory	SCU >1 TB	RAID hard disk array
Georeferencing	Applanix POS/DG navigation system with GPS and INS	Applanix POS IMU with GPS and INS	Not specified	POS Z/I 510 navigation system with GPS and INS

because many cities update their LU/LC registries annually or as an ongoing process, and the role of EO sensors for rapidly archiving and documenting these data cannot be overestimated. Most LU/LC analyses make use of the Anderson land cover classification system (Anderson et al., 1976) or a similar national/regional system that accommodates several levels in its classification hierarchy and is suited for automated classification techniques for medium- to high-level resolution sensors (Jensen, 2007). Determining LU/LC changes in urban areas, however, requires VHR images for which fully automated classification techniques are not

yet operational. Even with the development of knowledge-based classifiers and object recognition and feature extraction methods, manual interpretation of aerial photographs or VHR imagery is still the norm (Herold et al., 2003; Myint, 2006). Screen digitizing on VHR images may provide some cost reduction over the use of air photos, but does not present a desirable trend in the use of EO technology. To automate the procedure of urban mapping, integration of GIS information and RS data seems to offer huge potential (Stow et al., 2003), and data fusion methods for the integration of VHR panchromatic images into lower resolution multispectral images are being developed (Alparone et al., 2006). A new paradigm in the processing of VHR imagery involves the integration of object knowledge into the analysis process, and was recently coined GeoObject-Based Image Analysis (see Blaschke et al., 2008).

15.5.3 Monitoring Urban Growth and Planning

Monitoring of urban growth and detecting informal settlements that are not registered in cadastral databases require detailed topographic mapping. For structural and strategic planning such as building of new roads, bridges, or towns, large-scale site mapping is also essential. VHR satellite sensors and/or digital airborne stereo sensors can provide not only the necessary 2-D mapping information, but are also capable of producing automated surface models (Ehlers, 2007). EO data offer great potential for mapping, monitoring, and predicting accelerated growth of urban areas especially in newly industrialized and developing nations. For global assessment studies, use has been made of medium- and high-resolution satellite data such as Landsat and SPOT imagery (Lo, 1995; Civco et al., 2005; Hipple et al., 2006; Xian, 2007).

For structural analyses, 3-D information is vital. This can be extracted from stereo images of VHR spaceborne or airborne sensors using well-established photogrammetric techniques. LIDAR sensors provide another source of accurate height information that is rapidly becoming important as costs are reduced and data quality increased (Shan and Sampath, 2007). Depending on point density and the level of integration with auxiliary data (e.g., images, terrestrial laser scanning), 3-D applications range from box and prism modeling to accurately textured and geometrically detailed models. New investigations focus on the quality of interferometric synthetic aperture radar (IfSAR) for digital elevation model (DEM) extraction and reconstruction of urban buildings (Stilla et al., 2003; Zhang et al., 2004).

Detailed 3-D information is necessary not only for virtual reality modeling, 3-D geobrowsers, and general *geotainment*, but also for traffic planning, noise and pollution modeling, and emergency routing. Other application areas include slope and stability monitoring in mountainous areas, visual impact assessments, and facilities and infrastructure management. Figure 15.3 shows a 3-D view of a section of the city of Osnabrueck (Ehlers et al., 2003). Newly constructed buildings (yellow outline) block the flow of cold and fresh air (blue arrows) toward the center of the city. The 3-D model was constructed using HR digital stereo camera data from the HRSC sensor (see Table 15.4) for the calculation of DSM. Data from the city's digital cadastral database were used to extract the buildings and to create the 3-D building models.

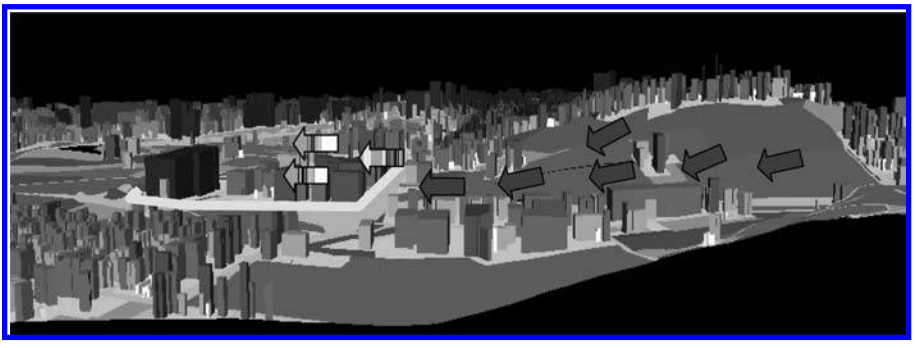

FIGURE 15.3 (See color insert following page 324.) Perspective view of a section of Osnabrueck: newly constructed buildings (yellow outline) block the flow of cold and fresh air toward the center of the city showing the impact that such a structure would have on the inner-city environment (exaggeration factor 5).

15.6 IMAGE FUSION

A cursory look at VHR satellite systems and digital airborne cameras reveals that almost all sensors have different spatial resolutions for their panchromatic and multispectral recording modes. The highest spatial information is only provided in the panchromatic mode, whereas multispectral images are of lower spatial resolution. The ratios between high-resolution panchromatic and lower-resolution multispectral images vary between 1:2 and 1:5 (Ehlers, 2004a). This ratio may increase if data from different sensors are used. For example, the resolution ratio between Ikonos panchromatic and SPOT 5 multispectral imagery is 1:10, and for SPOT 4 it is 1:20. Some sensors (e.g., EROS B or WorldView-1) provide only panchromatic imagery. To produce HR multispectral datasets required for many urban remote applications, the panchromatic information is merged with multispectral images.

The goals of the fusion process are many: to sharpen multispectral images, to improve geometric corrections, to provide stereo viewing capabilities for stereophotogrammetry, to enhance certain features not visible in either of the single datasets alone, to complement datasets for improved classification, to detect changes using multitemporal data, and to replace defective data (see Pohl and van Genderen, 1998).

In general, image fusion methods can be differentiated into three levels: pixel level (iconic), feature level (symbolic), and knowledge or decision level. Of highest relevance to RS applications are techniques for iconic image fusion, for which many different methods have been developed (see, e.g., Welch and Ehlers, 1987; Pohl and van Genderen, 1998; Alparone et al., 2006). The objective of iconic image fusion is to combine the high spatial and the multispectral information to form a fused multispectral image that retains the spatial information from the HR panchromatic image and the spectral characteristics of the lower resolution multispectral image. These methods have been proven to work well for many applications, especially in cases of single-sensor single-date fusion. Most methods, however, exhibit significant color distortions for multitemporal and multisensor case studies (Ehlers, 2004b; Klonus and Ehlers, 2007).

Consequently, a number of improved algorithms have been developed over the past years promising to minimize color distortion while maintaining the spatial improvement of the standard data fusion algorithms. The wavelet theory, in particular, has led to a number of new fusion methods (Otazu et al., 2005; Lillo-Saavedra and Gonzalo, 2006; Yunhao et al., 2006). Ehlers et al. (2008) tested the quality of a number of advanced algorithms for multitemporal multisensor fusion. The results of this research confirm previous findings that the standard as well as the most advanced fusion methods implemented in commercial image processing systems cannot cope with the demands that are placed on them by multisensor/multitemporal fusion, and should only be used for single-sensor, single-date images. Serious color distortions ranging from brightness reversion to a complete change of spectral characteristics are the results of many operational and often used fusion techniques. Conversely, wavelet-based fusion retains most of the spectral characteristics at the expense of spatial improvement. The research concluded that of the fusion methods used in the comparative study, only the Ehlers fusion technique recently implemented in the ERDAS Imagine Software delivers pansharpened images with almost no spectral changes (Ehlers et al., 2008; Figure 15.4).

A combined method for quantitative assessment of spatial improvement and spectral preservation in fusion techniques is still needed to act as a quality measure for

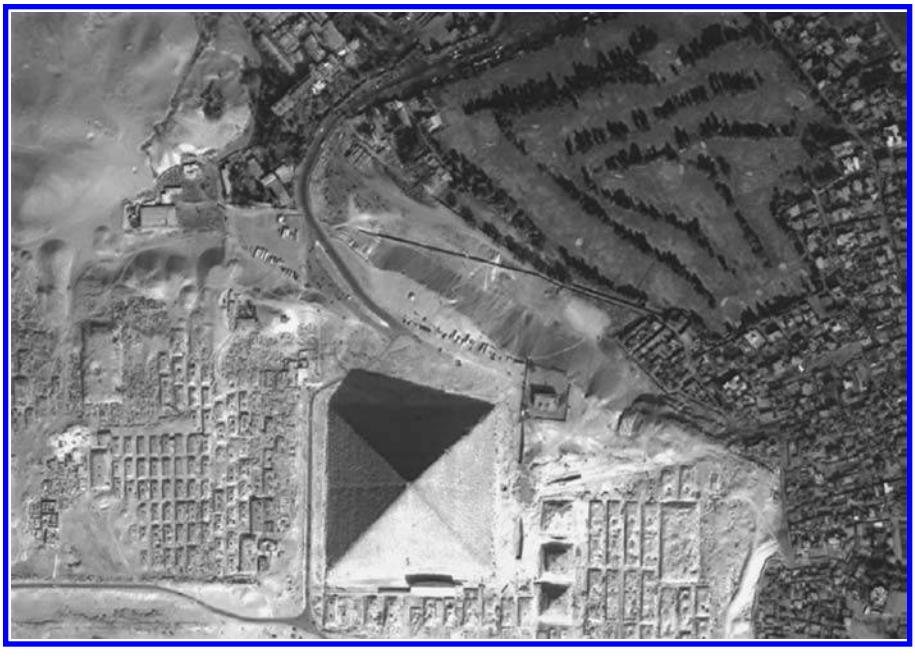

FIGURE 15.4 QuickBird panchromatic (see Figure 15.2) and multispectral image data are fused using the color-preserving Ehlers fusion algorithm. The fused image retains the spatial resolution of the panchromatic image and, at the same time, the spectral characteristics of the multispectral bands. (Image from DigitalGlobe®. Used with permission.)

fusion results. Nevertheless, it seems possible to fuse multitemporal and multisensor image data with sufficient spatial enhancement and spectral fidelity.

15.7 ROLE OF EO FOR THE GENERAL PUBLIC

One of the main advantages of VHR images is the impact that they have on the general public. For example, news companies, rescue organizations, and government agencies routinely use EO sensor information for disaster mapping and monitoring. Recent examples include the tsunami event in the Indian ocean on Christmas of 2004 (http://www.crisp.nus.edu.sg/tsunami/tsunami.html, accessed on June 4, 2008), the landfall of hurricane Katrina at New Orleans in August 2005 (http://www.nasa.gov/vision/earth/lookingatearth/h2005_katrina.html, accessed on June 4, 2008), or the May 2008 disasters, the Myanmar flooding (http://earthobservatory.nasa.gov/Newsroom/NewImages/images.php3?img_id=18019, accessed on June 4, 2008), and the Earthquake in China (http://www.universetoday.com/2008/05/16/satellite-images-of-china-earthquake/, accessed on June 4, 2008), where hundreds of thousands lost their lives. The usefulness of RS data for these examples is immediately evident. More important, in our opinion, is the use of RS by any citizen who has access to the Internet. Not only can Internet-based geobrowsers be used by anyone to locate his or her house and explore the neighborhood or foreign regions, but public awareness is frequently created by nongovernmental organizations (NGOs) and grassroot communities through the use of visual evidence provided by HR sensors.

This point will be illustrated by a couple of examples, which should not be judged by their political intentions, but rather by their use of EO data for their particular purpose. This can, in principle, be set up by any individual in an open and democratic society and also contested and argued in public. What makes this strategy unique is the convincing visual evidence that is provided by the EO sensors.

For example, the environmentalist group Appalachian Voices maintains a website that uses Landsat and QuickBird imagery to show the ongoing destruction of the Appalachian Mountains by mountaintop removal coal mining (http://www.ilovemountains.org, accessed on June 4, 2008). The second example is Amnesty International's project Eyes on Darfur. This project leverages the power of VHR satellite imagery to provide undisputable evidence of the atrocities being committed in Darfur — enabling actions by private citizens, policy makers, and international courts. Eyes on Darfur also breaks new ground in protecting human rights by allowing people around the world to literally "watch over" and protect 12 intact, but highly vulnerable, villages using commercially available satellite imagery (http://www.eyesondarfur.org, accessed on June 4, 2008). The following QuickBird images from their website show the Darfur village of Ishma before and after the attack by Sudanese government forces between November 2004 and early 2005. Figure 15.5 is a subset of an image taken before 2004 showing the structures of an intact village; Figure 15.6 was taken in 2007 after its almost complete destruction. These examples demonstrate the power of VHR imagery to give the public the opportunity to view "what goes on in my neighbor's backyard and beyond."

FIGURE 15.5 **(See color insert following page 324.)** The village of Ishma (Darfur) before destruction by government and Janjawid forces. (Image from DigitalGlobe®. Used with permission.)

FIGURE 15.6 **(See color insert following page 324.)** The village of Ishma after its destruction. (Image from DigitalGlobe®. Used with permission.)

15.8 CONCLUSIONS

The development of RS systems capable of very high and ultra high resolution has matured over the past several years. New airborne digital camera systems have the potential to finally end the reign of analog cameras when it comes to

image acquisition for large-scale applications, whereas spaceborne sensors offer increasing competitive advantages for acquisition of timely, accurate, and low-cost data. Radar, hyperspectral, and LIDAR information complement optical VHR imagery data and provide tremendous potential for urban applications. The 3-D capability of new airborne and satellite sensors is of particular advantage for applications such as city mapping, monitoring, and modeling. As almost all sensors have the highest spatial resolution in their panchromatic mode, image fusion for pansharpening is an essential tool for image analysis. Wider utilization of these data sources is mainly dependent on increased awareness of its availability and effectiveness among practitioners, cost reductions, and easier integration into existing work procedures. Of special importance is the access of EO data for the general public that allow NGOs, grassroot organizations, and individual citizens to make use of EO data.

For professionals, further research to increase automation in 3-D city modeling and land use mapping from HR and VHR images is essential. However, because every city is unique, the development of "black box" algorithms, implying complete automation is probably neither possible nor desirable and researchers are encouraged to work with end users to develop realistic local solutions. This entails a degree of change in workplace methodologies, which can best be facilitated by demonstrations of how EO technology can make peoples' jobs more efficient and productive.

REFERENCES

Alparone, L., Aiazzi, B., Baronti, S., Garzelli, A., and Nencini, F., A critical review of fusion methods for true colour display of very high resolution images of urban areas, 1st EARSeL Workshop of the SIG Urban Remote Sensing, Humboldt University, Berlin, 2–3 March 2006 (CD publication).

Anderson, J.R., Hardy, E.E., Roach, J.T., and Witmer, R.E., A land use and land cover classification system for use with remote sensor data, *US Geological Survey Professional Paper*, 964, Washington, DC, 1976.

Blaschke, T., Lang, S., and Hayes, G., eds., *Object-Based Image Analysis — Spatial Concepts for Knowledge-Driven Remote Sensing Application*, Springer Lecture Notes in Geoinformation and Cartography, 2008.

Civco, D.L., Chabaeva, A., Angel, S., and Sheppard, S., The urban growth management initiative — confronting the expected doubling of the size in the developing countries in the next thirty years — methods and preliminary results, *Proceedings, 2005 ASPRS Annual Convention*, Baltimore, MD, 12 pp. (CD publication), 2005.

Colwell, R.N., History and place of photographic interpretation, in: Philipson, W.R., ed., *Manual of Photographic Interpretation*, 2nd edition, American Society for Photogrammetry and Remote Sensing, Bethesda, MD, pp. 33–48, 1997.

Cowen, D.J., and Jensen, J.R., Extraction and modeling of urban attributes using remote sensing technology, in: Liverman, D., Moran, E.F., Rindfuss, R.R., and Stern, P.C., eds., *People and Pixels: Linking Remote Sensing and Social Science*, National Academic Press, Washington, D.C., pp. 164–188, 1998.

Dörstel, C., DMC — Practical experiences and photogrammetric system performance, in: Fritsch, D., ed., *Photogrammetric Week 03*, Wichmann Verlag, Heidelberg, pp. 59–66, 2003.

Ehlers, M., Schiewe, J., and Möller, M., 3D city modelling using high resolution and multi-sensoral remote sensing, *Geo-Informations-Systeme*, 6(3), 30–37, 2003.

Ehlers, M., Remote sensing for GIS applications: New sensors and analysis methods, in: Ehlers, M., Kaufmann, H.J., and Michel, U., eds., *Remote Sensing for Environmental Monitoring, GIS Applications, and Geology III*, *Proceedings of SPIE*, vol. 5239, Bellingham, WA, pp. 1–13, 2004a.

Ehlers, M., Spectral characteristics preserving image fusion based on Fourier domain filtering, in: Ehlers, M., Posa, F., Kaufmann, H.J., Michel, U., and De Carolis, G., eds., *Remote Sensing for Environmental Monitoring, GIS Applications, and Geology IV*, *Proceedings of SPIE*, vol. 5574, Bellingham, WA, pp. 1–13, 2004b.

Ehlers, M., New developments and trends for urban remote sensing, in: Weng, Q., and Quattrochi, D., eds., *Urban Remote Sensing*, CRC Press, Taylor and Francis Group, Boca Raton, London, pp. 357–375, 2007.

Ehlers, M., Jacobsen, K., and Schiewe, J., High resolution image data and GIS, in: Madden, M., ed., *ASPRS Manual of GIS*, American Society for Photogrammetry and Remote Sensing, Bethesda, MD, pp. 1721–1777, 2009.

Ehlers, M., Klonus, S., and Åstrand, P.J., Quality assessment for multi-sensor multi-date image fusion, *Proceedings of the XXXIst International Congress of ISPRS*, Beijing, China, IAPRS XXXV/ B4, pp. 498–506, 2008.

Fricker, P., Sandau, R., Tempelmann, U., and Walker, S., ADS 40 — Why LH systems took the three-line road, *GIM International*, pp. 45–47, 2000.

Herold, M., Liu, X., and Clarke, K.C., Spatial metrics and image texture for mapping urban land use, *Photogrammetric Engineering and Remote Sensing*, 69(9), 1151–1156, 2003.

Hipple, J.D., Butchart, T.A., Davis, C., Haithcoat, T.L., Heiden, U., Jensen, R.R., and Song, W., Characterizing and mapping human settlements, in: Ridd, M., and Hipple, J.D., eds., *The Manual of Remote Sensing*, 3rd edition, Vol. 5: *Remote Sensing of Human Settlements*, American Society for Photogrammetry and Remote Sensing, Bethesda, MD, pp. 149–206, 2006.

Hoffmann, A., and Lehmann, F., Vom Mars zur Erde — die erste digitale Orthobildkarte Berlin mit Daten der Kamera HRSC-A, *Kartographische Nachrichten*, 50(2), 61–71, 2000.

Jensen, J.R., *Remote Sensing of the Environment*, 2nd edition, Prentice-Hall, Upper Saddle River, NJ, 2007.

Klonus, S., and Ehlers, M., Image fusion using the Ehlers spectral characteristics preserving algorithm, *GIScience and Remote Sensing*, 44(2), 93–116, 2007.

Konecny, G., Schuhr, W., and Wu, J., Untersuchungen über die Interpretierbarkeit von Bildern unterschiedlicher Sensoren und Plattformen für die Kleinmaßstäbige Kartierung, *Bildmessung und Luftbildwesen*, 50, 187–200, 1982.

Leberl, F., and Gruber, M., Flying the new large format digital aerial camera ultracam, in: Fritsch, D., ed., *Photogrammetric Week 03*, Wichmann Verlag, Heidelberg, pp. 67–76, 2003.

Lillo-Saavedra, M., and Gonzalo, C., Spectral or spatial quality for fused satellite imagery? A trade-off resolution using the wavelet à trous algorithm. *International Journal of Remote Sensing*, 27(7), 1453–1464, 2006.

Lo, C.P., Automated population and dwelling unit estimation from high-resolution satellite images: A GIS approach, *International Journal of Remote Sensing*, 16(1), 17–34, 1995.

Moore, G., Cramming more components onto integrated circuits, *Electronics*, 38(8), 114–117, 1965.

Myint, S.W. Urban mapping with geospatial algorithms, in: Weng, Q., and Quattrochi, D., eds., *Urban Remote Sensing*, CRC Press, Taylor and Francis Group, Boca Raton, pp. 109–136, 2006.

Nichol, J., Remote sensing of urban heat islands by day and night, *Photogrammetric Engineering and Remote Sensing*, 71(5), 613–621, 2005.

Nichol, J., and Wong, M.S., Assessing urban environmental quality with multiple parameters, in: Weng, Q., and Quattrochi, D., eds., *Urban Remote Sensing*, CRC Press, Taylor and Francis Group, Boca Raton, pp. 253–268, 2007.

Nichol, J., King, B., Xiaol, D., Dowman, I., Quattrochi, D., and Ehlers, M., Policy document on earth observation for urban planning and management, *Photogrammetric Engineering and Remote Sensing*, 73(9), 973–979, 2007.

Otazu, X., González-Audícana, M., Fors, O., and Núnez, J., Introduction of sensor spectral response into image fusion methods: Application to wavelet-based methods, *IEEE Transactions on Geoscience and Remote Sensing*, 43(10), 2376–2385, 2005.

Pohl, C., and van Genderen, J.L., Multisensor image fusion in remote sensing: Concepts, methods and applications, *International Journal of Remote Sensing*, 59, 823–854, 1998.

Quattrochi, D.A., Luvall, J.C., Rickman, D.L., Estes, M.G., Laymon, C.A., and Howell, B.F., A Decision support information system for urban landscape management using thermal infrared data, *Photogrammetric Engineering and Remote Sensing*, 66(11), 1195–1207, 2000.

Shan, J., and Sampath, A., Urban terrain and building extraction from airborne LIDAR data, in: Weng, Q., and Quattrochi, D., eds., *Urban Remote Sensing*, CRC Press, Taylor and Francis Group, Boca Raton, pp. 21–45, 2007.

Small, C., Global analysis of urban population distribution and the physical environment, *Proceedings of the Open Meeting of the Human Dimension of Global Environmental Change Research Community*, Brazil Academy of Science, Rio de Janeiro, Brazil, 11 pp., 2001.

Stilla, U., Soergel, U., and Thoennessen, U., Potential and limits of InSAR data for building reconstruction in built-up areas, *ISPRS Journal of Photogrammetry and Remote Sensing*, 58(1–2), 113–123, 2003.

Stow, D., Coulter, L., Kaiser, J., Hope, A., Service, D., Schutte, K., and Walters, A., Irrigated vegetation assessments for urban environments, *Photogrammetric Engineering and Remote Sensing*, 69(4), 381–390, 2003.

Streutker, D.R., Satellite-measured growth of the urban heat island of Houston, Texas, *Remote Sensing of Environment*, 85, 282–289, 2003.

United Nations, 2006. Available at: http://www.guardian.co.uk/environment/2006/jun/16/internationalnews.

Voogt, J.A., and Oke, T.R., Thermal remote sensing of urban climates, *Remote Sensing of Environment*, 86, 370–384, 2003.

Watson, R.P., and Ehlers, M., New and emerging instruments and some emerging trends for remote sensing of human settlements, in: Ridd, M., and Hipple, J.D., eds., *The Manual of Remote Sensing*, 3rd edition, Vol. 5: *Remote Sensing of Human Settlements*, American Society for Photogrammetry and Remote Sensing, Bethesda, MD, pp. 713–738, 2006.

Welch, R., Spatial resolution requirements for urban studies, *International Journal of Remote Sensing*, 3(2), 139–146, 1982.

Welch, R., and Ehlers, M., Merging multiresolution SPOT HRV and Landsat TM data, *Photogrammetric Engineering and Remote Sensing*, 53(3), 301–303, 1987.

Xian, G., Assessing urban growth with subpixel impervious surface coverage, in: Weng, Q., and Quattrochi, D., eds., *Urban Remote Sensing*, CRC Press, Taylor and Francis Group, Boca Raton, pp. 179–219, 2007.

Yunhao, C., Lei, D., Jing, L., Xiaobing, L., and Peijun, S., A new wavelet-based image fusion method for remotely sensed data, *International Journal of Remote Sensing*, 27(7), 1465–1476, 2006.

Zhang, Y., Tao, C.V., and Mercer, J.B., An initial study on automatic reconstruction of ground DEMs from airborne IfSAR DSMs, *Photogrammetric Engineering and Remote Sensing*, 70(4), 427–438, 2004.

16 Methods and Challenges for Using High-Temporal Resolution Data to Monitor Urban Growth

Alexandre Boucher and Karen C. Seto

CONTENTS

16.1 THE NEED FOR HIGH TEMPORAL RESOLUTION DATA TO MAP URBAN GROWTH

Earth-observing satellites have collected remote sensing data for more than 30 years, yet most urban mapping studies do not take full advantage of the historical record and the temporal frequency of the observations available. That information is ever more important as remote sensing images are increasingly being used with other types of data such as demographics, economics, and policy to understand the link between human activity and impacts on the landscape (Lo and Faber, 1997; Wang and Zhang, 2001; Schneider et al., 2005; Seto and Kaufmann, 2005). Linking social processes with spatial patterns observed in remote sensing has been the subject of numerous studies (Homewood et al., 2001; Lambin et al., 2000; Reid et al., 2000; Nagendra et al., 2004). Yet, it is almost without exception that the spatial patterns in these studies are observed in only two or three periods. The underlying assumption

is that the relationship between landscape dynamics and social processes can be understood with several observations in time. Although this may hold true for relatively slow land use and land cover changes, the assumption is not valid for rapidly urbanizing landscapes.

Urban growth patterns — also called urban morphology — are complex. Despite decades of research in geography, economics, and urban studies, urban land-use change patterns are still not well understood nor characterized (Batty, 2008). Although the consensus is that compact urban form is critical for sustainable development, very little is known about how urban form evolves (Jabareen, 2006; Schneider and Woodcock, 2008). Many different methods have been proposed to model urban growth patterns, but what are lacking are real-world observations (Makse et al., 1995; Landis and Zhang, 1998; Fragkias and Seto, 2007). Due to the complex nature of urban growth patterns, using only a few observations in time will not provide accurate or meaningful information about the ways in which urban land-use change evolves. Rather, urban growth and associated land cover changes are complex nonlinear processes that require frequent observations through time to properly monitor and describe their morphology.

Understanding why and how cities grow requires linking landscape dynamics with socio-politico-economic processes. Urban growth patterns and the rate of growth are driven in large part by micro- and macrofactors at different temporal and spatial scales, including global economic activity (Beaverstock et al., 2000), local factors (Beauregard, 1995; Marcotullio, 2001), and socioeconomic changes (Knox, 1991). To understand the linkage between the socioeconomic drivers and the growth of cities, it is important to first understand how these cities have grown in space and time. Studies that have gone beyond the mapping process to link spatial patterns with socioeconomic drivers have relied on accurate urban land cover maps over a long time series at suitable spatial and temporal resolutions. From that perspective, knowing the rate of change or where these changes occurred over two or three periods may not be sufficient in making the linkages with demographic patterns and policy shifts and will require multiple observations. Rapid urban land conversion is occurring in many regions, most notably in China, India, and sub-Sahara Africa. It is not a phenomenon limited to a single country or region.

The scarcity of urban remote sensing studies using high-frequency temporal data, here defined by use of at least three images, can be partly explained by the limited algorithms available for such high-frequency multitemporal mapping. This chapter emphasizes the importance of high temporal resolution methods to map urban growth. It also surveys the existing algorithms for multitemporal urban mapping and proposes metrics to provide accuracy assessment for long times series studies.

16.2 GOALS OF MAPPING WITH HIGH TEMPORAL RESOLUTION DATA

Mapping is an exercise undertaken to answer specific questions. *Where* do the land covers of interest exist? *How* are they distributed geographically? *What* is the spatial configuration of the landscape? The choice of a classification algorithm, the land

cover types, as well as the validation metrics must be selected according to how these questions are to be answered. The classified map must provide information about land cover at temporal and spatial resolutions sufficient for the objectives. When the mapping exercise is not an end in itself, but only a starting point to link observed landscape patterns to their drivers or their consequences, the mapping output should:

- Provide high temporal resolution land cover transitions;
- Accurately map land cover/use change patterns in space and time.

The resulting multitemporal classification should yield the area, the spatial distribution, and the rate of change as well as the trajectories of the land covers (Lu et al., 2004). In addition, the accuracy of the change map, including the area estimates and spatial patterns of change, must be assessed.

The temporal resolution must be high enough to capture multiple land cover changes, such as the transition from forest to agriculture to urban. Furthermore, the rate of growth is usually not equally distributed through time, with faster growth during some periods and slower in others. The rate of growth and spatial pattern of growth will vary in time and often in response to exogenous stimuli such as demographic shifts (e.g., migration) or policy changes (e.g., farm subsidies). Linking landscape changes and social processes requires observations of the landscape at temporal frequencies that capture spatiotemporal dynamics.

16.3 AN EXAMPLE OF HIGH TEMPORAL RESOLUTION MAPPING

To understand the drivers of the change in the landscape, it is critical to have enough measurements through time to assess the effect of a political or economic event on land use patterns. Consider Figure 16.1, which shows the annual change in urban land use in the Pearl River Delta between 1988 and 1996. The annual rate of change is not constant and varies in times; one cannot model the variation using a single straight line. Furthermore, the more abrupt and interesting variations coincide with political

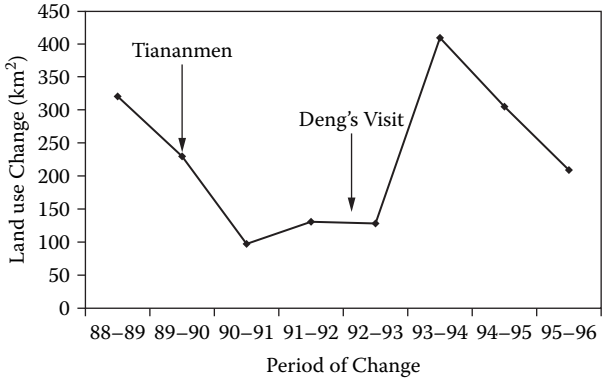

FIGURE 16.1 Annual urban land use change in km^2 for the Pearl River Delta.

events. The interesting feature is not so much the average growth between 1988 and 1996, but that the growth rate varies through time, corresponding to domestic and international events as well as local and national conditions. In the case of the Pearl River Delta, urban growth during the late 1980s and throughout the 1990s was largely driven by investment, particularly overseas funds. The Tiananmen Square incident in 1989 threatened investment flows to the region, which had significant and visible effects on land use change. It was not until after Deng Xiao Peng's visit to the region in 1992 that investors regained confidence in the government's commitment to reforms and investment flows returned, spurring another wave of urban expansion. Clearly, political events had important effects on the landscape evolution. Without high temporal frequency satellite data, the link between landscape patterns and socioeconomic-political processes would not be possible.

Considering only the two endpoints of the time series, that is, 1988 and 1996, it would have shown that approximately 2400 km^2 has changed but would not have shown the reduced rates of change after the Tiananmen Square event and the very rapid increase after Deng's visit in 1992. Even adding a middle point between the endpoints would still have masked the rapid increase in urban land use after Deng's visit. With that limited information, one would have to infer an average annual growth that is not representative of and would not have been as useful in identifying the political factor in urban growth. Only by classifying images at enough time steps can one generate the temporal resolution needed to understand the complex relationship between political and economic factors and the change in the urban landscape.

Similarly, there is evidence that, in some regions among all land cover types, high-quality agricultural lands are first converted into urban uses. To make policies to address these transitions, the planning agency must first know what the drivers of these losses were. The rate and the geographical location of these conversions must then be correlated with local or global policies. Sound policy grounded on a solid understanding of the growth drivers may have significant impact on sustainable development and food security.

Many of the current challenges in managing and understanding rapid anthropogenic landscape changes have such high temporal resolution requirements. Whenever it becomes necessary to understand these drivers of changes, the details provided by a time series of classified images are essential in correlating potential drivers to the landscape evolution. The trajectories of the urban landscape, defined over a long time series, are then linked to economic and immigration policy, investment, demography, infrastructure planning, and environmental regulation. This linkage between drivers and landscapes is a critical component in assessing existing planning policies and in developing better ones.

The temporal resolution has also been shown to be important in other fields such as vegetation monitoring (Lunetta et al., 2004). The built environment, especially in developing countries, often shows higher and more variable rate of change compared to the vegetation ecosystem, and requires higher temporal resolution. The change detection algorithms developed for monitoring vegetation may not be well suited for the longer time series required for mapping changes in urban areas.

Another need for long time series with good pattern accuracy is in training urban forecasting algorithm; see Clarke et al. (1997) and Fragkias and Seto (2007) for

examples of such algorithms. These algorithms are increasingly used in projecting current urbanization trends into the future. In general, these forecasting algorithms capture the growth of a city by learning how the city had grown based on satellite sensor images. It is thus important that growth patterns be correctly mapped both in space and time to provide a reliable basis for forecasting.

16.4 CURRENT METHODS FOR HIGH TEMPORAL RESOLUTION DATA ANALYSIS

The remote sensing literature is rich with change detection methods (Singh, 1989; Lu et al. 2004). These techniques include image regression, image subtraction, postclassification comparison, multidate principal components analysis, multidate tasseled cap transformation, change vector analysis, and neural networks (Fung, 1990; Lambin and Strahler, 1994; Collins and Woodcock, 1994; Gopal and Woodcock, 1996; Dai and Khorram, 1999). Numerous methods have been developed because of the variation in the types of study areas, the types of land cover changes being mapped, and the temporal and spatial resolution of the data. In turn, the variation in applications, study areas, and data constraints means that there is no such thing as a "best" technique.

Most change detection studies evaluate change between two periods (Howarth and Boasson, 1983; Green et al., 1994; Kwarteng and Chavez, 1998; Mas, 1999). Although studies that use more than two dates of imagery exist (Jensen et al., 1995; Pax Lenney et al., 1996; Collins and Woodcock, 1996), most do not use consecutive dates, nor do they extract annual estimates of land use or land cover. Furthermore, analyses that use more than two images are largely limited to AVHRR data (Eastman and Fulk, 1993; Barbosa et al., 1999; Lambin, 1996). Few methods have been developed or adapted for high temporal resolution data. A survey of the literature reveals that there are fewer than one dozen studies where the algorithm was developed for the purpose of high temporal frequency mapping (Kaufmann and Seto, 2001; Pan and Zhao, 2007; Xu et al., 2007).

The success of pixelwise change detection method is, first of all, a function of the quality of the registration (Townshend et al., 1992; Dai and Khorram, 1998). Coregistration of very long time series is difficult and can be an impediment to even the best multitemporal method. One cannot expect high accuracy of the results if the geographical location of pixels across the images is not reliable.

16.4.1 Postprocessing of Classified Images

The simplest change detection method classifies each image independently; changes are then identified by comparing the classified images. This is by far the least complex and most widely used change detection method. Although each map taken individually may be accurate, there is no guarantee that the time series will be well classified. The problem lies in the compounding of the errors across time. The time series accuracy is approximately the product of accuracy associated with each individually classified map (Singh, 1989). For example, a series of seven classified maps, each with an overall accuracy of 80%, may have a time series accuracy of 0.87, or

20% under the assumption of uncorrelated classification errors across time or space. Thus, a good single time classification on each map is no guarantee of an accurate time series.

16.4.2 Classification of Trajectories

A second change detection method consists of analyzing the stacked images concurrently and classifying the class trajectories (Singh, 1989). For example, instead of classifying a pixel as urban or agriculture, all the possible transitions between those classes (urban to urban, urban to agriculture, agriculture to urban, and agriculture to agriculture) are considered. The drawback of this method is that all pixel trajectories in time must be exhaustively stated before the classification. Furthermore, it requires having training data representing all these transitions. This technique is efficient and generates good accuracy when the time series is relatively short and contains few possible transitions. However, a long time series or the inclusion of just a few additional land cover classes can generate far too many possibilities to be manageable.

16.4.3 Econometrics Time Series

A third method models every pixel as a time series, where the time of change is estimated. For example, Kaufmann and Seto (2001) use time series econometrics to detect dates of change with better results than when the changes are obtained from postprocessing independently classified images. The method is efficient in finding the date of change on long time series but does not address which land cover types were involved in the changes.

16.4.4 The Cascade Approach

The cascade approach features a good balance between ease of use and performance in classifying long time series (Swain, 1978). It consists of sequentially classifying the land cover classes, usually in a chronological order. Past classifications are used to condition future classifications. The link between land cover at different times is parameterized with transition probabilities. The main drawback of doing the classification chronologically is that the accuracy will decrease as the time series increases. Moreover, if the first pixel is not well classified, the remaining portion of the time series, being conditioned to that misclassified pixel, is also likely to be misclassified.

Instead of a classical chronological classification, one can start by classifying the image that contains the most information relative to other images in the series. By first identifying this image, rather than the first image in the series, these high confidence classifications can be used to better classify the data in other periods where classification is more uncertain (Boucher et al., 2006). The image with the best information can be found with some information content metrics such as entropy. Thus, adding images with high information content to a time series can increase the mapping accuracy by constraining the images carrying less information.

The integration of satellite sensor data at different times is done with transition probabilities. The transition probability between land cover A and land cover B is the probability that a pixel will change from A to B within a defined period. The probability that no change occurred is the transition probability between land cover A and A or B and B. If there are L land cover types, then there are L^2 transition probabilities. It is misleading to assume that the transition probabilities are extra information that is not needed with the previous techniques; in fact, it can be shown that postprocessing independently classified images is equivalent of setting the transition probability from A to B to the global proportion of B. Not explicitly choosing a set of transition probabilities is simply equivalent to choosing an implicit, and likely incorrect, set of transition probabilities. Bruzzone and Serpico (1997) provide a technique for estimating these transition probabilities.

The cascade approach is the most scalable method for long time series. The algorithm complexity increases approximately linearly with the length of the time series. Furthermore, it does not require radiometric corrections or that the ground truth be colocated as required by the trajectory methods. It does, however, require the additional effort of obtaining the transition probability for any land cover to change into any other land cover in one time step. Ideally, each remote sensing image should have been taken at regular intervals, say every year in December. The transition probability matrix must be adjusted if the images are distributed irregularly in time.

A more rigorous approach would be to jointly classify all the dates through an iterative method such as expectation-maximization; such an iterative approach would be prohibitively and computationally costly for long time series and large images.

16.4.5 Issues of Spatial Resolution

The techniques discussed above assumed that the images have the same spatial resolution. This may not always be the case. For example, combining Landsat MSS with Landsat Thematic Mapper imagery has the additional challenges of integrating images with different radiometric and spatial resolution. Newer sensors provide spatial resolution that is finer than existing sensors. Combining images from sensors with different spatial resolution pose additional challenges that will be increasingly relevant if we wish to take advantage of the available information. At this point, one can either adjust the spatial scale of the images by upscaling or downscaling so that they will share the same spatial resolution.

16.5 ACCURACY ASSESSMENT OF HIGH TEMPORAL RESOLUTION TIME SERIES

A classified map is only useful if associated with an accuracy assessment. Moreover, that accuracy assessment must target the mapping objectives. Most change detection studies address issues of accuracy, but few address the issue of accuracy through time. In addition to cross-sectional accuracy, such as the confusion matrix and the kappa coefficient, the classification of land covers over time must also be accurate. The temporal component becomes as important as the spatial component when it is necessary to

know both when and where changes have occurred. Classifying a time series of remote sensing images differs from classifying each image independently. Independently classifying each image provides an accurate mapping of the urban area at each time, that is, cross-sectional accuracy. It may provide reasonable estimates of the rates of overall growth between two periods. It will not, however, provide an accurate temporal pattern of growth, that is, where, when, and how the changes occurred. The reader is referred to Biging et al. (1999) for a perspective on accuracy for change detection.

Ideally, a time series of georeferenced ground truth data would exist for each pixel in the training data set. Having enough of these fully known time series greatly eases the validation of the temporal mapping. Take the example of mapping five land covers (e.g., water, vegetation, agriculture, urban, and transition) over 8 years, from 1988 to 1996, in the Pearl River Delta, China. Figure 16.2 shows the accuracy of the time series as a function of its length; the accuracy assessment is performed on more than 2000 known time series with a fivefold cross-validation. The solid and the dashed lines are obtained with the cascade approach, whereas the gray line is obtained by classifying each image independently. Two measures of accuracy are displayed; the first one is the accuracy in mapping change. In this case, a time series is considered to be well classified if the dates of change have been correctly identified. The land covers involved in the change are not considered at this point. A second accuracy metric, also shown in Figure 16.2 (right), considers a time series well classified only if all the land cover types have been correctly identified for all points in time. This measures the *type* of land cover change — change from what to what land cover classes — as well as *when* the change occurred. This is a more stringent accuracy metric, but it is also more relevant when linking changes in land covers with socioeconomic policies.

As the length of the time series increases, the accuracy generally decreases. The rate of decrease is higher when the images are independently classified (shown by the gray line) than when the cascade approach is used (shown by the solid and dashed lines). For the cascade approach, accuracy is also a function of the sequencing. For instance, classifying the most informed pixels first (solid line) delivers a higher accuracy than doing a chronological classification (dashed line). Using temporal

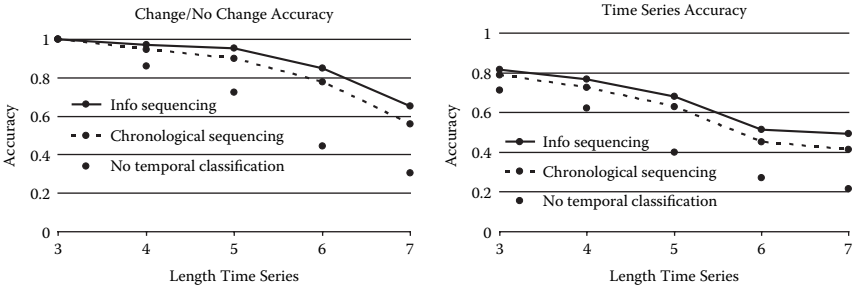

FIGURE 16.2 Computed accuracy for increasing length of time series for five land covers with a cascade approach with information-based sequencing (solid line), a chronological approach, and independently classified images (gray lines). Left: change/no change accuracy. Right: full time-series accuracy.

information — in this case, transition probabilities — increases the accuracy of a long time series.

For a given length of a time series, a useful accuracy indicator is the percentage of time series containing at least *n* consecutive pixels that are correctly classified. Consider the examples in Figure 16.2 with a time series length of seven. The first point in Figure 16.3 shows the percentage of time series that have at least two consecutive times, out of the seven, that are well classified. That same accuracy is computed for a consecutive sequence of three, four, up to seven, which yields the same values as in Figure 16.2.

In the most difficult case, where the ground truth data are not georeferenced through time, the validation of the time series becomes more difficult because there are no data to compare the classification over time. In that case, one cannot obtain a precise accuracy number. The issue of how to assess time series accuracy for long time series and high temporal frequency data will require significant research, especially as the satellite record continues to lengthen. New metrics, albeit imperfect, will be required that describes time series accuracy. One alternative is to search and count how many impossible or very unlikely transitions, based from expert knowledge, have been mapped (Liu and Zhou, 2004). For example, if it is impossible for an urban land cover to change into a forest within 2 years, one can then scan the classified maps searching for such a transition. If some are found, it is indicative of some of the errors contained in the map. Tabulating such impossible transitions would give the user a broad idea about its accuracy in mapping change patterns.

16.6 CONCLUSION

As the physical size and number of cities continue to grow, their impacts on the environment will also increase. The questions and challenges generated by these fast-growing cities required high-temporal resolution time series, and algorithms can

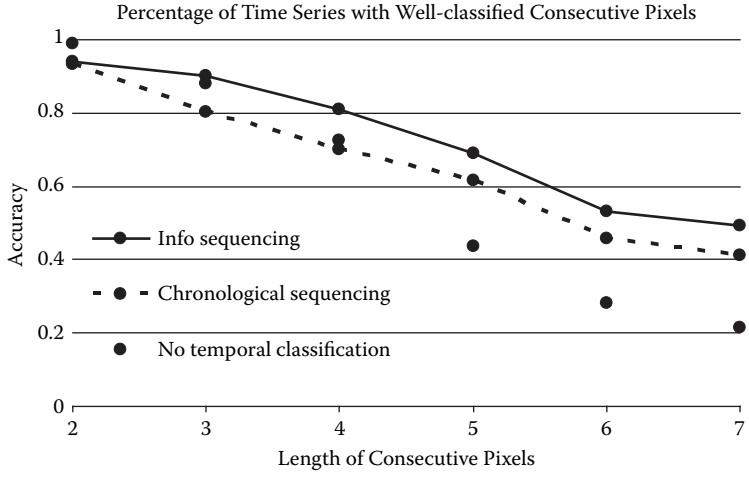

FIGURE 16.3 Percentage of time series with at least *n* consecutive years that are well-classified. The number of consecutive dates *n* is set to vary between 2 and 7.

efficiently process these images. Learning what influenced the growth patterns and linking urban growth with sociopolitical or economic events is essential in developing policies that will lead to more sustainable built places.

New methods for classifying and assessing these long time series are needed to reduce the time and effort required in generating these high-temporal resolution images. Most of the development about multitemporal mapping focuses on classifying only two or three images when, in fact, many more are needed to link urban growth with social and economics policies.

REFERENCES

Barbosa, P.M., Gregoire, J.-M., and Pereira, J.M.C., An algorithm for extracting burned areas from time series of AVHRR GAC data applied at a continental scale, *Remote Sensing of Environment*, 69, 253–263, 1999.

Batty, M., The size, scale, and shape of cities, *Science*, 319, 769–771, 2008.

Beauregard, R., Theorizing the global-local connection, in: Knox, P.L., and Taylor, P.J., eds., *World Cities in a World System*, Cambridge University Press, Cambridge, pp. 232–248, 1995.

Beaverstock, J.V., Smith, R.G., Taylor, P.J., Walker, D.R.F., and Lorimer, H., Globalization and world cities: Some measurement methodologies, *Applied Geography*, 20, 43–63, 2000.

Biging, G.S., Chrisman, N.R., Colby, D.R., Congalton, R.G., Dobson, J.E., Fergurson, R.L., Goodchild, M.F., Jensen, J.R., and Mace, T.H., in: Khorram, S., ed., *Accuracy Assessment of Remote Sensing-Detected Change Detection*, American Society for Photogrammetry and Remote Sensing, 1999.

Boucher, A., Seto, K.C., and Journel, A.G., A novel method for mapping land cover changes; Integrating space and time with geostatistics, *IEEE Transactions on Geosciences and Remote Sensing*, 44, 3427–3435, 2006.

Bruzzone, L., and Serpico, S.B., An iterative technique for the detection of land-cover transitions in multitemporal remote-sensing images, *IEEE Transactions on Geosciences and Remote Sensing*, 35, 858–867, 1997.

Clarke, K.C., Hoppen, S., and Gaydos, L., A self-modifying cellular automaton model of historical urbanization in the San Francisco Bay area, *Environment and Planning B: Planning and Design*, 24, 247–261, 1997.

Collins, J.B., and Woodcock, C.E., Change detection using the Gramm-Schmidt transformation applied to mapping forest mortality, *Remote Sensing of Environment*, 50, 267–279, 1994.

Collins, J.B., and Woodcock, C.E., An assessment of several linear change detection techniques for mapping forest mortality using multitemporal Landsat TM data, *Remote Sensing of Environment*, 56, 66–77, 1996.

Dai, X.L., and Khorram, S., The effects of image misregistration on the accuracy of remotely sensed change detection, *IEEE Transactions on Geosciences and Remote Sensing*, 36, 1566–1577, 1998.

Dai, X.L., and Khorram, S., Remotely sensed change detection based on artificial neural networks, *Photogrammetric Engineering and Remote Sensing*, 65, 1187–1194, 1999.

Eastman, R.J., and Fulk, M., Long sequence time series evaluation using standardized principal components, *Photogrammetric Engineering and Remote Sensing*, 59, 1307–1312, 1993.

Fragkias, M., and Seto, K.C., Modeling urban growth in data-sparse environments: A new approach, *Environment and Planning B*, 34, 858–883, 2007.

Fung, T., An assessment of TM imagery for land-cover change detection, *IEEE Transactions on Geoscience and Remote Sensing*, 28, 681–684, 1990.

Gopal, S., and Woodcock, C.E., Remote sensing of forest change using artificial neural networks, *IEEE Transactions on Geoscience and Remote Sensing*, 34, 398–404, 1996.

Green, K., Kempka, D., and Lackey, L., Using remote sensing to detect and monitor land-cover and land-use change, *Photogrammetric Engineering and Remote Sensing*, 60, 331–337, 1994.

Homewood, K., Lambin, E.F., Coast, E., Kariuki, A., Kikula, I., Kivalia, J., Said, M., Serneels, S., and Thompson, M., Long-term changes in Serengeti-Mara wildebeest and land cover: Pastoralism, population, or policies? *Proceedings of the National Academy of Sciences*, 98, 12544–12549, 2001.

Howarth, P.J., and Boasson, E., Landsat digital enhancements for change detection in urban environments, *Remote Sensing of Environment*, 13, 149–160, 1983.

Jabareen, Y.R., Sustainable urban forms: Their typologies, models, and concepts, *Journal of Planning Education and Research*, 26, 38–52, 2006.

Jensen, J.R., Rutchey, K., Koch, M.S., and Narumalani, S., Inland wetland change detection in the everglades water conservation area 2A using a time series of normalized remotely sensed data, *Photogrammetric Engineering and Remote Sensing*, 51, 199–209, 1995.

Kaufmann, R.K., and Seto, K.C., Change detection, accuracy and bias in a sequential analysis of Landsat imagery in the Pearl River Delta, China: Econometric techniques, *Agriculture, Ecosystem Environment*, 85, 95–105, 2001.

Knox, P.L., The restless urban landscape: Economic and sociocultural change and the transformation of metropolitan Washington, D.C., *Annals of the Association of American Geographers*, 81, 181–209, 1991.

Kwarteng, A.Y., and Chavez, P.S., Jr., Change detection study of Kuwait City and environs using multi-temporal Landsat Thematic Mapper data, *International Journal of Remote Sensing*, 19, 1651–1662, 1998.

Lambin, E.F., Change detection at multiple temporal scales: Seasonal and annual variations in landscape variables, *Photogrammetric Engineering and Remote Sensing*, 62, 931–938, 1996.

Lambin, E.F., Rounsevell, M., and Geist, H., Are agricultural land-use models able to predict changes in land use intensity? *Agriculture, Ecosystems & Environment*, 82, 321–331, 2000.

Lambin, E.F., and Strahler, A.H., Change-vector analysis in multitemporal space: A tool to detect and categorize land-cover change processes using high temporal-resolution satellite data, *Remote Sensing of Environment*, 48, 231–244, 1994.

Landis, J., and Zhang, M., The second generation of the California Urban Futures Model: Part 1. Model logic and theory, *Environment and Planning B: Planning and Design*, 25, 657–666, 1998.

Liu, H., and Zhou, Q., Accuracy analysis of remote sensing change detection by rule-based rationality evaluation with post-classification comparison, *International Journal of Remote Sensing*, 25, 1037–1050, 2004.

Lo, C.P., and Faber, B.J., Integration of Landsat Thematic Mapper and census data for quality of life assessment, *Remote Sensing of Environment*, 62, 143–157, 1997.

Lu, D., Mausel, P., Brondízio, E., and Moran, E., Change detection techniques, *International Journal of Remote Sensing*, 25, 2365–2407, 2004.

Lunetta, R.S., Johnson, D.M., Lyon, J.G., and Crotwell, J., Impacts of imagery temporal frequency on land-cover change detection monitoring, *Remote Sensing of the Environment*, 89, 444–454, 2004.

Makse, H.A., Havlin, S., and Stanley, H.E., Modeling urban growth patterns, *Nature*, 377, 608–612, 1995.

Marcotullio, P.J., Asian urban sustainability in the era of globalization, *Habitat International*, 25, pp. 577–598, 2001.

Mas, J.-F., Monitoring land-cover changes: A comparison of change detection techniques, *International Journal of Remote Sensing*, 20, 139–152, 1999.

Nagendra, H., Munroe, D.K., and Southworth, J., From pattern to process: Landscape fragmentation and the analysis of land use/land cover change, *Agriculture, Ecosystems, and Environment*, 101, 111–115, 2004.

Pan, X., and Zhao, Q., Measurement of urbanization process and the paddy soil loss in Yixing city, China between 1949 and 2000, *CATENA*, 69, 65–73, 2007.

Pax Lenney, M., Woodcock, C.E., and Collins, J.B., The status of agricultural lands in Egypt: The use of multitemporal NDVI features derived from Landsat TM, *Remote Sensing of Environment*, 56, 8–20, 1996.

Reid, R.S., Kruska, R.L., Muthul, N., Taye, A., Wotton, S., Wilson, C. J., and Mulatu, W., Land-use and land-cover dynamics in response to changes in climatic, biological and socio-political forces: The case of southwestern Ethiopia, *Landscape Ecology*, 15, 339–355, 2000.

Schneider, A., and Woodcock, C., Compact, dispersed, fragmented, extensive? A comparison of urban growth in twenty-five global cities using remote sensing data, pattern metrics, and census information, *Urban Studies*, 45, 659–692, 2008.

Schneider, A., Seto, K.C., and Webster, D., Urban growth in Chengdu, western China: Application of remote sensing to assess planning and policy outcomes, *Environment and Planning B*, 32, 323–345, 2005.

Seto, K.C., and Kaufmann, R.K., Using logit models to classify land cover and land-cover change from Landsat Thematic Mapper, *International Journal of Remote Sensing*, 26, 563–577, 2005.

Singh, A., Digital change detection techniques using remotely-sensed data, *International Journal of Remote Sensing*, 10, 989–1003, 1989.

Swain, P.H., Bayesian classification in a time-varying environment, *IEEE Transactions on Systems, Man, and Cybernetics*, 8, 879–883, 1978.

Townshend, J.R.G., Justice, C.O., Gurney, C., and McManus, J., The impact of misregistration on change detection, *IEEE Transactions on Geoscience and Remote Sensing*, 30, 1054–1060, 1992.

Wang, Y.Q., and Zhang, X.S., A dynamic modeling approach to simulating socioeconomic effects on landscape changes, *Ecological Economics*, 140, 141–162, 2001.

Xu, C., Liu, M., Zhang, C., An, S., Yu, W., and Chen, J.M., The spatiotemporal dynamics of rapid urban growth in the Nanjing metropolitan region of China, *Landscape Ecology*, 22, 925–937, 2007.

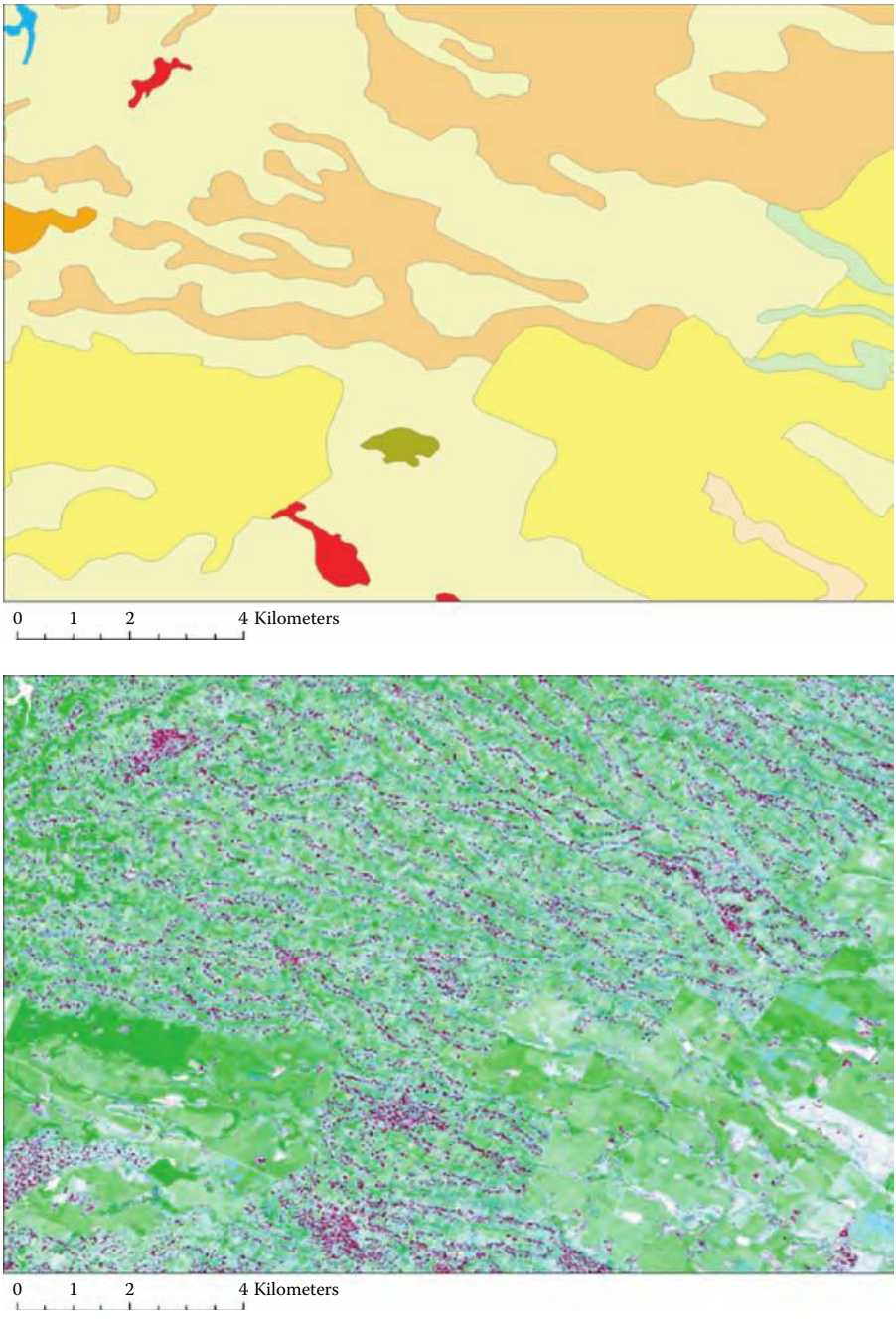

COLOR FIGURE 3.5 Settlements north of Nairobi, Kenya. Three examples of landscape representations: (a) land cover map produced in the Africover project based on Landsat 5 imagery; (b) built-up index map based on SPOT 5 imagery.

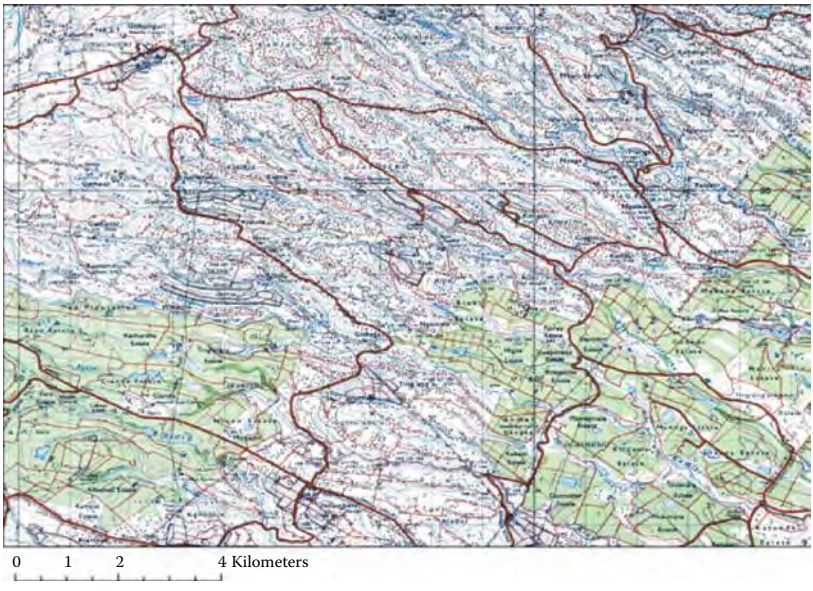

COLOR FIGURE 3.5 (Continued) (c) 1: 50.000 scale topographic map.

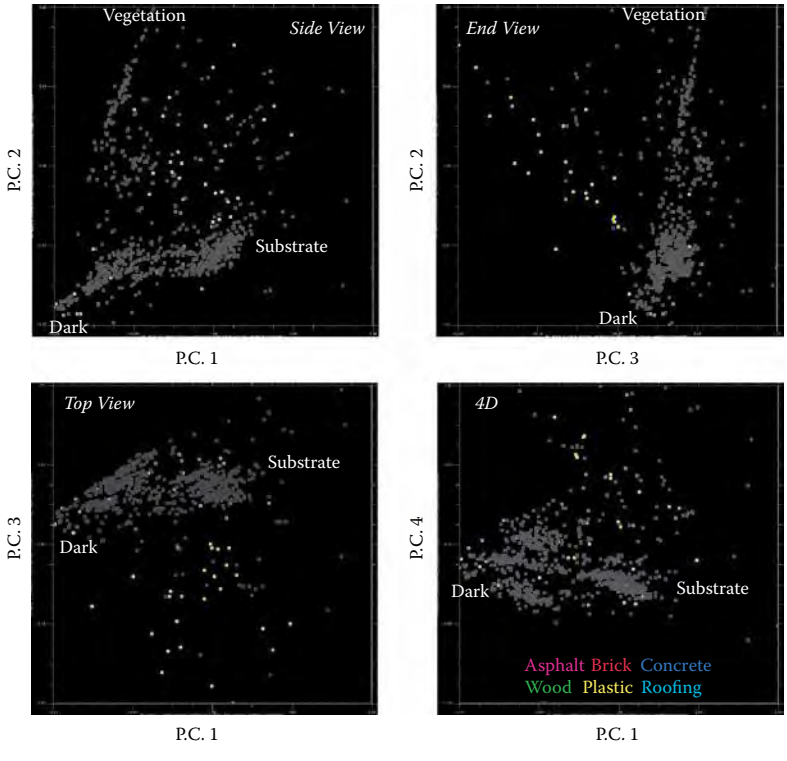

COLOR FIGURE 4.2 Anthropogenic materials in spectral mixing space. Scatterplots of the four primary principal components (P.C.s) of the laboratory spectra in Figure 4.1 show the geometric relationship of the anthropogenic spectra (in color) to vegetation and rock and soil substrates (gray). The latter non-anthropogenic spectra form a sub-planar, triangular distribution resulting from mixtures of bright substrates (e.g., sand) and dense vegetation (e.g., grass) with varying amounts of darker, more absorptive material (e.g., Fe-Mg minerals) or shadow.

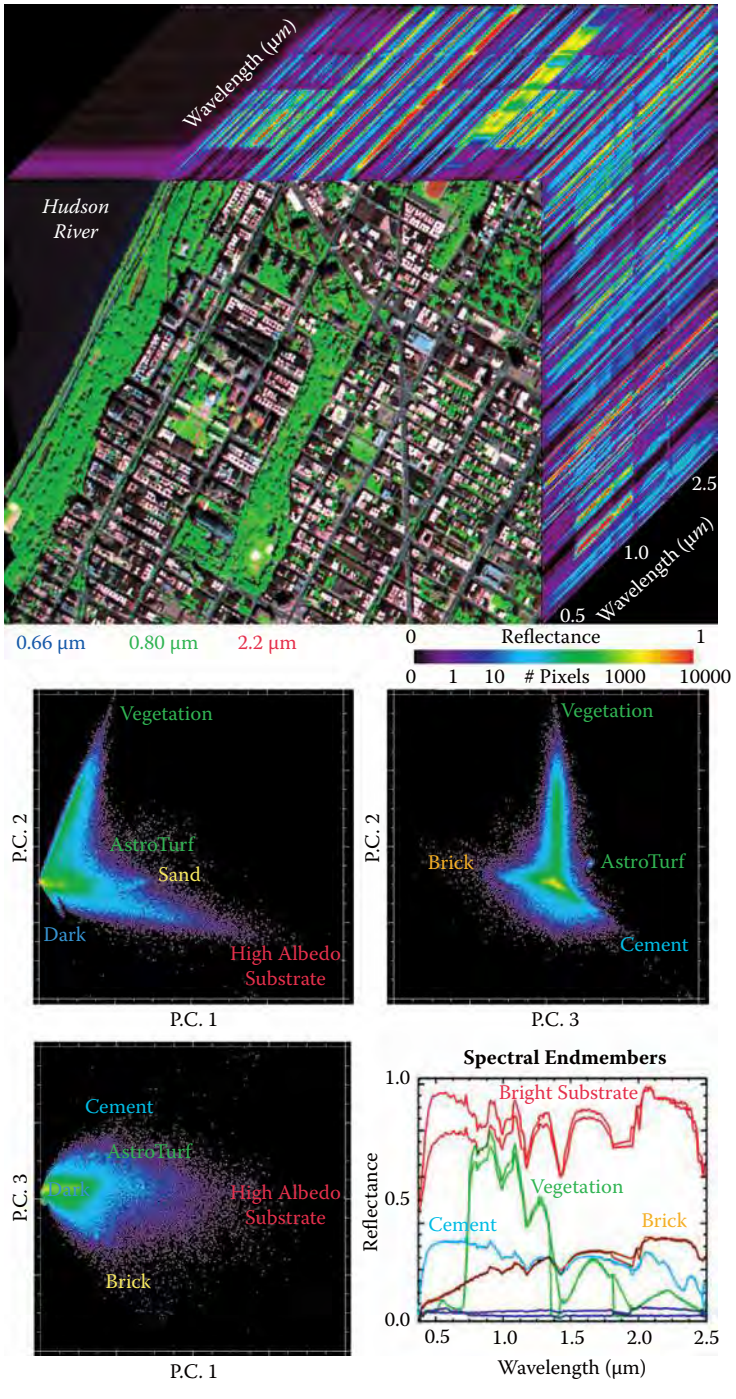

COLOR FIGURE 4.5 Hyperspectral urban diversity in New York City and California. AVIRIS hyperspectral cube shows the diversity and scale of urban reflectance in the densely built-up environment of upper Manhattan and in both Goleta and its undeveloped periphery. The "red edge" at 0.7 mm illustrates the abundance of fine scale vegetation in the urban mosaic. Mixing space topology has a skewed pyramid structure with the dark endmember at the apex and prominent mixing lines associated with asphalt and vegetation.

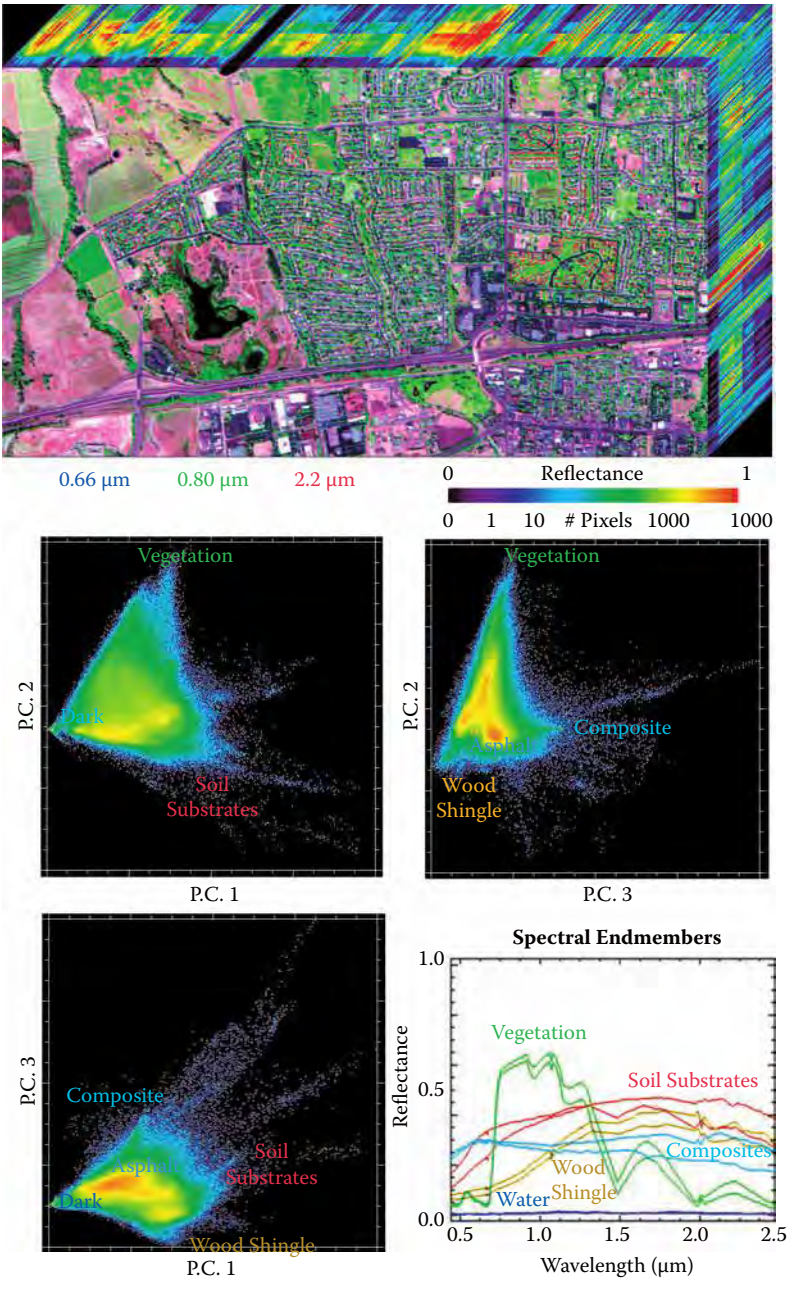

COLOR FIGURE 4.5 (Continued)

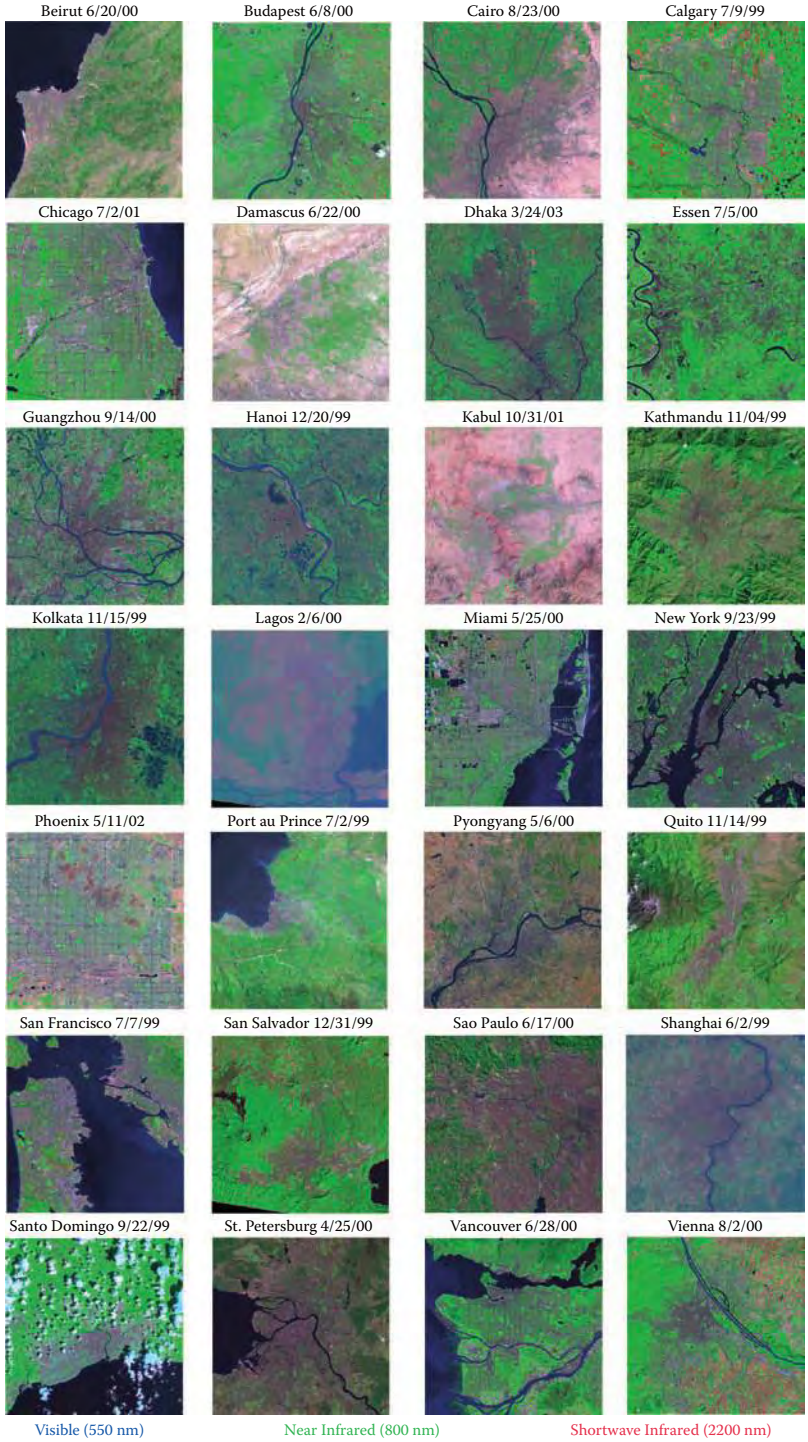

COLOR FIGURE 4.6 Inter-urban comparison of 28 cities as seen by Landsat 7. Each 30 × 30 km subscene has been calibrated to exoatmospheric reflectance and enhanced with the same 1% linear stretch so colors are comparable. Full resolution color images available at http://www.LDEO.columbia.edu/~small/Urban

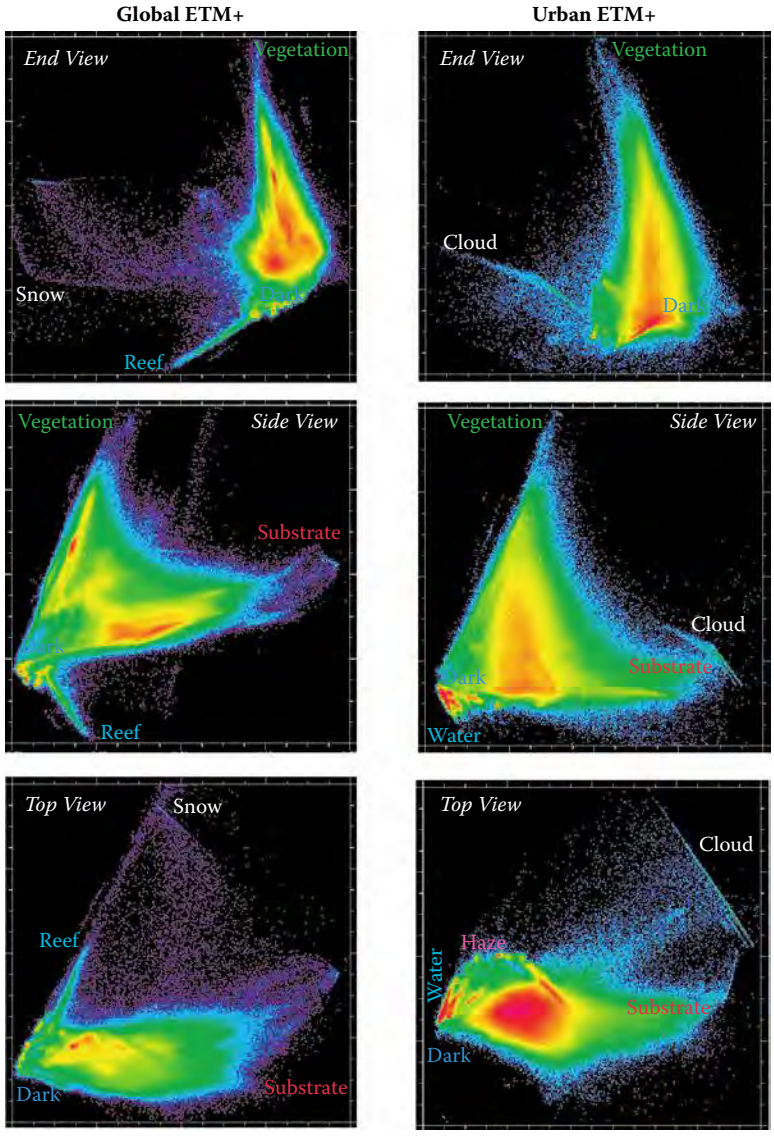

COLOR FIGURE 4.7 Comparison of Landsat ETM+ global composite mixing spaces for urban and non-urban environments for 30 cities, and for mixing spaces with 9×9 km cores of each of the 30 cities in the composite. Aside from spurs associated with reefs, ice and snow in the global composite, the topology of the mixing spaces is strikingly similar. The non-urban space has three distinct internal clusters (not including water) along vegetation and substrate mixing lines but the urban space has only one cluster for built-up cores. Note that even the most densely built-up cores together span almost the entire mixing space.

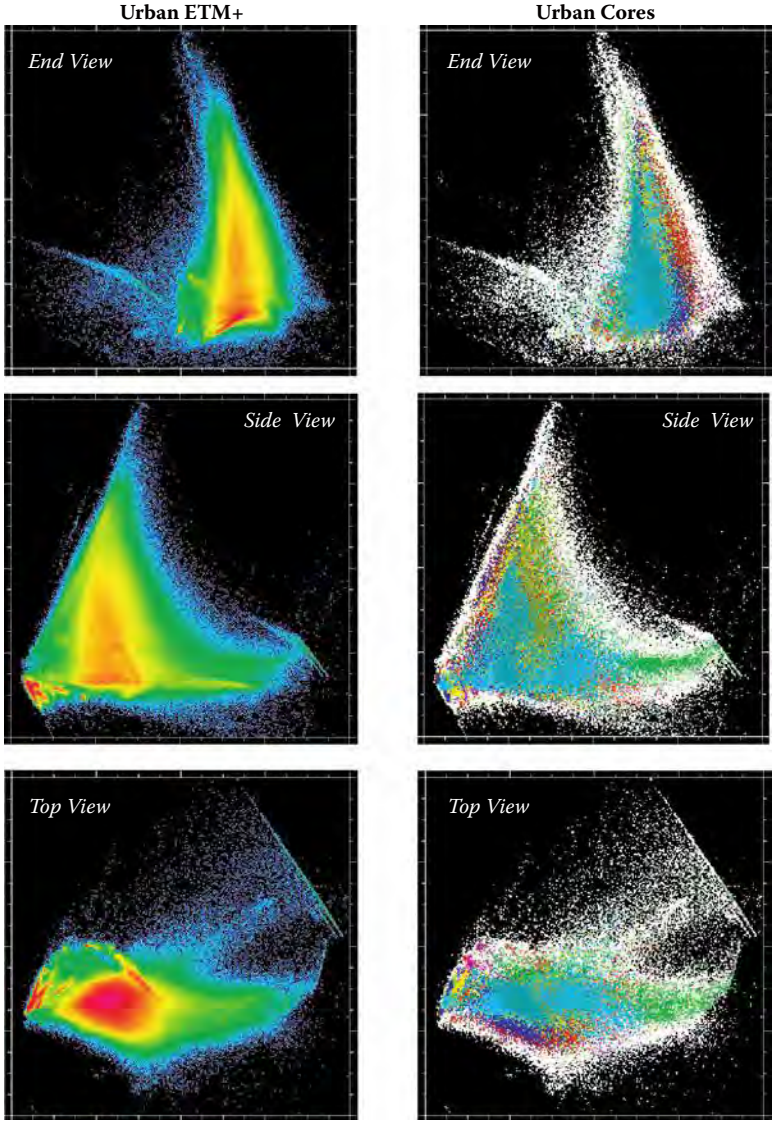

COLOR FIGURE 4.7 (Continued)

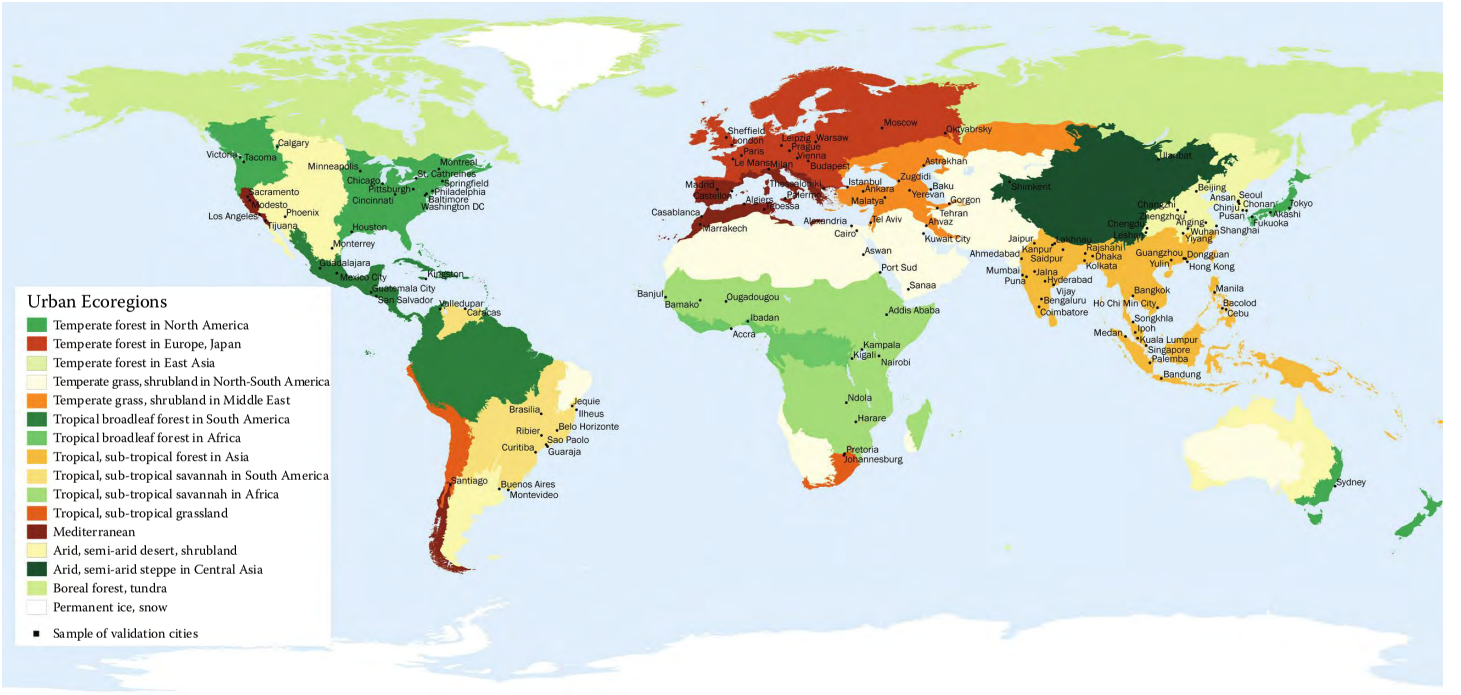

COLOR FIGURE 5.1 The map of urban ecoregions produced for this research to facilitate analysis and processing of the MODIS 463.3 data as well as assessment of the resultant global map of urban extent. The sample 135 cities used for validation purposes are indicated by dots.

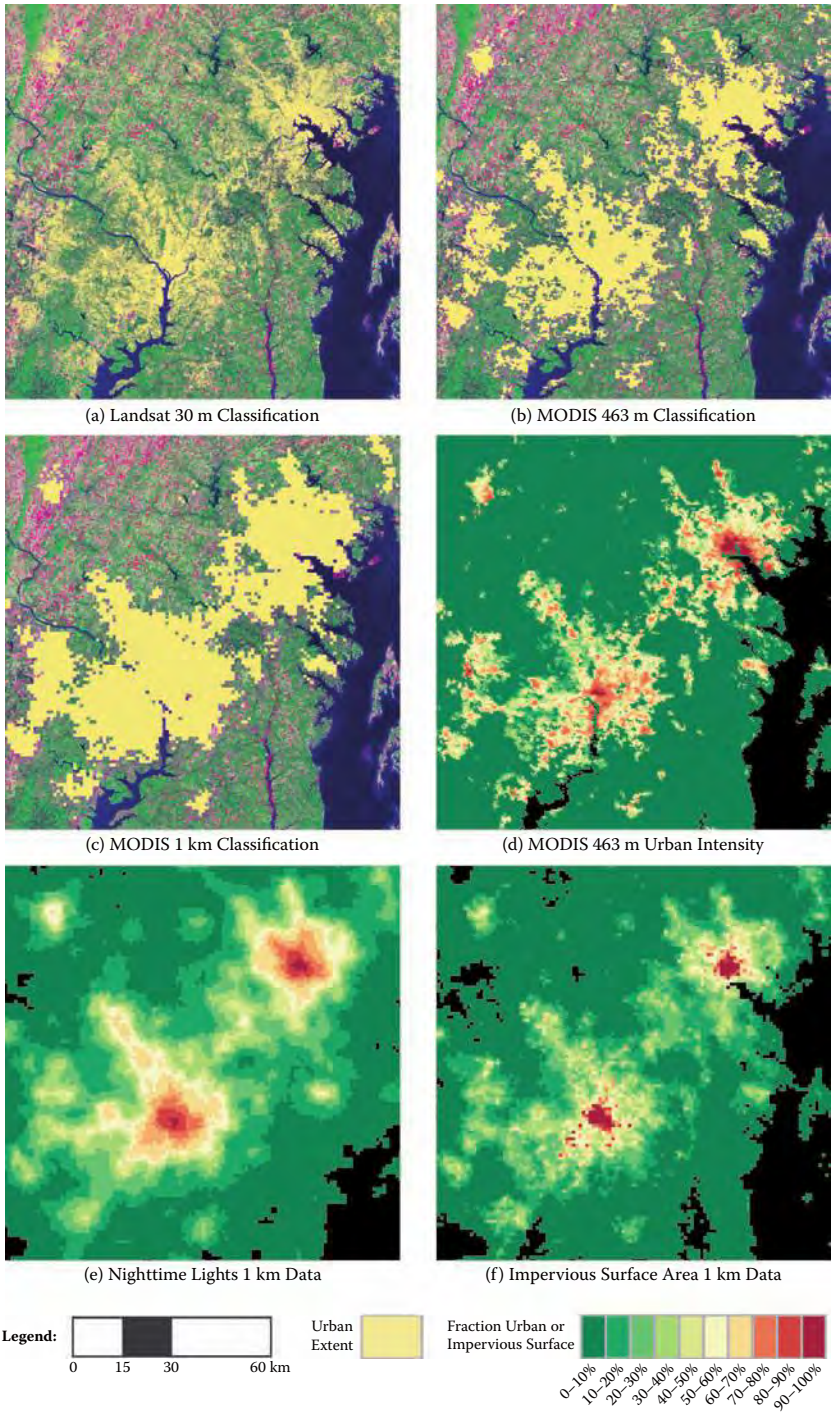

COLOR FIGURE 5.2 A comparison of maps for the Washington D.C.–Baltimore, Maryland conurbation depicting (a) a Landsat-based classification (30 m), (b) the MODIS-based classification (463 m resolution), (c) the prior version of the MODIS-based map (1 km resolution), (d) sub-pixel "urban intensity" from 463 m MODIS data, (e) nighttime lights data, and (f) NOAA's impervious surface area map.

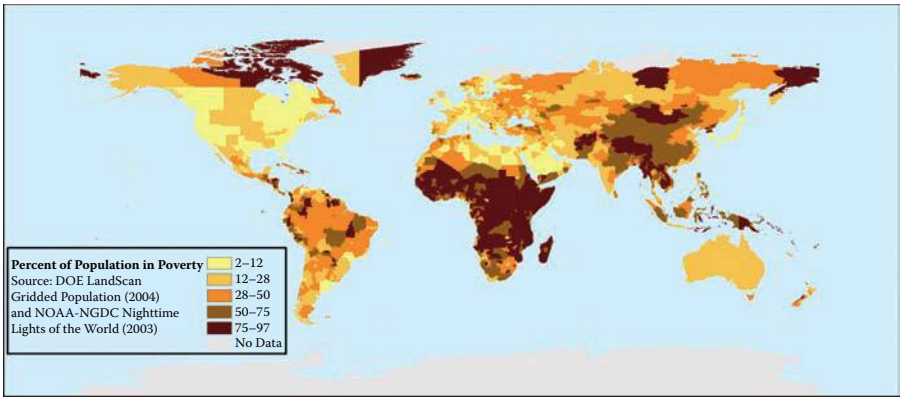

COLOR FIGURE 6.5 Map of poverty levels for 2,543 sub-national administrative units estimated based on the satellite data–derived poverty index.

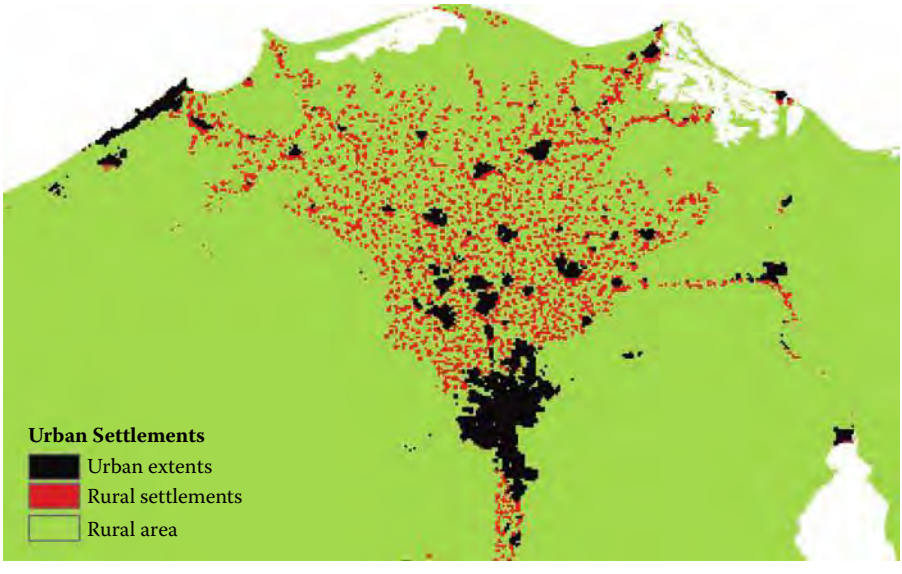

COLOR FIGURE 8.1 Urban extents and rural settlements in the Nile Delta (FAO-PMUR), 2000.

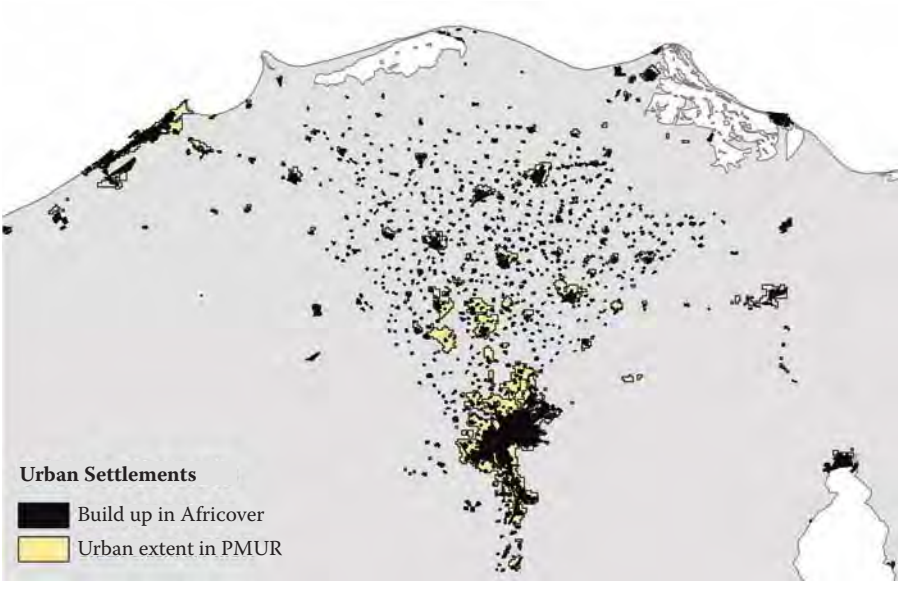

COLOR FIGURE 8.2 Overlay of built-up area from Africover on urban extents from PMUR in the Nile Delta, 2000.

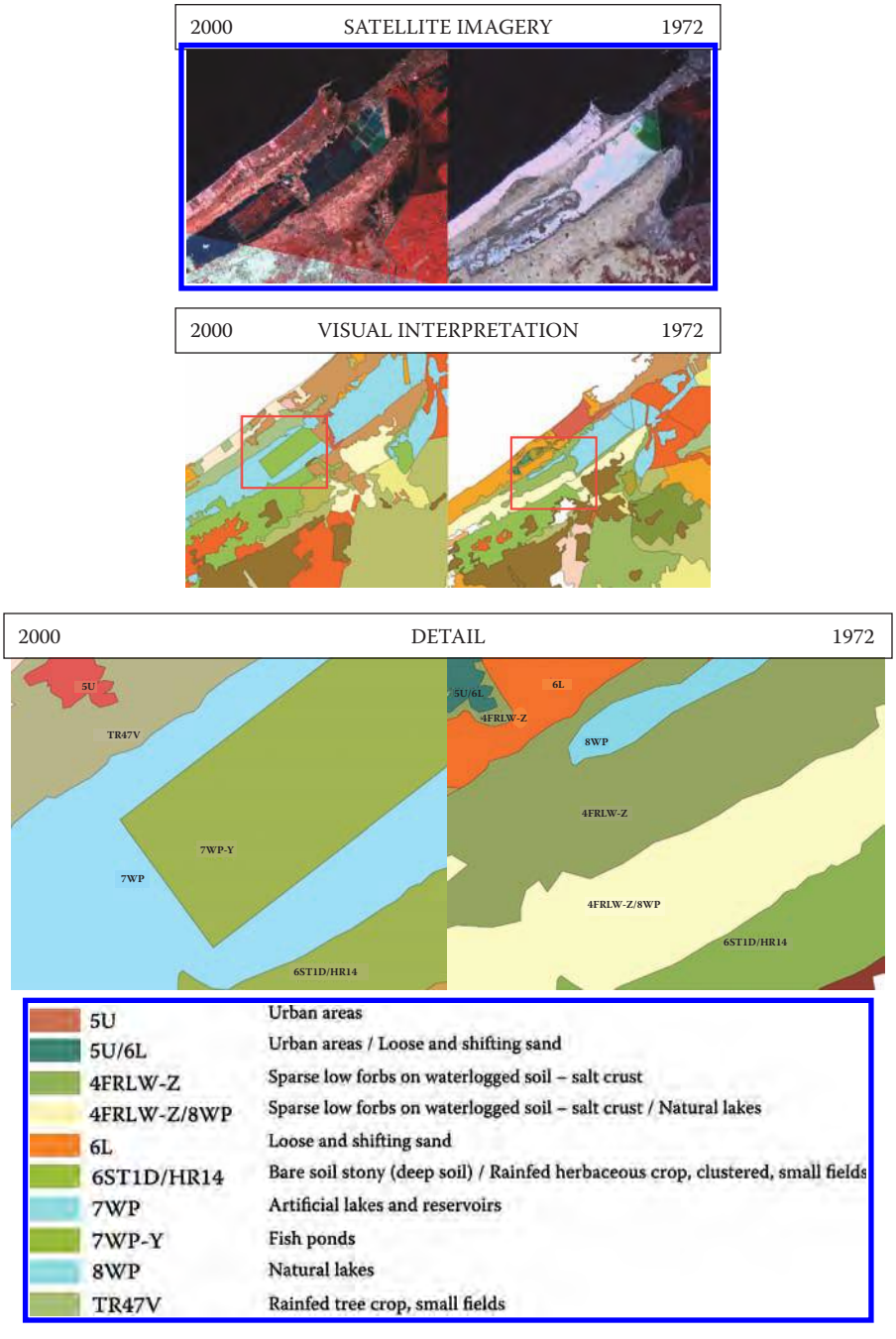

COLOR FIGURE 8.4 Transformation around the Nile Delta lagoon, changes from 1972 to 2000.

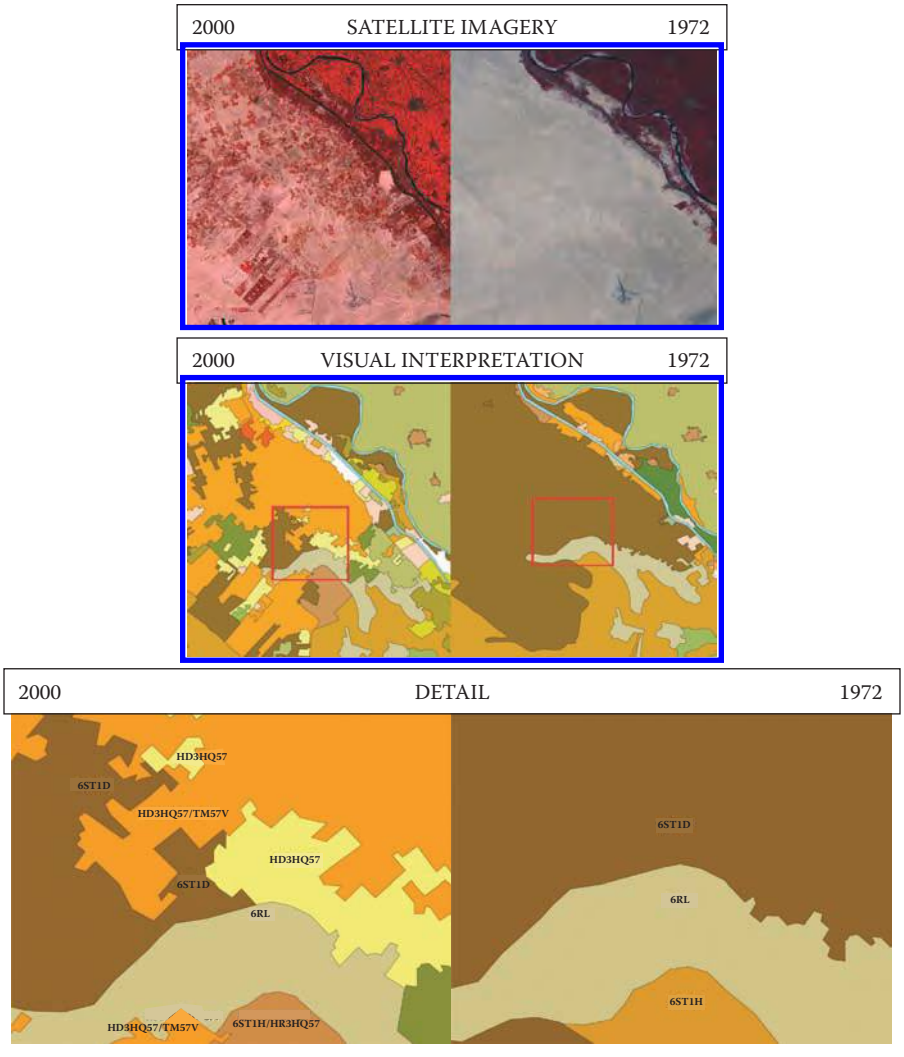

COLOR FIGURE 8.5 Land reclamation in the Nile Delta, changes from 1972 to 2000.

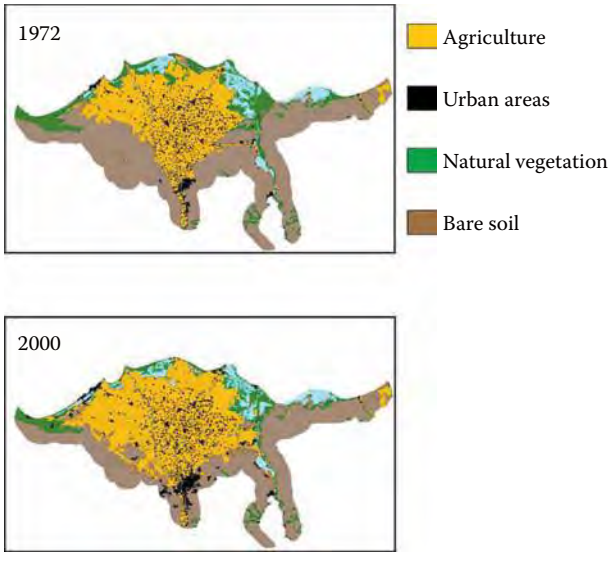

COLOR FIGURE 8.6 Land cover change in the Nile Delta from 1972 to 2000, Africover aggregations.

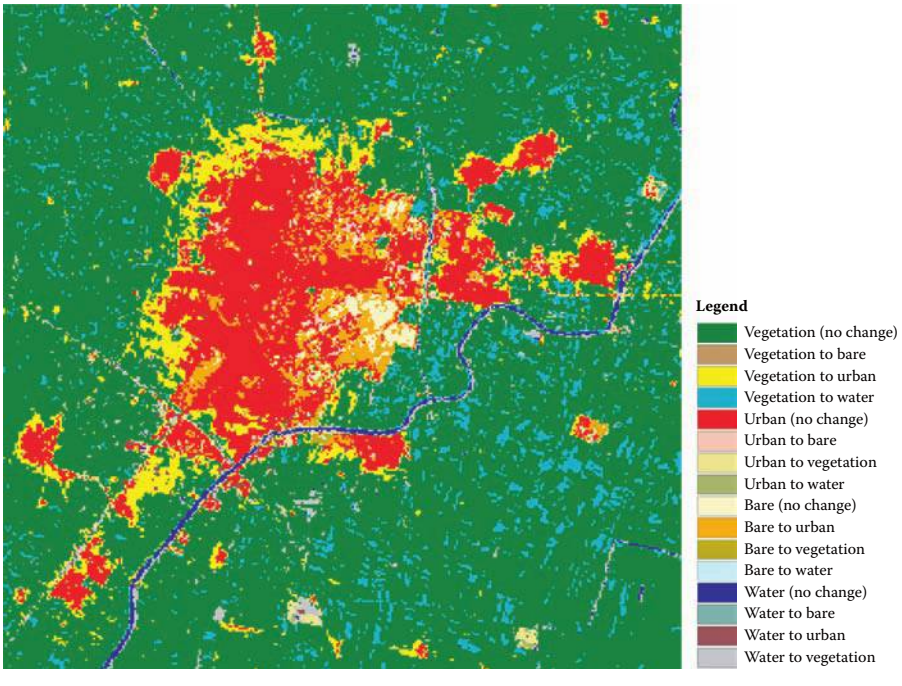

COLOR FIGURE 8.8 Land cover change in the Egyptian city of El Mahala El Kobra from 1984 to 2002, Africover aggregations.

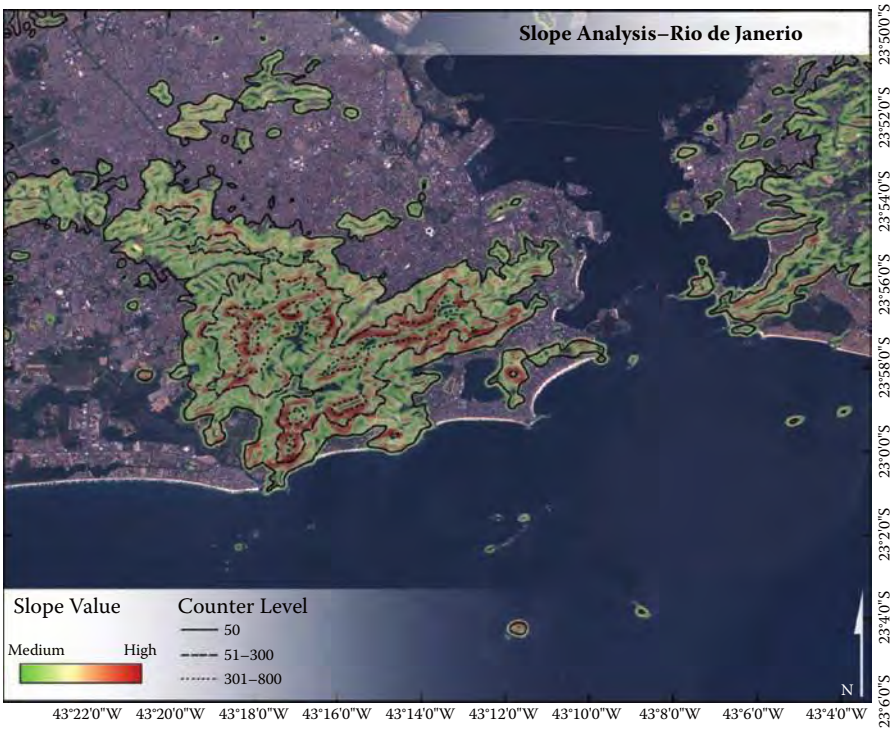

COLOR FIGURE 10.2 Overlapping of the DEM and Landsat data indicating areas of high landslide risk based on steepness of slopes in the megacity Rio de Janeiro, Brazil.

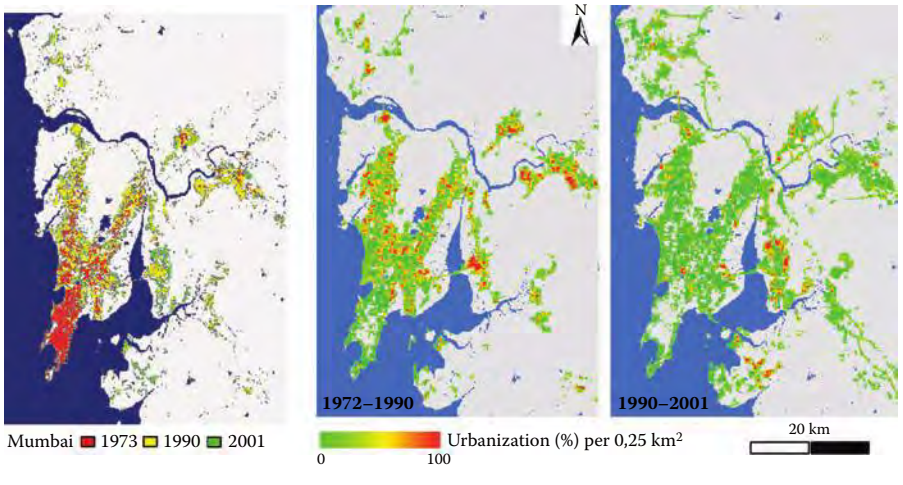

COLOR FIGURE 10.3 Change detection and urbanization rates in the megacity Mumbai, India.

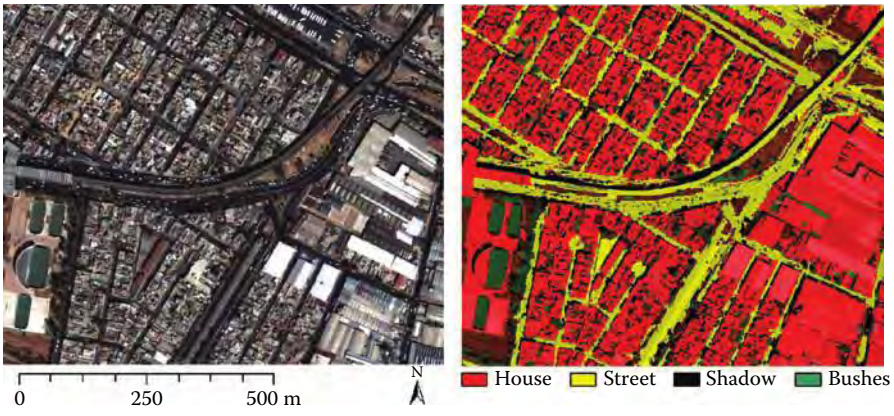

COLOR FIGURE 10.5 Land cover classification of the dense urban structures of Mexico City, Mexico, based on Quickbird data.

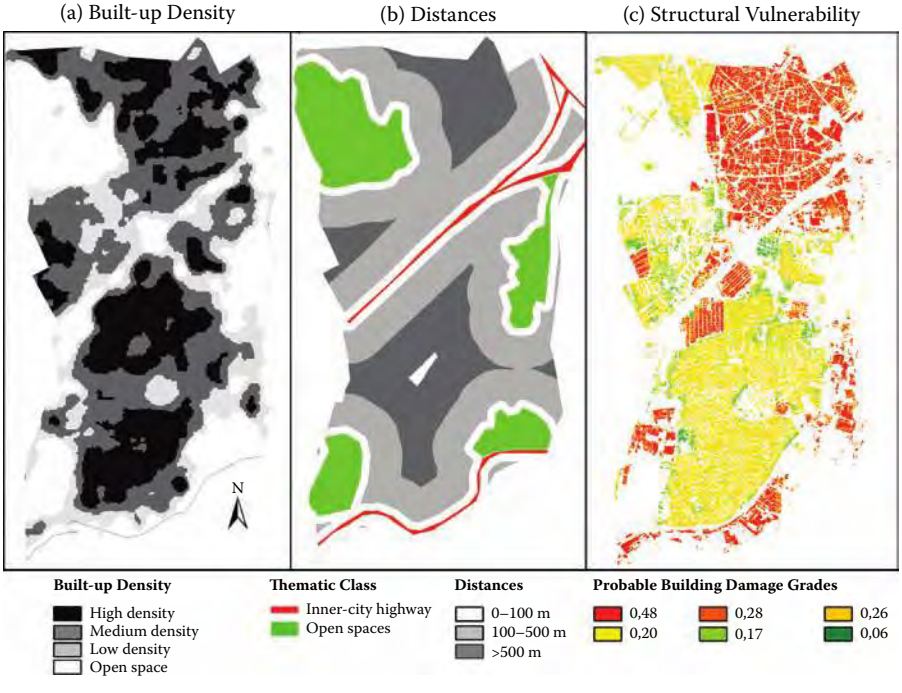

COLOR FIGURE 10.6 Indicators contributing to a holistic concept of risk and vulnerability.

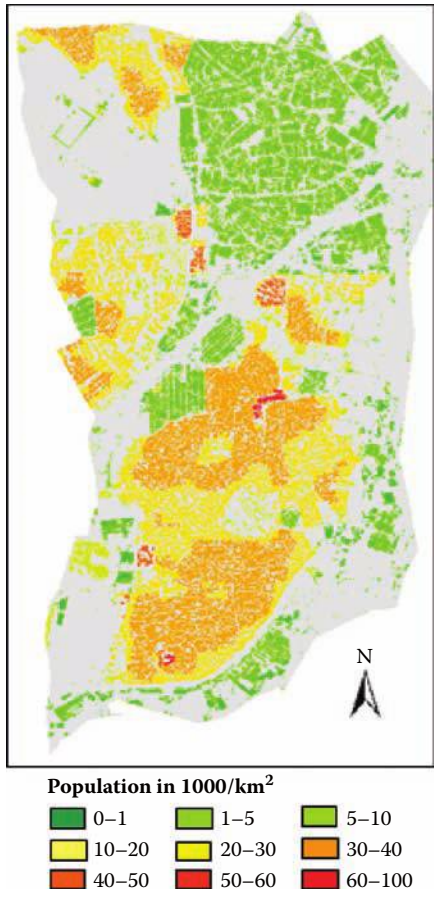

COLOR FIGURE 10.7 Nighttime population estimation.

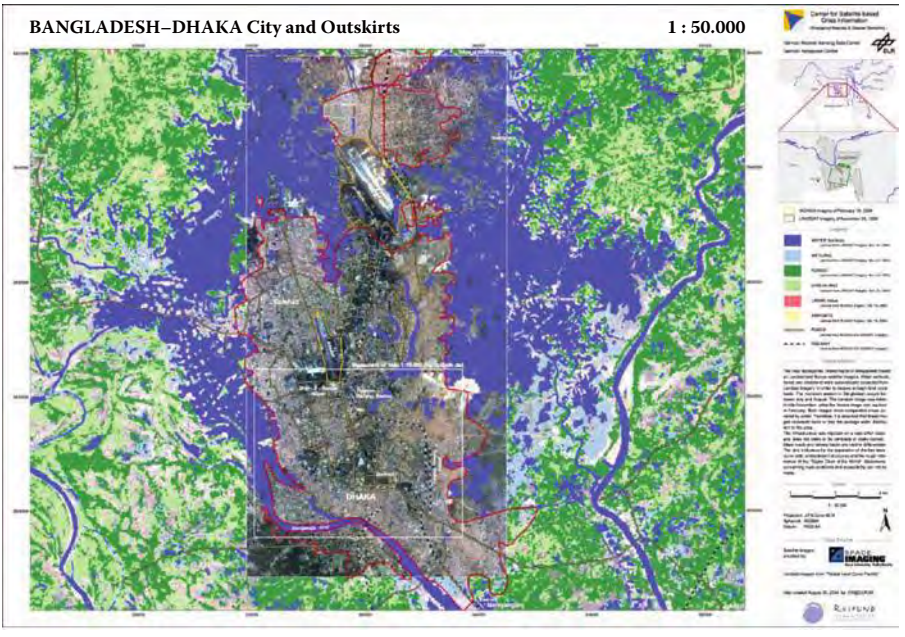

COLOR FIGURE 10.9 Flooding of the megacity Dhaka, Bangladesh. Rapid mapping product produced at DLR-ZKI to derive up-to-date spatial information for relief operations. (Image from the Center for Satellite-Based Crisis Information. With permission.)

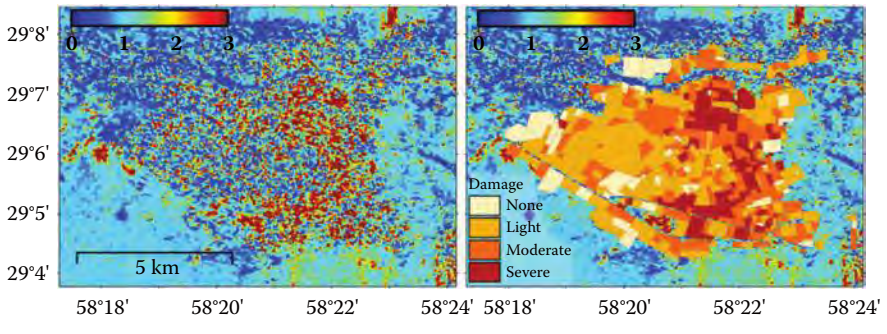

COLOR FIGURE 10.10 Mapping damage from an earthquake in an urban environment using interferometric coherence.

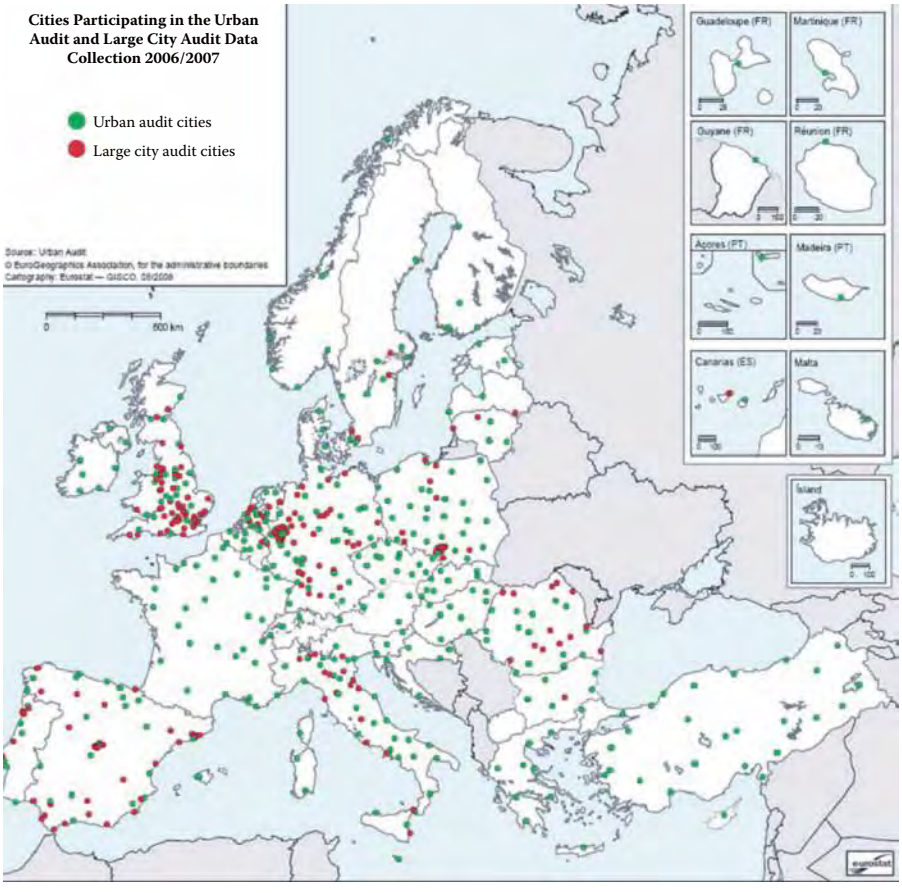

COLOR FIGURE 11.1 Cities participating in the Urban Audit, 2006–2007. (Courtesy of Urban Audit.)

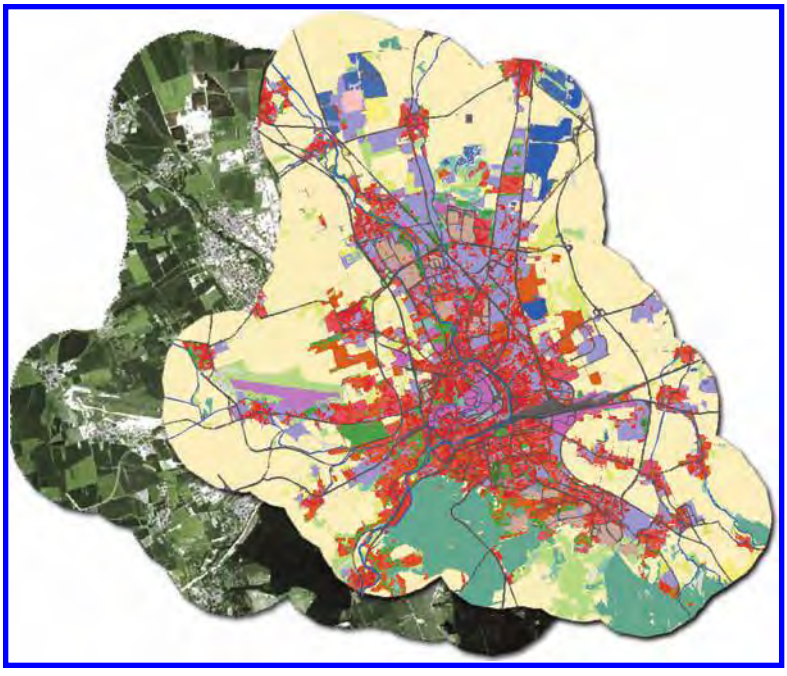

COLOR FIGURE 11.3 Satellite image and derived land use map from city of Erfurt, Germany. (Courtesy of GUS, H.G. Geo Data Solutions.)

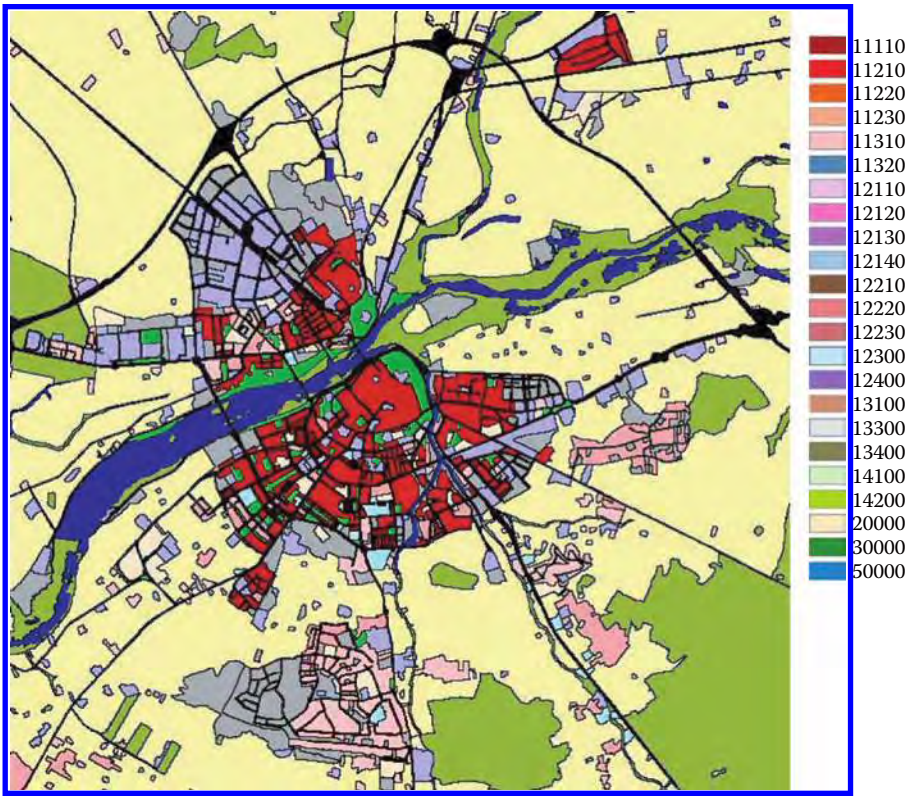

COLOR FIGURE 11.4 Badajoz, Spain, example of Urban Atlas classification. (Courtesy of GSE Land.)

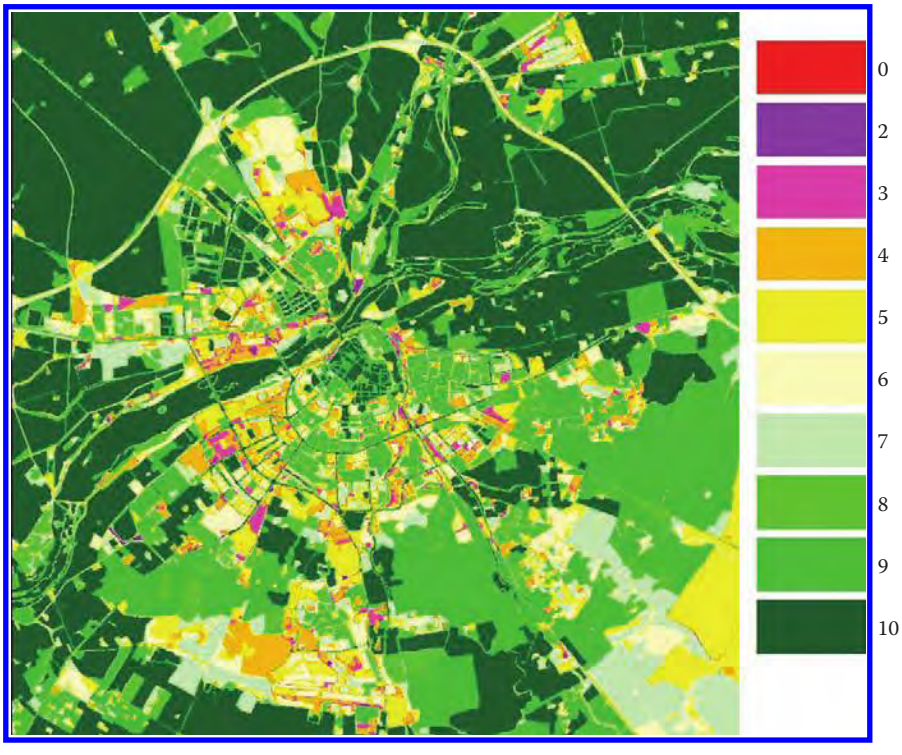

COLOR FIGURE 11.5 Badajoz divergence image — from red for no agreement to green for total agreement among the 10 service providers. (Courtesy of ETC-Lusi.)

COLOR FIGURE 11.6 Urban green map for the city of Poperinge, Belgium. (Courtesy of GUS – Eurosense.)

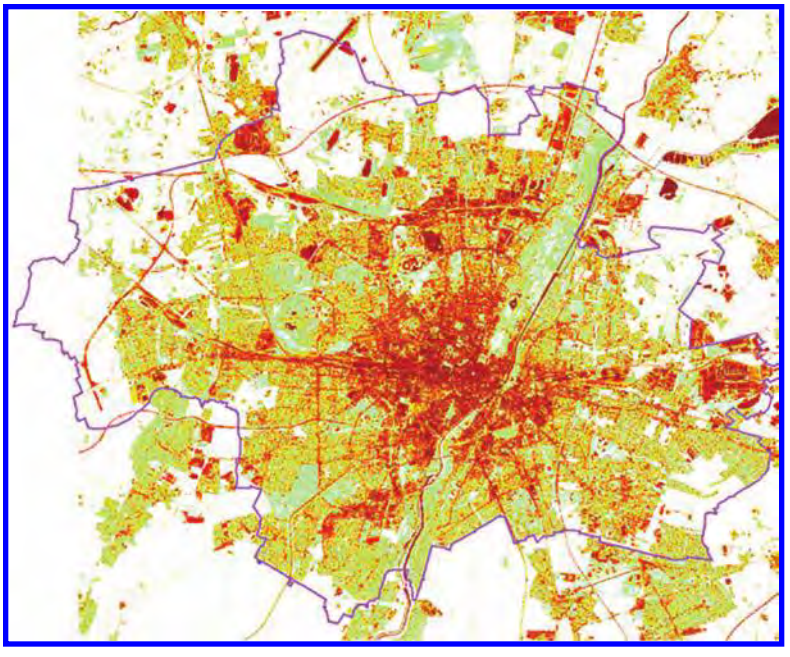

COLOR FIGURE 11.9 Pixel-based soil sealing map of Munich, Germany. (Courtesy of GSE Land – H.G. Geodata Solutions.)

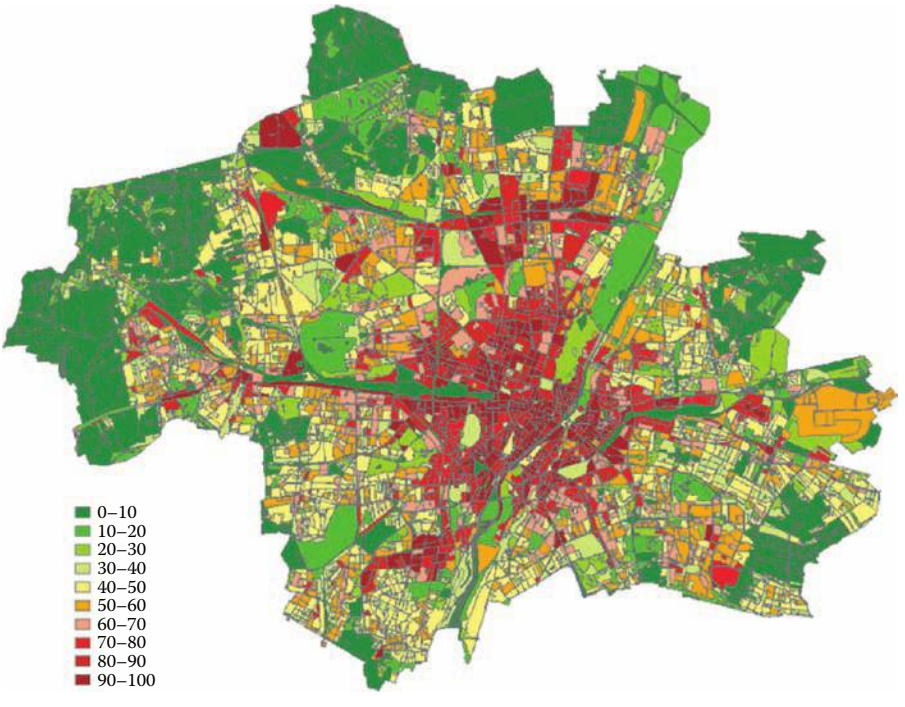

COLOR FIGURE 11.10 Object-based soil sealing map of Munich, Germany. (Courtesy of GSE Land – H.G. Geodata Solutions.)

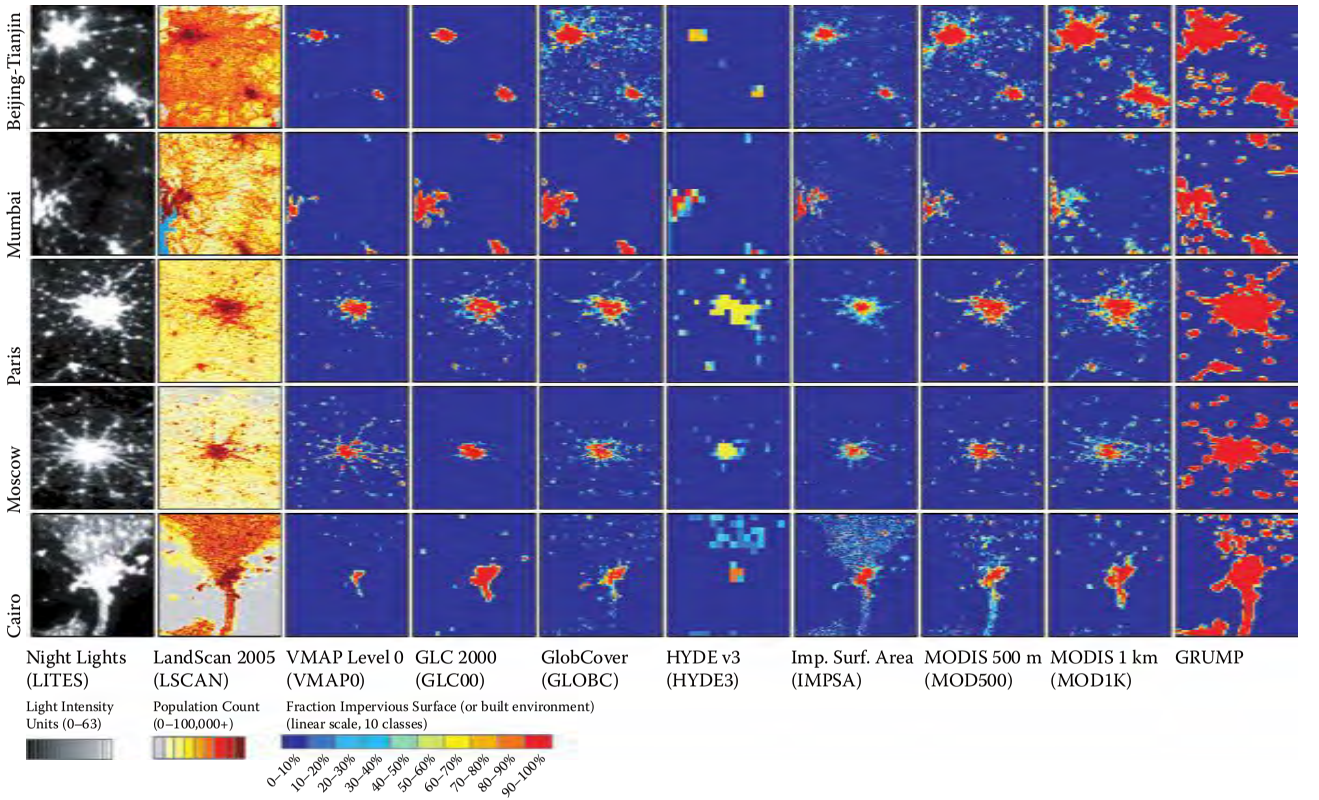

COLOR FIGURE 13.3 The eight global urban maps and two urban-related maps for Beijing–Tianjin, China; Mumbai, India; Paris, France; Moscow, Russia; and Cairo, Egypt. Each subset is approximately 150 × 150 km. LITES, LSCAN and IMPSA are at 30" arc-second resolution, HYDE3 is at 5' arc-minutes, and the remaining maps have been aggregated from 30" arc-seconds to 1.5' arc-minutes for display and comparison, effectively converting their legends from binary (urban/rural) to continuous (percentage urban). (From Potere, D. and Schneider, A. *GeoJournal*, 69: 55–80, 2007. With permission.)

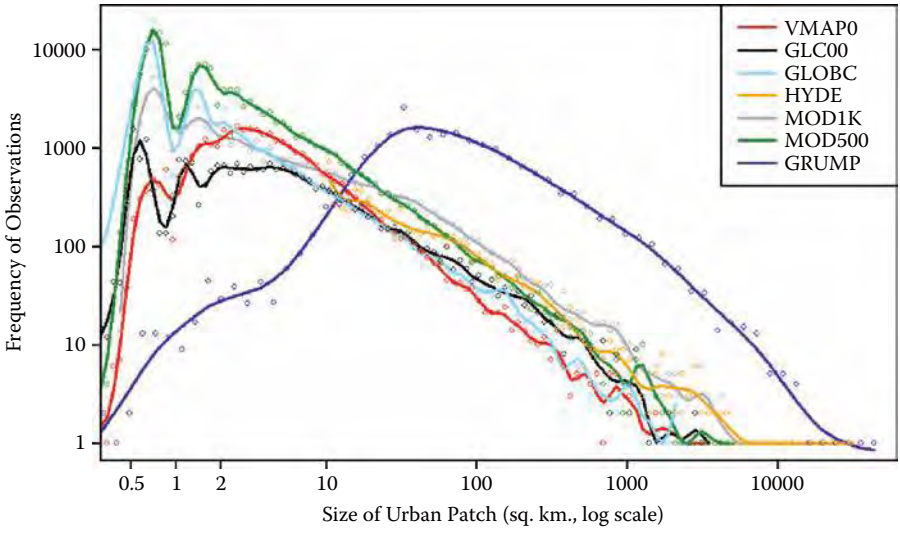

COLOR FIGURE 13.4 The frequency of urban patch sizes (log-log scale) for each map (excluding IMPSA). Observations are indicated with hollow circles and the solid line is a fitted spline. HYDE3 is plotted starting at 10 km^2 because of the coarse resolution of HYDE3 pixels (5' arc-minutes). (From Potere, D. and Schneider, A. *GeoJournal*, 69: 55–80, 2007. With permission.)

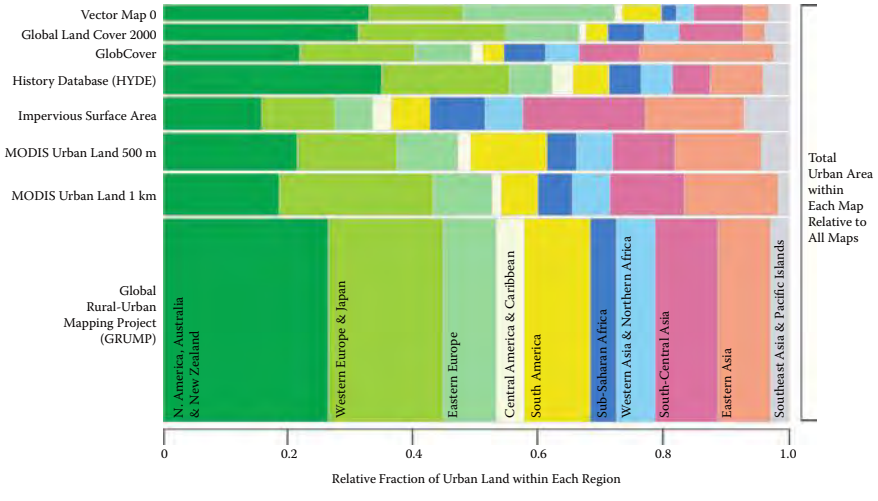

COLOR FIGURE 13.5 The distribution of urban land per continental region for eight global urban maps. The thickness of the horizontal bars reflects the relative amount of urban land within each of the eight maps. These horizontal bars are divided into sections representing the relative distribution of urban land area within each of the ten regions. (From Potere, D. and Schneider, A. *GeoJournal*, 69: 55–80, 2007. With permission.)

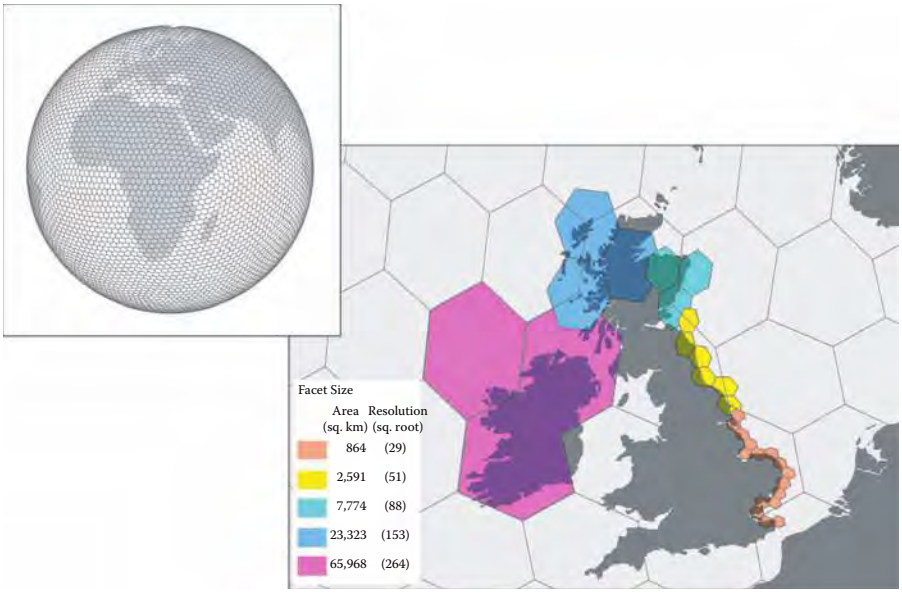

COLOR FIGURE 13.6 Five levels of a discrete global grid (DGG) system with hexagonal facets for the globe (upper left) and over the United Kingdom (lower right). The DGG displayed for the globe is at the coarsest facet size of 70,000 km^2 (purple facets in the lower right). The map legend also shows the effective spatial resolution for each facet size, estimated by the square root of the facet area. (From Potere, D. and Schneider, A. *GeoJournal*, 69: 55–80, 2007. With permission.)

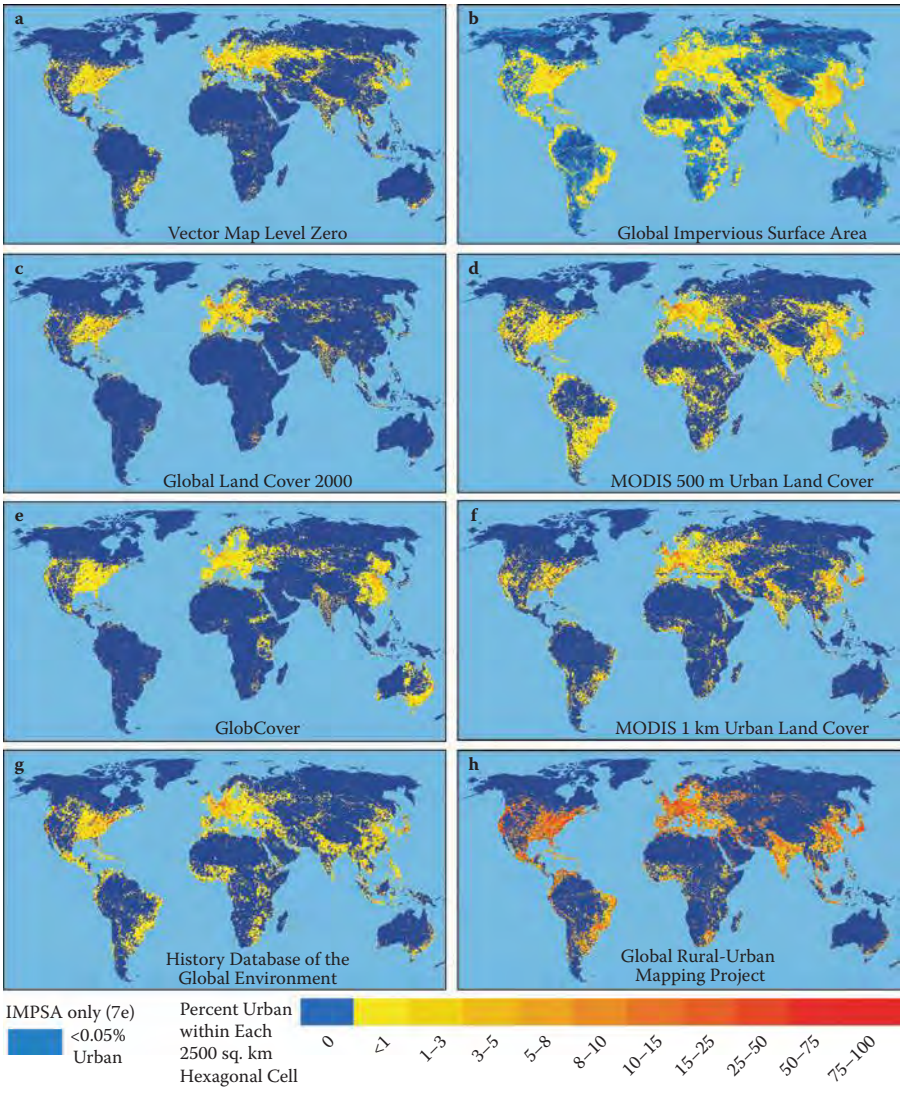

COLOR FIGURE 13.7 Depiction of the percentage of urban land per facet for all eight global urban maps, aggregated to a discrete global grid with hexagonal facets 2,591 km^2 in area (effective resolution of 51 km); (i) shows the amount of urban area for each grid cell averaged across all eight maps. Dark blue indicates absence of urban land. (From Potere, D. and Schneider, A. *GeoJournal*, 69: 55–80, 2007. With permission.)

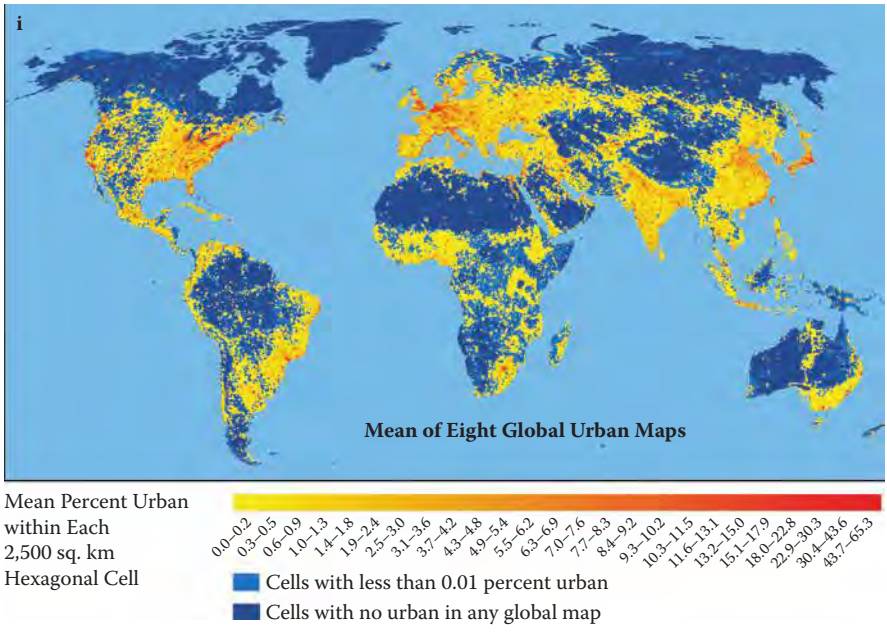

COLOR FIGURE 13.7 (Continued)

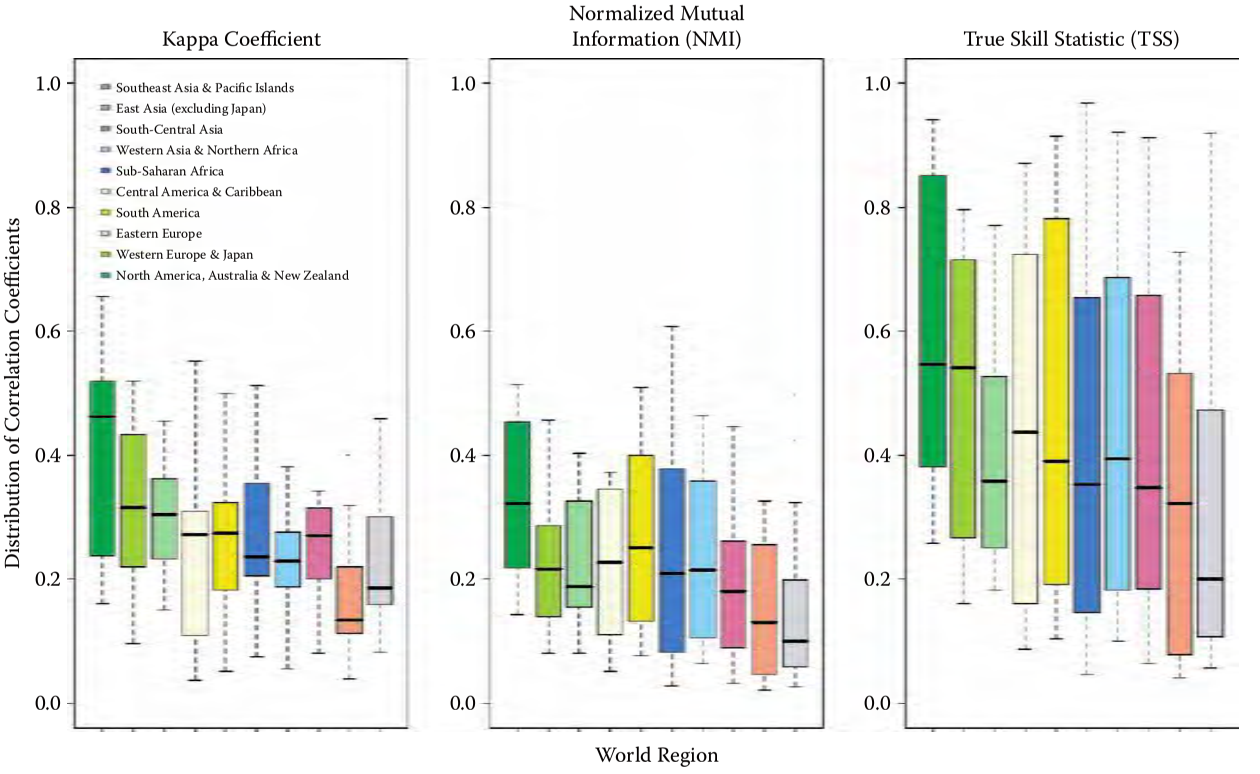

COLOR FIGURE 13.8 Regional box-plots for Cohen's Kappa, Normalized Mutual Information (NMI) and the True Skill Statistic (TSS) from contingency tables for all 28 inter-map comparisons, grouped by world region. All measures approach one when the maps are in complete agreement. (From Potere, D. and Schneider, A. *GeoJournal*, 69: 55–80, 2007. With permission.)

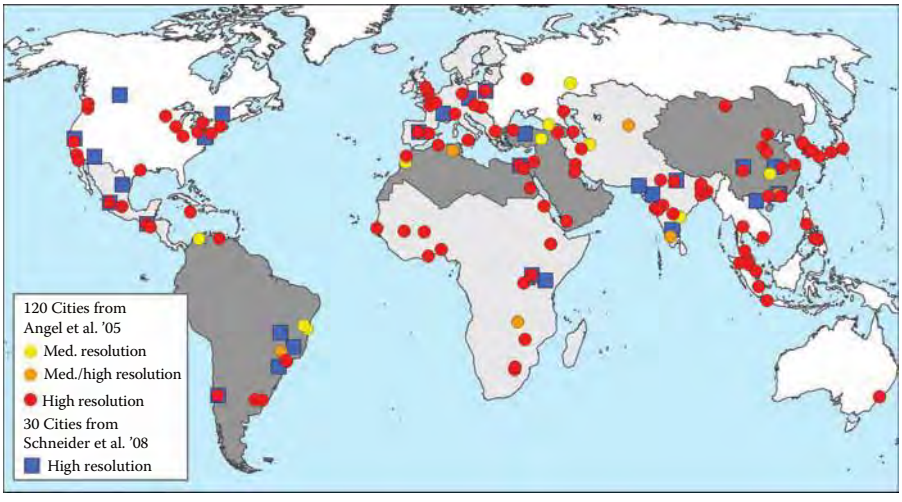

COLOR FIGURE 13.11 A global sample of 120 cities with populations greater than 100,000 from Angel et al. (2005) and 30 world cities from Schneider and Woodcock (2008). The Schneider and Woodcock cities are blue boxes, all of which are covered by high-resolution imagery from the Google Earth (GE) archive. The circles represent Angel et al. cities, and the color indicates the resolution of GE imagery available for that city as of March 2008, where "high" is QuickBird, Spot 5, or aerial photography, and "medium" is Landsat GeoCover. (From Potere, D. and Schneider, A. *GeoJournal*, 69: 55–80, 2007. With permission.)

COLOR FIGURE 15.3 Perspective view of a section of Osnabrueck: newly constructed buildings (yellow outline) block the flow of cold and fresh air toward the center of the city showing the impact that such a structure would have on the inner-city environment (exaggeration factor 5).

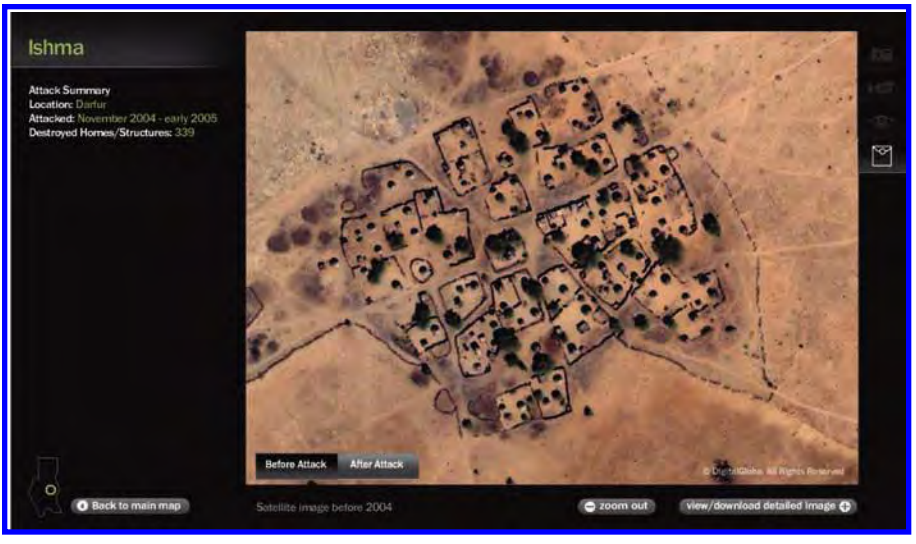

COLOR FIGURE 15.5 The village of Ishma (Darfur) before destruction by government and Janjawid forces. (Image from DigitalGlobe®. Used with permission.)

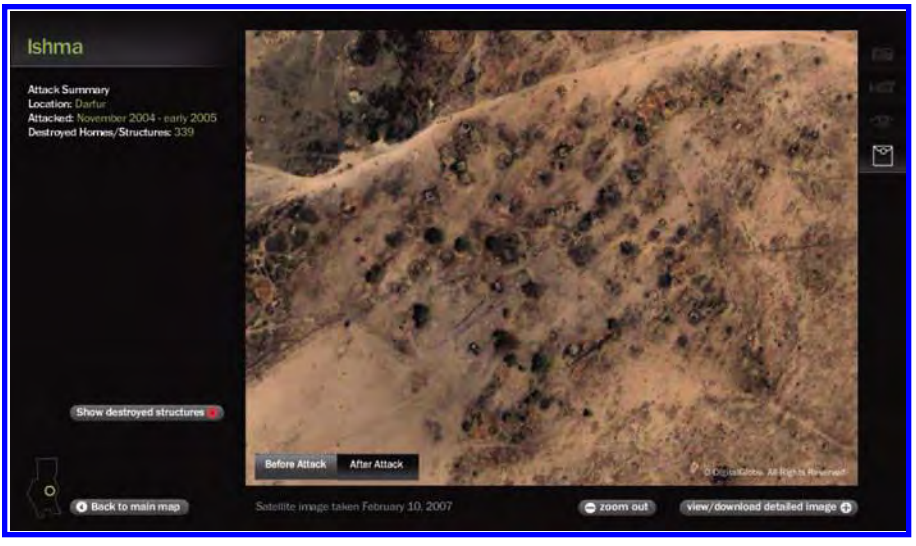

COLOR FIGURE 15.6 The village of Ishma after its destruction. (Image from DigitalGlobe®. Used with permission.)